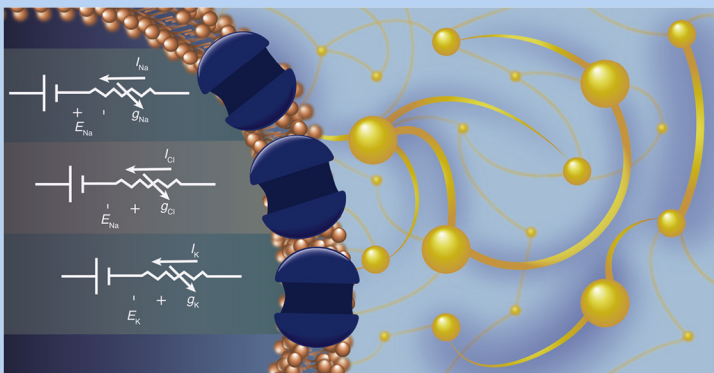


PROGRESS IN BRAIN RESEARCH

249

Mathematical Modelling in Motor Neuroscience: State of the Art and Translation to the Clinic. Gaze Orienting Mechanisms and Disease



EDITED BY
Stefano Ramat
Aasef G. Shaikh



Progress in Brain Research
Volume 249

Mathematical
Modelling in Motor
Neuroscience: State of
the Art and Translation
to the Clinic. Gaze
Orienting Mechanisms
and Disease

Serial Editor

Vincent Walsh

*Institute of Cognitive Neuroscience
University College London
17 Queen Square
London WC1N 3AR UK*

Editorial Board

Mark Bear, *Cambridge, USA.*
Medicine & Translational Neuroscience

Hamed Ekhtiari, *Tehran, Iran.*
Addiction

Hajime Hirase, *Wako, Japan.*
Neuronal Microcircuitry

Freida Miller, *Toronto, Canada.*
Developmental Neurobiology

Shane O'Mara, *Dublin, Ireland.*
Systems Neuroscience

Susan Rossell, *Swinburne, Australia.*
Clinical Psychology & Neuropsychiatry

Nathalie Rouach, *Paris, France.*
Neuroglia

Barbara Sahakian, *Cambridge, UK.*
Cognition & Neuroethics

Bettina Studer, *Dusseldorf, Germany.*
Neurorehabilitation

Xiao-Jing Wang, *New York, USA.*
Computational Neuroscience

Progress in Brain Research
Volume 249

Mathematical Modelling in Motor Neuroscience: State of the Art and Translation to the Clinic. Gaze Orienting Mechanisms and Disease

Edited by

Stefano Ramat

*Department of Electrical, Computer and Biomedical Engineering,
University of Pavia, Pavia, Italy*

Aasef G. Shaikh

*Department of Neurology,
University Hospitals Cleveland Medical Center;
Neurology Service, Louis Stokes Cleveland VA Medical Center,
Cleveland, OH, United States*



ACADEMIC PRESS

An imprint of Elsevier

Academic Press is an imprint of Elsevier
50 Hampshire Street, 5th Floor, Cambridge, MA 02139, United States
525 B Street, Suite 1650, San Diego, CA 92101, United States
The Boulevard, Langford Lane, Kidlington, Oxford OX5 1GB, United Kingdom
125 London Wall, London, EC2Y 5AS, United Kingdom

First edition 2019

Copyright © 2019 Elsevier B.V. All rights reserved.

No part of this publication may be reproduced or transmitted in any form or by any means, electronic or mechanical, including photocopying, recording, or any information storage and retrieval system, without permission in writing from the publisher. Details on how to seek permission, further information about the Publisher's permissions policies and our arrangements with organizations such as the Copyright Clearance Center and the Copyright Licensing Agency, can be found at our website: www.elsevier.com/permissions

This book and the individual contributions contained in it are protected under copyright by the Publisher (other than as may be noted herein).

Notices

Knowledge and best practice in this field are constantly changing. As new research and experience broaden our understanding, changes in research methods, professional practices, or medical treatment may become necessary.

Practitioners and researchers must always rely on their own experience and knowledge in evaluating and using any information, methods, compounds, or experiments described herein. In using such information or methods they should be mindful of their own safety and the safety of others, including parties for whom they have a professional responsibility.

To the fullest extent of the law, neither the Publisher nor the authors, contributors, or editors, assume any liability for any injury and/or damage to persons or property as a matter of products liability, negligence or otherwise, or from any use or operation of any methods, products, instructions, or ideas contained in the material herein.

ISBN: 978-0-444-64254-7

ISSN: 0079-6123

For information on all Academic Press publications
visit our website at <https://www.elsevier.com/books-and-journals>

Publisher: Zoe Kruze
Acquisition Editor: Sam Mahfoudh
Editorial Project Manager: Peter Llewellyn
Production Project Manager: Abdulla Sait
Cover Designer: Alan Studholme

Typeset by SPi Global, India



Working together
to grow libraries in
developing countries

www.elsevier.com • www.bookaid.org

Contributors

Zachariah O. Adham

Illinois Neurologic Institute, University of Illinois College of Medicine, Peoria, IL, United States

Chrystalina A. Antoniades

NeuroMetrology Lab, Nuffield Department of Clinical Neurosciences, University of Oxford, Oxford, United Kingdom

Laura J. Balcer

Department of Neurology; Department of Ophthalmology; Department of Population Health, New York University School of Medicine, New York, NY, United States

Mahya Beheshti

Department of Physical Medicine & Rehabilitation, NYU School of Medicine, New York, NY, United States

Elena Belova

Semenov Institute of Chemical Physics, Moscow, Russia

Sinem Balta Beylergil

Department of Biomedical Engineering, Case Western Reserve University; National VA Parkinson Consortium Center, Neurology Service, Daroff-Dell'Osso Ocular Motility and Vestibular Laboratory, Louis Stokes Cleveland VA Medical Center, Cleveland, OH, United States

Yash Chaudhry

Department of Neurology, New York University School of Medicine, New York, NY, United States

Tommaso Chiantini

Eye-tracking and Visual Application Lab (EVALab), Department of Medicine, Surgery and Neurosciences, University of Siena, Siena, Italy

Clara Chisari

Department of Neurology, University of Catania, Catania, Italy

Jeong-Yoon Choi

Department of Neurology, Dizziness Center, Clinical Neuroscience Center, Seoul National University Bundang Hospital, Seongnam; Department of Neurology, Seoul National University College of Medicine, Seoul, South Korea

Ayse I. Colpak

Department of Neurology, The Johns Hopkins University, Baltimore, MD, United States; Department of Neurology, Hacettepe University, Ankara, Turkey

John Douglas Crawford

York University, Toronto, ON, Canada

Weiwei Dai

Department of Neurology, New York University School of Medicine; Department of Electrical and Computer Engineering, New York University Tandon School of Engineering, New York, NY, United States

Emiliano De Schutter

Division de Neurologia, Hospital Del Carmen, Mendoza, Argentina

Mark J. Edwards

Motor Control and Movement Disorder Group, Institute of Molecular and Clinical Sciences, St George's University of London, London, United Kingdom

Thomas Eggert

Department of Neurology, University Hospital, LMU Munich, Munich, Germany

James J. Fitzgerald

NeuroMetrology Lab, Nuffield Department of Clinical Neurosciences; Nuffield Department of Surgical Sciences, University of Oxford, Oxford, United Kingdom

James Fung

Department of Physical Medicine & Rehabilitation, NYU School of Medicine, New York, NY, United States

Joseph Galea

School of Psychology, University of Birmingham, Birmingham, United Kingdom

Steven L. Galetta

Department of Neurology; Department of Ophthalmology, New York University School of Medicine, New York, NY, United States

Fatema F. Ghasia

Neurology Service, Daroff-Dell'Osso Ocular Motility Laboratory, Louis Stokes Cleveland VA Cole Eye Institute, Cleveland Clinic, Cleveland, OH, United States

Stefan Glasauer

Computational Neurosciences; German Center for Vertigo and Balance Disorders, University Hospital Munich, Munich; Institute of Medical Technology, Brandenburg University of Technology Cottbus-Senftenberg, Senftenberg; Graduate School of Systemic Neurosciences, Ludwig-Maximilians-University Munich, Planegg, Germany

Laurent Goffart

Aix Marseille University, CNRS, INT, Institut de Neurosciences de la Timone, Marseille; Aix Marseille University, CNRS, CGGG, Centre Gilles Gaston Granger, Aix-en-Provence, France

Marco Gori

University of Siena, Siena, Italy

Peter Henningsen

Department of Psychosomatic Medicine and Psychotherapy, Klinikum rechts der Isar, Technical University of Munich, Munich, Germany

Anja K.E. Horn

Institute of Anatomy and Cell Biology I, Ludwig-Maximilian University (LMU); Graduate School of Systemic Neurosciences (GSN), LMU, Munich, Germany

Maryam Hosseini

Department of Physical Medicine & Rehabilitation, NYU School of Medicine, New York, NY, United States

Todd E. Hudson

Department of Physical Medicine & Rehabilitation; Department of Neurology, NYU School of Medicine, New York, NY, United States

Jonathan B. Jacobs

Daroff-Dell'Osso Ocular Motility Laboratory, Department of Neurology, Louis Stokes Cleveland VA Medical Center; School of Medicine; Department of Biomedical Engineering, Case Western Reserve University, Cleveland, OH, United States

Hyder A. Jinnah

Departments of Neurology and Human Genetics, Emory University, Atlanta, GA, United States

Ileok Jung

Department of Neurology, Korea University College of Medicine, Korea University Ansan Hospital, Ansan, South Korea

Bahadir Kasap

Department of Biophysics, Radboud University, Donders Centre for Neuroscience, Nijmegen, The Netherlands

Jorge C. Kattah

Illinois Neurologic Institute, University of Illinois College of Medicine, Peoria, IL, United States

Amir Kheradmand

Department of Neurology; Department of Otolaryngology-Head and Neck Surgery, The Johns Hopkins University, Baltimore, MD, United States

Hyo-Jung Kim

Research Administration Team, Seoul National University Bundang Hospital, Seongnam, South Korea

Ji-Soo Kim

Department of Neurology, Dizziness Center, Clinical Neuroscience Center, Seoul National University Bundang Hospital, Seongnam; Department of Neurology, Seoul National University College of Medicine, Seoul, South Korea

Sung-Hee Kim

Department of Neurology, Kyungpook National University, Chilgok Hospital, Daegu, South Korea

Yoshiko Kojima

Washington National Primate Research Center, University of Washington, Seattle, WA, United States

Nadine Lehnen

Department of Psychosomatic Medicine and Psychotherapy, Klinikum rechts der Isar, Technical University of Munich; German Center for Vertigo and Balance Disorders, University Hospital Munich, Munich; Institute of Medical Technology, Brandenburg University of Technology Cottbus-Senftenberg, Senftenberg; Graduate School of Systemic Neurosciences, Ludwig-Maximilians-University Munich, Planegg, Germany

Karoline Lienbacher

Institute of Anatomy and Cell Biology I, Ludwig-Maximilian University (LMU); German Center for Vertigo and Balance Disorders, LMU, Munich, Germany

John Martone

Department of Neurology, New York University School of Medicine, New York, NY, United States

Ümit S. Mayadali

Institute of Anatomy and Cell Biology I, Ludwig-Maximilian University (LMU); German Center for Vertigo and Balance Disorders; Graduate School of Systemic Neurosciences (GSN), LMU, Munich, Germany

Cameron C. McIntyre

Department of Biomedical Engineering, Case Western Reserve University, Cleveland, OH, United States

Jordan Murray

Cole Eye Institute, Cleveland Clinic, Cleveland, OH, United States

Michael Mustari

Washington National Primate Research Center; Department of Ophthalmology, University of Washington, Seattle, WA, United States

Vladislav Myrov

Saint Petersburg Academic University, Saint Petersburg, Russia

Ludmila Myrova

Moscow Scientific Research Institute of Radio Engineering, Moscow, Russia

Paolo Nucci

San Giuseppe Eye Clinic; University of Milan, Milan, Italy

Lance M. Optican

Laboratory of Sensorimotor Research, NEI, NIH, DHHS, Bethesda, MD, United States

Jorge Otero-Millan

Department of Neurology, The Johns Hopkins University, Baltimore, MD, United States

Murat C. Ozdemir

Department of Neurology, University Hospital, LMU Munich, Munich, Germany

Sarah Ozinga

Department of Biomedical Engineering, Case Western Reserve University, Cleveland, OH, United States

Salil Patel

NeuroMetrology Lab, Nuffield Department of Clinical Neurosciences, University of Oxford, Oxford, United Kingdom

Pietro Piu

Eye-tracking and Visual Application Lab (EVALab), Department of Medicine, Surgery and Neurosciences, University of Siena, Siena, Italy

Elena Pretegiani

Eye-tracking and Visual Application Lab (EVALab), Department of Medicine, Surgery and Neurosciences, University of Siena, Siena, Italy; Laboratory of Sensorimotor Research-NEI, NIH, DHHS, Bethesda, MD, United States

Nataliya Pyatka

Department of Neurology, University Hospitals Cleveland Medical Center and Case Western Reserve University, Cleveland, OH, United States

Cecilia Ramaioli

Department of Psychosomatic Medicine and Psychotherapy, Klinikum rechts der Isar, Technical University of Munich; German Center for Vertigo and Balance Disorders, University Hospital Munich, Munich; Institute of Medical Technology, Brandenburg University of Technology Cottbus-Senftenberg, Senftenberg, Germany

John-Ross Rizzo

Department of Physical Medicine & Rehabilitation; Department of Neurology, NYU School of Medicine, New York, NY, United States

Francesca Rosini

Eye-tracking and Visual Application Lab (EVALab); Neurological and Neurometabolic Unit, Department of Medicine, Surgery and Neurosciences, University of Siena, Siena, Italy

Jaume Rosset-Llobet

Institut de l'Art. Medicina & Fisiologia, Terrassa, (Barcelona) Spain

Janet C. Rucker

Department of Neurology; Department of Ophthalmology, NYU School of Medicine, New York, NY, United States

Alessandra Rufa

Eye-tracking and Visual Application Lab (EVALab), Neurological and Neurometabolic Unit, Department of Medicine, Surgery and Neurosciences, University of Siena, Siena, Italy

Anna Sadnicka

Motor Control and Movement Disorder Group, Institute of Molecular and Clinical Sciences, St George's University of London; Clinical and Movement Neurosciences, UCL Queen Square Institute of Neurology, London, United Kingdom

Matteo Scaramuzzi

Cole Eye Institute, Cleveland Clinic, Cleveland, OH, United States; San Giuseppe Eye Clinic; University of Milan, Milan, Italy

Lena Schröder

Department of Psychosomatic Medicine and Psychotherapy, Klinikum rechts der Isar, Technical University of Munich, Munich; Graduate School of Systemic Neurosciences, Ludwig-Maximilians-University Munich, Planegg, Germany

Alexey Sedov

Semenov Institute of Chemical Physics, Russian Academy of Sciences; Russian Institute for Chemical Physics, Moscow, Russia

Ulia Semenova

Semenov Institute of Chemical Physics, Russian Academy of Sciences, Moscow, Russia

Alexandra J. Sequeira

Department of Neurology, New York University School of Medicine, New York, NY, United States

Valeria Serchi

Eye-tracking and Visual Application Lab (EVALab), Department of Medicine, Surgery and Neurosciences, University of Siena, Siena, Italy

Alessandro Serra

Daroff-Dell'Osso Ocular Motility Laboratory, Department of Neurology, Louis Stokes Cleveland VA Medical Center; School of Medicine, Case Western Reserve University; Department of Neurology, University Hospitals Cleveland Medical Center, Cleveland, OH, United States

Azadeh Shafieesabet

Department of Physical Medicine & Rehabilitation, NYU School of Medicine, New York, NY, United States

Aasef G. Shaikh

Department of Neurology, University Hospitals Cleveland Medical Center and Case Western Reserve University; Case Medical Center, Case Western Reserve University; Daroff-Dell'Osso Ocular Motility Laboratory and Neurology Service; National VA Parkinson Consortium Center and Neurology Service, Louis Stokes Cleveland VA Medical Center, Cleveland, OH, United States

Yoshikazu Shinoda

Department of Systems Neurophysiology, Graduate School of Medicine, Tokyo Medical and Dental University, Tokyo, Japan

Margaret M. Skelly

Daroff-Dell'Osso Ocular Motility Laboratory, Department of Neurology, Louis Stokes Cleveland VA Medical Center, Cleveland, OH, United States

Lawrence H. Snyder

Department of Neuroscience, Washington University School of Medicine, St. Louis, MO, United States

Andreas Straube

Department of Neurology, University Hospital, LMU Munich, Munich, Germany

Michael Strupp

German Center for Vertigo and Balance Disorders; Department of Neurology;
Graduate School of Systemic Neurosciences (GSN), LMU, Munich, Germany

Yuriko Sugiuchi

Department of Systems Neurophysiology, Graduate School of Medicine, Tokyo
Medical and Dental University, Tokyo, Japan

Mayu Takahashi

Department of Systems Neurophysiology, Graduate School of Medicine, Tokyo
Medical and Dental University, Tokyo, Japan

Alexey Tomskiy

N.N. Burdenko National Scientific and Practical Center for Neurosurgery,
Moscow, Russia

Svetlana Usova

Semenov Institute of Chemical Physics, Russian Academy of Sciences, Moscow,
Russia

A. John van Opstal

Department of Biophysics, Donders Institute for Brain, Cognition and Behaviour,
Radboud University Nijmegen, Nijmegen, The Netherlands

Mark F. Walker

National VA Parkinson Consortium Center; Neurology Service, Daroff-Dell'Osso
Ocular Motility and Vestibular Laboratory, Louis Stokes Cleveland VA Medical
Center, Cleveland, OH, United States

Benjamin L. Walter

Center for Neurological Restoration, Cleveland Clinic, Cleveland, OH,
United States

Domenica Zaino

Eye-tracking and Visual Application Lab (EVALab); Neurological and
Neurometabolic Unit, Department of Medicine, Surgery and Neurosciences,
University of Siena, Siena, Italy

Dario Zanca

University of Florence, Florence; University of Siena, Siena, Italy

David S. Zee

Department of Neurology; Department of Otolaryngology-Head and Neck
Surgery; Department of Neuroscience; Department of Ophthalmology, The Johns
Hopkins University, Baltimore, MD, United States

This page intentionally left blank

Contents

Contributors.....	v
Preface	xxv

SECTION I DIDACTIC: Modeling

CHAPTER 1 Sequential Bayesian updating as a model for human perception.....	3
<i>Stefan Glasauer</i>	
1. Introduction.....	3
2. A simple case: Temporal constancy	5
3. A more sophisticated case: Random changes over time	8
4. Implementing sequential updating.....	12
5. Perception-action coupling: Decision making.....	14
6. Summary	16
Acknowledgment.....	16
References.....	16
CHAPTER 2 Maps and sensorimotor transformations for eye-head gaze shifts: Role of the midbrain superior colliculus.....	19
<i>A. John van Opstal, Bahadir Kasap</i>	
1. Introduction.....	20
1.1. Eye-head gaze shifts.....	20
1.2. Brief background SC	21
2. Methods.....	22
2.1. Paradigm.....	23
2.2. Analysis.....	23
3. Results	24
3.1. Behavior.....	24
3.2. Neural responses	25
3.3. Model	27
4. Discussion	29
Acknowledgments	32
References.....	32
CHAPTER 3 Modeling gaze position-dependent opsoclonus.....	35
<i>Lance M. Optican, Janet C. Rucker, John-Ross Rizzo, Todd E. Hudson</i>	
1. Introduction	35

2. Methods	38
3. Results	39
4. New model of opsoclonus	40
4.1. Eye position neurons.....	42
4.2. Supplementary eye fields (SEF).....	42
4.3. Ocular motor cerebellum	43
4.4. Summary of cortical inputs.....	43
4.5. Nucleus prepositus hypoglossi (NPH).....	43
4.6. Omnidirectional and directional pause neurons (OPN and DPN).....	44
4.7. New hypothesis about OPN function.....	47
4.8. Smooth pursuit.....	48
4.9. Model implementation	49
4.10. Simulations.....	52
5. Discussion	55
Acknowledgments.....	56
References	56

SECTION II DIDACTIC: Translational

CHAPTER 4 Eye position-dependent opsoclonus in mild traumatic brain injury.....	65
<i>John-Ross Rizzo, Todd E. Hudson, Alexandra J. Sequeira, Weiwei Dai, Yash Chaudhry, John Martone, David S. Zee, Lance M. Optican, Laura J. Balcer, Steven L. Galetta, Janet C. Rucker</i>	
1. Introduction	66
2. Case description.....	66
3. Eye movement recording methods.....	67
4. Eye movement recording results.....	67
5. Discussion.....	68
5.1. Behavioral characteristics of opsoclonus/ocular flutter and “voluntary flutter”	68
5.2. Mechanisms of opsoclonus/ocular flutter and gaze position-dependence	72
5.3. Relationship with traumatic brain injury and potential mechanisms of gaze position-dependent opsoclonus/ ocular flutter.....	75
6. Conclusion	75
Acknowledgment	76
References	76

SECTION III RESEARCH: Saccades

CHAPTER 5 Saccades in Parkinson's disease: Hypometric, slow, and maladaptive	81
Aasef G. Shaikh, Fatema F. Ghasia	
1. Introduction.....	82
2. Methods.....	83
2.1. Experimental setup.....	83
2.2. Experimental protocol and data analysis.....	83
3. Results.....	84
3.1. Quantitative characteristics of saccade interruptions.....	84
3.2. Quantitative characteristics of saccade curvature.....	86
3.3. Saccade amplitude to velocity relationship.....	87
3.4. Do abnormal saccade characteristics correlate with the severity of PD?.....	89
4. Discussion.....	89
4.1. Impaired function of basal ganglia, superior colliculus, and impaired corollary discharge to the frontal eye fields...90	90
4.2. Impaired function of burst generators in PD	90
4.3. Superior colliculus activation and maladaptive changes in saccade trajectory	91
Acknowledgments	92
References	92
CHAPTER 6 Brainstem neural circuits for fixation and generation of saccadic eye movements	95
Yoshikazu Shinoda, Mayu Takahashi, Yuriko Sugiuchi	
1. Background.....	95
2. Synaptic inputs from the SC to Abd MNs and IBNs.....	97
3. Synaptic inputs from the rostral and caudal parts of the SC to OPNs	98
4. Discussion	100
Conflicts of Interest	102
References	102
CHAPTER 7 Morphological and electrophysiological characteristics of the commissural system in the superior colliculi for control of eye movements	105
Mayu Takahashi	
1. Introduction.....	106
2. Methods	107

3. Results	107
4. Discussion	112
References	114

CHAPTER 8 Potassium channels in omnipause neurons 117

**Ümit S. Mayadali, Karoline Lienbacher, Michael Mustari,
Michael Strupp, Anja K.E. Horn**

1. Introduction	118
2. Methods	118
3. Results	119
4. Discussion	121
Acknowledgments	122
References	122

**CHAPTER 9 The cerebellum improves the precision of
antisaccades by a latency-duration trade-off 125**

**Pietro Piu, Elena Pretegiani, Francesca Rosini,
Valeria Serchi, Domenica Zaino, Tommaso Chiantini,
Alessandra Rufa**

1. Introduction	126
2. Methods	127
2.1. Patients and controls	127
2.2. Eye movement recording	127
2.3. Signal processing	128
2.4. Latency decomposition	128
2.5. Statistical analysis	130
3. Results	131
3.1. Descriptive statistics	131
3.2. Ex-Wald parameters (drift and boundary): Mann-Whitney <i>U</i> test	133
3.3. Kolmogorov-Smirnov test of the DT and RT distributions	133
3.4. Logistic model	133
3.5. Sample entropy of saccadic end-points	135
4. Discussion	135
References	137
Further reading	139

**CHAPTER 10 Saccade variability in healthy subjects
and cerebellar patients 141**

Thomas Eggert, Andreas Straube

1. Introduction	141
------------------------------	-----

2. Methods	143
2.1. Subjects.....	143
2.2. Apparatus and procedure	143
2.3. Data analysis.....	144
2.4. Statistics	146
3. Results	146
3.1. Parametric approach for the analysis of motor feedback ..	147
3.2. Decomposition of the inter-trial variance of the saccade trajectory into accumulating noise and feedback noise....	148
4. Discussion	149
Acknowledgments	151
References	151

CHAPTER 11 Electrical stimulation in a spiking neural network model of monkey superior colliculus 153

A. John van Opstal, Bahadir Kasap

1. Introduction.....	153
2. Methods and results	155
2.1. Afferent mapping	155
2.2. Network characteristics	156
2.3. Current spread	159
2.4. Network tuning	159
2.5. Micro-stimulation	159
2.6. Kinematics	159
3. Discussion	160
3.1. Network tuning	162
3.2. Network normalization	162
3.3. In conclusion	163
Acknowledgments	164
Appendix: Parameter values used in the simulations	164
References	165
Further reading	166

SECTION IV RESEARCH: Adaptation

CHAPTER 12 A neuronal process for adaptive control of primate saccadic system 169

Yoshiko Kojima

1. Introduction	170
2. Saccade adaptation paradigm	170
3. The neuronal mechanism of saccades	171

4. The neural mechanism of saccade adaptation	173
5. Error signal for saccade adaptation	175
Acknowledgments	179
References	179

CHAPTER 13 A unified computational framework for visual attention dynamics 183

Dario Zanca, Marco Gori, Alessandra Rufa

1. Introduction	183
2. Convolutional feature activation maps are good saliency predictors	184
3. Eye movements guided by convolutional features	185
4. Discussion	187
References	187

CHAPTER 14 Improving the repeatability of two-rate model parameter estimations by using autoencoder networks 189

Murat C. Ozdemir, Thomas Eggert, Andreas Straube

1. Introduction	189
2. Methods	190
3. Results	192
4. Discussion	193
References	194

SECTION V RESEARCH: Nystagmus

CHAPTER 15 Rebound nystagmus, a window into the oculomotor integrator 197

**Jorge Otero-Millan, Ayse I. Colpak, Amir Kheradmand,
David S. Zee**

1. Introduction	197
2. Methods	199
3. Results	200
4. Discussion	202
4.1. Characterization of gaze holding	202
4.2. Modeling rebound nystagmus	205
4.3. Why rebound?	207
4.4. Other approaches to model neural integrators	207
Acknowledgments	208
References	208

CHAPTER 16 Central positional nystagmus: Characteristics and model-based explanations	211
Jeong-Yoon Choi, Ji-Soo Kim	
1. Introduction.....	212
2. Characteristics of central positional nystagmus.....	213
2.1. Paroxysmal CPN.....	213
2.2. Persistent CPN	216
3. Etiology and location of lesions	217
4. Mechanisms.....	218
5. Conclusion.....	221
Source of funding/support.....	221
Conflict of interest statement	222
Disclosure	222
Authors' contributions.....	222
References	222
CHAPTER 17 Modulation of acquired monocular pendular nystagmus in multiple sclerosis: A modeling approach.....	227
Ileok Jung, Sung-Hee Kim, Hyo-Jung Kim, Jeong-Yoon Choi, Ji-Soo Kim	
1. Introduction	228
2. Methods	228
2.1. Patient.....	228
2.2. Study protocol	229
2.3. Oculography	230
2.4. Analyses of nystagmus	230
2.5. Statistics	230
3. Results	230
3.1. The paradigm I for visual modulation.....	230
3.2. The paradigm II for saccadic modulation.....	231
4. Discussion	231
5. Conclusion	233
Acknowledgments	233
Disclosure	233
References	233
CHAPTER 18 Fixation instability in amblyopia: Oculomotor disease biomarkers predictive of treatment effectiveness	235
Matteo Scaramuzzi, Jordan Murray, Jorge Otero-Millan, Paolo Nucci, Aasef G. Shaikh, Fatema F. Ghasia	
1. Introduction	236

2. Methods	237
2.1. Eye movement recording and analysis.....	241
3. Clinical data and outcome measures.....	242
4. Results	243
5. Treatment outcome measures as a function of the clinical subtype of amblyopia.....	243
6. Treatment outcome measures as a function of fixation eye movement waveforms	245
7. Discussion.....	246
Acknowledgments.....	247
References.....	247
Further reading.....	248

SECTION VI RESEARCH: Dystonia

CHAPTER 19 What can kinematic studies tell us about the mechanisms of dystonia? 251

Anna Sadnicka, Joseph Galea, Mark J. Edwards

1. Dystonia	251
2. Why study kinematics?	252
3. Kinematic studies of dystonia.....	253
4. Variability in DYT1 dystonia	254
5. Directions for future work	258
6. Conclusions	259
References	259

CHAPTER 20 Implications of asymmetric neural activity patterns in the basal ganglia outflow in the integrative neural network model for cervical dystonia 261

**Alexey Sedov, Ulia Semenova, Svetlana Usova,
Alexey Tomskiy, John Douglas Crawford, Hyder A. Jinnah,
Aasef G. Shaikh**

1. Introduction	262
2. Materials and methods	263
3. Results	263
4. Discussion	267
Acknowledgments	267
References	267

CHAPTER 21 A motor control model of task-specific dystonia and its rehabilitation 269

Anna Sadnicka, Jaume Rosset-Llobet

1. Introduction	269
------------------------------	-----

2. Risk factors for task-specific dystonia.....	270
3. A motor control model of task-specific dystonia.....	273
3.1. Motor skill learning in health.....	273
3.2. Neural correlates of skill expertise.....	274
3.3. Psychology of motor control.....	275
3.4. Onset of dystonia.....	276
4. Management of task-specific dystonia.....	278
4.1. Prevention.....	278
4.2. Traditional management.....	279
4.3. Emerging treatments.....	279
5. Conclusions.....	281
References.....	281

CHAPTER 22 Tremor in chronic inflammatory demyelinating polyneuropathy: Proof of unifying network model for dystonia..... 285

**Nataliya Pyatka, Alexey Sedov, Benjamin L. Walter,
Hyder A. Jinnah, Aasef G. Shaikh**

1. Introduction.....	286
2. Methods.....	287
2.1. Clinical case.....	287
2.2. Data acquisition technique.....	288
2.3. Data analysis.....	289
3. Results.....	289
4. Discussion.....	292
Acknowledgments.....	293
References.....	293

SECTION VII RESEARCH: Parkinson's disease

CHAPTER 23 Oculomotor effects of medical and surgical treatments of Parkinson's disease..... 297

Salil Patel, James J. Fitzgerald, Chrystalina A. Antoniades

1. Introduction.....	297
2. Effects of PD medication on the oculomotor system.....	298
3. Effects of surgical intervention on PD on the oculomotor system.....	300
3.1. Computational modeling of oculomotor function in PD.....	301
References.....	303

CHAPTER 24 Vestibular heading perception in Parkinson's disease	307
Sinem Balta Beylergil, Sarah Ozinga, Mark F. Walker, Cameron C. McIntyre, Aasef G. Shaikh	
1. Introduction	308
2. Methods	308
2.1. Subjects	308
2.2. Experiment setup	310
2.3. Experiment protocol	310
2.4. Data analysis	311
3. Results	312
4. Discussion	314
5. Conclusion	316
References	316
CHAPTER 25 A new approach for estimation of spiketrain patterns in basal ganglia	321
Vladislav Myrov, Alexey Sedov, Alexey Tomskiy, Ludmila Myrova, Elena Belova	
1. Introduction	321
2. Materials and methods	322
2.1. Data description	322
2.2. Method description	322
3. Results	323
4. Discussion	324
Acknowledgment	324
References	324
SECTION VIII RESEARCH: Others	
CHAPTER 26 A model-based study of internuclear ophthalmoparesis and ocular-motor fatigue in multiple sclerosis	329
Jonathan B. Jacobs, Clara Chisari, Margaret M. Skelly, Mark F. Walker, Alessandro Serra	
1. Introduction	330
2. Methods	331
2.1. Eye movement recording	331
2.2. Model simulation	333
3. Results	336
3.1. Saccades parameters	336
3.2. Model simulation: PSR changes	337

3.3. Model simulation: PTD changes	338
3.4. Model simulation: Complex saccades	339
4. Discussion	339
Acknowledgment	343
Funding	343
Disclaimer	343
References	343
Further reading	344
CHAPTER 27 Central positional vertigo: A clinical-imaging study	345
Emiliano De Schutter, Zachariah O. Adham, Jorge C. Kattah	
1. Introduction	346
2. Methods	346
3. Results	347
3.1. General characteristics	347
3.2. CPV-first and imaging-first groups	354
3.3. Unilateral and bilateral lesion groups	355
4. Discussion	355
4.1. General clinical neurotology findings	357
5. Comparison between clinical-first and imaging-first subgroups	358
5.1. CPV lesion localization	358
6. Limitations	359
References	359
CHAPTER 28 Eye-hand re-coordination: A pilot investigation of gaze and reach biofeedback in chronic stroke ...	361
John-Ross Rizzo, Mahya Beheshti, Azadeh Shafieesabet, James Fung, Maryam Hosseini, Janet C. Rucker, Lawrence H. Snyder, Todd E. Hudson	
1. Introduction	362
2. Methods	363
2.1. Subjects	363
2.2. Inclusion and exclusion criteria	363
2.3. Experiment	365
2.4. Statistical analysis	366
2.5. Results	366
3. Eye and hand movement timing/duration	366
4. Spatial errors for look and reach	369
5. Discussion	370
References	372
Further reading	374

CHAPTER 29 Kinematics and the neurophysiological study of visually-guided eye movements	375
Laurent Goffart	
1. Gaze, target and measurements	375
2. Gaze direction as equilibrium	376
3. Transforming the location of a peripheral target into saccade duration	378
4. Tracking a moving target	379
5. Target velocity as a stimulus for pursuit	380
6. Pursuit as sustained imbalance	381
7. Conclusion	381
Acknowledgments	382
References	382
Further reading	384
CHAPTER 30 Deficient head motor control in functional dizziness: Experimental evidence of central sensory-motor dysfunction in persistent physical symptoms	385
Nadine Lehnken, Lena Schröder, Peter Henningsen, Stefan Glasauer, Cecilia Ramaioli	
1. Introduction	386
2. Materials and methods	388
2.1. Subjects	388
2.2. Experimental procedure	388
2.3. Data analysis	389
2.4. Statistical analysis	391
3. Results	392
3.1. Video head impulse test and head impulse testing device function test	392
3.2. Altering head mechanics during eye-head gaze shifts to visual targets	392
3.3. Comparison to previously acquired data from patients with chronic vestibular loss and cerebellar ataxia	393
4. Discussion	393
Conflict of interest	396
Author contribution	396
Funding	397
Data availability statement	397
References	397

Preface

Volume 249 of *Progress in Brain Research: Mathematical Modeling in Motor Neuroscience: State of the Art and Translation to the Clinic* is the second of two volumes that grew out of a conference, *Mathematical Modeling in Motor Neurosciences*, held at the University of Pavia, Italy, 6–8 June, 2018 to honor Lance Optican. Volume 248 focuses on the ocular motor plant and gaze stabilization mechanisms. This volume, 249, deals with gaze orienting mechanisms and disease. The reader is referred to the Foreword in Volume 248 for a summary of the motivation behind both the conference and publication, and the many contributions made by Lance Optican.

Stefano Ramat^a
Aasef G. Shaikh^b

^a*Department of Electrical, Computer and Biomedical Engineering, University of Pavia, Pavia, Italy*

^b*Department of Neurology, University Hospitals Cleveland Medical Center; Neurology Service,
Louis Stokes Cleveland VA Medical Center, Cleveland, OH, United States*

This page intentionally left blank

SECTION

DIDACTIC:
Modeling

I

This page intentionally left blank

Sequential Bayesian updating as a model for human perception

1

Stefan Glasauer*

*Computational Neuroscience, Brandenburg University of Technology Cottbus-Senftenberg,
Cottbus, Germany*

*Corresponding author: Tel.: +49-355-693270, e-mail address: stefan.glasauer@b-tu.de

Abstract

Sequential Bayesian updating has been proposed as model for explaining various systematic biases in human perception, such as the central tendency, range effects, and serial dependence. The present chapter introduces to the principal ideas behind Bayesian updating for the random-change model introduced previously and shows how to implement sequential updating using the exact method via probability distributions, the Kalman filter for Gaussian distributions, and a particle filter for approximate sequential updating. Finally, it is demonstrated how to couple perception to action by selecting an appropriate action based on the posterior distribution that results from sequential updating.

Keywords

Probabilistic model, Decision making, Central tendency, Range effect, Serial dependence, Particle filter, Kalman filter

1 Introduction

During the last decades probabilistic models have become successful in explaining particular features of human perception, and often even of cognition in general (e.g., Chater et al., 2006). A central idea behind the rise of probabilistic models is the ubiquitous uncertainty in sensory signals but also in neural processing in general. Because sensory inputs are noisy, central processing of these inputs should deal appropriately with the uncertainty. The optimal way to do so is to use methods from probability theory, which provides a normative optimum for processing uncertain inputs. Probability theory tells us how to infer the latent causes from uncertain and noisy stimuli: was that movement in the leaves caused by the wind or by a potentially dangerous animal?

Bayes's rules, which first was formulated in 1763 (Bayes and Price, 1763), is just one of the many statistical theorems that is utilized. However, it gave the name to what nowadays it called Bayesian probability, or Bayesian statistics, contrasting it to frequentist statistics (e.g., Rouder, 2014). The Bayesian view of probability is that it expresses a degree of belief in a certain hypothesis. This belief is then updated using Bayes' theorem by new evidence, for example, when new data come in. This type of inference is a useful strategy for statistical data analysis (e.g., Kruschke and Liddell, 2018 for an introduction), but can as well be used to model how the brain should process sensory information and prior knowledge to come up with beliefs about possible causes of the sensory inputs. The idea that the brain performs a process of inference not only when we think about logical deductions, but also when we simply perceive, has first been formulated by Helmholtz (1867): "... it may be permitted to designate the mental acts of ordinary perception as unconscious inferences..." (Helmholtz, 1867, chapter 26, translation by SG). While Helmholtz himself did not provide a mathematical foundation for these ideas, during the last decades theories of brain function were developed that implement Helmholtz' unconscious inference on the mathematical basis of probability theory (e.g., Chater et al., 2006; Dayan et al., 1995; Griffiths et al., 2008; Knill and Pouget, 2004).

The goal of this course chapter is not to provide a complete overview of the literature on probabilistic modeling of perception and cognition (for a recent critique, see Rahnev and Denison, 2018), but rather to concentrate on one particular case, sequential Bayesian updating, and to explain with simple examples how such models are formed and what they can explain.

A central feature of probabilistic models is that they assume that internal variables are represented as probability distributions rather than discrete values. Probability distributions express the probability of certain events, for example, the binomial distribution is used to describe how often one might see heads up when flipping a coin n times. Using such distributions, one can also make inferences: given that we observe the coin a certain number of times and record how often it showed the head, what's the probability of the coin showing a head? Here probability expresses a degree of belief (Rouder, 2014): when we say that for the coin the probability is 0.5 (or 50%), then we mean that it's equally likely that on the next trial the coin lands heads-up or tail-up. The probability is thus a parameter of the coin. While the binomial distribution is a discrete distribution, magnitudes such as distances, durations, brightness, loudness, etc., require continuous distributions such as the normal distribution. In all cases, the integral over the distribution yields unity, since the overall probability of all possible cases (or magnitudes) together is 100%, it is certain. Probabilities thus express the degree of belief in a hypothesis, e.g., the coin being fair (expressed as its probability being 0.5), in an experiment sound and light coming from the same source, etc. Bayes rule provides the principled way to update the belief when new evidence becomes available.

Representing probability distributions, be it on paper, on a computer, or in the brain, usually requires to hold more than just a single value: a normal distribution, for example, is described by its mean and its variance. While there have been many ideas of how neurons or neural networks might represent probability distributions,

for example, in population codes, the exact implementation is not important for the following. We just have to assume that it can be done, be it as parameterized version (e.g., mean and variance), as discrete approximation (e.g., a histogram), or as samples (representing exemplars of the actual distribution).

The probability distribution that expresses our belief about the aspects of external world we're interested in before having new evidence is called the prior distribution. It is the probability of our current hypothesis $P(H)$. The new evidence is gathered by observation or measurement and, importantly, is also subject to uncertainty. This uncertainty is expressed by another distribution, by the likelihood distribution. The likelihood distribution expresses the knowledge about the measurement uncertainty. For example, when hearing a sound, we can determine its direction or duration not exactly, but with a certain variability, which is due to measurement noise, because our ears are not perfect measurement instruments. The likelihood thus expresses the probability for observing the current data given the hypothesis, which is written as $P(D|H)$. Bayes law allows to determine from likelihood and prior what we're really interested in: the posterior probability of the hypothesis given the data $P(H|D)$:

$$P(H|D) = P(D|H) \cdot P(H)/P(D)$$

Note that one does not need to know $P(D)$, since $P(H|D)$ is a probability distribution and thus sums up to unity, so that we can simply normalize the product $P(D|H)*P(H)$ to yield the result $P(H|D)$. In other words, $P(D)$ is calculated as $P(D) = \int P(D|H)*P(H) dH$.

The core of sequential Bayesian updating is that we can use the posterior probability $P(H|D)$ as new prior distribution, because it represents our beliefs after observing the current data, and thus before observing the next evidence.

2 A simple case: Temporal constancy

In the most simple case, we repeatedly observe an event (such as the coin landing again, or another beep of the sound), and assume that the parameter associated with the event remains constant over time (the probability of the coin does not change, the sound comes from the same location). In such a case, sequential updating is particularly simple. The generative model that formulates our assumption, will simply state that the parameter x is constant: $x_k = x_{k-1}$, with k denoting the k th observation. Note that we do not observe x (the parameter or property that we're interested in) directly, but usually just a noisy version of it: $z_k = x_k + \varepsilon_z$, with ε_z being a random variable with a given distribution (for example, a normal distribution with zero mean) describing the measurement noise or uncertainty.

For a concrete example, let us assume that a signal is coming repeatedly from a location somewhere around us. Before the first event, we can either make no assumption about where the signal will come from (uninformed or neutral prior, same probability for all locations, Fig. 1A) or we can, for example, assume that the signal will come from somewhere in front of us (e.g., because we were told to point toward it).

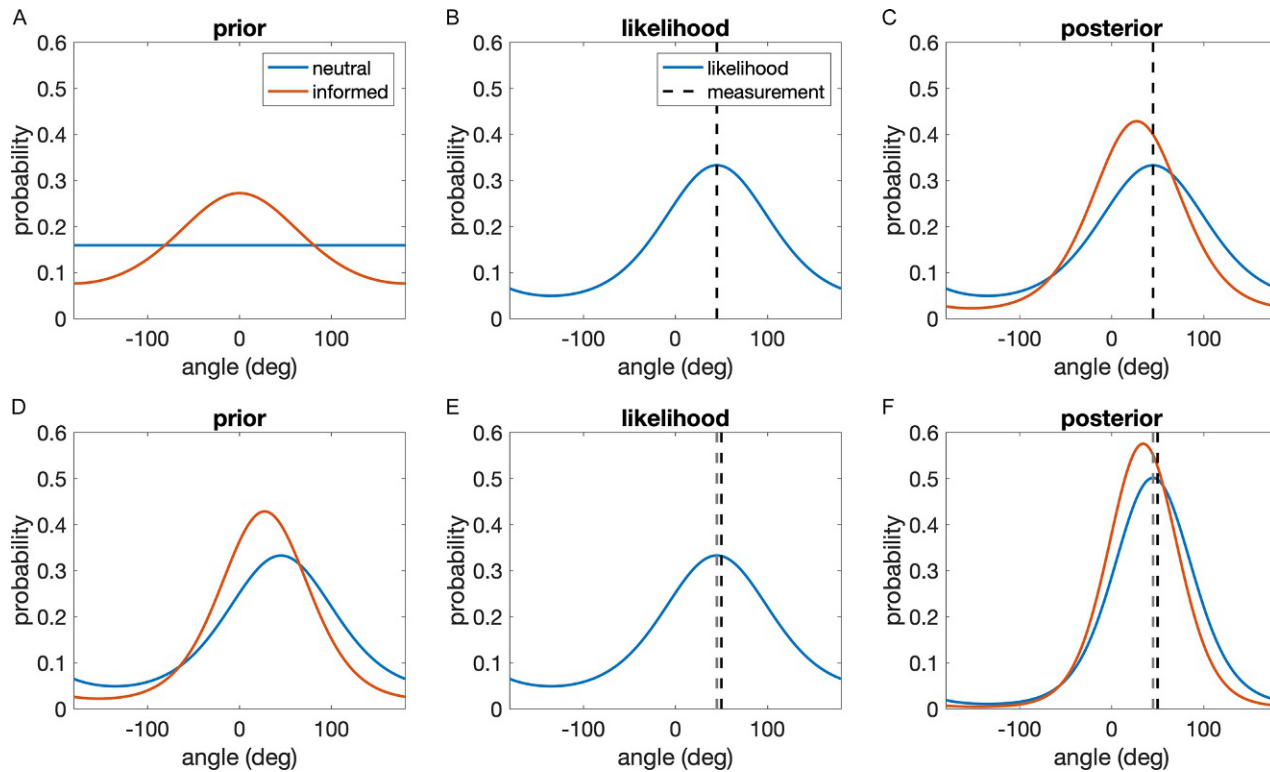


FIG. 1

Illustration of an example for Bayesian estimation of the location of a signal. (A) Two possible initial prior distributions (neutral or informed). (B) The likelihood function for a signal observed at 45 degree. It is assumed that the variability of our sensor is relatively high. (C) Posterior distributions for the two priors. Note that with a neutral prior the most likely location of the signal source is at 45 degree, but with the informed prior it is estimated to be closer to the middle (peak of the posterior is at about 28 degree). (D) Example continued: the use of the previous posterior distribution as new prior leads to sequential Bayesian updating of the estimated location of a signal. (E) The likelihood function for a signal observed at 50 degree (previous observation in gray). (F) Posterior distributions for the two priors.

This initial knowledge about the location x of the signal source is described by the prior distribution $p(x)$. Once we observed the first signal z_1 (dashed line in Fig. 1B), we assign the likelihood function to it (Fig. 1B), which is the probability of observing the signal given the location $p(z_1|x)$. Now we can estimate the location of its source by using Bayes theorem. We take our prior distribution and multiply it by the likelihood distribution:

$$p(x|z_1) = p(z_1|x) \cdot p(x)/p(z_1)$$

with $p(z_1)$ being a normalization factor. Now we have a posterior distribution $p(x|z_1)$ (Fig. 1C) that gives us the probability distribution for the location of the signal source. In the example (Fig. 1) the von-Mises distribution $p(x|\mu, \kappa)$ with mean μ and concentration κ is used as prior and likelihood function, which is the equivalent of a normal distribution on a circle (the signal can come from any direction around us). Note that the likelihood function is the probability expressed as function of the unknown parameter, in this case, as function of the mean of the von-Mises distribution as $f(\mu|\alpha, \kappa)$ with α being the observed angle and $1/\kappa$ corresponding to the uncertainty of the observation.

The posterior distribution is sharper than the prior, which means that we gained confidence in the estimated location. In the next step, we can now use the posterior as new prior (Fig. 1D). In Fig. 1E, the new measurement is slightly different, but the peak of the posterior continues to grow, indicating better confidence in the estimate.

Assuming that our participant has to point to the source of the signal after 5 presentations of the stimulus, we can now predict her performance. For the simulation (Fig. 2), we assume that each stimulus presentation is well-separated from the next

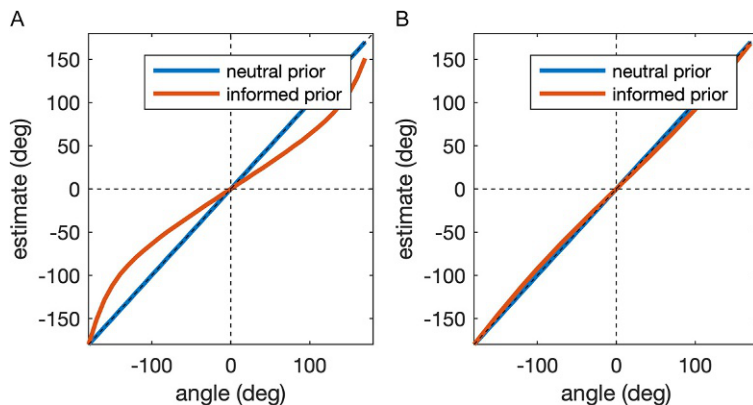


FIG. 2

Simulated estimation of a stimulus direction with a neutral prior or an informed prior (see Fig. 1A) after a single stimulus presentation (A) or after 5 consecutive presentations (B). The systematic bias induced by the prior becomes smaller if more confidence is given to the observation due to repeated presentation of the stimulus and sequential Bayesian updating.

one to avoid serial dependencies, which will be discussed below. Fig. 2A shows the putative estimation performance after a single presentation, Fig. 2B after 5 consecutive stimulus presentations. Note that the resulting estimate is biased toward the assumed straight ahead direction (angle 0 degree), but much less so after 5 presentations (Fig. 2B).

The curve shown in Fig. 2A is similar to the adjustment of a visually presented line to the vertical being tilted in different body positions (Mittelstaedt, 1983): the subjective visual vertical (SVV). And indeed, the systematic bias of the SVV is often explained as being due to a prior for upright body position, which then results in very similar dependencies (see, for example, Clemens et al., 2011).

3 A more sophisticated case: Random changes over time

The stationarity of the presented stimulus, which was assumed for the model presented above, is, however, very often not given, for example, because a stimulus moves or because stimuli of different magnitude are presented sequentially.

In this case, however, sequential Bayesian updating becomes more complicated. Our generative model (Fig. 3) now changes in the simplest case to $x_k = x_{k-1} + \varepsilon_x$, with ε_x being a random variable with zero mean. In other words we assume now that the property, which we want to estimate, changes from trial to trial by a random amount, which is described by the transition probability $p(x_k | x_{k-1})$. The initial knowledge is, as in the example above, described by the prior $p(x_0)$. Now the first measurement comes in, and we can calculate the new posterior by the update equation

$$p(x_1 | z_1) = p(z_1 | x_1) \cdot p(x_1) / p(z_1)$$

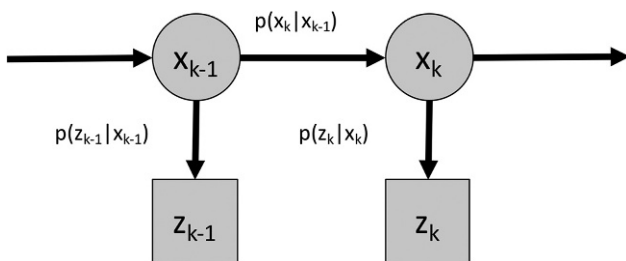


FIG. 3

Graphical visualization of the model underlying Bayesian sequential updating. The current observation z_k only depends on x_k , the actual state to be estimated. x_k only depends on the previous state x_{k-1} (the so-called Markov assumption). The probability $p(x_k | x_{k-1})$ describes how the state at time k depends on the previous state. $p(z_k | x_k)$ describes how the observation depends on the state.

Note that even for the first measurement, we still need to calculate $p(x_1)$, because the transition probability $p(x_1|x_0)$ now has a variance larger than zero^a:

$$p(x_1) = \int p(x_1|x_0) \cdot p(x_0) \cdot dx_0$$

This calculation is called the prediction step, because we predict the probability distribution of the location at the time of the first observation from just prior knowledge and the transition probability.

In the next time step, we get the second observation, and want to calculate the posterior distribution $p(x_2|z_2, z_1)$. Respectively, in time step k we calculate $p(x_k|z_k, \dots, z_1) = p(x_k|z_{1:k})$. To do so, we first predict the probability distribution $p(x_k|z_{1:k-1})$ of the current location depending on the past observations:

$$p(x_k|z_{1:k-1}) = \int p(x_k|x_{k-1}) \cdot p(x_{k-1}|z_{1:k-1}) \cdot dx_{k-1}$$

Note that this is an integral over all possible x_{k-1} , which means that the distributions involved are now two-dimensional (Fig. 4).

Now the posterior probability given the current measurement can be calculated:

$$p(x_k|z_{1:k}) = p(z_k|x_k) \cdot p(x_k|z_{1:k-1}) / p(z_k|z_{k-1})$$

with $p(z_k|x_k)$ being the likelihood distribution and $p(z_k|z_{k-1}) = \int p(z_k|x_k) \cdot p(x_k|z_{1:k-1}) \cdot dx_k$ being a normalization constant (Fig. 4D).

As stimuli we use a random sequence of 200 angles ranging from -90 to 90 degree presented sequentially to the model. The initial prior distribution is set to the informed prior of the previous example, but note that the initial prior

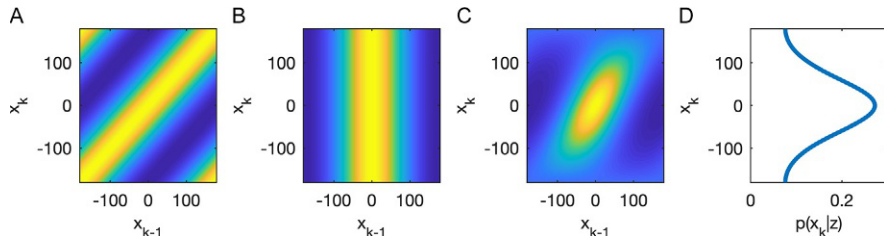


FIG. 4

The prediction step of Bayesian sequential updating. (A) The transition probability $p(x_k|x_{k-1})$. (B) The prior probability $p(x_{k-1}|z_{1:k-1})$. (C) Multiplication of (A) and (B). (D) The result of integral over x_{k-1} is the probability distribution $p(x_k|z_{1:k-1})$, which is the predicted probability for x at time k given all previous observations z.

^aStrictly speaking, in the first example the transition probability had zero variance, because it was assumed that $x_k = x_{k-1}$. This yields a Dirac function for $p(x_k|x_{k-1})$, so that $p(x_k) = p(x_k|z_{k-1})$.

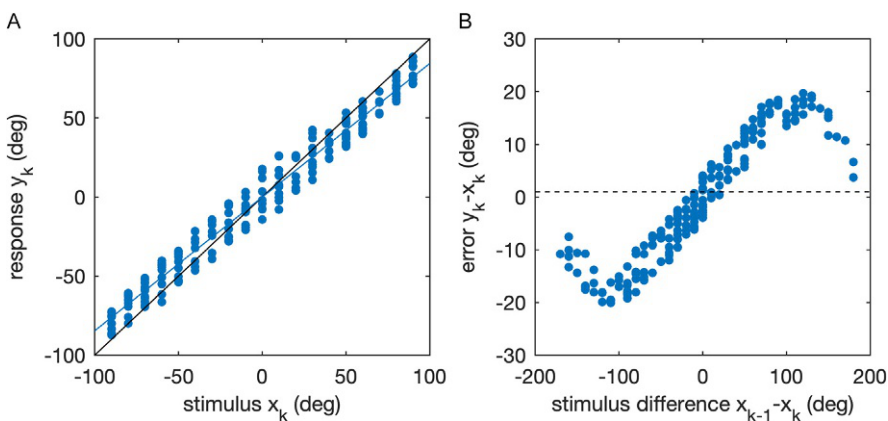
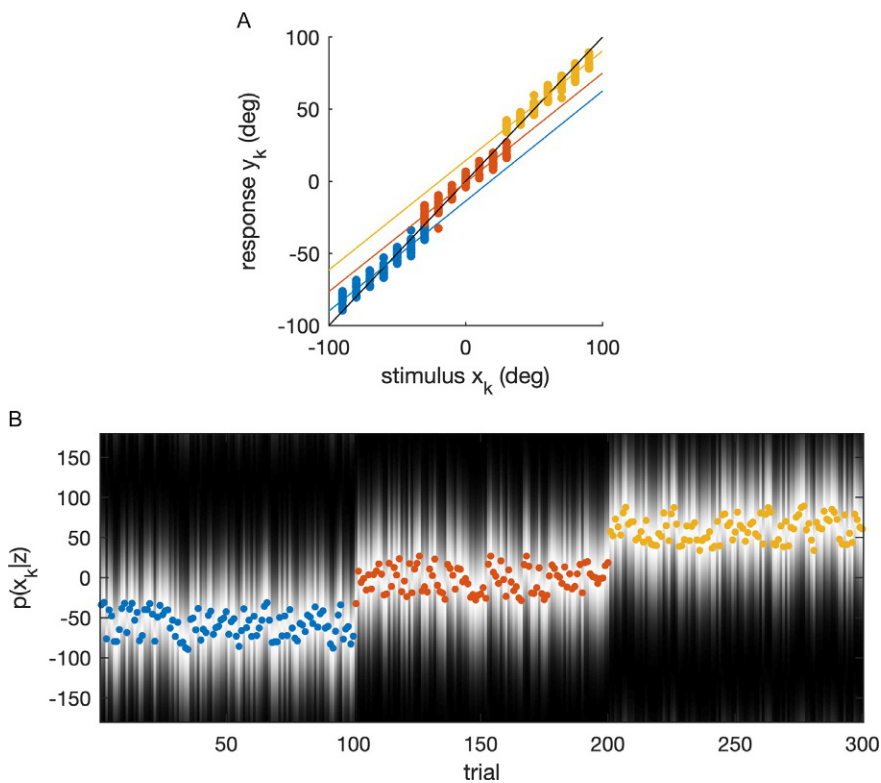


FIG. 5

Results of Bayesian sequential updating in an estimation task with a random sequence of stimuli (−90 to 90 degree). (A) Response magnitude plotted over stimulus magnitude. Regression line (blue line) shows central tendency (slope 0.84). (B) Serial dependence revealed by plotting current error over stimulus difference between previous and current trial.

is unimportant for the present model, since it only describes the belief about the first stimulus and is thus quickly modified by the updating. Matlab code for this and other examples in the paper can be found in the Supplemental Material in the online version at <https://doi.org/10.1016/bs.pbr.2019.04.025>. Fig. 5A shows the responses of the model plotted over the stimuli together with the best-fit linear regression line. Note that the regression line has a slope smaller than unity, that is, large stimulus values are under-estimated, thus exhibiting a “central tendency” (Hollingworth, 1910) or “regression to the mean” (Stevens and Greenbaum, 1966). Even though there are no random influences in the model (the estimation process is deterministic), the responses do not lie on a line or curve, because each response depends not just on the current stimulus, but via the prior also on previous stimuli. This serial dependence can be visualized, for example, by plotting the error at trial k over the difference of stimuli at trials $k - 1$ and k (Fig. 5B). However, note that both types of systematic errors are caused by the same mechanism, the sequential updating, and are not independent, as erroneously assumed in a recent study on facial age estimation (Clifford et al., 2018).

The sequential updating also leads to range effects (Teghtsoonian and Teghtsoonian, 1978) with the slope of the regression line depending on the range of stimuli. The slope in Fig. 5A is closer to 1 than in Fig. 6A, despite the model and the overall range of stimuli being exactly the same. Fig. 6 also shows that when the range of stimuli presented changes abruptly, the sequential updating leads to a posterior distribution that rapidly follows the stimulus range. Thus, within each sequence of stimuli associated with one range, a specific central tendency is found, which leads to differences between the ranges (Fig. 6). With sequential updating, for these range effects to occur there is no need of providing knowledge about the range of stimuli before the experiment starts

**FIG. 6**

Range effect as results of Bayesian sequential updating in an estimation task with three concatenated random sequences of 100 stimuli (-90 to -30 degree in blue, -30 to 30 degree in red, 30–90 degree in yellow). (A) Response magnitude plotted over stimulus magnitude. Separate regression lines for the three stimulus ranges each show a central tendency (slope 0.75) with an indifference point that clearly depends on the current stimulus range. (B) Temporal evolution of the posterior distribution (gray background) and the responses (colored dots, as in (A)). The posterior distribution switches rapidly from one range to the next.

(as suggested, for example, by [Jazayeri and Shadlen, 2010](#)), since the updating leads to concurrent learning of the stimulus statistics and thus to adaptation to the stimulus range.

Bayesian sequential updating with the simple generative model shown in [Fig. 3](#) thus provides a coherent explanation of the central tendency, serial dependence, and the range effect. We have previously suggested this explanation ([Petzschner and Glasauer, 2011; Petzschner et al., 2015](#)) with one additional detail: the estimation procedure was assumed to take place on a logarithmic scale, so that Weber's law could be implemented. The Bayesian updating taking place on a log-scale also explains the non-linear stimulus-response relation often seen for magnitude estimation

and was able to reproduce the well-known power-law relationship in magnitude estimation. However, for the present demonstration it is not important and thus will be neglected in the following.

4 Implementing sequential updating

Computationally, simulating the model in the examples shown here has been done by using a grid-based method, where the distributions are represented as values on a regular discrete grid (with small spacing to minimize numerical errors). This method works well in low-dimensional cases, but already requires a lot of computer memory, since the transition distribution is two-dimensional (Fig. 4A). For more complicated problems, the grid-based method is not suitable because the memory requirements and the computation time become too expensive.

In our previous work (Petzschner and Glasauer, 2011; Petzschner et al., 2015) we used the so-called Kalman filter (Kalman, 1960), which provides a fast and efficient method of sequential updating for the case of normal distributions. The basic idea behind the Kalman filter is that, when using Gaussian distributions for the prior, the likelihood, and the transition probability, then the posterior distribution will again be a Gaussian. Thus, instead of updating the whole distribution, it is sufficient to update the mean and the variance of the prior distribution (see Supplemental Material in the online version at <https://doi.org/10.1016/bs.pbr.2019.04.025> for an example corresponding to Fig. 3) without having to represent the whole distribution. Note, however, that in our example above the Kalman filter cannot be applied since the distributions involved are not Gaussian.

Fortunately, yet another method is available for computing sequential updating, which does not require the assumptions of the Kalman filter. The particle filter method (for review from the point of cognitive science, see Sanborn, 2017; for technical review and tutorial see Arulampalam et al., 2002), a sequential Monte Carlo technique, is based on representing probability distributions not by their parameters (as in the Kalman filter) or as discretized functions (as in the grid-based method), but as random samples from the respective distribution. This might at first sound difficult to comprehend, but it actually is what we do all the time when we deal with data. When we measure a particular variable many times, we can now estimate the mean, the variance, or other moments, but we can also represent the underlying probability distribution by generating a histogram of the measurements. Thus, any set of random samples can be translated into a distribution and thus represent this distribution. This is exactly what is used for particle filtering.

A basic particle filter is Sampling Importance Resampling (SIR) (Arulampalam et al., 2002), which is outlined here for the special case depicted in Fig. 3 and used for the example shown in Fig. 6 (see Supplemental Material in the online version at <https://doi.org/10.1016/bs.pbr.2019.04.025> for code corresponding to Fig. 7). To begin with, a set of n random samples (with large n estimates get closer to the optimal Bayes), the particles, has to be generated to represent the initial prior distribution.

Since an appropriate random number generator is not available for the von-Mises distribution used here, samples are generated using a Markov chain Monte Carlo algorithm (for the simulation we used the Metropolis sampler). For each particle, we then predict a value at the next timestep by simply adding a random number from the transition distribution, which here is also a von-Mises distribution. Next, the importance weights are calculated for each particle using the likelihood function of the current measurement. The n posterior samples are generated by randomly sampling from the n prior particles (which represent the candidate hypotheses) weighted by the importance weights. From the resulting posterior we can calculate the estimate as circular mean. The resulting simulation is shown in Fig. 7.

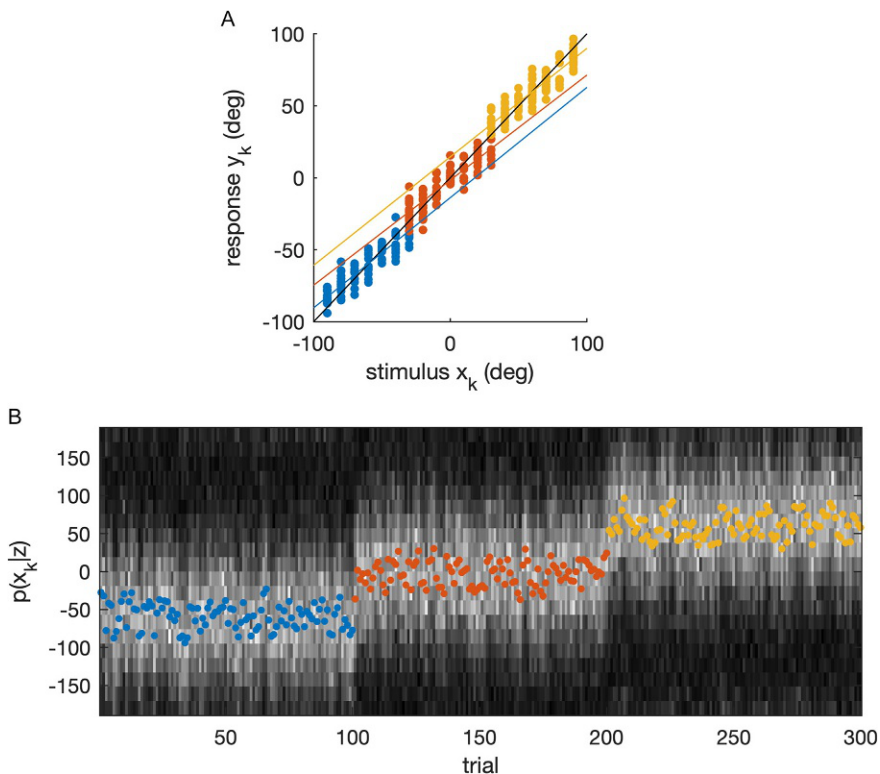


FIG. 7

Simulation using particle filter (1000 particles) for Bayesian sequential updating in the estimation task depicted in Fig. 6. (A) Response magnitude plotted over stimulus magnitude. Separate regression lines for the three stimulus ranges each show a central tendency (average slope approx. 0.75), compare to Fig. 6A. (B) Temporal evolution of the posterior distribution (gray background) and the responses (colored dots, as in (A)). The posterior distribution switches rapidly from one range to the next as in Fig. 6B.

Note that there are many different flavors of particle filters (Arulampalam et al., 2002) that could be used and that produce different systematic errors for smaller number of particles and/or large number of trials (e.g., the degeneracy problem of sampling). Some of the systematic errors due to approximate Bayesian inference could be the reason for cognitive biases (e.g., Brown and Steyvers, 2009; Sanborn, 2017; Shi et al., 2010). Other approximations such as variational Bayes, which is used for the free-energy model (Friston, 2008), are also possible (see Aitchison and Lengyel, 2017; Sanborn, 2017).

How Bayesian estimation or an approximation thereof is realized and represented in the brain is still an open question. Different levels of implementation have been proposed from single neurons and neural networks (using population coding, e.g., Ma et al., 2006) to interaction between different brain areas. In support of the latter, several studies have investigated how variables of Bayesian estimation models such as likelihoods and priors correlate with brain activity (e.g., Rohe and Noppeney, 2015; Vilares et al., 2012; Wiener et al., 2016), or how effects of deep brain stimulation can be explained by Bayesian mechanisms (Antoniades et al., 2014).

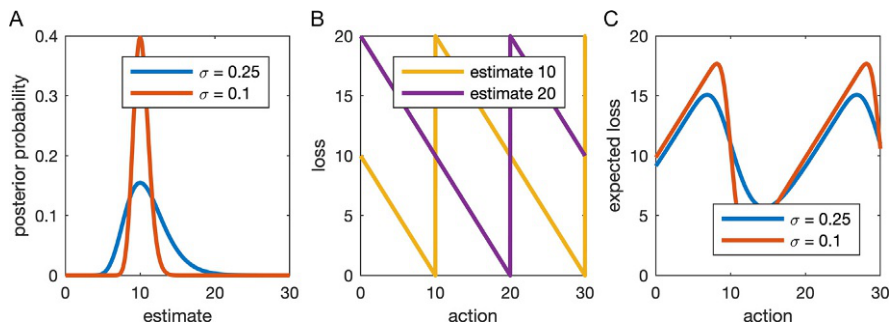
5 Perception-action coupling: Decision making

So far all examples resulted in a posterior distribution that represented the perception of the respective variable (in the example above the angular direction of the stimulus source). However, for an action to be performed, we need a single value, not a distribution. Thus, we have to select an appropriate value from the posterior. Intuitively, the most likely value (the maximum a-posteriori value), the mean of the distribution, or the median value seem to be good choices. Fortunately, the most appropriate choice is not a matter of intuition, but can be formalized within the Bayesian framework (Körding and Wolpert, 2006; Trommershäuser et al., 2008). All we need is to define a utility or cost function that describes the outcome of a particular action in terms of gain or loss. The loss function is thus defined as loss L depending on the action a and the estimate e : $L(a,e)$. Common cost functions are costs that depend linearly or quadratically on the error (being zero for zero error), or that have zero cost for a hit (small or zero error) and constant cost for misses (larger error).

Consequently, the optimal action is the one that minimizes the expected loss. Given our posterior distribution $p(e)$, the expected loss is

$$E_{loss}\{a\} = \int_e L(a, e) \cdot p(e) de$$

As an example, let's assume that we want to catch the bus. Our posterior distribution for the time needed to reach the bus stop is given by a log-normal distribution $p(e)$, which is a common distribution for duration estimation (e.g., Shi et al., 2013). The action is the time of departure at home before bus departure. The cost for arriving at the bus stop too early increases linearly because of unused waiting time. However, the cost of arriving too late assumes a high value, because we miss the bus and have to wait for the next one. The cost immediately after bus departure could depend, for

**FIG. 8**

Example for Bayesian decision making. (A) The assumed posterior distribution has a peak at 10min, the maximum a-posterior value for reaching the bus stop (see text). Two different distributions are shown. (B) Asymmetric cost function depending on action plotted for two estimates. The bus leaves every 20min, if our estimate for reaching the bus stop is exactly 10min, then the optimal action (zero loss) would evidently be to start 10min before bus departure. (C) since the actual duration for reaching the bus stop is uncertain (see (A)), the actual loss depends on the posterior probability and reaches a minimum at 14.56min (for the wide distribution) or 12.2min (for the narrow distribution) before bus departure.

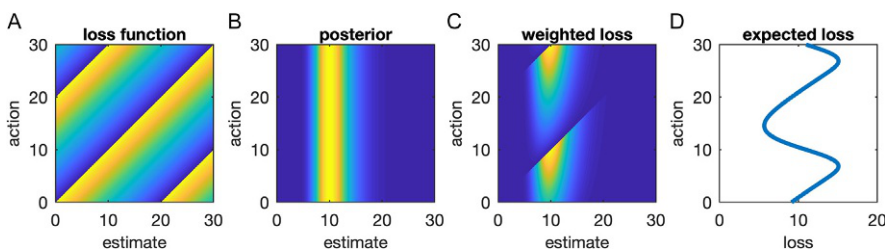
example, on the waiting time d until the next bus arrives, so that it decreases again over time:

$$L(a, e) = \begin{cases} a - e & \text{for } a > e \\ d + (a - e) & \text{for } a \leq e \end{cases}$$

Fig. 8 shows two versions of the assumed posterior distribution (with two different standard deviations), the loss function plotted over the action for two different estimates, and the expected loss given the posterior distributions. In the example, the posterior peaks at 10min, which is the most likely duration for reaching the bus stop. The bus arrives every 20min; for the loss function we assume that it makes no difference whether we take the first or the second bus (Matlab code for this example can be found in the Supplemental Material in the online version at <https://doi.org/10.1016/bs.pbr.2019.04.025>).

In **Fig. 9**, the computation of the expected loss is shown. For the lognormal distribution shown in **Fig. 8A**, the expected loss reaches a minimum for 14.5 min. In other words, it is optimal to leave for the bus stop 14.5 min before bus departure. Intuitively, this is a good choice.

Note that the expected loss depends on the width of the posterior distribution (**Fig. 8C**), which means that repeated observations leading to sharper posterior distributions (as in **Fig. 1**) lead to lower loss. Hence, in many cases the reaction time to start an action can be explained in the Bayesian framework as accumulating evidence until the expected cost falls below a threshold (see [Vul et al., 2014](#)). If the cost is assumed to increase with reaction time, then an optimal cost can be calculated from using reaction time as additional parameter of loss calculation. It has also been shown that traditional drift-diffusion models of evidence accumulation are equivalent to Bayesian inference ([Bitzer et al., 2014](#)).

**FIG. 9**

Computing the expected loss for Bayesian decision making example (see Fig. 8). (A) The loss function depends on estimate and action. (B) The posterior distribution is a function of the estimate independently of the action. (C) The loss function weighted by the posterior probability. (D) The integral over the weighted loss yields the expected loss depending on action.

6 Summary

In the present course chapter, I gave a brief overview of how to apply sequential Bayesian updating to model human perception and decision making. I have shown that sequential updating under the assumption of a very simple random-change model leads to the central tendency, the range effect, and to sequential dependencies (see also Petzschner et al., 2015). Note that the simple random-change model is based on a specific assumption of how stimuli change over time and thus is optimal only for that case, which, however, is not met in standard experimental protocols (Glasauer and Shi, 2018). The full implementation of sequential Bayesian updating can become computationally very demanding because of multi-dimensional probability distributions involved that need to be integrated (marginalized). However, there are less demanding implementations of sequential updating. The Kalman filter is equivalent to sequential Bayesian updating in the case of Gaussian noise and a linear system. Particle filters are a particularly elegant sampling-based approximative method for sequential Bayesian inference, which has also been used for explaining cognitive biases. Finally, I showed with an example how sequential updating is extended by appropriate cost or loss functions in order to select the optimal action based on the posterior distribution that represents perception.

Acknowledgment

This study was supported by German DFG research project GL 342/3-2.

References

- Aitchison, L., Lengyel, M., 2017. With or without you: predictive coding and Bayesian inference in the brain. *Curr. Opin. Neurobiol.* 46, 219–227.
- Antoniades, C.A., Bogacz, R., Kennard, C., FitzGerald, J.J., Aziz, T., Green, A.L., 2014. Deep brain stimulation abolishes slowing of reactions to unlikely stimuli. *J. Neurosci.* 34, 10844–10852.

- Arulampalam, M.S., Maskell, S., Gordon, N., Clapp, T., 2002. A tutorial on particle filters for online nonlinear/non-Gaussian Bayesian tracking. *IEEE Trans. Signal Process.* 50, 174–188.
- Bayes, T., Price, R., 1763. An essay towards solving a problem in the doctrine of chances. *Philos. Trans. R. Soc. Lond.* 53, 370–418.
- Bitzer, S., Park, H., Blankenburg, F., Kiebel, S.J., 2014. Perceptual decision making: drift-diffusion model is equivalent to a Bayesian model. *Front. Hum. Neurosci.* 8, 102.
- Brown, S.D., Steyvers, M., 2009. Detecting and predicting changes. *Cogn. Psychol.* 58, 49–67.
- Chater, N., Tenenbaum, J., Yuille, A., 2006. Probabilistic models of cognition: conceptual foundations. *Trends Cogn. Sci.* 10, 287–291.
- Clemens, I.A.H., da Vrijer, M., Selen, L.P.J., van Gisbergen, J.A.M., Medendorp, W.P., 2011. Multisensory processing in spatial orientation: an inverse probabilistic approach. *J. Neurosci.* 31 (14), 5365–5377.
- Clifford, C.W.G., Watson, T.L., White, D., 2018. Two sources of bias explain errors in facial age estimation. *R. Soc. Open Sci.* 5, 180841.
- Dayan, P., Hinton, G.E., Neal, R., 1995. The Helmholtz machine. *Neural Comput.* 7, 889–904.
- Friston, K., 2008. Hierarchical models in the brain. *PLoS Comput. Biol.* 4, e1000211.
- Glasauer, S., Shi, Z., 2018. 150 years of research on Vierordt's law—Fechner's fault? *bioRxiv* <https://doi.org/10.1101/450726>.
- Griffiths, T.L., Kemp, C., Tenenbaum, J.B., 2008. Bayesian models of cognition. In: Sun, R. (Ed.), *The Cambridge Handbook of Computational Psychology*. Cambridge University Press, pp. 59–100.
- Helmholtz, H., 1867. *Handbuch der Physiologischen Optik*. Leopold Voss, Leipzig.
- Hollingworth, H.L., 1910. The central tendency of judgment. *J. Philos. Psychol. Sci. Methods* 7, 461–469.
- Jazayeri, M., Shadlen, M.N., 2010. Temporal context calibrates interval timing. *Nat. Neurosci.* 13, 1020–1026.
- Kalman, R.E., 1960. A new approach to linear filtering and prediction problems. *J. Basic Eng.* 82, 35–45.
- Knill, D.C., Pouget, A., 2004. The Bayesian brain: the role of uncertainty in neural coding and computation. *Trends Neurosci.* 27, 712–719.
- Körding, K.P., Wolpert, D.M., 2006. Bayesian decision theory in sensorimotor control. *Trends Cogn. Sci.* 10, 319–326.
- Kruschke, J.K., Liddell, T.M., 2018. Bayesian data analysis for newcomers. *Psychon. Bull. Rev.* 25, 155–177.
- Ma, W.J., Beck, J.M., Latham, P.E., Pouget, A., 2006. Bayesian inference with probabilistic population codes. *Nat. Neurosci.* 9, 1432–1438.
- Mittelstaedt, H., 1983. A new solution to the problem of the subjective vertical. *Naturwissenschaften* 70, 272–281.
- Petzschner, F.H., Glasauer, S., 2011. Iterative Bayesian estimation as an explanation for range and regression effects: a study on human path integration. *J. Neurosci.* 31, 17220–17229.
- Petzschner, F.H., Glasauer, S., Stephan, K.E., 2015. A Bayesian perspective on magnitude estimation. *Trends Cogn. Sci.* 19, 285–293.
- Rahnev, D., Denison, R.N., 2018. Suboptimality in perceptual decision making. *Behav. Brain Sci.* 41 (e223), 1–107.
- Rohe, T., Noppeney, U., 2015. Cortical hierarchies perform Bayesian causal inference in multisensory perception. *PLoS Biol.* 13, e1002073.

- Rouder, J.N., 2014. Optional stopping: no problem for Bayesians. *Psychon. Bull. Rev.* 21, 301–308.
- Sanborn, A.N., 2017. Types of approximation for probabilistic cognition: sampling and variational. *Brain Cogn.* 112, 98–101.
- Shi, L., Griffiths, T.L., Feldman, N.H., Sanborn, A.N., 2010. Exemplar models as a mechanism for performing Bayesian inference. *Psychon. Bull. Rev.* 17, 443–464.
- Shi, Z., Church, R.M., Meck, W.H., 2013. Bayesian optimization of time perception. *Trends Cogn. Sci.* 17, 556–564.
- Stevens, S.S., Greenbaum, H.B., 1966. Regression effect in psychophysical judgment. *Percept. Psychophys.* 1, 439–446.
- Teghtsoonian, R., Teghtsoonian, M., 1978. Range and regression effects in magnitude scaling. *Percept. Psychophys.* 24, 305–314.
- Trommershäuser, J., Maloney, L.T., Landy, M.S., 2008. Decision making, movement planning and statistical decision theory. *Trends Cogn. Sci.* 12, 291–297.
- Vilares, I., Howard, J.D., Fernandes, H.L., Gottfried, J.A., Körding, K.P., 2012. Differential representations of prior and likelihood uncertainty in the human brain. *Curr. Biol.* 22, 1641–1648.
- Vul, E., Goodman, N., Griffiths, T.L., Tenenbaum, J.B., 2014. One and done? Optimal decisions from very few samples. *Cognit. Sci.* 38, 599–637.
- Wiener, M., Michaelis, K., Thompson, J.C., 2016. Functional correlates of likelihood and prior representations in a virtual distance task. *Hum. Brain Mapp.* 37, 3172–3187.

Maps and sensorimotor transformations for eye-head gaze shifts: Role of the midbrain superior colliculus

2

A. John van Opstal*, Bahadir Kasap*Department of Biophysics, Donders Institute for Brain, Cognition and Behaviour,
Radboud University Nijmegen, Nijmegen, The Netherlands***Corresponding author: e-mail address: j.vanopstal@donders.ru.nl*

Abstract

Single-unit recordings in head-restrained monkeys indicated that the population of saccade-related cells in the midbrain Superior Colliculus (SC) encodes the kinematics of desired straight saccade trajectories by the cumulative number of spikes. In addition, the nonlinear main sequence of saccades (their amplitude–peak velocity saturation) emerges from a spatial gradient of peak-firing rates of collicular neurons, rather than from neural saturation at brain-stem burst generators. We here extend this idea to eye-head gaze shifts and illustrate how the cumulative spike-count in head-unrestrained monkeys relates to the desired gaze trajectory and its kinematics. We argue that the output of the motor SC is an abstract desired gaze-motor signal, which drives in a feedforward way the instantaneous kinematics of ongoing gaze shifts, including the strong influence of initial eye position on gaze kinematics. We propose that the neural population acts as a vectorial gaze pulse-generator for eye-head saccades, which is subsequently decomposed into signals that drive both motor systems in appropriate craniocentric reference frames within a dynamic gaze-velocity feedback loop.

Keywords

Motor map, Neural code, Kinematics, Eye-head coupling, Reference frames, Nonlinear pulse generator, Initial eye position

1 Introduction

1.1 Eye-head gaze shifts

A saccadic eye-head gaze shift (ΔG) is the directional change of the fovea in space, which is determined by the sum of the changes of the eye-in-head and the head-on-neck orientations: $\Delta G = \Delta E + \Delta H$. The gaze-control system of human and non-human primates is optimally suited to reorient the fovea as fast and as accurately as possible to a target and to allow vision to identify objects with high resolution during intermittent fixations.

Although any particular gaze shift can in principle be generated by infinitely many combinations of eye and head contributions, under controlled initial conditions the system selects highly reproducible movement strategies. It has therefore been hypothesized (Goossens and Van Opstal, 2012; Harris and Wolpert, 1998, 2006; Kardamakis and Moschovakis, 2009; Sağlam et al., 2011) that gaze shifts result from a control principle that optimizes some performance criterion, such as speed-accuracy trade-off, which minimizes the impact of internal noise and uncertainty, or minimization of motor effort.

Fig. 1A illustrates a horizontal sound-evoked gaze saccade, in which the initial eye- and head orientations were aligned at straight ahead. It shows the different stages during and around the gaze shift: (i) the fixation phase, during which the vestibular-ocular reflex (VOR) ensures stable fixation, (ii) the gaze shift ($\Delta G = 26$ degree) consists of a large eye saccade ($\Delta E = 22$ degree) to E_{END} , and a small head-movement contribution ($\Delta H = 4$ degree) with the VOR attenuated. (iii) The gaze shift is followed by a remaining head movement (here 14 degree), during which gaze remains stable because of the VOR. (iv) At the end of the head movement (H_{off}), the eye orientation may be eccentric in the head (here, $E_{\text{off}} = 8$ degree).

Because of the different plant dynamics of eyes and head, and the eye's limited oculomotor range, not all eye-head combinations are possible or equally efficient in reorienting gaze. Typically, small gaze shifts are associated with small head movements, and large gaze shifts with larger head movements, but the latter also depends on initial eye orientation (e.g., Freedman and Sparks, 2000; Goossens and Van Opstal, 1997; Guitton and Volle, 1987; Kardamakis et al., 2010). Thus, when a large head movement contributes to the gaze shift, gaze peak-velocity is reduced. This point is illustrated in **Fig. 1B**. Because of the much larger head contribution, the gaze velocity of 60 degree gaze shifts tends to be considerably lower than for gaze shifts with an amplitude of 30 degree.

In this report, we propose a quantitative model that explains this behavior. The major novelty of our model with respect to earlier proposals (Daye et al., 2014; Freedman, 2001; Goossens and Van Opstal, 1997; Guitton and Volle, 1987; Kardamakis et al., 2010; Sağlam et al., 2011) resides in the assumed role of the mid-brain Superior Colliculus (SC) in the control of gaze shifts. Our model is based on results of recent single-unit recordings, taken from the SC of head-restrained and head-free monkeys, which support the idea that the motor SC acts as the nonlinear vectorial gaze-pulse generator of the system.

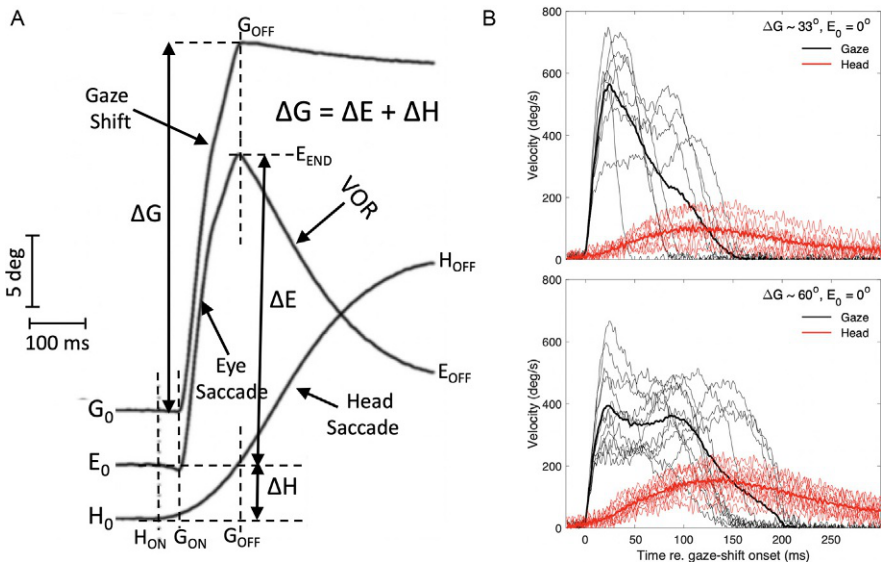


FIG. 1

(A) Example of a horizontal gaze shift (25.5 degree amplitude) to an auditory target with the eyes and head initially aligned (signals are shifted by a few degrees for illustrative reasons). The eye- and head displacements that contribute to the gaze shift are measured between gaze on- and offset (G_{ON}, G_{OFF} ; vertical dashed lines). Note that the contribution of the head to the gaze shift ($\Delta H = 3.8$ degree) differs markedly from the overall head displacement (17.6 degree). Note also that the head starts to move slightly earlier than the eyes (H_{ON}), inducing a small vestibular counter movement of the eyes to maintain stable gaze fixation. During the fully operating vestibular ocular reflex (VOR) after gaze offset, gaze remains stable (apart from a slow centripetal drift in darkness), while the head continues to move to its final position, H_{OFF} . (B) Example gaze- (black) and head- (red) velocity profiles for gaze shifts with an amplitude of about 33 degree (top) vs. 60 degree (bottom). In the latter case, the head contribution is considerably larger, causing the overall gaze velocity to drop (see also Fig. 2B). Solid lines: average profiles.

1.2 Brief background SC

The SC contains a topographic map of saccadic gaze shifts (Freedman and Sparks, 1997; Ottes et al., 1986; Robinson, 1972). Prior to and during saccades, a population of cells encodes amplitude and direction by the location of its center within the map (Ottes et al., 1986; Sparks and Mays, 1980). SC recordings in head-restrained monkeys demonstrated that the population also encodes saccade kinematics through their firing rates (Goossens and Van Opstal, 2006).

We thus proposed that the SC issues a desired (straight-line) dynamic eye-displacement signal by its total cumulative number of spikes in the saccade-related bursts. Moreover, all cells in the population synchronize their bursts, such that even

at the single-unit level each cell encodes the straight desired trajectory of any saccade within its movement field (Goossens and Van Opstal, 2012).

We formulated a simple computational model, in which each spike in the burst from each recruited neuron, k , contributes a tiny movement, \vec{m}_k , to the saccade. This “spike-vector” is determined by the cell’s location in the map, and specifies its connection strength with the brainstem burst generators via the SC-to-brainstem efferent mapping function (Ottes et al., 1986; Van Gisbergen et al., 1987). According to this dynamic ensemble-coding model, the saccade trajectory is encoded by linear cumulative integration of all SC spike vectors:

$$\Delta \vec{E}(t) = \sum_{k=1}^{N_{POP}} \sum_{s=1}^{N_{spk,k} < t} \delta(t - \tau_{k,s}) \cdot \vec{m}_k \quad (1)$$

where $\delta(t - \tau_{k,s})$ is a spike of cell k , fired at time $t = \tau_{k,s}$.

Simulations with measured spike trains and a *linear* brainstem burst generator demonstrated that the model fully accounted for the nonlinear main-sequence properties and velocity profiles of fast and slow saccades. As a logical consequence, the main-sequence nonlinearity has to reside in the distribution of spike trains and firing rates in the motor SC (Van Opstal and Goossens, 2008).

The hypothesis therefore holds that the SC may embed the neural correlate of the optimal controller underlying gaze shifts (Harris and Wolpert, 1998, 2006). Analysis of single-unit responses revealed that its neural mechanism could be described as follows:

- (I) A spatial gradient in the peak-firing rates of SC cells from rostral (small saccades, firing rates up to 900 spks/s) to caudal locations (large saccades, about 300–400 spks/s).
- (II) On average, cells fire the *same* number of spikes for their optimal saccade.
- (III) The population size is the same (diameter of about 1 mm) for all saccades. Hence, the total number of spikes in each recruited population is the same.
- (IV) All cells within the population synchronize their bursts.

We here extend these ideas to the head-unrestrained condition. Monkeys generated eye-head saccades with considerable natural variability in their kinematics, induced by varying the initial eye-in-head position. A critical prediction of Eq. (1) is that the *same* relation should hold for head-unrestrained saccades, regardless gaze-shift kinematics. Thus, the nonlinear gaze kinematics should be reflected in the burst properties of SC cells. To our knowledge, these properties have so far not been documented for head-unrestrained gaze shifts.

2 Methods

Experiments were performed in the laboratory of Dr. EG Freedman at the Department of Neurobiology and Anatomy, School of Medicine and Dentistry of the University of Rochester, NY, while one of the authors (A.J.v.O.) was a visiting

scientist. Two trained rhesus monkeys (P and S) participated in the experiments. Animals were trained to follow briefly flashed visual targets against a small liquid reward by generating rapid eye-head gaze shifts, while single-unit activity from the left SC was recorded. Details on the surgical procedures, training protocols, and experimental setup are described in full detail in [Quessey and Freedman \(2004\)](#), [Quessey et al. \(2010\)](#), and [Walton and Freedman \(2011\)](#). All experimental procedures were approved by the University of Rochester Animal Care and Use Committee, and fully adhered to the National Institutes of Health Guide for the Care and Use of Animals.

We recorded from a total of 52 cells, out of which 30 neurons were isolated long enough for detailed analysis. The movement fields were typically obtained from cells in the caudal SC, where optimal saccade amplitudes ranged from about 30 to 100 degree.

2.1 Paradigm

To vary movement kinematics, monkeys elicited gaze-saccades from different initial eye-in-head orientations. At the start of a trial, the animal looked at a straight-ahead LED while aligning one of three head-fixed lasers with the fixation point. The lasers were positioned such that the horizontal head orientation with respect to straight ahead would be either $[-18, 0, +18]$ degree. For example, a target presented at 60 degree rightward resulted in three different 60 degree eye-head gaze shifts: the head at -18 degree (i.e., the eyes directed 18 degree ipsilateral to the target), 0 degree (eye-head alignment), or $+18$ degree (the “eye-contra” condition).

2.2 Analysis

To determine the movement field, gaze saccades were elicited in and around the cell’s response field. We counted the number of spikes in the burst from 20ms before gaze-shift onset to 20ms before offset (e.g., [Fig. 3A](#)), and applied the afferent mapping function of [Ottes et al. \(1986\)](#) to each gaze shift to calculate its anatomical coordinates (u, v) in the SC map. In polar coordinates ($\Delta G, \Phi$):

$$\begin{aligned} u &= B_u \cdot \ln \left(\frac{\sqrt{\Delta G^2 + 2A \cdot \Delta G \cdot \cos \Phi + A^2}}{A} \right) \text{mm} \\ v &= B_v \cdot \tan \left(\frac{\Delta G \cdot \sin \Phi}{\Delta G \cdot \cos \Phi + A} \right) \text{mm} \end{aligned} \quad (2)$$

where $B_u = 1.4$ mm, $B_v = 1.8$ mm/rad, and $A = 3.0$ degree determine the shape of the monkey afferent mapping function ([Ottes et al., 1986](#); [Robinson, 1972](#); [Fig. 4](#)).

We first fitted the *static movement field* function to all gaze-saccade vectors, and included a potential eye-in-head gain-field modulation (Van Opstal et al., 1995) by the initial eye position, E_0 , to the total number of spikes in the burst, N , according to:

$$N(\Delta G, \Phi, E_0) = N_0 \cdot (1 + \epsilon \cdot E_0) \cdot \exp\left(-\frac{(u - u_0)^2 + (v - v_0)^2}{2\sigma_p^2}\right) \quad (3)$$

This model has five free parameters: N_0 is the number of spikes in the burst for the optimal saccade from straight ahead, (u_0, v_0) (in mm) are the SC coordinates of the optimal saccade (Eq. 2), ϵ (in #spikes/degree) is the eye-position gain, and σ_p (in mm) quantifies the tuning width. Optimal parameter values were obtained with the Nelder–Mead Simplex algorithm in MATLAB®.

Next, the *dynamic movement field* describes how the cumulative number of spikes in the burst evolves during the straight gaze-displacement along the line connecting start- and end-positions (Goossens and Van Opstal, 2006). According to this model, the cumulative spike count for any gaze shift, regardless its kinematics, obeys the following, linear, relation:

$$CS(\Delta G, \Phi, E_0, t) = \Delta G(t + \tau) \cdot \frac{N(\Delta G, \Phi, E_0)}{\Delta G} \quad (4)$$

where $\Delta G(t + \tau)$ is the desired straight trajectory (increasing monotonically from 0 to ΔG). The neuron's lead time, τ , was fixed at $\tau = 20\text{ms}$ for all neurons. The straight trajectory was obtained by projecting the actual trajectory $(x(t), y(t))$ onto gaze vector $\Delta G \cdot (\cos\Phi, \sin\Phi)$ (Goossens and Van Opstal, 2006):

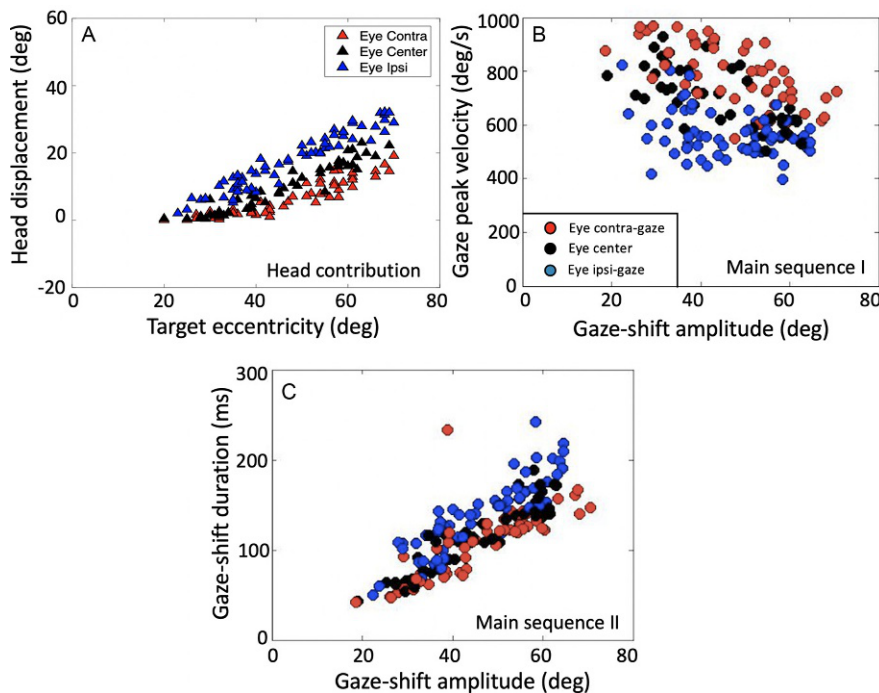
$$\Delta G(t) = x(t) \cdot \cos\Phi + y(t) \cdot \sin\Phi \quad (5)$$

The time-independent factor in Eq. (4), $N(\Delta G, \Phi, E_0)/\Delta G$, corresponds to the slope of the dynamic phase-relation. It should vary in a systematic way with gaze-shift amplitude and direction (Goossens and Van Opstal, 2006).

3 Results

3.1 Behavior

Fig. 2 shows an analysis of representative gaze shifts from monkey S for the three initial eye positions. These mainly horizontal gaze shifts (amplitudes between 20 and 75 degree) were directed into the movement field of neuron s1809. The contribution of the head movement to the gaze shift (see Fig. 1, for definition) depended systematically on the gaze-shift amplitude and initial eye-position (Fig. 2A), and had a strong influence on the peak gaze-velocity (Fig. 2B), and gaze-saccade duration (Fig. 2C). Note that for the largest gaze shifts, peak gaze velocity even tended to decrease with gaze-shift amplitude, which was highly significant for the contra- ($r = -0.46$) and centered ($r = -0.63$) eye positions. This property is due to two factors: first, for increasing gaze amplitudes the contribution of the (slower) head movement increases (Figs. 1B and 2A). Second, for large gaze shifts, the eyes will

**FIG. 2**

Properties of monkey eye-head gaze shifts, measured during single-unit recording of neuron s1809 (see Fig. 3). Rightward gaze shifts ($N = 180$) up to 75 degree amplitude were elicited into the cell's movement field, for three initial eye-in-head orientations (colors). (A) The contribution of the head movement varied systematically with initial eye position. (B,C) The initial fixation conditions had a strong influence on the gaze kinematics: larger/smaller head movements yielded slower/faster gaze shifts. Peak gaze velocities thus varied by >40%. Note also the significant decline of peak gaze velocity for the larger gaze shifts for the contralateral (red) and central (black) initial eye positions.

approach their oculomotor range so that the eye-in-head velocity starts to plateau. As a result, the later (slower) part of the head movement will increasingly dominate the gaze velocity. Ipsilateral eye orientations (blue symbols) caused consistently larger head movements, and the slowest gaze shifts. The fastest gaze shifts were obtained for contralateral initial eye orientations. These findings were robust for all recording sessions and for both monkeys.

3.2 Neural responses

The changes in initial eye-position also affected the activity of SC neurons. This is documented in Fig. 3 for neuron s1809. Fig. 3A shows the raw spike trains for the gaze shifts of Fig. 2. The neuron fires a prominent saccade-related burst associated with the upcoming saccade. Fig. 3B presents the phase plots for these spike trains.

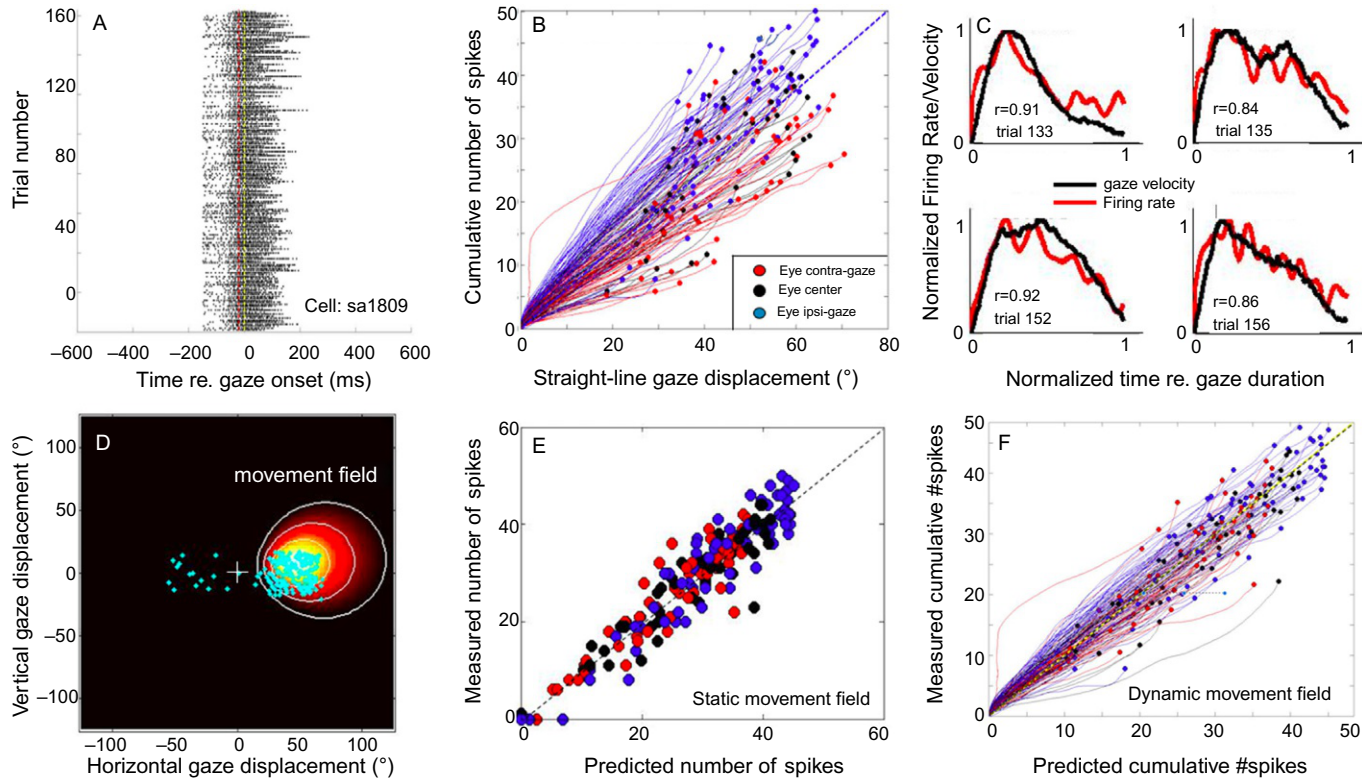


FIG. 3

(A) Raw spike trains of cell s1809 for all 180 trials into its movement field, aligned to gaze-movement onset (yellow-dashed line at $t=0$). The motor burst starts 20ms before gaze onset (red-dashed line). (B) Phase trajectories of the cumulative number of spikes as function of ongoing gaze displacement along the straight gaze vector. (C) Four example trials demonstrating a tight correlation between the cell's firing-rate profile and instantaneous gaze velocity. For ease of comparison, both variables were normalized to gaze duration and to their maxima. (D) Plot of the movement field (Eq. 3) in gaze-vector coordinates; color specifies number of spikes (dark: low, light: high). Cyan dots: endpoints of the gaze-shift vectors elicited during the neural recording. (E) The gain-field model captures the data well for all gaze shifts and initial conditions. (F) Test of Eq. (4) on the spike trains during all fast (red), intermediate (black), and slow (blue) gaze shifts into the movement field.

It shows the cumulative number of spikes, $CS(t+20)$, as function of the dynamic gaze-shift vector, $\Delta G(t)$. Note that each phase trajectory follows an approximately straight line, for which slope and end point differed considerably for each trial. According to Eq. (4), this slope should depend on the total number of spikes in the burst (as determined by Eq. 3), and gaze-saccade amplitude. It is immediately clear that the cumulative number of spikes in the burst also depends on initial eye position, as blue, black and red phase trajectories fall into different clusters. To test whether the dynamic movement-field model of Eq. (4) captures this variability in the cell's spiking behavior, we first determined the static movement field of the cell by fitting Eq. (3) to the total spike counts. Fig. 3D shows the movement field of the cell, together with all 180 gaze-saccade endpoints (cyan dots) for this experiment. The optimal parameters for this neuron were:

$N_0 = 40.3$ spikes	$\Delta G_0 = 57.2$ degree	$\Phi_0 = 9.4$ degree	$u_0 = 4.2$ mm	$v_0 = 0.28$ mm	$\sigma_P = 0.73$ mm	$\epsilon = 0.0063$ spikes/ degree
------------------------	-------------------------------	--------------------------	----------------	-----------------	----------------------	--

In Fig. 3E we show that the total number of spikes in the burst is predicted well by this model ($r = 0.96$). Fitting the movement field without eye-position modulation yielded $r = 0.90$, which is significantly lower ($P < 0.0001$). We next determined the predictions for the slopes of the spike-train phase trajectories of Fig. 3B (Eq. 4). Fig. 3F shows the predicted cumulative number of spikes for each response vs. the measured cumulative spike count. Note that this plot contains $>20,000$ data points. Yet, the correlation between measurements and predictions is very high: $r = 0.96$.

We observed that the neuron's firing rate had a remarkably good resemblance with instantaneous gaze velocity along the desired trajectory for a large fraction of trials. To illustrate this point, Fig. 3C shows four example trials with different gaze-velocity profiles. These normalized traces appeared to correlate very well. We obtained correlations $r > 0.7$ for nearly 50% of the trials in the majority of cells (results to be published elsewhere; see Section 4).

3.3 Model

Based on the behavioral and neurophysiological results we propose a computational model for the generation of eye-head gaze shifts, in which the SC provides the common drive for the eyes and head as a dynamic desired straight gaze trajectory, $\Delta G(t)$, by its total cumulative number of spikes. In other words, the instantaneous firing rate of the total population specifies the desired gaze velocity profile, and as such acts as a *vectorial gaze-pulse generator*. Details of the model, which is presented in its conceptual form in Fig. 4, including simulations, were published recently in Kasap and Van Opstal (2018a).

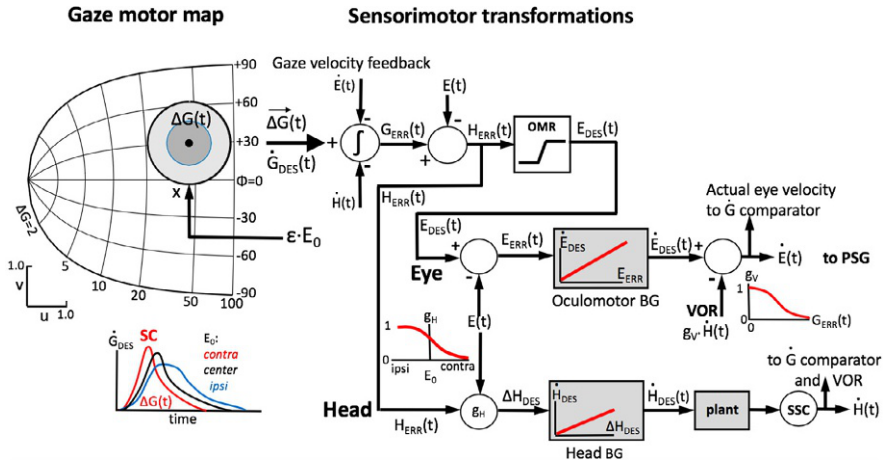


FIG. 4

Computational scheme for dynamic ensemble-coding of saccadic eye-head gaze shifts by the collicular population. The desired gaze-velocity profile along the straight trajectory, $\Delta G(t)$, is issued by the SC population, on which the initial eye position, E_0 , exerts a weak, multiplicative modulation. Thus, in line with our recordings, the number of spikes in the burst, and the spike timings, depends on eye position too (e.g., Fig. 3C and E). Eye and head are driven by different signals in head-centered reference frames. The actual contributions of the eye and head movements to the gaze shift, ΔE , and ΔH , depend on E_0 through gain g_H (inset) and on their relative timings. The VOR gain is modulated between 0 and 1 by ongoing gaze error, $G_{ERR}(t)$ (inset). PSG: pulse-step generator and oculomotor plant (not shown). The relative onsets of eye- and head movements depend on stimulus modality, initial eye position, and top-down task-related signals (not shown).

The SC output represents the desired straight-line gaze velocity, $\dot{G}_{DES}(t)$, which is compared with the true gaze velocity from the oculomotor and head-motor systems to determine a dynamic gaze-error signal:

$$G_{ERR}(t) = \int_{ON}^t (\dot{G}_{DES}(\tau) - \dot{E}(\tau) - \dot{H}(\tau)) d\tau \quad (6)$$

This gaze error is combined with eye position to represent the dynamic error of the gaze saccade in a *craniocentric* reference frame:

$$H_{ERR}(t) = G_{ERR}(t) + E(t) \quad (7)$$

This latter signal drives both the oculomotor and head-motor systems. For the eye, the signal can keep eye position within the (soft) oculomotor range (OMR). The dynamic desired eye-in-head position thus becomes:

$$E_{DES}(t) = OMR(H_{ERR}(t)) \quad (8)$$

This signal drives the (linear) oculomotor burst generator with dynamic eye motor-error:

$$E_{ERR}(t) = E_{DES}(t) - E(t) \quad (9)$$

The output of the oculomotor burst generator represents *desired* eye velocity:

$$\dot{E}_{DES}(t) = B_E \cdot E_{ERR}(t) \quad (10)$$

with B_E (in s^{-1}) a linear gain. Finally, the actual eye velocity during eye-head gaze shifts is obtained after combining this signal with the VOR:

$$\dot{E}(t) = \dot{E}_{DES}(t) - g_V(G_{ERR}(t)) \cdot \dot{H}(t) \quad (11)$$

where the VOR gain ($0 < g_V < 1$) is a nonlinear sigmoid function of instantaneous gaze error: it is close to one (fully engaged) when the gaze error is small, and approaches zero (it is off) for large gaze errors (inset in Fig. 4).

In our model also the head is driven by the dynamic head-motor error (see inset in Fig. 4):

$$\Delta H_{DES}(t) = g_H(E_0) \cdot H_{ERR}(t) \quad (12)$$

where the gain $0 < g_H < 1$ is a nonlinear function of initial eye position. The desired head velocity is subsequently generated by a linear head-burst generator:

$$\dot{H}_{DES}(t) = B_H \cdot \Delta H_{DES}(t) \quad (13)$$

where $B_H < B_E$. The actual head velocity results after passing the desired motor drive through the head-motor plant:

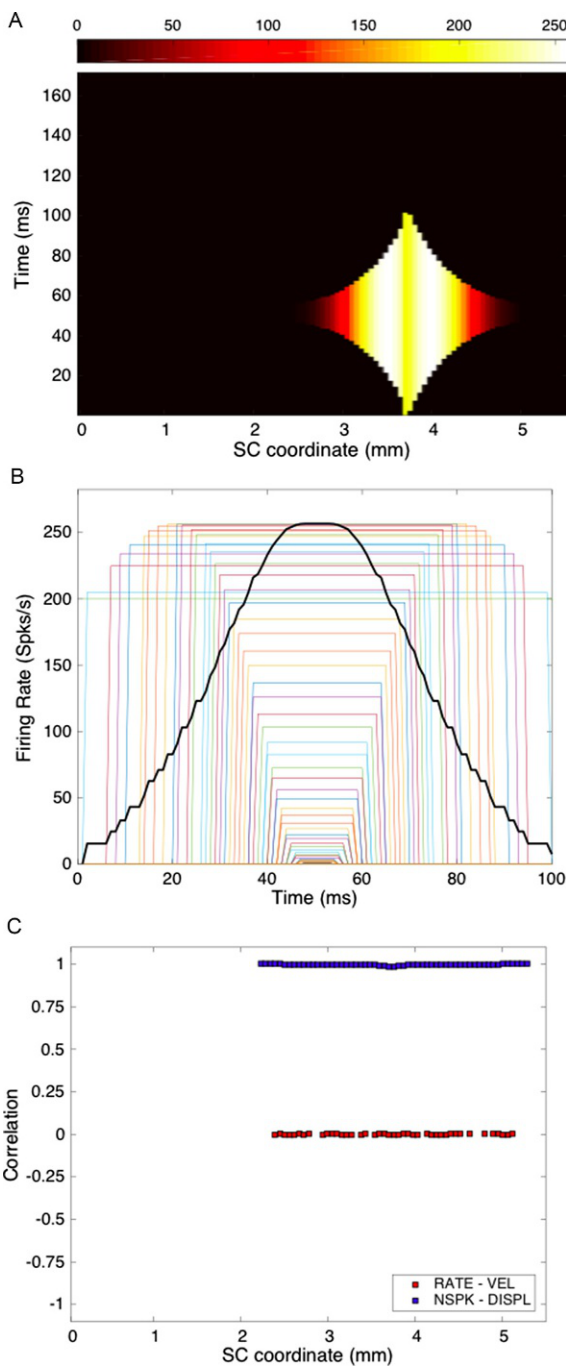
$$\dot{H}(t) = PLANT_{HEAD}(\dot{H}_{DES}(t)) \quad (14)$$

for which we took a simple first-order low-pass filter. Simulations with this model show that it faithfully captures the kinematics and eye-head cross-coupling properties of measured eye-head gaze shifts (Kasap and Van Opstal, 2018a).

4 Discussion

We extended our SC model of dynamic movement fields (Goossens and Van Opstal, 2006) by including a small, but significant, influence of initial eye-in-head position on the total number of spikes in the burst (gain-field model, Eq. 3). We noted that eye position systematically influenced the SC firing-rate profiles:

Ipsilateral eye	Lower firing rates	Longer burst durations	More spikes
Contralateral eye	Higher firing rates	Shorter burst durations	Fewer spikes

**FIG. 5**

See legend on opposite page.

In many trials ($\sim 50\%$) we found a tight correlation ($r > 0.7$) between the instantaneous firing rate of an SC cell and the straight-line gaze-velocity profile into their movement fields (e.g., Fig. 3C). An eye-position signal in the motor SC has been reported before (Van Opstal et al., 1995), but its potential role for the control of gaze kinematics in eye-head saccades has not been reported.

Note that the linear spike-counting model (Eq. 1) is a *population model*. As such, it predicts that the *total* collicular output faithfully reflects the instantaneous desired gaze displacement (cumulative spike count) and gaze velocity (total cumulative firing rate). The model does *not* necessarily predict that individual cells should reflect gaze kinematics on a trial-by-trial basis.

To illustrate this point, Fig. 5 shows a simulation with rectangular SC bursts (Fig. 5B), with the number of spikes determined by the static movement field. The total SC output still produced the required gaze-velocity (Fig. 5B) and gaze trajectory, even though none of the cells encode gaze velocity ($r = 0$; Fig. 5C). Therefore, the tight correlation illustrated in Fig. 3C underscores the role for the motor SC as the nonlinear vectorial pulse generator of the saccadic gaze-controller, as proposed in our model (Fig. 4).

In head-restrained monkeys, we found that spike trains correlated well with instantaneous eye-velocity because of the tight synchronization of burst profiles across the population (Goossens and Van Opstal, 2012). We recently reported that this important aspect of neural population activity can be understood from excitatory-inhibitory lateral interactions among the SC cells in a spiking neural network (Kasap and Van Opstal, 2017, 2018b; Van Opstal and Kasap, 2018).

We here conjecture that a similar control principle may hold for eye-head gaze saccades, whereby initial eye position influences the characteristics of SC cells in such a way that (i) their burst characteristics vary with initial eye orientation, and (ii) the total number of spikes changes too.

In our spiking neural network model (Kasap and Van Opstal, 2017, 2018b; Van Opstal and Kasap, 2018), the burst characteristics of spiking leaky-integrate-and-fire neurons depended on two parameters: the time constant of the membrane adaptation current, and the scaling strength of the synaptic weights that make up the lateral

FIG. 5

Simulation of a hypothetical SC–brainstem saccade model (one-dimensional, for clarity), in which all cells fire rectangular bursts. (A) Population activity in the SC motor map as function of time for a gaze shift of 30 degree. Color code represents mean firing rates. Cells at the fringes of the population start their shorter bursts later than the central cells, so that all cells reach their peak at the same time. (B) Rectangular bursts of all cells; the number of spikes of each cell is determined by the static movement field; burst duration decays exponentially with distance from the central hot spot at $u = 3.7$ mm. Continuous curve: instantaneous (normalized) firing rate (representing gaze velocity) of the population. (C) The cumulative number of spikes for each individual cell correlates well with instantaneous gaze displacement (blue), but firing rates of individual cells do not correlate at all with instantaneous gaze velocity (red).

excitatory-inhibitory interactions. To ensure a fixed number of spikes in the central burst of the population, and a systematic decrease of peak firing-rate with saccade amplitude, both parameters had to depend systematically on the cell's rostral-caudal location in the motor map. We here speculate that initial eye position may affect the values of these parameters for the upcoming gaze shift, leading to the observed modifications of the burst characteristics and ensuing gaze kinematics.

As a result of eye-head coupling, the inclusion of the VOR, the oculomotor range, and the eye-position influence on SC cells, each of which introduces its own nonlinearity in the system, the computational complexity of the model is markedly increased when compared to the simple linear eye-movement model of [Goossens and Van Opstal \(2006\)](#). Moreover, the variable onsets of eye- and head-movements in the gaze shift, and thus their contribution and kinematics, depend on various factors, such as initial eye position, stimulus modality, and task constraints. Thus, at first sight, one would not immediately expect that firing rates of SC neurons would correlate so well with the dynamic gaze trajectory.

As a final note, our model concentrated mainly on the role of the SC in gaze control, and less on the question whether downstream brainstem-cerebellar-spinal circuitry operates with a gaze feedback loop (like [Fig. 4](#), and in the models of [Goossens and Van Opstal, 1997](#); [Guitton and Volle, 1987](#); [Kasap and Van Opstal, 2018a](#); [Sağlam et al., 2011](#)), or without gaze-feedback by controlling independent, but coupled eye-head circuits (like in the models of [Daye et al., 2014](#); [Freedman, 2001](#); [Kardamakis et al., 2010](#)). We believe that our collicular data do not rule out either hypothesis, as the SC responses already seem to reflect all major properties of the ensuing gaze shifts and their kinematics.

Acknowledgments

This work was supported by EU Horizon 2020 ERC Advanced Grant ORIENT (nr. 693400, A.J.v.O., B.K.) and by the Radboud University (A.J.v.O.). The authors are highly indebted to Ed Freedman, Mark Walton, and Stephan Quesy from the Department of Neuroscience at the University of Rochester, NY, USA, for hosting A.J.v.O. in their lab (May–June 2009), to share their excellent facilities, their time and expertise that enabled the experiments, and for many fruitful discussions.

References

- [Daye, P.M., Optican, L.M., Blohm, G., Lefèvre, P., 2014. Hierarchical control of two-dimensional gaze saccades. *J. Comput. Neurosci.* 36, 355–382.](#)
- [Freedman, E.G., 2001. Interactions between eye and head control signals can account for movement kinematics. *Biol. Cybern.* 84, 453–462.](#)
- [Freedman, E.G., Sparks, D.L., 1997. Eye-head coordination during head-unrestrained gaze shifts in rhesus monkeys. *J. Neurophysiol.* 77, 2328–2348.](#)
- [Freedman, E.G., Sparks, D.L., 2000. Coordination of the eyes and head: movement kinematics. *Exp. Brain Res.* 131, 22–32.](#)

- Goossens, H.H.L.M., Van Opstal, A.J., 1997. Human eye-head coordination in two dimensions under different sensorimotor conditions. *Exp. Brain Res.* 114, 542–560.
- Goossens, H.H.L.M., Van Opstal, A.J., 2006. Dynamic ensemble-coding of saccades in the monkey superior colliculus. *J. Neurophysiol.* 95, 2326–2341.
- Goossens, H.H.L.M., Van Opstal, A.J., 2012. Optimal control of saccades by spatial-temporal activity patterns in monkey superior colliculus. *PLoS Comput. Biol.* 8 (5), e1002508.
- Guitton, D., Volle, M., 1987. Gaze control in humans: eye-head coordination during orienting movements to targets within and beyond the oculomotor range. *J. Neurophysiol.* 58, 427–459.
- Harris, C.M., Wolpert, D.M., 1998. Signal-dependent noise determines motor planning. *Nature* 394, 780–784.
- Harris, C.M., Wolpert, D.M., 2006. The main sequence of saccades optimizes speed-accuracy trade-off. *Biol. Cybern.* 95, 21–29.
- Kardamakis, A.A., Moschovakis, A.K., 2009. Optimal control of gaze shifts. *J. Neurosci.* 29, 7723–7730.
- Kardamakis, A.A., Grantyn, A., Moschovakis, A.K., 2010. Neural network simulations of the primate oculomotor system. V. Eye–head gaze shifts. *Biol. Cybern.* 102, 209–225.
- Kasap, B., Van Opstal, A.J., 2017. A spiking neural network model of the midbrain superior colliculus that generates saccadic motor commands. *Biol. Cybern.* 111, 249–268.
- Kasap, B., Van Opstal, A.J., 2018a. Double stimulation in a spiking neural network model of the midbrain superior colliculus. *Front. Appl. Math. Stat.* 4, 47. <https://doi.org/10.3389/fams.2018.00047>.
- Kasap, B., Van Opstal, A.J., 2018b. A model for auditory-visual evoked eye-head gaze shifts in dynamic multi-steps. *J. Neurophysiol.* 119, 1796–1808.
- Ottes, F.P., Van Gisbergen, J.A.M., Eggermont, J.J., 1986. Visuomotor fields of the superior colliculus: a quantitative model. *Vision Res.* 12, 1795–1808.
- Quessy, S., Freedman, E.G., 2004. Electrical stimulation of rhesus monkey nucleus reticularis gigantocellularis. I. Characteristics of evoked head movements. *Exp. Brain Res.* 156, 342–356.
- Quessy, S., Quinet, J., Freedman, E.G., 2010. The locus of motor activity in the superior colliculus of the rhesus monkey is unaltered during saccadic adaptation. *J. Neurosci.* 30, 14235–14244.
- Robinson, D.A., 1972. Eye movements evoked by collicular stimulation in the alert monkey. *Vision Res.* 12, 1795–1808.
- Sağlam, M., Lehnert, N., Glasauer, S., 2011. Optimal control of natural eye-head movements minimizes the impact of noise. *J. Neurosci.* 31, 16185–16193.
- Sparks, D.L., Mays, L.E., 1980. Movement fields of saccade-related burst neurons in the monkey superior colliculus. *Exp. Brain Res.* 39, 39–50.
- Van Gisbergen, J.A.M., Van Opstal, A.J., Tax, A.A.M., 1987. Collicular ensemble coding of saccades based on vector summation. *Neuroscience* 21, 541–555.
- Van Opstal, A.J., Goossens, H.H.L.M., 2008. Linear ensemble coding in midbrain superior colliculus specifies the saccade kinematics. *Biol. Cybern.* 98, 561–577.
- Van Opstal, A.J., Kasap, B., 2018. Electrical stimulation in a spiking neural network model of monkey superior colliculus. In: Mathematical Modeling in Motor Neuroscience: State of the Art and Translation to the Clinic. *Progress in Brain Research*, vol. 248. Elsevier.
- Van Opstal, A.J., Hepp, K., Suzuki, Y., Henn, V., 1995. Influence of eye position on activity in monkey superior colliculus. *J. Neurophysiol.* 74, 1593–1610.
- Walton, M.M.G., Freedman, E.G., 2011. Gaze-shift duration, independent of amplitude, influences the number of spikes in the burst for medium-lead burst neurons in pontine reticular formation. *Exp. Brain Res.* 214, 225–239.

This page intentionally left blank

Modeling gaze position-dependent opsoclonus

3

Lance M. Optican^{a,*}, Janet C. Rucker^b, John-Ross Rizzo^b, Todd E. Hudson^b

^aLaboratory of Sensorimotor Research, NEI, NIH, DHHS, Bethesda, MD, United States

^bNYU School of Medicine, New York, NY, United States

*Corresponding author: Tel.: +1-301-496-9375, e-mail address: lanceoptic@nih.gov

Abstract

Opsoclonus/flutter (O/F) is a rare disorder of the saccadic system. Previously, we modeled O/F that developed in a patient following abuse of anabolic steroids. That model, as in all models of the saccadic system, generates commands to make a *change* in eye position. Recently, we saw a patient who developed a unique form of opsoclonus following a concussion. The patient had postsaccadic ocular flutter in both directions of gaze, and opsoclonus during fixation and pursuit in the left hemifield. A new model of the saccadic system is needed to account for this gaze-position dependent O/F. We started with our prior model, which contains two key elements, mutual inhibition between inhibitory burst neurons on both sides and a prolonged reactivation time of the omnipause neurons (OPNs). We included new inputs to the OPNs from the nucleus prepositus hypoglossi and the frontal eye fields, which contain position-dependent neurons. This provides a mechanism for delaying OPN reactivation, and creating a gaze-position dependence. A simplified pursuit system was also added, the output of which inhibits the OPNs, providing a mechanism for gaze-dependence during pursuit. The rest of the model continues to generate a command to change eye position.

Keywords

Opsoclonus, Saccade, Smooth pursuit, Model

1 Introduction

Abnormal eye movements characterized by bursts of involuntary, back-to-back (i.e., without an intersaccadic interval), conjugate saccades at frequencies in the range of 10–35 Hz are called opsoclonus (if multidirectional) or ocular flutter (if horizontal only) (Averbuch-Heller and Remler, 1996; Cogan, 1954, 1968; Leigh and Zee, 2015; Pretegiani et al., 2017a; Wong et al., 2001). We recently proposed that opsoclonus/flutter (O/F) was due to the OPNs being held off after a saccade, perhaps

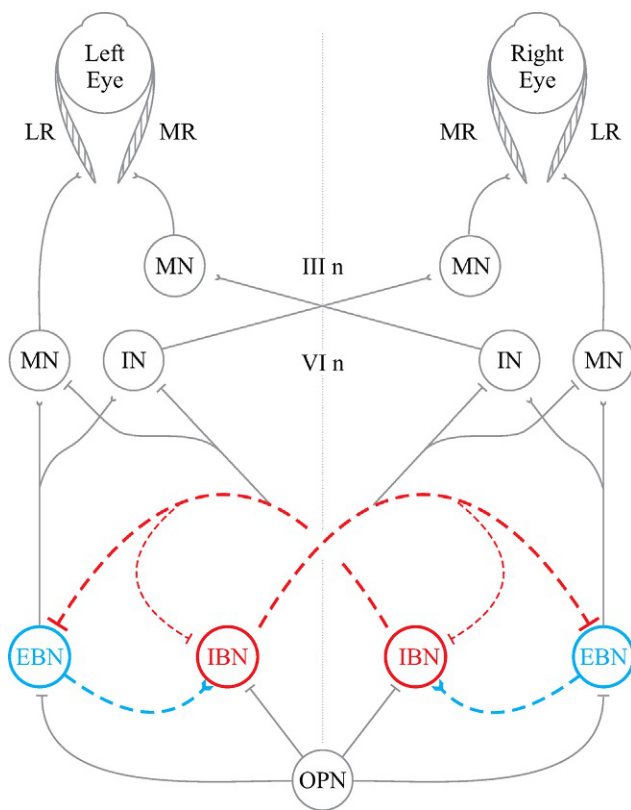
only for saccades in one direction (Optican and Pretegiani, 2017a). However, the dependence of the flutter on orbital position cannot be explained by that model.

Recently, Rucker and colleagues identified a novel, gaze position-dependent O/F in a patient following a concussion (see the companion paper in this volume for the clinical description). The patient made hypometric saccades in both directions followed by postsaccadic flutter for a few half-cycles (oscillating at 25–30 Hz). Opsoclonus occurred when the eyes were fixating in the left hemifield, or during smooth pursuit when the eyes were in the left or lower hemifield. Follow-up 7 months later showed a marked reduction in the number of occurrences of opsoclonus, along with significant recovery from concussion, but saccades were still followed by ocular flutter. Our concussion patient showed signs of frontal lobe, particularly frontal eye field (FEF), injury (Rivaud et al., 1994). The subject had an increased latency during visually-guided prosaccades, overlap and antisaccades, but no increased latency during the gap task. There were no differences in error rates in anti-saccade tasks. The subject also made hypometric saccades. These findings suggest that the concussion led to chronic FEF dysfunction.

Previous studies have also reported opsoclonus with pontine lesions. A patient with a head injury developed synchronous horizontal, vertical and torsional macrosaccadic oscillations during fixation. MRI revealed a unilateral pontine lesion, which included the area of the raphe interpositus nucleus (RIP), (Averbuch-Heller et al., 1996). The authors attributed this deficit to a loss of function in the omnipause neurons (OPNs). Tychsen et al. (1990) reported on a patient with essential hypertension who showed square-wave jerks, dynamic overshoot, opsoclonus (0.5–1° in amplitude and 20–25 Hz in frequency) and tinnitus. The tinnitus co-occurred with episodes of opsoclonus. The authors attributed this disorder to pontine dysfunction. Thus, the pons appears to be important in generating posttraumatic saccadic intrusions.

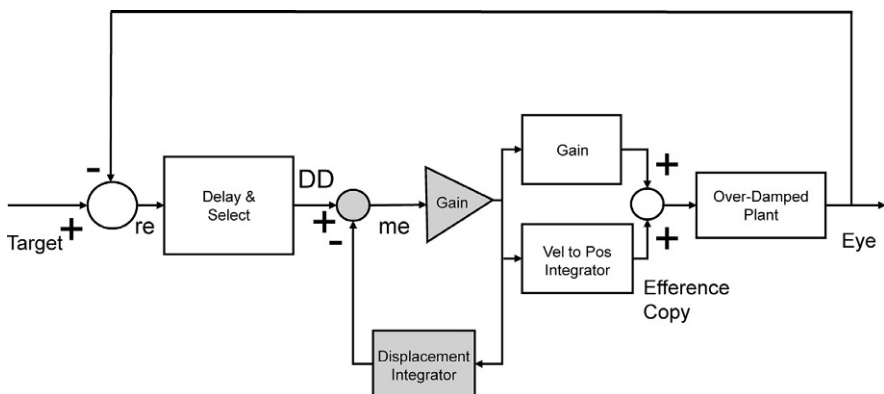
From these results we infer that a mechanism involving the frontal lobe and the pons may be important for gaze-position related oscillations. Here, we demonstrate that a mechanism based on differential inputs from the frontal lobe and the brain stem to the OPNs can account for the delayed reactivation of the OPNs that leads to ocular flutter during saccades and fixation when eccentricity is large. To account for opsoclonus during pursuit at smaller eccentricities than during fixation requires yet another input, of smooth pursuit velocity, to the OPNs, as suggested previously (Keller and Missal, 2003; Missal and Keller, 2002).

What mechanism generates opsoclonus? The neurons that control initiation and termination of a saccade lie mostly in the midbrain, pons, brain stem and cerebellum. Areas of the cerebrum are also involved in saccades, primarily in selecting the target. Fig. 1 shows a schematic of the premotor circuit for driving the motor neurons that make saccades. This circuit is inherently unstable because of the feedback loops between excitatory (EBNs, cyan) and inhibitory (IBNs, red) burst neurons on both sides (Ramat et al., 2005). These premotor burst neurons are normally inhibited by omnipause neurons (OPNs). Previous theories of opsoclonus and similar saccadic oscillations assumed that it is disinhibition in an inherently unstable linear system that leads to oscillation (Wong et al., 2001). However, such theories produce only

**FIG. 1**

Brain stem circuit for horizontal saccades. Eye movements are made by the horizontal recti muscles (medial and lateral recti, MR and LR), which are innervated by the motor neurons of the abducens (VIn) and oculomotor (IIIIn) nuclei. The motor neurons are controlled by burst neurons in the paramedian pontine reticular formation (wherein lie the excitatory burst neurons, or EBNs), and in the nucleus paragiganto-cellularis dorsalis (wherein lie the inhibitory burst neurons, or IBNs). The burst neurons are held off by the omnipause neurons (OPNs) in the raphe interpositus nucleus. To make a rightward saccade, the OPNs first shut off, then the right EBNs and IBNs turn on. The EBNs drive the abducens motor neurons (MN) and interneurons (IN), while the IBNs inhibit the left abducens nucleus, and the left EBNs and IBNs. If the OPNs are held off, the mutually inhibitory connections between the IBNs (red) can lead to oscillations.

sinusoidal oscillations, and are thus unable to account for the quasi-sinusoidal waveforms usually seen in O/F. Nor could they account for the gaze position-dependence of our patient. Recently, we analyzed data from two patients with opsoclonus following abuse of anabolic steroids (Pretegiani et al., 2017b). This led us to propose a new model of O/F, based on dysfunction in a circuit involving the brain stem premotor

**FIG. 2**

Schematic diagram of lumped saccadic system. The drive to the saccadic system comes from the inner feedback loop (gray blocks). The input to that loop is a desired eye displacement (DD), which is derived from retinal error (re). Desired displacement is compared with the progress of the current saccade from the resettable displacement integrator. This provides the motor error (me) that drives the saccade. The only place in this model corresponding to eye position is the output of the velocity to position integrator, which provides an efference copy of eye position. However, that efference copy is derived after the burst is generated. Thus, neither this model nor any other model based solely on desired displacement can produce gaze position-dependent opsoclonus/flutter.

neurons (EBNs, IBNs and OPNs) and the cerebellum (oculomotor vermis and fastigial nuclei oculomotor region) (Optican and Pretegiani, 2017a). The new model reproduced the waveforms seen in those patients by assuming an increase in the inhibitory GABA_A receptor sensitivity.

The latter model cannot account for gaze position-dependence of O/F as seen in our concussion patient, because it has only neurons that are sensitive to *changes* in eye position, and not eye position itself. Fig. 2 shows a simple model of saccadic motor control. The problem with this type of model is that there is no explicit or implicit information about eye position. The model generates a burst to move the eyes based on a desired eye *displacement* signal. Nonetheless, there are neurons in the brain that are sensitive to eye position, and the purpose of this modeling study is to show that an improved model, extended by including just a few new connections, explains the position-dependent O/F seen in the postconcussion patient.

2 Methods

The patient was seen twice, 3 years after the concussion and again 7 months later. Eye movements were recorded with the EyeLink 1000+ video-oculography system (SR Research, Ontario, Canada). Data from the tracker had a mean interval of

2.00 ms but a range of 1.9–2.1 ms. To more accurately determine measures of duration, the data were resampled at a uniform interval of 1.00 ms (Matlab's interp1 function, with the piecewise cubic hermite interpolating polynomial), and filtered and differentiated (Matlab's Savitzky–Golay filter, order = 2, frame length = 11).

The model was simulated in Matlab and Simulink (The Mathworks, Natick, MA), version R2017b. The solver used to compute the states of the model was the third order Bogacki–Shampine method for nonstiff, ordinary differential equations (ode23), with a fixed step size of 0.1 ms.

3 Results

Examples of our patient's data on the first visit are shown in Figs. 3–4. Fig. 3 shows eye position traces when the eye follows two horizontal target jumps. Fig. 3 shows the three key features of the patient's eye movements during saccades and fixation: the saccades in both directions are hypometric, saccades to the right and left are followed by a few half-cycles of postsaccadic flutter, and opsoclonus occurs in leftward eccentric fixation beyond about 15° of eccentricity.

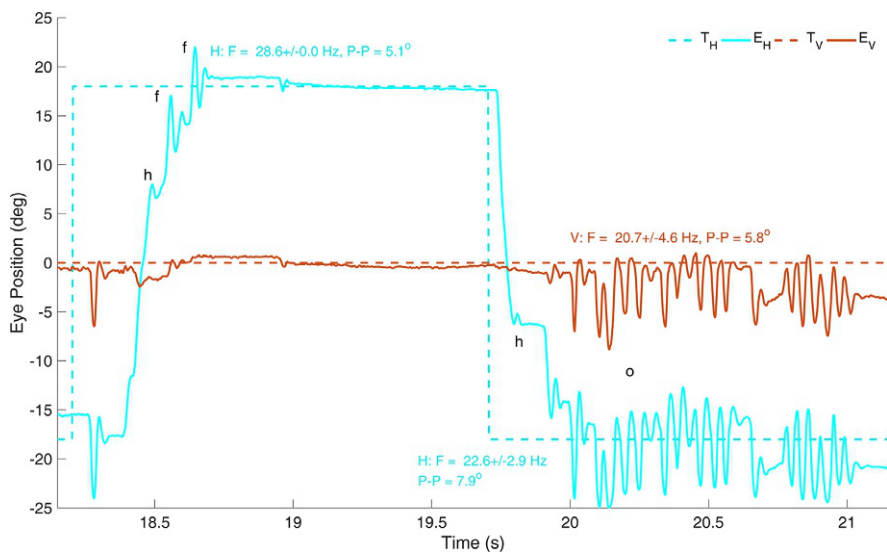
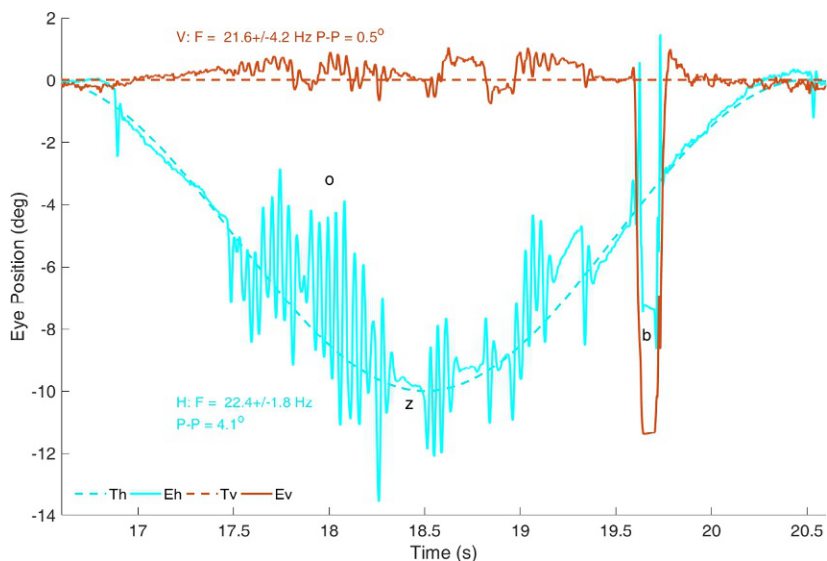


FIG. 3

Example of patient's eye movements during saccades and fixation. Note that the saccades are hypometric (h) and followed by one or two half-cycles of back-to-back saccades (flutter, f). During fixation to the left, when the eye is beyond about 15° of eccentricity, the eyes oscillate continuously both horizontally and vertically (o). F is frequency \pm std. dev, P–P is the median positive peak minus the negative peak of the oscillations.

**FIG. 4**

Example of patient's record showing opsoclonus (o) during smooth pursuit of a sinusoidal target in the left hemifield. The opsoclonus is stronger when the patient is moving leftward. Note that the opsoclonus tends to stop near the point where the target turns around (i.e., where eye velocity is nearing zero, z). Compared to Fig. 3, we can see that the opsoclonus occurs when the eye is in the left hemifield, but with a much smaller eccentricity than needed to elicit opsoclonus during fixation. Whenever there is an oscillation on the horizontal trace, there is also one of the same frequency, albeit smaller, on the vertical trace. Blink artifact (b). Other labels as in Fig. 3.

Fig. 4 shows the patient's eye movements during pursuit of a sinusoidal target in the left hemifield. Note that the opsoclonus occurs when the eye is only about 5° left of center, which is less than the 15° of eccentricity needed for opsoclonus during fixation. The opsoclonus is stronger when the eye is moving to the left. There is a tendency for the opsoclonus to stop when the eye nears the turning point of the pursuit target (i.e., when pursuit velocity is zero).

4 New model of opsoclonus

The new model proposed here (Fig. 5) is an extension of our previous model of opsoclonus (Optican and Pretegiani, 2017a), which was an extension of our previous neuromimetic models of saccades (Daye et al., 2013, 2014; Lefevre et al., 1998; Optican and Pretegiani, 2017b; Optican and Quaia, 2002; Quaia et al., 1999). Many of the underlying principles of the model are available in those papers, and most of the parameters of the current model are from the previous opsoclonus paper

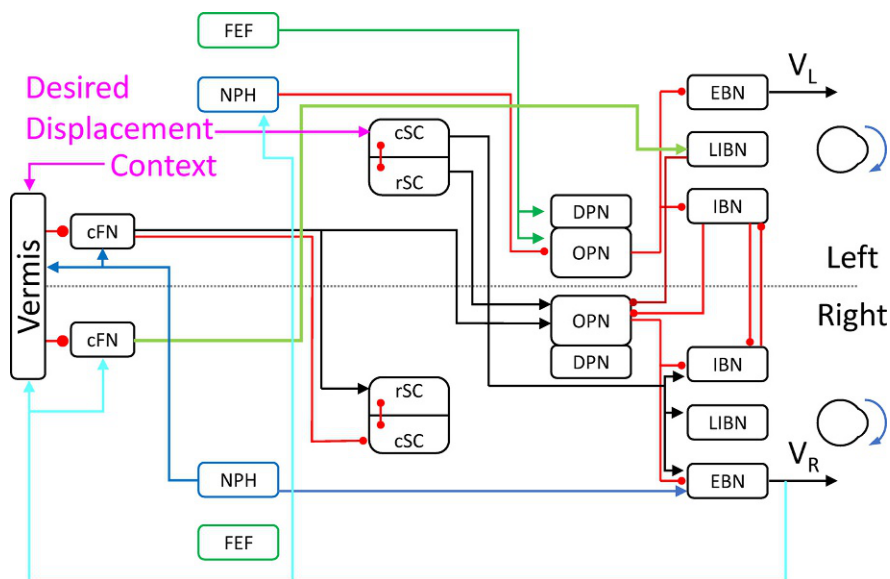


FIG. 5

Schematic of a neuromimetic model of the saccadic system. The model's connections are symmetric, but here we show only the connections needed to make a rightward eye movement (arrowheads: excitatory; disk heads: inhibitory). Before the movement, the oculomotor vermis, the cFN, both rostral SC (rSC) and omnipause neurons (OPN) are on, and the premotor burst neurons (EBN, IBN and LIBN) are off. At the start of a rightward saccade, cerebral cortex sends target information to the left caudal SC (cSC) (desired displacement, magenta arrow). The left cSC begins to fire, which inhibits the left rSC and excites the right excitatory burst neurons (EBN), inhibitory burst neurons (IBN), and long-lead inhibitory burst neurons (LIBN). However, the OPNs are holding the EBNs and IBNs off. The right LIBNs are not held off, and they can now inhibit the OPNs. This allows the right EBNs and IBNs to fire, which starts the movement. As the movement proceeds, an efference copy of eye velocity is fed back from the right EBNs to the vermis (cyan line). This causes a wave of inhibition to spread across the vermis to the right. When the wave of inhibition reaches the location corresponding to the ending point of the saccade on the right side of the vermis, the right cFN is disinhibited (red line). The right cFN excites the left IBNs, overcoming the inhibition by the right IBNs. The left IBNs activate and inhibit the right PBN, choking off the drive to the right motor neurons and stopping the movement. The OPNs and rSC reactivate, because of the right cFN input, preventing saccadic oscillations and holding the eyes on target. This model now shows two other areas, the NPH and the FEF. These send inhibitory and excitatory signals (respectively) to the OPNs. This introduces an eccentricity sensitivity to the model, which otherwise works only with eye movement displacements. The FEF also projects to the DPNs, but we do not show any output from the DPNs, because it is not known to where their efferents project.

(Optican and Pretegiani, 2017a). Here, we describe the new elements of the model, the nucleus prepositus hypoglossi (NPH) and the frontal eye fields (FEF). The most essential element in our new model of opsoclonus is the change to the inputs of the omnipause neuron (OPN), which will be discussed at length below.

4.1 Eye position neurons

4.1.1 Frontal eye fields (FEF)

The FEF are intimately involved in eye movements and target selection. Stimulation of the FEF elicits contralateral saccades of size and off-horizontal direction that depends upon the stimulation site (Bruce et al., 1985; Robinson and Fuchs, 1969). FEF neurons can be divided into two groups (Bizzi, 1968; Bizzi and Schiller, 1970). Group one neurons fire during saccades in a preferred direction. Group two neurons fire during fixation and smooth pursuit, whenever the eye is in a specific eccentric position. The rate of activity increases with eccentricity during both fixation and pursuit. In addition, some group two neurons fire for central eye positions (Bizzi, 1968). The fixation neurons reduce their firing rate during smooth pursuit (Izawa and Suzuki, 2014).

This suggests that the FEF play both excitatory and inhibitory roles in eye movements. Indeed, electrical stimulation of the FEF shows two types of saccade suppression: a widely distributed response that suppresses initiation of ipsiversive saccades, and a more localized area that suppresses saccades in any direction (Izawa et al., 2004a,b). The FEF may play a role in the maintenance of visual fixation by activating OPNs directly (Stanton et al., 1988) or indirectly via the SC (Pare and Guitton, 1994).

The FEF projects ipsilaterally to the rostral SC, and bilaterally to the nucleus reticularis segmenti pontis (NRTP) and the paramedian pontine reticular formation (PPRF); it also projects bilaterally, but primarily ipsilaterally, to the RIP, the site of the OPNs (Huerta et al., 1986; Segraves, 1992; Shook et al., 1990; Stanton et al., 1988).

4.2 Supplementary eye fields (SEF)

The SEF contain saccade- and pursuit-related neurons. Microstimulation of the SEF evokes contralateral saccades (Schlag and Schlag-Rey, 1987). Position-dependent activity, during both fixation and smooth pursuit, is found in a significant proportion of neurons in the SEF. In addition, some of these cells fire during fixation or smooth pursuit of a target with a rate proportional to eye eccentricity, above a threshold (which can be in the non-preferred direction) (Schlag et al., 1992). The SEF sends an excitatory projection directly to the OPN region (Missal and Heinen, 2017; Shook et al., 1988), bilaterally, but predominantly ipsilaterally. It also projects to the FEF (Huerta and Kaas, 1990; Stanton et al., 2005) and bilaterally to the SC (Shook et al., 1990). The SEF also projects to the cerebellum via the basal pontine nuclei (BPN) and the NRTP (Thier and Mock, 2006).

4.3 Ocular motor cerebellum

4.3.1 Vermis

Purkinje cells (PuC) in the vermis (lobules VIc and VII, called the oculomotor vermis, or OMV) have saccade-related activity that differs in the timing for the response depending upon the direction of the movement, being earlier for contraversive saccades and later for ipsiversive saccades (Noda and Fujikado, 1987; Ohtsuka and Noda, 1995). The OMV projects ipsilaterally to the fastigial oculomotor region (FOR) (Yamada and Noda, 1987), which is in the caudal fastigial nucleus (cFN).

Several studies have found position-dependent tonic units in the OMV (Kase et al., 1980; Ohtsuka and Noda, 1992, 1995). The NPH is the site of part of the neural integrator that provides the signal for holding the eyes at an eccentric position. Yamada and Noda (1987) found that the NPH projects to the vermis. This could be the source of the position-dependent mossy fiber (MF) signals.

4.3.2 Caudal fastigial nuclei

The tonic activity of most cFN neurons does not change significantly with eye position. However, Ohtsuka and Noda (1991) found a small population of fastigial neurons with a position dependence; they were located between the saccade- and vestibular-related regions of the fastigial nuclei. Fuchs et al. (1993) also found 8 of 13 fastigial neurons that had activity correlated with eye position. The NPH projects bilaterally to the cFN (Noda et al., 1990), and could be a source of the position-dependent signals.

4.4 Summary of cortical inputs

From the above discussion it is possible that several areas, including the cerebellum, the FEF and the SEF might send a position-dependent signal to the OPNs. For simplicity, we collapse all these possibilities in the model, and refer to all the excitatory position-dependent signals as coming from the FEF. More experimental evidence will be needed to tease out the contributions of each area to this signal.

4.5 Nucleus prepositus hypoglossi (NPH)

The orbital tissues have an elastic restoring force that tends to bring the eye toward the center of the orbit (Robinson, 1964). To hold the eye in an eccentric position, a tonic level of neuronal activity in the motor neurons is needed to generate enough force to overcome that restoring force. As all eye movement commands are in the velocity domain, one way to obtain a position-related signal is to simply integrate the velocity commands (Robinson, 1975). The neuronal circuits that perform this function are called the neural integrator, or NI, and for horizontal movements are formed by the nucleus prepositus hypoglossi (NPH), the medial vestibular nuclei (MVN), and the cerebellum (flocculus and paraflocculus).

Evidence suggests that the NI is not a perfect integrator, but “leaks.” Thus, as the eye is held eccentrically, it drifts back exponentially toward the center with a long time constant. A saccade occurs to keep the eye from drifting back too much. The pattern of drift back to the center followed by eccentric saccades is called gaze-paretic nystagmus. The drift time constant is not constant, but rather decreases (drift velocity increases) as the eye is held more eccentric (Bertolini et al., 2013; Chan and Galiana, 2005; Eizenman et al., 1990). Thus, the NI is leaky with a time constant that is a nonlinear function of eccentricity (Chan and Galiana, 2008; Khojasteh et al., 2013).

Neurons in the NPH/MVN display a variety of firing patterns, ranging from position-like to velocity-like (McFarland and Fuchs, 1992). The class of neurons of most interest to us is the position neuron, which changes its firing rate in proportion to eye position. The position cell lags the eye movement by ~10ms (McFarland and Fuchs, 1992).

Afferents to the NPH arise from the perihypoglossal nuclei (including NPH itself), vestibular nuclei, the contralateral nucleus paragiganto-cellularis dorsalis (PGD) (i.e., IBN area), ipsilateral PPRF (i.e., the EBN area), extraocular motor nuclei, the cerebellum (flocculus and caudal fastigial nuclei). The NPH also receives inputs from the superior colliculus, the FEF, the SEF, and the posterior parietal cortex, and the RIP (i.e., the OPN area) (Langer and Kaneko, 1983).

The efferent projections of the NPH are widespread throughout the cerebellum and brain stem (McCrea and Horn, 2006). The NPH projects directly to the three motor nuclei (III α , IV α , and VI α), providing the necessary tonic activity to hold the eye steady against the elastic restoring forces in the orbit. The NPH neurons use a variety of both excitatory and inhibitory neurotransmitters, including GABA, glycine (Gly), and glutamate (Glu) (McCrea and Horn, 2006). Spike-triggered averaging and autoradiography revealed that NPH neurons which project to the ipsilateral abducens nucleus gave rise to excitatory postsynaptic currents via Glu, whereas NPH neurons that project to the contralateral abducens nucleus evoked inhibitory postsynaptic currents via Gly (Escudero et al., 1992; Spencer et al., 1989).

The NPH also projects bilaterally to the cerebellum (floccular-nodular lobe, ventral paraflocculus, posterior vermis, fastigial nuclei, and hemispheres), but more ipsilaterally than contralaterally, the PPRF (wherein lie the EBNs) and the PGD (wherein lie the IBNs). The NPH projects bilaterally to the intermediate SC, although the contralateral projection is heavier (McCrea and Horn, 2006).

Importantly for our purposes, the NPH/MVN sends a weak, bilateral projection to the pontine raphe nuclei, including the RIP, which contains the OPNs (Ito et al., 1984; Langer and Kaneko, 1984; McCrea and Baker, 1985). We will assume that this projection provides an inhibitory signal proportional to eye position in the head (eccentricity).

4.6 Omnidirectional and directional pause neurons (OPN and DPN)

Oscillations are the natural consequence of the reciprocal inhibition between neurons that exhibit postinhibitory rebound (Wang and Rinzel, 1992). Mutual inhibition between IBNs on both sides thus leads to flutter if the OPNs cannot resume firing after a saccade (Ramat et al., 2005). Here, we give a detailed discussion of pause

neurons because they play the key role in our model of opsoclonus (Pretegiani et al., 2017b). The pause neurons are found in a small, midline region in the caudal PPRF, called the RIP, and have large dendritic fields that cross the midline (Buttner-Ennever et al., 1988). Pause neurons fire at a steady rate during the intersaccadic interval and pause during saccades in some or all directions (Keller, 1974; Luschei and Fuchs, 1972). Pause neurons stop discharging during sleep (Henn et al., 1984). Pause neurons are glycinergic (Horn et al., 1994).

Pause neurons can be divided into two groups, those that pause only for ipsilateral saccades, called directional pause neurons (DPNs), and those that pause for saccades in all directions, called omnipause neurons (OPNs). Although all early studies of pause neurons found both DPNs and OPNs (Cohen and Henn, 1972; Keller, 1974; Luschei and Fuchs, 1972), subsequent studies, and all models of the saccadic system, ignored the DPNs. For our purposes, the DPNs may help to explain how OPN firing rates are determined. Whereas the OPNs fire at a steady rate during fixation irrespective of eye position in the orbit, the activity of DPNs during fixation increases with eye eccentricity to the ipsilateral side.

Luschei and Fuchs (1972) found that, of 32 pause units, 12 paused for saccades in all directions, nine paused only for ipsilateral saccades, three paused only for contralateral saccades, and eight paused for both ipsilateral and contralateral saccades. Cohen and Henn (1972) reported that neurons paused for both saccades and quick phases of nystagmus, and some paused only in one direction. They also reported that fixation activity in some pause neurons increased with eccentricity. Keller (1974) found that of 20U, 12 OPNs showed no correlation between eye position and fixation activity, whereas eight DPNs increased their activity with ipsilateral eye position eccentricity. The OPN tonic rate ranged from 180 to 250 sp/s, whereas the DPN rate never exceeded 150 sp/s. The start of the pause in both types of neurons preceded the saccade by 12–25 ms. The OPNs did not change their activity during different fixation positions or the slow phases of rotatory nystagmus, but the DPNs changed rate in proportion to eye position (firing faster for more ipsilateral positions).

Bergeron and Guitton (2001) looked at the gaze position error dependence of OPNs in cats. They found that OPN firing rates were more or less constant above 10° of error. However, when the error was between 0 and 10° the activity decreased from about 143 sp/s to 60 sp/s, with a slope of -4 spikes/deg. (i.e., activity was highest when error was zero). There is a difference in the timing of OPN activity in head unrestrained cats and monkeys. In cats, the OPNs are tightly coupled to gaze (eye + head) movements (Pare and Guitton, 1998). In monkeys, they are more tightly coupled to eye movements (Coble et al., 1994). However, the main difference appears to be in how crisply the gaze shift ends (being less crisp in cats), so there may be no difference in the gaze control circuit for OPNs (Pare and Guitton, 1998).

Although the OPN firing rate during fixation is not a function of eye position, it is not constant. Bergeron and Guitton (2002) showed that during multiple step saccades in head unrestrained cats, the activity of the OPN after the pause was greater, the closer the eye was to the target. This is also true for rSC neurons, so it is possible that the OPN activity is simply reflecting the rSC input.

4.6.1 Afferents

Several systems converge on the OPNs, including visual, vestibular, and saccadic systems. [Prsa and Galiana \(2007\)](#) showed with extensive model simulations that much of the behavior of saccadic and vestibular activity during head unrestrained movements could be captured by a model of the OPNs whose input was a weighted sum of gaze motor error (from the SC), head velocity (from the medial vestibular nuclei, MVN) and eye velocity (from the excitatory burst neurons, EBNS, and long-lead inhibitory burst neurons, LIBNs).

Electrical stimulation of the vestibular nerve or labyrinths causes polysynaptic suppression of the OPNs, ([King et al., 1978, 1980](#)). The MVN project bilaterally to the RIP, but predominantly ipsilaterally ([Ito et al., 1984](#)). Electrical stimulation of the MVN inhibits the OPNs ([Ito et al., 1986](#)). The MVN are active during saccades, even if the head is not moving, and inhibits the OPNs (see review by [Galiana, 1991](#)). There is also a bilateral projection from the NPH to the RIP, predominantly ipsilateral ([Ito et al., 1984; Langer and Kaneko, 1984, 1990](#)). As the NPH/MVN form the neural integrator, and the MVN projections are inhibitory, we shall assume in our model that the NPH projection to the OPNs is also inhibitory.

OPNs receive glutamatergic, GABAergic and glycinergic inputs ([Horn et al., 1994; Wang et al., 2013](#)). Receptors for Glu are restricted to OPN dendrites, whereas GABA and Gly receptors are on both OPN dendrites and somata ([Horn et al., 1994](#)). The OPNs receive excitatory, monosynaptic input from bilateral rSC ([Buttner-Ennever et al., 1988; Harting, 1977; Raybourn and Keller, 1977](#)), contralateral cFN ([Noda et al., 1990](#)) and FEF ([Stanton et al., 1988](#)).

They also receive inputs from LIBNs ([Kamogawa et al., 1996](#)). The LIBNs are monosynaptically excited by the contralateral cSC and disynaptically inhibited from the ipsilateral cSC (via the contralateral IBNs) ([Sugiuchi et al., 2005](#)). IBNs also received disynaptic inhibition from the rostral SC via the OPNs. Thus, OPNs receive monosynaptic excitation from the rSC, and disynaptic inhibition (via IBNs) from the cSC ([Shinoda et al., 2011](#)).

The rSC excites the contralateral OPNs directly ([Buttner-Ennever et al., 1988](#)), and indirectly through excitatory projections in the ipsilateral central mesencephalic reticular formation (cMRF, [Wang et al., 2013](#)). The cSC also inhibits the OPNs via GABAergic neurons in the ipsilateral cMRF ([Wang et al., 2013](#)). The cSC inhibits ipsilateral OPNs via contralateral glycinergic LIBNs and IBNs ([Shinoda et al., 2011; Wang et al., 2013](#)). During the gap paradigm (fixation point goes off, and after a gap in time the target light comes on) the activity in rSC neurons begins to decrease, but the activity in OPNs remains steady ([Everling et al., 1998](#)). Some OPNs also had a phasic increase in activity immediately after target onset. At the end of the saccade, rSC neurons begin firing at a steady rate, whereas OPN activity increases gradually over the first three spikes. OPN discharge after the pause is variable, with some neurons showing an increase relative to pre-pause activity, and some showing a decrease. Thus, the input to the OPNs cannot come solely from the rSC. One possibility is that the loss of input from the rSC is made up by buildup neurons in the cSC before the saccade ([Everling et al., 1998](#)). Alternatively, activity could be made up by input from the SEF and FEF ([Burman and Bruce, 1997](#)).

OPNs project to contralateral EBNs and IBNs, but not LIBNs (Curthoys et al., 1984; Scudder et al., 1988; Takahashi et al., 2005). Projections of the DPNs have not been studied and will not be included in the model.

4.7 New hypothesis about OPN function

The OPNs receive projections from many places, including the SC, the cMRF, the IBNs and LIBNs, the cFN, the NPH/MVN, and the cortical FEF and SEF. We do not include all these connections in the model, because they are redundant. We shall assume for the purposes of our model that the inputs from the cFN, the rSC and the FEF are glutamatergic (excitatory); from the NPH are GABAergic (inhibitory); and from the IBNs and the LIBNs are glycinergic (inhibitory).

We assume that the tonic firing rate of the OPNs between saccades is due to the balance between the Glu inputs from cFN, SC, and FEF, the Gly inputs from LIBNs and the GABA inputs from the NPH. This is consistent with the findings of Kanda et al. (2007). The GABAergic inputs could also be controlling OPNs during slow movements, such as smooth pursuit (Missal and Keller, 2002) and vergence (Busettini and Mays, 2003).

The major new hypothesis here relates to the role of the NPH projection to the OPNs. Why should the NPH send a signal to the OPNs? The neural integrator (NI) is not perfect, but “leaks,” i.e., in eccentric positions, the eye will drift back to center. During nystagmus, an increase in head velocity increases the probability of a quick phase occurring (Galiana, 1991). During a sustained head turn, the quick phases of nystagmus carry the eye further than the slow phases, so the eye gradually moves ahead in the orbit, perhaps so that it can see what is in the direction of the head turn earlier (Chun and Robinson, 1978; Galiana, 1991; Ramat et al., 2003). Also, as the eye moves more eccentrically in the orbit, the neural integrator becomes leakier, causing a faster gaze paretic nystagmus. The further eccentric the eye, the faster it drifts back. Thus, more frequent quick phases are able to keep the eye more eccentric (Bertolini et al., 2013; Bockisch et al., 2013; Chan and Galiana, 2005, 2008, 2010; Crawford and Vilis, 1993; Khojasteh et al., 2013).

We hypothesize that to keep the eye as eccentric as possible in lower animals (e.g., rabbits), the NPH sends an inhibitory signal to the OPNs. As the eye position becomes more and more eccentric, this signal increases, and thereby reduces the activity in the OPNs, which makes it more likely that a saccade will occur to counteract the drift. According to this hypothesis, OPN activity should decrease as the eye moves more eccentrically. However, OPN activity is independent of orbital eccentricity (Cohen and Henn, 1972; Keller, 1974; Luschei and Fuchs, 1972). To reconcile this discrepancy between our hypothesis and the data, we suggest that in higher animals (e.g., monkeys) the need to counteract gaze-paretic nystagmus is less acute, and thus the inhibitory position-dependent input from the NPH is canceled by an excitatory position-dependent input from the FEF/SEF/Cerebellum. If we assume that this excitatory signal goes to both OPNs and DPNs, but the inhibitory signal from NPH/MVN goes only to OPNs, we can create the observed dichotomy in pause neurons:

$$DPN = FEF + \dots \quad (1a)$$

$$OPN = (FEF - NPH) + \dots \quad (1b)$$

In a normal subject, the Glu and GABA outputs from these position-dependent areas set the baseline activity for the OPNs. We assume that in our patient the output from cerebral cortex (FEF/SEF) and possibly the cerebellum has become imbalanced because of the concussion. In particular, the Glu signals are diminished and/or delayed. Thus, the membrane potential is pulled down by the GABA signals. This makes the OPNs more likely to turn off, if they are on, and less likely to turn on, if they are off. If a saccade is made, the OPN membrane potential is lowered by Gly, and part of the restoration of the membrane potential comes from the withdrawal of Gly from the IBNs. However, there will also be less Glu, so the time it takes for the GABA-determined baseline to recover is extended. During this extended time the left-right IBN reciprocal circuit oscillates. This creates a position-dependent nystagmus, because the size of the Glu signals coming from the SEF, FEF and cerebellum are position-dependent.

The key feature in our patient was the eye position-dependence of the opsoclonus. Saccades in both directions were hypometric and followed by a brief opsoclonus, but sustained oscillations during fixation only occurred when the eyes were deviated to the left by more than $\sim 15^\circ$. As was shown previously, opsoclonus may be caused by reciprocal inhibition in the cerebellum and brain stem when the OPN reactivate later than normal ([Optican and Pretegiani, 2017a](#)). In the new model opsoclonus occurs because the FEF drive to the OPNs is too late and/or too weak, causing the NPH inhibition to keep the OPNs hyperpolarized for too long. This same mechanism can account for postsaccadic opsoclonus in our patient. The finding that saccades in both directions were hypometric and followed by opsoclonus means that the FEF was delayed after rightward saccades and delayed and weak after leftward saccades.

The delayed reactivation of OPN activity hypothesized above would cause rightward saccades to become hypermetric. However, we assume that the adaptive capability of the cerebellum would reduce saccade gain (G_{saccade}) so that the eyes got on target, and thus both hypometria and oscillations would be observed.

4.8 Smooth pursuit

Why should opsoclonus in our concussion patient be so prominent during smooth pursuit in leftward positions, especially at eccentricities that are smaller than those required to elicit opsoclonus during fixation? To answer this question, we must consider how the output from the smooth pursuit system influences the OPNs. The OPNs were long thought to be exclusively part of the saccadic system, but in a seminal paper [Missal and Keller \(2002\)](#) showed that activity in about half of OPNs declined (by about 30–40%) during smooth pursuit movements. Some of these OPNs showed a strong burst at the time of target onset, but that will be ignored in this discussion. Furthermore, they showed that electrical microstimulation of OPNs induced a strong deceleration in ongoing pursuit.

In another paper, [Keller and Missal \(2003\)](#) recorded from a small population of burst neurons in the PPRF near the OPN region. They found a new type of neuron that responded to both smooth pursuit and saccadic eye movements, which they called saccade/pursuit neurons (SPNs). They proposed that the SPNs received inputs from the saccadic EBNs, and from the pursuit drive neurons (PNs). The SPNs then inhibited the OPNs, acting as a latch to keep OPNs off during saccades or to increase the gain of the PNs during pursuit movements (which they called gain control).

Their results suggest that the saccade-related drop in the OPN membrane potential can be completely accounted for by the inputs described above, and that the time course of the OPNs is very fast. In their examples, we found the dominant time constant (T_p) to be ~ 2.4 ms. This is consistent with a glycine receptor channel model of OPN inhibition during saccades ([Kanda et al., 2007](#); [Optican, 2008](#); [Yoshida et al., 1999](#)). In contrast, the relationship between the smooth pursuit signal and eye velocity was much slower. The eye velocity drive does not exactly match the OPN activity. Instead, the input to the OPN shows some evidence of acceleration sensitivity, and a low pass filter with a time constant of ~ 20 ms. This suggests that the glycinergic mechanism may not be operating. Instead, we propose that the pursuit signal goes through the GABA_A receptors on the OPNs. This is consistent with a dominant time constant between SPN and OPN activity of ~ 96 ms.

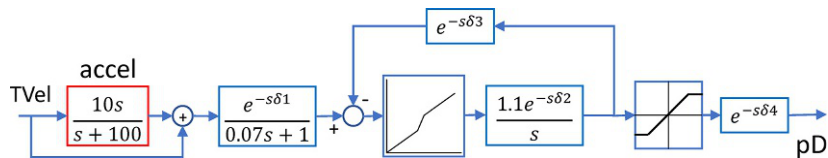
Although it is speculative to make inferences about time courses from such limited and indirect experiments, we think that it is reasonable to propose that the two sources of inhibition to the OPNs (glycinergic and GABAergic) have much different time courses.

If we assume that the OPNs are only weakly inhibited by the NPH to begin with, then a reduction in OPN activity caused by the SPN input may be enough to release the reciprocal-inhibition in the brain stem and cause ocular oscillations. This would allow opsoclonus to occur during pursuit at smaller eccentricities than are required to elicit fixation opsoclonus. Note that one prediction of this model is that for pursuit targets with eccentricities smaller than for fixation opsoclonus, the opsoclonus will stop when eye speed drops to zero, as the SPNs will then not be inhibiting the OPNs. To include smooth pursuit in our model, we had to include a mechanism for tracking moving targets. This is a very complicated topic, especially because tracking can occur with zero lag. For our purposes, a simple system proposed earlier by [Robinson et al. \(1986\)](#) was used, but modified with an acceleration term on the input to achieve zero-lag tracking ([Fig. 6](#)).

4.9 Model implementation

The model developed here is almost the same as the model in our previous paper on opsoclonus ([Optican and Pretegiani, 2017a](#)). We briefly describe the elements of the model with a focus on the new parts. All neurons were represented as adaptive low pass filters, with postinhibitory rebound (PIR) ([Ramat et al., 2005](#)):

$$\min \left(\left[\left[1 + \frac{sG_a T_a}{sT_a + 1} \right] \frac{G_l}{sT_l + 1} \right] e^{-s\delta}, 800 \right) \quad (2)$$

**FIG. 6**

Schematic of Pursuit System. An acceleration term (accel, red) has been added on the left to allow the model to track sinusoids with zero lag. Input is target velocity (TVel) and output is pursuit drive (pD). Delays ($\delta_1 - \delta_4$) are 0.001s, 0.035s, 0.030s, and 0.001s.

Model is taken from Robinson, D.A., Gordon, J.L., Gordon, S.E., 1986. A model of the smooth pursuit eye movement system. Biol. Cybern. 55, 43–57.

where s is the Laplace variable. The adaptation factor has gain and time constant G_a and T_a (typically 0.05–0.10 and 1–200 ms). The low pass filter has gain and time constant G_l and T_l (typically 1.0 and 2 ms). The floor corner brackets ($\lfloor \rfloor$) imply that the output is always nonnegative. The min() function indicates a saturation at 800 sp/s. The output is delayed by the synaptic delay, δ (0.8 ms). Each neuron has three inputs that are summed, one excitatory, one inhibitory, and a dominant inhibition from OPN (with three gains, G_e , G_i and G_o , typically 4, 4 and 10).

4.9.1 Pursuit system

We used a simple pursuit system (Fig. 6) developed by Robinson et al. (1986). This model always tracks with a phase delay, but our patient showed tracking with almost no delay. Thus, an acceleration term was added to the input of the pursuit model:

$$\frac{10s}{(s+100)} \quad (3)$$

to allow the eye to track a sinusoidal target without a delay. The output of the model was P_{drive} . It contributed to the velocity drive in the final common path with a gain of $pDriveGain$.

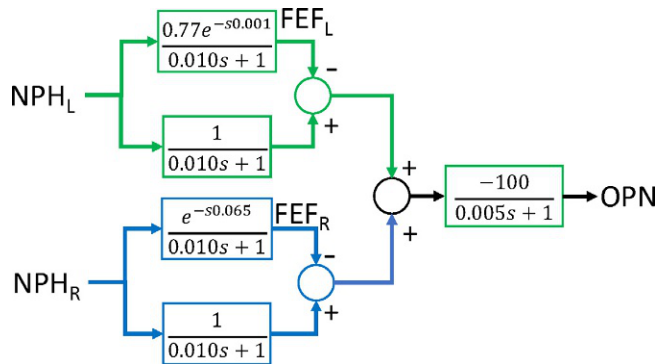
4.9.2 Nucleus prepositus hypoglossi (NPH)

The NPH output was taken as the output of the neural integrator:

$$\frac{20}{(20s+1)} \quad (4)$$

The NPH position signal was split into rightward and leftward signals (Fig. 7). These went through a delay (FEFdelR or FEFdell), and created two new signals, NPHlpR and NPHlpL representing a lowpass filtered version of the one-sided NPH output according to:

$$\frac{1}{(0.01s+1)} \quad (5)$$

**FIG. 7**

Schematic of FEF/NPH input to OPNs. The NPH provides a position dependent signal to the FEF. The FEF signal lags the NPH signal. The factor of -100 in the last transfer function reverses the sign so that the NPH inhibits, and the FEF excites, the OPNs. The delays and gains of the FEF lowpass filters are different on the left and right, giving the position-dependence exhibited by our patient.

Table 1 Model parameters needed in the new model, as compared with the older model (Optican and Pretegiani, 2017a).

$G_{\text{FEFL}} = 0.77$	$G_{\text{FEFR}} = 1.0$	$\text{EBN}_{\text{TC}} = 0.010$	$\text{IBN}_{\text{TC}} = 0.001$
$\text{TC}_{\text{FEFL}} = 0.010$	$\text{TC}_{\text{FEFR}} = 0.010$	$\text{EBN}_{\text{aGain}} = 3$	$\text{IBN}_{\text{aGain}} = 8$
$\text{FEFdelL} = 0.001$	$\text{FEFdelR} = 0.065$	$\text{EBN}_{\text{TCadapt}} = 0.001$	$\text{IBN}_{\text{TCadapt}} = 0.005$
$\text{SPN}_{\text{Gain}} = 57$	$G_{\text{Saccade}} = 0.80$	$\text{pDriveGain} = 0.40$	

Time constants (TC) and delays (del) are in seconds.

4.9.3 Frontal eye fields (FEF)

The FEF position signals were derived from the position signals in the NPH. The NPH signals were delayed and sent into lowpass filters for left and right signals, called FEFlpR and FEFlpL (Fig. 7):

$$\frac{G_{\text{FEF}}}{T_{\text{FEFs}} s + 1} \quad (6)$$

These lowpass filters were constructed so that they could be reset to zero if the eye position was on the opposite side. See Table 1 for parameter values.

4.9.4 Omnipause neurons (OPN)

A difference signal was then created for each side:

$$D_{nph,fef} L = [L_1 \{L_2(e^{-s\delta} \text{FEFL}) - L_2(NPHL)\}] \quad (7)$$

$$D_{nph,fef} R = [L_1 \{L_2(e^{-s\delta} \text{FEFR}) - L_2(NPHR)\}] \quad (8)$$

where L_1 is a lowpass filter with gain 100 and time constant 0.005s; L_2 is a lowpass filter with gain 1.0 and time constant 0.010s. The time delay of the FEF signal is δ . This difference signal was input to the OPNs.

The OPNs were modeled as a single, lumped neuron, as in Eq. 1b. The inputs to the OPN were:

$$\begin{aligned} OPN_{in} = & (cFN + rSC + 200) \\ & - (LIBN_L + LIBN_R + D_{nph,fef}L + D_{nph,fef}R + SPN_{Gain}|P_{drive}|). \end{aligned} \quad (9)$$

4.10 Simulations

[Fig. 8](#) shows simulated saccades and fixation for a normal subject. Note that the difference between NPH and FEF eye position signals (B) is only noticeable during very large saccades (A). Thus, the OPN activity (red trace in A) is not affected, and saccades are normal. Simulated smooth pursuit tracking is shown in [Fig. 9A](#). The eye tracks the target very closely for the first 2s, after which it begins to lag the target.

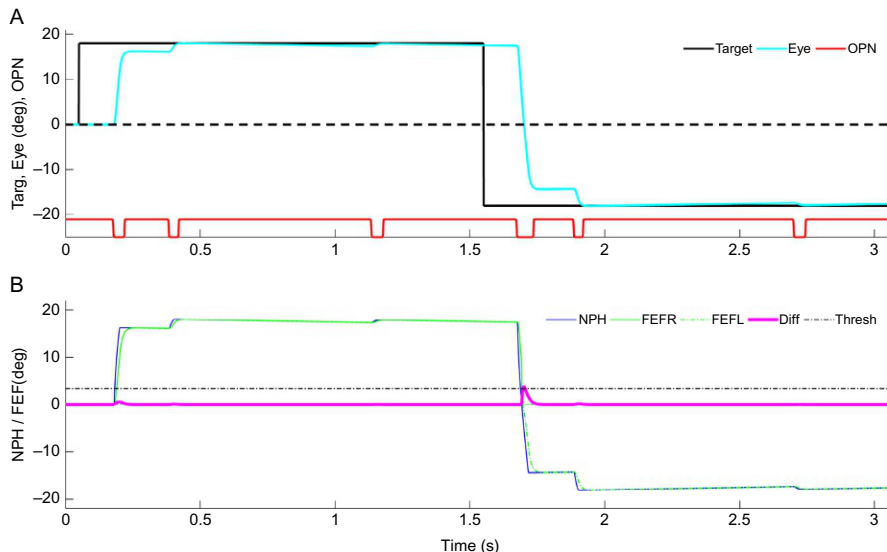
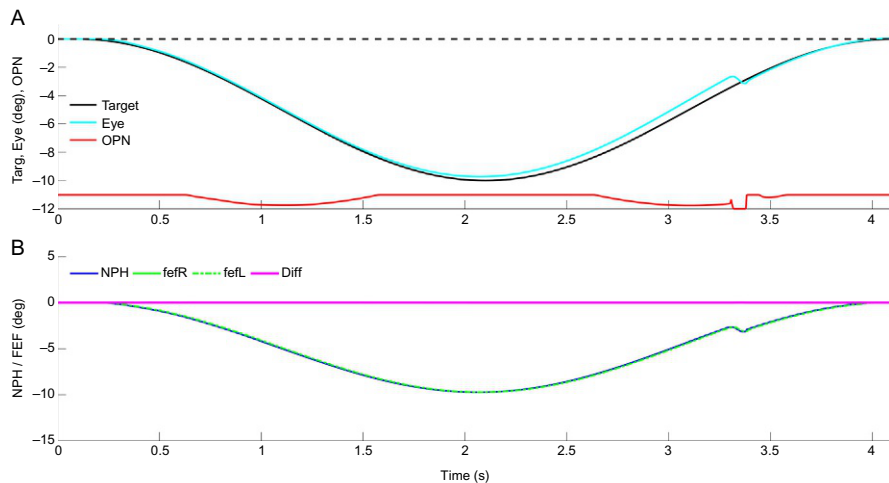


FIG. 8

Simulation of normal saccade tracking. (A) Large leftward and rightward saccades are slightly hypometric. Red trace shows the activity of the OPNs. (B) Internal signals related to eye eccentricity (NPH, blue; FEF, green). The signals from the left and right FEF are slightly delayed and lowpass filtered relative to the NPH signal. Their difference (magenta) inhibits the OPNs, but is significant only during large saccades, so it has no effect on the postsaccadic period.

**FIG. 9**

Simulated smooth pursuit tracking. (A) Eye movement follows target very closely up until about 2s. The eye then lags the target until it is corrected by a small saccade at about 3.3s. The red trace shows that the activity of the OPN is not constant during pursuit. The OPNs receive inhibition from the smooth pursuit drive signal, so OPN activity declines slightly during leftward and rightward movements, but not when the eye velocity is near zero. Note the complete pause in the OPNs at the time of the catch-up saccade. (B) NPH (blue) and FEF (green) traces and their difference (magenta). There is essentially no difference between NPH and FEF signals because of the low speed of pursuit. Thus, their difference provides no net inhibition to the OPNs.

A catch-up saccade corrects this at about 3.3s. The eye movements are slow, so the difference between the NPH and FEF signals is negligible (Fig. 9B). Nonetheless, the OPN activity (red trace in Fig. 9A) shows a dip when pursuit velocity is high. This is because of the inhibition of the OPNs by the smooth pursuit drive signal.

Fig. 10A shows a simulation of saccades and fixation in our patient, which can be compared with Fig. 3. The essential features from Fig. 3 are reproduced (hypometria, postsaccadic flutter, and fixation opsoclonus beyond -15°). Fig. 9B shows the internal signals in the model. The blue trace is the NPH output. The green traces are the FEF output (split into left (dashed) and right (solid)). The magenta trace is the absolute value of the difference between the NPH and the FEF signals. Whenever the difference is greater than $\sim 3^\circ$ (Thresh), the OPNs (red trace in Fig. 9A) are off. This allows postsaccadic flutter and opsoclonus. As the flutter would carry the eyes beyond the target, we assume that adaptation in the cerebellum lowers the saccadic gain from 1.0 to 0.8, thus causing the saccades to become hypometric.

A simulation of the patient's smooth pursuit tracking is shown in Fig. 11A, which can be compared with Fig. 4. Note that all the essential features of the patient's performance are captured in the model (pursuit opsoclonus at smaller eccentricities

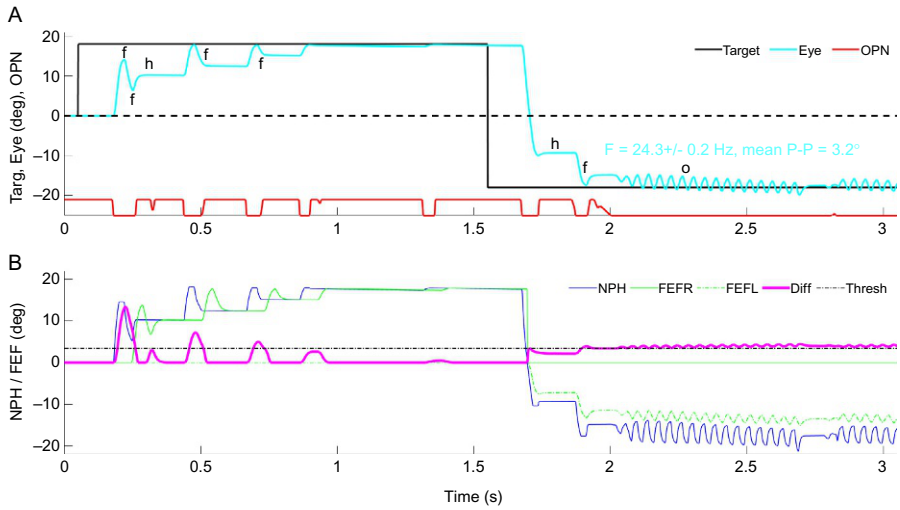


FIG. 10

Simulation of patient's eye movements during saccades and fixation. (A) Saccades in both directions are hypometric (h) and followed by one or two half-cycles of back-to-back saccades (flutter, f). The red trace shows the OPN activity. (B) The NPH (blue) and FEF (left and right, green) activity in the model are shown. Their difference ($|NPH - FEF|$) is shown in magenta. During fixation on the left, when the eye is beyond about 15° of eccentricity, the difference signal exceeds the threshold (Thresh $\sim 3^\circ$), the OPNs are held off (red trace in A) and the system oscillates (opsclonus, o). Frequency label as in Fig. 3.

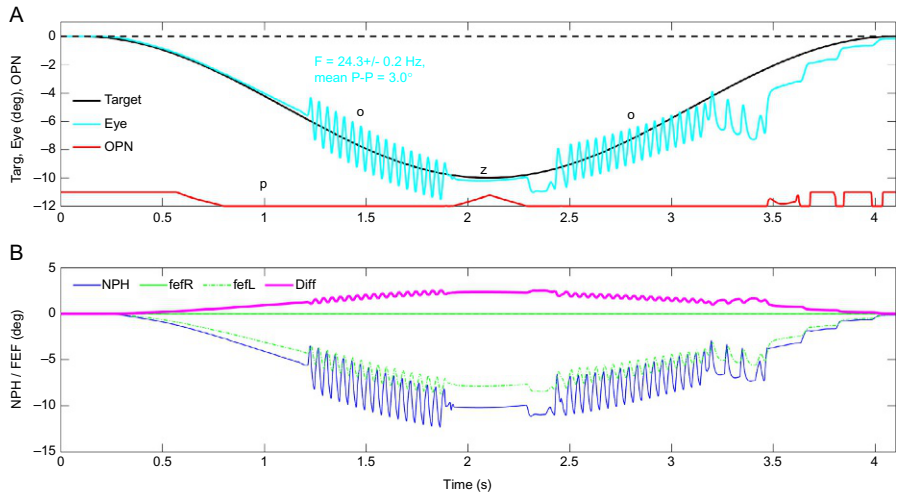


FIG. 11

Simulation of patient's smooth pursuit. (A) The essential features of the patient's smooth pursuit are captured (flutter at small eccentricities, o, and no flutter at zero pursuit speed, z). OPN activity is shown in the red trace. (B) The NPH and FEF signals, and their difference, are shown. Note that when the difference is only about 2° , the OPNs are already off, because they are inhibited by both the difference signal and the smooth pursuit drive signal. Frequency label as in Fig. 3.

than required for fixation opsoclonus, and a termination of opsoclonus when the eye velocity drops to zero). The opsoclonus in our simulation is symmetrical, being equally strong for rightward and leftward movements in the left hemifield. Our patient showed a more marked opsoclonus when the eye was moving to the left. This could be captured in the model by splitting the pursuit drive into leftward and rightward drives and using a different gain for their inhibition of the OPNs. Fig. 10B shows the NPH, FEF and difference signals. The difference signal is smaller than during saccades or fixation (cf. Fig. 10), but the OPN activity is shut off (red trace, Fig. 11A), because of the input from the smooth pursuit velocity drive.

5 Discussion

Our new model has been able to explain how OPN reactivation can be delayed, how opsoclonus can occur when the eyes are eccentric in one hemifield, and how pursuit tracking can lead to opsoclonus. The key elements of the new model are the excitatory signal from the FEF, SEF or cerebellum to the OPNs, and the inhibitory signal from the NPH to the OPNs. More research will be needed to determine the roles of the FEF, SEF, cerebellum and NPH in providing the position-dependent signals. We have also incorporated smooth pursuit drive inhibition of the OPNs (Keller and Missal, 2003; Missal and Keller, 2002).

Our patient developed these symptoms following a concussion. How this could lead to the kinds of defects used here in the model is not clear. Concussion may cause a diffuse axonal injury, involving the white matter of the cerebrum, the corpus callosum, the brain stem, and the cerebellum (Adams et al., 1989). Concussion has also been reported to cause short-term eye movement abnormalities, such as nystagmus, if the cerebellum is involved (Fumeya and Hideshima, 1994). Following concussion, extracellular fluids show an increase in levels of taurine, glutamate, aspartate, and GABA (Nilsson et al., 1990). It is assumed that glutamate and aspartate (excitatory neurotransmitters) are the mediators in traumatic brain injury. In contrast, the concomitant release of adenosine, taurine and GABA (inhibitory neurotransmitters) may protect the brain or ameliorate the excitotoxicity of glutamate and aspartate. In general, concussion can cause a neurometabolic cascade of events, including disruption of neuronal cell membranes, axonal stretching, and transient membrane defects (Barkhoudarian et al., 2011; Giza and Hovda, 2014; Smith et al., 1997). The axonal stretching can cause diffuse depolarization. One study showed that multiple concussions lead to specific, long-term dysfunction of intracortical inhibitory mechanisms, mediated through GABA_B receptors (Tremblay et al., 2011). It is not yet possible to separate the effects of concussion on neurotransmitters vs. axonal injury, but overall the effect seems to be cognitive problems (e.g., attention and memory), and slowing of reaction times (Eckner et al., 2014; Giza and Hovda, 2014).

Based on these studies, we assume that concussion decreases the activity of the FEF, SEF and/or cerebellar neurons that carry eye position signals. This would be most notable at saccade end, when the ipsilateral cFN must reactivate the OPNs.

Failure to reactivate the OPNs at the appropriate time would result in hypermetric saccades and postsaccadic oscillations. Thus, we assume that the right FEF pathway is delayed (causing delay in OPN reactivation and thus postsaccadic flutter). However, we assume that the hypermetria is offset by a gain reduction in the goal of the saccade (e.g., by learning where to initiate the locus of the pause in the vermis, [Optican and Quaia, 2002](#)). Thus, saccades become hypometric, with postsaccadic flutter.

We do not know the exact point of impact in our patient, or whether the damage occurred under or opposite to the point of contact ([Ommaya et al., 1971](#)). Nonetheless, the position-dependence of sustained opsoclonus (only on the left side in our patient), can be explained by assuming that the left FEF pathway has a reduced gain. Thus, it would be unable to cancel the inhibition from the NPH, causing sustained OPN inactivity with eccentric eye positions in the left hemifield.

Although opsoclonus is a rare disease, we have learned much about how the brain controls eye movements by recording, analyzing and modeling these movements. For example, opsoclonus in our concussion patient required us to propose the first model of the saccadic system incorporating a gaze position-dependent signal. Further study of rare ocular motor diseases should provide further insights into how the brain controls movement that may not be apparent from the study of normal systems.

Acknowledgments

This research was supported (in part) by the Intramural Research Program of the NEI, NIH.

References

- Adams, J.H., Doyle, D., Ford, I., Gennarelli, T.A., Graham, D.I., Mclellan, D.R., 1989. Diffuse axonal injury in head injury: definition, diagnosis and grading. *Histopathology* 15, 49–59.
- Averbuch-Heller, L., Remler, B., 1996. Opsoclonus. *Semin. Neurol.* 16, 21–26.
- Averbuch-Heller, L., Kori, A.A., Rottach, K.G., Dell’osso, L.F., Remler, B.F., Leigh, R.J., 1996. Dysfunction of pontine omnipause neurons causes impaired fixation: macrosaccadic oscillations with a unilateral pontine lesion. *Neuroophthalmology* 16, 99–106.
- Barkhoudarian, G., Hovda, D.A., Giza, C.C., 2011. The molecular pathophysiology of concussive brain injury. *Clin. Sports Med.* 30, 33–48, VII–iii.
- Bergeron, A., Guitton, D., 2001. The superior colliculus and its control of fixation behavior via projections to brainstem omnipause neurons. *Prog. Brain Res.* 134, 97–107.
- Bergeron, A., Guitton, D., 2002. In multiple-step gaze shifts: omnipause (OPNs) and collicular fixation neurons encode gaze position error; OPNs gate saccades. *J. Neurophysiol.* 88 (4), 1726–1742.
- Bertolini, G., Tarnutzer, A.A., Olasagasti, I., Khojasteh, E., Weber, K.P., Bockisch, C.J., Straumann, D., Marti, S., 2013. Gaze holding in healthy subjects. *PLoS One* 8, E61389.
- Bizzi, E., 1968. Discharge of frontal eye field neurons during saccadic and following eye movements in unanesthetized monkeys. *Exp. Brain Res.* 6, 69–80.
- Bizzi, E., Schiller, P.H., 1970. Single unit activity in the frontal eye fields of unanesthetized monkeys during eye and head movement. *Exp. Brain Res.* 10, 150–158.

- Bockisch, C.J., Khojasteh, E., Straumann, D., Hegemann, S.C., 2013. Eye position dependency of nystagmus during constant vestibular stimulation. *Exp. Brain Res.* 226, 175–182.
- Bruce, C.J., Goldberg, M.E., Bushnell, M.C., Stanton, G.B., 1985. Primate frontal eye fields. II. Physiological and anatomical correlates of electrically evoked eye movements. *J. Neurophysiol.* 54, 714–734.
- Burman, D.D., Bruce, C.J., 1997. Suppression of task-related saccades by electrical stimulation in the primate's frontal eye field. *J. Neurophysiol.* 77, 2252–2267.
- Busettini, C., Mays, L.E., 2003. Pontine omnipause activity during conjugate and disconjugate eye movements in macaques. *J. Neurophysiol.* 90, 3838–3853.
- Buttner-Ennever, J.A., Cohen, B., Pause, M., Fries, W., 1988. Raphe nucleus of the pons containing omnipause neurons of the oculomotor system in the monkey, and its homologue in man. *J. Comp. Neurol.* 267, 307–321.
- Chan, W.W., Galiana, H.L., 2005. Integrator function in the oculomotor system is dependent on sensory context. *J. Neurophysiol.* 93, 3709–3717.
- Chan, W.W., Galiana, H.L., 2008. Modeling the nonlinear context dependency of the neural integrator in the vestibuloocular reflex. *IEEE Trans. Biomed. Eng.* 55, 1946–1955.
- Chan, W., Galiana, H.L., 2010. A nonlinear model of the neural integrator improves detection of deficits in the human Vor. *IEEE Trans. Biomed. Eng.* 57, 1012–1023.
- Chun, K.S., Robinson, D.A., 1978. A model of quick phase generation in the vestibuloocular reflex. *Biol. Cybern.* 28, 209–221.
- Coble, E.T., Ling, L., Phillips, J.O., Fuchs, A.F., 1994. The role of omnipause neurons during gaze shifts. In: Van Rensbergen, J., d'Ydewalle, G. (Eds.), *Visual and Oculomotor Functions, Studies in Visual Information Processing*. vol. 5. Elsevier/North Holland, Amsterdam, pp. 285–293.
- Cogan, D.G., 1954. Ocular dysmetria; flutterlike oscillations of the eyes, and opsoclonus. *AMA Arch. Ophthalmol.* 51, 318–335.
- Cogan, D.G., 1968. Opsoclonus, body tremulousness, and benign encephalitis. *Arch. Ophthalmol.* 79, 545–551.
- Cohen, B., Henn, V., 1972. Unit activity in the pontine reticular formation associated with eye movements. *Brain Res.* 46, 403–410.
- Crawford, J.D., Vilis, T., 1993. Modularity and parallel processing in the oculomotor integrator. *Exp. Brain Res.* 96, 443–456.
- Curthoys, I.S., Markham, C.H., Furuya, N., 1984. Direct projection of pause neurons to nystagmus-related excitatory burst neurons in the cat pontine reticular formation. *Exp. Neurol.* 83, 414–422.
- Daye, P.M., Optican, L.M., Roze, E., Gaymard, B., Pouget, P., 2013. Neuromimetic model of saccades for localizing deficits in an atypical eye-movement pathology. *J. Transl. Med.* 11, 125.
- Daye, P.M., Optican, L.M., Blohm, G., Lefevre, P., 2014. Hierarchical control of two-dimensional gaze saccades. *J. Comput. Neurosci.* 36, 355–382.
- Eckner, J.T., Kutcher, J.S., Broglio, S.P., Richardson, J.K., 2014. Effect of sport-related concussion on clinically measured simple reaction time. *Br. J. Sports Med.* 48, 112–118.
- Eizenman, M., Cheng, P., Sharpe, J.A., Frecker, R.C., 1990. End-point nystagmus and ocular drift: an experimental and theoretical study. *Vision Res.* 30, 863–877.
- Escudero, M., De La Cruz, R.R., Delgado-Garcia, J.M., 1992. A physiological study of vestibular and prepositus hypoglossi neurones projecting to the abducens nucleus in the alert cat. *J. Physiol.* 458, 539–560.

- Everling, S., Pare, M., Dorris, M.C., Munoz, D.P., 1998. Comparison of the discharge characteristics of brain stem omnipause neurons and superior colliculus fixation neurons in monkey: implications for control of fixation and saccade behavior. *J. Neurophysiol.* 79, 511–528.
- Fuchs, A.F., Robinson, F.R., Straube, A., 1993. Role of the caudal fastigial nucleus in saccade generation. I. Neuronal discharge pattern. *J. Neurophysiol.* 70, 1723–1740.
- Fumeya, H., Hidemitsu, H., 1994. Cerebellar concussion—three case reports. *Neurol Med Chir (Tokyo)* 34, 612–615.
- Galiana, H.L., 1991. A nystagmus strategy to linearize the vestibulo-ocular reflex. *IEEE Trans. Biomed. Eng.* 38, 532–543.
- Giza, C.C., Hovda, D.A., 2014. The new neurometabolic cascade of concussion. *Neurosurgery* 75 (Suppl. 4), S24–S33.
- Harting, J.K., 1977. Descending pathways from the superior colliculus: an autoradiographic analysis in the rhesus monkey (*Macaca mulatta*). *J. Comp. Neurol.* 173, 583–612.
- Henn, V., Baloh, R.W., Hepp, K., 1984. The sleep-wake transition in the oculomotor system. *Exp. Brain Res.* 54, 166–176.
- Horn, A.K., Buttner-Ennever, J.A., Wahle, P., Reichenberger, I., 1994. Neurotransmitter profile of saccadic omnipause neurons in nucleus raphe interpositus. *J. Neurosci.* 14, 2032–2046.
- Huerta, M.F., Kaas, J.H., 1990. Supplementary eye field as defined by intracortical microstimulation: connections in macaques. *J. Comp. Neurol.* 293, 299–330.
- Huerta, M.F., Krubitzer, L.A., Kaas, J.H., 1986. Frontal eye field as defined by intracortical microstimulation in squirrel monkeys, owl monkeys, and macaque monkeys: I. Subcortical connections. *J. Comp. Neurol.* 253, 415–439.
- Ito, J., Markham, C.H., Curthoys, I.S., 1984. Projections to eye movement-related pause neuron region in cat using HRP. *Exp. Neurol.* 86, 93–104.
- Ito, J., Markham, C.H., Curthoys, I.S., 1986. Direct projection of type II vestibular neurons to eye movement-related pause neurons in the cat pontine reticular formation. *Exp. Neurol.* 91, 331–342.
- Izawa, Y., Suzuki, H., 2014. Activity of fixation neurons in the monkey frontal eye field during smooth pursuit eye movements. *J. Neurophysiol.* 112, 249–262.
- Izawa, Y., Suzuki, H., Shinoda, Y., 2004a. Suppression of visually and memory-guided saccades induced by electrical stimulation of the monkey frontal eye field. II. Suppression of bilateral saccades. *J. Neurophysiol.* 92, 2261–2273.
- Izawa, Y., Suzuki, H., Shinoda, Y., 2004b. Suppression of visually and memory-guided saccades induced by electrical stimulation of the monkey frontal eye field. I. Suppression of ipsilateral saccades. *J. Neurophysiol.* 92, 2248–2260.
- Kamogawa, H., Ohki, Y., Shimazu, H., Suzuki, I., Yamashita, M., 1996. Inhibitory input to pause neurons from pontine burst neuron area in the cat. *Neurosci. Lett.* 203, 163–166.
- Kanda, T., Iwamoto, Y., Yoshida, K., Shimazu, H., 2007. Glycinergic inputs cause the pause of pontine omnipause neurons during saccades. *Neurosci. Lett.* 413, 16–20.
- Kase, M., Miller, D.C., Noda, H., 1980. Discharges of Purkinje cells and mossy fibres in the cerebellar vermis of the monkey during saccadic eye movements and fixation. *J. Physiol.* 300, 539–555.
- Keller, E.L., 1974. Participation of medial pontine reticular formation in eye movement generation in monkey. *J. Neurophysiol.* 37, 316–332.
- Keller, E.L., Missal, M., 2003. Shared brainstem pathways for saccades and smooth-pursuit eye movements. *Ann. N. Y. Acad. Sci.* 1004, 29–39.

- Khojasteh, E., Bockisch, C.J., Straumann, D., Hegemann, S.C., 2013. A dynamic model for eye-position-dependence of spontaneous nystagmus in acute unilateral vestibular deficit (Alexander's law). *Eur. J. Neurosci.* 37, 141–149.
- King, W.M., Precht, W., Dieringer, N., 1978. Connections of behaviorally identified cat omnipause neurons. *Exp. Brain Res.* 32, 435–438.
- King, W.M., Precht, W., Dieringer, N., 1980. Afferent and efferent connections of cat omnipause neurons. *Exp. Brain Res.* 38, 395–403.
- Langer, T.P., Kaneko, C.R., 1983. Efferent projections of the cat oculomotor reticular omnipause neuron region: an autoradiographic study. *J. Comp. Neurol.* 217, 288–306.
- Langer, T.P., Kaneko, C.R., 1984. Brainstem afferents to the omnipause region in the cat: a horseradish peroxidase study. *J. Comp. Neurol.* 230, 444–458.
- Langer, T.P., Kaneko, C.R., 1990. Brainstem afferents to the oculomotor omnipause neurons in monkey. *J. Comp. Neurol.* 295, 413–427.
- Lefevre, P., Quaia, C., Optican, L.M., 1998. Distributed model of control of saccades by superior colliculus and cerebellum. *Neural Netw.* 11, 1175–1190.
- Leigh, R.J., Zee, D.S., 2015. *The Neurology of Eye Movements*. vol. 90. Oxford University Press, USA.
- Luschei, E.S., Fuchs, A.F., 1972. Activity of brain stem neurons during eye movements of alert monkeys. *J. Neurophysiol.* 35, 445–461.
- McCrea, R.A., Baker, R., 1985. Anatomical connections of the nucleus prepositus of the cat. *J. Comp. Neurol.* 237, 377–407.
- McCrea, R.A., Horn, A.K., 2006. Nucleus prepositus. *Prog. Brain Res.* 151, 205–230.
- McFarland, J.L., Fuchs, A.F., 1992. Discharge patterns in nucleus prepositus hypoglossi and adjacent medial vestibular nucleus during horizontal eye movement in behaving macaques. *J. Neurophysiol.* 68, 319–332.
- Missal, M., Heinen, S.J., 2017. Stopping smooth pursuit. *Philos. Trans. R. Soc. Lond. B Biol. Sci.* 372.
- Missal, M., Keller, E.L., 2002. Common inhibitory mechanism for saccades and smooth-pursuit eye movements. *J. Neurophysiol.* 88, 1880–1892.
- Nilsson, P., Hillered, L., Ponten, U., Ungerstedt, U., 1990. Changes in cortical extracellular levels of energy-related metabolites and amino acids following concussive brain injury in rats. *J. Cereb. Blood Flow Metab.* 10, 631–637.
- Noda, H., Fujikado, T., 1987. Topography of the oculomotor area of the cerebellar vermis in macaques as determined by microstimulation. *J. Neurophysiol.* 58, 359–378.
- Noda, H., Sugita, S., Ikeda, Y., 1990. Afferent and efferent connections of the oculomotor region of the fastigial nucleus in the macaque monkey. *J. Comp. Neurol.* 302, 330–348.
- Ohtsuka, K., Noda, H., 1991. Saccadic burst neurons in the oculomotor region of the fastigial nucleus of macaque monkeys. *J. Neurophysiol.* 65, 1422–1434.
- Ohtsuka, K., Noda, H., 1992. Burst discharges of mossy fibers in the oculomotor vermis of macaque monkeys during saccadic eye movements. *Neurosci. Res.* 15, 102–114.
- Ohtsuka, K., Noda, H., 1995. Discharge properties of Purkinje cells in the oculomotor vermis during visually guided saccades in the macaque monkey. *J. Neurophysiol.* 74, 1828–1840.
- Ommaya, A.K., Grubb Jr., R.L., Naumann, R.A., 1971. Coup and contre-coup injury: observations on the mechanics of visible brain injuries in the rhesus monkey. *J. Neurosurg.* 35, 503–516.
- Optican, L.M., 2008. The role of omnipause neurons: why glycine? *Prog. Brain Res.* 171, 115–121.

- Optican, L.M., Pretegiani, E., 2017a. A Gabaergic dysfunction in the olivary–cerebellar–brainstem network may cause eye oscillations and body tremor. II. Model simulations of saccadic eye oscillations. *Front. Neurol.* 8, 372.
- Optican, L.M., Pretegiani, E., 2017b. What stops a saccade? *Philos. Trans. R. Soc. Lond. B Biol. Sci.* 372, 20160194.
- Optican, L.M., Quaia, C., 2002. Distributed model of collicular and cerebellar function during saccades. *Ann. N. Y. Acad. Sci.* 956, 164–177.
- Pare, M., Guitton, D., 1994. The fixation area of the cat superior colliculus: effects of electrical stimulation and direct connection with brainstem omnipause neurons. *Exp. Brain Res.* 101, 109–122.
- Pare, M., Guitton, D., 1998. Brain stem omnipause neurons and the control of combined eye-head gaze saccades in the alert cat. *J. Neurophysiol.* 79, 3060–3076.
- Pretegiani, E., Rosini, F., Federico, A., Optican, L.M., Rufa, A., 2017a. Eye movements in genetic Parkinsonisms affecting the alpha-synuclein, Park9, and manganese network. *Clin. Neurophysiol.* 128, 2450–2453.
- Pretegiani, E., Rosini, F., Rocchi, R., Ginanneschi, F., Vinciguerra, C., Optican, L.M., Rufa, A., 2017b. GABAergic dysfunction in the olivary–cerebellar–brainstem network may cause eye oscillations and body tremor. *Clin. Neurophysiol.* 128, 408–410.
- Prsa, M., Galiana, H.L., 2007. Visual–vestibular interaction hypothesis for the control of orienting gaze shifts by brain stem omnipause neurons. *J. Neurophysiol.* 97, 1149–1162.
- Quaia, C., Lefevre, P., Optican, L.M., 1999. Model of the control of saccades by superior colliculus and cerebellum. *J. Neurophysiol.* 82, 999–1018.
- Ramat, S., Schmid, R., Zambarbieri, D., 2003. Eye–head coordination in darkness: formulation and testing of a mathematical model. *J. Vestib. Res.* 13, 79–91.
- Ramat, S., Leigh, R.J., Zee, D.S., Optican, L.M., 2005. Ocular oscillations generated by coupling of brainstem excitatory and inhibitory saccadic burst neurons. *Exp. Brain Res.* 160, 89–106.
- Raybourn, M.S., Keller, E.L., 1977. Colliculoreticular organization in primate oculomotor system. *J. Neurophysiol.* 40, 861–878.
- Rivaud, S., Muri, R.M., Gaymard, B., Vermersch, A.I., Pierrot-Deseilligny, C., 1994. Eye movement disorders after frontal eye field lesions in humans. *Exp. Brain Res.* 102, 110–120.
- Robinson, D.A., 1964. The mechanics of human saccadic eye movement. *J. Physiol.* 174, 245–264.
- Robinson, D.A., 1975. Oculomotor control signals. In: Lennerstrand, G., Bach-y-Rita, P. (Eds.), *Basic Mechanisms of Ocular Motility and Their Clinical Implication*. Pergamon, New York, pp. 337–374.
- Robinson, D.A., Fuchs, A.F., 1969. Eye movements evoked by stimulation of frontal eye fields. *J. Neurophysiol.* 32, 637–648.
- Robinson, D.A., Gordon, J.L., Gordon, S.E., 1986. A model of the smooth pursuit eye movement system. *Biol. Cybern.* 55, 43–57.
- Schlag, J., Schlag-Rey, M., 1987. Evidence for a supplementary eye field. *J. Neurophysiol.* 57, 179–200.
- Schlag, J., Schlag-Rey, M., Pigarev, I., 1992. Supplementary eye field: influence of eye position on neural signals of fixation. *Exp. Brain Res.* 90, 302–306.
- Scudder, C.A., Fuchs, A.F., Langer, T.P., 1988. Characteristics and functional identification of saccadic inhibitory burst neurons in the alert monkey. *J. Neurophysiol.* 59, 1430–1454.
- Segraves, M.A., 1992. Activity of monkey frontal eye field neurons projecting to oculomotor regions of the pons. *J. Neurophysiol.* 68, 1967–1985.

- Shinoda, Y., Sugiuchi, Y., Takahashi, M., Izawa, Y., 2011. Neural substrate for suppression of omnipause neurons at the onset of saccades. *Ann. N. Y. Acad. Sci.* 1233, 100–106.
- Shook, B.L., Schlag-Rey, M., Schlag, J., 1988. Direct projection from the supplementary eye field to the nucleus raphe Interpositus. *Exp. Brain Res.* 73, 215–218.
- Shook, B.L., Schlag-Rey, M., Schlag, J., 1990. Primate supplementary eye field: I. Comparative aspects of mesencephalic and pontine connections. *J. Comp. Neurol.* 301, 618–642.
- Smith, D.H., Chen, X.H., Pierce, J.E., Wolf, J.A., Trojanowski, J.Q., Graham, D.I., McIntosh, T.K., 1997. Progressive atrophy and neuron death for one year following brain trauma in the rat. *J. Neurotrauma* 14, 715–727.
- Spencer, R.F., Wenthold, R.J., Baker, R., 1989. Evidence for glycine as an inhibitory neurotransmitter of vestibular, reticular, and prepositus hypoglossi neurons that project to the cat abducens nucleus. *J. Neurosci.* 9, 2718–2736.
- Stanton, G.B., Goldberg, M.E., Bruce, C.J., 1988. Frontal eye field efferents in the macaque monkey: II. Topography of terminal fields in midbrain and pons. *J. Comp. Neurol.* 271, 493–506.
- Stanton, G.B., Friedman, H.R., Dias, E.C., Bruce, C.J., 2005. Cortical afferents to the smooth-pursuit region of the macaque monkey's frontal eye field. *Exp. Brain Res.* 165, 179–192.
- Sugiuchi, Y., Izawa, Y., Takahashi, M., Na, J., Shinoda, Y., 2005. Physiological characterization of synaptic inputs to inhibitory burst neurons from the rostral and caudal superior colliculus. *J. Neurophysiol.* 93, 697–712.
- Takahashi, M., Sugiuchi, Y., Izawa, Y., Shinoda, Y., 2005. Synaptic inputs and their pathways from fixation and saccade zones of the superior colliculus to inhibitory burst neurons and pause neurons. *Ann. N. Y. Acad. Sci.* 1039, 209–219.
- Thier, P., Mock, M., 2006. The oculomotor role of the pontine nuclei and the nucleus reticularis segmenti pontis. *Prog. Brain Res.* 151, 293–320.
- Tremblay, S., De Beaumont, L., Lassonde, M., Theoret, H., 2011. Evidence for the specificity of intracortical inhibitory dysfunction in asymptomatic concussed athletes. *J. Neurotrauma* 28, 493–502.
- Tychsen, L., Engelken, E.J., Austin, E.J., 1990. Periodic saccadic oscillations and tinnitus. *Neurology* 40, 549–551.
- Wang, X.J., Rinzel, J., 1992. Alternating and synchronous rhythms in reciprocally inhibitory model neurons. *Neural Comput.* 4, 84–97.
- Wang, N., Perkins, E., Zhou, L., Warren, S., May, P.J., 2013. Anatomical evidence that the superior colliculus controls saccades through central mesencephalic reticular formation gating of omnipause neuron activity. *J. Neurosci.* 33, 16285–16296.
- Wong, A.M., Musallam, S., Tomlinson, R.D., Shannon, P., Sharpe, J.A., 2001. Opsoclonus in three dimensions: oculographic, neuropathologic and modelling correlates. *J. Neurol. Sci.* 189, 71–81.
- Yamada, J., Noda, H., 1987. Afferent and efferent connections of the oculomotor cerebellar vermis in the macaque monkey. *J. Comp. Neurol.* 265, 224–241.
- Yoshida, K., Iwamoto, Y., Chimoto, S., Shimazu, H., 1999. Saccade-related inhibitory input to pontine omnipause neurons: an intracellular study in alert cats. *J. Neurophysiol.* 82, 1198–1208.

This page intentionally left blank

SECTION

DIDACTIC:
Translational

II

This page intentionally left blank

4

Eye position-dependent opsoclonus in mild traumatic brain injury

John-Ross Rizzo^{a,b}, Todd E. Hudson^{a,b}, Alexandra J. Sequeira^b, Weiwei Dai^{b,c}, Yash Chaudhry^b, John Martone^b, David S. Zee^d, Lance M. Optican^e, Laura J. Balcer^{b,f,g}, Steven L. Galetta^{b,f}, Janet C. Rucker^{b,f,*}

^aDepartment of Physical Medicine and Rehabilitation, New York University School of Medicine, New York, NY, United States

^bDepartment of Neurology, New York University School of Medicine, New York, NY, United States

^cDepartment of Electrical and Computer Engineering, New York University Tandon School of Engineering, New York, NY, United States

^dDepartment of Neurology, The Johns Hopkins University, Baltimore, MD, United States

^eLaboratory of Sensorimotor Research, NEI, NIH, DHHS, Bethesda, MD, United States

^fDepartment of Ophthalmology, New York University School of Medicine, New York, NY, United States

^gDepartment of Population Health, New York University School of Medicine, New York, NY, United States

*Corresponding author: Tel.: +212-263-7744, e-mail address: janet.rucker@nyulangone.org

Abstract

Opsoclonus consists of bursts of involuntary, multidirectional, back-to-back saccades without an intersaccadic interval. We report a 60-year-old man with post-concussive headaches and disequilibrium who had small amplitude opsoclonus in left gaze, along with larger amplitude flutter during convergence. Examination was otherwise normal and brain MRI was unremarkable. Video-oculography demonstrated opsoclonus predominantly in left gaze and during pursuit in the left hemifield, which improved as post-concussive symptoms improved. Existing theories of opsoclonus mechanisms do not account for this eye position-dependence. We discuss theoretical mechanisms of this behavior, including possible dysfunction of frontal eye field and/or cerebellar vermis neurons; review ocular oscillations in traumatic brain injury; and consider the potential relationship between the larger amplitude flutter upon convergence and post-traumatic ocular oscillations.

Keywords

Concussion, Ocular flutter, Opsoclonus, Saccades, Eye position-dependence

1 Introduction

Opsoclonus and ocular flutter are saccadic intrusions characterized by bursts of involuntary, back-to-back saccades without an intersaccadic interval. The oscillations are termed ocular flutter when they exist in the horizontal plane only and opsoclonus when they are multidirectional in horizontal, vertical, and torsional planes. Pathologic opsoclonus and ocular flutter occur most commonly with paraneoplastic autoimmune disorders and parainfectious brainstem encephalitis; reports are very rare with traumatic brain injury (Digre, 1986; Turazzi et al., 1977)—especially mild traumatic brain injury (Manta et al., 2018). We report a patient with mild traumatic brain injury, large amplitude flutter upon convergence, and opsoclonus/ocular flutter with distance viewing with two unusual features: (1) eye position-dependence manifested as opsoclonus predominantly in left gaze and (2) accompanying hypometric saccades to visual targets. Further, we discuss hypothetical mechanisms underlying these features and their potential relationships with larger amplitude flutter upon convergence and with mild traumatic brain injury.

2 Case description

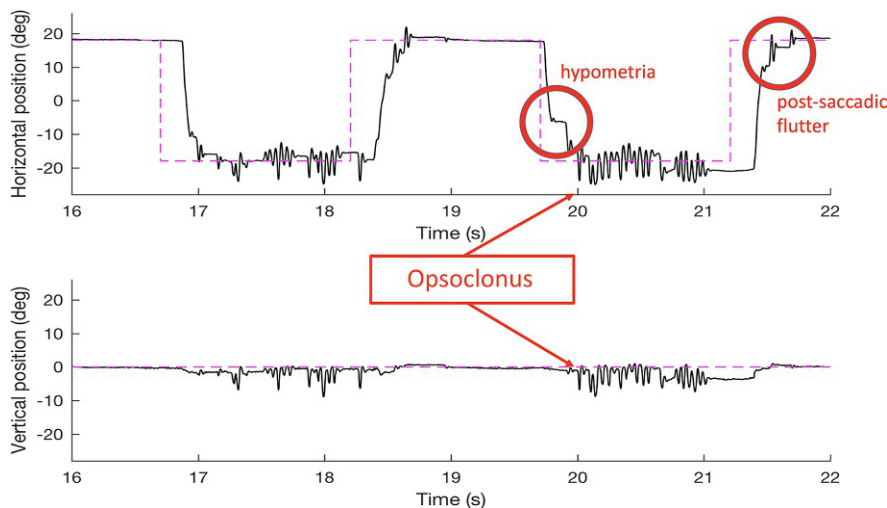
A 60-year-old man sustained a concussion 3 years prior when he was thrown from his bicycle after colliding with a suddenly-opened car door. He had brief loss of consciousness and his helmet was cracked in two sites. The location of direct head impact was unknown. Head CT revealed no intracranial contusion or hemorrhage. He immediately developed severe headaches, intolerance of motion and busy environments, and difficulty reading. In the ensuing 3 years, he had persistent post-concussive chronic right-sided headaches and disequilibrium without visual symptoms or oscillopsia. Quantitative eye movement recordings were initially obtained as part of a clinical trial of ocular motility in concussed participants. Upon discovery of abnormal findings on eye movement recordings, neuro-ophthalmologic consultation was performed. Examination detected very small amplitude oscillations in left gaze that were too small to characterize further (Video 1 in the online version at <https://doi.org/10.1016/bs.pbr.2019.04.016>, Segments 1 and 3). During otherwise normal convergence movements, larger amplitude oscillations were seen (Video 1 in the online version at <https://doi.org/10.1016/bs.pbr.2019.04.016>, Segment 2). The patient was unaware of abnormal eye movements prior to and during the examination. Ocular ductions and versions were full. There was no ocular misalignment with distant target fixation. No oscillations were present in central gaze following gaze shifts or behind Frenzel goggles in upright or supine positions. Vestibulo-ocular reflexes were normal. Visual acuity and fields, pupils, optic nerves, neurological examination, and brain MRI were normal.

3 Eye movement recording methods

Horizontal and vertical eye movements of both eyes were recorded with infrared video-oculography (Eyelink 1000+, SR Research, Ontario, Canada) (sampling frequency 500Hz, spatial accuracy 0.5 degrees), following a 13-point spatial calibration. The head was stabilized with a forehead cradle. The visual stimulus was a solid white circle displayed on a computer screen with a dark gray background. Gaze stability during visual fixation was assessed centrally and eccentrically at ± 18.5 degrees horizontally and ± 11 degrees vertically. Saccades were tested to target jumps through a range of amplitudes up to ± 18 degrees horizontally and ± 11 degrees vertically. A peripheral target was triggered after fixating on a central target for 1.1 s. Horizontal antisaccades were assessed with the same parameters, with instructions to look in the same but opposite mirror location of the stimulus. Gap and overlap saccades were measured to target jumps through a range of amplitudes up to ± 14.8 degrees horizontally. For the gap paradigm, the peripheral target appeared 150ms after the central fixation target disappeared. For the overlap paradigm, the central fixation target and peripheral target were displayed simultaneously for 150ms before the central fixation target disappeared. Pursuit movements were tested as the visual target moved sinusoidally at $0.25\text{ Hz} \pm 10$ degrees horizontally and vertically. Eye movement data were analyzed off-line using custom MATLAB[®] software.

4 Eye movement recording results

Back-to-back saccades oscillating about the fixation target without an intersaccadic interval in horizontal and vertical position traces, consistent with opsoclonus, were seen in left gaze (for horizontal component: mean peak-to-peak amplitude [SD], 5.94 [5.47] degrees; mean peak velocity [SD], 343.79 [45.51] degrees/s; frequency, 16Hz) (Fig. 1). Post-saccadic horizontal oscillations (flutter) occurred following rightward saccades (Fig. 1). Left and rightward saccades were persistently hypometric (Fig. 1). The main sequence amplitude to peak velocity relationships showed that horizontal visually-guided saccades had velocities near or above the upper limits of normal, especially in the leftward direction, and peak velocities of the horizontal saccades during flutter were higher than expected for saccade amplitude (Fig. 2). Opsoclonus, with a larger horizontal than vertical component was also superimposed on pursuit, predominantly when tracking targets in the left hemifield (Fig. 3). Average latencies of horizontal saccades were 222.7 [± 96.0] ms for pro-saccades, 219.4 [± 117.1] ms for saccades with the gap paradigm, and 234.0 [± 112.8] ms for saccades with the overlap paradigm. Normative control values in our lab are 176 [± 13] ms for pro-saccades, 149 [± 13] ms for saccades with the gap paradigm, and 187 [± 27] ms for saccades with the overlap paradigm. Antisaccade latency was 368 [± 97.3] ms (normative control values in our lab are 294 [± 62.5] ms), with 7/18 (38.9%) made in the incorrect direction. Repeat video-oculography 7 months

**FIG. 1**

Horizontal (upper) and vertical (lower) eye position traces during saccade testing demonstrate opsoclonus in left gaze, bursts of post-saccadic ocular flutter with rightward saccades, and hypometric saccades in right and left directions. Upward deflections represent rightward movements.

later, when post-concussive symptoms had nearly resolved, showed marked lessening of the saccadic oscillations. Transient opsoclonus occurred in left gaze (for horizontal component: mean peak-to-peak amplitude [SD], 2.78 [4.83] degrees; mean peak velocity [SD], 163.05 [33.44] degrees/s; frequency, 5 Hz) (Fig. 4). Post-saccadic flutter following rightward saccades was markedly reduced and saccadic hypometria was lessened. A few oscillations remained superimposed on leftward pursuit.

5 Discussion

5.1 Behavioral characteristics of opsoclonus/ocular flutter and “voluntary flutter”

Our patient demonstrated two unusual features of opsoclonus/ocular flutter: the oscillations varied with the position of the eye in the orbit and saccades to visual targets were hypometric. We will first comment on the atypical features of the opsoclonus/flutter of our patient and then on the concept of flutter upon convergence.

Our patient showed opsoclonus with many typical features, including back-to-back, conjugate, multidirectional saccades without an intersaccadic interval and with an average amplitude between 1 and 5 degrees and a frequency range between 10 and 25 Hz (Bergenius, 1986; Zee and Robinson, 1979). As seen in our patient, saccadic peak velocities in the presence of opsoclonus/ocular flutter are either faster than

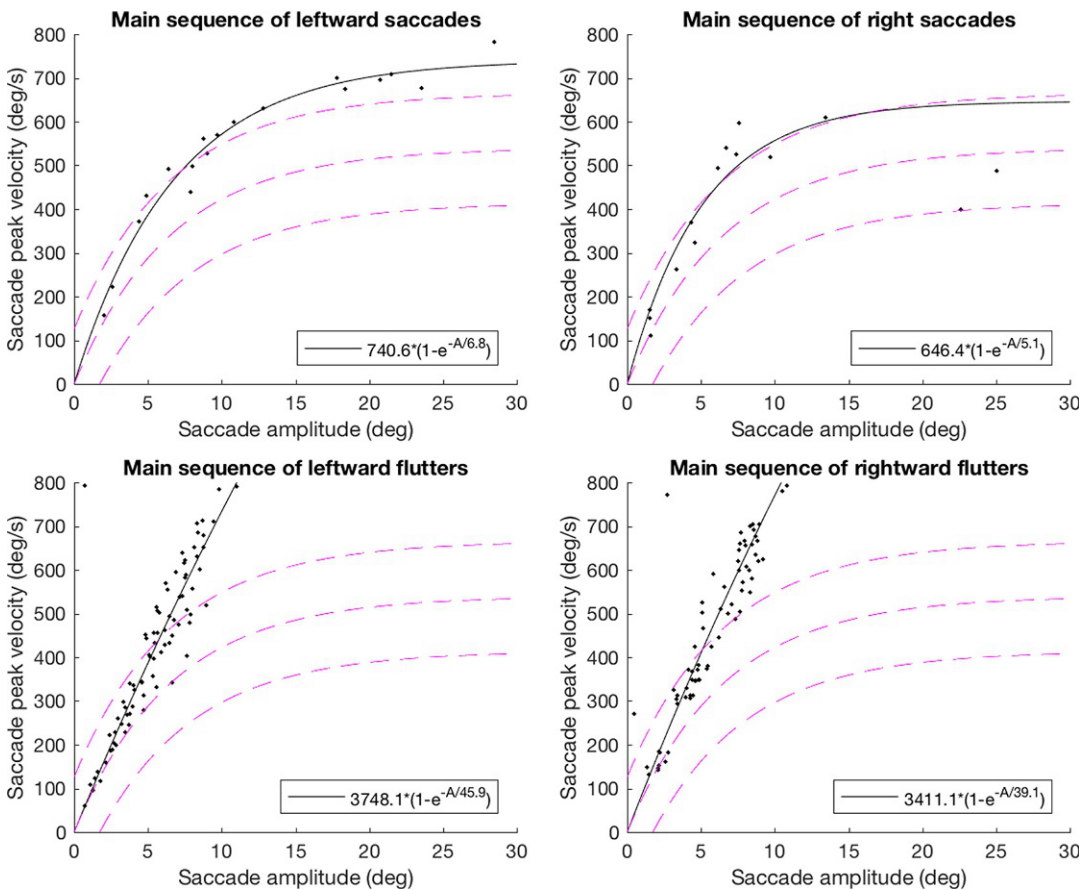
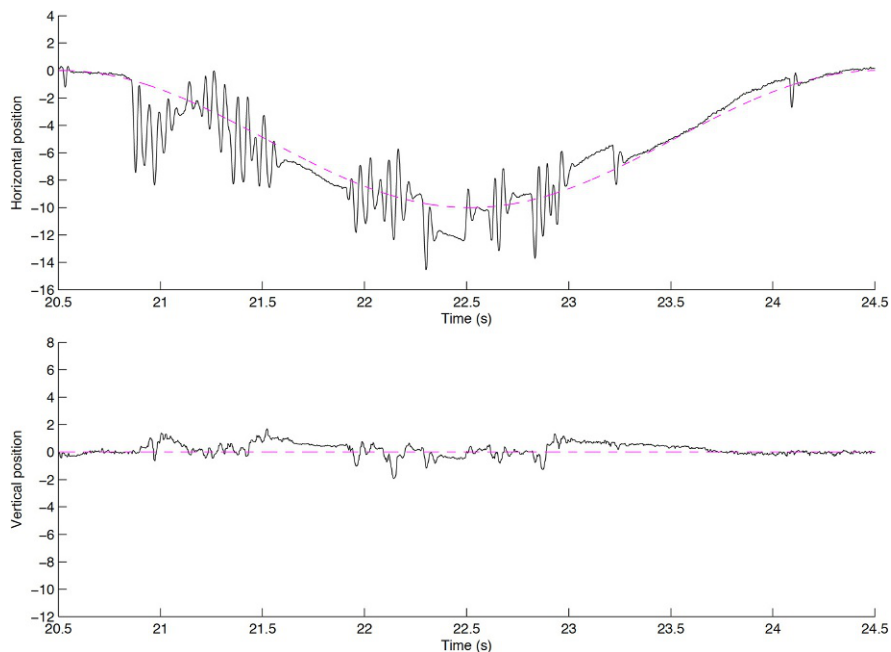


FIG. 2

Main sequence relationships of peak velocity to amplitude for leftward (upper left panel) and rightward (upper right panel) visually-guided saccades and for leftward (lower left panel) and rightward (lower right panel) flutter saccades demonstrating saccades near or above the upper limits of normal peak velocity, especially in the leftward direction, and flutter saccades faster than expected for saccade amplitude. Patient data are represented in black. Data are fit with an exponential equation: $\text{peak velocity} = V_{\max} \times (1 - e^{-AC})$, where V_{\max} is the asymptotic peak velocity, A is the amplitude, and C is a constant defining the exponential rise. Normative control data from our lab, along with normative 5th and 95th prediction intervals, are plotted (hatched pink lines).

**FIG. 3**

Horizontal (upper) and vertical (lower) eye position traces during pursuit testing show opsoclonus superimposed on pursuit, predominantly with tracking targets in the left hemifield. Upward deflections represent rightward movements.

(Bergenius, 1986) or appropriate for (Ellenberger et al., 1972; Zee and Robinson, 1979) saccade amplitude and can differ for visually-guided prosaccades versus flutter saccades (Pretegiani et al., 2017). Saccades in the presence of opsoclonus/ocular flutter may land on target, show dynamic overshoots, or be hypermetric (Daye et al., 2013; Pretegiani et al., 2017; Zee and Robinson, 1979); however, saccades in both horizontal directions in our patient were hypometric. Another characteristic feature of opsoclonus/ocular flutter is a tendency to be provoked in central gaze by gaze shifts from an eccentric gaze position (Bergenius, 1986; Zee and Robinson, 1979), which was not seen in our patient.

A striking feature in our patient was the relation of his saccadic oscillations to the position of the eye in the orbit. Opsoclonus/ocular flutter tends to occur in central gaze position and may also occur in eccentric gaze positions. Positional ocular flutter and opsoclonus evoked by supine positioning have been described (Brodsky and Hunter, 2011; Kim et al., 2013; Martins et al., 2018). The eye position-dependence with opsoclonus only in left post-saccadic gaze holding seen in our patient, however, has not. Two prior cases described what was termed “unidirectional flutter” (Kobayashi, 2015; Verhaeghe et al., 2007). However, eye movement recording traces in those cases were inconsistent with flutter, as the abnormal spontaneous

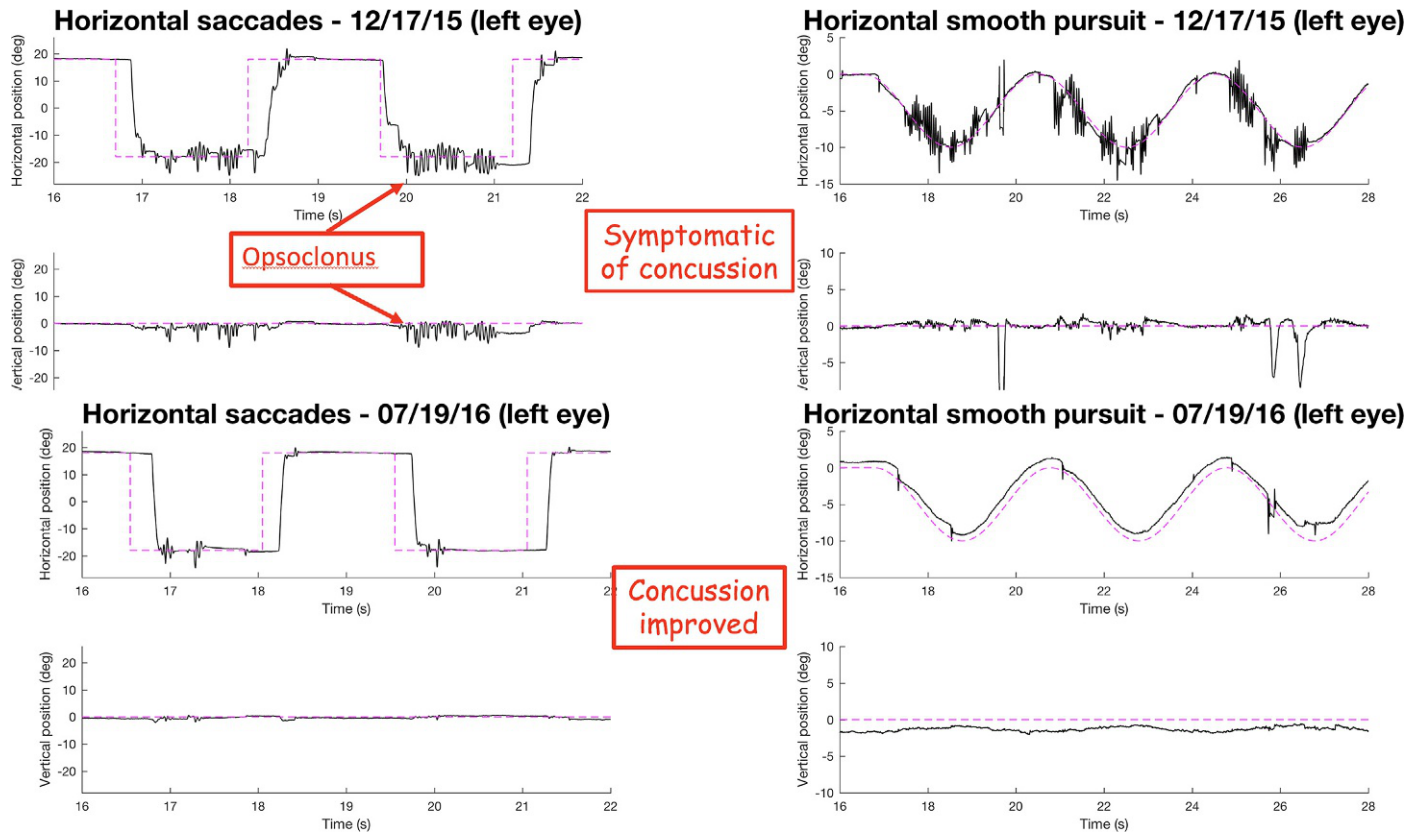


FIG. 4

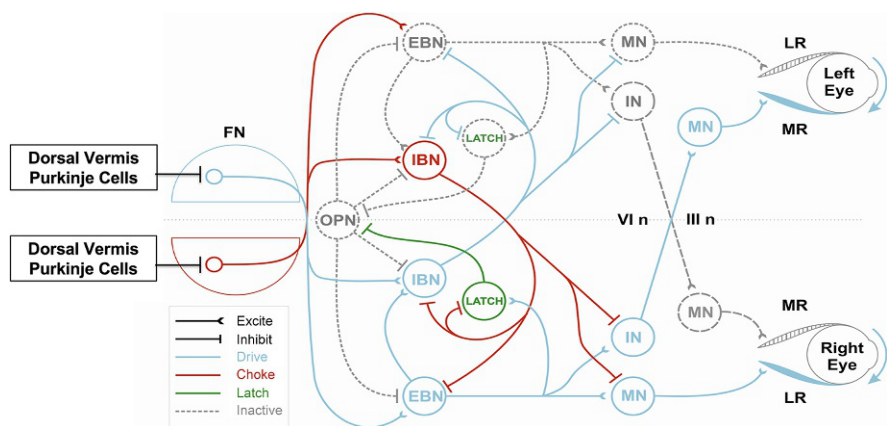
Saccade (left panels) and pursuit (right panels) eye position traces at time of initial recording (upper panels) and 7 months later (lower panels), showing marked lessening of oscillations and diminished saccade hypometria at the later date. Upward deflections represent rightward movements.

saccades did not oscillate about the midline. The eye movements more closely resembled double saccadic pulses (DSP), which consist of a saccade away from fixation followed immediately by a return saccade back to fixation, with no intersaccadic interval and no crossing of the midline. A third case of DSP (Kim et al., 2007), reported by Kim et al., was due to a focal right-sided demyelinating pontine lesion. These three reports each described abnormal spontaneous DSP oscillations in the rightward direction that did not oscillate across the midline and that occurred in central, right, and left eye positions. Interestingly, in one of these cases (Verhaeghe et al., 2007), there was some modulation with eye position, with a higher amplitude and frequency of the saccadic pulses in right gaze compared to central gaze and in central gaze compared to left gaze.

Our patient generated ocular flutter upon convergence of the eyes that had a larger amplitude than the oscillations seen with distance fixation in left gaze. About 5–10% of the general population have the ability to voluntarily generate back-to-back saccadic oscillations that mimic pathologic ocular flutter, usually—but not always—provoked by converging the eyes (Blair et al., 1967; Jarrett et al., 1977; Nagle et al., 1980; Zahn, 1978). There may a hereditary component of this capability; however, it is also a behavior that can be learned, providing support to the concept that the saccadic system is inherently prone to oscillation in normal healthy individuals (Hotson, 1984). These voluntary oscillations can only be sustained for 5–30 s at a time and tend to be of lower amplitude and higher frequency than pathologic ocular flutter. Some individuals, however, are capable of generating larger amplitude movements in the horizontal plane and even of producing voluntary multidirectional opsoclonus (Yee et al., 1994). Though these voluntary eye oscillations are often called “voluntary nystagmus,” they are better termed “voluntary flutter,” since they consist of back-to-back saccades with no slow-phase movements of the type that characterize nystagmus. Given the presence of flutter upon convergence in our patient, the possibility was considered that our patient’s opsoclonus in left gaze and during leftward pursuit may have been voluntary. This was, however, thought unlikely, given the patient’s visually asymptomatic state without oscillopsia (i.e., subjective sense of visual motion), improvement in opsoclonus upon recovery from his concussion, and the patient’s lack of awareness of any abnormal eye movements before they were detected on infrared video-oculography.

5.2 Mechanisms of opsoclonus/ocular flutter and gaze position-dependence

Current theories and models of the mechanisms underlying opsoclonus/ocular flutter do not account for a relation to eye position or saccadic hypometria as seen in our patient. Opsoclonus/ocular flutter is attributed to intrinsic properties of the saccade-generating brainstem machinery that render it inherently unstable and prone to oscillation. Saccades are generated by glutaminergic excitatory burst neurons (EBN) that send signals to agonist motoneurons to activate extraocular muscles (Fig. 5). EBN for horizontal saccades are located in the paramedian pontine reticular

**FIG. 5**

Schematic of pathways involved in saccade control, with demonstration of neuronal activity during a rightward saccade. Reciprocal innervation in the circuit of excitatory and inhibitory burst neurons renders it vulnerable to internally-generated oscillations, which are normally inhibited by omnipause neurons. Disinhibition of this reciprocally-innervated system results in oscillations. Abbreviations: FN, fastigial nucleus; OPN, omnipause neurons; EBN, excitatory burst neurons; IBN, inhibitory burst neurons; MN, motoneurons; IN, internuclear neurons; VI n, sixth nerve nucleus; III n, third nerve nucleus; MR, medial rectus; LR, lateral rectus.

Figure adapted from Optican, L.M., Rucker, J.C., Keller, E.L., Leigh, R.J., 2008. Mechanism of interrupted saccades in patients with late-onset Tay-Sachs disease. Prog. Brain Res. 171, 567–570.

formation (PPRF) and EBN for vertical and torsional saccades, in the rostral interstitial medial longitudinal fasciculus (RIMLF). Inhibitory burst neurons (IBN) ipsilateral to horizontal saccade direction inhibit contralateral antagonist muscles to facilitate saccade onset; this occurs via signals received from the contralateral cerebellar fastigial nucleus (FN). Contralateral IBN assist in saccade termination via a “choke signal” received at saccade end from the ipsilateral FN. FN neuronal discharge is modulated by Purkinje cells in the overlying posterior ocular motor vermis (Yamada and Noda, 1987). Except during saccades, EBN and IBN are tonically inhibited by glycinergic omnipause neurons (OPN) in the raphe interpositus nucleus in the caudal pons (Optican and Quaia, 2002).

The properties of this system that predispose it to generating oscillations include (1) positive feedback loops due to reciprocal inhibition between IBN and (2) the EBN membrane property of post-inhibitory rebound (PIR) mediated by low-threshold calcium channels that leads to increased neuronal firing upon inhibitory release from glycinergic omnipause neurons (OPN) in the raphe interpositus, which tonically inhibit all burst neurons during fixation (Ramat et al., 2005, 2008; Shaikh et al., 2008). Several types of interruptions in brainstem and/or cerebellar circuits may lead to saccadic oscillations via heightened EBN membrane excitability, increased PIR, and/or

decreased glycinergic inhibition (Shaikh et al., 2008). An increase in the frequency of discharge of EBN relative to the size of a saccade may account for saccades with higher than normal velocities with opsoclonus/flutter (Bergenius, 1986); whereas, decreased glycinergic inhibition has been proposed as a potential mechanism for “voluntary flutter,” due to the potential to voluntarily inhibit OPN tone in such individuals (Hain et al., 1986; Ramat et al., 2005). A similar mechanism may account for superimposition of opsoclonus/flutter upon pursuit, as partial OPN inhibition also occurs during pursuit (Missal and Keller, 2002).

The dependence of opsoclonus on eye position, appearing predominantly in left gaze is not likely due to direct EBN or IBN pathology, since EBN and IBN do not modulate their discharge with changes in eye position within the orbit (Cullen and Guittion, 1997; Van Horn et al., 2008). The OPN are also unlikely to be the sole cause of the oscillations since lesions of OPN lead to slowing of saccades but not to oscillations (Kaneko, 1996). Rather, the likely source of the dependence of opsoclonus on eye position in our patient is dysfunction of an inhibitory input to the OPN from neurons that do encode eye position in the orbit, such as those in the cerebellar ocular motor vermis and fastigial oculomotor region or in the cerebral cortex, possibly the frontal eye fields. The cerebellar ocular motor vermis contains neurons that burst during saccades in either both directions or one direction with variable timing during the saccade to enhance onset or facilitate offset. There is a subset of vermis pause cells that decrease their discharge just before contralateral saccades (Ohtsuka and Noda, 1995). Unilateral cerebellar dysfunction might theoretically alter the balance of discharge between vermis burst and pause cells and enhance FN output (Helmchen et al., 1994, 2003), leading to reduced OPN inhibition and increased EBN firing, and predispose to oscillations in one direction of gaze. Furthermore, some of these neurons in the ocular motor vermis neurons modulate their firing rates with changes in orbital position of the eye (Ohtsuka and Noda, 1995). Disruption of input from the frontal eye fields to OPN as a mechanism of the relation of opsoclonus to eye position is supported in our patient by his substantial increase of overlap and anti-saccade latencies (Rivaud et al., 1994).

The hypometria of saccades in our patient could hypothetically be caused by either a cerebellar or a frontal lobe mechanism. The saccadic hypermetria and dynamic overshooting that often accompany saccades in individuals with pathological saccadic oscillations were initially hypothesized to be due to inhibitory hyperpolarization of OPN cell membranes, rendering them momentarily refractory to excitatory stimulation and resumption of firing at saccade end (Zee and Robinson, 1979). Alternatively, saccadic hypermetria could be due to a delayed “choke signal” from the ipsilateral FN to the contralateral IBN (Daye et al., 2013; Optican and Quaia, 2002). In contrast, hypometric saccades may be due to impaired input from the cerebellum or frontal lobes to OPN, leading to premature resumption of OPN discharge (Hain et al., 1986). Direct damage to the dorsal cerebellar vermis or frontal eye field might also cause hypometric saccades (Tusa et al., 1986).

5.3 Relationship with traumatic brain injury and potential mechanisms of gaze position-dependent opsoclonus/ocular flutter

Concussion results in neurological injury, including a cascade of neurochemical and neurometabolic events with neurophysiologic cortical alterations that can be protracted (Giza and Hovda, 2014; Tremblay et al., 2011). Saccadic abnormalities are not uncommon following mild traumatic brain injury; however, opsoclonus and ocular flutter are rare (Manta et al., 2018). These oscillations have been reported in the setting of severe head injury (Robins et al., 1976; Turazzi et al., 1977); however, when present after mild injury, they often have features suggesting that they more likely represent “voluntary flutter” than pathologic oscillations (Yee et al., 1994). The saccadic deficits typically reported in mild traumatic brain injury include prolonged latencies and higher error rates with memory-guided saccade and antisaccade paradigms (Crevits et al., 2000; Heitger et al., 2002, 2004, 2009), suggesting injury to frontal lobe cortical eye centers including the frontal eye fields and the dorsolateral prefrontal cortex, which is compatible with the propensity of the frontal lobes to injury from trauma. Indeed, in our patient, injury to the frontal lobe was suggested by the substantial increase of overlap and anti-saccade latencies (Rivaud et al., 1994). Other evidence from mild traumatic brain injury supports a role for altered intracortical mechanisms in the motor cortex due to impaired gamma-amino-butyric acid (GABA) receptor activity (Tremblay et al., 2011). This idea may provide a link between concussion-related cortical injury and abnormal ocular oscillations, as alterations in the sensitivity of brainstem saccadic neurons to GABA have been directly implicated in several causes of opsoclonus/ocular flutter (Petit-Pedrol et al., 2014; Pretegiani et al., 2017; Shaikh and Wilmot, 2016), and GABA receptors are present both in the forebrain and in the cerebellum. Thus, based on the likely location of injury in our patient, impaired inhibitory input from the frontal eye field to OPN may be the more likely explanation for opsoclonus than direct injury to the cerebellum—which is less common with mild traumatic brain injury (Kepski, 1983; Meabon et al., 2016). However, future consideration of mechanisms for gaze-dependence opsoclonus from frontal lobe injury will have to take into account the rarity of frontal lobe lesions as a cause of ocular oscillations. It may be that an inherently unstable saccade system is a necessary requisite for saccadic oscillations to emerge after traumatic brain injury.

6 Conclusion

We have reported an unusual patient with abnormal eye movement findings following mild traumatic brain injury, including eye position-dependent opsoclonus, unidirectional ocular flutter, and hypometric saccades to visual targets. We propose that the eye position-dependence of the opsoclonus may be due to impaired inhibitory input to OPN from a neuronal source that modulates its firing rate based on the orbital

position of the eye, such as the cerebellar ocular motor vermis and/or frontal eye fields. This case exemplifies both the contributions of clinical eye movement physiology to expanding understanding of eye movement control in the brain, as well as the limitations of clinical cases. To further understand the potential underlying anatomy, application of a neuromimetic model to the behavior is required. Further contributions of this approach can be reviewed in the companion paper in this volume (Modeling Gaze Position-Dependent Opsoclonus, Optican et al.).

Acknowledgment

This research was supported, in part, by the Intramural Research Program of the NEI, NIH.

References

- Bergenius, J., 1986. Saccade abnormalities in patients with ocular flutter. *Acta Otolaryngol.* 102, 228–233.
- Blair, C.J., Goldberg, M.F., Von Noorden, G.K., 1967. Voluntary nystagmus. Electro-oculographic findings in four cases. *Arch. Ophthalmol.* 77, 349–354.
- Brodsky, M.C., Hunter, J.S., 2011. Positional ocular flutter and thickened optic nerves as sentinel signs of Krabbe disease. *J. AAPOS* 15, 595–597.
- Crevits, L., Hanse, M.C., Tummers, P., Van Maele, G., 2000. Antisaccades and remembered saccades in mild traumatic brain injury. *J. Neurol.* 247, 179–182.
- Cullen, K.E., Guitton, D., 1997. Analysis of primate IBN spike trains using system identification techniques. II. Relationship to gaze, eye, and head movement dynamics during head-free gaze shifts. *J. Neurophysiol.* 78, 3283–3306.
- Daye, P.M., Optican, L.M., Roze, E., Gaymard, B., Pouget, P., 2013. Neuromimetic model of saccades for localizing deficits in an atypical eye-movement pathology. *J. Transl. Med.* 11, 125.
- Digre, K.B., 1986. Opsoclonus in adults. Report of three cases and review of the literature. *Arch. Neurol.* 43, 1165–1175.
- Ellenberger Jr., C., Keltner, J.L., Stroud, M.H., 1972. Ocular dyskinesia in cerebellar disease. Evidence for the similarity of opsoclonus, ocular dysmetria and flutter-like oscillations. *Brain* 95, 685–692.
- Giza, C.C., Hovda, D.A., 2014. The new neurometabolic cascade of concussion. *Neurosurgery* 75 (Suppl. 4), S24–S33.
- Hain, T.C., Zee, D.S., Mordes, M., 1986. Blink-induced saccadic oscillations. *Ann. Neurol.* 19, 299–301.
- Heitger, M.H., Anderson, T.J., Jones, R.D., 2002. Saccade sequences as markers for cerebral dysfunction following mild closed head injury. *Prog. Brain Res.* 140, 433–448.
- Heitger, M.H., Anderson, T.J., Jones, R.D., Dalrymple-Alford, J.C., Frampton, C.M., Ardagh, M.W., 2004. Eye movement and visuomotor arm movement deficits following mild closed head injury. *Brain* 127, 575–590.
- Heitger, M.H., Jones, R.D., Macleod, A.D., Snell, D.L., Frampton, C.M., Anderson, T.J., 2009. Impaired eye movements in post-concussion syndrome indicate suboptimal brain function beyond the influence of depression, malingering or intellectual ability. *Brain* 132, 2850–2870.

- Helmchen, C., Straube, A., Buttner, U., 1994. Saccade-related activity in the fastigial oculomotor region of the macaque monkey during spontaneous eye movements in light and darkness. *Exp. Brain Res.* 98, 474–482.
- Helmchen, C., Rambold, H., Sprenger, A., Erdmann, C., Binkofski, F., fMRI study, 2003. Cerebellar activation in opsoclonus: an fMRI study. *Neurology* 61, 412–415.
- Hotson, J.R., 1984. Convergence-initiated voluntary flutter: a normal intrinsic capability in man. *Brain Res.* 294, 299–304.
- Jarrett, A., Emery, J.M., Coats, A.C., Justice Jr., J., 1977. Voluntary nystagmus. *Ann. Ophthalmol.* 9, 853–859.
- Kaneko, C.R., 1996. Effect of ibotenic acid lesions of the omnipause neurons on saccadic eye movements in rhesus macaques. *J. Neurophysiol.* 75, 2229–2242.
- Kepski, A., 1983. Clinical aspects and prognosis in cerebellar concussion syndromes. *Neurol. Neurochir. Pol.* 17, 239–243.
- Kim, J.S., Choi, K.D., Oh, S.Y., et al., 2007. Double saccadic pulses and macrosaccadic oscillations from a focal brainstem lesion. *J. Neurol. Sci.* 263, 118–123.
- Kim, J.S., Kim, J.S., Youn, J., et al., 2013. Ocular motor characteristics of different subtypes of spinocerebellar ataxia: distinguishing features. *Mov. Disord.* 28, 1271–1277.
- Kobayashi, M., 2015. Unidirectional ocular flutter: report of a case with abnormal saccadic characteristics. *Neurol. Sci.* 36, 1273–1276.
- Manta, A., Ugradar, S., Theodorou, M., 2018. Ocular flutter after mild head trauma. *J. Neuroophthalmol.* 38, 476–478.
- Martins, A.I., Nunes, C., Macario, M.C., Lemos, J., 2019. Positional ocular flutter associated with middle cerebellar peduncle demyelination. *J. Neuroophthalmol.* 39, 117–119.
- Meabon, J.S., Huber, B.R., Cross, D.J., et al., 2016. Repetitive blast exposure in mice and combat veterans causes persistent cerebellar dysfunction. *Sci. Transl. Med.* 8, 321ra6.
- Missal, M., Keller, E.L., 2002. Common inhibitory mechanism for saccades and smooth-pursuit eye movements. *J. Neurophysiol.* 88, 1880–1892.
- Nagle, M., Bridgeman, B., Stark, L., 1980. Voluntary nystagmus, saccadic suppression, and stabilization of the visual world. *Vision Res.* 20, 717–721.
- Ohtsuka, K., Noda, H., 1995. Discharge properties of Purkinje cells in the oculomotor vermis during visually guided saccades in the macaque monkey. *J. Neurophysiol.* 74, 1828–1840.
- Optican, L.M., Quaia, C., 2002. Distributed model of collicular and cerebellar function during saccades. *Ann. N. Y. Acad. Sci.* 956, 164–177.
- Petit-Pedrol, M., Armangue, T., Peng, X., et al., 2014. Encephalitis with refractory seizures, status epilepticus, and antibodies to the GABA_A receptor: a case series, characterisation of the antigen, and analysis of the effects of antibodies. *Lancet Neurol.* 13, 276–286.
- Pretegiani, E., Rosini, F., Rocchi, R., et al., 2017. GABAergic dysfunction in the olivary-cerebellar-brainstem network may cause eye oscillations and body tremor. *Clin. Neurophysiol.* 128, 408–410.
- Ramat, S., Leigh, R.J., Zee, D.S., Optican, L.M., 2005. Ocular oscillations generated by coupling of brainstem excitatory and inhibitory saccadic burst neurons. *Exp. Brain Res.* 160, 89–106.
- Ramat, S., Leigh, R.J., Zee, D.S., Shaikh, A.G., Optican, L.M., 2008. Applying saccade models to account for oscillations. *Prog. Brain Res.* 171, 123–130.
- Rivaud, S., Muri, R.M., Gaymard, B., Vermersch, A.I., Pierrot-Deseilligny, C., 1994. Eye movement disorders after frontal eye field lesions in humans. *Exp. Brain Res.* 102, 110–120.
- Robins, A., Vallat, M., Tapie, P., et al., 1976. Opsoclonus et troubles neurologiques accocies. *Arch. Ophtalmol.* 36, 645–656.

- Shaikh, A.G., Wilmot, G., 2016. Opsoclonus in a patient with increased titers of anti-GAD antibody provides proof for the conductance-based model of saccadic oscillations. *J. Neurol. Sci.* 362, 169–173.
- Shaikh, A.G., Ramat, S., Optican, L.M., Miura, K., Leigh, R.J., Zee, D.S., 2008. Saccadic burst cell membrane dysfunction is responsible for saccadic oscillations. *J. Neuroophthalmol.* 28, 329–336.
- Tremblay, S., de Beaumont, L., Lassonde, M., Theoret, H., 2011. Evidence for the specificity of intracortical inhibitory dysfunction in asymptomatic concussed athletes. *J. Neurotrauma* 28, 493–502.
- Turazzi, S., Alexandre, A., Bricolo, A., Rizzuto, N., 1977. Opsoclonus and palatal myoclonus during prolonged post-traumatic coma. A clinico-pathologic study. *Eur. Neurol.* 15, 257–263.
- Tusa, R.J., Zee, D.S., Herdman, S.J., 1986. Effect of unilateral cerebral cortical lesions on ocular motor behavior in monkeys: saccades and quick phases. *J. Neurophysiol.* 56, 1590–1625.
- Van Horn, M.R., Sylvestre, P.A., Cullen, K.E., 2008. The brain stem saccadic burst generator encodes gaze in three-dimensional space. *J. Neurophysiol.* 99, 2602–2616.
- Verhaeghe, S., Diallo, R., Nyffeler, T., Rivaud-Pechoux, S., Gaymard, B., 2007. Unidirectional ocular flutter. *J. Neurol. Neurosurg. Psychiatry* 78, 764–766.
- Yamada, J., Noda, H., 1987. Afferent and efferent connections of the oculomotor cerebellar vermis in the macaque monkey. *J. Comp. Neurol.* 265, 224–241.
- Yee, R.D., Spiegel, P.H., Yamada, T., Abel, L.A., Suzuki, D.A., Zee, D.S., 1994. Voluntary saccadic oscillations, resembling ocular flutter and opsoclonus. *J. Neuroophthalmol.* 14, 95–101.
- Zahn, J.R., 1978. Incidence and characteristics of voluntary nystagmus. *J. Neurol. Neurosurg. Psychiatry* 41, 617–623.
- Zee, D.S., Robinson, D.A., 1979. A hypothetical explanation of saccadic oscillations. *Ann. Neurol.* 5, 405–414.

SECTION

RESEARCH:
Saccades

III

This page intentionally left blank

Saccades in Parkinson's disease: Hypometric, slow, and maladaptive

5

Aasef G. Shaikh^{a,b,c,*}, Fatema F. Ghasia^{b,d}^a*Department of Neurology, University Hospitals Cleveland Medical Center and Case Western Reserve University, Cleveland, OH, United States*^b*Daroff-Dell'Osso Ocular Motility Laboratory and Neurology Service, Louis Stokes Cleveland VA Medical Center, Cleveland, OH, United States*^c*National VA PD Consortium Center, Louis Stokes Cleveland VA Medical Center, Cleveland, OH, United States*^d*Cole Eye Institute, Cleveland Clinic, Cleveland, OH, United States***Corresponding author: Tel.: +1-313-850-8604, e-mail address: aasefshaikh@gmail.com*

Abstract

Visuomotor impairments, such as hypometria of visually guided saccades, are common in Parkinson's disease (PD). Explaining the mechanistic underpinning of such abnormal voluntary (eye) movements can provide insights into the pathophysiology of limb movement disorders in PD. We measured visually guided saccades in 20 PD patients using quantitative high-resolution oculography. The experiments source to determine whether common motor deficits in PD, such as those affecting visually-guided saccades reflect excessive inhibition of the superior colliculus or rather involvement of brainstem saccade generators. We found slowing, interruptions, and curvatures in the saccade trajectory. The curvature not only reflected the mismatch in the velocity of relatively slower vertical (compared to horizontal) saccades, but could be due to aberrant activation of the superior colliculus. The irregularities in the saccade trajectory and slowing were prominent in the vertical direction. We suggest that abnormal saccades in PD not only reflect abnormal tectal function, but also suggest abnormal oscillatory behavior in the reciprocally innervating circuit of excitatory and inhibitory burst neurons. Impaired function of excitatory and inhibitory burst neurons causing maladaptive feedback and premature activation of the superior colliculus can cause irregularity in saccade trajectory.

Keywords

Eye movement, Superior colliculus, Basal ganglia, Burst neurons

1 Introduction

Parkinson's disease (PD), the second most common neurodegenerative disorder, affects approximately 10 million individuals world-wide. Devastating motor consequences of PD, such as episodic interruption of gait (freezing), lateral drift while walking (veering), impaired visuospatial navigation, and falls are frequently linked to impaired visuomotor function. The clinical description of the visuomotor deficits in PD include hypometria of saccades (rapid eye movements) made to visual targets (visually guided saccades) and to remembered target locations (memory-guided saccades), saccadic intrusions during gaze holding, convergence insufficiency, and deficient motion perception (Blekher et al., 2009; Chambers and Prescott, 2010; DeJong and Jones, 1971; Herishanu and Sharpe, 1981; Kimmig et al., 2002; Otero-Millan et al., 2013; Rascol et al., 1989, 1991; Repka et al., 1996; Rottach et al., 1996; Terao et al., 2011; Shaikh et al., 2011a,b; White et al., 1983). In order to delineate the physiology of complex motor and perceptual phenomena, it is often useful to first understand what leads to abnormality in physiologically less complex visuomotor function, such as visually-guided saccades. Delineating the pathophysiology of visually-guided saccades in PD may lead to better understanding of linked complex motor and perceptual phenomenologies and thereby offer conceptual understanding (i.e., prototype) for other complex movement disorders in PD which are not directly linked to the visuomotor deficits, e.g., bradykinesia and hypokinesia.

The superior colliculus is instrumental for visuomotor coordination, and its dysfunction can lead to abnormal scaling of saccades in PD (Terao et al., 2011, 2013). It was proposed that impairment of visually-guided saccades that clinically appear hypometric is due to increased inhibition of the superior colliculus through abnormal basal ganglia output (via substantia nigra pars reticulata) (Basso and Liu, 2007; Hikosaka and Wurtz, 1985; Wurtz and Hikosaka, 1986). The PD patients may have impairment in pre-attentional visual processing and saccade execution (Lieb et al., 1999). Functional MRI has shown reduced activation of the frontal eye fields in patients with PD during the preparatory phase of the visually-guided saccades (Javaid et al., 2010; Rieger et al., 2008). The underlying physiology may refer to the superior colliculus as it sends corollary signals to both frontal ocular motor and occipital visual regions at the onset of eye movement (Javaid et al., 2012; Sommer and Wurtz, 2008). Fundamentally important, yet unanswered, questions are: (1) Whether hypometric visually-guided saccades in PD depict an “interruption” of ongoing eye movement due to excessive phasic inhibition transmitted through the substantia nigra pars reticulata to the superior colliculus. (2) Whether saccades are malprogrammed due to impaired preparatory phase in the frontal eye fields. (3) Whether the saccade abnormality that appears like “hypometria” are the irregularities in the saccade trajectory due to the abnormal function of the brainstem burst generators such as paramedian pontine reticular formation and rostral interstitial nucleus of the medial longitudinal fasciculus (Horn et al., 1999; Leigh and Zee, 2015). Answer to these questions will address an important dichotomy whether visually-guided saccade abnormalities (i.e., abnormal voluntary motor behavior) in PD reflects excessive

inhibition of the superior colliculus and cortical malprogramming; or it suggests an involvement of brainstem mechanisms such as burst generators that are anatomically distinct for horizontal and vertical saccades. The goal of this study was to understand the abnormal kinematic properties of visually-guided saccades and their mechanistic underpinning in PD.

2 Methods

We studied visually-guided saccades from 20 PD subjects (12 men and 8 women, age 69.7 ± 8.5 years). The diagnosis of PD was made clinically by movement disorders neurologist. By definition, all PD subjects had robust responsiveness to dopaminergic medications. Average daily dopamine dose was 797 ± 253 mg. There was $44.9 \pm 16.3\%$ improvement in the motor part of Unified Parkinson's Disease Rating Scale (UPDRS III) during levodopa response testing. The studies were conducted in dopamine off period. The study and consent form were approved by The Cleveland Clinic and The Emory University Institutional Review Boards. The experiments were performed in accordance with the ethical standards laid down in the 1964 Declaration of Helsinki and its later amendments. The subjects signed written consent before the experiment.

2.1 Experimental setup

High-resolution video-based eye tracker (EyeLink 1000[®], SR Research, Ontario, Canada; spatial resolution = 0.01° and temporal resolution = 500Hz) was used to non-invasively measure horizontal and vertical eye positions in PD patients and matched healthy subjects. The video-based eye tracker uses the corneal reflection (first Purkinje image) and the center of the pupil to measure the coordinates of the gaze position. It does not rely on pupil size which may change with light reflex or cognitive processes including thoughts and behaviors. The calibration process used the saccades made to target shifts of known distance; in order to compensate for hypometria we used the final eye position after corrective saccades. The data were further processed and analyzed with previously published techniques using custom software (MATLAB[®], MathworksTM, Natick, MA) ([Ghasia and Shaikh, 2015a,b](#); [Ghasia et al., 2016](#)).

2.2 Experimental protocol and data analysis

The subjects stabilized their head on the chin rest. The head stability through the experiment was assured by measuring head velocity using synchronized gyroscope. A circular target with 0.5° visual angle was displayed on the computer monitor that was 55 cm away from the chin rest. The subjects were instructed to look at the target projected straight-ahead or 5° , 10° , 15° , and 20° to the right and left and 5° , 10° , 15° , and 20° up or down. We measured eye movements as the subjects held gaze steady or rapidly changed the line of sight from one target position to the other.

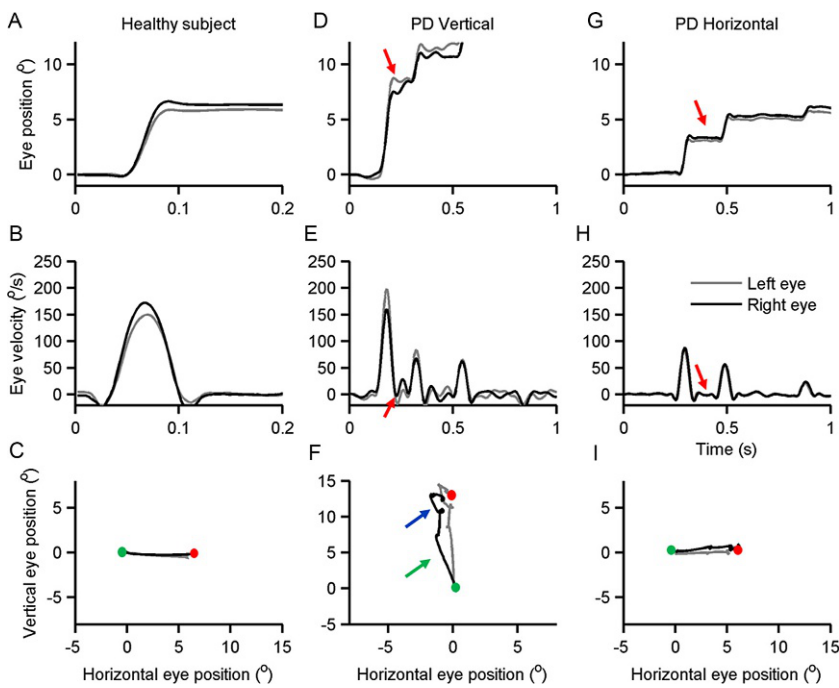
The key analyzed variables were the amplitude, velocity, acceleration, and deceleration of saccades. Eye position was differentiated and smoothed with a Savitzky-Golay filter (polynomial order: 3; frame length: 21) to compute eye velocity. Due to the irregular trajectory and fluctuations in the velocity, the onset and offset of saccades were determined interactively. The saccade onset was determined when eye position shifted 2 degrees away from the steady baseline after the target shift. Such position threshold was used to exclude square-wave jerks. The end was when the eyes reached new baseline. Breaks in the saccades were determined using the velocity trace. The troughs in the velocity trace corresponded to breaks; those reaching zero indicated a complete pause in the movement. MATLAB[®] toolboxes were used for the statistical analyses and curve fitting.

3 Results

[Fig. 1A](#) and [B](#) depicts an example of a visually guided saccade captured from a healthy subject. The eye position ([Fig. 1A](#)) and velocity ([Fig. 1B](#)) is plotted on the y-axis, while corresponding time is plotted on the x-axis. The visually guided saccade in a healthy subject is uninterrupted as it is evident from a single peak in the velocity profile ([Fig. 1B](#)). The path of the illustrated eye movement followed a straight trajectory as evident in [Fig. 1C](#). Unlike healthy subject, the saccades were interrupted in a PD patient. [Fig. 1D–I](#) depict an example of interrupted vertical saccade measured from the PD patient. We saw three types of interruptions; in one type the eyes did not stop but continued to move at much slower velocity compared to preceding saccade segment (red arrow in [Fig. 1D](#) and [E](#)). Two other types of interruptions (not shown in [Fig. 1D](#) and [E](#)) were either complete cessation of the eye movement or the eyes moved at much slower speed in the direction opposite of the ongoing saccade. The vertical saccade in the illustrated example was not only interrupted but it also had a curved and irregular trajectory. For instance, in an example depicted in [Fig. 1F](#), the initial trajectory was directed upward and to the right and then upward and to the left ([Fig. 1F](#), green arrow). After a halt (not visible in [Fig. 1F](#)), the eyes made another curved movement ([Fig. 1F](#), blue arrow). Like vertical saccades, the interruptions were present in the horizontal saccades ([Fig. 1G](#) and [H](#)), but unlike the vertical saccades the curvature or irregularity of the horizontal saccades was much smaller ([Fig. 1I](#)). The example of the horizontal saccade described in [Fig. 1G](#) shows an example of an interruption (red arrows, [Fig. 1G](#) and [H](#)). During such break, the velocity reached zero (red arrows [Fig. 1H](#)), it was then followed by a catchup saccade bringing the eyes to their destination. Such deficits of horizontal and vertical saccades were consistently seen in all subjects, as summarized and quantitatively analyzed in sections below.

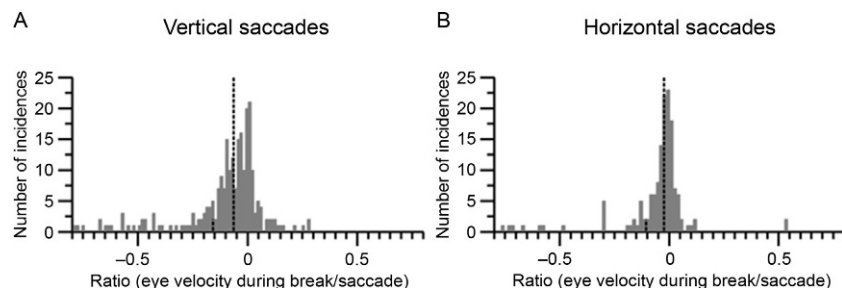
3.1 Quantitative characteristics of saccade interruptions

This section quantifies the kinematic characteristics of the eye movements during saccade interruptions for all trials in all PD patients. First we asked whether the eyes stop during saccade interruption or they continue to move at a slower velocity.

**FIG. 1**

Examples of visually guided saccades from healthy subject and PD patient. In first row of subplots the eye position is plotted on the y-axis while x-axis depicts corresponding time in seconds. Black line depicts right eye, gray trace is left eye. Red arrows depict interruption in ongoing saccades. Panel (A) illustrates normal visually guided vertical saccade from a healthy subject. Panels (D,G) depict examples of visually guided vertical and horizontal saccades from the same PD subject. Middle row of subplots depicts eye velocity. Panel (B) depicts eye velocity of normal visually guided saccade recorded from a healthy subject, while panels (E,H) depict vertical and horizontal eye velocity respectively from a PD patient. In these subplots the eye velocity is plotted on y-axis while x-axis illustrates corresponding time. Red arrows illustrate interruption in saccade when eye velocity was zero (panel H) or when eye moved at slower velocity in the opposite direction (panel E). The bottom row of the subplots depict trajectories of horizontal and vertical saccades. Panel (C) depicts normal saccade from the healthy subject, panel (F,I) depicts vertical and horizontal saccades in PD. Green dot is start point, red dot is stop point. Arrows in panels (F, I) depict curvature in saccade trajectory.

We measured the ratio of the eye velocity during the interrupted segment and the peak velocity of the preceding saccadic pulse. The ratio would be zero in instances when the interruption leads to a complete cessation of the eye movement. A non-zero value of the ratio suggests slow eye movement during the interruption. A positive value of the ratio depicts slow eye movement in the same direction as the ongoing saccade, while the negative value would suggest that the slow eye

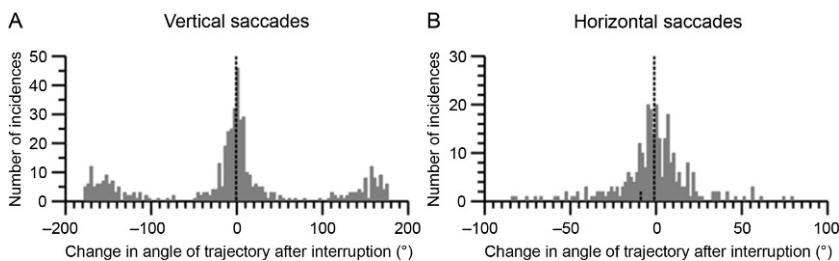
**FIG. 2**

Summary of ratio of eye velocity during interruption and saccade segment of interrupted horizontal and vertical saccades in PD. Panel (A) depicts vertical saccade, while panel (B) illustrates horizontal saccade. Both panels provide the cumulative summary of ratio from all PD patients. Ratio near zero suggests that eyes movements completely paused during interruption; while positive value of the ratio depicts slow eye movement in the same direction as saccade. Negative value suggests slow eye movement in the opposite direction (like an oscillation). X-axis depicts bins of ratio, while y-axis is number of incidences in the given bin. Tall dashed line depicts mean, while short dashed line is median value.

movements are in the opposite direction. We found that the ratios in most instances were a non-zero value, and its value spanned between positive to negative in all subjects. This analysis suggested that in PD patients the eyes did not stop in most instances when the saccade was interrupted. Instead, they slowly moved either in the direction of ongoing saccade or in the opposite direction. The histograms in Fig. 2A and B depict the summary of ratios from all patients during horizontal (Fig. 2A) and vertical (Fig. 2B) saccades. The dashed lines in Fig. 2A and B graphically illustrate the mean value of the ratio (vertical saccade ratio: 0.03 ± 0.06 , horizontal saccade ratio: 0.04 ± 0.1). The difference in the distributions of ratios measured from the horizontal saccade group was significantly different when compared with the vertical saccade group (Kolmogorov-Smirnov test, $P < 0.001$). The range of ratio spanning 66% area under the curve was -0.64 to 0.01 for vertical saccades; it was -0.59 to -0.005 for the horizontal saccades. These results suggest that the eye velocity during interruption of the vertical and horizontal saccades reached upto 60% of the peak saccade velocity; hence the eyes were still in motion during interruption.

3.2 Quantitative characteristics of saccade curvature

Change in the direction of saccade trajectory leading to irregularity was evident in all subjects. The change in saccade trajectory in the example of one saccade is illustrated with green and blue arrows in Fig. 1F. Fig. 3 depicts the summary of the differences in the direction of the trajectories of saccade segments before and after the interruption. The mean difference in the direction of the trajectory from all subjects was a non-zero value. Fig. 3A and B depicts the summary of deviation of all saccades

**FIG. 3**

Cumulative summary of change in angle of trajectory after interruption of vertical (A) and horizontal (B) saccades in all PD subjects. Angle of zero suggests no change in saccade trajectory after the interruption, while the non-zero value suggests a change in the trajectory. X-axis depicts bins of trajectory angles, while y-axis is number of incidences in the given bin. Tall dashed line depicts mean, while short dashed line is the median value.

measured from all subjects. The mean value of the changes in the vertical saccade trajectory was -4.2 ± 93.62 degrees, while it was -1.6 ± 21.84 degrees for the horizontal. The range of values encompassing 66% area under the curve was -132.7 to 148.3 degrees for vertical saccades, while it was -19.3 to 13.6 degrees for the horizontal. The comparison of the histograms representing the distributions of the directional changes in the trajectories revealed statistical significance (Kolmogorov-Smirnov test, $P = 0.003$). The results suggest that interrupted saccades in PD patients were invariably misdirected and PD patients had to make multiple changes in the trajectory to reach the intended target. The irregularity in the trajectory (i.e., the curvatures) were much more robust in vertical saccades compared to horizontal saccades.

3.3 Saccade amplitude to velocity relationship

We assessed the amplitude-to-velocity relationship (i.e., the main-sequence) of vertical and horizontal saccades. There were two components to this analysis as schematized in the inset of Fig. 4B. In the first part, we compared desired saccade amplitude ("Ad," inset of Fig. 4B, and filled symbols in Fig. 4A and B) with the peak velocity (Vmax) during the gaze shift required to accomplish such movement. The second part of the analysis compared the amplitude of segmented saccade ("A1," inset Fig. 4B, and open symbols in Fig. 4A and B) with the velocity of the corresponding saccade segment (V1). Filled symbols in Fig. 4A depict the main-sequence of the desired saccade, i.e., comparison of desired amplitude (Ad) with peak velocity (Vmax) for vertical saccades. In this figure each color represents one subject. Open symbols in Fig. 4A illustrate the main-sequence relationship of the segmented saccades, i.e., the comparison of segmented saccade amplitude (A1) with corresponding saccade velocity (V1). Again each color depicts one subject and each symbol depicts one saccade. Gray lines in Fig. 4A represent the normative range determined from age and gender matched control subjects. As shown in Fig. 4A the distribution of the filled symbols, i.e., the comparison of desired amplitude

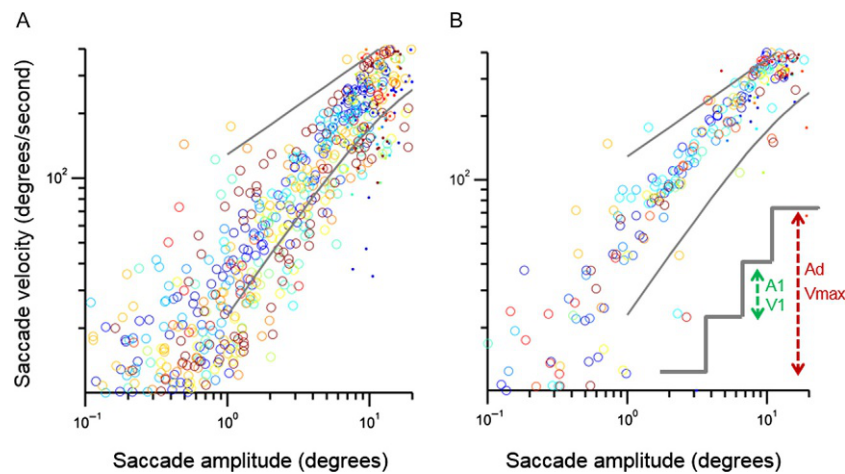


FIG. 4

Comparison of saccade velocity and corresponding amplitude in main sequence analysis for vertical (A) and horizontal (B) saccades. Saccade velocity is plotted on y-axis while x-axis depicts saccade amplitude. Each color depict one subject, each symbol depicts one saccade. Filled symbols depict the relationship of peak saccade velocity with the desired amplitude of saccade, while open symbols show the relationship between the amplitude of the broken segment of the saccade and corresponding velocity. Gray lines are normative range. Inset of panel B schematizes analysis strategy. In this inset a multistep saccade is schematized. Analysis (green arrow) of the second component of the saccade (after velocity has decreased and then increased again) renders change in position A1 with its corresponding velocity (V1). Compare this with the desired change of eye position, i.e., the red arrow depicting desired saccade amplitude (Ad) and maximal velocity (Vmax).

change with peak velocity did not follow the main-sequence. In contrast, the segmented saccade amplitude and their corresponding velocity relationship did follow the main-sequence. We quantified the main-sequence by measuring the goodness-of-fit to the equation: $V = K \cdot A^L$. In this equation V is peak saccade velocity, A is saccade amplitude, two parameters K and L determine the amplitude dependence of the saccade velocity. This analysis was separately done for two types of main-sequence comparison—desired saccade amplitude and segmented saccade amplitude. Main-sequence for vertical and horizontal saccades were separately analyzed. For vertical saccades, the goodness-of-fit of the main-sequence equation (r^2 value) was 0.26 ± 0.25 when desired saccade amplitude was compared with the peak saccade velocity. The goodness-of-fit for the main-sequence comparison was 0.8 ± 0.14 for the comparison of segmented vertical saccade amplitude with corresponding saccade velocity. For the horizontal saccades, the goodness-of-fit for the main-sequence equation was 0.44 ± 0.28 for the comparison of desired saccade and peak velocity. For the comparison of segmented saccade and corresponding peak velocity, the goodness-of-fit was 0.9 ± 0.1 .

The open datapoints from 6 of 20 subjects in Fig. 4A, suggesting the relationship of segmented saccade amplitude and corresponding velocity, were below the normative range suggesting slowing of segmented vertical saccades (Fig. 4A). This observation in vertical saccade contrasted with the horizontal saccades, where in most instances the relationship of segmented amplitude (or even desired amplitude) and velocity of the saccade segment (or the peak horizontal saccade velocity) depicted by the open and filled datapoints respectively in Fig. 4B fell within the normal range. These results suggest that the segmented portion of vertical saccades are often slow, but such slowing is not evident in horizontal saccades.

3.4 Do abnormal saccade characteristics correlate with the severity of PD?

The differences in the kinematic properties of saccades, i.e., only in 6 of 20 subjects vertical saccade segments were slow, led to question whether reduced saccade velocity and corresponding difference in the main-sequence parameters correlate with overall motor manifestation of the disease state measured with UPDRS III score. Table 1 depicts r^2 values and slopes comparing the main-sequence parameters **K** and **L** and the severity of motor impairment in PD measured with UPDRS III. We found the lack of correlation in the of values of parameters **K** and **L** for the main-sequence relationship of desired as well as interrupted saccades in horizontal and vertical directions and the severity of motor impairment in PD as measured with UPDRS III.

Taken together we found three types of abnormalities in visually-guided saccades in PD subjects. (1) Frequent interruption of the ongoing saccade. (2) Irregularity in the saccade trajectory resulting in longer duration to complete the movement; and (3) Slowing of segmented saccade velocity, especially vertically. None of these saccade abnormalities correlated with the motor severity of PD quantified by UPDRS III score.

4 Discussion

Visuomotor deficits such as hypometric memory- and visually-guided saccades and deficient motion perception are present in PD despite their ability to accurately perceive the visual stimulus (Blekher et al., 2009; Chambers and Prescott, 2010; DeJong and Jones, 1971; Herishanu and Sharpe, 1981; Kimmig et al., 2002;

Table 1 Fit parameters for vertical and horizontal saccades.

	L		K	
	r^2	Slope	r^2	Slope
Vertical Desired	0.05	0.19	0.001	0.003
Vertical Segmented	0.001	0.4	0.005	12.5
Horizontal Desired	0.6	0.03	0.4	27.5
Horizontal Segmented	0.4	0.01	0.02	-6.7

Otero-Millan et al., 2013; Rascol et al., 1989, 1991; Repka et al., 1996; Rottach et al., 1996; Terao et al., 2011; Shaikh et al., 2011a,b; White et al., 1983). The fundamental question is: How does PD cause transient interruption of ongoing saccades that clinically appear hypometric? Dysfunction of the superior colliculus secondary to the abnormal outflow from the substantia nigra pars reticulata in disease states such as PD can lead to direct inhibition of the superior colliculus or altered activation of the frontal eye field (Javaid et al., 2010; Lieb et al., 1999; Rieger et al., 2008). Such mechanism expects relatively equal impairment of horizontal and vertical saccades, and during interruption the eye velocity would be next to null. Another fundamentally critical possibility is that hypometric visually guided saccades in PD are due to the abnormal function of the brainstem saccade generators. Our experiments probed these two hypotheses.

4.1 Impaired function of basal ganglia, superior colliculus, and impaired corollary discharge to the frontal eye fields

Substantia nigra pars reticulata maintains tonic GABAergic inhibition of the superior colliculus (Fisher et al., 1986; Francois et al., 1984). Transient cessation of these neurons, in preparation for the voluntary saccade, leads to timely saccade initiation (Handel and Glimcher, 1999; Hikosaka and Wurtz, 1983). Pharmacological inhibition of substantia nigra pars reticulata after muscimol injection results in saccadic intrusions and contralaterally directed spontaneous saccades (Hikosaka and Wurtz, 1985; Wurtz and Hikosaka, 1986). Electrical stimulation of the substantia nigra pars reticulata causes reduced latency and hypometric visually guided saccades (Basso and Liu, 2007). Disinhibition of the substantia nigra pars reticulata, as expected in PD, can prematurely interrupt ongoing saccade by imposing phasic inhibition to the superior colliculus. This mechanism, however, suggests equal impairment of the horizontal and vertical saccades. This theory also suggested that the saccade velocity should always reach zero (eyes should completely stop) during each break. We found interruptions in horizontal and vertical saccades in PD patients, but the involvement of horizontal saccades was at much lesser extent. Furthermore, during interruptions, the eyes did not completely pause. Hence we concluded that increased activation of the substantia nigra pars reticulata and its subsequent influence on the activity of superior colliculus and the frontal eye field could be one of the underlying abnormalities but not the sole deficit for impaired visually-guided saccade in PD.

4.2 Impaired function of burst generators in PD

Saccades are initiated by the circuits within the frontal and parietal eye fields in the cerebral cortex. Cortical saccade-related signals follow two main pathways; one projecting to the nucleus reticularis tegmenti pontis (NRTP) of the pontine reticular formation while the other to the superior colliculus. Neurons of NRTP then project to the oculomotor vermis (OMV) (lobules 5–7) of the cerebellar cortex that sends

GABAergic inhibitory signals to the underlying caudal fastigial nucleus (fastigial oculomotor region (FOR)). The FOR projects to the omnidirectional pause neurons (OPN) of the saccadic burst generator area in the nucleus raphe interpositus of the midline pons as well as to the burst neurons themselves. OPNs and inhibitory burst neurons (IBNs) are two sources of sustained inhibitory influence on the excitatory burst neurons (EBNs). Sudden cessation of external inhibition leading to abrupt increase in the excitability, the post-inhibitory rebound (PIR), is critical for high-velocity of saccades (Enderle and Engelken, 1995; Miura and Optican, 2006; Shaikh et al., 2007, 2008, 2010, 2011a,b). Abrupt cessation of the sustained OPN activity matches with the high-acceleration of saccades; at the end of sustained inhibition of the EBNs, there is an abrupt increase in their firing due to PIR (Enderle and Engelken, 1995; Miura and Optican, 2006; Shaikh et al., 2008, 2010, 2011a,b). Simultaneously the activity of ipsilateral IBNs inhibits contralateral EBNs, hence preventing the activation of antagonistic eye muscles. Reactivation of contralateral IBNs offsets the EBNs activity hence abruptly stopping the moving eyes during a saccade. Also the OPNs turn on at the end of the saccade further assuring steady gaze holding. Impaired activation of the EBNs could lead to slow saccades, while early activation of the OPNs and IBNs could result in premature breaks in the ongoing saccade resulting in early interruptions in the trajectory and resultant hypometria.

OPNs equally affect horizontal and vertical saccades via its influence on the nucleus reticularis tagmenti pontis and rostral interstitial nucleus of medial longitudinal fasiculus, respectively. However, PD patients have prominent involvement of vertical saccades. Therefore the malfunction of OPNs is less likely to cause saccade abnormality. The EBNs for horizontal and vertical saccades are located in anatomically distinctly regions. Therefore it is likely that impaired excitation of vertical saccade sensitive EBNs results in abnormal vertical saccades in PD patients.

4.3 Superior colliculus activation and maladaptive changes in saccade trajectory

Stimulation of the superior colliculus fixation zone during the saccade can cause directional changes of the ongoing eye movement (Gandhi and Keller, 1999; Munoz and Wurtz, 1993a,b). The path of the redirected saccades is dependent upon the co-ordinates of the stimulated site in the collicular fixation zone (Gandhi and Keller, 1999). Premature activation of the various locations in the fixation zone of the superior colliculus in PD patients may explain idiosyncratically determined trajectory of the redirected saccade and subsequent irregular saccade trajectory.

What causes the premature stimulation of the superior colliculus and why it predominantly affects the vertical saccades? We speculate that PD first affects EBNs and IBNs responsible for the vertical saccades. Due to degenerative insult the IBNs discharge asynchronously and irregularly. Such discharge pattern of IBNs during an ongoing vertical saccade is not only inferred as a signal to pause the eye movement causing interruption but it is also forwarded in the feedback circuit to the superior

colliculus (Waitzman et al., 1991). Subsequent undesired activation of the collicular fixation zone leads to redirected saccades in an arbitrary direction. These predictions underlying pathophysiology of abnormal visually guided saccades are also supported by the histopathological findings in PD suggesting the early involvement of midbrain reticular formation, the area for vertical saccade generation (Braak et al., 2003; Halliday et al., 1990, 2006).

Slow, curved and multistep saccades are well known phenomenon in parkinsonism, typically in its atypical forms (Quinn, 1996; Rottach et al., 1996). Here we report unique kinematic properties of visually guided saccades in PD. The features include well-recognized hypometria, but also we noted slowing, interruptions, and irregularities and curvatures in the saccade trajectory. We speculate that curvature and irregularity in the saccade trajectory in PD is not merely due to the mismatch in the velocity of relatively slower vertical component, but it is due to aberrant activation of the superior colliculus. We further predict that the irregularities and slowing, prominently seen in the vertical saccades, could be due to impaired function of EBNs and IBNs leading to maladaptive feedback causing the premature activation of the superior colliculus.

Acknowledgments

A.G.S. is supported by career development award from the American Academy of Neurology, George Cotzias Memorial Fellowship (American Parkinson's Disease Association), and Dystonia Medical Research Foundation. F.F.G is supported by grants from Blind Children's Foundation, Knights Templar Eye Foundation, and Fight for Sight grant. There are no financial conflict of interests. On behalf of all authors, the corresponding author states that there is no conflict of interest.

References

- Basso, M.A., Liu, P., 2007. Context-dependent effects of substantia nigra stimulation on eye movements. *J. Neurophysiol.* 97, 4129–4142.
- Blekher, T., Weaver, M.R., Cai, X., Hui, S., et al., 2009. Test-retest reliability of saccadic measures in subjects at risk for Huntington disease. *Invest. Ophthalmol. Vis. Sci.* 50, 5707–5711.
- Braak, H., Del Tredici, K., Rub, U., de Vos, R.A., Jansen Steur, E.N., Braak, E., 2003. Staging of brain pathology related to sporadic Parkinson's disease. *Neurobiol. Aging* 24, 197–211.
- Chambers, J.M., Prescott, T.J., 2010. Response times for visually guided saccades in persons with Parkinson's disease: a meta-analytic review. *Neuropsychologia* 48, 887–899.
- DeJong, J.D., Jones, G.M., 1971. Akinesia, hypokinesia, and bradykinesia in the oculomotor system of patients with Parkinson's disease. *Exp. Neurol.* 32, 58–68.
- Enderle, J., Engelken, E., 1995. Simulation of oculomotor post-inhibitory rebound burst firing using a Hodgkin-Huxley model of a neuron. *Biomed. Sci. Instrum.* 31, 53–58.
- Fisher, R.S., Buchwald, N.A., Hull, C.D., Levine, M.S., 1986. The GABAergic striatonigral neurons of the cat: demonstration by double peroxidase labeling. *Brain Res.* 398, 148–156.
- Francois, C., Percheron, G., Yelnik, J., 1984. Localization of nigrostriatal, nigrothalamic and nigrotectal neurons in ventricular coordinates in macaques. *Neuroscience* 13, 61–76.

- Gandhi, N.J., Keller, E.L., 1999. Comparison of saccades perturbed by stimulation of the rostral superior colliculus, the caudal superior colliculus, and the omnipause neuron region. *J. Neurophysiol.* 82, 3236–3253.
- Ghasia, F.F., Shaikh, A.G., 2015a. Experimental tests of hypotheses for microsaccade generation. *Exp. Brain Res.* 233, 1089–1095.
- Ghasia, F.F., Shaikh, A.G., 2015b. Uncorrected myopic refractive error increases microsaccade amplitude. *Invest. Ophthalmol. Vis. Sci.* 56, 2531–2535.
- Ghasia, F.F., Wilmot, G., Ahmed, A., Shaikh, A.G., 2016. Strabismus and micro-opsoclonus in Machado-Joseph disease. *Cerebellum* 15, 491–497.
- Halliday, G.M., Li, Y.W., Blumbergs, P.C., Joh, T.H., Cotton, R.G., Howe, P.R., Blessing, W.W., Geffen, L.B., 1990. Neuropathology of immunohistochemically identified brainstem neurons in Parkinson's disease. *Ann. Neurol.* 27, 373–385.
- Halliday, G.M., Del Tredici, K., Braak, H., 2006. Critical appraisal of brain pathology staging related to presymptomatic and symptomatic cases of sporadic Parkinson's disease. *J. Neural Transm. Suppl.*, 70, 99–103.
- Handel, A., Glimcher, P.W., 1999. Quantitative analysis of substantia nigra pars reticulata activity during a visually guided saccade task. *J. Neurophysiol.* 82, 3458–3475.
- Herishanu, Y.O., Sharpe, J.A., 1981. Normal square wave jerks. *Invest. Ophthalmol. Vis. Sci.* 20, 268–272.
- Hikosaka, O., Wurtz, R.H., 1983. Visual and oculomotor functions of monkey substantia nigra pars reticulata. IV. Relation of substantia nigra to superior colliculus. *J. Neurophysiol.* 49, 1285–1301.
- Hikosaka, O., Wurtz, R.H., 1985. Modification of saccadic eye movements by GABA-related substances. I. Effect of muscimol and bicuculline in monkey superior colliculus. *J. Neurophysiol.* 53, 266–291.
- Horn, A.K., Buttner, U., Buttner-Ennever, J.A., 1999. Brainstem and cerebellar structures for eye movement generation. *Adv. Otorhinolaryngol.* 55, 1–25.
- Javaid, M.A., Weeden, J., Flom, P., Avitable, M., Glazman, S., Bodis-Wollner, I., 2010. Perisaccadic gamma modulation in Parkinson disease patients and healthy subjects. *Clin. EEG Neurosci.* 41, 94–101.
- Javaid, M.A., Amassian, V., Glazman, S., Fesharaki, A., Stefanov, D., Bodis-Wollner, I., 2012. Cortical control of voluntary saccades in Parkinson's disease and pre-emptive perception. *Parkinsonism Relat. Disord.* 18 (Suppl. 1), S100–S103.
- Kimmig, H., Haussmann, K., et al., 2002. What is pathological with gaze shift fragmentation in Parkinson's disease? *J. Neurol.* 249, 683–692.
- Leigh, R.J., Zee, D.S., 2015. *The Neurology of Eye Movements*. Oxford University Press, New York.
- Lieb, K., Brucker, S., Bach, M., Els, T., Lucking, C.H., Greenlee, M.W., 1999. Impairment in pre-attentive visual processing in patients with Parkinson's disease. *Brain* 122 (Pt. 2), 303–313.
- Miura, K., Optican, L.M., 2006. Membrane channel properties of premotor excitatory burst neurons may underlie saccade slowing after lesions of omnipause neurons. *J. Comput. Neurosci.* 20, 25–41.
- Munoz, D.P., Wurtz, R.H., 1993a. Fixation cells in monkey superior colliculus. I. Characteristics of cell discharge. *J. Neurophysiol.* 70, 559–575.
- Munoz, D.P., Wurtz, R.H., 1993b. Fixation cells in monkey superior colliculus. II. Reversible activation and deactivation. *J. Neurophysiol.* 70, 576–589.
- Otero-Millan, J., Schneider, R., Leigh, R.J., Macknik, S.L., Martinez-Conde, S., 2013. Saccades during attempted fixation in parkinsonian disorders and recessive ataxia: from microsaccades to square-wave jerks. *PLoS One* 8, e58535.

- Quinn, N., 1996. The “round the houses” sign in progressive supranuclear palsy. *Ann. Neurol.* 40, 951.
- Rascol, O., Clanet, M., Montastruc, J.L., Simonetta, M., Soulier-Esteve, M.J., Doyon, B., Rascol, A., 1989. Abnormal ocular movements in Parkinson's disease. Evidence for involvement of dopaminergic systems. *Brain* 112 (Pt. 5), 1193–1214.
- Rascol, O., Sabatini, U., Simonetta-Moreau, M., Montastruc, J.L., Rascol, A., Clanet, M., 1991. Square wave jerks in parkinsonian syndromes. *J. Neurol. Neurosurg. Psychiatry* 54, 599–602.
- Repka, M.X., Claro, M.C., Loupe, D.N., Reich, S.G., 1996. Ocular motility in Parkinson's disease'. *J. Pediatr. Ophthalmol. Strabismus* 33, 144–147.
- Rieger, J.W., Kim, A., Argyelan, M., Farber, M., Glazman, S., Liebeskind, M., Meyer, T., Bodis-Wollner, I., 2008. Cortical functional anatomy of voluntary saccades in Parkinson disease. *Clin. EEG Neurosci.* 39, 169–174.
- Rottach, K.G., Riley, D.E., DiScenna, A.O., Zivotofsky, A.Z., Leigh, R.J., 1996. Dynamic properties of horizontal and vertical eye movements in parkinsonian syndromes. *Ann. Neurol.* 39, 368–377.
- Shaikh, A.G., Miura, K., Optican, L.M., Ramat, S., Leigh, R.J., Zee, D.S., 2007. A new familial disease of saccadic oscillations and limb tremor provides clues to mechanisms of common tremor disorders. *Brain* 130, 3020–3031.
- Shaikh, A.G., Ramat, S., Optican, L.M., Miura, K., Leigh, R.J., Zee, D.S., 2008. Saccadic burst cell membrane dysfunction is responsible for saccadic oscillations. *J. Neuroophthalmol.* 28, 329–336.
- Shaikh, A.G., Wong, A.L., Optican, L.M., Miura, K., Solomon, D., Zee, D.S., 2010. Sustained eye closure slows saccades. *Vis. Res.* 50, 1665–1675.
- Shaikh, A.G., Xu-Wilson, M., Grill, S., et al., 2011a. Staircase' square-wave jerks in early Parkinson's disease. *Br. J. Ophthalmol.* 95, 705–709.
- Shaikh, A.G., Zee, D.S., Optican, L.M., Miura, K., Ramat, S., Leigh, R.J., 2011b. The effects of ion channel blockers validate the conductance-based model of saccadic oscillations. *Ann. N. Y. Acad. Sci.* 1233, 58–63.
- Sommer, M.A., Wurtz, R.H., 2008. Visual perception and corollary discharge. *Perception* 37, 408–418.
- Terao, Y., Fukuda, H., Yugeta, A., Hikosaka, O., Nomura, Y., Segawa, M., Hanajima, R., Tsuji, S., Ugawa, Y., 2011. Initiation and inhibitory control of saccades with the progression of Parkinson's disease—changes in three major drives converging on the superior colliculus. *Neuropsychologia* 49, 1794–1806.
- Terao, Y., Fukuda, H., Ugawa, Y., Hikosaka, O., 2013. New perspectives on the pathophysiology of Parkinson's disease as assessed by saccade performance: a clinical review. *Clin. Neurophysiol.* 124, 1491–1506.
- Waitzman, D.M., Ma, T.P., Optican, L.M., Wurtz, R.H., 1991. Superior colliculus neurons mediate the dynamic characteristics of saccades. *J. Neurophysiol.* 66, 1716–1737.
- White, O.B., Saint-Cyr, J.A., Tomlinson, R.D., Sharpe, J.A., 1983. Ocular motor deficits in Parkinson's disease. II. Control of the saccadic and smooth pursuit systems. *Brain* 106 (Pt. 3), 571–587.
- Wurtz, R.H., Hikosaka, O., 1986. Role of the basal ganglia in the initiation of saccadic eye movements. *Prog. Brain Res.* 64, 175–190.

Brainstem neural circuits for fixation and generation of saccadic eye movements

6

Yoshikazu Shinoda*, Mayu Takahashi, Yuriko Sugiuchi

Department of Systems Neurophysiology, Graduate School of Medicine, Tokyo Medical and Dental University, Tokyo, Japan

*Corresponding author: Tel.: +81-3-5803-5152, e-mail address: yshinoda.phy1@tmd.ac.jp

Abstract

We review neural connections of the superior colliculus (SC) and brainstem saccade-related neurons in relation to saccade generation mechanism. The caudal and rostral SC play a role in saccade generation and visual fixation, respectively. This functional differentiation suggests that different connections should exist between these two SC areas and their brainstem target neurons. We examined synaptic potentials evoked by stimulation of the rostral and caudal SC in inhibitory burst neurons (IBNs) and omnipause neurons (OPNs) in anesthetized cats. The caudal and rostral SC produced monosynaptic excitation and disynaptic inhibition in IBNs, respectively. Intracellular HRP staining showed that single IBNs sent their axons to abducens motoneurons, IBNs and OPNs on the opposite side. OPNs received monosynaptic excitation from the rostral SC, and disynaptic inhibition from the caudal SC via opposite IBNs. These neural connections are discussed in relation to the saccade triggering system and the model proposed by Miura and Optican.

Keywords

Superior colliculus, Saccade, Omnipause neuron (OPN), Saccade trigger, Fixation, Inhibitory burst neuron (IBN), Excitatory burst neuron (EBN), Abducens motoneuron, T-type Ca channel

1 Background

Saccades are the fast eye movements that rapidly redirect a line of sight (Leigh and Zee, 2015). Various types of neurons were found in relation to saccadic eye movements in the brainstem. Premotor burst neurons for saccade generation consist of long lead burst neurons (LLBNs) and medium lead burst neurons (MLBNs). LLBNs start firing much earlier than MLBNs at the onset of saccades, so that it is believed that SC output neurons activate LLBNs and then LLBNs activate MLBNs in a sequential way (Fig. 1, left). MLBNs consist of excitatory and inhibitory burst neurons (EBNs and IBNs, respectively) and are distributed in the midbrain, pons

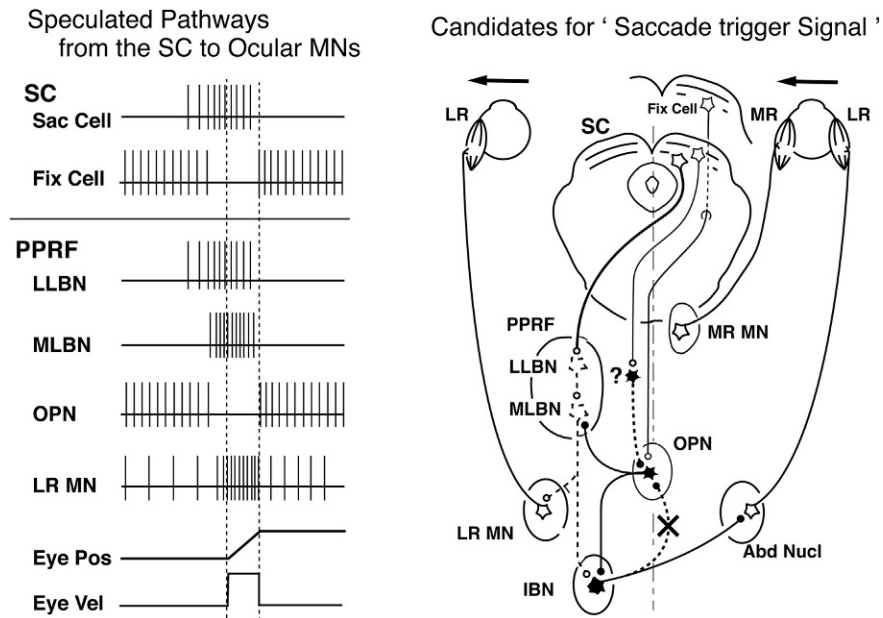


FIG. 1

Left: Patterns of spike activity of various superior colliculus (SC) output neurons and brainstem premotor and motor neurons in relation to visually-guided horizontal saccades. Vertical broken lines indicate onset and end of horizontal saccade. Eye Pos and Vel, eye position and velocity; Sac Cell, saccade neuron in the caudal SC; Fix Cell, fixation cell in the rostral SC; LLBN, MLBN, long and medium lead burst neuron; LR and MR MN, lateral and medial rectus motoneuron; Abd nucleus, abducens nucleus; PPRF, paramedian pontine reticular formation. Right: Presumed brainstem neural connections from the SC to an omnipause neuron (OPN) and an inhibitory burst neuron (IBN) for generation of horizontal saccades. Open and closed neurons, excitatory and inhibitory neurons. Broken lines are speculated neural connections. A question mark indicates an unknown inhibitory interneuron that inhibits OPNs to trigger saccades. Note that the shortest excitatory and inhibitory pathways from the SC to Abd MNs are presumed to be trisynaptic and quadrисynaptic, respectively.

and medulla. EBNs for horizontal saccades are in the paramedian pontine reticular formation (PPRF), projecting to the ipsilateral abducens nucleus, and IBNs for horizontal saccades are in the paramedian pontomedullary reticular formation (PPMRF), projecting to the contralateral abducens nucleus. Accordingly, it is generally accepted that the shortest excitatory pathway from the SC to Abd MNs is trisynaptic and the shortest inhibitory pathway is quadrисynaptic via EBNs (Fuchs et al., 1985; Hepp et al., 1989; Scudder et al., 2002) (Fig. 1, right). The activities of these MLBNs are closely related to the duration and velocity of saccades (Keller, 1974). Thus, the ipsilateral EBNs provide the saccadic drive to the agonist

muscle's final common pathway, and the ipsilateral IBNs inhibit the antagonist muscle's premotor neurons on the contralateral side. However, one group of neurons was different in that they stop firing during saccades. This group of neurons shows tonic activity between saccades, and stops firing during saccades (pause neurons) (Fig. 1, left OPN) (Cohen and Henn, 1972; Keller, 1974; Luschei and Fuchs, 1972). Since most of them cease firing during saccades in all directions, they are called omnipause neurons (OPNs). OPNs are located in the nucleus raphe interpositus (RIP) (Büttner-Ennever et al., 1988; Ohgaki et al., 1987). Stimulation of the OPN area in the midline pons could prevent the occurrence of saccades in all directions during stimulation (Keller, 1977; Keller and Edelman, 1994).

The superior colliculus (SC) contains a motor map that reflects direction and size of saccades (Guitton et al., 1980; McIlwain, 1986; Robinson, 1972). The rostral SC reflects the foveal region of the retina, and contains neurons that discharge continuously during visual fixation (Munoz and Guitton, 1989, 1991; Munoz and Wurtz, 1993). Its stimulation suppresses generation of saccadic eye movements (Gandhi and Keller, 1999; Pare and Guitton, 1994). On the other hand, stimulation of the caudal SC evokes saccades directed to the contralateral side. Therefore, the rostral and caudal parts of the SC are considered to have different functions; the caudal "saccade zone" that encodes saccade generation, and the rostral "fixation zone" that encodes visual fixation. If two different systems of reciprocal functions, i.e., maintaining fixation vs. generating saccades do exist in the rostral and caudal SC, respectively, then the respective parts of the SC should have different neural connections with abducens motoneurons (Abd MNs), EBNs, IBNs and OPNs in the saccade generator of the brainstem. However, the projections from the rostral and caudal parts of the SC to brainstem saccade generators still require clarification. Robinson (1973, 1975) proposed a famous model for generation of saccades, in which he postulated two command signals in parallel; one was a saccade driving signal to oculomotor burst neurons and the other was a saccade triggering signal to OPNs (Fig. 1, right). Since then, many researchers have tried to identify inhibitory interneurons that inhibit OPNs at the onset of saccades (neuron indicated by a question mark in Fig. 1, right), but a neural substrate for triggering saccades by inhibiting OPN activity still remains controversial. To understand the neural mechanisms of generation of saccades and their suppression during visual fixation, we investigated the neural pathways from the rostral and caudal SC to Abd MNs, IBNs and OPNs in anesthetized cats by recording intracellular potentials from them. Before discussing the saccade trigger system, the detailed neural pathways from the SC to ocular motoneurons for the saccade driving system will be described first.

2 Synaptic inputs from the SC to Abd MNs and IBNs

To investigate synaptic inputs from the SCs to Abd MNs, we recorded intracellular potentials from Abd MNs and examined effects of stimulation of each SC. Abd MNs received excitation from the contralateral SC and inhibition from the ipsilateral SC

(not shown) (Izawa et al., 1999). We found that both of these excitation and inhibition were disynaptic, although these were assumed to be trisynaptic and quadrisynaptic, respectively. Medial rectus MNs received trisynaptic excitation from the ipsilateral SC via contralateral EBNs and internuclear interneurons located in the contralateral abducens nucleus (not shown). All lateralities in the present review are described with reference to the recording site. To determine the interneurons mediating disynaptic inhibition from the SC to Abd MNs, we searched for neurons in the IBN region that is located caudomedial to the abducens nucleus, and about 0.8 mm lateral to the midline (Hikosaka and Kawakami, 1977). Penetrated neurons were identified as IBNs, based on their location in the pontomedullary junction (PPMRF), antidromic activation from the contralateral abducens nucleus, and monosynaptic excitation from the contralateral caudal SC (Sugiuchi et al., 2005). Two examples of IBNs are shown in Fig. 2B (right IBN) and C (left IBN). When recordings were made from a single IBN in control, stimulation of the rostral and caudal parts of the ipsilateral SC evoked disynaptic inhibition similar to Fig. 2B 5–8, whereas stimulation of the contralateral SC evoked monosynaptic excitation similar to Fig. 2C 5–8, which usually increased as stimulation sites moved more caudally in the SC. In addition, the most rostral site in the contralateral SC was different from the more caudal sites in that stimulation of the most rostral site evoked inhibition in the IBN, which followed the preceding excitation (Fig. 2C 5). This input pattern from the contralateral SC was different from that in Abd MNs, because Abd MNs received only excitation from the contralateral entire SC (Izawa et al., 1999). To determine the pathways from the rostral and caudal SCs to IBNs, we transected the predorsal bundle on one side at the level rostral to the location of OPNs and recorded from IBNs on the either side (Fig. 2A). The transection on the contralateral side completely eliminated the disynaptic inhibition from the ipsilateral rostral and caudal SC (Fig. 2C 1–4), indicating that the disynaptic inhibition evoked by ipsilateral rostral and caudal SC stimulation was mediated via inhibitory interneurons that are located on the contralateral side. However, the same transverse section of the contralateral predorsal bundle could not eliminate contralateral SC-evoked inhibition (Fig. 2C 5), indicating that this disynaptic inhibition from the rostral SC was mediated via inhibitory interneurons located on the ipsilateral side other than IBNs (most likely OPNs). Ipsilateral IBNs can not be a candidate for this inhibition, because IBNs project only contralaterally and exert inhibitory influences on their target neurons (Sugiuchi et al., 2005; Yoshida et al., 1982).

3 Synaptic inputs from the rostral and caudal parts of the SC to OPNs

To demonstrate that disynaptic inhibition from the rostral SC to IBNs is mediated by OPNs, we recorded synaptic potentials from OPNs in the RIP (Takahashi et al., 2005). Since OPNs could not be identified by their characteristic firing pattern in our anesthetized preparation, they were identified by their antidromic activation

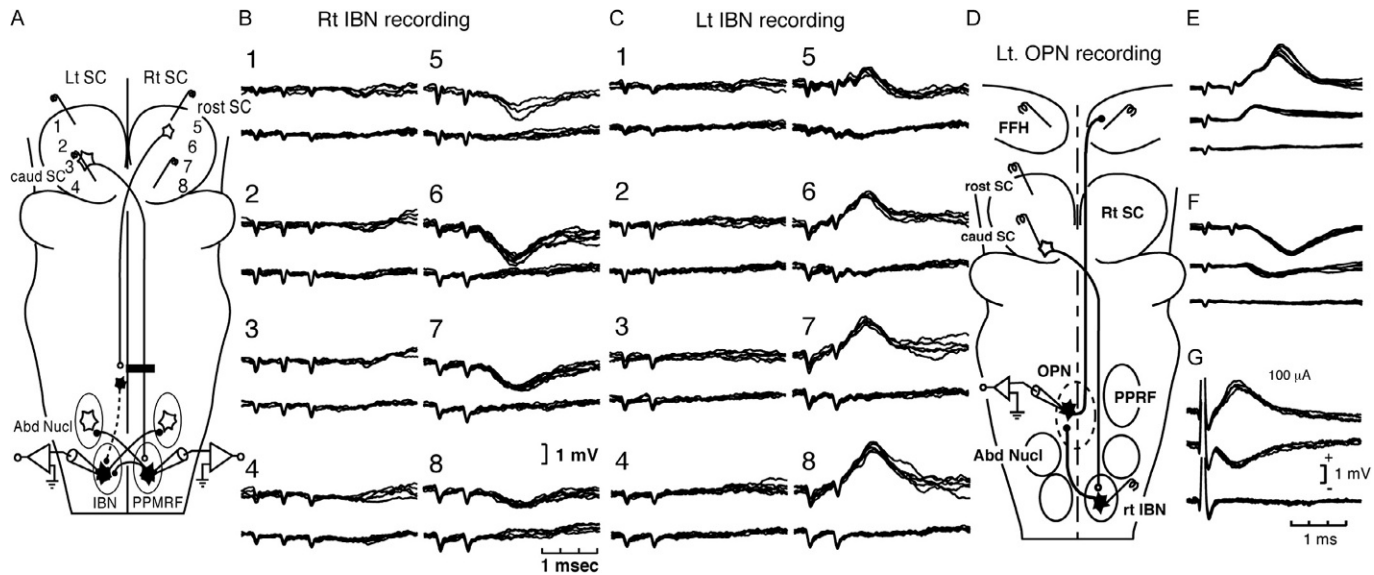


FIG. 2

Intracellular potentials recorded from IBNs during stimulation of the rostral and caudal parts of the SCs (A–C): Synaptic inputs from the bilateral SCs in a right (B) and a left IBN (C). (A) Experimental setup. (B) Synaptic inputs from the left SC (1–4) and the right SC (5–8) in the right IBN after the transverse section of the right predorsal bundle. Stimulating electrodes are arranged rostrocaudally along the horizontal meridian of the SC motor map (McIlwain, 1986). (C) Synaptic inputs from the left SC (1–4) and the right SC (5–8) stimulus sites in another left IBN in the same preparation as in B. Note all responses from 1 to 4 stimulus sites in the SC disappeared, while all responses from 5 to 8 stimulus sites remained unaffected after the lesion. Intracellular potentials recorded from left OPNs (D–G): Synaptic inputs from the SC (E and F) and the IBN region (G) to left omnipause neurons (OPNs). (D) Experimental setup. E and F: (E) Excitation evoked by stimulation of the left rostral SC, and (F) inhibition evoked by stimulation of the left caudal SC in the same left OPN. Upper and middle traces; double and single stimulation, respectively. Lower traces; juxtacellular field potentials. G: Monosynaptic inhibition (middle traces) and reversed (depolarized) inhibition after C₁⁻ injection (upper traces) evoked by stimulation of the right IBN region in another left OPN.

Panels A–C: Reproduced from Sugiuchi, Y., Izawa, Y., Takahashi, M., Na, J., Shinoda, Y., 2005. Physiological characterization of synaptic inputs to inhibitory burst neurons from the rostral and caudal superior colliculus. *J. Neurophysiol.* 93, 697–712; Panels D–G: Reproduced from Shinoda, Y., Sugiuchi, Y., Izawa, Y., Takahashi, M., 2008. Neural circuits for triggering saccades in the brainstem. In: C. Kennard and R.J. Leigh (Eds.). *Using Eye Movements as an Experimental Probe of Brain Function*, Progress in Brain Research, vol. 171, 79–85.

from the Forel's Field H (FFH) or the contralateral IBN area, or by their characteristic morphology visualized by intracellular injection of HRP, because OPNs are known to send their axons to the EBN area (PPRF), IBN area (PPMRF) and also the burst neuron area in the FFH (Ohgaki et al., 1987). Stimulation of the rostral SC evoked excitation with a monosynaptic latency in an OPN (Fig. 2E). The rather long latency is due to the fact that the conduction velocity of output neurons of the rostral SC is slower than that of the caudal SC. In contrast, stimulation of the ipsilateral caudal SC evoked disynaptic inhibition in the same cell (Fig. 2F). The reason why this inhibition is disynaptic is that inhibitory interneurons must intervene between the SC and the OPN, because output neurons of the caudal SC are excitatory. Since output fibers in the predorsal bundle from the contralateral SC are known to terminate extensively on IBNs (Langer and Kaneko, 1990; Strassman et al., 1987), the IBN area on the contralateral side was stimulated at 100 µA, and inhibition was evoked at a monosynaptic latency in the same OPN (Fig. 2G). These results together with the transection experiment of the predorsal bundle indicate that OPNs receive monosynaptic excitatory input from the rostral SC and disynaptic inhibition from the contralateral caudal SC via contralateral IBNs.

In summary, the present analysis of the brainstem neural connections between the SC and horizontal premotor neurons showed that OPNs that project to the burst premotor neurons are monosynaptically excited by the rostral SC, and are disynaptically inhibited via IBNs by the caudal SC. In contrast, IBNs are excited monosynaptically by the contralateral caudal SC, and inhibited disynaptically by the ipsilateral caudal SC via contralateral IBNs, and additionally inhibited disynaptically by the rostral SC via OPNs.

4 Discussion

Our studies reveal the brainstem circuits from the rostral and caudal parts of the SCs to Abd MNs, EBNs, IBNs, and OPNs. Two important questions concerning the physiological properties of OPNs remained controversial in fixation and saccade. As to the first question: which excitatory neurons maintain sustained activity of OPNs during steady visual fixation?, we determined output neurons in the rostral SC as a responsible source for tonic excitation of OPNs, because OPNs receive monosynaptic excitation only from the rostral parts of the SCs where tonically active neurons during fixation are located. These neurons are called fixation neurons (Munoz and Guitton, 1989, 1991; Munoz and Wurtz, 1993) or microsaccade neurons (see Krauzlis et al., 2017). These two kinds of neurons are located in the most rostral part of the SC, tonically active during fixation and stop firing during large-amplitude saccades. In addition to these properties, microsaccade neurons show firing during contralateral microsaccades. Therefore, although it is often accepted that these two regions in the SC have different functions; the caudal "saccade zone" that encodes saccade generation, and the rostral "fixation zone" that encodes visual fixation, it is

proposed that even the most rostral zone is only an extension of the caudal saccade zone (see [Krauzlis et al., 2017](#)). Our experimental condition in anesthetized preparations could not determine whether these two groups of neurons exist or not. But our data can only conclude that the most rostral SC output neurons, not the more caudal SC neurons, exert excitation in OPNs. The rostral SC neurons most likely receive inputs from the “suppression area” of the FEF, because neurons there are tonically active during fixation and stop firing during saccades, and are known to project to the rostral part of the SC ([Izawa et al., 2004](#)). Furthermore, stimulation of the FEF “suppression area” suppresses saccade initiation, which is very similar to the rostral SC whose stimulation suppresses generation of saccades in both directions ([Pare and Guitton, 1994](#)).

As to the second question; which inhibitory neurons suppress activity of OPNs? Our result showed that IBNs inhibit OPNs at the onset of saccades. As shown in [Fig. 1](#) right, Robinson proposed two parallel pathways for triggering saccades and driving saccades. However, he did not indicate the origin of a triggering signal but the existence of a triggering signal that inhibits OPNs. Since then, many researchers tried to identify the location of interneurons to inhibit OPNs. Our data show that IBNs inhibit OPNs by mediating a saccade drive signal from the caudal SC. Accordingly, there is no need to postulate the origin of a triggering signal in the SC. IBNs were not considered to be such a candidate for inhibiting OPNs as a triggering signal, but for a latch signal during saccades. Single unit recordings have demonstrated that the pause of OPNs starts just before MLBNs begin firing ([Keller, 1974](#); [Yoshida et al., 1999](#)). Since IBNs were speculated to be activated trisynaptically from the SC, IBNs were not considered to be such a candidate ([Yoshida et al., 2002](#)). However, our data have shown that IBNs are activated monosynaptically from the SC, and IBNs terminate on OPNs directly. Previous morphological data could not support the existence of the projection from IBNs to the OPN area ([Strassman et al., 1986](#); [Yoshida et al., 1982](#)). Our data suggest possible roles of IBNs that may trigger saccades by actively inhibiting the tonic activity of OPNs at the onset of saccades and also maintain saccades by continuously inhibiting OPN activity during saccades. Recently, the brainstem neural circuits for vertical saccades were identified from the SC to vertical ocular motoneurons (see the details in [Takahashi and Shinoda, 2018](#)). Vertical IBNs are found in the interstitial nucleus of Cajal ([Sugiuchi et al., 2013](#)), but the relation of IBNs and OPNs remains undetermined in the vertical saccade system.

To examine the functional role of OPNs, [Kaneko \(1996\)](#) made a lesion in the OPN area (the nucleus raphe interpositus), and found that the peak velocity of saccades was decreased without a delay of saccade onset. This finding suggests that they must also contribute to the saccade drive signal. The slow saccades suggest that the RIP lesion makes the firing rate of the EBNs and IBNs smaller. Thus, Miura and Optican thought that this experimental finding gives a clue to the sources of the currents that form the activity of EBNs, which, in turn, determines the dynamics of saccades. So, Miura and Optican, by extending their dynamic model

(Miura and Optican, 2003), constructed a conductance-based model of EBNs and simulated saccades using a simple lumped model with two EBN units (Miura and Optican, 2006). Their simulation indicated that the inclusion of the T-type Ca^{++} channel in the model of EBNs can reproduce the saccade slowing following OPN lesion/inactivation, because the T-current is reduced after OPN inactivation. Thus, they propose that the reduction in T-current may be one of the causes of saccade slowing seen after OPN lesion/ inactivation. In relation to this simulation model, our data of the neural circuits suggest that output neurons in the most rostral part of the SC, which are tonically firing during fixation, stop firing at the onset of saccade, so that OPNs that receive tonic input from these SC neurons must decrease firing. At the same time, such OPNs receive strong inhibition from IBNs, and their activities are quickly shut down. The tonic inhibition of EBNs and IBNs by OPNs during fixation hyperpolarizes the membrane potentials of the MLBNs, and prevents inactivation of the T-type Ca^{++} channel. At the onset of saccades, quick decrease of this tonic hyperpolarization caused by quick shutdown of OPN firing activates T-type Ca^{++} currents, and quick excitatory input from the caudal SC simultaneously depolarizes the membrane potentials to causes strong burst spike activity in the MLBNs. Although the properties of neural circuits related to saccade generation have been the primary focus so far (Fig. 1, right), the combination of biophysical membrane properties of MLBNs and the output of OPNs may play an important role in determining the size of the velocity command for saccades. The direct experimental evidence is required to support the existence of T-type Ca^{++} currents in MLBNs.

Conflicts of Interest

The authors declare no conflicts of interest.

References

- Büttner-Ennever, J.A., Cohen, B., Pause, M., Fries, W., 1988. Raphe nucleus of the pons containing omnipause neurons of the oculomotor system in the monkey, and its homologue in man. *J. Comp. Neurol.* 267, 307–321.
- Cohen, B., Henn, V., 1972. Unit activity in the pontine reticular formation associated with eye movements. *Brain Res.* 46, 403–410.
- Fuchs, A.F., Kaneko, C.R., Scudder, C.A., 1985. Brainstem control of saccadic eye movements. *Ann. Rev. Neurosci.* 8, 307–337.
- Gandhi, N.J., Keller, E.L., 1999. Comparison of saccades perturbed by stimulation of the rostral superior colliculus, the caudal superior colliculus, and the omnipause neuron region. *J. Neurophysiol.* 82, 3236–3253.
- Guitton, D., Crommelinck, M., Roucoux, A., 1980. Stimulation of the superior colliculus in the alert cat. I. Eye movements and neck EMG activity evoked when the head is restrained. *Exp. Brain Res.* 39, 63–73.

- Hepp, K., Henn, V., Vilis, T., Cohen, B., 1989. Brainstem regions related to saccade generation. In: Wurtz, R.H., Goldberg, M.E. (Eds.), *The Neurobiology of Saccadic Eye Movements, Reviews of Oculomotor Research. vol. III*. Elsevier, Amsterdam, pp. 105–212.
- Hikosaka, O., Kawakami, T., 1977. Inhibitory reticular neurons related to the quick phase of vestibular nystagmus—their location and projection. *Exp. Brain Res.* 27, 377–396.
- Izawa, Y., Sugiuchi, Y., Shinoda, Y., 1999. Neural organization from the superior colliculus to motoneurons in the horizontal oculomotor system of the cat. *J. Neurophysiol.* 81, 2597–2611.
- Izawa, Y., Suzuki, H., Shinoda, Y., 2004. Suppression of visually and memory-guided saccades induced by electrical stimulation of the monkey frontal eye field. II. Suppression of bilateral saccades. *J. Neurophysiol.* 92, 2261–2273.
- Kaneko, C.R., 1996. Effect of ibotenic acid lesions of the omnipause neurons on saccadic eye movements in rhesus macaques. *J. Neurophysiol.* 75, 2229–2242.
- Keller, E.L., 1974. Participation of medial pontine reticular formation in eye movement generation in monkey. *J. Neurophysiol.* 37, 316–332.
- Keller, E.L., 1977. Control of saccadic eye movements by midline brain stem neurons. In: Baker, R., Bethoz, A. (Eds.), *Control of Gaze by Brain Stem Neurons*. Elsevier, Amsterdam, pp. 2327–2336.
- Keller, E.L., Edelman, J.A., 1994. Use of interrupted saccade paradigm to study spatial and temporal dynamics of saccadic burst cells in superior colliculus in monkey. *J. Neurophysiol.* 72, 2754–2770.
- Krauzlis, R.J., Goffart, L., Hafed, Z.M., 2017. Neuronal control of fixation and fixational eye movements. *Philos. Trans. R. Soc. Lond. B Biol. Sci.* 372, 20160205.
- Langer, T.P., Kaneko, C.R., 1990. Brainstem afferents to the oculomotor omnipause neurons in monkey. *J. Comp. Neurol.* 295, 413–427.
- Leigh, R.J., Zee, D.S., 2015. *The Neurology of Eye Movements*. Oxford, New York.
- Luschei, E.S., Fuchs, A.F., 1972. Activity of brain stem neurons during eye movements of alert monkeys. *J. Neurophysiol.* 35, 445–461.
- Mellwain, J.T., 1986. Effects of eye position on saccades evoked electrically from superior colliculus of alert cats. *J. Neurophysiol.* 55, 97–112.
- Miura, K., Optican, L.M., 2003. Membrane properties of medium-lead burst neurons may contribute to dynamical properties of saccades. In: Proceedings of the 1st International IEEE EMBS Conference on Neural Engineering, pp. 20–23.
- Miura, K., Optican, L.M., 2006. Membrane channel properties of premotor excitatory burst neurons may underlie saccade slowing after lesions of omnipause neurons. *J. Comput. Neurosci.* 20, 25–41.
- Munoz, D.P., Guitton, D., 1989. Fixation and orientation control by the tecto-reticulo-spinal system in the cat whose head is unrestrained. *Rev. Neurol. (Paris)* 145, 567–579.
- Munoz, D.P., Guitton, D., 1991. Control of orienting gaze shifts by the tectoreticulospinal system in the head-free cat. II. Sustained discharges during motor preparation and fixation. *J. Neurophysiol.* 66, 1624–1641.
- Munoz, D.P., Wurtz, R.H., 1993. Fixation cells in monkey superior colliculus. I. Characteristics of cell discharge. *J. Neurophysiol.* 70, 559–575.
- Ohgaki, T., Curthoys, I.S., Markham, C.H., 1987. Anatomy of physiologically identified eye-movement-related pause neurons in the cat: pontomedullary region. *J. Comp. Neurol.* 266, 56–72.

- Pare, M., Guittot, D., 1994. The fixation area of the cat superior colliculus: effects of electrical stimulation and direct connection with brainstem omnipause neurons. *Exp. Brain Res.* 101, 109–122.
- Robinson, D.A., 1972. Eye movements evoked by collicular stimulation in the alert monkey. *Vision Res.* 12, 1795–1808.
- Robinson, D.A., 1973. Models of the saccadic eye movement control system. *Kybernetik* 14, 71–83.
- Robinson, D.A., 1975. Oculomotor control signals. In: Lennerstrand, G., Bach-y-Rita, P. (Eds.), *Basic Mechanisms of Ocular Motility and Their Clinical Implications*. Pergamon Press, Oxford, pp. 337–374.
- Scudder, C.A., Kaneko, C.S., Fuchs, A.F., 2002. The brainstem burst generator for saccadic eye movements: a modern synthesis. *Exp. Brain Res.* 142, 439–462.
- Strassman, A., Highstein, S.M., McCrea, R.A., 1986. Anatomy and physiology of saccadic burst neurons in the alert squirrel monkey. II. Inhibitory burst neurons. *J. Comp. Neurol.* 249, 358–380.
- Strassman, A., Evinger, C., McCrea, R.A., Baker, R.G., Highstein, S.M., 1987. Anatomy and physiology of intracellularly labelled omnipause neurons in the cat and squirrel monkey. *Exp. Brain Res.* 67, 436–440.
- Sugiuchi, Y., Izawa, Y., Takahashi, M., Na, J., Shinoda, Y., 2005. Physiological characterization of synaptic inputs to inhibitory burst neurons from the rostral and caudal superior colliculus. *J. Neurophysiol.* 93, 697–712.
- Sugiuchi, Y., Takahashi, M., Shinoda, Y., 2013. Input-output organization of inhibitory neurons in the interstitial nucleus of Cajal projecting to the contralateral trochlear and oculomotor nucleus. *J. Neurophysiol.* 110, 640–657.
- Takahashi, M., Shinoda, Y., 2018. Brain stem neural circuits of horizontal and vertical saccade systems and their frame of reference. *Neuroscience* 392, 281–328.
- Takahashi, M., Sugiuchi, Y., Izawa, Y., Shinoda, Y., 2005. Synaptic inputs and their pathways from fixation and saccade zones of the superior colliculus to inhibitory burst neurons. *Ann. N. Y. Acad. Sci.* 1039, 209–219.
- Yoshida, K., McCrea, R.A., Berthoz, A., Vidal, P.P., 1982. Morphological and physiological characteristics of inhibitory burst neurons controlling horizontal rapid eye movements in the alert cat. *J. Neurophysiol.* 48, 761–784.
- Yoshida, K., Iwamoto, Y., Chimoto, S., Shimazu, H., 1999. Saccade-related inhibitory input to pontine omnipause neurons: an intracellular study in alert cats. *J. Neurophysiol.* 82, 1198–1208.
- Yoshida, K., Iwamoto, Y., Chimoto, S., Shimazu, H., 2002. Disynaptic inhibition of omnipause neurons following electrical stimulation of the superior colliculus in alert cats. *J. Neurophysiol.* 85, 2639–2642.

7

Morphological and electrophysiological characteristics of the commissural system in the superior colliculi for control of eye movements

Mayu Takahashi*

Department of Systems Neurophysiology, Graduate School of Medicine, Tokyo Medical and Dental University, Tokyo, Japan

*Corresponding author: Tel.: +81-3-5803-5155; Fax: +81-3-5803-5155,
e-mail address: takahashi.phy1@tmd.ac.jp

Abstract

Commissural connections between the superior colliculi (SCs) were well known anatomically, and assumed to be only inhibitory in relation to visual inputs. However, by recording intracellular potentials, we revealed that a strong monosynaptic excitatory commissural connection exists between the rostral SCs of the cat. Commissural excitation existed between the medial-medial or lateral-lateral parts of both SCs, while commissural inhibition existed between the medial SC on one side and the lateral SC on the opposite side. These commissural excitation and inhibition were also confirmed morphologically with the double-labeling method of HRP-conjugated gold particle and GABA. Similarity of the topography of commissural inhibition between the SC system and the vestibuloocular system supported the conclusion that the saccadic eye movement system uses the same semicircular canal coordinate as the vestibuloocular system. The commissural excitation may help to maintain Listing's law in saccadic eye movements.

Keywords

Superior colliculus, Saccade, VOR, Commissural connection, Listing's law, Vertical eye movement, Sprague effect, Forel's field H

1 Introduction

The anatomical commissural connection between the two superior colliculi (SCs) has been well known (Behan and Kime, 1996; Edwards, 1977; Fish et al., 1982; Magalhães-Castro et al., 1978; Moschovakis and Karabelas, 1985), and was considered to be mainly inhibitory (Hoffman and Straschill, 1971; Maeda et al., 1979). This commissural inhibition was originally thought to mediate the “Sprague effect,” because cats that received unilateral lesions in the visual cortex recovered from the contralateral hemianopsia in response to either ablation of the SC opposite the cortical lesion or transection of the collicular commissure (Sprague, 1966). Many anatomical and behavioral studies on the collicular commissural connections have been devoted to showing the neural mechanism of the Sprague effect. However, more recent studies have shown that this Sprague effect is mediated by a pathway other than intrinsic collicular commissural neurons (CNs), because transection of the rostral commissure in the SC, where fibers of the intrinsic collicular CNs are known to run, produced no effect, whereas transection of the caudal commissure produced the Sprague effect (Wallace et al., 1989). The other basis of support for the Sprague effect, the idea that the commissural projection is purely inhibitory, has also been shown to be incorrect. Anatomical studies have shown that about one-half of the characterized tectotectal projection is gamma-aminobutyric acid (GABA)-positive, and the other half is glutamatergic (Appell and Behan, 1990; Olivier et al., 2000). This ran counter to earlier physiological studies that suggested that the projection was only inhibitory.

Tectal output neurons related to saccadic eye movements were inhibited during ipsiversive orienting movements or by electrical stimulation of the contralateral SC (Munoz and Istvan, 1998). Maeda et al. (1979) first demonstrated the existence of commissural monosynaptic inhibitory postsynaptic potentials (IPSPs) by intracellular recordings from tectal neurons. Consistent with these physiological observations, Appell and Behan (1990) found that commissural cells constitute a major source of GABAergic projection to the contralateral SC in the cat. On the other hand, stimulation of the contralateral SC sometimes evoked very tiny monosynaptic EPSPs followed by larger monosynaptic IPSPs in tectal neurons (Maeda et al., 1981), suggesting that there is an excitatory component of the tectotectal pathway. More recently, Takahashi et al. (2005) found very strong monosynaptic commissural excitation mainly in rostral tectoreticular neurons (TRNs) that projected to the Forel’s Field H (FFH) where burst neurons of vertical saccades are located. How these inhibitory and excitatory commissural connections are organized in the bilateral SCs is very important, because it will be a key to understand the functional relationship between the medial upward saccade system and the lateral downward system in each SC. The spatial distribution of CNs and their terminals in the SC has been examined anatomically. Tectotectal connections are generally restricted to the rostral half of the SC, but their projections show diverse patterns (Edwards, 1977; Fish et al., 1982; Magalhães-Castro et al., 1978). Intracellularly-labeled neurons showed that labeled axons and terminals of individual neurons were widely

spread in the contralateral SC, and some of them (“T-cells”) sent their main axons to the predorsal bundle (PDB) and the ventral ascending tract in the cat (Grantyn, 1988; Moschovakis and Karabelas, 1985) and the monkey (Moschovakis et al., 1988a,b). Previous anatomical studies have shown the laminar location and rostrocaudal distribution of commissural neurons, but no detailed data are available to show the correlation between this laminar arrangement and the topographical distribution of excitatory and inhibitory commissural neurons in the SC, and their connections with output TRNs in the SC. Since this information is required to understand the functional roles of excitatory and inhibitory CNs in eye movement control, a series of electrophysiological and morphological studies were performed to determine SC commissural effects on TRNs that project to last-order premotor neurons for saccades in the brainstem with intracellular recording and their underlying neural correlates morphologically (Takahashi et al., 2005, 2007, 2010, 2011).

2 Methods

Experiments were performed in 14 anesthetized cats weighing 2.5–5.0 kg. The experimental arrangements for electrophysiological studies were described in detail previously (Takahashi et al., 2005, 2007). Briefly, four concentric bipolar stimulating electrodes (ID and OD, 0.1 and 0.3 mm, respectively; interelectrode distance along the longitudinal axis, 1.0 mm) with a 1.0–1.2 mm rostrocaudal separation were placed along the presumed horizontal meridian of the motor map in the SC on the right side (McIlwain, 1986). The tips of the SC electrodes were positioned in the intermediate or deep layer (1.5–2.0 mm from the surface) of the SC. For antidromic activation of TRNs projecting to the FFH region and PDB, an array of two concentric bipolar electrodes was stereotactically placed on each side in the FFH (A: 7.0–7.5, L: 1.0, 2.5), and separate electrode arrays were placed in the right PDB contralateral to the recording site in the SC (Takahashi et al., 2005, 2007). The protocols of anatomical works were the same as those described in detail (Takahashi et al., 2010). In cases that were used for double labeling, injections of WGA conjugated to apo-HRP conjugated to gold particles (GPs) (15-nm particle size, E-Y Laboratories) was injected into the left SC (Lee et al., 2001). The survival period after the GP injection was 7–28 days. To examine whether GP-labeled CNs were inhibitory or excitatory, sections with GP-labeled CNs were treated for GABA immunohistochemistry.

3 Results

To examine the patterns of input from the contralateral SC to TRNs, intracellular recordings were made from a TRN, while stimulating the medial or lateral part of the contralateral SC. Fig. 1(A–C) shows an example of intracellular records in a medial TRN of the rostral SC. In this medial TRN, antidromic spikes were evoked by

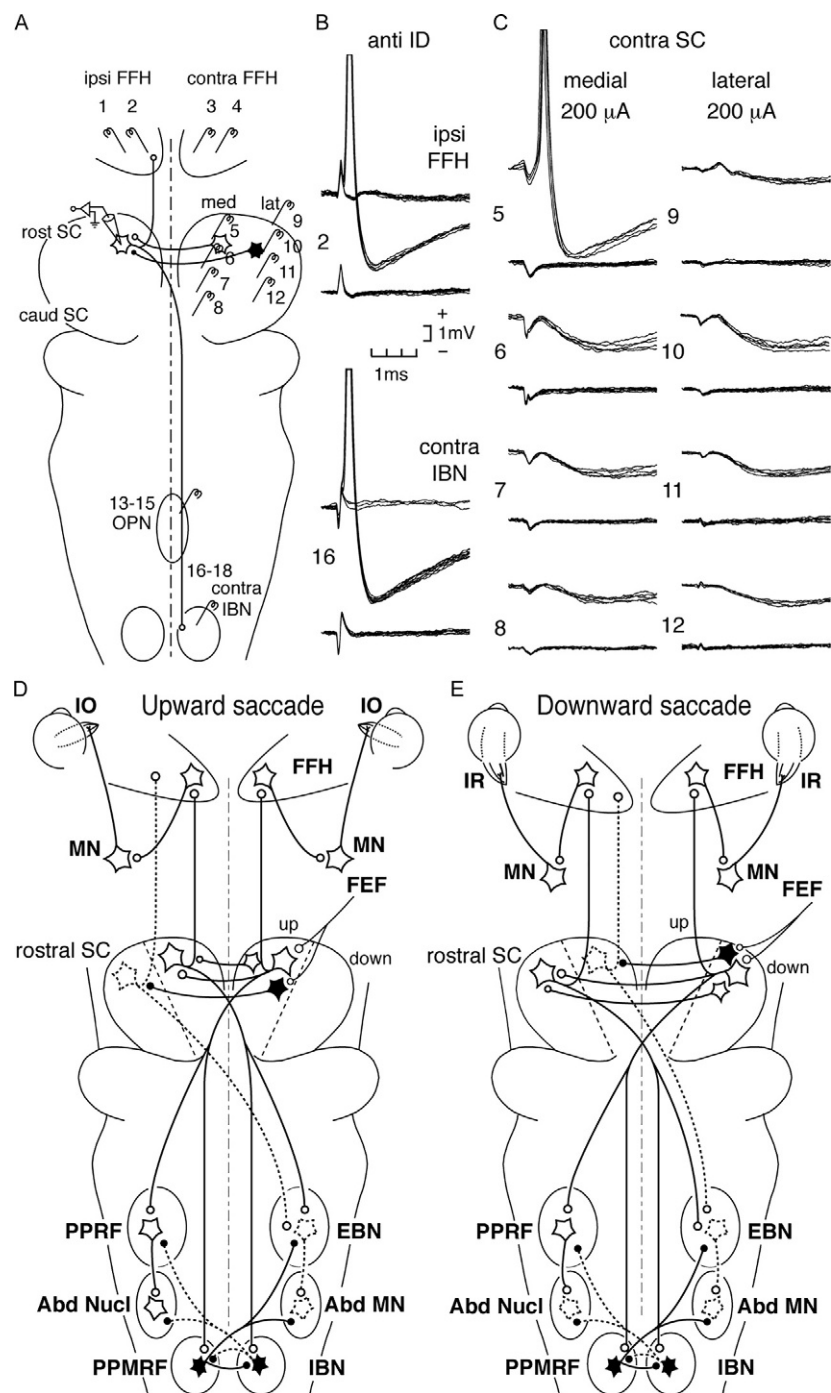


FIG. 1

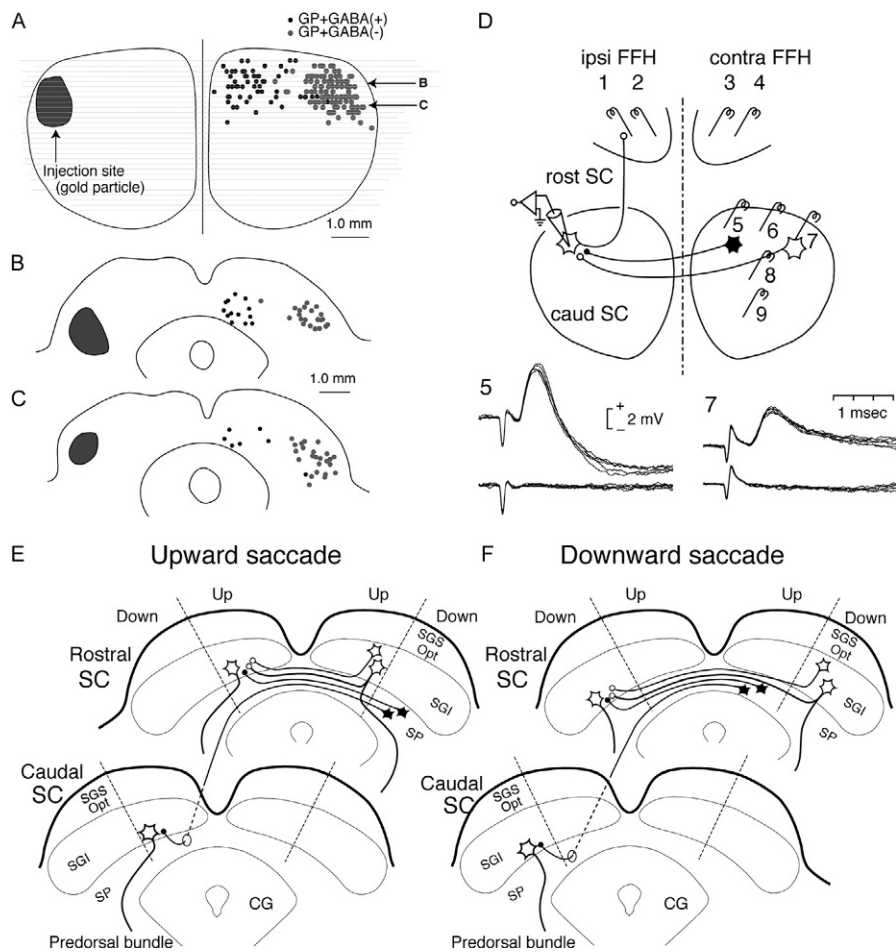
See legend on opposite page.

stimulation of the ipsilateral FFH (Fig. 1B, site 2) and the contralateral inhibitory burst neuron (IBN) area (Fig. 1B, site 16), indicating that this neuron is a SC output neuron that projects to the burst neuron area and is related to saccadic eye movements. The strong excitation was evoked only from the rostromedial part of the contralateral SC (Fig. 1C, site 5). In contrast, the commissural inhibition was evoked from the entire contralateral SC (Fig. 1C, sites 6–12), but the inhibition evoked by stimulation of the medial SC (sites 6–8) was due to activation of the passing fibers of inhibitory CNs located in the lateral SC. In a lateral TRN of the rostral SC, stimulation of the lateral SC on the contralateral side (site 7 in Fig. 2D) evoked pure excitation, while stimulation of the medial SC on the contralateral side evoked excitation followed by inhibition (site 5 in Fig. 2D). This medial excitation was due to activation of the passing fibers of lateral excitatory CNs, because the onset of this excitation was slightly shorter than that of the lateral SC. The later inhibition was not disynaptic but monosynaptic from the contralateral SC, because the inhibitory CNs were small and their axonal conduction velocity was slow. These electrophysiological results are summarized in Fig. 1D and E. Excitatory commissural connection existed between the medial and medial (D), or lateral and lateral parts of the two rostral SCs (E), while inhibitory commissural connection existed from the medial to the lateral (D), or from the lateral to the medial parts of the SCs (E). These excitatory and inhibitory commissural effects were exerted on TRNs that projected to horizontal burst neurons in the paramedian pontine reticular formation

FIG. 1

(A–C): Properties of commissural inputs from the medial and lateral parts of the contralateral superior colliculus (SC) to a tectoreticular neuron (TRN) in the medial part of the rostral SC (A–C). (A) Experimental setup. Intracellular potentials were recorded from a TRN in the medial part of the left rostral SC. (B) Antidromic spikes of the TRN evoked in an all-or-none manner at threshold by stimulation of the ipsilateral field of Forel H (FFH) (site 2) and the contralateral inhibitory burst neuron (IBN) area (site 16) at $500\mu A$. (C) Properties of EPSPs and IPSPs evoked by stimulation of the medial (sites 5–8) and lateral parts (sites 9–12) of the contralateral SC at $200\mu A$ in the same TRN as in (B). (D, E) Summary diagrams of commissural excitation and inhibition for upward (D) and downward saccades (E). (D) Upward oblique or pure upward saccades. (E) Downward oblique or pure downward saccades. Open and filled neurons indicate excitatory and inhibitory neurons, respectively. Solid and broken lines indicate excited and suppressed pathways, respectively. *Abd MN*, abducens motoneuron; *Abd Nucl*, abducens nucleus; *EBN*, excitatory burst neuron; *FEF*, frontal eye field; *FFH*, field of Forel H; *IBN*, inhibitory burst neuron; *IO*, inferior oblique muscle; *IR*, inferior rectus muscle; *MN*, motoneuron; *PPMRF*, paramedian pontomedullary reticular formation; *PPRF*, paramedian pontine reticular formation

Panels (A–E): From Takahashi, M., Sugiuchi, Y., Shinoda, Y., 2007. Commissural mirror-symmetric excitation and reciprocal inhibition between the two superior colliculi and their roles in vertical and horizontal eye movements. J. Neurophysiol. 98, 2664–2682.

**FIG. 2**

(A–C): Tectal distribution of GABA-positive and GABA-negative commissural neurons (CNs) that projected to the lateral part of the opposite rostral SC (unpublished data). (A) Dorsal view of the site of a gold particle (GP) injection into the lateral part of the left rostral SC and the distribution of retrogradely labeled neurons in the right SC. GP solution (1 track, total 0.7 μ L) was injected into the rostralateral SC (1.6–1.8 mm deep from the surface). Survival time, 20 days. In (A–C), black dots indicate single CNs that were double-labeled with GP and GABA (GABA-positive CNs) (their soma areas smaller than $200 \mu\text{m}^2$), and gray dots represent neurons that were single-labeled with GP (GABA-negative CNs) (their soma areas larger than $200 \mu\text{m}^2$). (B, C) Distribution of labeled CNs in representative frontal planes at the levels indicated as (B) and (C) in (A). (D) Commissural inputs to a TRN in the lateral part of the rostral SC from the medial and the lateral part of the opposite rostral SC. Experimental setup (upper drawing). Intracellular records from a rostralateral TRN during stimulation of the medial (site 5) and lateral (site 7) of the opposite rostral SC at 200 μ A. Note that lateral

(PPRF) or vertical burst neurons in the rostral interstitial nucleus of medial longitudinal fasciculus (riMLF) or both (Takahashi et al., 2005, 2007).

To examine morphologically the distribution of excitatory and inhibitory CNs in the SC, we injected WGA conjugated to apo-HRP conjugated to gold particles (GPs) into the lateral part of the left SC to label CNs in the opposite SC, and performed double staining with GABA to identify whether the labeled CNs were either GABAergic or not (Fig. 2A). An injection of GP into the SC showed that the retrogradely stained CNs were located only in the rostral part of the contralateral SC. Only CNs with small soma area ($<200\mu\text{m}^2$) were labeled by an injection of GP into the caudal SC, while both CNs with small and larger soma areas ($>200\mu\text{m}^2$) were labeled by its injection into the rostral SC. Within this area, double stained CNs were restricted to the medial part of the right SC, and labeled neurons only with GP were restricted to the lateral part of the right SC (Fig. 2A). These two groups of the stained CNs were segregated in the mediolateral direction; the two groups were almost segregated approximately at the presumed horizontal meridian of the motor map (McIlwain, 1986) (Fig. 2A). In the dorsoventral direction, double-labeled neurons were located in the deeper layer (layer VI), whereas single-labeled neurons were located in the more superficial layer (layer IV) (Fig. 2B and C). These results indicate that the GABAergic CNs in the medial SC projected to the opposite lateral SC, and non-GABAergic CNs in the lateral SC projected to the opposite lateral SC (Fig. 2A–C). These anatomical findings fit very well with the electrophysiological data as mentioned about Fig. 2D in that lateral TRNs receive excitation and inhibition from the lateral and the medial SC on the opposite side, respectively. In a similar way, the distribution of GABAergic and non-GABAergic CNs was examined after an injection of GP into the rostromedial part of the SC. GABAergic CNs were mainly observed in the lateral SC, whereas non-GABAergic CNs were more abundantly observed in the medial SC on the contralateral side (not shown). The summary of the obtained morphological data is shown in Fig. 2E and F. GABAergic inhibitory CNs were small (their soma areas were $<200\mu\text{m}^2$) and located in the deeper layers (filled neurons in Fig. 2E and F), whereas non-GABAergic excitatory CNs (open neurons) were larger and located in layer IV with two types (one is a pure CN, and the other a TRN with a commissural collateral) (Takahashi et al., 2010).

stimulation mainly evoked excitation, but medial stimulation evoked excitation followed by inhibition. (E, F) Summary diagrams of excitatory and inhibitory CNs in the medial and lateral parts of the SC for upward (E) and downward saccades (F). Filled neurons, small GABAergic inhibitory neurons; open neurons, small, medium-sized and large excitatory neurons. CG, central gray; SGI, stratum griseum intermedium; SGS, stratum griseum superficiale; SO, stratum opticum; SP, stratum griseum and album profundum.

Panels (D–F): From Takahashi, M., Sugiuchi, Y., Shinoda, Y., 2010. Topographic organization of excitatory and inhibitory commissural connections in the superior colliculi and their functional roles in saccade generation. J. Neurophysiol. 104, 3146–3167.

In summary, for the upward saccade system, TRNs in the medial SC (upward saccade representing area) receive excitation from the contralateral medial SC (upward saccade representing area) and inhibition from the lateral SC (downward saccade representing area), whereas TRNs in the lateral SC receive excitation from the contralateral lateral SC and inhibition from the contralateral medial SC.

4 Discussion

Our study showed that CNs could be classified into two types: those that project mainly to the rostral part of the contralateral SC and those that project to the entire rostrocaudal extent of the contralateral SC (Takahashi et al., 2005, 2010). The former is excitatory and the latter is inhibitory, because monosynaptic commissural excitation was recorded only from TRNs in the rostral SC and monosynaptic inhibition was recorded from TRNs in the entire rostrocaudal extent of the SC. Many rostral CNs have axon collaterals spreading rostrocaudally in the contralateral SC, and these CNs are considered to be inhibitory. Other CNs have only collaterals terminating in the rostral SC, and these CNs are considered to be excitatory (Takahashi et al., 2005). We investigated how tectotectal commissural excitation and inhibition are distributed with respect to the mediolateral dimension of the SC (Takahashi et al., 2007), because the medial and lateral halves of the SC represent saccades into the upper and the lower visual field, respectively. In summary of electrophysiological studies, rostromedial TRNs receive commissural inhibition from the lateral SC and commissural excitation from the medial SC on the opposite side, whereas rostralateral TRNs receive commissural inhibition from the medial SC and commissural excitation from the lateral SC on the opposite side. However, caudal TRNs do not receive commissural excitation and receive only commissural inhibition from the contralateral SC. This commissural inhibition is responsible for reciprocity of right and left horizontal saccadic eye movement systems, because TRNs in the caudal SC are mainly involved in horizontal saccades.

Morphological study further characterized the SC commissural excitation and inhibition (Takahashi et al., 2010). An injection of WGA-HRP into the lateral or medial SC retrogradely labeled many larger neurons (GABA negative neurons) in the lateral or medial part of the contralateral SC, respectively. In contrast, a WGA-HRP injection into the lateral or medial SC retrogradely labeled small neurons (GABA positive neurons) in the medial or lateral part of the contralateral rostral SC, respectively. These results indicate that excitatory commissural connections exist between the medial and medial parts or between the lateral and lateral parts of the rostral SCs. It is generally assumed that the point-to-point mirror-symmetric commissural connections exist between the two SCs (Behan and Kime, 1996; Edwards, 1977; Fish et al., 1982), but this statement is an oversimplification and only true for excitatory commissural connections, because mirror-symmetric relationship did not exist for inhibitory commissural connections between the homonymous parts

of the rostral SCs; instead, the reciprocal inhibitory commissural connections existed between the lateral part of one SC and the medial part of the other SC. In favor of this point-to-point mirror-symmetric excitatory connection, some TRNs in the lateral SC have a commissural collateral to the lateral part of the contralateral SC and another TRNs in the medial SC have a commissural collateral to the medial part of the contralateral SC. Accordingly, when a pure vertical upward (downward) saccade occurs, TRNs in the medial (lateral) parts of the two SCs will be excited simultaneously by commissural excitation and TRNs in the lateral (medial) parts of the two SCs will be suppressed simultaneously by tectal commissural inhibition. As a consequence, the upward and downward saccadic systems appear to be reciprocal. However, the reciprocal commissural inhibition between the lateral and medial parts of the two SCs implies that the medial region representing upward torsional saccades inhibits the contralateral lateral region representing downward torsional saccades and vice versa. Therefore, this commissural inhibition between the SCs gives evidence that the upward torsional saccade system on one side and the downward torsional saccade system on the opposite side are mutually inhibited (antagonistic), and are the basic structure of reciprocity for vertical saccades (Takahashi and Shinoda, 2018). This pattern of commissural reciprocal inhibitions between upward saccade system on one side and downward system on the other is similar to the pattern of commissural reciprocal inhibitions between the anterior canal system on one side and the posterior canal system on the other for vestibuloocular reflex (VOR). In the VOR, such commissural reciprocal inhibition existed between the bilateral vestibular nuclei (Shimazu and Precht, 1966). Comparing the well-known vestibuloocular pathways with our findings of commissural inhibition between both superior colliculi, we proposed that the saccade system uses the same frame of reference as the vestibuloocular system, common semicircular canal coordinate. In spite of using the semicircular coordinate, the saccadic eye movement system must still hold Listing's law; saccades from the primary position do not have torsional components around the visual axis and have only vertical and horizontal components (Helmholtz, 1867). The present proposed circuit suggests that activation of the rostral-lateral SC on the right side directly produces downward and clockwise torsional eye movements (from the point of view of the subject), and activation of the rostral-lateral SC on the left side produces downward and counterclockwise eye movements (Takahashi and Shinoda, 2018; Takahashi et al., 2011). During vertical downward saccades, coactivation of TRNs in mirror-symmetric rostral-lateral locations of the two SCs might occur through the tectal commissural excitatory connections, so that the torsional components of individual eyes, which are induced in opposite directions by the two SCs, seem to cancel each other, leaving mainly vertical components of saccades. Similar coactivation of TRNs in the mirror-symmetric rostromedial SCs on both sides might occur during vertical upward saccades. These tectotectal commissural functions may seem to minimize torsional movements of eyes and help to maintain Listing's law in the saccade system. Future experiments to test this hypothesis are required to see what would be the effects of a lesion damaging a part of this commissural excitatory connection on vertical saccades.

References

- Appell, P.P., Behan, M., 1990. Sources of subcortical GABAergic projections to the superior colliculus in the cat. *J. Comp. Neurol.* 302, 143–158.
- Behan, M., Kime, N.M., 1996. Spatial distribution of tectotectal connections in the cat. *Prog. Brain Res.* 112, 131–142.
- Edwards, S.B., 1977. The commissural projection of the superior colliculus in the cat. *J. Comp. Neurol.* 173, 23–40.
- Fish, S., Goodman, D.K., Kuo, D.C., Polcer, J.D., Rhoades, R.W., 1982. The intercollicular pathway in the golden hamster: an anatomical study. *J. Comp. Neurol.* 204, 6–20.
- Grantyn, R., 1988. Gaze control through superior colliculus: structure and function. In: Büttner-Ennever, J.A. (Ed.), *Neuroanatomy of the Oculomotor System*. Elsevier Science, New York, pp. 273–333.
- Helmholtz, H.V., 1867. *Handbuch der Physiologischen Optik*. Voss, Hamburg.
- Hoffman, K.P., Straschill, M., 1971. Influence of cortico-tectal and intertectal connections on visual responses in the cat's superior colliculus. *Exp. Eye Res.* 12, 120–131.
- Lee, P.H., Schmidt, M., Hall, W.C., 2001. Excitatory and inhibitory circuitry in the superficial gray layer of the superior colliculus. *J. Neurosci.* 21, 8145–8153.
- Maeda, M., Shibasaki, T., Yoshida, K., 1979. Monosynaptic inhibition evoked in superior colliculus neurons following contralateral collicular stimulation. In: Ito, M. (Ed.), *Integrative Control Functions of the Brain*. Elsevier, Amsterdam/North-Holland, pp. 68–71.
- Maeda, M., Shibasaki, T., Yoshida, K., 1981. The role of tecto-reticular and tecto-spinal pathways in eye-head coordination. In: Fuchs, A., Becker, R. (Eds.), *Progress in Oculomotor Research*. Elsevier, North-Holland, Amsterdam, pp. 317–324.
- Magalhães-Castro, H.H., de Lima, A.D., Saraiva, P.E.S., Magalhães-Castro, B., 1978. Horseradish peroxidase labeling of cat tectotectal cells. *Brain Res.* 148, 1–13.
- McIlwain, J.T., 1986. Effects of eye position on saccades evoked electrically from superior colliculus of alert cats. *J. Neurophysiol.* 55, 97–112.
- Moschovakis, A.K., Karabelas, A.B., 1985. Observations on the somatodendritic morphology and axon trajectory of intracellularly HRP-labeled efferent neurons located in the deeper layers of the superior colliculus of the cat. *J. Comp. Neurol.* 239, 276–308.
- Moschovakis, A.K., Karabelas, A.B., Highstein, S.M., 1988a. Structure–function relationships in the primate superior colliculus. I. Morphological classification of efferent neurons. *J. Neurophysiol.* 60, 232–262.
- Moschovakis, A.K., Karabelas, A.B., Highstein, S.M., 1988b. Structure–function relationships in the primate superior colliculus. II. Morphological identity of presaccadic neurons. *J. Neurophysiol.* 60, 263–302.
- Munoz, D.P., Istvan, P.J., 1998. Lateral inhibitory interactions in the intermediate layers of the monkey superior colliculus. *J. Neurophysiol.* 79, 1193–1209.
- Olivier, E., Corvisier, J., Pauluis, Q., Hardy, O., 2000. Evidence for glutamatergic tectotectal neurons in the cat superior colliculus: a comparison with GABAergic tectotectal neurons. *Eur. J. Neurosci.* 12, 2354–2366.
- Shimazu, H., Precht, W., 1966. Inhibition of central vestibular neurons from the contralateral labyrinth and its mediating pathway. *J. Neurophysiol.* 29, 467–492.
- Sprague, J.M., 1966. Interaction of cortex and superior colliculus in mediation of visually guided behavior in the cat. *Science* 153, 1544–1547.

- Takahashi, M., Shinoda, Y., 2018. Brain stem neural circuits of horizontal and vertical saccade systems and their frame of reference. *Neuroscience* 392, 281–328.
- Takahashi, M., Sugiuchi, Y., Izawa, Y., Shinoda, Y., 2005. Commissural excitation and inhibition by the superior colliculus in tectoreticular neurons projecting to omnipause neuron and inhibitory burst neuron regions. *J. Neurophysiol.* 94, 1707–1726.
- Takahashi, M., Sugiuchi, Y., Shinoda, Y., 2007. Commissural mirror-symmetric excitation and reciprocal inhibition between the two superior colliculi and their roles in vertical and horizontal eye movements. *J. Neurophysiol.* 98, 2664–2682.
- Takahashi, M., Sugiuchi, Y., Shinoda, Y., 2010. Topographic organization of excitatory and inhibitory commissural connections in the superior colliculi and their functional roles in saccade generation. *J. Neurophysiol.* 104, 3146–3167.
- Takahashi, M., Sugiuchi, Y., Shinoda, Y., 2011. Commissural inhibition between bilateral superior colliculi for saccades and bilateral vestibular nuclei for vestibulo-ocular reflex (VOR). *Ann. N. Y. Acad. Sci.* 1233 (Suppl), 152–174.
- Wallace, S.F., Rosenquist, A.C., Sprague, J.M., 1989. Recovery from cortical blindness mediated by destruction of nontectotectal fibers in the commissure of the superior colliculus in the cat. *J. Comp. Neurol.* 284, 429–450.

This page intentionally left blank

Potassium channels in omnipause neurons

8

Ümit S. Mayadali^{a,b,d,*}, Karoline Lienbacher^{a,b}, Michael Mustari^{e,f},
Michael Strupp^{b,c,d}, Anja K.E. Horn^{a,d}

^a*Institute of Anatomy and Cell Biology I, Ludwig-Maximilian University (LMU), Munich, Germany*

^b*German Center for Vertigo and Balance Disorders, LMU, Munich, Germany*

^c*Department of Neurology, LMU, Munich, Germany*

^d*Graduate School of Systemic Neurosciences (GSN), LMU, Munich, Germany*

^e*Washington National Primate Research Center, University of Washington, Seattle, WA,
United States*

^f*Department of Ophthalmology, University of Washington, Seattle, WA, United States*

*Corresponding author: Tel.: +49 89-2180-72668,
e-mail address: umit.mayadali@med.uni-muenchen.de

Abstract

Potassium (K^+) channels are major contributors to fast and precise action potential generation. The aim of this study was to establish the immunoreactivity profile of several potassium channels in omnipause neurons (OPNs), which play a central role in premotor saccadic circuitry. To accomplish this, we histochemically examined monkey and human brainstem sections using antibodies against the voltage gated K^+ -channels Kv1.1, Kv3.1b and K^+-Cl^- cotransporter (KCC2). We found that OPNs of both species were positive for all three K^+ -antibodies and that the staining patterns were similar for both species. In individual OPNs, Kv3.1b was detected on the somatic membrane and proximal dendrites, while Kv1.1 was mainly confined to soma. Further, KCC2 immunoreactivity was strong in distal dendrites, but was weak in the somatic membrane. Our findings allow the speculation that the alterations in K^+ -channel expression in OPNs could be the underlying mechanism for several saccadic disorders through neuronal and circuit-level malfunction.

Keywords

Saccade, Fast-firing neurons, Perineuronal nets, Immunohistochemistry, Kv1.1, Kv3.1b, Potassium-chloride cotransporter, Monkey, Human

1 Introduction

The generation and accurate execution of saccades relies on the timely interaction of premotor burst neurons and omnipause neurons (OPNs) in the brainstem (Leigh and Zee, 2015). During fixation and non-saccadic eye movements, OPNs prevent burst neurons from firing via a continuous tonic inhibition with frequencies approaching 200Hz (Gandhi and Keller, 1999). Conceivably, a malfunction of the OPN firing pattern could result in saccadic disorders such as saccadic intrusions/oscillations (e.g., ocular flutter, opsoclonus) or saccadic slowing (Leigh and Kennard, 2004). Although some histochemical properties of OPNs that may contribute to the firing characteristics have been studied (Horn et al., 2003), not much is known about their ion channel expression profiles. Investigation of ion channels in OPNs would not only provide essential parameters of the saccadic circuitry, but also would enable the investigation of possible mechanisms of OPN failure that could contribute to saccadic intrusions/oscillations or slowing (Shaikh et al., 2008).

Due to their central role in determining and maintaining membrane potentials in highly active neurons (Johnston et al., 2010), it is reasonable to assume that voltage-gated potassium channel subunits (K_V) contribute significantly to OPN firing characteristics. Therefore, we provide here $K_V1.1$, $K_V3.1b$ and K^+-Cl^- cotransporter (KCC2) expression profiles of OPNs in monkey and human tissue specimen.

2 Methods

Five monkey brainstems (three *Macaca nemestrina*, obtained from Washington National Primate Research Center, two *Macaca mulatta* sections from previous studies—all fixed with 4% paraformaldehyde), and four post mortem human cases (fixed in 10% formaline) with no prior oculomotor symptoms obtained from the Reference Center for Neurodegenerative Disorders of the LMU were examined. Free-floating monkey brainstem sections were processed for the simultaneous immunofluorescence detection of one K^+ channel together with either SMI-32, a non-phosphorylated neurofilament (NP-NF) marker, or perineuronal net (PNN) marker hyaluronan and proteoglycan link protein 1 (HAPLN1), or with γ -aminobutyric acid (GABA)-A receptor (GABA_AR). Sections were subsequently visualized with a laser-scanning confocal microscope (Leica SP5, Mannheim, Germany) as described previously (May et al., 2016). Paraffin sections from human and monkey brainstems were processed for the detection of one K^+ channel together with either SMI-32 or PNN marker aggrecan (ACAN) using an immunoperoxidase protocol (see Table 1). The specificity of antibodies was validated by antibody-antigen preabsorption tests (data not shown). Since K^+ channels have been extensively

Table 1 Overview of the antibodies used in this study.

Antibody antigen	Dilution IF	Dilution IHC	Immunogen	Antibody details
K _v 1.1	1:250	1:500 (human) 1:750 (monkey)	AA residues 416–495 of mouse KCNA1	Alomone APC-009 rabbit polyclonal
K _v 3.1b	1:2000	1:6000	Residues 567–585 of rat K _v 3.1b, KCNC1	Alomone APC-014 rabbit polyclonal
KCC2	1:500	1:4000	Residues 932–1043 of rat KCC2	Millipore 07-432 rabbit polyclonal
SMI-32 (NP-NF)	1:2500	1:2500	Neurofilament heavy polypeptide, 200 kDa	Sternberger 801701 mouse monoclonal
ACAN	–	1:75	Purified human articular cartilage aggrecan	Acris SM1353 mouse monoclonal
HAPLN1	1:100	1:400	Residues 16–354 of human HAPLN1	R&D AF2608 goat polyclonal

IF: immunofluorescence; IHC: immunohistochemistry; NP-NF: non-phosphorylated neurofilaments; ACAN: aggrecan; HAPLN1: hyaluronan and proteoglycan link protein 1.

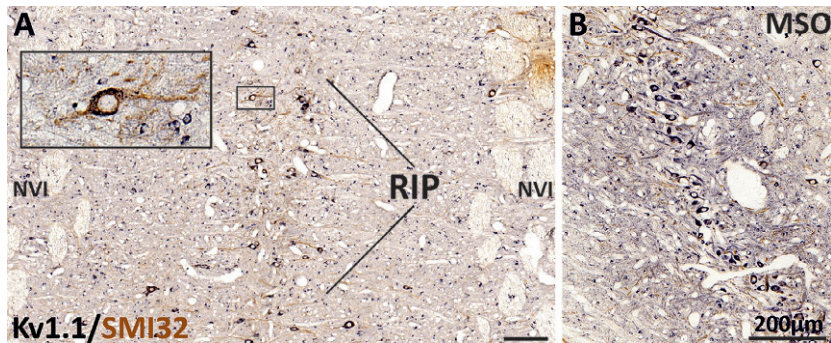
studied in the auditory nuclei, the medial superior olive (MSO) in the same sections served as the internal positive control for both species (Johnston et al., 2010; Mathews et al., 2010).

3 Results

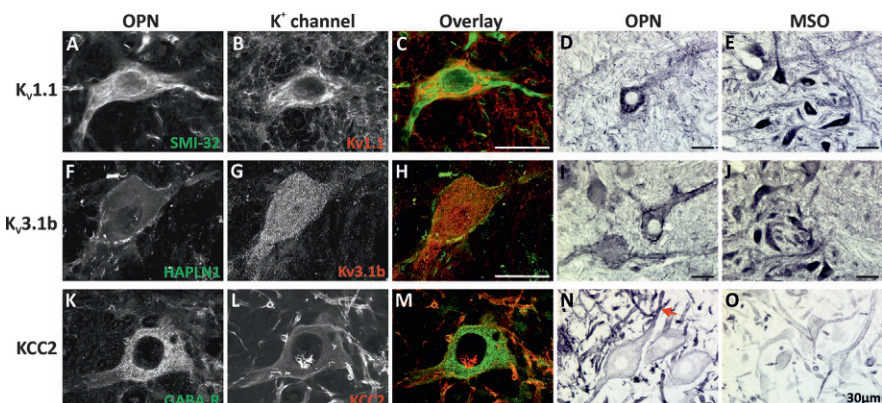
In monkey and human, OPNs were identified at the level of the traversing fibers of the abducens nerve by either SMI-32 or PNN immunostaining, which outlines their characteristic morphology (Figs. 1A and 2A,F) (Horn et al., 2003). The MSO was located ventrolateral to the OPNs in the same sections (Fig. 1B).

K_v1.1: OPNs showed positive K_v1.1 immunoreactivity in both monkey and human (Figs. 1A and 2A–D). Notably, K_v1.1 labeling in the OPNs was confined to the soma in both species, while K_v1.1 immunoreactivity in MSO neurons extended to somatic and dendritic membranes (Figs. 2E and 3D).

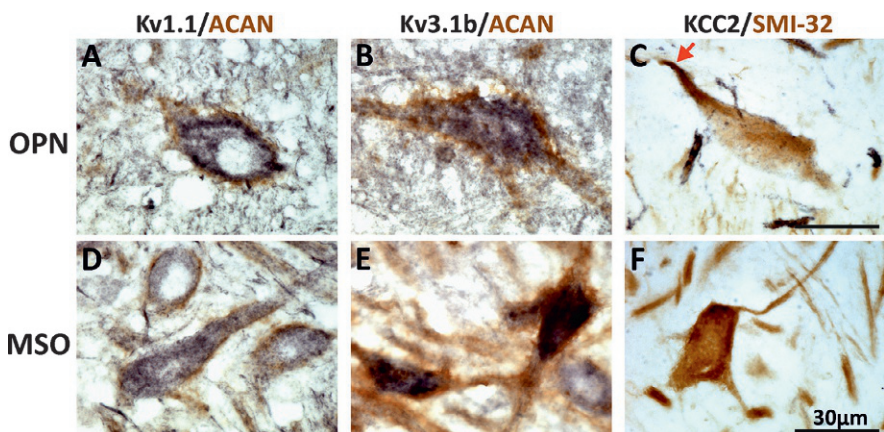
K_v3.1b: OPNs exhibited strong K_v3.1b immunoreactivity in both species (Figs. 2F–I and 3B). Confocal microscopy revealed that K_v3.1b expression was primarily present in the cell membrane of soma and proximal dendrites and moderately in the cytoplasm (Figs. 2G–I and 3B). A similar pattern of K_v3.1b immunoreactivity was found in MSO neurons of both species (Figs. 2J and 3E).

**FIG. 1**

Overview of OPNs located within raphe interpositus (RIP) (A), between traversing fibers of the abducens nerve (NVI) and medial superior olive (MSO, B) found ventrolateral to the OPNs on the same frontal section of a monkey pontine brainstem. Scale bars = 200 μm.

**FIG. 2**

K⁺ channels in monkey OPNs: Kv1.1 labeling in OPNs identified by either SMI-32 (A, C) or HAPLN1 immunostaining (F, H) was confined to the somatic cytoplasm (A–D), while Kv3.1b was primarily found in the cell membrane of the soma and proximal dendrites (F–H). MSO neurons within the same section showed strong somatic and dendritic immunoreactivity for Kv1.1 and Kv3.1b (E, J). KCC2 immunoreactivity was weak in the somatic membranes (L, N), but strong in the dendrites of OPNs (L, N, arrow) similar to that of MSO neurons (O). A strong co-expression of GABA_A-Receptor immunoreactivity was present in OPNs (K). Scale bars = 30 μm.

**FIG. 3**

K^+ channels in human OPNs: Immunostaining for $Kv1.1$ and $Kv3.1b$ (A–B) in human OPNs that were outlined by ACAN (aggrecan, brown) were similar to those of monkey OPNs. Comparable to KCC2 expression in monkey OPNS, KCC2 immunoreactivity was stronger in dendrites (C, arrow) than somatic membrane. MSO neurons on the same sections as the $Kv1.1$, $Kv3.1b$ and KCC2 stainings are shown in their respective columns (D–F). Scale bars = 30 μ m.

KCC2: Strong KCC2 immunoreactivity was present in the dendrites of OPNs, whereas in their somatic membranes the signal was weak (Figs. 2K–N and 3C). The KCC2 positive OPNs co-expressed GABA_AR immunoreactivity (Fig. 2K–M). KCC2 staining patterns of the OPNs were similar to that of MSO neurons, but the latter expressed less overall immunoreactivity (Figs. 2O and 3F).

4 Discussion

This study demonstrates by specific immunohistochemical staining that saccadic OPNs in monkey and human express the potassium channels $Kv1.1$, $Kv3.1b$ and KCC2. Expression of $Kv1$ and $Kv3$ subunits in particular, suggests a direct contribution to the fast and precise firing properties of OPNs, as previously demonstrated in auditory brainstem circuitry (Johnston et al., 2010; Mathews et al., 2010). For instance, $Kv1$ subunits are known to raise the action potential firing threshold and to reduce the time constant by opening with only small perturbations (Johnston et al., 2010). $Kv3$ subunits, on the other hand, facilitate high firing rates by opening only at high membrane potentials, and short refractory periods by their fast closure kinetics (Kaczmarek and Zhang, 2017). Specifically, $Kv3.1b$ expression is often found in neurons with fast-firing properties that contain the calcium-binding protein

parvalbumin, and that are ensheathed by PNNs (Härtig et al., 1999) as seen in OPNs (Horn et al., 2003). Further, KCC2 maintains chloride homeostasis in neurons and determines the polarity and efficacy of GABA_{AR} and glycine receptors (Chamma et al., 2012). As GABAergic and glycinergic input to the OPNs had been already found (Horn et al., 1994), the co-expression of KCC2 and GABA_{AR} in OPNs in the present study is in line with the functional implications of the transporter (Fig. 2K–M) (Chamma et al., 2012).

These findings on OPNs have clinical implications as irregularities in all of the tested potassium channels result in disorders related to neuronal excitability (Kaczmarek and Zhang, 2017; Shieh et al., 2000; Vinay and Jean-Xavier, 2008). Such a failure of a key cell group in the saccadic circuitry could manifest itself as saccadic flutter/oscillations, as suggested by Shaikh et al. (2008). Therefore, investigation of potassium channel expression in OPNs (or other functional groups of the saccadic circuitry) in such saccadic disorders as found in autoantibody-mediated autoimmune disorders, paraneoplastic syndromes and brainstem encephalitis (Torres-Vega et al., 2016; Tüzün et al., 2010) would provide valuable insight into their pathophysiology.

Acknowledgments

We thank Christine Unger and Ahmed Messoudi, MPh for their excellent technical assistance, and Prof. Dr. med. Waschke for his continuous support. This work was supported by BMBF (IFB-01E0901, Brain-Net-01GI0505) and National Institutes of Health (EY06069; P51 OD010425).

References

- Chamma, I., Chevy, Q., Poncer, J.C., Levi, S., 2012. Role of the neuronal K-cl co-transporter KCC2 in inhibitory and excitatory neurotransmission. *Front. Cell. Neurosci.* 6, 5.
- Gandhi, N.J., Keller, E.L., 1999. Comparison of saccades perturbed by stimulation of the rostral superior colliculus, the caudal superior colliculus, and the omnipause neuron region. *J. Neurophysiol.* 82, 3236–3253.
- Härtig, W., Derouiche, A., Welt, K., Brauer, K., Grosche, J., Mäder, M., Reichenbach, A., Brückner, G., 1999. Cortical neurons immunoreactive for the potassium channel Kv3.1b subunit are predominantly surrounded by perineuronal nets presumed as a buffering system for cations. *Brain Res.* 842, 15–29.
- Horn, A.K.E., Büttner-Ennever, J.A., Wahle, P., Reichenberger, I., 1994. Neurotransmitter profile of saccadic omnipause neurons in nucleus raphe interpositus. *J. Neurosci.* 14, 2032–2046.
- Horn, A.K.E., Brückner, G., Härtig, W., Messoudi, A., 2003. Saccadic omnipause and burst neurons in monkey and human are ensheathed by perineuronal nets but differ in their expression of calcium-binding proteins. *J. Comp. Neurol.* 455, 341–352.
- Johnston, J., Forsythe, I.D., Kopp-Scheinplug, C., 2010. Going native: voltage-gated potassium channels controlling neuronal excitability. *J. Physiol.* 588, 3187–3200.

- Kaczmarek, L.K., Zhang, Y., 2017. Kv3 channels: enablers of rapid firing, neurotransmitter release, and neuronal endurance. *Physiol. Rev.* 97, 1431–1468.
- Leigh, R.J., Kennard, C., 2004. Using saccades as a research tool in the clinical neurosciences. *Brain* 127, 460–477.
- Leigh, R.J., Zee, D.S., 2015. *The Neurology of Eye Movements*, fifth ed. Oxford University Press, New York.
- Mathews, P.J., Jercog, P.E., Rinzel, J., Scott, L.L., Golding, N.L., 2010. Control of submillisecond synaptic timing in binaural coincidence detectors by Kv1 channels. *Nat. Neurosci.* 13, 601–609.
- May, P.J., Warren, S., Bohlen, M.O., Barnessoi, M., Horn, A.K., 2016. A central mesencephalic reticular formation projection to the Edinger-Westphal nuclei. *Brain Struct. Funct.* 221, 4073–4089.
- Shaikh, A.G., Ramat, S., Optican, L.M., Miura, K., Leigh, R.J., Zee, D.S., 2008. Saccadic burst cell membrane dysfunction is responsible for saccadic oscillations. *J. Neuroophthalmol.* 28, 329–336.
- Shieh, C.C., Coghlan, M., Sullivan, J.P., Gopalakrishnan, M., 2000. Potassium channels: molecular defects, diseases, and therapeutic opportunities. *Pharmacol. Rev.* 52, 557–594.
- Torres-Vega, E., Durán-Moreno, M., Sánchez Del Pino, M., Yáñez, Y., Cañete, A., Castel, V., López-Cuevas, R., Vilchez, J.J., Dalmau, J., Graus, F., García Verdugo, J.M., Bataller, L., 2016. Immunoproteomic studies on paediatric opsoclonus-myoclonus associated with neuroblastoma. *J. Neuroimmunol.* 297, 98–102.
- Tüzün, E., Kurtüncü, M., Lang, B., Içöz, S., Akman-Demir, G., Eraksoy, M., Vincent, A., 2010. Bickerstaff's encephalitis and Miller Fisher syndrome associated with voltage-gated potassium channel and novel anti-neuronal antibodies. *Eur. J. Neurol.* 17, 1304–1307.
- Vinay, L., Jean-Xavier, C., 2008. Plasticity of spinal cord locomotor networks and contribution of cation-chloride cotransporters. *Brain Res. Rev.* 57, 103–110.

This page intentionally left blank

The cerebellum improves the precision of antisaccades by a latency-duration trade-off

9

Pietro Piu^a, Elena Pretegiani^{a,c}, Francesca Rosini^{a,b}, Valeria Serchi^a,
Domenica Zaino^{a,b}, Tommaso Chiantini^a, Alessandra Rufa^{a,b,*}

^a*Eye-tracking and Visual Application Lab (EVALab), Department of Medicine, Surgery and Neurosciences, University of Siena, Siena, Italy*

^b*Neurological and Neurometabolic Unit, Department of Medicine, Surgery and Neurosciences, University of Siena, Siena, Italy*

^c*Laboratory of Sensorimotor Research-NEI, NIH, DHHS, Bethesda, MD, United States*

*Corresponding author: Tel.: +39-0577-585760, e-mail address: rufa@unisi.it

Abstract

The cerebellum adapts motor responses by controlling the gain of a movement, preserving its accuracy and by learning from endpoint errors. Adaptive behavior likely acts not only in the motor but also in the sensory, behavioral, and cognitive domains, thus supporting a role of cerebellum in monitoring complex brain performances. Here, we analyzed the relationship between saccade latency, duration and endpoint error of antisaccades in a group of 10 idiopathic cerebellar atrophy (ICA) patients compared to controls. The latency distribution was decomposed in a decision time and a residual time. Both groups showed a trade-off between duration and decision time, with a peak of entropy within the range of this trade-off where the information flow was maximized. In cerebellar patients, greater reductions of duration as the time of decision increased, were associated with a lower probability for a saccade to fall near the target, with a constant low entropy outside the optimal time window. We suggest a modulation of saccade duration, depending on the latency-related decision time (accumulation of sensory and motor evidences in favor of a goal-directed movement), normally adopted to perform efficient trajectories in goal-directed saccades. This process is impaired in cerebellar patients suggesting a role for the cerebellum in monitoring voluntary motor performance by controlling the movement onset until the ambiguity of planning is resolved.

Keywords

Antisaccades, Latency, Cerebellum, Optimization, End-point error

1 Introduction

Motor adaptation is a fundamental property of our brain: by monitoring a brain function, it allows the optimization of its performance, which results in reduction of the magnitude and rate of errors. In the ocular motor system, the cerebellar vermis is considered a crucial structure for the adaptation of saccades, the rapid eye movements that move our gaze to a target (Catz et al., 2005; Chen-Harris et al., 2008; Hopp and Fuchs, 2004; Kojima et al., 2010). Since vision is impaired during the execution of saccades and visual acuity sharply decreases outside the fovea, efficient saccades need to be short (duration) and accurate. The cerebellum optimizes involuntary reflexive saccades in response to external visual stimuli through a duration/accuracy trade-off, which minimizes the end-point variability also related to signal inherent noise (Golla et al., 2008; Izawa et al., 2008; Xu-Wilson et al., 2009). Such duration/accuracy trade-off is obtained by monitoring the dynamic error signal and by modulating the motor command for upcoming saccades via an internal feedback (Joiner and Shelhamer, 2009; Xu-Wilson et al., 2009). This mechanism is demonstrated to be efficient for reflexive visually guided saccades, where there is no ambiguity related to the needed motor plan. Nevertheless, it is not known whether a comparable mechanism regulates more sophisticated voluntary internally triggered saccades. Antisaccade task, in which the subject is instructed to make a mirror saccade to the opposite direction with respect to the eccentric stimulus, is an effective tool to study goal directed voluntary actions under cortical control since the underlying neural network has been largely clarified (Everling and Munoz, 2000; Ford et al., 2005; Hallett, 1978; Pierrot-Deseilligny et al., 2004). Correctly executed antisaccades require the resolution of a conflict regarding saccade direction and the solving of uncertainty related to an unmarked landing position. The high computational cost related to this complex process is reflected into the pre-motor time (latency) of antisaccades.

Patients with pathophysiologically defined neurological disorders offer insights into understanding of normal human brain function. In previous studies, we found that patients with neurogenetic and neurodegenerative cerebellar diseases show antisaccades with longer latency and significantly greater trial by trial latency variability, as compared to controls (Pretegiani et al., 2018; Rosini et al., 2017). We postulated that the latency is composed by a decision phase the duration of which is related to the accumulation of sensory motor information and a non-decisional, residual phase. Our hypothesis is that the cerebellum controls voluntary actions by monitoring the pre-motor, *decision phase*, until the desired action goal is clarified. To verify this hypothesis, we investigated whether antisaccades are regulated by a cerebellar mechanism analogous to that utilized by reflexive saccades by assessing the duration/accuracy trade-off in 10 patients with idiopathic adult onset pure cerebellar atrophy and 34 controls.

2 Methods

2.1 Patients and controls

Ten patients (five males) with idiopathic cerebellar ataxia (ICA) (mean age 42.4 years, range 27–53 years) and 34 healthy age-matched subjects (13 males) (mean age 36 years, range 19–65 years) participated to the study. In normal subjects, the latency of antisaccades is more dependent from aging than the latency of reflexive saccades; however, the effect of aging on antisaccade latency is evident from the age of 60–85 years. ICA is a sporadic and genetically heterogeneous neurodegenerative process confined to the cerebellum (Kerber et al., 2005). All neurological patients underwent complete neurological, neuro-ophthalmological and International Cooperative Ataxia Rating Scale (ICARS) (Trouillas et al., 1997) examination, a conventional brain MRI and the recommended clinical protocol for ataxias, including genetic and laboratory testing when pertinent. Exclusion criteria included any known causes of recessive and dominant ataxias (Friedreich ataxia, fragile X-premutation, ataxia-telangiectasia, ataxias associated with mutation of aprataxin, senataxin or sactsin, metabolic causes of ataxia such as abetalipoproteinemia, vitamin E deficiency, late-onset Tay–Sachs disease, cerebrotendinous xanthomatosis, autosomal dominant spinocerebellar ataxias due to de novo mutations).

All participants gave their informed consent and the study was approved by the local Ethics Committee (Comitato Etico Locale Azienda Ospedaliera Universitaria Senese, EVAlab protocol CEL no. 48/2010).

2.2 Eye movement recording

Eye-movements were recorded in one eye using an ASL-504 eye-tracker device (Applied Science Laboratories) sampling the image of the eye at 240Hz. Stimulation and data acquisition were controlled by a PC (3GHz Pentium) running a custom software dedicated to real-time data acquisition. The visual stimulus was a red dot (63 cd/m^2) with diameter subtending a visual angle of 0.4 deg on a black background LCD screen (2.5 cd/m^2 , $310 \times 510\text{ mm}$, 1024×768 pixels) placed at 720 mm from the subject. Subjects were seated in a darkened room and movements were minimized by a chinrest. Recording sessions were preceded by a 9-point calibration and validation. The task was a sequence of at least 40 horizontal anti-saccade trials. After the disappearance of a central fixation point (gap, 200 ms), a peripheral target appeared randomly to the right or left (10 deg) for 2500 ms. The subjects were requested to make a mirror saccade to the opposite direction with respect to the eccentric stimulus. Data analyses of the main antisaccades characteristics were previously reported (Federighi et al., 2011).

2.3 Signal processing

Signal processing was conducted off-line in MATLAB® (The MathWorks). Data were filtered using a third-order Butterworth low-pass digital filter (-3 dB , 25 Hz). A velocity threshold of 10 deg/s was used to determine the starting and ending times of saccades. Saccades with latency $<100\text{ ms}$ and direction exceeding $>30\text{ deg}$ the horizontal plane were excluded from the analyses. Only correctly executed antisaccades were considered in this study. A correctly executed antisaccade was defined as a mirror saccade to the opposite direction with respect to the eccentric stimulus.

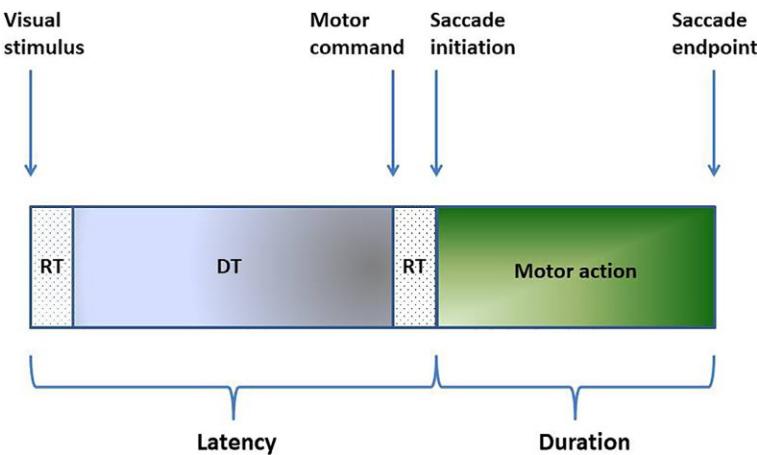
For each antisaccade movement, latency, duration and amplitude were computed. Latency was the time delay between target presentation and saccade onset, in milliseconds. Duration was the time interval between saccade onset and the end, in milliseconds. Amplitude was the difference between eye position at the saccade onset and end, in degrees of visual angle. Amplitude expressed the location of the saccadic end-point error, computed as $|\text{target amplitude} - \text{saccadic amplitude}|$. The most effective antisaccades show over- or under-estimation of the target within a radius of 1.5 deg from it. Therefore, saccades with a landing end-point error lower than a radius of 1.5 deg were considered accurate saccades and taken into consideration as such.

2.4 Latency decomposition

Perceptual sensory and motor planning decision stages take place between the stimulus appearance and the saccade onset (Cutsuridis, 2010; Gomez et al., 2007; Hutton, 2008; Noorani, 2014; Van Rullen and Thorpe, 2001). In this sense, the latency interval reflects the time taken by a decision-making process for driving the saccade to a specific desired target among a set of potential alternatives (Hutton, 2008; Noorani, 2014). The process entails an information stream, proceeding from low-level stimulus encoding mechanisms to high-level action planning mechanisms (Van Rullen and Thorpe, 2001), such that the visual stimulus is firstly detected (perceptual process), then the target is identified and the saccade toward the selected placement is planned and initiated (sensory motor-decision process) (Cutsuridis, 2010; Hutton, 2008).

According to our hypothesis, the cerebellum was expected to modulate the eye-movements through a visible action on the decisional time. Therefore, the Ex-Wald distribution function (Schwarz, 2001) was used to decompose the latency time series into decision time (DT, sensory-motor -decision stage) and residual time (RT, non-decisional component stage) (Fig. 1).

DT is the time for perceiving a visual stimulus, recognizing the target and planning the saccade trajectory. RT, in contrast, includes the neural encoding: the time for the transduction of the stimulus into a neural signal for its sensory detection, the transition time for the motor command to reach the muscle group and the time to inhibit reflexive responses (Gomez and Perea, 2014; Luce, 1986; Schwarz, 2001; Voss et al., 2015; White et al., 2010).

**FIG. 1**

Sensory-planning-action map. Most part of the latency (around 97%) is covered by the decision time (DT) which reflects the diffusive process for the perception of the stimulus and the decision of the trajectory. The residual part (RT) embodies the sensory process of neural encoding of the visual signal, and the synaptic delays of the motor command (before and after the decision process, respectively).

The Ex-Wald probability density is a four-parameter (μ, σ, a, γ) function given by the convolution of an inverse Gaussian and an independent exponential random variable. The mean and variance of an ex-Wald distributed random variable x are showed in Eqs. (1–2):

$$E[x] = \frac{a}{\mu} + \frac{1}{\gamma} \quad (1)$$

$$\text{var}(x) = \frac{a \cdot \sigma^2}{\mu^3} + \frac{1}{\gamma^2} \quad (2)$$

The interaction among μ, σ and a , drives the speed-accuracy trade-off during the decisional process:

- μ estimates the mean drift rate (i.e., accumulation of evidence per unit of time), and it relates to the task difficulty and the perceptual uncertainty about the stimulus, such that if the stimulus is easily classified (high quality of information) the drift rate increases;
- σ is a scaling parameter which measures the volatility of the drift rate;
- a is the absorbing boundary which indicates the amount of evidence needed to come to a decision, and it reflects to the response caution, that is, the a priori confidence about the best choice.

The exponential parameter of the Ex-Wald distribution, γ , expresses the residual stage of the latency (McGill, 1963; Palmer et al., 2011; Schwarz, 2001; White et al., 2010).

The Ex-Wald parameters were calculated applying a maximum likelihood estimation procedure based on the Nelder-Mead simplex search algorithm (Lagarias et al., 1998), with starting values of μ_0 randomly selected within $[-5, +5]$, $\sigma_0 = 1$, a_0 equal to the median of the latency time series, and $\gamma_0 = 0.0025$. The estimated parameters of the Ex-Wald distribution were subsequently used to evaluate DT and RT. The mean values of DT and RT were calculated from Eq. 1 as the first ratio (a/μ) and the second ratio ($1/\gamma$), respectively.

Afterward, a simulation was implemented to assess the relationship between amplitude, DT, RT, and duration in each group. A t-copula was used to generate 200 correlated multivariate data of latency, duration and amplitude across 1000 iterations. The correlated multivariate data were re-ordered based on their latency (ascending order). Three individual matrices (200×1000) of latencies, durations and amplitudes were then formed from the latency-based sorted values. The Ex-Wald distribution was fitted over each row of the matrix of latencies, which yielded mean vectors (200×1) of DT and RT. Row-based averages and standard deviations values were computed for the matrix of durations and of amplitudes, respectively.

2.5 Statistical analysis

Prior to the application of the t-copula, the relationship among latency, duration and amplitude in the observed antisaccades of controls and ICA was investigated through Spearman correlation test. In fact, the correlation between the observed data variables is a necessary condition in order to perform the simulation.

For each group, the Ex-Wald parameters were tested through the Mann-Whitney statistic. The distributions of the DT and RT values between groups were compared through Kolmogorov-Smirnov tests.

Three-predictor logistic regression models were implemented to estimate whether and to what extent DT, RT, and duration influenced the probability of performing efficient saccades. For this purpose, the copula-generated amplitude time series underwent a binary transformation, such that the saccades with error in amplitude ranging from ± 1.5 deg were encoded as “+1,” and as “-1” elsewhere. The number of end-points falling outside the 1.5 deg radius was 132/200 for controls and 137/200 for ICA. The results of the logistic model were used to compute the probabilities of making efficient saccades (saccades with shorter duration and better accuracy), which allowed to form curves of DT-duration balance in correspondence of different probability values. For probabilities >0.8 , the relationship between DT and duration was further investigated and linear models were accordingly fitted.

All the tests were at the nominal significance level of 1%.

Sample entropy (SampEn) was used to assess the variability in the saccadic end-points. The higher the SampEn value, the more complex is the time series (Pincus, 1991; Pincus and Goldberger, 1994; Richman and Moorman, 2000).

A window of size 18 (17/18 overlap ratio) was moved over the saccadic end-points vector (Ahmad and Chappell, 2008). For each window, the SampEn was calculated (tolerance parameter = $0.2 \times$ standard deviation of the end-points data, embedding dimension = 2). The SampEn time series was, then, built and plotted against the DT and duration time series. Peaks in the SampEn were investigated in relation to the variability of the saccadic end-point. In fact, the presence of such peaks might suggest the occurrence of event-related responses driven by the sensory-planning-execution path.

3 Results

To verify the hypothesis that, in AS, the latency duration is composed by a decision time and a non-decision time, we used the Ex-Wald distribution. (Gomez and Perea, 2014). Indeed, under the hypothesis that the decision stage involves a Wiener stochastic process where information is continuously accumulated until the attainment of a threshold, the ex-Wald parameters (μ , σ , a) fully describe this diffusion process which unravels during the decision time. In addition, the exponential parameter (γ) determines the residual non-diffusive stages of the latency, which precede and/or follow the decision making, like the encoding of the stimulus, the neural conduction and synaptic delays of the motor commands (McGill, 1963; Palmer et al., 2011; Schwarz, 2001; White et al., 2010). The application of the ex-Wald distribution function facilitated the standing out and analysis of the stages involved in the latency period. Moreover the ex-Wald function fits well with the skewed distributions of the latency. Finally the ex-Wald function is a convolution of an inverse Gaussian variable and an independent exponential random variable, it enables the jointly estimation of the parameters of the two sub-processes involved in the latency period-decision stage and residual non-decisional stage.

3.1 Descriptive statistics

Correlation coefficients among latency, duration and amplitude of the observed correctly executed antisaccades are reported in Table 1.

The observed antisaccadic variables significantly correlated in both groups, legitimating the t-copula employment in this study.

The relevant parameters of the generated antisaccades are displayed in Table 2.

The distributions of the end-point error, latency and duration for the healthy controls and ICA patients are represented in Fig. 2.

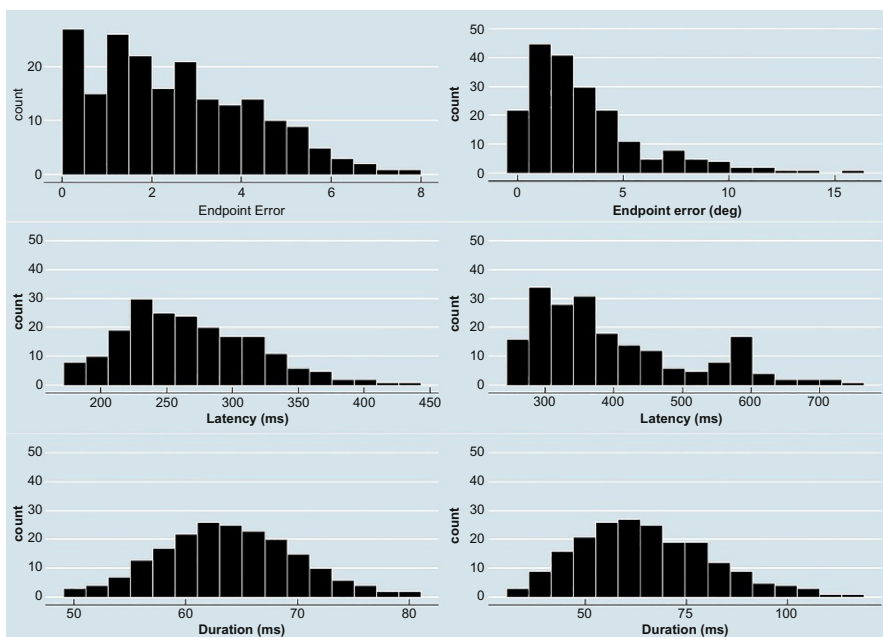
Significant differences were detected in latency ($z = -12.89$, $P < 0.0001$), DT ($z = -12.89$, $P < 0.0001$), and RT ($z = -7.56$, $P < 0.0001$), with controls having on average the shortest latency, DT and RT. On average, the contribution of DT to latency amounted to approximately 97% in both groups. ICA and controls did not differ significantly either in duration ($z = 0.35$, $P = 0.73$) or in end-point errors, ($z = -1.17$, $P = 0.24$).

Table 1 Spearman's correlation coefficients measured in antisaccade task.

Correlation	CTR		ICA	
	rho	P value	rho	P value
Latency-duration	-0.19	0.007	-0.48	0.002
Latency-amplitude	-0.26	0.003	-0.47	0.003
Duration-amplitude	0.84	<0.0001	0.84	<0.0001

Table 2 Descriptive statistics of the copula-generated data.

	CTR			ICA		
	Skew	Mean	sd	Skew	Mean	sd
Latency	0.8	269.7	54.7	0.9	399.7	114.9
Duration	0.2	63.9	6.1	0.5	64.8	16.3
Error	0.7	2.6	1.8	1.7	3.2	2.9
DT	0.7	261.4	54.3	1.0	388.4	112.3
RT	2.1	10.0	3.1	0.2	15.4	6.6

**FIG. 2**

The distributions of end-point error (top row), latency (middle row) and duration (bottom row) of healthy subjects (left column) and ICA patients (right column) are shown.

The latencies were distributed asymmetrically with positive skewness, supporting the groundwork for the implementation of the ex-Wald function. The end-point errors of ICA showed longer tail (skewness = 1.7) than controls (skewness = 0.7). The duration distribution was right-skewed in both ICA (skewness = 0.5) and controls (skewness = 0.2).

3.2 Ex-Wald parameters (drift and boundary): Mann-Whitney *U* test

During the decision stage, the drift did not differ between ICA and controls ($z = -0.90, P = 0.37$). Instead, ICA showed significant higher value of the boundary parameter than controls ($z = -12.4, P < 0.0001$).

3.3 Kolmogorov-Smirnov test of the DT and RT distributions

ICA and controls did not differ significantly in duration ($z = 0.35, P = 0.73$) and in the end-point errors ($z = -1.17, P = 0.24$), whereas their distributions of DT and RT were significantly different ($P < 0.00001$).

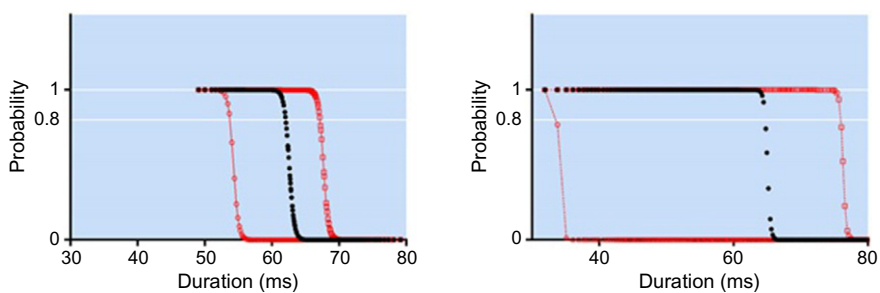
3.4 Logistic model

The model with all three covariates fitted significantly better than the reduced model with only the intercept both in ICA ($\text{LR} = 146.6, P < 0.0001$; $W = 16.0, P = 0.0011$) and controls ($\text{LR} = 120.5, P < 0.0001$; $W = 40.6, P < 0.0001$). The logistic regression model explained 73% and 63% of the variance (Nagelkerke R²) of the end-point errors in ICA and controls, respectively.

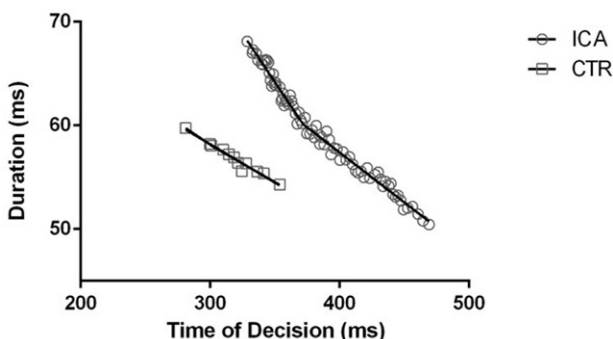
Both groups showed a negative relationship between the predictors DT (control: $P < 0.0001$; ICA: $P = 0.0002$) and duration (control: $P < 0.0001$; ICA: $P = 0.0001$) and the likelihood of saccadic end-points falling in a neighborhood of radius 1.5 deg from the target. Specifically, the predicted logit of the saccadic end-point was equal to $459.12 - (0.51 \times \text{DT}) - (4.25 \times \text{Duration})$ for ICA and $218.05 - (0.20 \times \text{DT}) - (2.68 \times \text{Duration})$ for controls. Increases of 1 ms in duration highly influenced the probability of performing efficient saccades both for ICA (~99%) and controls (~93%), with the odds ratios of duration equal to 0.01 and 0.07, respectively (Table 4, $e^{(\beta)}$). Instead, unit increases in DT generated lower percentage reductions in the probability of performing efficiently (ICA, ~40%; controls, ~18%).

RT was not significantly explicative of the variability of end-point and it was left out of the latency-duration trade-off analysis. The curves of probability of efficient saccades were built as function of the duration with given values of DT (Fig. 3).

The probability of performing efficient saccadic eye movements within a radius of 1.5 deg from the target depended on the DT-duration equilibrium. Prolonged DTs had to be balanced by shorter duration so as to attain high probability of ending the movement nearby the target. This inverse relationship produced the left-ward shifting of the probability curves with the increasing of DT. As the DT gets longer, the

**FIG. 3**

DT duration trade-off estimated for the group of healthy subjects (top panel) and ICA patients (bottom panel). The dashed thin line represents the curve of probability as function of duration for the given 95th percentile of DT (ICA, 611.2; controls, 366.1 ms), the central thick line corresponds to the median value of DT (ICA, 355.3 ms; controls, 253.6 ms) and the thin line on the right is obtained from the fifth percentile of DT (ICA, 262.4 ms; controls, 184.4 ms).

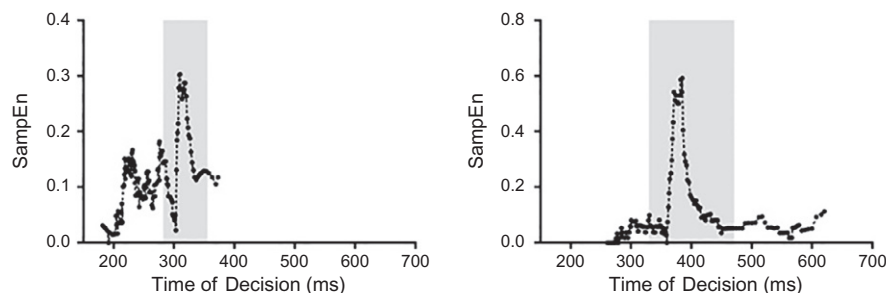
**FIG. 4**

The set of all points in the DT-duration plane, whose location satisfies the condition of yielding the highest probabilities (>0.8) to approach the target.

curve on the plot shifts to left, and shorter durations (in narrower ranges of values) are necessary to keep the probability of “success” in that interval.

Over the interval of probabilities >0.8 of getting closer to the target, linear regressions were estimated to predict the duration based on the DT (Fig. 4).

Controls showed a significant regression equation between duration and DT ($\text{Duration} = 80.4 - 0.07 \times \text{DT}$, $F(1,10) = 280.3$, $P < 0.0001$, $R^2 = 0.96$), with DT within 281 and 354 ms. ICA instead, did not show a constant responsiveness of duration to DT, having a change point for DT equal to 371.7 ms. For ICA, a further segmental regression analysis was therefore applied. The analysis highlighted

**FIG. 5**

Time course of the SampEn measurements with respect to DT for the healthy controls (left panel) and the ICA patients (right panel). The most efficient intervals of DT are highlighted in gray.

two segments with different slope (DT: 328.5–371.7 ms, slope: -0.19 ; and DT: 371.7–469 ms, slope: -0.09). The DT-duration regression lines for controls had steeper slopes than ICA in both segments ($F(1,43)=122.9$, $P < 0.0001$) and ($F(1,51)=8.4$, $P = 0.005$). These findings suggested that ICA needed to change abruptly the pace of the DT-duration balance to keep the probability to attain the target maximized. Therefore, for the ICA patients as the DT increased, durations had to be reduced faster not only compared to healthy controls, but also in the first segment relative to the second segment. Longer latency (DT) allowing the accumulation of new information, is associated with more efficient antisaccades. In addition, the interval of optimal duration values for the ICA group spanned a larger range (from 50.4 to 68.1 ms) than for healthy controls (from 54.3 to 59.7 ms).

3.5 Sample entropy of saccadic end-points

The analysis of the saccadic end-point variability through SampEn is reported in Fig. 5.

For both groups, peaks in the entropy occurred in the most efficient time windows of DT and duration, associated with probabilities >0.8 of a saccadic end-point nearby the target.

4 Discussion

The cerebellum optimizes the saccadic movement by a duration/accuracy trade-off, which minimizes the end-point variability due to motor noise and inherent neuronal activity noise (Golla et al., 2008; Izawa et al., 2008; Xu-Wilson et al., 2009). While this mechanism alone is efficient for externally triggered visually guided saccades, in which there is no ambiguity regarding motor planning, other optimization

mechanisms should be considered in antisaccades. The cognitive cost related to this complex process resides in the pre-motor time of antisaccades.

Through the comparison of antisaccade latency, duration and accuracy in ICA and controls, we demonstrate, for the first time in both groups, a duration/decision time latency trade-off for optimizing the probability of getting the saccade end-point closer to the target. A peak of entropy occurred within the range of this trade-off in correspondence to the maximization of the information flow. Importantly, cerebellar patients showed a greater reduction of duration as the time of decision increased, associated with a lower probability to be accurate and a constant lower entropy outside the optimal time window. Although both ICA and controls showed the trade-off between latency-duration and accuracy, suggesting a general behavior adopted by the brain for accumulating evidence in favor of well executed movements, this mechanism is less efficient in cerebellar patients, who are less efficient in performing a precise movement, beside longer latencies.

Latency of antisaccades is usually more variable (trial by trial) and longer than those of visually-guided saccades (Olk and Kingstone, 2003). An influential model explaining the response time distribution in a simple decisional process such as prosaccades vs antisaccade, is the LATER (linear approach to threshold with ergodic rate) model, a race-to-threshold model in which two different options compete for the final decision. According to race-to-threshold models of antisaccades (Kristjánsson et al., 2001; Munoz and Everling, 2004; Schlag-Rey et al., 1997), longer and variable latencies either reflect the unpredictable timing for the accumulation of information concerning the execution of a correct antisaccade (Noorani and Carpenter, 2013) or may depend on noisy accumulation of information during the decisional process (Cutsuridis et al., 2007; Cutsuridis et al., 2014). The analysis of the diffusion parameters of our model indicated that the ability of accumulating evidence was not spoiled in the ICA group, rather cerebellar patients had greater uncertainty about the motor planning and metrics generation of the antisaccade (Table 3). In agreement with previous studies, our cerebellar patients had increased and more variable antisaccadic latency, but also longer latency associated with a reduced probability to execute a precise antisaccade. Long decision times would reveal low confidence on the sensory-motor encoding, and consequently a high boundary envelops the prior probability.

In that case, the response caution exerts major control on the decision, while the rate of accumulation of evidence is relatively slow. On the contrary, short decision

Table 3 Ex-Wald parameters from the latency decomposition (median values).

	CTR	ICA	U test	P value
Drift (μ)	1.09	1.09	-0.90	0.37
Boundary (a)	266.60	381.80	-12.40	<0.0001
Diffusion (σ)	1.01	1.01	-1.10	0.25
Exponential (γ)	0.14	0.12	-5.50	<0.0001

Table 4 Results of the logistic regression analysis in antisaccade task for each group.

	Predictor	Beta	SE	e^(beta)	99% CI low	99% CI up	Wald stat	P value
CTR	Constant	218.05	40.84	5.0E+94	112.85	323.24	5.34	<0.0001
	DT	-0.20	0.04	0.82	-0.30	-0.09	-4.93	<0.0001
	RT	0.13	0.08	1.14	-0.08	0.35	1.56	0.12
	Duration	-2.68	0.49	0.07	-3.95	-1.42	-5.48	<0.0001
ICA	Constant	459.12	120.89	2.5E+199	147.72	770.53	3.80	0.0001
	DT	-0.51	0.14	0.60	-0.87	-0.16	-3.76	0.0002
	RT	-0.19	0.08	0.83	-0.40	0.03	-2.22	0.03
	Duration	-4.25	1.11	0.01	-7.11	-1.39	-3.83	0.0001

times can be associated with unambiguous sensory-motor encoding and visual spatial processing which in turn require low boundary; hence, the decision is mainly based on high-quality evidence and can therefore speed up. Since a cerebellar dysfunction alone seems to be sufficient to delay the latency of a wanted movement, a specific role of the cerebellum in controlling the onset of a voluntary movement is likely. The cerebellum, thus, through its connections, might speed up the information accumulation or reduce the noise in pre-frontal areas like the supplemental eye-field and pre-supplemental motor area, and parietal areas as the pre-frontal eye field, which are involved in determining the antisaccade onset. Moreover, the cerebellum forms reciprocal, closed-loop circuits with much of the cerebral cortex as well as subcortical regions such as basal ganglia and superior colliculus, suggesting a more extensive participation in complex cognitive functions including decision making. In addition, the left cerebellar hemisphere, is interconnected with the right parietal cortex for spatial orienting and attention, indicating a cerebellar role in early stages of visual spatial processing (Stoodley, 2016).

In conclusion, we suggest a latency-related modulation of duration adopted by the brain to increase the probability of reducing end-point errors in goal directed saccades. Specifically, the duration could be modulated depending on the latency-related decision time in order to perform efficient saccadic trajectories.

References

- Ahmad, S., Chappell, P.H., 2008. Moving approximate entropy applied to surface electromyographic signals. *Biomed. Signal Process. Control* 3, 88–93.
- Catz, N., Dicke, P.W., Thier, P., 2005. Cerebellar complex spike firing is suitable to induce as well as to stabilize motor learning. *Curr. Biol.* 15, 2179–2189.
- Chen-Harris, H., Joiner, W.M., Ethier, V., Zee, D.S., Shadmehr, R., 2008. Adaptive control of saccades via internal feedback. *J. Neurosci.* 28, 2804–2813.
- Cutsuridis, V., 2010. Neural accumulator models of decision making in eye movements. *Adv. Exp. Med. Biol.* 657, 61–72.

- Cutsuridis, V., Smyrnis, N., Evdokimidis, I., Perantonis, S., 2007. A neural model of decision-making by the superior colliculus in an antisaccade task. *Neural Netw.* 20, 690–704.
- Cutsuridis, V., Kumari, V., Ettinger, U., 2014. Antisaccade performance in schizo-phrenia: a neural model of decision making in the superior colliculus. *Front. Neurosci.* 8, 13.
- Everling, S., Munoz, D.P., 2000. Neuronal correlates for preparatory set associated with pro-saccades and anti-saccades in the primate frontal eye field. *J. Neurosci.* 20, 387–400.
- Federighi, P., Cevenini, G., Dotti, M.T., Rosini, F., Pretegiani, E., Federico, A., Rufa, A., 2011. Differences in saccade dynamics between spinocerebellar ataxia 2 and late-onset cerebellar ataxias. *Brain* 134, 879–891.
- Ford, K.A., Goltz, H.C., Brown, M.R., Everling, S., 2005. Neural processes associated with antisaccade task performance investigated with event-related fMRI. *J. Neurophysiol.* 94, 429–440.
- Golla, H., Tziridis, K., Haarmeier, T., Catz, N., Barash, S., Thier, P., 2008. Reduced saccadic resilience and impaired saccadic adaptation due to cerebellar disease. *Eur. J. Neurosci.* 27, 132–144.
- Gomez, P., Perea, M., 2014. Decomposing encoding and decisional components in visual-word recognition: a diffusion model analysis. *Q. J. Exp. Psychol. (Hove)* 67, 2455–2466.
- Gomez, P., Ratcliff, R., Perea, M., 2007. A model of the go-nogo task. *J. Exp. Psychol.* 136, 389–413.
- Hallett, P.E., 1978. Primary and secondary saccades to goals defined by instructions. *Vision Res.* 18, 1279–1296.
- Hopp, J.J., Fuchs, A.F., 2004. The characteristics and neuronal substrate of saccadic eye movement plasticity. *Prog. Neurobiol.* 72, 27–53.
- Hutton, S.B., 2008. Cognitive control of saccadic eye movements. *Brain Cogn.* 68, 327–340.
- Izawa, J., Rane, T., Donchin, O., Shadmehr, R., 2008. Motor adaptation as a process of reoptimization. *J. Neurosci.* 28, 2883–2891.
- Joiner, W.M., Shelhamer, M., 2009. A model of time estimation and error feedback in predictive timing behavior. *J. Comput. Neurosci.* 26, 119–138.
- Kerber, K.A., Jen, J.C., Perlman, S., Baloh, R.W., 2005. Late-onset pure cerebellar ataxia: differentiating those with and without identifiable mutations. *J. Neurol. Sci.* 238, 41–45.
- Kojima, Y., Soetedjo, R., Fuchs, A.F., 2010. Changes in simple spike activity of some Purkinje cells in the oculomotor vermis during saccade adaptation are appropriate to participate in motor learning. *J. Neurosci.* 30, 3715–3727.
- Kristjánsson, A., Chen, Y., Nakayama, K., 2001. Less attention is more in the preparation of antisaccades, but not prosaccades. *Nat. Neurosci.* 4, 1037–1042.
- Lagarias, J., Reeds, J., Wright, M., Wright, P., 1998. Convergence properties of the Nelder-Mead simplex method in low dimensions. *SIAM J. Optim.* 9, 112–147.
- Luce, R.D., 1986. Response Times: Their Role in Inferring Elementary Mental Organization. Oxford University Press, New York.
- McGill, W.J., 1963. Stochastic latency mechanisms. In: Luce, R.D., Bush, R.R., Galanter, E. (Eds.), *Handbook of Mathematical Psychology*. vol. 1. Wiley, New York, pp. 309–360.
- Munoz, D.P., Everling, S., 2004. Look away: the anti-saccade task and the voluntary control of eye movement. *Nat. Rev. Neurosci.* 5, 218–228.
- Noorani, I., 2014. LATER models of neural decision behavior in choice tasks. *Front. Integr. Neurosci.* 8, 67.
- Noorani, I., Carpenter, R.H., 2013. Antisaccades as decisions: LATER model predicts latency distributions and error responses. *Eur. J. Neurosci.* 37, 330–338.

- Olk, B., Kingstone, A., 2003. Why are antisaccades slower than prosaccades? A novel finding using a new paradigm. *Neuroreport* 14, 151–155.
- Palmer, E.M., Horowitz, T.S., Torralba, A., Wolfe, J.M., 2011. What are the shapes of response time distributions in visual search? *J. Exp. Psychol. Hum. Percept. Perform.* 37, 58–71.
- Pierrot-Deseilligny, C., Milea, D., Müri, R.M., 2004. Eye movement control by the cerebral cortex. *Curr. Opin. Neurol.* 17, 17–25.
- Pincus, S.M., 1991. Approximate entropy as a measure of system complexity. *Proc. Natl. Acad. Sci. U.S.A.* 88, 2297–2301.
- Pincus, S.M., Goldberger, A.L., 1994. Physiological time-series analysis: what does regularity quantify? *Am. J. Physiol.* 266, H1643–H1656.
- Pretegiani, E., Piu, P., Rosini, F., Federighi, P., Serchi, V., Tumminelli, G., Dotti, M.T., Federico, A., Rufa, A., 2018. Anti-saccades in cerebellar ataxias reveal a contribution of the cerebellum in executive functions. *Front. Neurol.* 9, 274.
- Richman, J.S., Moorman, J.R., 2000. Physiological time-series analysis using approximate entropy and sample entropy. *Am. J. Physiol. Heart Circ. Physiol.* 278, H2039–H2049.
- Rosini, F., Pretegiani, E., Mignarri, A., Optican, L.M., Serchi, V., De Stefano, N., Battaglini, M., Monti, L., Dotti, M.T., Federico, A., Rufa, A., 2017. The role of dentate nuclei in human oculomotor control: insights from cerebrotendinous xanthomatosis. *J. Physiol.* 595, 3607–3620.
- Schlag-Rey, M., Amador, N., Sanchez, H., Schlag, J., 1997. Antisaccade performance predicted by neuronal activity in the supplementary eye field. *Nature* 390, 398–401.
- Schwarz, W., 2001. The ex-Wald distribution as a descriptive model of response times. *Behav. Res. Methods Instrum. Comput.* 33, 457–469.
- Stoodley, C.J., 2016. The cerebellum and neurodevelopmental disorders. *Cerebellum* 15, 34–37.
- Trouillas, P., Takayanagi, T., Hallett, M., Currier, R.D., Subramony, S.H., Wessel, K., Bryer, A., Diener, H.C., Massaquoi, S., Gomez, C.M., Coutinho, P., Ben Hamida, M., Campanella, G., Filla, A., Schut, L., Timann, D., Honnorat, J., Nighoghossian, N., Manyam, B., 1997. International cooperative ataxia rating scale for pharmacological assessment of the cerebellar syndrome. The ataxia neuropharmacology committee of the World Federation of Neurology. *J. Neurol. Sci.* 145, 205–211.
- Van Rullen, R., Thorpe, S.J., 2001. Rate coding versus temporal order coding: what the retinal ganglion cells tell the visual cortex. *Neural Comput.* 13, 1255–1283.
- Voss, A., Voss, J., Lerche, V., 2015. Assessing cognitive processes with diffusion model analyses: a tutorial based on fast-dm-30. *Front. Psychol.* 6, 336.
- White, C.N., Ratcliff, R., Vasey, M.W., McKoon, G., 2010. Using diffusion models to understand clinical disorders. *J. Math. Psychol.* 54, 39–52.
- Xu-Wilson, M., Chen-Harris, H., Zee, D.S., Shadmehr, R., 2009. Cerebellar contributions to adaptive control of saccades in humans. *J. Neurosci.* 29, 12930–12939.

Further reading

- Harris, C.M., Wolpert, D.M., 2006. The main sequence of saccades optimizes speed-accuracy trade-off. *Biol. Cybern.* 95, 21–29.

This page intentionally left blank

Saccade variability in healthy subjects and cerebellar patients

10

Thomas Eggert*, Andreas Straube

Department of Neurology, University Hospital, LMU Munich, Munich, Germany

*Corresponding author: Tel.:+49 (0) 89-44007-4834; Fax:+49 (0) 89-44007-4801,
e-mail address: eggert@lrz.uni-muenchen.de

Abstract

In a previous study we developed a model for the inter-trial variance of saccade trajectories in the rhesus macaque. The analysis of that model showed that signal-dependent noise results in different effector variabilities depending on whether the noise is propagated feedforward through the system (accumulating noise) or whether the noise originates from inside of a premotor feedback loop (feedback noise). This allowed the gain of the premotor feedback loop to be estimated directly from behavioral data. In the present study, we applied the model in healthy human subjects and in patients with chronic isolated cerebellar lesions due to ischemic stroke. Humans showed smaller noise coefficients of variation for both accumulating noise and feedback noise and smaller feedback gain than the monkeys. Despite these differences in the model parameters, the qualitative differences between the two noise types were similar in both species.

Cerebellar patients showed larger inter-trial variance of saccade amplitude compared to controls, but saccade metrics and dynamics were well compensated. The parameters of the noise model did not differ significantly between groups. The variance of the saccade amplitude correlated highly ($r=0.95$) with the coefficient of variation of accumulating noise but not with the other model parameters. The results suggest that the cerebellum plays a role not only in premotor feedback but also in feedforward saccade control and that the latter is responsible for increased endpoint variance in cerebellar patients.

Keywords

Human, Eye movements, Saccade, Signal proportional noise

1 Introduction

Various noise sources within the sensorimotor system contribute to movement variability when visually guided movements are repeated under similar stimulus conditions (Faisal et al., 2008). For saccadic eye movements, the most important components are (1) motor noise due to the statistics of the recruitment of muscle-fibers

(Harris and Wolpert, 2006; Jones et al., 2002); (2) noise in the activity of premotor burst neurons which are supposed to be part of a motor feedback loop involving the brainstem and the cerebellum (Chen-Harris et al., 2008; Jürgens et al., 1981; Quaia et al., 2000; Robinson, 1975); and (3) planning noise related to the limited precision of target selection processes and of target representations in retinotopic maps (sensory and motor maps). Previous studies have mostly analyzed the variance and covariances of saccade parameters, such as amplitude, peak velocity and duration, to estimate the contribution of different noise sources (van Beers, 2007). In a recent study (Eggert et al., 2016), we extended these approaches by treating the entire saccade trajectory as a multivariate observation and developed a model which decomposed the variance/covariance structure of the trajectory into two distinct noise components, *feedback noise*, defined as noise which is generated within a premotor feedback loop, and *accumulating noise*, defined as noise which propagates through the motor system in a feedforward manner. Both planning noise and motor noise are examples of accumulating noise. These definitions were motivated by our observation that the variance/covariance structure of the saccade trajectory induced by planning noise and motor noise are similar, which makes it difficult to disentangle them. Consequently, we constrained our model to two components and subsumed motor noise and planning noise under the common term *accumulating noise*. The main advantage of this model is the possibility to estimate two characteristic features of the premotor feedback mechanism: the feedback gain and the strength of the feedback noise.

In our previous study (Eggert et al., 2016), we developed this model (Fig. 1), applied it to saccades of rhesus macaques (Robinson et al., 1993), and showed that the variance of eye displacement induced by accumulating noise increases

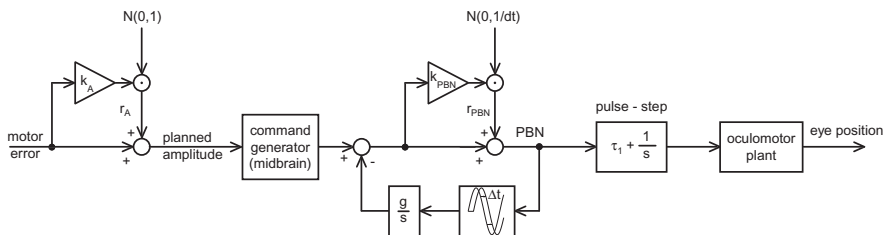


FIG. 1

Principal flowchart of the model (Eggert et al., 2016) accounting for two different noise sources: The noise (r_A) contaminates the sensory representation of the motor error (=retinal target eccentricity at saccade onset). This noise and the resulting planned saccade amplitude are scalar values evaluated before each saccade. The second noise is a stochastic process (r_{PBN}) which contaminates the premotor burst signal (PBN). In contrast to the first noise, which is propagated feedforward, r_{PBN} enters inside of a premotor feedback loop characterized by an integrator gain (g) and a delay $\Delta t = 4 \text{ ms}$. The standard deviation of both noise components is proportional to the respective signal with the coefficients of variation k_A and k_{PBN} .

monotonically during the entire saccade duration, whereas feedback noise caused increased variance during the saccade but played a minor role for endpoint variance. Feedback noise contributed substantially to the variance of eye displacement during the acceleration period but played only a minor role in the variance at the saccade end (i.e., the variance of the amplitude). Fitting this model to saccades executed during temporal inactivation of the caudal fastigial nucleus on one side of the cerebellum revealed, for saccades ipsiversive to the lesion, a significant decrease of the feedback gain compared to control conditions. This is in line with the previously suggested role of the cerebellum in premotor feedback because the caudal fastigial nucleus projects directly to the premotor burst neurons in the brainstem (Ohtsuka and Noda, 1991). In some monkeys, accumulating noise increased strongly during fastigial inactivation.

The current study investigates whether our model can also mimic the variance/covariance structure of saccades in healthy human subjects and in patients with isolated chronic lesions due to ischemic infarcts in the cerebellum. It also addresses the question whether increased variability of movement amplitude in cerebellar patients is caused by deficits of premotor feedback.

2 Methods

2.1 Subjects

A group of healthy control subjects (age: 53.7 ± 14.1 years; $N=9$) and a slightly older group of patients with cerebellar infarcts (age: 69.3 ± 15.2 years; $N=9$) participated in the study. All patients showed cerebellar signs in eye movement control such as fixation instabilities ($N=5$), nystagmus ($N=1$) or hypermetric saccades (gain >1.1 ; $N=3$). The infarcts were diagnosed by standard clinical magnetic resonance imaging (MRI). The cerebellar lesions were unilateral (left: $N=4$, right: $N=3$), or bilateral ($N=1$). The stroke occurred on average 11.1 ± 4.5 years before the study. All subjects were unexperienced in eye movement experiments. The experimental procedure was in accordance with the Declaration of Helsinki and was approved by the Ethics Committee of the Medical Faculty of the Ludwig-Maximilians University Munich (280-10).

2.2 Apparatus and procedure

Subjects sat in a darkened room at a viewing distance of 128 cm in front of a screen on which a red laser spot (diameter <2 mm) was projected. It was controlled by a mirror galvanometer (General Scanning 120D Watertown, MA, USA) and served as a fixation target which stepped between five different positions on the horizontal meridian ($0, \pm 5, \pm 10$ deg). The target steps were randomized in direction (right/left) and amplitude (5, 10 deg). The inter-target interval was 1.5 s. In each of two subsequent measurement blocks, subjects performed 80 visually guided saccades to this target. Eye movements were recorded with a head-mounted eye tracker

(Schneider et al., 2009) at a sampling frequency of 220 Hz. The eye tracker was synchronized with a real-time system (Hays et al., 1982) running on 1 kHz used to control the laser target. To minimize sampling artifacts, the eye position data were resampled offline into the frame rate of the stimulus generator (1 kHz) by linear interpolation. Eye velocity was then computed by a three-point differentiator applied after filtering the position data with a digital symmetric (zero-phase) Gaussian lowpass with a cut-off frequency of 33 Hz (attenuation of 0.1 at 85 Hz).

2.3 Data analysis

Saccade onset and end were defined as the time when eye velocity increased above or decreased below 10% of the peak velocity. Saccades with peak velocities smaller than 150 deg/s and amplitudes smaller than 3 deg were excluded from the analysis. The saccade gain was defined as the ratio between the saccade amplitude and the retinal eccentricity of the target at the time of saccade onset. Except for one patient with hypermetria of saccades directed toward the lesion side, none of the subjects showed a gain asymmetry between rightward and leftward saccades. Therefore, we mirrored the eye position trace of leftward saccades and pooled them with the rightward saccades.

To focus on the saccade variability due to internal noise sources, only a carefully selected subgroup of saccades responding to similar initial motor errors was submitted to the analysis of inter-trial saccade variability. Of all primary saccades, only those to the 10 deg target steps for which the initial motor error (i.e., the retinal target eccentricity at the time of saccade onset) ranged between 7.5 and 12.5 deg were selected. To make our estimates of inter-trial variance robust against outliers, we further excluded from this preselection all saccades in which either duration or amplitude differed from their respective median by more than three times the median-quartile distance (Velleman and Hoaglin, 1981). This outlier analysis was performed separately for each subject. After this selection, 45 ± 9 saccades remained to be analyzed for each subject.

Two different approaches were applied to describe the inter-trial variability of these saccades: A parametric approach in which saccade variability was expressed by the variance and covariance of saccade duration and amplitude, and a non-parametric approach in which the sampled saccade trajectory (eye displacement at each time point during the saccade) was directly considered as a multivariate random vector (Eggert et al., 2016). The main question of the parametric approach is whether the parameters of saccades with similar initial motor error vary along the main sequence, which would be expected in the case of pure planning noise. This was tested by computing the slope (α_{10} [deg/ms]) specifying the average increase of saccade amplitude per increase in saccade duration for saccades with initial motor errors of 10 deg. The slope α_{10} was estimated by linear regression of amplitude on duration, separately for each subject and pooling only across the saccades selected as described above. This slope was then compared with the slope (α_{all} [deg/ms]) specifying the increase of amplitude with duration along the main

sequence (Bahill et al., 1975; Becker, 1989; Van Opstal and Van Gisbergen, 1987). In contrast to α_{10} , α_{all} was computed by a regression of amplitude on duration across all primary saccades (pooling across all initial motor errors). $\alpha_{10} < \alpha_{all}$ suggests that the saccade amplitude is stabilized against variation of saccade duration by online motor-feedback. Similar approaches have been used previously (Jürgens et al., 1981; Quaia et al., 2000). This method is robust in demonstrating the incompatibility of the observed parameter variance with the assumption of pure planning noise, but it does not provide a direct estimate of the size of potentially involved noise sources or the feedback gain. This is attempted by our second approach, the non-parametrical approach which estimates the multivariate variance/covariance structure of the trajectories of saccades with similar initial motor error. Each of the selected saccade trajectories was treated as a single multivariate observation. The saccade onsets were aligned in time and all saccades were cut off to the duration of the shortest. Fig. 2 shows typical examples of these saccade trajectories.

From these selected traces, the inter-trial variance of eye displacement and its covariance with total eye displacement at saccade end was computed for each of

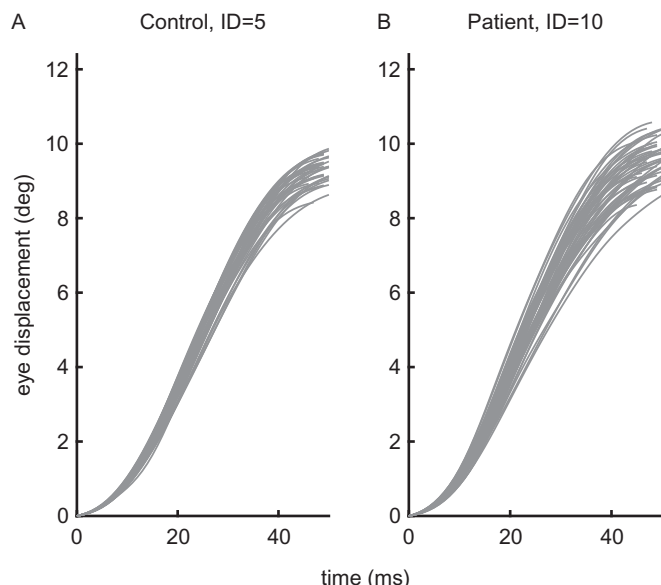


FIG. 2

Traces of eye displacement of a representative control subject (A, $N=40$) and a patient with a cerebellar infarct (B, $N=53$). Trials representing outliers in saccade duration or amplitude were eliminated. Each line shows a single saccade trajectory with an initial motor error between 7.5 and 12.5 deg. Even though this patient did not show systematic saccade dysmetria, the variance of the saccade amplitude (B: 0.33 deg^2) was larger than in the control subject (A: 0.14 deg^2).

the sampling points. These two time-courses are called the *variance trajectory* and the *covariance trajectory*, respectively. They represent the inter-trial variance/covariance structure of the saccade.

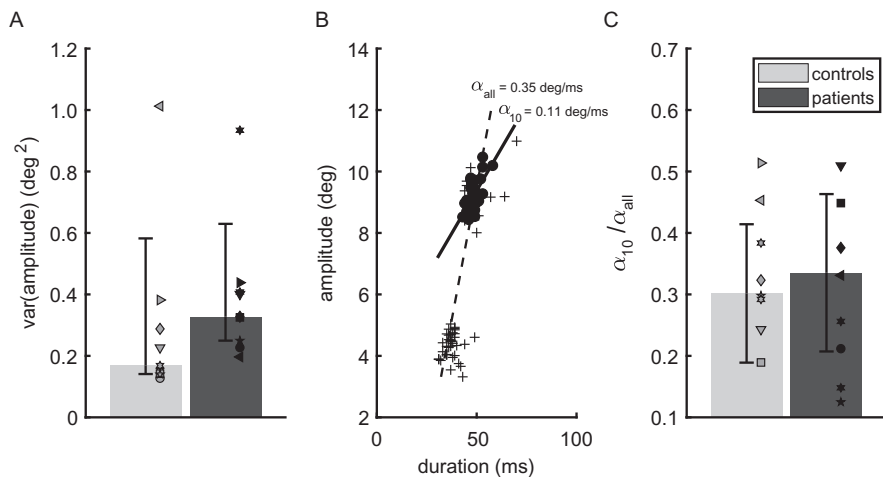
The variance and covariance trajectories were then decomposed into two components related to (1) noise generated within a premotor feedback loop, and (2) noise that is propagated feedforward through the motor system. For each individual subject, these two different noise components were fitted by our model (Eggert et al., 2016) with three parameters: the coefficient of variation of the planning noise (k_A), the coefficient of variation of the noise within the premotor feedback loop (k_{PBN}), and the feedback gain (g). To demonstrate that the noise component due to premotor feedback noise contributes significantly to the explanation of the observed saccade variance, two versions of the model were fitted to the data. The simplified version assumed that saccade noise was dominated by planning noise ($k_{PBN}=0$) and had only a single parameter (k_A) to minimize the mean squared distance between the observed and the modeled variance and covariance trajectories. The performance of this simplified model was compared with that of the full model with three parameters by means of the Akaike Information Criterion (Akaike, 1974; Burnham and Anderson, 2002). Positive differences $\Delta AIC = AIC(\text{simplified}) - AIC(\text{full})$ larger than 10 indicate that the simplified model performs worse than the full model in explaining the empirical data.

2.4 Statistics

Comparisons of saccade or model parameters between groups were performed with two-sample *t*-tests. The normality assumption of this test was confirmed by using the Lilliefors test. Since the inter-trial variances of saccade duration and amplitude were not normally distributed within the population, they were compared with the Wilcoxon rank-sum test. Normal distributions were characterized by mean \pm standard deviation, and non-normal distribution by median [interquartile range (iqr)]. The 95% confidence interval of the median of the amplitude-variance, shown by the whiskers in Fig. 3A, was computed using the function wilcox.test of the “stats” package in the R environment (R Core Team, 2012).

3 Results

Only three of the patients showed saccade hypermetria with saccade gains larger than two standard deviations above the mean of the control group. We pooled patients across saccade gains because the gains did not correlate with the variance of the saccade amplitude ($r = -0.24$; $t(16) = -0.99$; $P = 0.34$). The distribution of the gain of the selected saccades did not differ significantly between patients and controls. The mean gain, averaged across all subjects, was 0.99 ± 0.07 . Saccade latency was 235 ± 44 ms.

**FIG. 3**

Inter-trial variability of saccade parameters: (A) The variance of saccade amplitudes, pooled across saccades with similar initial motor error, was larger in patients than in controls. (B) Saccade duration and amplitudes of a typical subject. Filled circles: Selected trials with similar initial motor error. Crosses: trials with other initial motor errors. The increase of amplitude with duration was smaller for the selected trials (solid, slope α_{10}) than the one averaged across all trials (dashed, slope α_{all}). (C) The ratio α_{10}/α_{all} was smaller than one indicating that saccade amplitude was stabilized against variation in duration. This stabilization did not differ between patients and controls. Each symbol in A/C shows the data of one subject. Bars: median (A) or the mean (C) across the population; Whiskers: 95% confidence interval of the bars.

3.1 Parametric approach for the analysis of motor feedback

Investigating the inter-trial variability of the selected saccades with initial motor errors around 10 deg revealed that the inter-trial variance of the saccade amplitude (**Fig. 3A**) was larger (Wilcoxon: $P=0.05$) in the patients (0.33 [iqr= 0.17] deg 2) than in controls (0.17 [iqr= 0.17] deg 2). Amplitude variance did not correlate with age ($r=0.33$; $t(16)=1.38$; $P=0.19$). Neither the saccade duration (46.9 ± 4.1 ms) nor its inter-trial variance (4.53 [iqr= 7.77] ms 2) differed significantly between patients and controls. Within this pool of saccades responding to targets with similar retinal eccentricities, the saccade amplitude increased only by $\alpha_{10}=0.13 \pm 0.07$ deg/ms with increasing saccade duration, whereas the increase averaged across trials with any initial motor error was $\alpha_{all}=0.41 \pm 0.13$ deg/ms. This effect is illustrated in a representative subject in **Fig. 3B**. **Fig. 3C** shows that the ratio $\alpha_{10}/\alpha_{all}=0.32 \pm 0.15$ was significantly ($T(17)=-18.9$; $P<0.0001$) smaller than 1, indicating that saccade amplitude was stabilized against variation of saccade duration by an online motor-feedback. Neither α_{10} , nor α_{all} , nor the ratio α_{10}/α_{all} differed between patients and controls ($P>0.8$). Thus, the stabilization effects achieved by motor feedback did not differ between patients and controls.

3.2 Decomposition of the inter-trial variance of the saccade trajectory into accumulating noise and feedback noise

To verify that our model was able to differentiate between the two noise components (accumulating noise and feedback noise), we compared this model with a simplified version accounting for accumulating noise only. The AIC-difference between the simplified and the complete model was $\Delta AIC = 31.2 \pm 11.9$ and did not differ between patients and controls ($P > 0.3$). Thus, including the feedback noise in the model improved its ability to explain the measured variance/covariance trajectories.

Fig. 4 shows how the measured variance trajectories (blue) were decomposed into accumulating noise (green) and feedback noise (magenta). The characteristic difference between these two noise components is that the accumulating noise increases monotonically, whereas the feedback noise shows a bell-shaped profile

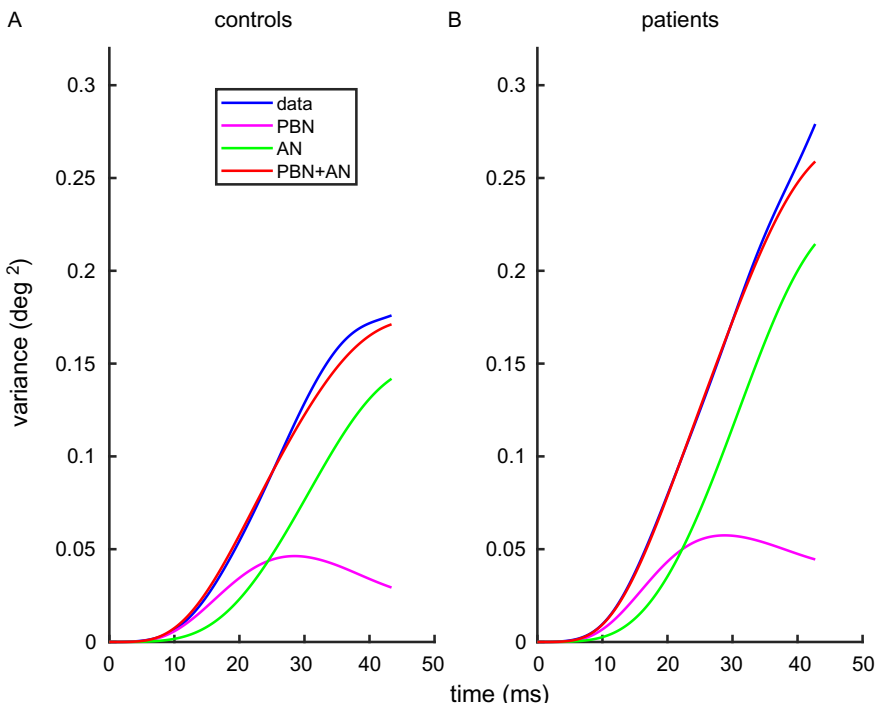


FIG. 4

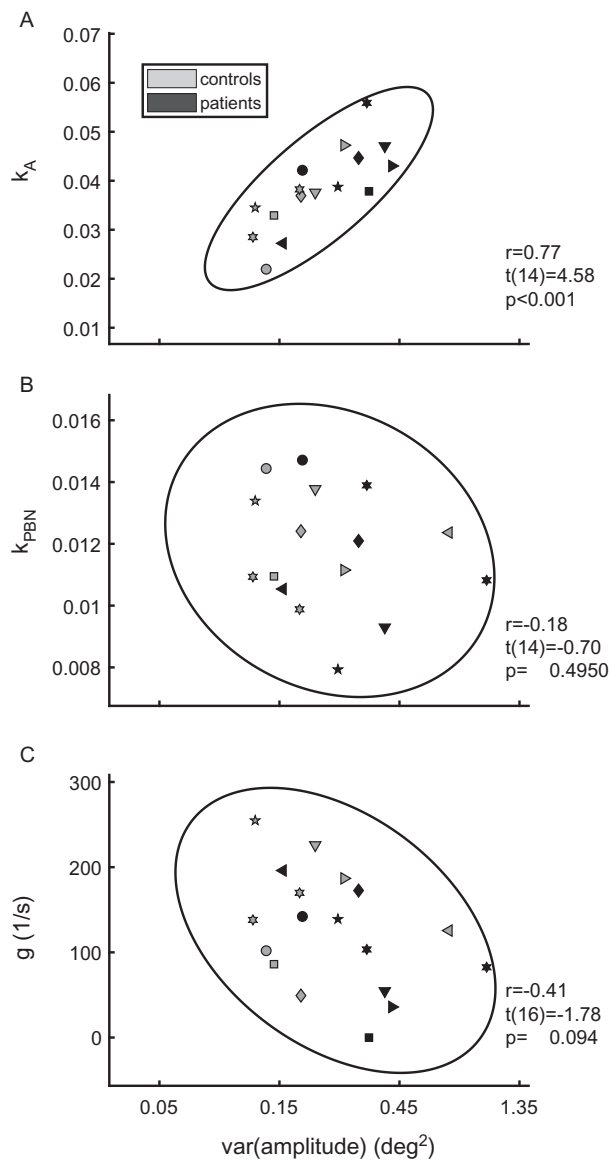
The mean variance trajectories (blue), decomposed into the mean variance related to signal-dependent noise entering inside of a premotor feedback loop (PBN, magenta), and the mean accumulating noise (AN, green). The mean model prediction (red) shows the sum of feedback noise and accumulating noise. Traces were computed by averaging the variance trajectories across all controls (A) and all patients (B) and across all models fitted separately to the data of each subject.

(due to feedback compensation). The positive ΔAIC reflects the observation that the eye displacement increased during the acceleration phase of the saccade faster than predicted by pure accumulating noise. This allowed not only the size of the accumulating noise (quantified by k_A), but also the size and the width of the variance component due to feedback noise (quantified by k_{PBN} and g) to be estimated. The individual fits achieved coefficients of determination close to one ($R^2=0.979\pm 0.015$), despite the considerable inter-subject difference of the variance trajectories. The three fitted model parameters ($k_A=0.0425\pm 0.0143$; $k_{PBN}=0.0117\pm 0.0030$; $g=126\pm 68\text{ s}^{-1}$) did not differ significantly between patients and controls ($P>0.16$). Thus, the increased variance of the saccade amplitude in patients compared to controls was not reflected in significant group effects on the model parameters. This is because the variance trajectories varied between subjects (also within groups) in more than a single dimension. This 3D-variation masked the group effect on the variance of the saccade amplitude which constitutes only one particular aspect of the overall movement variability. However, the group effect sizes (Cohen's d : $k_A:+0.5561$, $k_{PBN}:-0.3205$, $g:-0.6925$) on k_A and g could be classified as "medium" (Cohen, 1988) and were larger than the group effect on k_{PBN} . Power analysis showed that the corresponding increase of the planning noise coefficient ($\Delta k_A=+0.008$) and the decrease of the feedback gain ($\Delta g=-45\text{ s}^{-1}$) in the patient group would require 52 subjects in each group in order to be detectable at a type I error probability of 0.05 with a power of 0.8.

Fig. 5 shows that the variance of saccade amplitude was positively correlated (Pearson's: $r=0.77$, $P<0.001$) with the planning noise coefficient k_A , but not with the feedback noise coefficient k_{PBN} . The variance of saccade amplitude tended to decrease with increasing feedback gain g ($r=-0.41$; $P=0.09$). This reflects the model feature that at the saccade end, the feedback noise is relatively small compared to the accumulating noise (see Fig. 4), and that increased variance of saccade amplitude was predominantly explained by increased accumulating noise and only marginally by decreased feedback gain.

4 Discussion

The results showed that variance/covariance structure of human saccades consists of different components similar to in the rhesus macaque. The AIC-analyze showed, in line with the parametric approach, that planning noise (or accumulating noise) alone cannot explain the measured inter-trial variance. By taking the feedback noise into account, the model achieved very high coefficients of determination (R^2) when fitted to the data of individual subjects, despite considerably inter-individual differences. This allowed the two main characteristics of feedback noise: the coefficient of variation k_{PBN} and the feedback gain g to be estimated in addition to the coefficient of variation of the planning noise (k_A). The humans examined in the current study showed smaller noise-coefficients of variation and smaller feedback gain compared to our previous estimates (Egger et al., 2016) of the model parameters in rhesus

**FIG. 5**

Correlation between the inter-trial variance of the saccade amplitude and the three fitted model parameters for all subjects (symbols). The coefficient of variation of the planning noise k_A (A) showed a significant positive correlation and the feedback gain g (C) showed a marginal tendency for a negative correlation with the endpoint variance. The coefficient of variation of the feedback noise k_{PBN} (B) was uncorrelated with endpoint variance.

macaques ($k_A = 0.106 \pm 0.048$; $k_{PBN} = 0.028 \pm 0.008$; $g = 240 \pm 59 \text{ s}^{-1}$). These differences may be related to the fact that rhesus macaques usually show smaller latencies, smaller saccade durations, and larger peak velocity than humans. Despite these differences in the model parameters, the characteristic difference between the two noise components was the same for human and non-human primates: The accumulating noise increased monotonically, whereas the feedback noise peaked during the saccade and decreased toward its end. This feature, as well as the correlation pattern shown in Fig. 5 shows that individual differences of the endpoint variance are primarily due to differences in accumulating noise rather than to differences in feedback noise.

The observation that neither saccade duration and gain, nor the parameters of the noise model differed significantly between our patient group and our controls may reflect the clinical observation, that patients with focal, unilateral cerebellar lesions are in general less severely affected than patients with bilateral lesions. None of our patients showed an isolated lesion of the deep cerebellar nuclei comparable to the pharmacological inactivation study (Robinson et al., 1993). Nevertheless, the patient group showed increased variance of the saccade amplitude, which was explained by the model by increased planning noise. The direction of the (non-significant) differences of the model parameters between patients and controls pointed toward increased planning noise and decreased feedback gain associated with a cerebellar lesion. Like in monkeys, substantial premotor feedback was preserved while the cerebellar was lesioned.

In summary, both the human and the monkey data suggest that the cerebellum plays a role in inter-trial saccade variability. The cerebellum contributes to premotor feedback but is most probably not the only structure involved. Moreover, increased variance of saccade amplitude induced by cerebellar lesions is not primarily related to impaired feedback but rather explained by increased planning noise. Such an effect may be due to a role of the cerebellum in the feedforward path of saccadic control (Glasauer, 2003) or to a more indirect effect on the motor planning in response to the need to compensate for the cerebellar deficit.

Acknowledgments

The study was supported by the German Federal Ministry of Education and Research (initiative IFB—grant number: IFB DSGZ 01EO1401).

References

- Akaike, H., 1974. A new look at the statistical model identification. *IEEE Trans. Autom. Control* 19, 716–723.
- Bahill, A.T., Clark, M.R., Stark, L., 1975. The main sequence, a tool for studying human eye movements. *Math. Biosci.* 24, 191–204.
- Becker, W., 1989. The neurobiology of saccadic eye movements. *Metrics. Rev. Oculomot. Res.* 3, 13–67.

- Burnham, K.P., Anderson, D.R., 2002. Model Selection and Multimodel Inference: A Practical Information-Theoretic Approach. Springer Science & Business Media.
- Chen-Harris, H., Joiner, W.M., Ethier, V., Zee, D.S., Shadmehr, R., 2008. Adaptive control of saccades via internal feedback. *J. Neurosci.* 28, 2804–2813.
- Cohen, J., 1988. Statistical Power Analysis for the Behavioral Sciences. 2nd. Erlbaum, Hillsdale, NJ.
- Eggert, T., Robinson, F.R., Straube, A., 2016. Modeling inter-trial variability of saccade trajectories: effects of lesions of the oculomotor part of the fastigial nucleus. *PLoS Comput. Biol.* 12, e1004866.
- Faisal, A.A., Selen, L.P., Wolpert, D.M., 2008. Noise in the nervous system. *Nat. Rev. Neurosci.* 9, 292–303.
- Glasauer, S., 2003. Cerebellar contribution to saccades and gaze holding. *Ann. N. Y. Acad. Sci.* 1004, 206–219.
- Harris, C.M., Wolpert, D.M., 2006. The main sequence of saccades optimizes speed-accuracy trade-off. *Biol. Cybern.* 95, 21–29.
- Hays, A.V.J., Richmond, B.J., Optican, L.M., 1982. Unix-Based Multiple-Process System, for Real-Time Data Acquisition and Control. Electron Conventions, El Segundo, CA. None.
- Jones, K.E., Hamilton, A.F.D.C., Wolpert, D.M., 2002. Sources of signal-dependent noise during isometric force production. *J. Neurophysiol.* 88, 1533–1544.
- Jürgens, R., Becker, W., Kornhuber, H., 1981. Natural and drug-induced variations of velocity and duration of human saccadic eye movements: evidence for a control of the neural pulse generator by local feedback. *Biol. Cybern.* 39, 87–96.
- Ohtsuka, K., Noda, H., 1991. Saccadic burst neurons in the oculomotor region of the fastigial nucleus of macaque monkeys. *J. Neurophysiol.* 65, 1422–1434.
- Quaia, C., Paré, M., Wurtz, R.H., Optican, L.M., 2000. Extent of compensation for variations in monkey saccadic eye movements. *Exp. Brain Res.* 132, 39–51.
- R Core Team, 2012. R: A Language and Environment for Statistical Computing. R Foundation for Statistical Computing, Vienna, Austria, ISBN 3-900051-07-0, URL <http://www.R-project.org/>. [software].
- Robinson, D.A., 1975. Oculomotor control signals. In: Bach-y-rita, P., Lennerstrand, G. (Eds.), Basic Mechanisms of Ocular Motility and Their Clinical Implications. Oxford: Pergamon Press.
- Robinson, F.R., Straube, A., Fuchs, A.F., 1993. Role of the caudal fastigial nucleus in saccade generation. II. Effects of muscimol inactivation. *J. Neurophysiol.* 70, 1741–1758.
- Schneider, E., Villgrattner, T., Vockeroth, J., Bartl, K., Kohlbecher, S., Bardins, S., Ulbrich, H., Brandt, T., 2009. Eyeseecam: an eye movement–driven head camera for the examination of natural visual exploration. *Ann. N. Y. Acad. Sci.* 1164, 461–467.
- Van Beers, R.J., 2007. The sources of variability in saccadic eye movements. *J. Neurosci.* 27, 8757–8770.
- Van Opstal, A.J., Van Gisbergen, J.A., 1987. Skewness of saccadic velocity profiles: a unifying parameter for normal and slow saccades. *Vision Res.* 27, 731–745.
- Velleman, P.F., Hoaglin, D.C., 1981. Applications, Basics, and Computing of Exploratory Data Analysis. Duxbury Press.

Electrical stimulation in a spiking neural network model of monkey superior colliculus

11

A. John van Opstal^{a,*}, Bahadir Kasap^b

^a*Department of Biophysics, Donders Institute for Brain, Cognition and Behaviour, Radboud University Nijmegen, Nijmegen, The Netherlands*

^b*Department of Biophysics, Radboud University, Donders Centre for Neuroscience, Nijmegen, The Netherlands*

*Corresponding author: Tel.: +31-243-614-251, e-mail address: j.vanopstal@donders.ru.nl

Abstract

The superior colliculus (SC) generates saccades by recruiting a population of cells in its topographically organized motor map. Supra-threshold electrical stimulation in the SC produces a normometric saccade with little effect of the stimulation parameters. Moreover, the kinematics of electrically evoked saccades strongly resemble natural, visual-evoked saccades. These findings support models in which the saccade vector is determined by a center-of-gravity computation of activated neurons, while trajectory and kinematics arise in brainstem-cerebellar feedback circuits. Recent single-unit recordings, however, have indicated that the SC population also specifies the instantaneous saccade kinematics, supporting an alternative model, in which the saccade trajectory results from dynamic summation of movement effects of all SC spike trains. Here we reconcile the linear summation model with stimulation results, by assuming that the electric field directly activates a relatively small set of neurons around the electrode tip, which subsequently sets up a large population response through lateral synaptic interactions.

Keywords

Saccades, Motor map, Spatial-temporal transformation, Lateral synaptic interactions, Population coding, Vector averaging, Linear summation

1 Introduction

The midbrain superior colliculus (SC) is an important common terminal for cortical and subcortical inputs involved in saccade generation, and specifies a gaze-displacement command for downstream eye-head motor circuitries (Moschovakis et al., 1998; Robinson, 1972; Scudder, 1988). It contains a topographic map of

saccade vectors, in which amplitude is represented logarithmically along its rostral-caudal axis, and saccade direction maps roughly linearly along the medial-lateral axis (Ottes et al., 1986; Robinson, 1972).

Each saccade is associated with a translation-invariant Gaussian population, the center of which corresponds to the site of the saccade vector in the map (Ottes et al., 1986; Van Opstal et al., 1990). It is assumed that each recruited neuron encodes a tiny movement contribution, determined by its location in the motor map, and by its activity.

Two competing models have been proposed for decoding this population: weighted averaging of the cells' vector contributions (Lee et al., 1988; Port and Wurtz, 2003; Walton et al., 2005) vs. their linear summation (Goossens and Van Opstal, 2006, 2012; Van Gisbergen et al., 1985):

$$S_{AVG} = \frac{\sum_{n=1}^N F_n \cdot \mathbf{M}_n}{\sum_{n=1}^N F_n} \quad (1a)$$

versus

$$S_{SUM}(t) = \sum_{n=1}^N \sum_{k=1}^{K_n < t} \delta(t - \tau_{n,k}) \cdot \mathbf{m}_n \quad (1b)$$

N is the number of active neurons in the population, $K_n < t$ is the number of spikes from neuron n up to time t , F_n is mean firing rate, and \mathbf{M}_n is the saccade vector encoded at the SC site of cell n ; $\mathbf{m}_n = \zeta \mathbf{M}_n$ is the tiny contribution of cell n in the direction of \mathbf{M}_n for each of its spikes (the cell's “spike vector”); ζ is a fixed scaling, $\delta(t - \tau_{k,n})$ the k 'th spike of neuron n , fired at time $\tau_{k,n}$.

The vector-averaging scheme only specifies the amplitude and direction of the saccade vector, and places the SC motor map outside the kinematic control loop of its trajectory. The nonlinear amplitude-peak velocity relationship of saccades is thus generated by dynamic feedback circuits in brainstem-cerebellar pathways (Jürgens et al., 1981; Lee et al., 1988; Lefèvre et al., 1998; Quaia et al., 1999; Robinson, 1975).

In contrast, the linear spike-vector summation model encodes the full kinematics of the saccade trajectory at the level of the SC motor map through the temporal distribution of all spikes in the population (Goossens and Van Opstal, 2006, 2012). As a result, the instantaneous firing rates of all neurons together encode the saccadic velocity profile.

Clearly, the models of Eqs. (1a) and (1b) cannot both be right. Yet, each is supported by different lines of evidence. For example, micro-stimulation with rectangular current pulse-profiles produces fixed-vector E-saccades with normal kinematics that remain invariant to changing stimulation parameters (Katnani and Gandhi, 2012; Robinson, 1972; Van Opstal et al., 1990; Stanford et al., 1996). The vector-averaging scheme can readily account for this, since the center of gravity of the population only specifies the saccade vector. However, although

the vector-averaging model also predicts the observed pattern of saccadic dysmetrias to focal reversible lesions, it fails to explain the concurrent substantial slowing of saccades (Lee et al., 1988). As this latter observation is accounted for by the linear summation model (Goossens and Van Opstal, 2006), it further supports the idea that the SC population encodes both the saccade-vector and its kinematics.

Micro-stimulation experiments have also shown that at low current strengths, around threshold, E-saccades become smaller and slower than main sequence (Van Opstal et al., 1990; Katnani and Gandhi, 2012). These results do not follow from vector averaging either, but are explained by dynamic summation.

Clearly, if stimulation would produce a population profile that mimics the imposed rectangular current pulse (as is typically assumed), the summation model would generate severely distorted saccade-velocity profiles. Yet, little is known about the actual activity profiles in the motor map during micro-stimulation, as neural recordings during stimulation are not available, or remain obscured by large artifacts.

Two factors determine neuronal activation by micro-stimulation: (1) direct (feed-forward) current stimulation of cell bodies and axons, and (2) synaptic activation through lateral (feedback) connections among the neurons in the motor map. How each factor contributes to the population activity is not known. It is conceivable, however, that the electric field drops rapidly with distance from the electrode tip, so that a relatively small number of neurons would be directly stimulated by the electrode.

Indeed, two-photon imaging in frontal eye fields (FEF) revealed that only a sparse set of neurons was activated directly around the immediate vicinity of the stimulation site (Histed et al., 2009), suggesting that the major factor may be synaptic transmission.

We recently constructed a spiking neural network model with lateral interactions in the SC that explains the single-unit activity patterns around saccades (Kasap and Van Opstal, 2017). It accounts for the observed firing rates of collicular cells (Goossens and Van Opstal, 2006, 2012) in response to neural input from upstream sources (e.g., FEF). This paper provides a brief overview on how the model might cope with the effects of electrical micro-stimulation (see Kasap and Van Opstal, 2019, for a full account).

2 Methods and results

2.1 Afferent mapping

The afferent mapping function maps the target (R, ϕ) , in visual space, to the anatomical coordinates, (u, v) (in mm), of the SC motor map (Ottes et al., 1986). We here simplified this mapping by the complex logarithm:

$$u(R) = B_u \cdot \ln(R) \text{ and } v(\phi) = B_v \cdot \phi \quad (2)$$

with $B_u = 1.0$ mm and $B_v = 1.0$ mm/rad (isotropic map). Thus, the infinitesimal movement contribution, $\mathbf{m} = (m_x, m_y)$, of a single spike at site (u, v) to the eye movement (Eq. 1b) is given by the scaled efferent mapping:

$$m_x = \zeta \cdot \exp(u) \cdot \cos(v) \text{ and } m_y = \zeta \cdot \exp(u) \cdot \sin(v) \quad (3)$$

2.2 Network characteristics

We constructed a 2D spiking neural network model as a rectangular grid of 201×201 neurons (e.g., Fig. 3A), and simulated the network dynamics in C++/CUDA (Nickolls et al., 2008). In the simulations we employed dynamic parallelism to accelerate spike propagation on a GPU (Kasap and Van Opstal, 2018).

Neurons were modeled as adaptive exponential integrate-and-fire (AdEx; Brette and Gerstner, 2005), which reduces the Hodgkin-Huxley equations to two state variables: membrane potential, $V(t)$, and adaptation current, $q(t)$. The neuronal dynamics are determined by two coupled, nonlinear differential equations and a spiking-reset (Fig. 1B). For neuron n :

$$C \frac{dV_n}{dt} = -g_L(V_n - E_L) + g_L \eta \exp\left(\frac{V_n - V_T}{\eta}\right) - q_n + I_{inp,n}(t) \quad (4a)$$

$$\tau_{q,n} \frac{dq_n}{dt} = a(V_n - E_L) - q_n \quad (4b)$$

$$\text{at } t = \tau_{spk} : V(\tau_{spk}) \rightarrow V_{rst} \text{ and } q(\tau_{spk}) \rightarrow q(\tau_{spk}) + b \quad (4c)$$

with C the membrane capacitance, g_L the leak conductance, E_L the leak reversal potential, η a slope, V_T the neural spiking threshold, V_{rst} the reset potential, $\tau_{q,n}$ the adaptation time constant, and a the sub-threshold adaptation constant. Fig. 1C shows the response patterns of three AdEx neurons to different input currents and membrane properties.

In Eq. (4a), $I_{inp,n}$ is the neuron's total synaptic input current, provided by the lateral interactions with other neurons, and the externally applied micro-stimulation current (Fig. 1A):

$$I_{inp,n}(t) = g_n^{exc}(t)(E_e - V_n(t)) + g_n^{inh}(t)(E_i - V_n(t)) + I_E(u_n, v_n, t) \quad (5)$$

The lateral synaptic connections of neuron n with other neurons in the map are described by a Mexican-hat profile (Trappenberg et al., 2001), with local (σ_{exc}) excitatory and global (σ_{inh}) inhibitory projections ($\sigma_{exc} > \sigma_{inh}$; Fig. 2B). This profile has an overall synaptic scaling factor, s_n , depending on a cell's location (Fig. 2A). Neurons thus underwent strong short-range excitatory and weak long-range inhibitory influences through a dynamic soft winner-take-all mechanism. The “winner” governs the activity patterns of all other active neurons, inducing spike-train synchronization in the population (Goossens and Van Opstal, 2012; Kasap and Van Opstal, 2017; Fig. 2C).

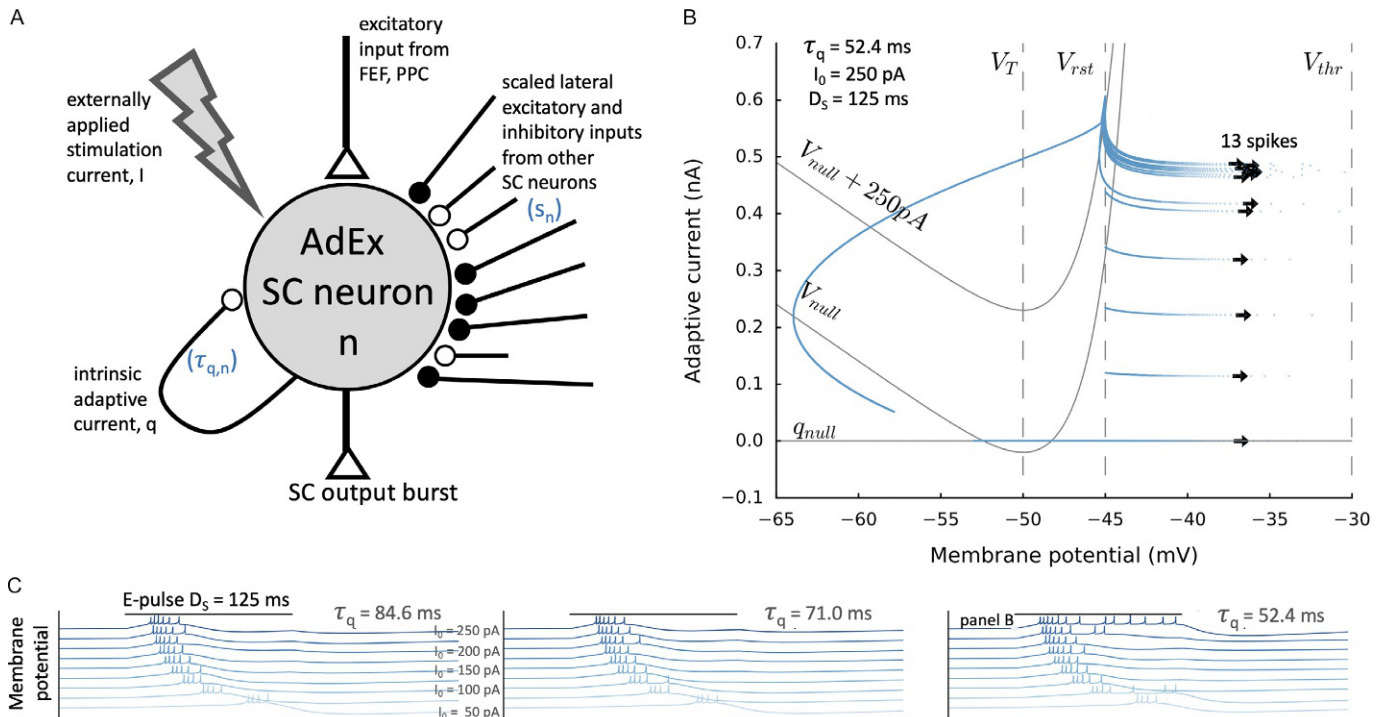


FIG. 1

(A) Schematic representation of an AdEx spiking SC neuron; two tuning parameters, s_n and $\tau_{q,n}$ determine its spiking behavior. (B) Phase plot (membrane potential vs. adaptive current) of the neuronal response (with $\tau_q=52.4 \text{ ms}$) to micro-stimulation ($I_0 = 250 \text{ pA}$, $D_S=125 \text{ ms}$). V - and q -nullclines are fixed-point trajectories of Eq. (4a) and (4b). Spike occurrences are indicated by arrows. (C) Responses of three model neurons ($\tau_q=84.6 \text{ ms}$, $\tau_q=70.95 \text{ ms}$, and $\tau_q=52.4 \text{ ms}$) to micro-stimulation at different current strengths (colored traces; $D_S = 125 \text{ ms}$).

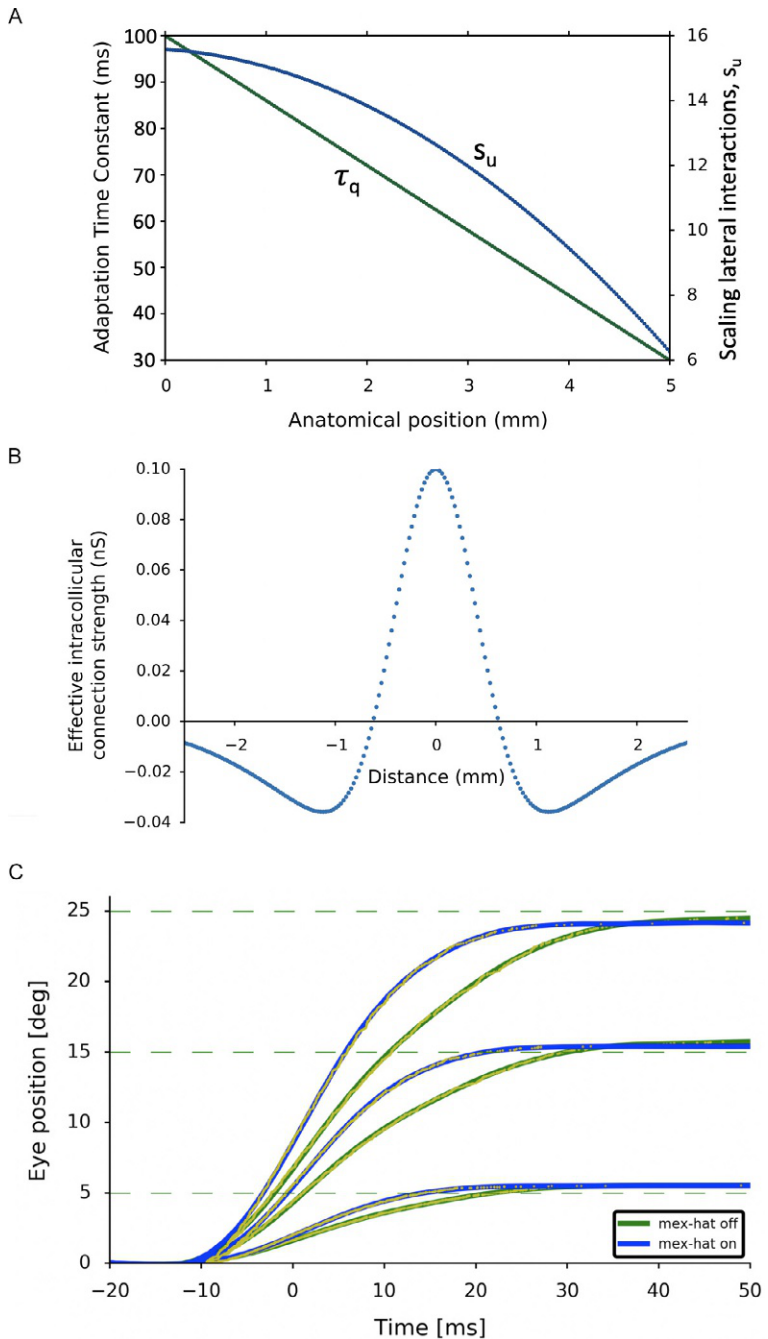


FIG. 2

(A) Result of tuning the site-dependent parameters in the model: $\tau_{q,n}$ (green line) and s_n (blue line), as function of u . (B) Lateral-interaction profile in the network, for a neuron in the center of the motor map. (C) Result of simulated saccades for two situations: without lateral interactions (green) and with lateral interactions (blue). The latter saccades are considerably faster, because of synchronization of neural activity in the population with the most-active neuron (see Fig. 3B).

2.3 Current spread

We applied electrical stimulation with an external current, centered around $[u_E, v_E]$, with an exponential spatial decay of the effective electric field:

$$I_E(u, v, t) = I_0 \cdot \exp\left(-\lambda \cdot \sqrt{(u - u_E)^2 + (v - v_E)^2}\right) \cdot P(t) \quad (6)$$

with λ (mm^{-1}) the spatial decay constant, I_0 the current intensity (in pA), and a rectangular stimulation pulse, $P(t)$, with duration D_S .

2.4 Network tuning

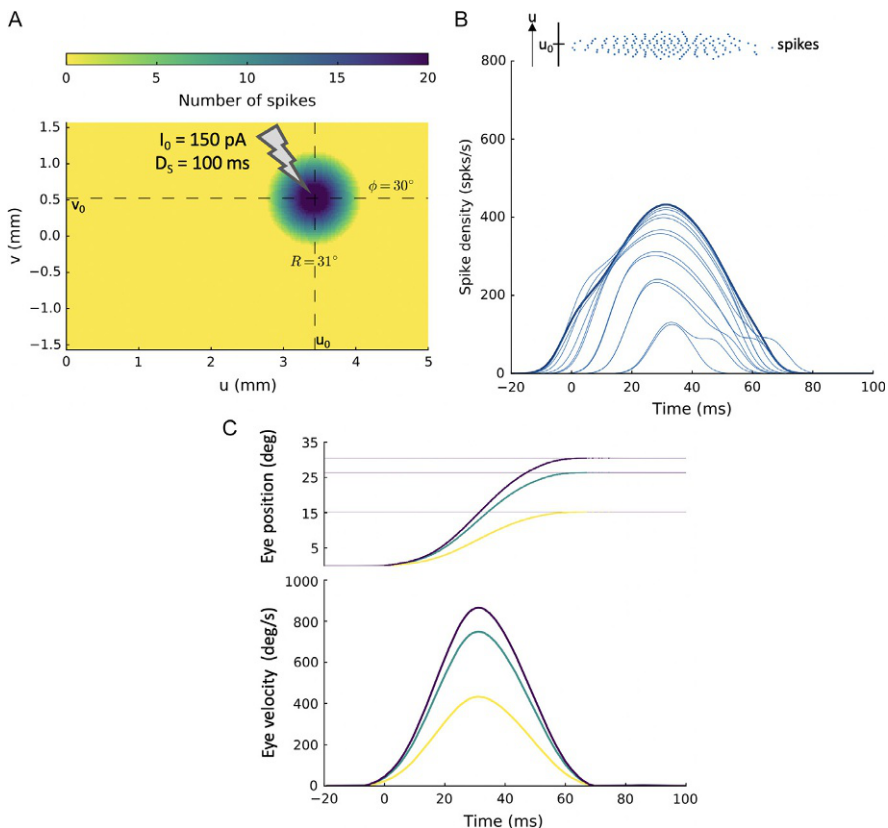
Intrinsic biophysical properties of the neurons were enforced by systematically varying the adaptation time constant, $\tau_{q,n}$, and the synaptic weight-scaling parameter, s_n . By tuning these two parameters, we accounted for the systematically changing firing properties of SC cells along the rostral-caudal axis of the motor map, while keeping a fixed number of spikes for the neurons' preferred saccades across the map. We used a genetic algorithm to find appropriate location-dependent $[\tau_{q,n}, s_n]$ pairs for the neurons, to ensure a fixed number of spikes per neuron under a given micro-stimulation condition, and the subsequent excitation profile through the lateral interactions (Fig. 3A). All parameters are summarized in [Appendix](#).

2.5 Micro-stimulation

[Fig. 3A–C](#) shows the effect of micro-stimulation at a caudal location in the motor map, yielding an oblique saccade with an amplitude of 31 deg. The size of the resulting population is very similar to that of a visual stimulus ($\sigma_{\text{POP}} = 0.5$ mm; [Kasap and Van Opstal, 2017](#)), and also the number of spikes elicited by the cells ($N = 20$ for the central cell, see color bar) corresponds to the normal condition. The peak firing rates of the neurons reached a maximum of about 450 spikes/s, with burst durations up to about 70 ms. The saccade reached a peak velocity of ~ 900 deg/s, while horizontal and vertical velocity profiles have identical shapes, indicating a straight oblique trajectory.

2.6 Kinematics

[Fig. 4A](#) and B presents E-saccades for nine stimulation sites along the horizontal meridian. Note that saccade duration increases with saccade amplitude, and that peak eye velocity shows a less than linear increase with saccade size. The nonlinear, saturating main sequence of these E-saccades is shown in [Fig. 4C](#). We also verified that the saccades remained invariant to a wide range of stimulation parameters, which is illustrated in [Fig. 4D](#). Around the threshold (around 80 pA), the peak velocity decreased substantially, but without affecting E-saccade amplitudes (not shown).

**FIG. 3**

(A) Spike counts in the motor map from the recruited population to micro-stimulation at $(u_E, v_E) = (3.2, 0.5)$ mm. (B) Burst profiles of the model neurons (at 0.1 mm intervals from the central cell along the u -direction) portray synchronized population activity. (C) Eye displacement and eye velocity from linear dynamic ensemble-coding (Eq. 1b; horizontal (green), vertical (yellow), and vectorial (purple) traces).

3 Discussion

The linear ensemble-coding model of Eq. (1b) (Goossens and Van Opstal, 2006; Van Gisbergen et al., 1987; Van Opstal and Goossens, 2008) is inconsistent with micro-stimulation results, when it is assumed that (i) a rectangular stimulation input profile (Eq. 6) directly imposes the firing patterns on the neural population, and (ii) neurons are independent, without synaptic interactions.

We here argued that these assumptions are neither supported by experimental observations, nor do they incorporate the possibility that a major factor determining the recruitment of SC neurons is caused by synaptic transmission within the motor map, rather than by direct activation through the electrode's electric field. We

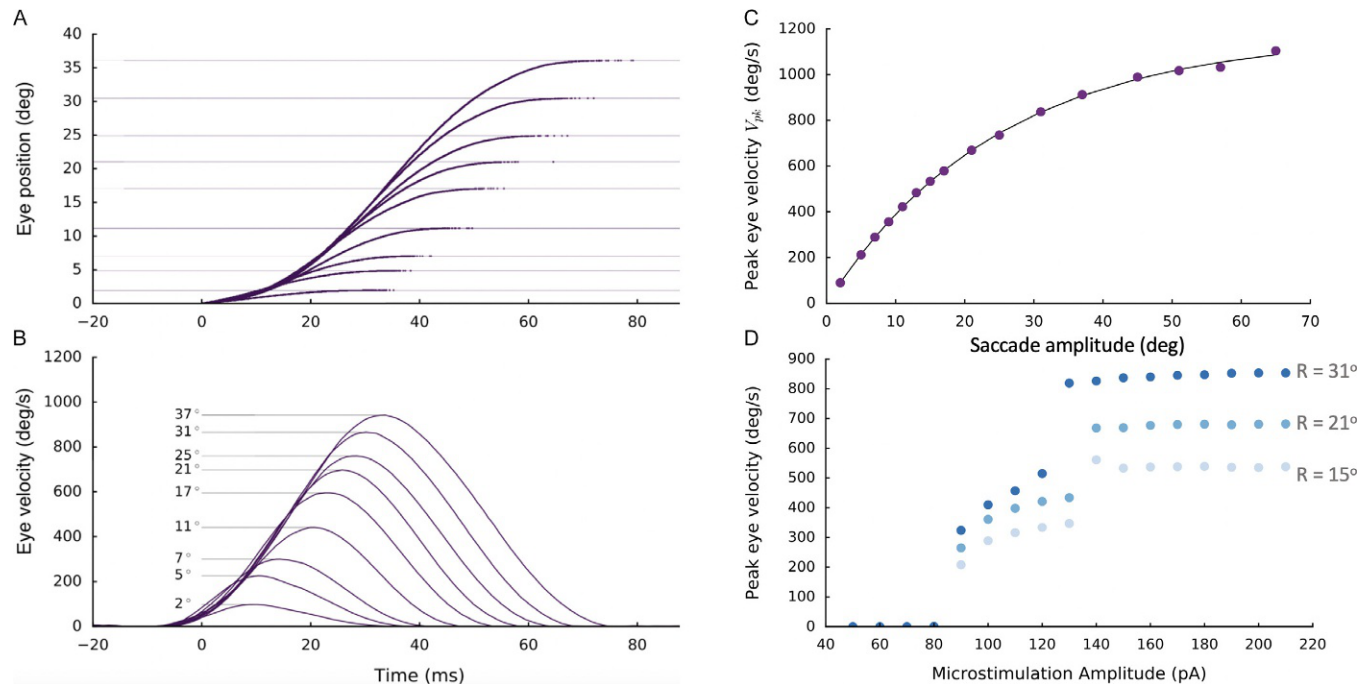


FIG. 4

- (A) Eye-displacement traces for nine horizontal E-saccades, elicited with $I_0 = 150$ pA, $D_S = 100$ ms at different sites in the motor map.
- (B) Eye-velocity profiles for the position traces in A. Note the clear increase in saccade duration, and the sublinear increase of peak eye-velocity with saccade amplitude. (C) A nonlinear, saturating main sequence, despite fully linear weighting of SC spike vectors (Eq. 1b). (D) Above 125 pA, saccade kinematics remained invariant for a large range of stimulation strengths. Near threshold (~ 80 pA), they became markedly slower.

implemented circular-symmetric, Mexican-hat like interactions in a spiking neural network model of the SC motor map and assumed that the current profile from the electrode rapidly decreased with distance from the electrode tip. As a consequence, only neurons in the direct vicinity (<0.1 mm) of the electrode were activated by the external electric field (Histed et al., 2009), insufficient to generate the saccade according to spike-vector summation (Eq. 1b).

Once neurons were recruited by the stimulation pulse, however, local excitatory synaptic transmission among nearby cells rapidly spread the activation to create a neural activity pattern which, within 10–15 ms, was dictated by the bursting dynamics of the most active central cells in the population (Fig. 3B, top). As a result, all cells synchronized their peak firing rates, and burst shapes within the population were highly correlated. Similar response properties have been reported in recordings for natural, sensory-evoked saccades (Goossens and Van Opstal, 2012). According to the dynamic spike-summation model (Eq. 1b), such high level of neuronal synchronization ensures an optimally strong input to the brainstem saccadic burst generator to accelerate the eye with the maximally possible innervation.

3.1 Network tuning

The lateral excitatory-inhibitory synaptic interactions, in combination with the site-dependent tuning of the neurons' biophysical parameters (Fig. 2A), ensured three important aspects of collicular firing patterns observed during saccade execution: (i) they set up a large, but limited, population of cells, invariant across the SC motor map, in which the total activity (quantified by the number of spikes elicited by the recruited cells) can be described by a circular-symmetric Gaussian with a width (standard deviation) of approximately 0.5 mm, (ii) the temporal firing patterns of the central cells (their peak firing rate, burst shape, and burst duration) depend uniquely on their location in the motor map, while the number of spikes in the burst remains invariant across the map, and for a wide range of micro-stimulation parameters, and (iii) already within the first couple of spikes, the recruited neurons all became synchronized throughout the population, in which the most active cells (those in the center) determined the spike-density profiles of all the others.

3.2 Network normalization

Only close to stimulation threshold, the evoked activity remained much lower than for supra-threshold stimulation currents, leading to excessively slow eye movements (Fig. 4D), starting at a longer latency. Similar results have been reported for micro-stimulation experiments (e.g., Katnani and Gandhi, 2012; Van Opstal et al., 1990). The peak eye-velocity of our model saccades followed a psychometric curve as function of the applied current strength (Fig. 4D), whereas the kinematics of eye movements evoked near-threshold became much slower than main sequence. This property is readily predicted by the linear spike-vector summation model (Eq. 1b), but does not follow from center-of-gravity computational schemes (like Eq. 1a), in which the activity patterns themselves are immaterial for evoked saccade kinematics.

Conceptually, the lateral interactions serve to normalize the population activity, and to synchronize neural activity across cells. As a result, the total number of spikes emanating from the SC population is constant across the motor map for a large range of (sensory or electrical) stimulation parameters. The nonlinear normalization of Eq. (1b) is thus automatically implemented through the intrinsic organization of the SC network dynamics, and does not require an additional downstream “spike-counting” mechanism to terminate the saccade, as suggested earlier by [Van Opstal and Goossens \(2008\)](#) (but see, e.g., [Van Opstal and Van Gisbergen, 1989a](#)).

Although other network architectures, relying, e.g., on presynaptic inhibition across the dendritic tree, can accomplish normalization of the population and implement vector averaging ([Carandini and Heeger, 1994](#); [Groh, 2001](#); [Van Opstal and Goossens, 2008](#); [Van Opstal and Van Gisbergen, 1989a,b](#)), anatomical evidence to support such nonlinear mechanisms is lacking. We here showed that simple linear summation of the effective synaptic inputs at the cell’s membrane, which is a well-recognized physiological mechanism of basic neuronal functioning, can implement such normalization when it is combined with excitatory-inhibitory communication among the neurons within the same, topographically organized structure. Such a simple mechanism could suffice to ensure (nearly) invariant gaze-motor commands across a wide range of competing neuronal inputs.

3.3 In conclusion

The spatial dependence of the lateral excitatory-inhibitory synaptic interactions and the adaptation time constants of collicular neurons in the collicular motor map ([Fig. 2A](#)), betrays a neural organization that aims to optimize speed-accuracy trade-off for saccades ([Harris and Wolpert, 2006](#)). As emerging properties of our linear model, cells in the neural population synchronize their bursts to provide a maximally effective pulse to the brainstem saccadic circuitry ([Goossens and Van Opstal, 2012](#)), and oblique saccades follow straight trajectories with saccade-component cross-coupling ([Smit et al., 1990](#)). Because of the simple linear population read-out (spike-vector summation), there is no need for either a nonlinear weighting mechanism of the SC population, like vector averaging ([Walton et al., 2005](#)), a nonlinear threshold mechanism in a putative downstream spike counter ([Goossens and Van Opstal, 2006](#)), or presynaptic inhibition ([Carandini and Heeger, 1994](#); [Groh, 2001](#)). Furthermore, because in the model the saccade kinematics are encoded by the spatial gradient in the SC motor map, the nonlinear saturating burst generators in the brainstem ([Harris and Wolpert, 2006](#); [Jürgens et al., 1981](#); [Van Gisbergen et al., 1981](#)) may, in fact, operate as linear component pulse generators.

We here investigated the neural population dynamics, by assuming that micro-stimulation merely provides direct electrical input to a small group of cells near the electrode. Due to the lateral interactions, the population rapidly grows to an activity profile that is virtually indistinguishable from the visual-evoked condition. As described in our companying paper ([Van Opstal and Kasap, 2019](#); this volume), this simple organization may be readily extended to the full eye-head gaze-control system.

Acknowledgments

This work was supported by the European Commission through a Horizon 2020 ERC Advanced Grant, project ORIENT (grant 693400; A.J.v.O.; B.K.). The Tesla K40 used for this research was donated by the NVIDIA Corporation.

Appendix: Parameter values used in the simulations

Micro-stimulation parameters		
λ	10mm^{-1}	Spatial decay constant
I_0	150 (40–280) pA	Intracellular current intensity
$P(t)$	I_0 (for $0 < t < D_s$)	Rectangular stimulus pulse
D_s	100 (25–250) ms	Stimulation duration
Neural parameters		
C	600 pF	Membrane capacitance
g_L	20 nS	Leak conductance
E_L	-53 mV	Leak reversal potential
η	2 mV	Spike slope factor
V_T	-50 mV	Exponential threshold
V_{peak}	-30 mV	Spiking threshold
V_{rst}	-45 mV	Reset potential
a	0 nS	Sub-threshold adaptation
b	120 pA	Spike-triggered adaptation
$\tau_{q,n}$	100–30 ms	Location-dependent adaptation time constant; varies with (u_n) , see Fig. 2A.
ζ	$5.087 \cdot 10^{-5}$	Efferent map mini-vector scaling factor
Synaptic parameters		
E_{exc}	0 mV	Excitatory reversal potential
E_{inh}	-80 mV	Inhibitory reversal potential
τ_{exc}	5 ms	Excitatory conductance decay
τ_{inh}	10 ms	Inhibitory conductance decay
Lateral connectivity parameters		
\bar{W}_{exc}	45 pS	Fixed excitatory scaling factor
σ_{exc}	0.4 mm	Range of excitatory synapses
\bar{W}_{inh}	14 pS	Fixed inhibitory scaling factor
σ_{inh}	1.2 mm	Range of inhibitory synapses
S_n	0.0112–0.0147	Location-dependent synaptic scaling factor; varies with (u_n) , see Fig. 2A.

References

- Brette, R., Gerstner, W., 2005. Adaptive exponential integrate-and-fire model as an effective description of neuronal activity. *J. Neurophysiol.* 94, 3637–3642.
- Carandini, M., Heeger, D.J., 1994. Summation and division by neurons in primate visual cortex. *Science* 264, 1333–1336.
- Goossens, H.H.L.M., Van Opstal, A.J., 2006. Dynamic ensemble coding of saccades in the monkey superior colliculus. *J. Neurophysiol.* 95, 2326–2341.
- Goossens, H.H.L.M., Van Opstal, A.J., 2012. Optimal control of saccades by spatial-temporal-activity patterns in monkey superior colliculus. *PLoS Comput. Biol.* 8 (5),e1002508.
- Groh, J.M., 2001. Converting neural signals from place codes to rate codes. *Biol. Cybern.* 85, 159–165.
- Harris, C.M., Wolpert, D.M., 2006. The main sequence of saccades optimizes speed-accuracy trade-off. *Biol. Cybern.* 95, 21–29.
- Histed, M.H., Bonin, V., Reid, R.C., 2009. Direct activation of sparse, distributed populations of cortical neurons by electrical microstimulation. *Neuron* 63, 508–522.
- Jürgens, R., Becker, W., Kornhuber, H., 1981. Natural and drug-induced variations of velocity and duration of human saccadic eye movements: evidence for a control of the neural pulse generator by local feedback. *Biol. Cybern.* 96, 87–96.
- Kasap, B., Van Opstal, A.J., 2017. A spiking neural network model of the midbrain superior colliculus that generates saccadic motor commands. *Biol. Cybern.* 111, 249–268.
- Kasap, B., Van Opstal, A.J., 2018. Dynamic parallelism for synaptic updating in GPU-accelerated spiking neural network simulations. *Neurocomputing* 302, 55–65.
- Kasap, B., Van Opstal, A.J., 2019. Micro-stimulation in a spiking neural network model of the midbrain superior colliculus. *PLoS Comput. Biol.* 15 (4), e1006522. <https://doi.org/10.1371/journal.pcbi.1006522>.
- Katnani, H.A., Gandhi, N.J., 2012. The relative impact of microstimulation parameters on movement generation. *J. Neurophysiol.* 108, 528–538.
- Lee, C., Rohrer, W.H., Sparks, D.L., 1988. Population coding of saccadic eye movements by neurons in the superior colliculus. *Nature* 332, 357–360.
- Lefèvre, P., Quaia, C., Optican, L.M., 1998. Distributed model of control of saccades by superior colliculus and cerebellum. *Neural Netw.* 11, 1175–1190.
- Moschovakis, A.K., Kitama, T., Dalezios, Y., Petit, J., Brandi, A.M., Grantyn, A.A., 1998. An anatomical substrate for the spatiotemporal transformation. *J. Neurosci.* 18, 10219–10229.
- Nickolls, J., Buck, I., Garland, M., Skadron, K., 2008. Scalable parallel programming with CUDA. *AMC Queue* 6, 40–53.
- Ottes, F.P., Van Gisbergen, J.A.M., Eggermont, J.J., 1986. Visuomotor fields of the superior colliculus: a quantitative model. *Vis. Res.* 26, 857–873.
- Port, N.L., Wurtz, R.H., 2003. Sequential activity of simultaneously recorded neurons in the superior colliculus during curved saccades. *J. Neurophysiol.* 90, 1887–1903.
- Quaia, C., Lefèvre, P., Optican, L.M., 1999. Model of the control of saccades by superior colliculus and cerebellum. *J. Neurophysiol.* 82, 999–1018.
- Robinson, D.A., 1972. Eye movements evoked by collicular stimulation in the alert monkey. *Vis. Res.* 12, 1795–1808.

- Robinson, D.A., 1975. Oculomotor control signals. In: Lennerstrand, G., Bach-Y-Rita, P. (Eds.), *Basic Mechanisms of Ocular Motility and their Clinical Implications*. Pergamon Press, pp. 337–374.
- Scudder, A., 1988. A new local feedback model of the saccadic burst generator. *J. Neurophysiol.* 59, 1455–1475.
- Smit, A.C., Van Opstal, A.J., Van Gisbergen, J.A.M., 1990. Component stretching in fast and slow oblique saccades in the human. *Exp. Brain Res.* 81, 325–334.
- Stanford, T.R., Freedman, E.G., Sparks, D.L., 1996. Site and parameters of microstimulation: evidence for independent effects on the properties of saccades evoked from the primate superior colliculus. *J. Neurophysiol.* 76, 3360–3381.
- Trappenberg, T.P., Dorris, M.C., Munoz, D.P., Klein, R.M., 2001. A model of saccade initiation based on the competitive integration of exogenous and endogenous signals in the Superior Colliculus. *J. Cogn. Neurosci.* 13, 256–271.
- Van Gisbergen, J.A.M., Robinson, D.A., Gielen, S., 1981. A quantitative analysis of generation of saccadic eye movements by burst neurons. *J. Neurophysiol.* 45, 417–442.
- Van Gisbergen, J.A.M., Van Opstal, A.J., Schoenmakers, J.J.M., 1985. Experimental test of two models for the generation of oblique saccades. *Exp. Brain Res.* 57, 321–336.
- Van Gisbergen, J.A.M., Van Opstal, A.J., Tax, A.A.M., 1987. Collicular ensemble coding of saccades based on vector summation. *Neuroscience* 21, 541–555.
- Van Opstal, A.J., Goossens, H.H.L.M., 2008. Linear ensemble coding in midbrain superior colliculus specifies the saccade kinematics. *Biol. Cybern.* 98, 561–577.
- Van Opstal, A.J., Kasap, B., 2019. Maps and sensorimotor transformations for eye-head gaze shifts: role of the midbrain superior colliculus. In: *Mathematical Modeling in Motor Neuroscience: State of the Art and Translation to the Clinic. Progress in Brain Research.* vol. 248. Elsevier.
- Van Opstal, A.J., Van Gisbergen, J.A.M., 1989a. A nonlinear model for collicular spatial interactions underlying the metrical properties of electrically elicited saccades. *Biol. Cybern.* 60, 171–183.
- Van Opstal, A.J., Van Gisbergen, J.A.M., 1989b. A model for collicular efferent mechanisms underlying the generation of saccades. *Brain Behav. Evol.* 33, 90–94.
- Van Opstal, A.J., Van Gisbergen, J.A.M., Smit, A.C., 1990. Comparison of saccades evoked by visual stimulation and collicular electrical stimulation in the alert monkey. *Exp. Brain Res.* 79, 299–312.
- Walton, M.M.G., Sparks, D.L., Gandhi, N.J., 2005. Simulations of saccade curvature by models that place superior colliculus upstream from the local feedback loop. *J. Neurophysiol.* 93, 2354–2358.

Further reading

- Georgopoulos, A.P., Schwartz, A.B., Kettner, R.E., 1986. Neuronal population coding of movement direction. *Science* 233, 1416–1419.
- Katnani, H.A., Van Opstal, A.J., Gandhi, N.J., 2012. A test of spatial-temporal decoding mechanisms in the superior colliculus. *J. Neurophysiol.* 107, 2442–2452.
- Van Opstal, A.J., 2016. *The Auditory System and Human Sound Localization Behavior*. Elsevier Publishers, Academic Press, Amsterdam.
- Van Opstal, A.J., Van Gisbergen, J.A.M., 1987. Skewness of saccadic velocity profiles: a unifying parameter for normal and slow saccades. *Vis. Res.* 27, 731–745.

SECTION

RESEARCH: Adaptation

IV

This page intentionally left blank

A neuronal process for adaptive control of primate saccadic system

12

Yoshiko Kojima*

*Washington National Primate Research Center, University of Washington, Seattle,
WA, United States*

*Corresponding author: Tel.: + 1-206-543-2490; Fax: + 1-206-685-0305;
e-mail address: ykojima@u.washington.edu

Abstract

In 1980, Dr. Optican established the existence of an adaptive plasticity of saccades and its dependence on the cerebellum with Dr. Robinson. The advantage of saccades is that the neuronal mechanisms underlying their generation have been well established. This knowledge allows us to identify the neuronal elements that participate in saccade adaptation. Briefly, the superior colliculus (SC) produces a saccade command signal, which reaches motoneurons in the abducens nucleus via the brainstem burst generator. The SC saccade command also is sent to the oculomotor vermis (OMV), a saccade-related area of the cerebellar cortex, and finally converges on the same motoneurons via the caudal fastigial nucleus (cFN) and inhibitory burst neurons (IBN). During adaptation, the saccade-related burst of SC neurons does not change; however, the activity of the cerebellum and its downstream targets do. We demonstrate that the SC is the source of the error signal to the OMV, and the error signal increases the probability of complex spike occurrence and decreases simple spike activity in the OMV. This decrease, in turn, is delivered through the cFN and IBN neurons to decrease motoneuron activity and hence saccade amplitude.

Keywords

Motor learning, Error signal, Saccade, Superior colliculus, Cerebellum

Abbreviations

BG	saccade burst generator
cf	climbing fibers
cFN	caudal fastigial nucleus
CS	complex spikes
IBN	inhibitory burst neuron
IO	inferior olive

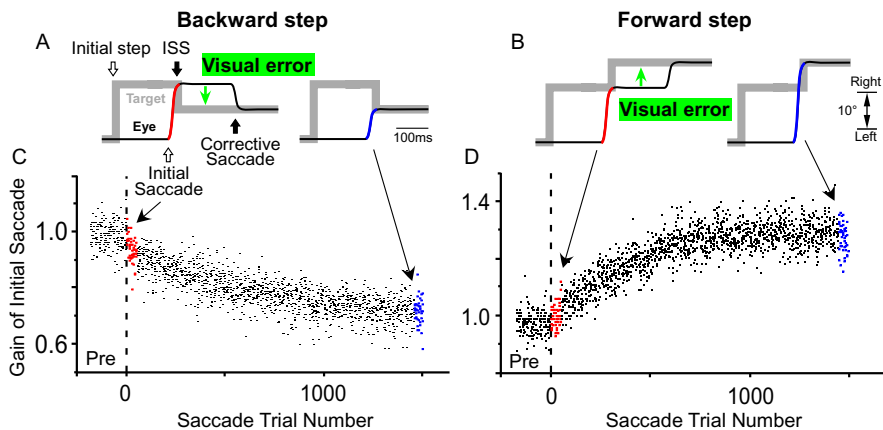
ISS	intra saccadic step, which creates a visual error to elicit saccade adaptation
mf	mossy fibers
MN	abducens motoneuron
N RTP	nucleus reticularis segmenti pontis
OMV	oculomotor vermis
P-cell	Purkinje cell
SC	superior colliculus
VOR	vestibuloocular reflex

1 Introduction

Motor learning got the attention of Dr. Robinson and other oculomotor researchers by the discovery of vestibuloocular reflex (VOR) plasticity in the early 1970s ([Robinson, 1987](#)). At about the same time, a general theory of cerebellar motor learning was presented by Drs. Marr and Albus and later refined by Dr. Ito for the VOR ([Albus, 1971; Ito, 1982; Marr, 1969; Robinson, 1987](#)). Since then, the cerebellum has been considered as the “repair shop” of the motor deficits produced in experiments involving rabbits, cats, and human patients. In the late ‘70s, Dr. Optican started to examine the “repair shop” for saccades in non-human primates in Dr. Robinson’s lab. However, they had no idea what part of the cerebellum was involved in such adaptation. Therefore, they tried to remove as much cerebellum as possible. The surgery was very difficult. They invited a neuro surgeon, tried many times, and finally published their classical study of the saccade adaptation “Cerebellar-Dependent Adaptive control of Primate Saccadic System” ([Optican and Robinson, 1980](#)). In that study, they weakened the horizontal recti muscles of one eye to make its saccades hypometric. When the weak eye viewed for several days with a patch on the intact eye, the saccades gradually became larger and recovered to be normometric. This recovery of the saccade dysmetria was abolished by cerebellectomy. Thus, they established the existence of adaptive plasticity of the saccades and its dependence on the cerebellum. In the discussion of their article, they raised two concerns: “It is impossible to say anything about the neural mechanism behind these cerebellar-dependent adaptive process,” and “Another major problem that remains unresolved concerns the nature of the error signal used by the adaptive mechanisms.” In this review, I will address these two issues and provide strong evidence they both now have been resolved.

2 Saccade adaptation paradigm

We can elicit saccade adaptation without weakening the recti muscles by a trick of target presentation. In this behavioral adaptation paradigm ([McLaughlin, 1967](#)), the target is displaced as the saccade is underway (Intrasaccadic step, ISS), and the subject must make a subsequent corrective saccade to reach it ([Fig. 1](#)). With a backward ISS, the initial saccade overshoots the target, and adaptation produces a gradual

**FIG. 1**

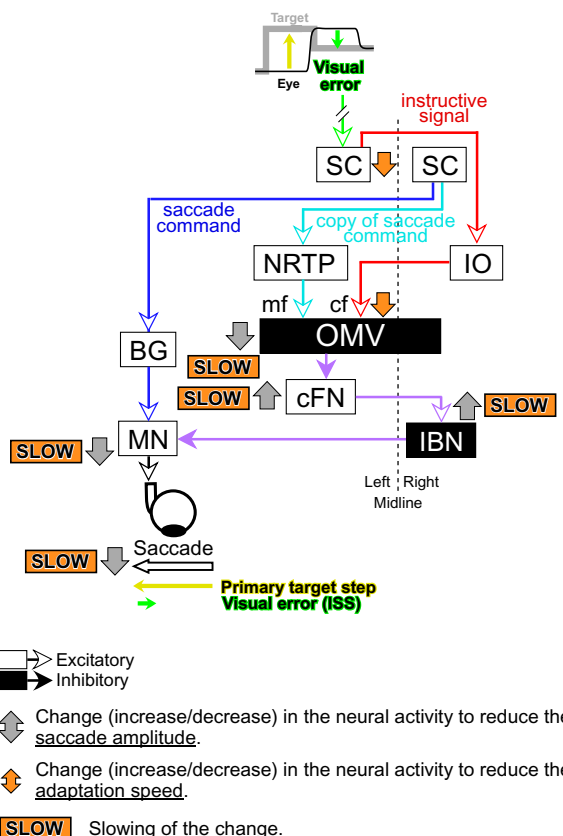
Intrasaccadic step (ISS) paradigm and saccadic gain change in the monkey. (A, B) target (gray) and eye movements (black). (C, D) gain change in the primary saccade amplitude with saccade trial number. Black dots represent individual saccades. First (red) and last (blue) 50 saccades are highlighted. In the backward step condition, the target steps back during the initial saccade to create a visual error and the monkey makes a corrective saccade (A). As a result, the gain of the initial saccade gradually decreases (C). In the forward step paradigm, the target steps forward (B) and the gain of the initial saccade gradually increases (D).

reduction of initial saccade size to reduce the visual error so that the eye once again lands near the target (Fig. 1A). A forward ISS, which causes the saccade to fall short, leads to a gradual size increase (Fig. 1B). With many repetitions of this paradigm, the saccade gain (initial saccade amplitude/target step amplitude) gradually changes to become almost normometric over the course of about 1000 trials in monkeys (Fig. 1C and D) (Scudder et al., 1998; Straube et al., 1997) and about 100 saccades in healthy human subjects (Albano, 1996; Deubel et al., 1986; Frens and van Opstal, 1994). Saccade adaptation typically follows an exponential time course, i.e., adaptation speed slows as adaptation progresses (Hopp and Fuchs, 2004).

3 The neuronal mechanism of saccades

The neuronal mechanisms underlying the generation of saccades have been studied over the past several decades (Scudder et al., 2002). This knowledge allows us to identify the neuronal elements that participate in saccade adaptation and what roles they play.

Fig. 2 shows a simplified schematic of the neural circuits that have been implicated in the generation of leftward saccades. The right superior colliculus (SC) produces a contraversive (leftward) saccade command signal that reaches contralateral motoneurons (MN) in the abducens nucleus via the brainstem burst generator (BG)

**FIG. 2**

Schematic of saccade neural circuits and changes that occur there during adaptation.

(blue pathway in Fig. 2). In addition to this direct pathway, a copy of the SC saccade command is sent to the oculomotor vermis (OMV), a saccade-related area of the cerebellar cortex, through the nucleus reticularis tegmenti pontis (N RTP) (cyan pathway). This signal is processed in the OMV and finally converges on the abducens motoneurons (MN) via the caudal fastigial nucleus (cFN) and inhibitory burst neurons (IBNs) (purple pathway). This secondary path through the cerebellum (cyan and purple) is required for saccades to be accurate because inactivation of the N RTP (Kaneko and Fuchs, 2006) or OMV (Barash et al., 1999; Kojima et al., 2010b; Optican and Robinson, 1980; Ritchie, 1976; Takagi et al., 1998) causes ipsiversive saccades (leftward saccades in Fig. 2 circuit) to become hypometric. cFN inactivation causes ipsiversive saccades to become hypermetric (Goffart et al., 2004; Iwamoto and Yoshida, 2002; Kojima et al., 2014; Robinson et al., 1993). The reciprocal effects of OMV and cFN inactivation occur because the OMV projection to the cFN is inhibitory.

4 The neural mechanism of saccade adaptation

During adaptation, the saccade-related burst of SC neurons exhibits either no apparent change (Frens and Van Opstal, 1997; Quessy et al., 2010) or inconsistent changes from cell to cell (Takeichi et al., 2007), suggesting that the saccade command signal does not change during adaptation (blue “saccade command” pathway in Fig. 2). Although the saccade command signal from the SC to the OMV does not change during adaptation (cyan pathway with “copy of saccade command”) (Takeichi et al., 2005), the activity of cells in the OMV and its downstream structures (purple pathway) does, suggesting that the cerebellum is the key place to induce the neuronal change for saccade adaptation.

How does cerebellar activity change during adaptation? In models of cerebellar plasticity (Albus, 1971; Ito, 1982; Marr, 1969), an error signal increases the complex spike activity of Purkinje cells (P-cells), which weakens the synaptic strength of the parallel fibers on the P-cell. The resultant decrease in P-cell simple spike activity is known as a long-term depression (Ito, 2005). Consistent with this model, the visual error induced by the ISS in the saccade adaptation paradigm increases the probability of complex spike occurrence in the OMV (Catz et al., 2005; Herzfeld et al., 2018; Soetedjo and Fuchs, 2006; Soetedjo et al., 2008a, 2008b) and decreases simple spike activity during adaptation (Catz et al., 2008; Herzfeld et al., 2018; Kojima et al., 2010a).

Fig. 3A–C shows the complex spike activity of a Purkinje cell in the OMV (Soetedjo et al., 2008b) associated with an ISS. A contraversive error increases the probability of complex spike occurrence (Fig. 3A left panel) but an ipsiversive error weakly suppresses their occurrence (Fig. 3A right panel). Fig. 3B shows the complex spike probability. It was largest for the contraversive (right) error direction. The preferred directions for most P-cells are contraversive to their recording side, i.e., neurons in the left OMV have rightward preferred directions and vice versa (Fig. 3C). Thus, the contraversive visual error increases the complex spike activity in the OMV.

The simple spike activity of most OMV P-cells also changes during saccade adaptation (Kojima et al., 2010a) as is illustrated for the “bursting” cell in Fig. 3D–F. Adaptation produced by backward target steps caused a reduction of saccade gain (Fig. 3D). As adaptation reduced saccade amplitude (Fig. 3E), the saccade related burst decreased (Fig. 3F).

How do these cerebellar changes work on the neural circuits of Fig. 2? The rightward ISS (backward step, green arrow below the eye in Fig. 2) elicits complex spikes of the Purkinje cells in the left OMV and decreases simple spike activity during adaptation (thick gray downward arrow next to OMV in Fig. 2). This decreased simple spike activity increases the activity of neurons in the cFN (Inaba et al., 2003; Scudder and McGee, 2003), consistent with the OMV P-cell inhibition of the cFN. The activity of cFN target neurons, the IBNs, increases (Kojima et al., 2008). Finally, IBN inhibition decreases the activity of MN, which, in turn, causes saccade amplitude to decrease. In contrast, inactivation of the cFN increases the MN activity (Kojima et al., 2014).

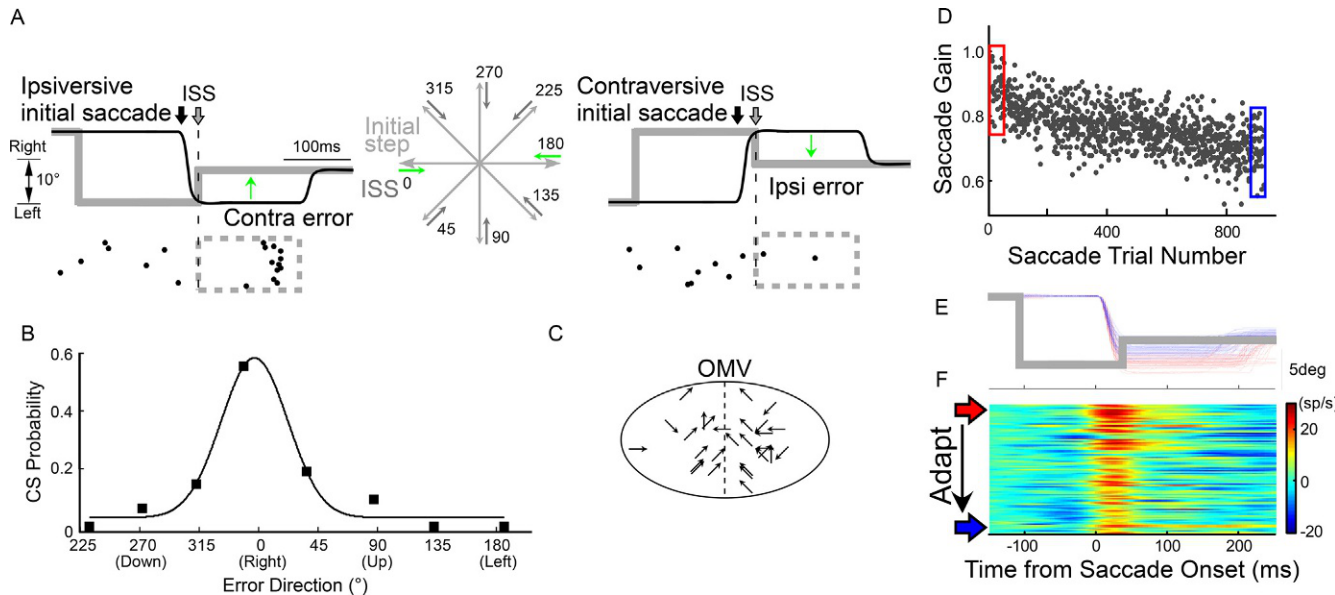


FIG. 3

Purkinje cell (P-cell) activity during saccade adaptation. (A–C) Probability of complex spike (CS) occurrence. (A) CS activity of a P-cell in the OMV (black dots). Gray line, target movement; black line, eye movement. Gray dashed box highlights the time between the ISS and corrective saccade when the CS probability changed from resting. (B) CS tuning for the error direction of a P-cell. (C) Preferred error direction of each P-cell in the OMV. CS probability is tuned for contraversive error. (D–F) Change of Simple spike activity during adaptation for a P-cell which exhibits burst for saccade. (D) Saccade gain change during adaptation. (E) Eye traces of the first (red) and last (blue) 50 saccades during adaptation. Aligned on saccade onset. (F) Course of change in the average Simple spike activity. The activity above and below resting rate is indicated by hotter and colder colors, respectively.

5 Error signal for saccade adaptation

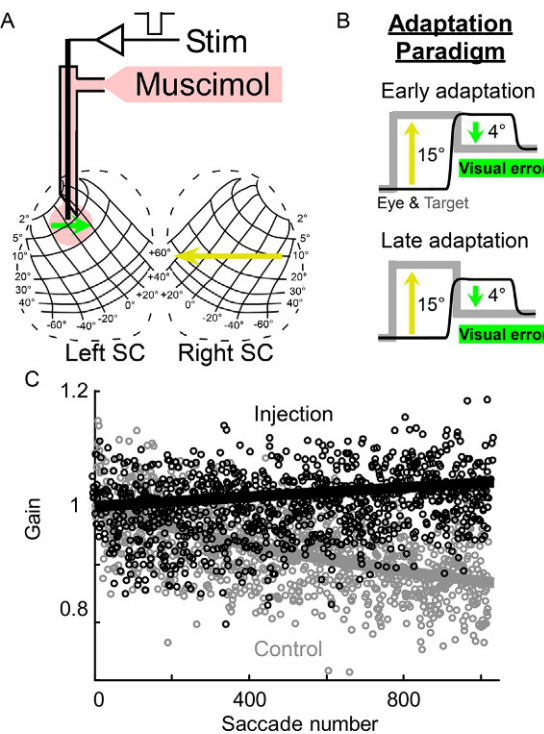
Climbing fibers in the OMV originate in the medial accessory nucleus of the contralateral inferior olive (IO in Fig. 2) (Kralj-Hans et al., 2007; Yamada and Noda, 1987), and the IO receives a projection from the contralateral SC (Harting, 1977; Huerta and Harting, 1984) (red pathway in Fig. 2). Therefore, we hypothesized that the SC is a source of the complex spikes in the OMV that induce saccade adaptation.

Three of our studies have supported this hypothesis. First, electrical stimulation of the rostral SC increases complex spike activity in the OMV (unpublished data) and when SC stimulation is timed to occur between the primary and corrective saccades, i.e., when there is a visual error, saccade adaptation is induced (Kaku et al., 2009; Soetedjo et al., 2009). This surrogate error signal caused adaptations with time courses like those induced by natural visual errors. Although this study showed that stimulation of the rostral SC could simulate an error signal and drive saccade adaptation, it did not provide the causal link between the natural SC error activity and saccade adaptation.

Therefore, in a second study, we examined the effect of SC inactivation on saccade adaptation (Kojima and Soetedjo, 2018). We injected muscimol into the rostral SC. We identified the injection site by observing its visual and saccade-related multi-unit activity and by evoking saccades with micro-stimulation through an electrode (Fig. 4A). In the representative experiment shown in Fig. 4, stimulation of the left SC evoked 4° rightward saccades (green arrow in Fig. 4). A small amount of muscimol (500 nL) injected into this site increased the reaction time of rightward 4° saccades, but did not affect the amplitude of saccades in the opposite direction (yellow arrow in Fig. 4, leftward 15°). The goal of this study was to eliminate only the error signal without affecting the adapting saccade, so we used the leftward saccade (yellow) as the adapted saccade and the rightward (green) vector as the visual error signal (Fig. 4B).

However, the conventional adaptation paradigm poses a problem for this experiment. In that paradigm, the size of the ISS is constant during adaptation so the visual error between the eye and target position decreases as adaptation progresses (Fig. 5A and B). Had we used the conventional paradigm, the location of the SC site activated during adaptation would have gradually moved rostrally away from the injection location. Therefore, to avoid this confound, we used a “constant error paradigm” in which the eye position at the end of the saccade is detected and the target is displaced relative to that position so the visual error remains constant during adaptation (Fig. 5D and E) (Kojima et al., 2015; Robinson et al., 2003). As seen in Fig. 5C and F, the adaptation curves are similar in the conventional and constant error paradigms.

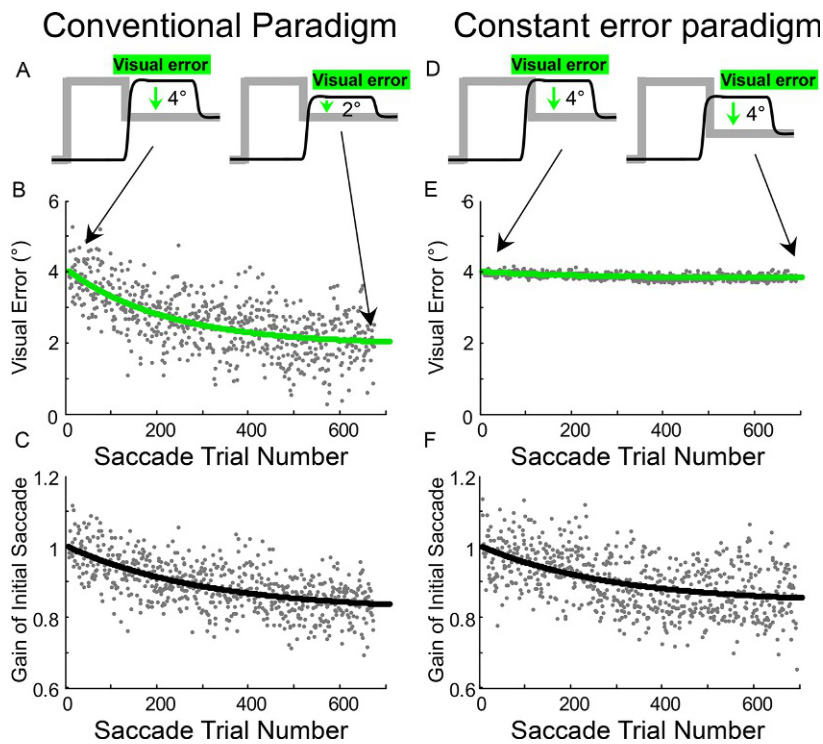
As shown in Fig. 4C, there was no gain decrease after the injection (black points). This result contrasts with the expected gain decrease observed in a no-injection control experiment performed 2 days later after the muscimol had dissipated (gray points). Thus, activity in the rostral SC is required to induce saccade adaptation.

**FIG. 4**

Muscimol injection to rostral SC. (A) Injectrode delivers micro-stimulation to evoke a saccade and muscimol to inactivate that portion of SC (pink). A unilateral injection inactivates the contraversive saccades evoked by the stimulation (green arrow) but does not affect ipsiversive saccades (yellow arrow), which are coded by the other SC. (B) Target step vectors used in the constant error paradigm are the same as those in A. (C) Comparison of the time course of saccade adaptation after rostral SC inactivation (black) and during a no-injection control experiment (gray). Each circle denotes a saccade; lines are exponential fits. Adaptation is abolished after the injection.

Finally, we tested what kind of information the SC provides to the OMV by recording SC activity during adaptation (Kojima and Soetedjo, 2017a). We focused on the visual related activity of SC neurons because they are timed to occur when complex spike probability increases in the OMV to a visual error signal, i.e., ~80–120 ms from the ISS (Soetedjo et al., 2008a, 2008b). Once we isolated a SC neuron, we identified its optimal vector (Muñoz and Wurtz, 1995; Sparks and Mays, 1980), which we used as the error signal in the constant error adaptation paradigm (Fig. 6A).

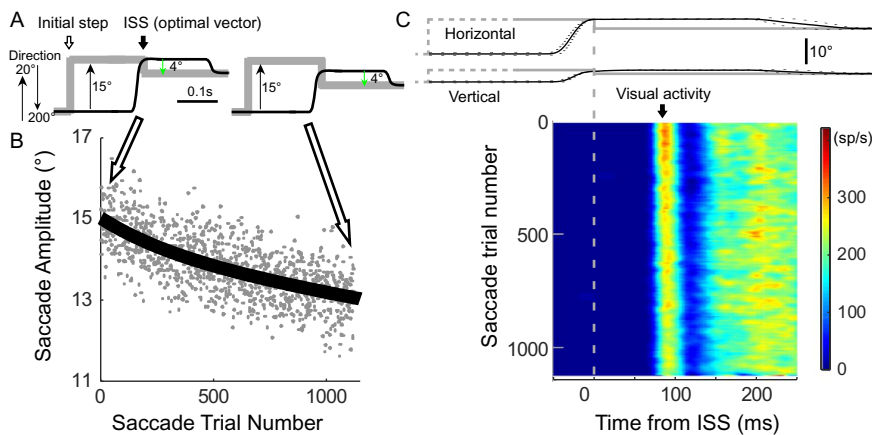
As adaptation progressed, saccade amplitude decreased and the adaptation rate slowed (Fig. 6B). Because the visual error was held constant, the slowing of the adaptation rate represents a decrease in the sensitivity to the constant error. The visual

**FIG. 5**

Two adaptation paradigms. (A–C) Conventional adaptation paradigm. (D–F) Constant error paradigm. In A–C, the backward target step size stays constant (A) and the visual error size changes (B). In (D–F), the backward target step size changes (D) to maintain a constant visual error (E). Both paradigms change the gain of saccades to the initial target; the data are fitted with exponential curves (C, F). Each dot denotes data from a single saccade trial.

activity, which occurred ~ 90 ms after the ISS, also decreased during adaptation (Fig. 6C, color changed red to yellow), reflecting a similar decrease in visual error sensitivity. SC visual sensitivity decreased with adaptation rate whether adaptation increased or decreased the saccade amplitude and whether the primary saccade was ipsi- or contraversive, suggesting that the activity change is not caused by the change in the metrics of the primary saccade.

To summarize, let's interpret these results on the saccade neural circuit in Fig. 2 to address the two questions posed by Optican and Robinson (1980). The visual error (green arrow at the top of Fig. 2) elicits complex spikes in Purkinje cells in the OMV via the SC and IO (red pathway); the complex spikes gradually decrease simple spike activity during adaptation (thick gray downward arrow next to OMV). This decreased simple spike activity modulates the activities of the downstream structures, i.e., cFN, IBN, and MN (thick gray arrows next to each structure),

**FIG. 6**

Activity of a visuo-motor neuron in the right SC during amplitude decrease adaptation. (A) schematic of target (gray lines) and eye (black lines) movements for the beginning and end of adaptation. Target stepped along the neuron's optimal direction, in this case 20°. During adaptation, the visual error was held constant at 4° (green arrow), this neuron's optimal amplitude. (B) decrease in primary saccade amplitude with saccade trial number. Gray dots represent individual saccades; black line is an exponential fit. (C) colorized visual activity during adaptation aligned on ISS onset (time = 0). Upper panel, target (gray) and eye movements (black) for the first 15 saccades during adaptation aligned on ISS onset at end of the primary saccade. Black broken lines indicate 1 standard deviation (SD) of eye movement; gray broken lines of target approximate the time of the initial target step (because the latency of the primary saccade is variable).

and decrease the saccade amplitude. This could be a cerebellar mechanism to change the saccade gain during adaptation. A weaker SC instructive signal would produce weaker complex spike activity in the OMV (thick orange arrows next to SC and OMV). In turn, the weaker complex spike activity would reduce the speed of cerebellar plasticity, leading to a slower decrease in simple spike activity in the OMV and consequently a slower decrease in saccade amplitude (Fig. 2, “SLOW” sign). This could be a neural mechanism for the error signal.

For the past half century, understanding the neural mechanism for motor learning has been a central goal of neuroscience because such adaptation is critical to keep the movement accurate and to allow recovery from a motor deficit. Since Drs. Optican and Robinson began, saccadic adaptation has been a valuable model to study the neural mechanisms underlying motor learning because the basic circuitry for saccade generation is well studied (Scudder et al., 2002) and the adaptation paradigm is well established (Hopp and Fuchs, 2004). Here we suggest the basic structure of how the brain could produce saccade adaptation and how the error signal drives the adaptation.

However, there are still many questions. For example, how can the SC error sensitivity be modulated during adaptation? Motivation affects the error sensitivity (Kojima and Soetedjo, 2017b), but how does the brain do it? Why does adaptation stop even though there still is an error signal, i.e., constant error adaptation paradigm? The adaptation characteristics of higher order saccades, such as memory-guided saccades, are different from the simple visually-guided saccade (Hopp and Fuchs, 2004, 2010; Kojima et al., 2015); does it also involve the cerebellum? Etc. The field started by Optican and Robinson (1980) is fertile indeed.

Acknowledgments

This study was supported by National Institute of Health (NIH) grants EY023277 (R01 for Y.K.), EY019258 (R01 for R.S.), OD010425 (P51 for WaNPRC), Vision Research Core (P30EY001730 for UW), and National Science Foundation BCS-1724176. The contents of this paper are solely the responsibility of the authors and do not necessarily represent the official views of NCRR or NIH. Robijanto Soetedjo and Albert Fuchs helped with the editing.

References

- Albano, J.E., 1996. Adaptive changes in saccade amplitude: oculocentric or orbitocentric mapping? *Vision Res.* 36, 2087–2098.
- Albus, J.S., 1971. A theory of cerebellar function. *Math. Biosci.* 10, 25–61.
- Barash, S., Melikyan, A., Sivakov, A., Zhang, M., Glickstein, M., Thier, P., 1999. Saccadic dysmetria and adaptation after lesions of the cerebellar cortex. *J. Neurosci. Off. J. Soc. Neurosci.* 19, 10931–10939.
- Catz, N., Dicke, P.W., Thier, P., 2005. Cerebellar complex spike firing is suitable to induce as well as to stabilize motor learning. *Curr. Biol.* 15, 2179–2189.
- Catz, N., Dicke, P.W., Thier, P., 2008. Cerebellar-dependent motor learning is based on pruning a Purkinje cell population response. *Proc. Natl. Acad. Sci. U. S. A.* 105, 7309–7314.
- Deubel, H., Wolf, W., Hauske, G., 1986. Adaptive gain control of saccadic eye movements. *Hum. Neurobiol.* 5, 245–253.
- Frens, M.A., van Opstal, A.J., 1994. Transfer of short-term adaptation in human saccadic eye movements. *Exp. Brain Res.* 100, 293–306.
- Frens, M.A., Van Opstal, A.J., 1997. Monkey superior colliculus activity during short-term saccadic adaptation. *Brain Res. Bull.* 43, 473–483.
- Goffart, L., Chen, L.L., Sparks, D.L., 2004. Deficits in saccades and fixation during muscimol inactivation of the caudal fastigial nucleus in the rhesus monkey. *J. Neurophysiol.* 92, 3351–3367.
- Harting, J.K., 1977. Descending pathways from the superior colliculus: an autoradiographic analysis in the rhesus monkey (*Macaca mulatta*). *J. Comp. Neurol.* 173, 583–612.
- Herzfeld, D.J., Kojima, Y., Soetedjo, R., Shadmehr, R., 2018. Encoding of error and learning to correct that error by the Purkinje cells of the cerebellum. *Nat. Neurosci.* 21, 736–743.
- Hopp, J.J., Fuchs, A.F., 2004. The characteristics and neuronal substrate of saccadic eye movement plasticity. *Prog. Neurobiol.* 72, 27–53.

- Hopp, J.J., Fuchs, A.F., 2010. Identifying sites of saccade amplitude plasticity in humans: transfer of adaptation between different types of saccade. *Exp. Brain Res.* 202, 129–145.
- Huerta, M.F., Harting, J.K., 1984. The mammalian superior colliculus studies of its morphology and connections. In: Vanegas, H. (Ed.), *Comparative Neurology of the Optic Tectum*. Plenum Press, New York, pp. 687–773.
- Inaba, N., Iwamoto, Y., Yoshida, K., 2003. Changes in cerebellar fastigial burst activity related to saccadic gain adaptation in the monkey. *Neurosci. Res.* 46, 359–368.
- Ito, M., 1982. Cerebellar control of the vestibulo-ocular reflex—around the flocculus hypothesis. *Annu. Rev. Neurosci.* 5, 275–296.
- Ito, M., 2005. Bases and implications of learning in the cerebellum—adaptive control and internal model mechanism. *Prog. Brain Res.* 148, 95–109.
- Iwamoto, Y., Yoshida, K., 2002. Saccadic dysmetria following inactivation of the primate fastigial oculomotor region. *Neurosci. Lett.* 325, 211–215.
- Kaku, Y., Yoshida, K., Iwamoto, Y., 2009. Learning signals from the superior colliculus for adaptation of saccadic eye movements in the monkey. *J. Neurosci.* 29, 5266–5275.
- Kaneko, C.R., Fuchs, A.F., 2006. Effect of pharmacological inactivation of nucleus reticularis tegmenti pontis on saccadic eye movements in the monkey. *J. Neurophysiol.* 95, 3698–3711.
- Kojima, Y., Fuchs, A.F., Soetedjo, R., 2015. Adaptation and adaptation transfer characteristics of five different saccade types in the monkey. *J. Neurophysiol.* 114, 125–137.
- Kojima, Y., Iwamoto, Y., Robinson, F.R., Noto, C.T., Yoshida, K., 2008. Premotor inhibitory neurons carry signals related to saccade adaptation in the monkey. *J. Neurophysiol.* 99, 220–230.
- Kojima, Y., Robinson, F.R., Soetedjo, R., 2014. Cerebellar fastigial nucleus influence on ipsilateral abducens activity during saccades. *J. Neurophysiol.* 111, 1553–1563.
- Kojima, Y., Soetedjo, R., 2017a. Change in sensitivity to visual error in superior colliculus during saccade adaptation. *Sci. Rep.* 7, 9566.
- Kojima, Y., Soetedjo, R., 2017b. Selective reward affects the rate of saccade adaptation. *Neuroscience* 355, 113–125.
- Kojima, Y., Soetedjo, R., 2018. Elimination of the error signal in the superior colliculus impairs saccade motor learning. *Proc. Natl. Acad. Sci. U. S. A* (in press).
- Kojima, Y., Soetedjo, R., Fuchs, A.F., 2010a. Changes in simple spike activity of some Purkinje cells in the oculomotor vermis during saccade adaptation are appropriate to participate in motor learning. *J. Neurosci. Off. J. Soc. Neurosci.* 30, 3715–3727.
- Kojima, Y., Soetedjo, R., Fuchs, A.F., 2010b. Effects of GABA agonist and antagonist injections into the oculomotor vermis on horizontal saccades. *Brain Res.* 1366, 93–100.
- Kralj-Hans, I., Baizer, J.S., Swales, C., Glickstein, M., 2007. Independent roles for the dorsal paraflocculus and vermal lobule VII of the cerebellum in visuomotor coordination. *Exp. Brain Res.* 177, 209–222.
- Marr, D., 1969. A theory of cerebellar cortex. *J. Physiol.* 202, 437–470.
- McLaughlin, S., 1967. Parametric adjustment in saccadic eye movements. *Percept. Psychophys.* 2, 359–362.
- Munoz, D.P., Wurtz, R.H., 1995. Saccade-related activity in monkey superior colliculus. I. Characteristics of burst and buildup cells. *J. Neurophysiol.* 73, 2313–2333.
- Optican, L.M., Robinson, D.A., 1980. Cerebellar-dependent adaptive control of primate saccadic system. *J. Neurophysiol.* 44, 1058–1076.
- Quesy, S., Quinet, J., Freedman, E.G., 2010. The locus of motor activity in the superior colliculus of the rhesus monkey is unaltered during saccadic adaptation. *J. Neurosci.* 30, 14235–14244.

- Ritchie, L., 1976. Effects of cerebellar lesions on saccadic eye movements. *J. Neurophysiol.* 39, 1246–1256.
- Robinson, D.A., 1987. The windfalls of technology in the oculomotor system. Proctor lecture. *Investig. Ophthalmol. Vis. Sci.* 28, 1912–1924.
- Robinson, F.R., Noto, C.T., Bevans, S.E., 2003. Effect of visual error size on saccade adaptation in monkey. *J. Neurophysiol.* 90, 1235–1244.
- Robinson, F.R., Straube, A., Fuchs, A.F., 1993. Role of the caudal fastigial nucleus in saccade generation. II. Effects of muscimol inactivation. *J. Neurophysiol.* 70, 1741–1758.
- Scudder, C.A., Batourina, E.Y., Tunder, G.S., 1998. Comparison of two methods of producing adaptation of saccade size and implications for the site of plasticity. *J. Neurophysiol.* 79, 704–715.
- Scudder, C.A., Kaneko, C.S., Fuchs, A.F., 2002. The brainstem burst generator for saccadic eye movements: a modern synthesis. *Exp. Brain Res.* 142, 439–462.
- Scudder, C.A., McGee, D.M., 2003. Adaptive modification of saccade size produces correlated changes in the discharges of fastigial nucleus neurons. *J. Neurophysiol.* 90, 1011–1026.
- Soetedjo, R., Fuchs, A.F., 2006. Complex spike activity of purkinje cells in the oculomotor vermis during behavioral adaptation of monkey saccades. *J. Neurosci.* 26, 7741–7755.
- Soetedjo, R., Fuchs, A.F., Kojima, Y., 2009. Subthreshold activation of the superior colliculus drives saccade motor learning. *J. Neurosci. Off. J. Soc. Neurosci.* 29, 15213–15222.
- Soetedjo, R., Kojima, Y., Fuchs, A., 2008a. Complex spike activity signals the direction and size of dysmetric saccade errors. *Prog. Brain Res.* 171, 153–159.
- Soetedjo, R., Kojima, Y., Fuchs, A., 2008b. Complex spike activity in the oculomotor vermis of the cerebellum: a vectorial error signal for saccade motor learning? *J. Neurophysiol.* 100, 1949–1966.
- Sparks, D.L., Mays, L.E., 1980. Movement fields of saccade-related burst neurons in the monkey superior colliculus. *Brain Res.* 190, 39–50.
- Straube, A., Fuchs, A.F., Usher, S., Robinson, F.R., 1997. Characteristics of saccadic gain adaptation in rhesus macaques. *J. Neurophysiol.* 77, 874–895.
- Takagi, M., Zee, D.S., Tamargo, R.J., 1998. Effects of lesions of the oculomotor vermis on eye movements in primate: saccades. *J. Neurophysiol.* 80, 1911–1931.
- Takeichi, N., Kaneko, C.R., Fuchs, A.F., 2005. Discharge of monkey nucleus reticularis tegmenti pontis neurons changes during saccade adaptation. *J. Neurophysiol.* 94, 1938–1951.
- Takeichi, N., Kaneko, C.R., Fuchs, A.F., 2007. Activity changes in monkey superior colliculus during saccade adaptation. *J. Neurophysiol.* 97, 4096–4107.
- Yamada, J., Noda, H., 1987. Afferent and efferent connections of the oculomotor cerebellar vermis in the macaque monkey. *J. Comp. Neurol.* 265, 224–241.

This page intentionally left blank

A unified computational framework for visual attention dynamics

13

Dario Zanca^{a,b,*}, Marco Gori^b, Alessandra Rufa^b

^aUniversity of Florence, Florence, Italy

^bUniversity of Siena, Siena, Italy

*Corresponding author: e-mail address: dario.zanca@unifi.it

Abstract

Eye movements are an essential part of human vision as they drive the fovea and, consequently, selective visual attention toward a region of interest in space. Free visual exploration is an inherently stochastic process depending on image statistics but also individual variability of cognitive and attentive state. We propose a theory of free visual exploration entirely formulated within the framework of physics and based on the general Principle of Least Action. Within this framework, differential laws describing eye movements emerge in accordance with bottom-up functional principles. In addition, we integrate top-down semantic information captured by deep convolutional neural networks pre-trained for the classification of common objects. To stress the model, we used a wide collection of images including basic features as well as high level semantic content. Results in a task of saliency prediction validate the theory.

Keywords

Visual attention, Scanpath, Saliency, Convolutional neural networks, Visual features, Principle of least action

1 Introduction

In the past three decades, many attempts have been made in the direction of modeling visual attention. Basing on the feature integration theory of attention of Koch and Ullman (1987) and Treisman and Gelade (1980) provided a description of human attention that operates in an early representation, which is basically a set of feature maps. They assume that these maps are then combined in a central representation, namely the *saliency map*, which plays a central role in driving attention mechanisms. A first implementation of this scheme was proposed by Itti et al. (1998). Several other models have been proposed by the computer vision community, in particular

to address the problem of refining saliency maps estimation (Borji and Itti, 2013; Bruce and Tsotsos, 2007; Cornia et al., 2018; Judd et al., 2009; Kruthiventi et al., 2017; Vig et al., 2014). However, these models do not produce a temporal sequence of eye movements, which can be of great importance for understanding human vision as well as for building systems that deal with video streams.

Some preliminary attempts to model sequences of fixations (i.e., scanpaths) are already present in the literature. Works are often only descriptive (Lee and Stella, 2000) or task specific (Renninger et al., 2005). A description of visual attention as a dynamic process has been proposed by Zanca and Gori (2017). The authors derive differential equations describing eye-movements, based on three bottom-up functional principles: boundedness of the retina, curiosity for details and brightness invariance. Dynamic laws are derived within the framework of variational calculus. This approach exhibits the important advantage of avoiding the global computation of a saliency map in advance, making it suitable for real-time applications. In this paper we extend our previous model with the top-down semantic information captured by deep convolutional neural networks pre-trained for the classification of common objects. This information is added in a natural way as fourth functional component. The approach is validated on the benchmark of saliency prediction CAT2000 described by Borji and Itti (2015).

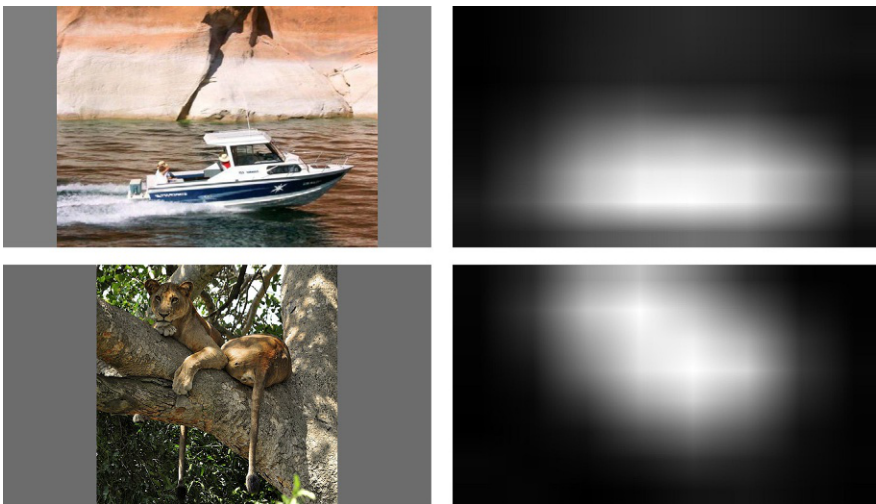
2 Convolutional feature activation maps are good saliency predictors

In the case of the Convolutional Neural Networks (CNNs) trained for the task of recognizing common objects, some methods (Selvaraju et al., 2017; Zhou et al., 2016) allow to visualize internal activation and understand which locations of the original input image were crucial for the system response. Class-specific activation maps are then obtained by averaging feature maps from the last convolutional tensor with the weights of the corresponding class. We claim that semantic maps obtained by averaging the activation of the units in the last convolutional layer are good predictors for human fixations distribution. In our experiments, we used an instance of the model described by Szegedy et al. (2016), pre-trained for classification on the ImageNet benchmark.^a For a given input image, let $f_u(x)$ represent the activation of unit u in the last convolutional layer U at spatial location $x = (x_1, x_2)$. Then, we can average the activations by setting

$$M(x) = \frac{1}{|U|} \sum_{u \in U} f_u(x) \quad (1)$$

defined on each spatial location x . Examples of these maps are given in Fig. 1.

^a<http://image-net.org>.

**FIG. 1**

Convolutional feature activation map M . In the left-hand column, examples of images from CAT2000 [Borji and Itti \(2015\)](#). In the right-hand column the corresponding map M obtained from the pre-trained instance of inception-v3 [Szegedy et al. \(2016\)](#).

We evaluate this visualization technique for the task of saliency prediction on the dataset CAT2000 ([Borji and Itti, 2015](#)). Performance improves by optimizing maps with blurring and histogram matching ([Bylinskii et al., 2018](#)). Scores are reported in [Table 1](#). From now on, we will refer to this model as the Convolutional Feature activation map (CF).

3 Eye movements guided by convolutional features

In our previous work ([Zanca and Gori, 2017](#)), a dynamic model of visual attention is derived by three bottom-up functional principles. First, let the retina be defined in a rectangular area determined by the coordinates $(0, 0)$, $(l_1, 0)$, (l_1, l_2) , $(0, l_2)$. Eye movements are required to be *bounded inside the definite area of the retina*. This gives the potential term

$$V(x) = k \sum_{i=1,2} \left((l_i - x_i)^2 \cdot [x_i > l_i] + (x_i)^2 \cdot [x_i < 0] \right), \quad (2)$$

where $i \in \{1, 2\}$ to sum up the contributions of both spatial coordinates, and k is a positive real number. Please notice that here we use the Iverson's notation, according to which $[cond]=1$ if a condition $cond$ is true and $[cond]=0$ otherwise.

The second principle states that locations with high values of the *brightness gradient are attractive*. Let b be the brightness function and p a blurred version of b .

Table 1 Results on CAT2000 Borji and Itti (2015).

Model version	Maps optimization	CAT2000	
		AUC	NSS
CF	–	0.80 (0.001)	1.177 (0.046)
CF	center bias	0.844 (0.001)	1.168 (0.009)
CF	center bias, hist. match.	0.834 (0.001)	1.684 (0.085)
EYMOL	blur	0.838 (0.001)	1.810 (0.014)
CF-EYMOL	blur	0.843 (0.001)	1.822 (0.064)
Itti-Koch	Itti et al. (1998)	0.77	1.06
AIM	Bruce and Tsotsos (2007)	0.76	0.89
Judd Model	Judd et al. (2009)	0.84	1.30
{One-human}	(baseline)	0.76	1.54
DeepFix	Kruthiventi et al. (2017)	0.87	2.28
SAM	Cornia et al. (2018)	0.88	2.38

Between brackets is indicated the standard error. Two different metrics AUC and NSS are used to compare results on the saliency prediction task. AUC (Area Under the ROC curve) is obtained by treating the saliency map as a binary classifier to separate positive from negative samples at various thresholds. NSS is measured as the mean value of the normalized saliency map at fixation locations.

Let indicate with b_x and p_x the spatial gradient of b and p , respectively. Then, with the potential term

$$C(t, x) = b_x^2 \cos^2(\omega t) + p_x^2 \sin^2(\omega t) \quad (3)$$

attention is attracted toward locations where the magnitude of the gradient of the brightness is high.

Finally, trajectories are required to preserve the property of *brightness invariance*, which brings to fixation and tracking behaviors. This is guaranteed by the soft satisfaction of the constraint

$$B(t, x, \dot{x}) = (b_t + b_x \dot{x})^2 \quad (4)$$

to be as small as possible. Here, b_t indicates the partial derivative of the brightness with respect to the time variable t .

Following the idea described by [Zanca and Gori \(2017\)](#), we construct a generalized action

$$S = \int_0^T (K - \hat{U}) dt \quad (5)$$

where K is the kinetic energy

$$K(\dot{x}) = -\frac{1}{2} m \dot{x}^2. \quad (6)$$

In the original work ([Zanca and Gori, 2017](#)), U is the generalized potential energy defined as

$$U(t, x, \dot{x}) = V(x) - \eta C(t, x) + \lambda B(t, x, \dot{x}). \quad (7)$$

In the present work, we extend it by adding the information carried by the map [\(1\)](#) simply by

$$\hat{U}(t, x, \dot{x}) = V(x) - \eta C(t, x) + \lambda B(t, x, \dot{x}) - M(x). \quad (8)$$

Please notice that, both C and M potential terms have minus sign since they come from attractive forces. By the Principle of Least Action, the true path of a mass m within the defined potential fields is given by the Euler-Lagrange equations

$$m\ddot{x} - \lambda \frac{d}{dt} B_{\dot{x}} + V_x - \eta C_x + \lambda B_x - \gamma M_x = 0. \quad (9)$$

These equations can be numerically integrated to simulate processes of free visual exploration. Saliency maps are obtained by summing up the most visited locations. From now on, we will refer to the basic model defined by principles [\(2\)](#), [\(3\)](#) and [\(4\)](#) as EYMOL, and to the model enriched with convolutional features CF with CF-EYMOL. [Table 1](#) reports scores for saliency prediction and comparison with state-of-the-art models.

4 Discussion

We have shown that an inherent model of visual attention is present in deep convolutional neural networks that are trained for a different task. The experimental results show that the convolutional features lead good human saliency predictors. However, the main contribution of this paper is to integrate the information brought by these maps with the bottom-up differential model of eye-movements defined by [Zanca and Gori \(2017\)](#), with the final purpose of simulating visual attention scanpaths. The proposed integration enriches the eye movement model thanks to the additional peripheral information that comes from the convolutional filters. Even if the calculation of the saliency comes as a by-product of the eye movements laws, results in saliency prediction show that the model competes with state-of-the-art models.

References

- Borji, A., Itti, L., 2013. State-of-the-art in visual attention modeling. *IEEE Trans. Pattern Anal. Mach. Intell.* 35 (1), 185–207.
- Borji, A., Itti, L., 2015. Cat2000: a large scale fixation dataset for boosting saliency research. *arXiv*. preprint arXiv:1505.03581.
- Bruce, N., Tsotsos, J., 2007. Attention based on information maximization. *J. Vis.* 7 (9), 950–950.

- Bylinskii, Z., Judd, T., Oliva, A., Torralba, A., Durand, F., 2018. What do different evaluation metrics tell us about saliency models? *IEEE Trans. Pattern Anal. Mach. Intell.*
- Cornia, M., Baraldi, L., Serra, G., Cucchiara, R., 2018. Predicting human eye fixations via an LSTM-based saliency attentive model. *IEEE Trans. Image Process.* 27 (10), 5142–5154.
- Itti, L., Koch, C., Niebur, E., 1998. A model of saliency-based visual attention for rapid scene analysis. *IEEE Trans. Pattern Anal. Mach. Intell.* 20 (11), 1254–1259.
- Judd, T., Ehinger, K., Durand, F., Torralba, A., 2009. Learning to Predict Where Humans Look. *IEEE*, pp. 2106–2113.
- Koch, C., Ullman, S., 1987. Shifts in selective visual attention: towards the underlying neural circuitry. In: *Matters of Intelligence*. Springer, pp. 115–141.
- Kruthiventi, S.S., Ayush, K., Babu, R.V., 2017. Deepfix: a fully convolutional neural network for predicting human eye fixations. *IEEE Trans. Image Process.* 26 (9), 4446–4456.
- Lee, T.S., Stella, X.Y., 2000. An information-theoretic framework for understanding saccadic eye movements. In: *Adv. Neural Inf. Process. Syst.*, pp. 834–840.
- Renninger, L.W., Coughlan, J.M., Verghese, P., Malik, J., 2005. An information maximization model of eye movements. In: *Adv. Neural Inf. Process. Syst.*, pp. 1121–1128.
- Selvaraju, R.R., Cogswell, M., Das, A., Vedantam, R., Parikh, D., Batra, D., 2017. Grad-cam: Visual Explanations From Deep Networks via Gradient-Based Localization. In: *IEEE International Conference on Computer Vision*, pp. 618–626.
- Szegedy, C., Vanhoucke, V., Ioffe, S., Shlens, J., Wojna, Z., 2016. Rethinking the Inception Architecture for Computer Vision. In: *IEEE Conference on Computer Vision and Pattern Recognition*, pp. 2818–2826.
- Treisman, A.M., Gelade, G., 1980. A feature-integration theory of attention. *Cogn. Psychol.* 12 (1), 97–136.
- Vig, E., Dorr, M., Cox, D., 2014. Large-Scale Optimization of Hierarchical Features for Saliency Prediction in Natural Images. In: *IEEE Conference on Computer Vision and Pattern Recognition*, pp. 2798–2805.
- Zanca, D., Gori, M., 2017. Variational Laws of Visual Attention for Dynamic Scenes. In: *Adv. Neural Inf. Process. Syst.*, pp. 3823–3832.
- Zhou, B., Khosla, A., Lapedriza, A., Oliva, A., Torralba, A., 2016. Learning Deep Features for Discriminative Localization. In: *IEEE Conference on Computer Vision and Pattern Recognition*, pp. 2921–2929.

Improving the repeatability of two-rate model parameter estimations by using autoencoder networks

14

Murat C. Ozdemir*, Thomas Eggert, Andreas Straube

Department of Neurology, University Hospital, LMU Munich, Munich, Germany

*Corresponding author: Tel.: +49-0-89-44007-4836; Fax: +49-0-89-44007-4801,
e-mail address: murat.ozdemir@lrz.uni-muenchen.de

Abstract

The adaptive changes elicited in visuomotor adaptation experiments are usually well explained at group level by two-rate models (Smith et al., 2006), but parameters fitted to individuals show considerable variance. Data cleaning can mitigate this problem, but the assumption of smoothness can be problematic due to fast adaptive changes with discontinuous derivatives. In this paper, we collected time-series data from an experimental paradigm involving repeated training and investigated the effect of various cleaning methods, including an autoencoder network (AE), on the parameter estimation. We compared changes in the fitted parameters across different methods and across training repetitions. The results suggest that AE performed best overall, without introducing an underestimation bias on b_f like moving average or piecewise polynomials, and that it reduced the within-subject variance overall and especially that of the fast retention rate a_f by >50%.

Keywords

Human, Visuomotor adaptation, Two-rate models, Autoencoder, Data cleaning

1 Introduction

Two-rate models (Smith et al., 2006) have frequently modeled goal-directed arm movements under visual disturbances, to elucidate the Bayesian relationship between error size and learning rate b_* (Herzfeld et al., 2014), and retention rate a_* (Vaswani and Shadmehr, 2013), simultaneously. These linear systems, consisting of “fast” and “slow” processes (and hence model parameters $[a_f, a_s, b_f, b_s]$), driven by

the error between the actual target location and the initial pointing direction, were largely successful due to an increase in explanatory power, in comparison to a one-rate model, for motor learning and many other aftereffects (Colagiorgio et al., 2015; Sing and Smith, 2010). Previous attempts at explaining the error sensitivity (Herzfeld et al., 2014), the time constants (Criscimagna-Hemminger and Shadmehr, 2008) or the retention rate (Vaswani and Shadmehr, 2013) separately have been done on an individual level, albeit the fitting of these model parameters for individuals is another interesting way of dimensionality reduction. However, their simultaneous estimation has been problematic due to repeatability issues caused by high variance in estimation. Therefore, this paper includes a comparison of common cleaning algorithms, along with the introduction of an advanced data cleaning technique utilizing autoencoder networks (Ballard, 1987), to improve parameter estimation with the aim of bias-free reduction of within-subject variation.

2 Methods

We designed an experiment, inspired by the idea of alternating closed loop trials and error clamp trials (Herzfeld et al., 2014). 19 Subjects were recruited for an experiment dealing with upper limb reaching movements (age: 31.7 ± 11.08 years, 5 of them were later left out due to very poor performance), using the same experiment equipment setup in Henriques et al. (2014). Each trial in our design could point to either of three target locations at $[-15, 0, 15]$ degrees. In the beginning of the session, 40 closed loop trials (CL) and 40 error clamp trials (EC) served as baseline trials, followed by 2 training phases for ± 30 degree visual discrepancy. In the first part, 10 iterations of 3 CL and 3 EC, henceforth known as alternating block (AL), were followed by 30 EC trials and 30 CL trials. The second part began with 30 trials of zero discrepancy CL washout, followed by AL and 30 EC at ± 30 degree visual discrepancy. We computed the adaptive change from initial movement directions from the first half of the acceleration period, which were referenced to the biases for each target location, calculated from respective baseline trials as their mean (henceforth known as raw session data). Afterward, the model parameters of the two-rate model (Smith et al., 2006) were estimated by least square minimization of the model errors on this raw data. However, a thorough exploration of the variability of the model parameters and the raw data, especially in AL, and its principal components made an exploration of data cleaning methods necessary.

Common data cleaning methods assume that the underlying signal is smooth and the noise has unwanted components only at higher frequencies. Therefore they are designed to have the characteristics of a low-pass filter, e.g., the moving average or outlier removal (McDougle et al., 2015). This might not be a viable assumption for our experiment design due to frequent changes of training conditions in AL. Therefore, we compared an outlier selection method (OS) with additional linear algorithms

of piecewise polynomial estimation (PP), a simple moving average (MA) and finally, with autoencoder networks (AE) as the sole nonlinear algorithm in our comparison.

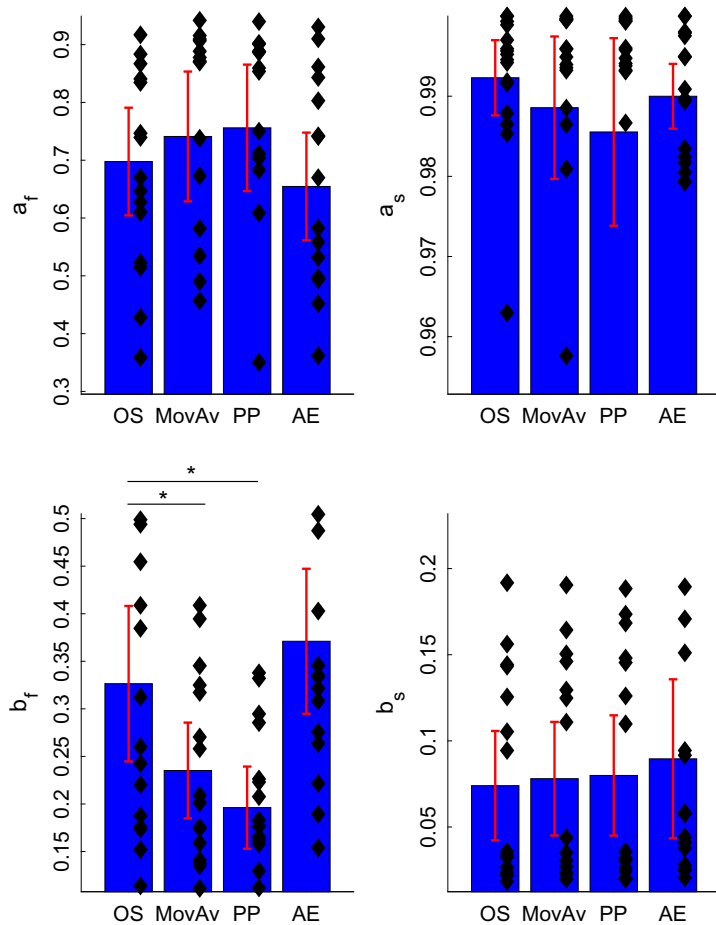
AE learns to compress (encodes) the training data into a code vector, with the capability of reconstructing (decoding) it at the output layer. If the training data is a good representation of the underlying signal, the network learns a low dimensional representation. Therefore, AE can be used to clean the raw data by simply running it through the trained network. Due to nonlinearities of AE during training and prediction phases, the output has the characteristics of both the raw data and the training data; therefore, AE is not necessarily a low-pass filter. The loss function for the training of this network comprised three error terms in summation,

$$E = \frac{1}{N} \sum_{n=1}^N \sum_{k=1}^K (x_{kn} - \hat{x}_{kn})^2 + \lambda * \Omega_{weights} + \beta * \Omega_{sparsity}$$

where the first term is the mean squared error of the reconstruction of each raw data point k for each subject n , the second term regularizes the sum of the L₂ norm of the encoder and decoder weights, and the third term punishes deviations from the average desired activation level for each neuron in the hidden layer(s) through Kullback-Leibler divergence (Kullback and Leibler, 1951). The third part, unlike a typical neural network, allows individual neurons in the hidden layer to specialize on specific subsets of the input data. Thus, the optimization of this network relies on λ , the L₂ norm regularizer; β , the sparsity regularizer; and ρ , the average desired activation level. We optimized these hyperparameters by using evolutionary algorithms, but it is not strictly necessary in this context.

We implemented OS as the baseline cleaning method, where the outlier detection threshold was two standard deviations away from the difference between raw data and MA. MA had the window size of five. We implemented PP with 4th degree polynomials for each large block of constant stimulus condition and 1st degree for the short blocks during AL with length three, totaling 42 continuous piecewise polynomials with no constraints on the derivatives at the borders. We implemented AE with one layer of eight hidden neurons, one autoencoder network for each part of the experiment paradigm. We prepared the training data for AE using a noisy set of the two-rate model output using the raw data only, and then contaminated them with Gaussian noise estimated from the residuals in OS.

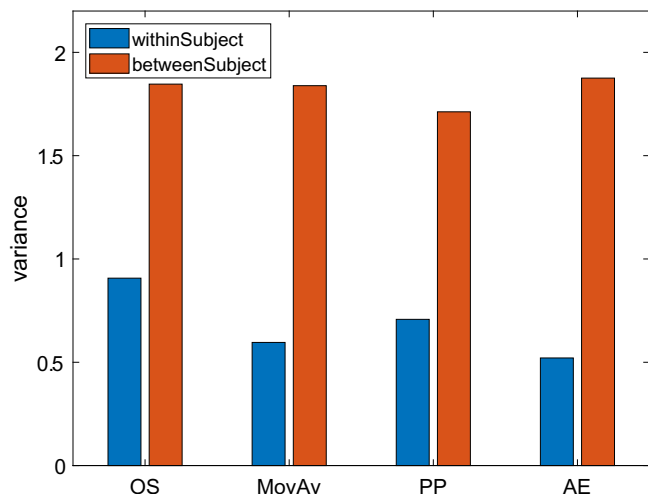
Our two main evaluation criteria are the bias introduced to parameter estimation, which is undesirable, and reduction of within-subject variance in a repeated measures experiment. For the first one, we compared OS with other cleaning methods. Since these differences were not normally distributed, as revealed by Royston's normality test (Royston, 1983), we applied non-parametric tests (multivariate: Randles sign test (Oja and Randles, 2004); univariate: Wilcoxon signed-rank test). For the second one, we performed a multivariate repeated measures ANOVA with two levels (first/s training) on the model parameters for each cleaning method.

**FIG. 1**

Mean of the fitted parameters across the first and the second part of the experiment, along with individual results marked in diamonds. Whiskers indicate the 95% confidence interval of the mean. a_s and b_s were consistently estimated by all cleaning methods. The estimation of a_f tended ($P = 0.1$) to be larger and that of b_f was significantly ($P < 0.001$, marked by *) lower in MA and PP compared to OS.

3 Results

Fig. 1 shows the mean of the model parameters of part 1 and part 2. The mean of the model parameters fitted for MA and PP differed systematically (Randles sign test: $P < 0.05$ for both) compared to OS, whereas AE did not show any bias ($P > 0.4$). The systematic bias of MA and PP originated from significant underestimation of b_f compared to OS (Wilcoxon: $P < 0.001$, $P < 0.0001$).

**FIG. 2**

The decomposition of total random variance into within-subject, between-subjects variances for OS, MA, PP and AE. Compared to OS, the within-subject variance was reduced for all other methods, but the greatest reduction was achieved with AE. Between-subjects variances were not affected.

Fig. 2 shows the decomposition of the noise in within-subject and between-subjects variance as provided by the repeated measures ANOVA. The between-subjects variability was similar for all cleaning methods, whereas the within-subject variance was lowest in AE. In terms of parameters, the greatest reduction was in a_f , with over 50% reduction and no visible change in other parameters.

4 Discussion

The overall effect of nearly all cleaning algorithms working on time series data is that they usually attenuate the signal on all frequency bands, therefore losing important information in the high frequency regime. This is significantly observable in Moving Average and Piecewise Polynomial approaches, where b_f is consistently underestimated, introducing a systemic bias. An outlier selection algorithm assumes less bias on the smoothness of data, but it does not help with variability of the fitted parameters, which ultimately clouds the comparisons between sets of model parameters. Autoencoders, on the other hand, did not induce any systematic bias on the model parameters.

Comparing within-subject variance, OS had the highest value and AE the lowest. Thus, cleaning by the AE was more efficient than the other methods. Our method also improved the estimation of a_f , which has been problematic (Tanaka et al., 2012). We envision that AE can clean noisy datasets, e.g., obtained in patient studies

(Wong et al., 2018). AE could even help distinguish possible subgroups of subjects. In conclusion, we propose AE to be a viable cleaning method for adaptive change time-series data.

References

- Ballard, D.H., 1987. Modular Learning in Neural Networks. AAAI, pp. 279–284.
- Colagiorgio, P., Bertolini, G., Bockisch, C.J., Straumann, D., Ramat, S., 2015. Multiple time-scales in the adaptation of the rotational VOR. *J. Neurophysiol.* 113, 3130–3142.
- Criscimagna-Hemminger, S.E., Shadmehr, R., 2008. Consolidation patterns of human motor memory. *J. Neurosci.* 28, 9610–9618.
- Henriques, D.Y., Filippopoulos, F., Straube, A., Eggert, T., 2014. The cerebellum is not necessary for visually driven recalibration of hand proprioception. *Neuropsychologia* 64c, 195–204.
- Herzfeld, D.J., Vaswani, P.A., Marko, M.K., Shadmehr, R., 2014. A memory of errors in sensorimotor learning. *Science* 345, 1349–1353.
- Kullback, S., Leibler, R.A., 1951. On information and sufficiency. *Ann. Math. Stat.* 22, 79–86.
- McDougle, S.D., Bond, K.M., Taylor, J.A., 2015. Explicit and implicit processes constitute the fast and slow processes of sensorimotor learning. *J. Neurosci.* 35, 9568–9579.
- Oja, H., Randles, R.H., 2004. Multivariate nonparametric tests. *Stat. Sci.* 19, 598–605.
- Royston, J., 1983. A simple method for evaluating the Shapiro-Francia W'test of non-normality. *J. R. Stat. Soc.*, 297–300.
- Sing, G.C., Smith, M.A., 2010. Reduction in learning rates associated with anterograde interference results from interactions between different timescales in motor adaptation. *PLoS Comput. Biol.* 6, E1000893.
- Smith, M.A., Ghazizadeh, A., Shadmehr, R., 2006. Interacting adaptive processes with different timescales underlie short-term motor learning. *PLoS Biol.* 4, E179.
- Tanaka, H., Krakauer, J.W., Sejnowski, T.J., 2012. Generalization and multirate models of motor adaptation. *Neural Comput.* 24, 939–966.
- Vaswani, P.A., Shadmehr, R., 2013. Decay of motor memories in the absence of error. *J. Neurosci.* 33, 7700–7709.
- Wong, A.L., Marvel, C.L., Taylor, J.A., Krakauer, J.W., 2018. Can Patients With Cerebellar Disease Switch Learning Mechanisms to Reduce Their Adaptation Deficits? *Biorxiv*, p. 386466.

SECTION

RESEARCH:
Nystagmus

V

This page intentionally left blank

Rebound nystagmus, a window into the oculomotor integrator

15

Jorge Otero-Millan^{a,*}, Ayse I. Colpak^{a,e}, Amir Kheradmand^{a,b}, David S. Zee^{a,b,c,d}

^aDepartment of Neurology, The Johns Hopkins University, Baltimore, MD, United States

^bDepartment of Otolaryngology-Head and Neck Surgery, The Johns Hopkins University, Baltimore, MD, United States

^cDepartment of Neuroscience, The Johns Hopkins University, Baltimore, MD, United States

^dDepartment of Ophthalmology, The Johns Hopkins University, Baltimore, MD, United States

^eDepartment of Neurology, Hacettepe University, Ankara, Turkey

*Corresponding author: Tel.: +1-602-696-3943, e-mail address: jotero@jhu.edu

Abstract

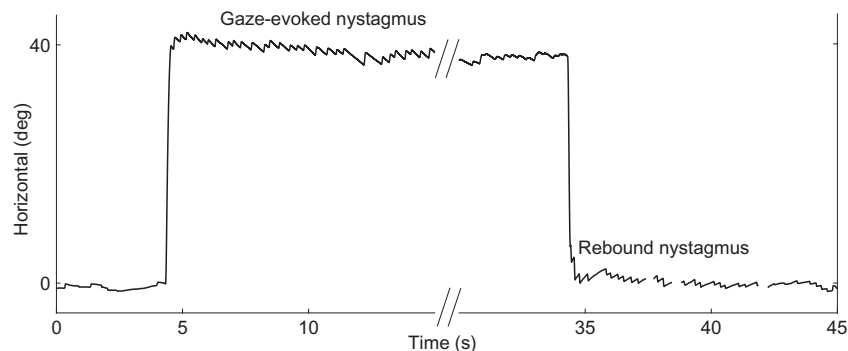
Rebound nystagmus, a common cerebellar sign, is a transient nystagmus that appears on returning to straight-ahead gaze after prolonged eccentric gaze. The slow phases of rebound nystagmus are in the direction of prior eccentric gaze. After eccentric gaze, healthy subjects also show rebound nystagmus when fixation is removed. Rebound nystagmus is thought to be related to the function of the oculomotor neural integrator—the circuit that ensures accurate gaze holding after any eye movement—but the exact mechanism of rebound nystagmus is unknown. Here, we combine experimental data with mathematical modeling to test several hypotheses for the generation of rebound nystagmus. We show that two mechanisms contribute, one relies on vision and the other does not. Future experiments must determine if (1) the non-visual mechanism is related to eye position or to eye velocity signals and (2) whether these signals are based on afferent (proprioception) or efferent (corollary) information.

Keywords

Cerebellum, Drift, Gaze-evoked nystagmus

1 Introduction

Rebound nystagmus (RN) is a transient nystagmus that occurs when the eyes return to straight ahead position following a period of prolonged eccentric gaze holding ([Fig. 1](#)). In RN the slow phases are directed toward the former eccentric gaze position and the quick-phases away from it ([Leigh and Zee, 2015](#)). Hood first described RN in

**FIG. 1**

Example of rebound nystagmus. A healthy subject looks at a flashing target, first at center (i.e., straight ahead), then eccentrically at 40 degrees to the right for 30 s, and then back to the center. During eccentric fixation at 40 degrees there is a gaze-evoked nystagmus with the slow phase drifting toward the center, which gradually decreases in intensity. During the rebound period, the slow phase drifts toward the previously-held, eccentric position.

a group of patients with cerebellar disorders (Hood et al., 1973) and it is typically considered to be a sign of abnormal cerebellar function (Lin and Young, 1999; Sharpe, 1974; Zee et al., 1976). Less intense RN can also be found in healthy subjects (Gordon et al., 1986; Shallo-Hoffmann et al., 1990; Zee et al., 1976), especially in the absence of a fixation target upon return of gaze to center.

Stable gaze holding is achieved by a neural network within the brainstem and cerebellum. This neural network must integrate (in the mathematical sense) signals that encode the velocity of eye movement commands such as saccades, smooth pursuit, or the vestibular ocular reflex, into position commands for holding the eyes still. The motor neurons receive the direct command encoding the velocity of the desired movement and the position command from the output of the neural integrator. These two signals combine in what is known, for saccades, as the pulse-step signal. The pulse helps overcome the viscous drag of the tissues surrounding the eye and the step provides the sustained drive to hold the eye at its new position (Robinson, 1981).

The neural integrator for gaze holding is not perfect, and even in some normal subjects, the eyes drift centripetally after an eccentric saccade, i.e., toward the straight-ahead position of gaze. This centripetal drift causes a nystagmus that is commonly referred to as gaze-evoked nystagmus. Gaze-evoked nystagmus tends to be larger at more eccentric eye positions and there is a null position where there is no drift and where the eye drifts toward from other positions. If we assume the drift can be approximated with an exponential curve, it can be parameterized by its time constant. In this case, the combination of time constant and null position determines the velocity of the drift from a given eye position.

The existence of rebound nystagmus indicates that the properties of the integrator may not be constant over time and instead depend on the prior eye movements and eye positions. If patients with gaze-evoked nystagmus are encouraged to sustain their attempt to look eccentrically, their nystagmus may quiet down and, on some occasions, even reverse direction, so that the eyes begin to drift centrifugally (Hood et al., 1973; Leech et al., 1977; Zee et al., 1976). This adaptability to past ocular motor behavior may represent mechanisms to optimize the behavior of the integrator. Understanding these mechanisms may help interpret the rebound nystagmus present in patients and improved their diagnosis and treatment.

In this study, we examined rebound nystagmus in healthy subjects with a briefly flashing target (to eliminate image motion on the retina due to the nystagmus itself) vs. continuously illuminated targets and tested whether bringing the eye to eccentric positions with different types of eye movements (smooth pursuit or saccades) affects either the intensity or duration of the rebound nystagmus. We also implemented a computational model to simulate the current results and make predictions of the results of future experiments to test the possible mechanisms of rebound nystagmus.

2 Methods

Six healthy human volunteers (two women) participated in the study. The experimental procedures were approved by Johns Hopkins Institutional Review Board and written informed consent was obtained from each subject. Subjects had no history of neurological nor vestibular disorders and were not taking sedative or psychiatric medications.

All experiments were performed in a dark room. Subjects sat upright with the head immobilized by a dental bite bar 135 cm away from a light-transmissive horizontal screen. Red laser targets were rear-projected on the screen and moved by a mirror galvanometer. Horizontal eye movements were recorded with an infrared video goggle system (RealEyes xDVR system, Micromedical Technologies Inc., Chatham, IL) controlled by custom software (Otero-Millan et al., 2015) at a frame rate of 100Hz. Each subject participated in two experiments.

Experiment I measured the difference on rebound nystagmus between holding eccentric gaze with a flashing target and with a continuous target. Each subject was asked to fix on a flashing target (illuminated for 10 ms every second) in the straight-ahead position. After 5 s, the target jumped eccentrically ($\pm 40^\circ$) and either flashed or remained on continuously. After 30 s holding the eccentric gaze position, the target jumped back to straight-ahead position and flashed (10 ms on per second) for 15 s. After the trial finished subjects had a 10-s break before the next trial began. For each condition (flashing or continuous target), two blocks of five trials were performed, one for each direction (left or right).

Experiment II measured the difference in rebound nystagmus after bringing the eye to an eccentric position by different types of eye movements. Three experimental conditions were used: single saccade, smooth pursuit, and a stair-case of saccades. For all conditions, the target was flashing at the straight-ahead position and at the 40° position but continuously on during the movements toward the eccentric target. For single saccade trials, we used the data from Experiment I where after 5 s recordings in the straight-ahead position, the subjects were asked to make a saccade to an eccentricity of 40°. After 30 s the target jumped back to the straight-ahead position where it remained for another 15 s. For smooth pursuit movements, after 5 s recordings in the straight-ahead position, the subjects were asked to track a small red laser dot, moving at 4°/s to reach an eccentricity of 40° which took 10 s. After a further 20 s of eccentric fixation, the target jumped back to the straight-ahead position where it remained for another 15 s. For staircase saccades, after 5 s with flashing light in the straight-ahead position, the target jumped four degrees every second until reaching an eccentricity of 40° (a total of 10 saccades which took 10 s.). After a further 20 s of eccentric fixation the target jumped back to the straight-ahead position where it remained for another 15 s. Note that in all cases the time spent away from the straight-ahead position was 30 s. For each condition, two blocks of five trials were performed, one for each direction (left or right).

To quantify rebound nystagmus, we measured the velocity of the slow phase of the nystagmus over time as the median velocity within windows of 500 ms (excluding samples belonging to quick phases, identified with a velocity threshold of 10 deg/s in either direction). Then we fit an exponential curve to the data corresponding to the first 15 s after returning to the straight-ahead position. From the exponential fit we obtained the maximum slow-phase velocity of the nystagmus and the time constant of the decay of the slow-phase velocity over time.

3 Results

In Experiment I we found that rebound nystagmus was more pronounced after subjects fixated eccentrically at the continuously illuminated target than at the flashing target. The average maximum slow-phase velocity, as measured with an exponential fit, was $3.5 \pm 0.7^\circ/\text{s}$ for the continuous target and $2.3 \pm 0.5^\circ/\text{s}$ for the flashing target ($P = 0.036$ paired *t*-test). The average time constant was 9 ± 3 s for the continuous target and 6 ± 1 s for the flashing target ($P = 0.1$ paired *t*-test). In Experiment II we found that the velocity of the rebound nystagmus did not depend on how the eyes reached the peripheral target: with a single saccade, 10 small saccades, or smooth pursuit. The average maximum slow-phase velocity was $2.3 \pm 0.5^\circ/\text{s}$, $1.9 \pm 0.4^\circ/\text{s}$, and $1.6 \pm 0.2^\circ/\text{s}$ for each of the conditions, respectively ($P = 0.2$ repeated measures ANOVA). The time constant of the rebound nystagmus was 6 ± 1 s, 6 ± 2 s, and 6 ± 2 s, respectively ($P = 0.7$ repeated measures ANOVA). Fig. 2 shows the average slow-phase velocity across subjects as well as the individual subjects for each of the experiments for the first 15 s after the subjects returned to straight ahead position.

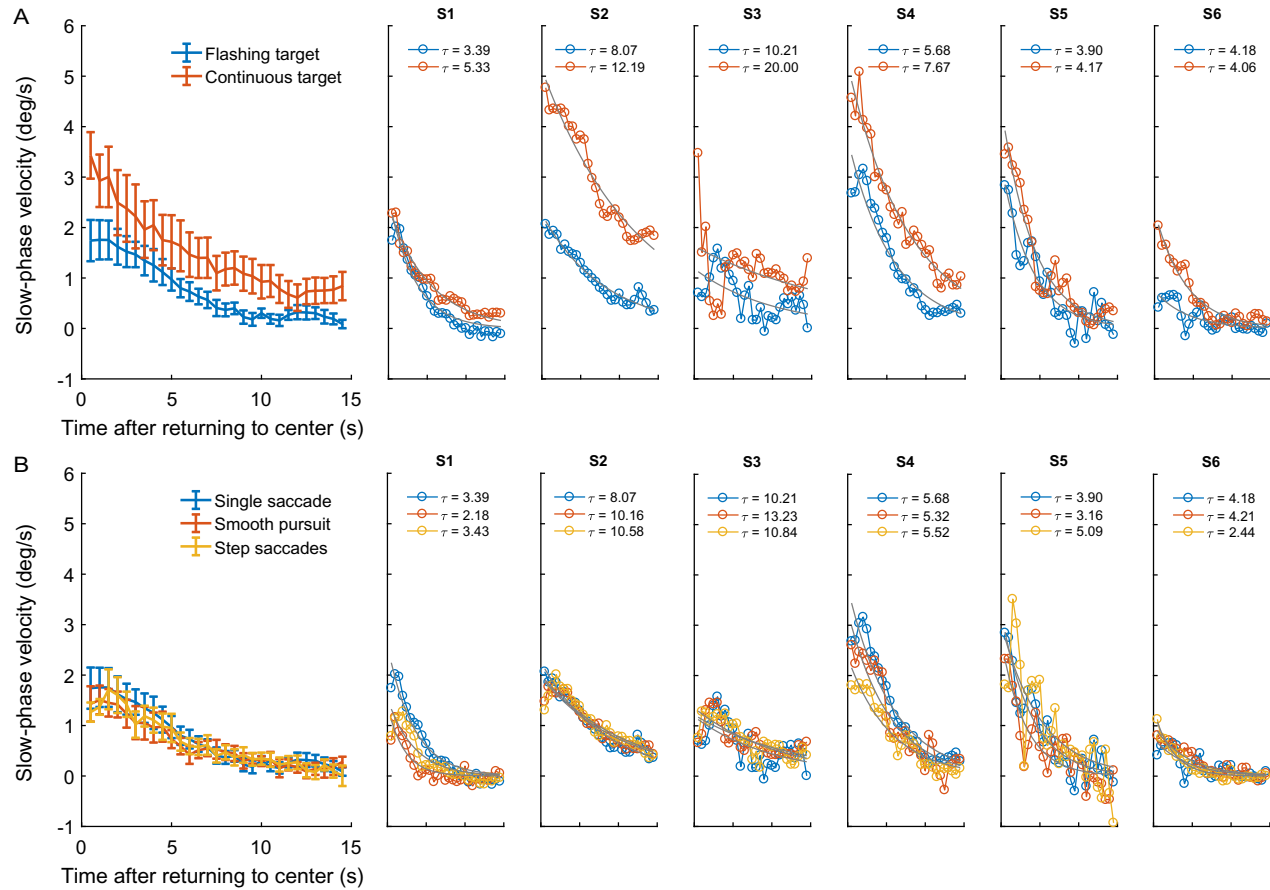


FIG. 2

Results of Experiments I (A) and Experiment II (B). The first columns show the average across subjects with error bars displaying the standard error of the mean. Subsequent columns show the results for each individual subject.

4 Discussion

4.1 Characterization of gaze holding

Gaze-holding behavior can be characterized by measuring the velocity of the gaze-evoked nystagmus as a function of the eye position eccentricity. This relationship is usually not linear (Abel et al., 1978; Bertolini et al., 2013) and can be characterized with a tangent function (Bertolini et al., 2013). Specifically, the relationship between eccentricity and drift (slow phase) velocity can be described with the simple equation (Romano et al., 2017; Tarnutzer et al., 2015):

$$V_E = \frac{k_2}{k_1} \tan(k_1 * E) + c_2$$

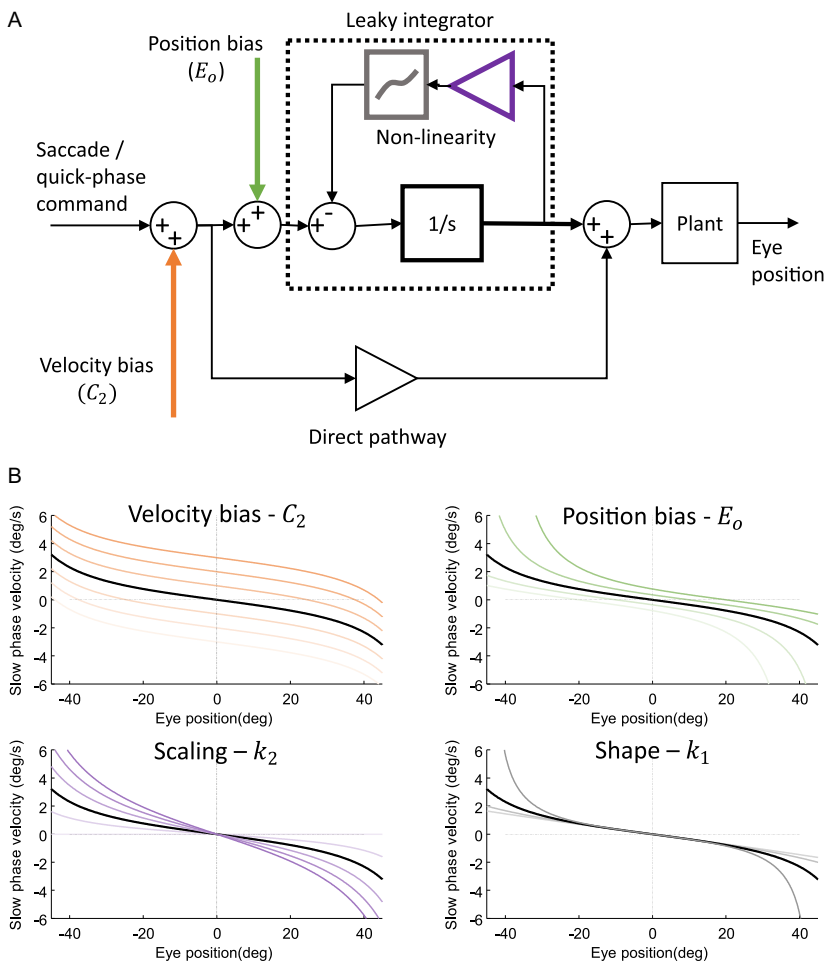
where V_E is the slow-phase velocity of the nystagmus at eccentricity E , k_1 is a parameter that defines the shape of the curve, that is, how non-linear it is, k_2 is a scaling factor that changes the overall slope of the curve, and c_2 is a velocity bias that corresponds with a possible eye drift present at straight ahead position. They used this approach to characterize the behavior of the neural integrator for gaze holding in healthy individuals (Bertolini et al., 2013), patients with different neurological disorders (Tarnutzer et al., 2015), and individuals with alcohol intoxication (Romano et al., 2017).

The parameters that characterize the tangent function need not be stable over time and may be affected by the recent history of eye movements, as is the case in rebound nystagmus. In this context the parameters of the tangent function become functions of time. Additionally, we added another parameter E_o that represents a possible shift in the null position of the integrator over time and moves the curve horizontally.

$$V_E(t) = \frac{k_2(t)}{k_1(t)} \tan(k_1(t) * (E - E_o(t))) + c_2(t)$$

Thus, it is possible that initially E_o and c_2 are zero, resulting in no nystagmus at straight-ahead position. However, after holding gaze eccentrically, those parameters may change resulting in a curve that corresponds with rebound nystagmus at straight-ahead position. The other parameters k_1 and k_2 may also change as a result of holding gaze eccentrically. Their changes, however, would not lead to rebound nystagmus by themselves. Instead, they would interact with the potential changes to E_o and c_2 affecting the amount of rebound nystagmus that would be generated.

This analytical characterization of the integrator can be implemented using a control system approach (Fig. 3). A leaky integrator is the most basic form of a gaze-holding control system. It is a system that accumulates the input it receives, in this case eye velocity, creating a memory of eye position. However, the integrator forgets (leaks) at some rate, which results in the memory of the eye position drifting over time. Two main parameters determine the behavior of the integrator: the null position, that is, the position that the eye tends to drift toward in the absence of an input and the time constant, which determines how fast the eye drifts toward the null

**FIG. 3**

Characterization of gaze-holding behavior. (A) Control systems diagram of the main elements of the gaze-holding circuit. (B) Effect of changing each of the parameters of the tangent equation describing the drift velocity of the eye as a function of the eye position. The elements in (A) that correspond to each of the parameters are highlighted with the same color.

position. The slow-phase velocity is determined by both parameters: the lower the time constant the faster the drift; the farther the null position from the current position the faster the drift. If the time constant does not depend on the eye position, the relationship between eye position and drift velocity is linear. To achieve the tangent curve described previously it is necessary for the time constant of the integrator to decrease with eccentricity as determined by k_1 and k_2 . The parameter E_o corresponds with the null position of the integrator and the parameter c_2 with a constant-velocity bias that is added to the input or output of the integrator.

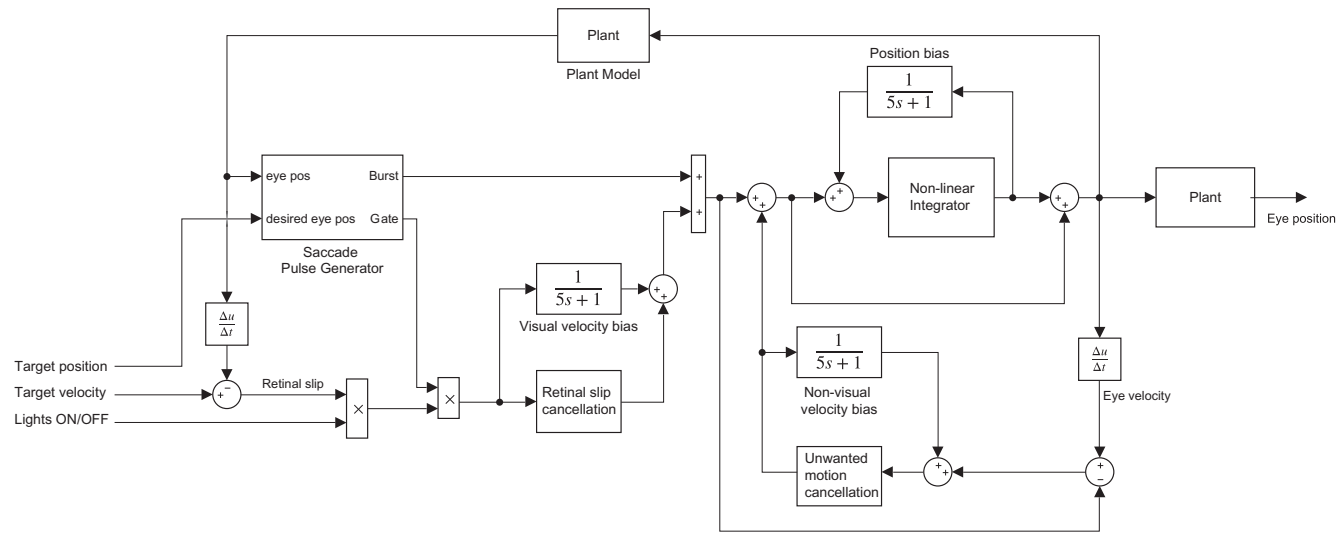


FIG. 4

Diagram of the control system model implemented to simulate rebound nystagmus. Three different elements contribute to rebound nystagmus: position bias, visual velocity bias, and non-visual velocity bias. The non-linear integrator was implemented simply with two different leaks, one for eccentricities within $\pm 25^\circ$ and a larger leak for eccentricities outside of $\pm 25^\circ$. The saccade generator generates a pulse of constant velocity whenever the difference between the target position and the output of the integrator is more than 0.2° until it corrects for that difference. The plant and retinal slip and unwanted motion cancellation systems are modeled as simple first order systems.

4.2 Modeling rebound nystagmus

Here, we set out to implement a control systems model that simulates rebound nystagmus under different conditions, including our results, and can help us design future experiments to test these ideas (Fig. 4). From our results, we know there must be at least two different mechanisms for rebound nystagmus: one independent of vision to account for rebound with the flashing target and one dependent on vision to account for the increased rebound in the continuous target condition. In this model, we implement three mechanisms that may contribute to rebound nystagmus. First, a system like smooth-pursuit, perhaps special for fixation (Luebke and Robinson, 1988), driven by motion of images on the retina (retinal slip) produced by the nystagmus itself, which creates a signal that attempts to cancel the nystagmus. By averaging this signal over time, using a first order system, a velocity bias is introduced. Second, a position bias is generated by averaging the output of the integrator over time and feeding it back to its input. This shifts the null of the integrator toward the current eye position. Finally, a system that may use efference copies of eye movement commands or extraocular proprioception to monitor unwanted drift of the eye also generates a signal that attempts to cancel the nystagmus even in the absence of light. This signal is also averaged over time resulting in another source of velocity bias.

First, we simulated the results of our experiments. Fig. 5A shows the simulation of Experiment I. As in our results, the velocity of the rebound nystagmus is larger in the light condition (equivalent to the continuously on target) than the “dark” condition (equivalent to the flashing target). Fig. 5B shows the simulation of Experiment II. As in the data from our experiments the model produces equivalent velocities of the rebound using smooth pursuit and large or step saccades.

Second, we simulated the results from Chung and Bedell (1995) studying the “dumping” of rebound nystagmus by the presence of a sustained visual target. They found that if a fixation target appeared shortly after returning to the straight-ahead position, the nystagmus would resume after the target disappeared but with a speed lower than would have been without a fixation target. Fig. 5C shows the result of the simulations with a fixation target visible for 4s. The rebound resumes after the target disappears but the velocity of the nystagmus is lower than for the same timepoint without any visual target having been presented. In this model, the source of this suppression is the velocity bias created by the retinal slip while the fixation target was on.

Finally, we simulated the results of a hypothetical experiment (Fig. 5D and E) where we could measure the contributions of some of the non-visual components. In this experiment, subjects would fix eccentrically for a period of time and then would return not to the straight-ahead position, but to different eye positions covering the entire range of eccentricities. Measuring the velocities of the rebound we could build the curve describing the relationship between eye position and drift velocity to describe how the integrator has changed after holding eccentric gaze. Then, by comparing with the same curve obtained without prior eccentric gaze holding, we could measure the contribution of the different components (position bias and velocity bias) to rebound nystagmus.

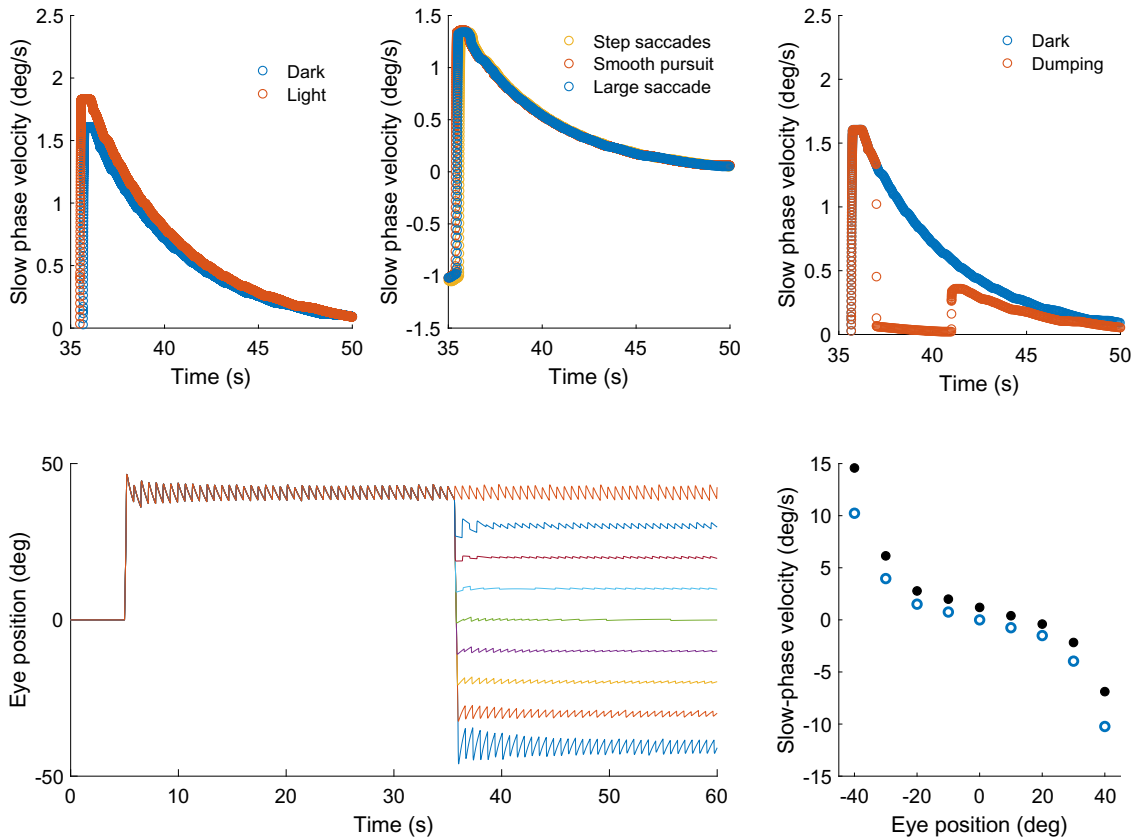


FIG. 5

Results of simulations of the model. (A) Simulations of Experiment I. (B) Simulations of Experiment II. (C) Simulations of Chung and Bedell (1995) experiments. (D and E) Simulations of hypothetical experiment to measure the eye position vs. drift velocity curve during rebound nystagmus. (D) Eye position traces when measuring rebound at each eccentricity after holding gaze always at 40°. (E) Corresponding slow-phase velocities of the rebound nystagmus. Blue dots indicate the velocity of the nystagmus during normal eccentric gaze and black dots represent the velocity of the rebound nystagmus after holding eccentric gaze and then moving to different eye positions.

4.3 Why rebound?

One may ask why the integrator should behave in a way that results in rebound nystagmus. A possible explanation is that there are mechanisms that calibrate the integrator to ensure that most of the time we do not suffer from gaze-evoked nystagmus. This would be part of a general strategy of the brain to eliminate unwanted biases in order to produce “quiet” zones or set-points that allow for optimal sensory and motor behavior (Zee et al., 2017). Based on this idea, the adaptive mechanisms of the brain could keep track of the most common gaze positions, and then change the properties of the integrator to reduce any drift at these positions, but perhaps at the expense of less stability for gaze at uncommon positions. This strategy would correspond with a continuous shift of the null position of the integrator toward the more common eye positions. Indeed, when such a mechanism goes awry, for example, in cerebellar disease, the null position becomes unstable and unwanted drift of the eyes occurs (Leech et al., 1977; Robinson, 1974).

The oculomotor integrator for gaze holding, which also operates upon vestibular signals, would also help compensate for any long-term bias in the vestibular system as another form of set-point adaptation (Khojasteh et al., 2013; Robinson et al., 1984). In this case, there could be a mechanism that continuously monitors the output of the integrator and detects biases in its rate of change (eye velocity). This would correspond with a velocity bias that attempts to compensate and remove unwanted image motion of the retina from instability of gaze. In both cases, the mechanisms must estimate the statistics of signals within the integrator, its inputs, or its outputs. Those estimates must be calculated over a period of time and thus would lag any change of the signals. This lag may not be noticeable under most circumstances. However, if the subject is presented with a sudden and large change, outside of the normal range, the consequences of the lag may be apparent as it is the case in rebound nystagmus.

A slightly different variant on these ideas, which emphasizes the flexibility of these adaptive circuits, is the ability of the brain to change the time constant of the oculomotor integrator to adjust the phase of the vestibulo-ocular reflex to eliminate unwanted retinal image motion during head movements. Normally, such a change in the time constant of the integrator would also lead to unwanted drift of the eyes after every movement ends (Kramer et al., 1995). The adaptive circuits, however, selectively alter integrator function for the vestibular system without causing unwanted drift during fixation after saccades (Kramer et al., 1998).

4.4 Other approaches to model neural integrators

Here, we have focused on a control systems approach to study the gaze-holding integrator and the possible mechanisms responsible for rebound nystagmus. However, there are other models of neural integration (Goldman et al., 2009). For example, Cannon and colleagues (Cannon and Robinson, 1985; Cannon et al., 1983) developed a neural network model that relies on laterally inhibited neurons that

simulate the behavior of neurons identified as part of the neural integrator as well as the expected eye movement behavior. Seung and colleagues developed a model based on a network of neurons with recurrent excitatory connections that behave as an “attractor” (Seung, 1996; Seung et al., 2000). Other models of neural integrators used to account for activity of head direction cells (Song and Wang, 2005) behave as maps where the desired output eye position is encoded by the location of activity in the map. These approaches could also be used to study rebound nystagmus and rebound nystagmus may emerge as an intrinsic property of these implementations. Nonetheless, a simple, control-systems approach as used here accounts for many aspects of rebound nystagmus and suggests future experiments.

Acknowledgments

We thank Dale Roberts for technical assistance, and Jing Tian for her comments. This work was supported by the National Eye Institute (Award K99EY027846 to J.O.M.), the National Institute of Deafness and Other Communication Disorders (NIDCD) (Award 5K23DC013552 to A.K.), and the Leon Levy, Fight for Sight foundations.

References

- Abel, L.A., Parker, L., Daroff, R.B., Dell’Osso, L.F., 1978. End-point nystagmus. *Invest. Ophthalmol. Vis. Sci.* 17 (6), 539–544.
- Bertolini, G., Tarnutzer, A.A., Olasagasti, I., Khojasteh, E., Weber, K.P., Bockisch, C.J., Straumann, D., Marti, S., 2013. Gaze holding in healthy subjects. *PLoS One* 8, e61389. <http://dx.plos.org/10.1371/journal.pone.0061389>.
- Cannon, S.C., Robinson, D.A., 1985. An improved neural-network model for the neural integrator of the oculomotor system: more realistic neuron behavior. *Biol. Cybern.* 53 (2), 93–108. <https://doi.org/10.1007/BF00337026>.
- Cannon, S.C., Robinson, D.A., Shamma, S., 1983. A proposed neural network for the integrator of the oculomotor system. *Biol. Cybern.* 49 (2), 127–136. <https://doi.org/10.1007/BF00320393>.
- Chung, S.T.L., Bedell, H.E., 1995. ‘Dumping’ of rebound nystagmus and optokinetic afternystagmus in humans. *Exp. Brain Res.* 107 (2), 306–314. <https://doi.org/10.1007/BF00230050>.
- Goldman, M.S., Compte, A., Wang, X.-J., 2009. Neural integrator models. In: Squire, L.R. (Ed.), *Encyclopedia of Neuroscience*. Academic Press, Oxford, pp. 165–178. <https://doi.org/10.1016/B978-008045046-9.01434-0>.
- Gordon, S.E., Hain, T.C., Zee, D.S., Fetter, M., 1986. Rebound nystagmus. In: 16th Annual Meeting of the Society for Neuroscience, Washington, DC. 1091.
- Hood, J.D., Kayan, A., Leech, J., et al., 1973. Rebound nystagmus. *Brain* 96 (3), 507–526.
- Khojasteh, E., Bockisch, C.J., Straumann, D., Hegemann, S.C.A., 2013. A dynamic model for eye-position-dependence of spontaneous nystagmus in acute unilateral vestibular deficit (Alexander’s Law). *Eur. J. Neurosci.* 37 (1), 141–149. <https://doi.org/10.1111/ejn.12030>.

- Kramer, P.D., Shelhamer, M., Zee, D.S., 1995. Short-term adaptation of the phase of the vestibulo-ocular reflex (VOR) in normal human subjects. *Exp. Brain Res.* 106 (2), 318–326. <https://doi.org/10.1007/BF00241127>.
- Kramer, P.D., Shelhamer, M., Peng, G.C.Y., Zee, D.S., 1998. Context-specific short-term adaptation of the phase of the vestibulo-ocular reflex. *Exp. Brain Res.* 120 (2), 184–192.
- Leech, J., Gresty, M., Hess, K., Rudge, P., 1977. Gaze failure, drifting eye movements, and centripetal nystagmus in cerebellar disease. *Br. J. Ophthalmol.* 61 (12), 774–781. <https://doi.org/10.1136/bjo.61.12.774>.
- Leigh, R.J., Zee, D.S., 2015. *The Neurology of Eye Movements*. Oxford University Press.
- Lin, C.-Y., Young, Y.-H., 1999. Clinical significance of rebound nystagmus. *Laryngoscope* 109 (11), 1803–1805.
- Luebke, A.E., Robinson, D.A., 1988. Transition dynamics between pursuit and fixation suggest different systems. *Vis. Res.* 28 (8), 941–946. [https://doi.org/10.1016/0042-6989\(88\)90103-4](https://doi.org/10.1016/0042-6989(88)90103-4).
- Otero-Millan, J., Roberts, D.C., Lasker, A., Zee, D.S., Kheradmand, A., 2015. Knowing what the brain is seeing in three dimensions: a novel, noninvasive, sensitive, accurate, and low-noise technique for measuring ocular torsion. *J. Vis.* 15 (14), 11. <https://doi.org/10.1167/15.14.11>.
- Robinson, D.A., 1974. The effect of cerebectomy on the cat's vestibulo-ocular integrator. *Brain Res.* 71 (2–3), 195–207. [https://doi.org/10.1016/0006-8993\(74\)90961-5](https://doi.org/10.1016/0006-8993(74)90961-5).
- Robinson, D.A., 1981. The use of control systems analysis in the neurophysiology of eye movements. *Annu. Rev. Neurosci.* 4 (1), 463–503. <https://doi.org/10.1146/annurev.ne.04.030181.002335>.
- Robinson, D.A., Zee, D.S., Hain, T.C., Holmes, A., Rosenberg, L.F., 1984. Alexander's law: its behavior and origin in the human vestibulo-ocular reflex. *Ann. Neurol.* 16 (6), 714–722. <https://doi.org/10.1002/ana.410160614>.
- Romano, F., Tarnutzer, A.A., Straumann, D., Ramat, S., Bertolini, G., 2017. Gaze-evoked nystagmus induced by alcohol intoxication. *J. Physiol.* 595 (6), 2161–2173. <https://doi.org/10.1113/JP273204>.
- Seung, H.S., 1996. How the brain keeps the eyes still. *Proc. Natl. Acad. Sci. U. S. A.* 93 (23), 13339–13344. <https://doi.org/10.1073/pnas.93.23.13339>.
- Seung, H.S., Lee, D.D., Reis, B.Y., Tank, D.W., 2000. Stability of the memory of eye position in a recurrent network of conductance-based model neurons. *Neuron* 26 (1), 259–271.
- Shallo-Hoffmann, J., Schwarze, H., Simonsz, H.J., Mühlendyck, H., 1990. A reexamination of end-point and rebound nystagmus in normals. *Invest. Ophthalmol. Vis. Sci.* 31 (2), 388–392.
- Sharpe, J.A., 1974. Rebound nystagmus—a cerebellar sign? *JAMA* 227 (6), 648–649.
- Song, P., Wang, X.-J., 2005. Angular path integration by moving 'hill of activity': a spiking neuron model without recurrent excitation of the head-direction system. *J. Neurosci.* 25 (4), 1002–1014. <https://doi.org/10.1523/JNEUROSCI.4172-04.2005>.
- Tarnutzer, A.A., Weber, K.P., Schuknecht, B., Straumann, D., Marti, S., Bertolini, G., 2015. Gaze holding deficits discriminate early from late onset cerebellar degeneration. *J. Neurol.* 262 (8), 1837–1849. <https://doi.org/10.1007/s00415-015-7773-9>.
- Zee, D.S., Yee, R.D., Cogan, D.G., Robinson, D.A., Engel, W.K., 1976. Ocular motor abnormalities in hereditary cerebellar ataxia. *Brain J. Neurol.* 99 (2), 207–234.
- Zee, D.S., Jareconsettasin, P., Leigh, R.J., 2017. Ocular stability and set-point adaptation. *Philos. Trans. R. Soc., B* 372 (1718) 20160199. <https://doi.org/10.1098/rstb.2016.0199>.

This page intentionally left blank

Central positional nystagmus: Characteristics and model-based explanations

16

Jeong-Yoon Choi^{a,b}, Ji-Soo Kim^{a,b,*}

^a*Department of Neurology, Dizziness Center, Clinical Neuroscience Center, Seoul National University Bundang Hospital, Seongnam, South Korea*

^b*Department of Neurology, Seoul National University College of Medicine, Seoul, South Korea*

*Corresponding author: Tel.: +82-31-787-7463; Fax: +82-31-719-6828,

e-mail address: jisookim@snu.ac.kr

Abstract

The central vestibular system operates to precisely estimate the rotational velocity and gravity orientation using the inherently ambiguous information from peripheral vestibular system. Therefore, any lesions disrupting this function can generate positional nystagmus. Central positional nystagmus (CPN) can be classified into the paroxysmal (transient) and persistent forms. The paroxysmal CPN has the features suggesting a semicircular canal origin regarding the latency, duration, and direction of nystagmus. Patients with paroxysmal CPN commonly show several different types of nystagmus classified according to the provoking positioning. The persistent form of CPN mostly appears as downbeat nystagmus while prone or supine, or apogeotropic or geotropic horizontal nystagmus when the head is turned to either side while supine. CPN may be ascribed to erroneous neural processing within the velocity-storage circuit that functions in estimating angular head velocity, gravity direction, and inertia. Paroxysmal CPN appears to be post-rotatory rebound nystagmus due to lesions involving the cerebellar nodulus and uvula. In contrast, persistent CPN may arise from erroneous gravity estimation. The overlap of lesion location responsible for both paroxysmal and persistent CPN may account for the frequent coexistence of both forms of nystagmus in a single patient.

Keywords

Vertigo, Nystagmus, Central positional nystagmus, Velocity-storage, Nodulus, Uvula

1 Introduction

Positional nystagmus may occur in central as well as peripheral pathologies (Buttner et al., 1999; Harrison and Ozsahinoglu, 1972). Due to its potentially grave underlying pathology (Buttner et al., 1999; Harrison and Ozsahinoglu, 1972), central positional nystagmus (CPN) has been the subject of clinical interest. According to its temporal characteristics, CPN may be specified into either paroxysmal or persistent type (Buttner et al., 1999) (Fig. 1). A typical form of paroxysmal CPN is short-lasting down-beat nystagmus with prominent vertigo that occurs when the patient lies down (Baloh and Spooner, 1981; Barber, 1984). Because of the similarity of clinical presentation with benign paroxysmal positional vertigo (BPPV), there have been attempts to define the characteristics of paroxysmal CPN in comparison to BPPV (Buttner et al., 1999). On the other hand, the persistent form of CPN is characterized by long lasting nystagmus in specific head positions (Buttner et al., 1999; Glasauer et al., 2001).

Recently, several patterns of positional nystagmus with the features previously known as central have also been described in peripheral pathologies such as anterior canal canalolithiasis (Bertholon et al., 2002; Cambi et al., 2013; Lopez-Escamez et al., 2006), horizontal canal cupulolithiasis (Baloh et al., 1995; Kim et al., 2012a;

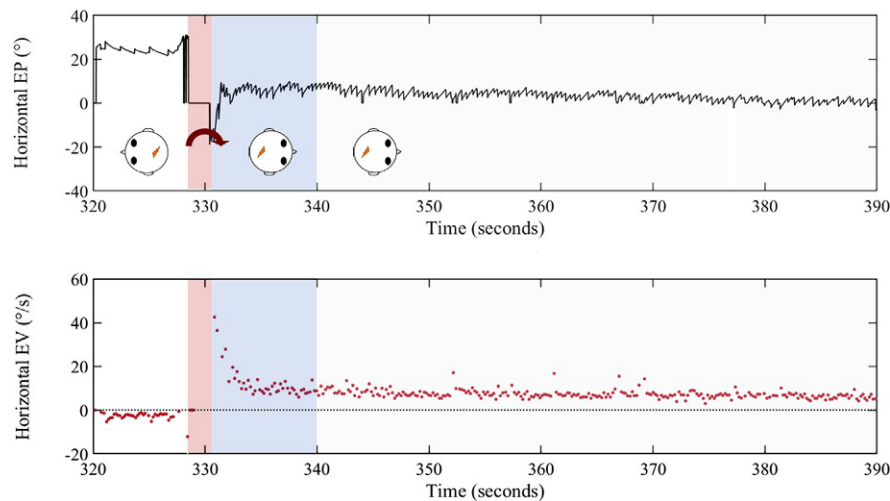


FIG. 1

Two types of central positional nystagmus (CPN). When the head is moved from left ear-down to right ear-down position, right beating horizontal nystagmus changes into left beating nystagmus. The velocity of left beating nystagmus shows a peak initially (about $40^{\circ}/s$) and then decreases exponentially. After about 10s of positioning, the slow eye velocity becomes stable at about $10^{\circ}/s$. The red column indicates the period of head motion. The blue and gray columns indicate paroxysmal and persistent components of CPN, respectively. EP, eye position ($^{\circ}$); EV, eye velocity ($^{\circ}/s$). Positive values indicate rightward eye position or velocity.

Oh et al., 2009), or light cupula (Choi et al., 2017; Kim et al., 2014, 2018). The characteristics of these atypical forms of BPPV are similar to those of CPN. Thus, it becomes more challenging to differentiate central from peripheral positional nystagmus. In this chapter, we will give an overview of the recent advances in the characteristics and mechanisms of CPN in comparison with BPPV.

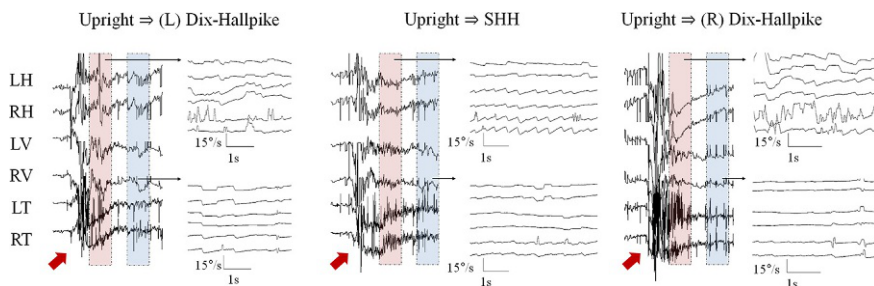
2 Characteristics of central positional nystagmus

Even though the paroxysmal and persistent CPN frequently co-exist in a single patient (Fig. 1), we will describe the characteristics of each CPN separately in this part.

2.1 Paroxysmal CPN

As the term implies, the paroxysmal CPN has a short latency and duration. Paroxysmal CPN has been reported to have a latency less than a few seconds (0–5 s) (Buttner et al., 1999). Recent observations have also confirmed that the paroxysmal CPN mostly occurs immediately after head motion (Choi et al., 2015; Macdonald et al., 2017). The intensity of paroxysmal CPN is peak at its onset or within 3–5 s of its onset, usually along with severe vertigo, and then decreases exponentially (Fig. 1). The time constant (TC) of paroxysmal CPN is about 4–6 s (Choi et al., 2015), and is similar to that of the cupula in the vertical semicircular canals (Goldberg and Fernandez, 1971) or that of the velocity-storage (VS) for the vertical rotational vestibulo-ocular reflex (VOR) (Bertolini and Ramat, 2011; Bertolini et al., 2008). Accordingly, the paroxysmal CPN mostly has a duration of 10–15 s (about three times of the TC) though a few patients with an exceptionally strong nystagmus may show a rather longer duration (Choi et al., 2015). This implies that evaluation of paroxysmal CPN should be focused on the initial 3–5 s after positioning given its rapidly decreasing pattern. However, the latency and duration may not be helpful in distinguishing paroxysmal CPN from BPPV (Buttner et al., 1999).

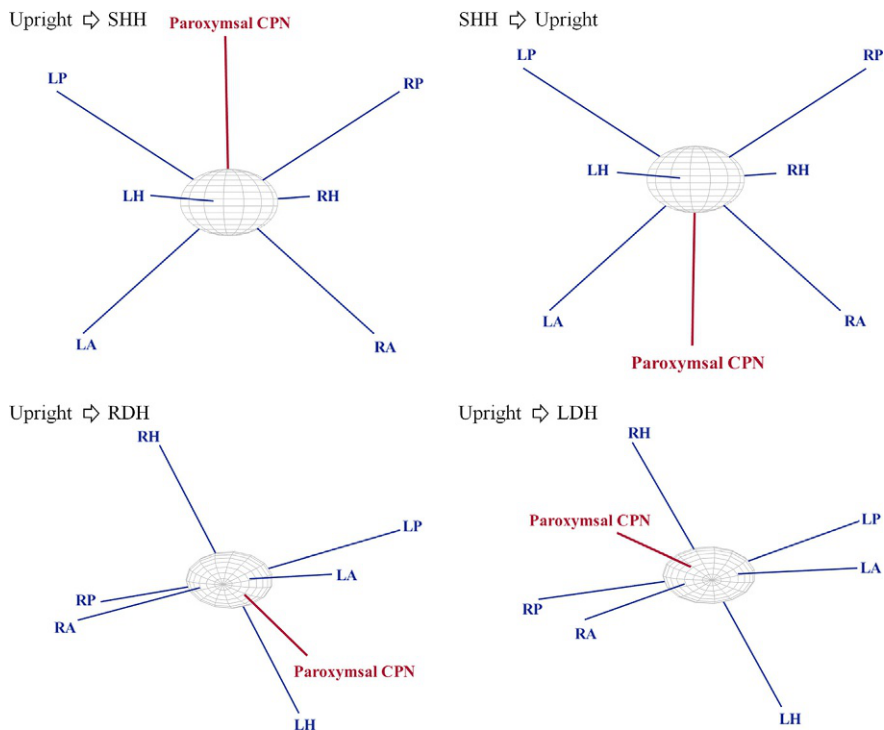
The representative form of paroxysmal CPN is pure vertical or torsional, which cannot be attributable to stimulation of a single semicircular canal (Buttner et al., 1999). Even though these directional characteristics have been well recognized in CPN, detailed patterns of nystagmus induced during each positional change require further elucidation. A recent study analyzed the patterns of paroxysmal CPN according to the provoking positional changes and disclosed three distinct subtypes (Choi et al., 2015). The first is paroxysmal downbeat CPN that mostly emerges when the head is rotated back while lying down, straight head hanging or Dix-Hallpike maneuver (Fig. 2). This paroxysmal downbeat CPN may accompany horizontal and torsional components depending on the semicircular canals stimulated or inhibited during the positioning. The second is paroxysmal upbeat CPN that appears when the head is rotated forward when resuming the upright position from the supine, straight-head hanging, or Dix-Hallpike position. This paroxysmal upbeat CPN

**FIG. 2**

Paroxysmal downbeat central positional nystagmus (CPN). The red columns indicate the paroxysmal component of CPN, while the blue columns represent the persistent component of CPN. During straight-head hanging (middle) and right Dix-Hallpike (right) maneuvers, the direction of initial nystagmus is mainly downward and counter-clockwise. During the left Dix-Hallpike maneuver (left), spontaneous counter-clockwise nystagmus is suppressed initially. Red arrows indicate the time period of head motion. LH, left eye horizontal position; LV, left eye vertical position; LT, left eye torsional position; RH, right eye horizontal position; RV, right eye vertical position; RT, right eye torsional position; HHV, horizontal head velocity; VHV, vertical head velocity; THV, torsional head velocity.

may also accompany horizontal and torsional components depending on the canals affected during each positioning. The third is paroxysmal apogeotropic CPN during the supine head roll tests. In these instances, the provoked nystagmus occurs in the opposite direction of head motion (i.e., right beating nystagmus after head rotation to the left and left beating nystagmus after head rotation to the right). From these findings, it may be concluded that paroxysmal CPN is frequently a mixture of horizontal, vertical, and torsional nystagmus and its direction depends on the canals stimulated during each positional change.

The relationship between the direction of paroxysmal CPN and the canals stimulated during each positioning is best demonstrated by analyzing the rotational vector of the induced nystagmus (Choi et al., 2015) (Fig. 3). With these analyses, it was disclosed that the rotational vector of paroxysmal CPN is mostly aligned with the rotational axes of the semicircular canals inhibited during the positioning. For instance, during right Dix-Hallpike maneuver, right posterior (excitation) and left anterior semicircular (inhibition) canals are mainly stimulated, but the ipsilateral (excitation) and contralateral (inhibition) horizontal canals are also stimulated in part. Accordingly, the rotational axis of paroxysmal CPN triggered during right Dix-Hallpike maneuver is aligned with the vector sum of the rotational axes of left anterior and left horizontal canals that are normally inhibited during this positioning. Given that canalolithiasis of the anterior canal can also generate paroxysmal torsional downbeat nystagmus during Dix-Hallpike or straight-head hanging maneuvers (Bertholon et al., 2002), differentiation of paroxysmal CPN from BPPV may be challenging when only based on the direction of nystagmus.

**FIG. 3**

Rotational vector for paroxysmal type of central positional nystagmus. The blue lines indicate a rotational vector of each semicircular canal. The red thick lines indicate the rotational vectors of paroxysmal central positional nystagmus. The data from the 17 patients in the previous report (Choi et al., 2015). CPN, central paroxysmal nystagmus; LA, left anterior canal; LDH, left Dix-Hallpike position; LH, left horizontal canal; LP, left posterior canal; RA, right anterior canal; RDH, right Dix-Hallpike position; RH, right horizontal canal; RP, right posterior canal; SHH, straight-head hanging position.

Another feature of paroxysmal CPN is the coexistence of several types. In a recent study, various types of paroxysmal CPN co-existed in a single patient (Choi et al., 2015). Of 17 patients with paroxysmal downbeat CPN, 16 also showed paroxysmal upbeat nystagmus and 13 exhibited apogeotropic horizontal nystagmus. Furthermore, about a half of the patients with paroxysmal CPN also showed persistent downbeat or apogeotropic CPN (Choi et al., 2015). Thus, this cooccurrence of various types of paroxysmal and persistent nystagmus may be a distinct feature of CPN.

Another feature of paroxysmal CPN is accompanied neurological signs suggestive of a central pathology. Therefore, ocular motor signs such as spontaneous downbeat nystagmus (Huh and Kim, 2011), direction-changing gaze-evoked nystagmus

(Cnyrim et al., 2008; Kattah et al., 2009), perverted head-shaking nystagmus (Choi et al., 2016), and saccadic hypermetria (Waespe and Wichmann, 1990) should be sought carefully in patients with positional vertigo and nystagmus.

2.2 Persistent CPN

Persistent nystagmus in a specific head position from a central lesion implies an involvement of the central gravity processing (Glasauer et al., 2001). Since the persistent and paroxysmal CPN often co-exist, the characteristics of persistent CPN can be assessed only after the paroxysmal component disappears. In most studies, the persistence of CPN has been defined by the duration of induced nystagmus of more than 1 min with a stable intensity (Bisdorff et al., 2009).

Until now, three common types of persistent CPN have been identified. One is persistent downbeat CPN. The downbeat nystagmus with the head upright has been mostly ascribed to cerebellar dysfunction (Zee et al., 1974), and is under the effect of static head position. Downbeat nystagmus usually increases in the face-down (prone) and decreases in the face-up (supine) position (Gresty et al., 1986; Marti et al., 2002). Even healthy subjects may show downbeat nystagmus when stand upside down (Kim et al., 2000). The effects of head position on downbeat nystagmus were investigated by analyzing the gravity-dependent and gravity-independent components of vertical eye velocity (Marti et al., 2002). In both patients with downbeat nystagmus and healthy subjects, the gravity-dependent component of downbeat nystagmus showed an upward velocity bias (generating downbeat nystagmus) in the face-down position and a downward velocity bias (generating upbeat nystagmus) in the face-up position (Marti et al., 2002). However, the effects of gravity on vertical velocity bias were significantly greater in patients with downbeat nystagmus than in normal subjects. These results can also explain the conversion of downbeat into upbeat nystagmus in straight-head hanging position (Helmchen et al., 2004). Therefore, the persistent downbeat CPN in the prone position may be considered an augmented form of downbeat nystagmus in the upright head position. Of interest, the patterns of positional modulation quite differ between paroxysmal and persistent form of downbeat CPN. Since both forms of downbeat CPN frequently co-exist, however, detection of downbeat nystagmus may require a longer period of observation in either supine or prone position.

Another type is persistent apogeotropic CPN observed when the head is turned to either side while supine. This nystagmus should be differentiated from the apogeotropic type of horizontal canal BPPV (apogeotropic HC-BPPV) (Baloh et al., 1995; Kim et al., 2012a; Oh et al., 2009). The persistent apogeotropic CPN is commonly observed in patients with cerebellar dysfunction (Macdonald et al., 2017). A recent study determined the patterns of positional modulation in persistent apogeotropic CPN (Choi et al., 2018a). Unilateral cerebellar lesions usually give rise to ipsilesional spontaneous horizontal nystagmus both in the head upright and supine positions without a difference in the intensity of nystagmus between the positions. Even though the apogeotropic positional nystagmus was stronger when its direction was

same as that of spontaneous nystagmus (synergistic effect between the spontaneous and positional nystagmus), the apogeotropic component induced by turning the head to the right or left while supine was symmetric when the intensity of spontaneous nystagmus while supine was subtracted from that of the nystagmus observed in the ear-down positions (Choi et al., 2018a). Given that the lying-down nystagmus is mostly ipsilesional and the apogeotropic nystagmus is stronger when the head is turned to the intact side in apogeotropic type of HC-BPPV (Koo et al., 2006; Lee et al., 2007), the patterns of positional modulation do not guarantee differentiation of persistent apogeotropic CPN from apogeotropic HC-BPPV. However, spontaneous horizontal nystagmus usually increases in the supine position in apogeotropic HC-BPPV (Koo et al., 2006; Lee et al., 2007). Otherwise, associated neurological symptoms and signs and coexistent of paroxysmal form CPN aid in differential diagnosis (Choi et al., 2015).

The third type is persistent geotropic CPN (Choi et al., 2018b; Lee et al., 2014; Yang and Oh, 2014). With introduction of persistent geotropic nystagmus from light cupula (Choi et al., 2017; Kim et al., 2014, 2018), diagnosis of persistent geotropic CPN became a challenge. Unlike for persistent apogeotropic CPN, no consistent patterns of positional modulation are known for persistent geotropic CPN (Choi et al., 2018b). In addition, the peak intensity and asymmetry of geotropic nystagmus were reported to be similar in those with central lesions and with presumed light cupula (Choi et al., 2018b). However, the characteristics of persistent geotropic CPN require further exploration.

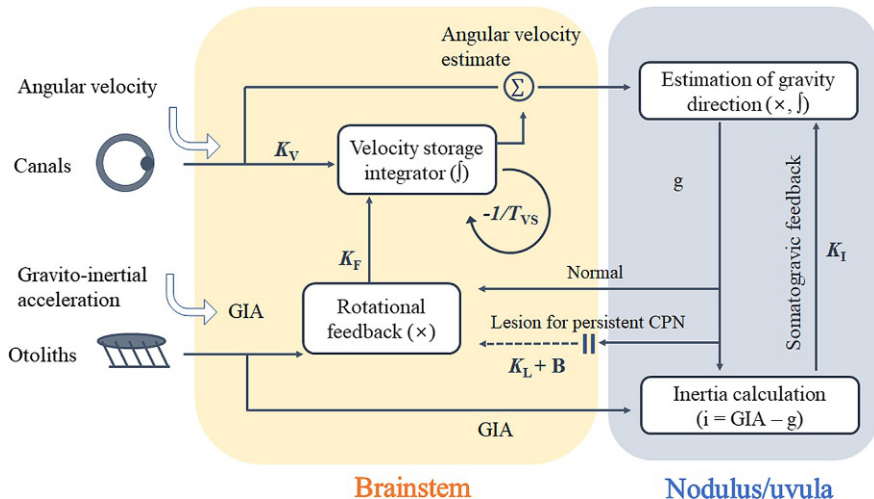
3 Etiology and location of lesions

In general, CPN has been considered a sign suggestive of a lesion involving the infratentorial structures (Buttner et al., 1999; Harrison and Ozsahinoglu, 1972). Even though paroxysmal CPN has mostly been highlighted in patients with Chiari malformation or posterior fossa tumor (Baloh and Spooner, 1981; Barber, 1984; Choi et al., 2018a; Yee et al., 1984), it has also been described in patients with strokes (Choi et al., 2015), multisystem atrophy (Lee et al., 2009), hereditary cerebellar ataxia (Jen et al., 2007; Kim et al., 2013; Yabe et al., 2003), anti-epileptic drug intoxication (Choi et al., 2014b; Oh et al., 2006), heat strokes (Jung et al., 2017), X-linked adrenoleukodystrophy (Kim et al., 2016), and paraneoplastic or parainfectious autoimmune cerebellitis (Choi et al., 2014a,c). Persistent CPN also has similar etiologies (Anderson et al., 2008; Cho et al., 2017; Choi et al., 2014a, 2015, 2018a,b; Helmchen et al., 2004; Kim et al., 2012b; Lee et al., 2014; Nam et al., 2009). Recently, there have been attempts to delineate the location of lesions responsible for either type of CPN. In both paroxysmal and persistent types of CPN, however, the lesions mostly involved the midline vestibulocerebellar structures such as the nodulus, uvula, and tonsil (Cho et al., 2017; Choi et al., 2015, 2018a,b; Lee et al., 2014). Isolated brainstem lesions have also been found in patients with CPN (Macdonald et al., 2017).

4 Mechanisms

The recently proposed mechanisms for both paroxysmal and persistent CPN are based on the neural processing that occurs in the central vestibular system during positional changes (Choi and Kim, 2017; Choi et al., 2015, 2018a,c). When our head changes its orientation in relation to gravity, two vestibular inputs are sent to our brain, the rotational velocity of the head and the new gravity direction in the head coordinate frame. The rotational velocity information relayed from the semicircular canals is basically inaccurate since it is derived from the relative difference between the head and endolymph velocities in space (Laurens and Angelaki, 2011; Merfeld et al., 1999). During prolonged constant-velocity rotation, this inaccuracy is the source for the exponential decay of per-rotational signals and emergence of post-rotatory signals (secondary phenomenon). This inaccuracy can affect the neural responses even during a brief head motion for a few seconds (Laurens and Angelaki, 2011). Estimation of gravity direction in the head coordinate frame also has an inherent ambiguity. The otolith organs do not provide information on the gravity direction but the sum of gravitational and inertial accelerations. This is known as “the tilt (gravity) and translational (inertia) ambiguity” (Angelaki et al., 2004; Merfeld et al., 1999; Yakusheva et al., 2007). Therefore, our brain should discriminate the gravity direction and inertial cue to maintain appropriate head orientation with regard to the gravity. The VS circuit (Green and Angelaki, 2004), which is comprised of bilateral vestibular nuclei, nodulus/uvula, and their reciprocal neural connections, is known to carry out this function (Laurens and Angelaki, 2011; Laurens et al., 2010; Merfeld et al., 1999; Yakusheva et al., 2007). This VS circuit estimates the rotational velocity first, and then calculates the gravity direction after each head rotation. Several experiments have also disclosed additional loops, such as the rotational and somatogravice feedback loops, within the VS circuit to enhance the accuracy of its function (Laurens and Angelaki, 2011; Laurens et al., 2010) (Fig. 4). Both types of CPN can be readily explained by dysfunction of this neural processing.

As described earlier, the paroxysmal CPN occurs in the opposite direction of head motion immediately after positioning, has a peak at its onset, and then exponentially decays with a TC of the vertical canals (Choi et al., 2015). These characteristics support that the paroxysmal CPN is driven by the canal cues. Of the regular and irregular primary vestibular nerve fibers (Goldberg and Fernandez, 1971), the irregular afferents are linked to high adaptive properties and VS circuit (Angelaki and Perachio, 1993; Clendaniel et al., 2001). One of the adaptive responses is the secondary phenomenon (post-rotatory response) (Goldberg and Fernandez, 1971). Although this post-rotatory response may cause a bias in estimating the rotational velocity and gravity direction, the feedback loops within the VS circuit can minimize this bias (Laurens and Angelaki, 2011) (Fig. 4). However, central lesions involving the vestibulocerebellum where the VS circuit is implemented may result in a loss of inhibitory effects on the irregular afferents and enhancement of the post-rotatory cue (Choi et al., 2015). This would induce

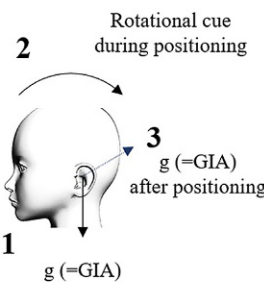
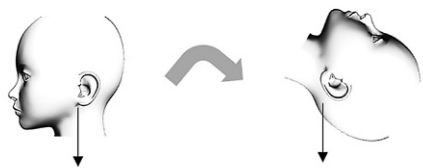
**FIG. 4**

A simplified diagram of the velocity-storage circuit proposed previously (Laurens and Angelaki, 2011). g , estimated gravity; GIA, gravitoinertial acceleration; i , inertia; x and \int are mathematical terms representing a vector cross product and integral. The parameter values of K_V (gain for velocity storage), T_{VS} (time constant of velocity storage), K_F (gain for rotational feedback), and K_I (gain for somatogravitic feedback) used in the simulation for normal subjects are 0.2, 15, 0.38, and 0.65, respectively. The persistent type of apogeotropic central positional nystagmus shown in Fig. 6 was simulated by implementing the lesions between the brainstem and cerebellum. The parameters adopted for the lesions are K_L (gain=0) and B (bias=0.02 g for the naso-occipital axis).

a prominent bias that cannot be corrected by the feedback loops in a real time manner, and thereby generate post-rotatory rebound nystagmus (Choi and Kim, 2017; Choi et al., 2015, 2018c) (Fig. 5).

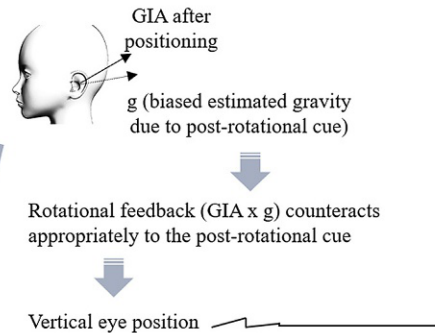
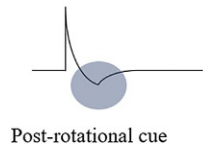
The gravity-dependent (induced) component of persistent downbeat CPN shows a sinusoidal pattern with regard to gravity orientation of the head (Marti et al., 2002). This implies that the gravity can generate oppositely directed nystagmus depending on its orientation in the head coordinate system. When a chemical lesion was made in the nodulus of monkeys, the gravity-induced apogeotropic horizontal nystagmus also showed a sinusoidal pattern of modulation according to head orientation in the roll plane (Sheliga et al., 1999). Likewise, in patients with persistent apogeotropic CPN, the gravity-induced (dependent) nystagmus between the right and left ear-down positions while supine showed the same intensities, but in the opposite directions (Choi et al., 2018a). These findings support that an erroneous central gravity processing is the cause of persistent CPN. A recent study implemented lesions into the VS model to simulate persistent CPN (Choi et al., 2018a). In this simulation, central lesions causing impaired gravity information and adding the bias successfully generated variable patterns of persistent CPN even without an actual

Theoretical neural processing during positional change



Healthy subjects

Response of vestibular nucleus neuron to the irregular afferents



Patients with paroxysmal central positional nystagmus

Response of vestibular nucleus neuron to the irregular afferents

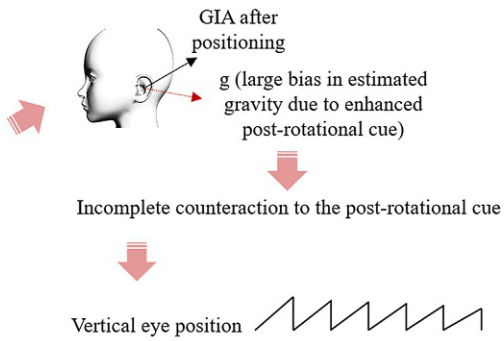
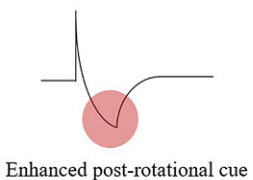
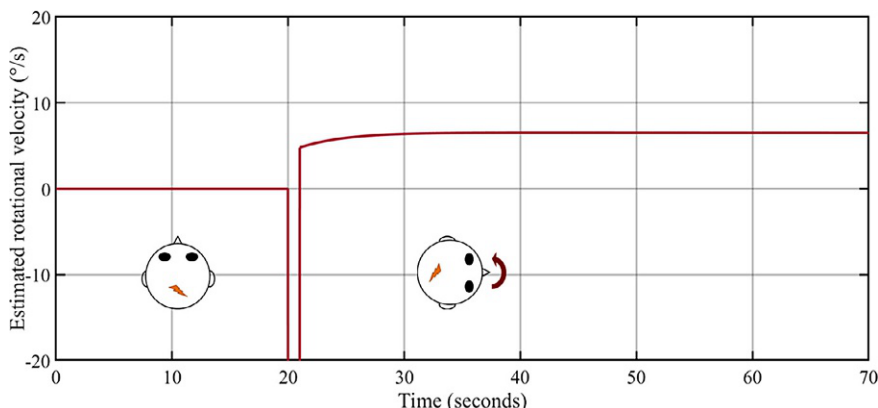


FIG. 5

Mechanism of the paroxysmal type of central positional nystagmus. Abbreviations; GIA, gravito-inertial acceleration, g , internally estimated gravity, NU, nodulus and uvula.

**FIG. 6**

Simulation of persistent type of central positional nystagmus (CPN). The positive values indicate leftward rotational direction. In patients with persistent type of CPN, central lesions that impair gravity information and add a bias to the velocity-storage circuit generate a persistent leftward rotational cue in the right ear-down position, thereby generating persistent left beating (apogeotropic) nystagmus.

rotational cue (Choi et al., 2018a). For example, when the bias is toward the nose and the head is turned to either side while supine, there would be sustained apogeotropic nystagmus because of an inappropriate feedback signal indicating that the head is rotating when it is not (Fig. 6). Likewise, downbeat nystagmus can be simulated in the supine or straight head hanging position when the bias is toward the chin. Therefore, by summing the gravity-dependent and independent components, any positional modulation of persistent CPN could be explained.

5 Conclusion

The overlap of the lesions responsible for either the paroxysmal or persistent form of CPN may explain the frequent co-existence of both types of CPN in a single patient. Both types of CPN may be ascribed to erroneous processing of the signals in the VS circuit that normally function to estimate the rotational velocity of the head and gravity direction. The paroxysmal CPN may be a post-rotatory rebound nystagmus due to enhanced post-rotatory canal signals and the persistent CPN may result from erroneous gravity estimation. The characteristics of CPN and associated findings may allow differentiating central from peripheral positional nystagmus.

Source of funding/support

This research was supported by Basic Science Research Program through the National Research Foundation of Korea (NRF) funded by the Ministry of Science and ICT (NRF-2017R1C1B1008582).

Conflict of interest statement

The authors declare they have no conflicts of interest.

Disclosure

J.-Y.C. has nothing to disclose. J.-S.K. serves as an Associate Editor of *Frontiers in Neuro-Otology* and on the editorial boards of the *Journal of Clinical Neurology*, *Frontiers in Neuro-ophthalmology*, *Journal of Neuro-Ophthalmology*, *Journal of Vestibular Research*, *Journal of Neurology*, and *Medicine*.

Authors' contributions

J.-Y.C. acquired and analyzed the data, and drafted the manuscript; J.-S.K. conceptualized the study, analyzed the data and revised the manuscript.

References

- Anderson, T., Luxon, L., Quinn, N., Daniel, S., David Marsden, C., Bronstein, A., 2008. Oculomotor function in multiple system atrophy: clinical and laboratory features in 30 patients. *Mov. Disord.* 23 (7), 977–984.
- Angelaki, D.E., Perachio, A.A., 1993. Contribution of irregular semicircular canal afferents to the horizontal vestibuloocular response during constant velocity rotation. *J. Neurophysiol.* 69 (3), 996–999.
- Angelaki, D.E., Shaikh, A.G., Green, A.M., Dickman, J.D., 2004. Neurons compute internal models of the physical laws of motion. *Nature* 430 (6999), 560–564.
- Baloh, R.W., Spooner, J.W., 1981. Downbeat nystagmus: a type of central vestibular nystagmus. *Neurology* 31 (3), 304–310.
- Baloh, R.W., Yue, Q., Jacobson, K.M., Honrubia, V., 1995. Persistent direction-changing positional nystagmus: another variant of benign positional nystagmus? *Neurology* 45 (7), 1297–1301.
- Barber, H.O., 1984. Positional nystagmus. *Otolaryngol. Head Neck Surg.* 92 (6), 649–655.
- Bertholon, P., Bronstein, A.M., Davies, R.A., Rudge, P., Thilo, K.V., 2002. Positional down beating nystagmus in 50 patients: cerebellar disorders and possible anterior semicircular canalithiasis. *J. Neurol. Neurosurg. Psychiatry* 72 (3), 366–372.
- Bertolini, G., Ramat, S., 2011. Velocity storage in the human vertical rotational vestibulo-ocular reflex. *Exp. Brain Res.* 209 (1), 51–63.
- Bertolini, G., Bockisch, C.J., Straumann, D., Zee, D.S., Ramat, S., 2008. Chapter 3.9—Do humans show velocity-storage in the vertical rVOR? In: Kennard, C., Leigh, R.J. (Eds.), *Progress in Brain Research*. Elsevier, pp. 207–210.
- Bisdorff, A., Von Brevern, M., Lempert, T., Newman-Toker, D.E., 2009. Classification of vestibular symptoms: towards an international classification of vestibular disorders. *J. Vestib. Res.* 19 (1–2), 1–13.
- Buttner, U., Helmchen, C., Brandt, T., 1999. Diagnostic criteria for central versus peripheral positioning nystagmus and vertigo: a review. *Acta Otolaryngol.* 119 (1), 1–5.

- Cambi, J., Astore, S., Mandala, M., Trabalzini, F., Nuti, D., 2013. Natural course of positional down-beating nystagmus of peripheral origin. *J. Neurol.* 260 (6), 1489–1496.
- Cho, B.H., Kim, S.H., Kim, S.S., Choi, J.Y., Lee, S.H., 2017. Central positional nystagmus associated with cerebellar tumors: clinical and topographical analysis. *J. Neurol. Sci.* 373, 147–151.
- Choi, J.Y., Kim, J.S., 2017. Nystagmus and central vestibular disorders. *Curr. Opin. Neurol.* 30 (1), 98–106.
- Choi, J.Y., Kim, J.S., Jung, J.M., Kwon, D.Y., Park, M.H., Kim, C., Choi, J., 2014a. Reversed corrective saccades during head impulse test in acute cerebellar dysfunction. *Cerebellum* 13 (2), 243–247.
- Choi, J.Y., Park, Y.M., Woo, Y.S., Kim, S.U., Jung, J.M., Kwon, D.Y., 2014b. Perverted head-shaking and positional downbeat nystagmus in pregabalin intoxication. *J. Neurol. Sci.* 337 (1–2), 243–244.
- Choi, S.Y., Park, S.H., Kim, H.J., Kim, J.S., 2014c. Paraneoplastic downbeat nystagmus associated with cerebellar hypermetabolism especially in the nodulus. *J. Neurol. Sci.* 343 (1–2), 187–191.
- Choi, J.Y., Kim, J.H., Kim, H.J., Glasauer, S., Kim, J.S., 2015. Central paroxysmal positional nystagmus: characteristics and possible mechanisms. *Neurology* 84 (22), 2238–2246.
- Choi, J.Y., Jung, I., Jung, J.M., Kwon, D.Y., Park, M.H., Kim, H.J., Kim, J.S., 2016. Characteristics and mechanism of perverted head-shaking nystagmus in central lesions: video-oculography analysis. *Clin. Neurophysiol.* 127 (9), 2973–2978.
- Choi, J.Y., Lee, E.S., Kim, H.J., Kim, J.S., 2017. Persistent geotropic positional nystagmus after meningitis: evidence for light cupula. *J. Neurol. Sci.* 379, 279–280.
- Choi, J.Y., Glasauer, S., Kim, J.H., Zee, D.S., Kim, J.S., 2018a. Characteristics and mechanism of apogeotropic central positional nystagmus. *Brain* 141 (3), 762–775.
- Choi, S.Y., Jang, J.Y., Oh, E.H., Choi, J.H., Park, J.Y., Lee, S.H., Choi, K.D., 2018b. Persistent geotropic positional nystagmus in unilateral cerebellar lesions. *Neurology* 91 (11), e1053–e1057.
- Choi, J.Y., Lee, S.H., Kim, J.S., 2018c. Central vertigo. *Curr. Opin. Neurol.* 31 (1), 81–89.
- Clendaniel, R.A., Lasker, D.M., Minor, L.B., 2001. Horizontal vestibulocular reflex evoked by high-acceleration rotations in the squirrel monkey. IV. Responses after spectacle-induced adaptation. *J. Neurophysiol.* 86 (4), 1594–1611.
- Cnyrim, C.D., Newman-Toker, D., Karch, C., Brandt, T., Strupp, M., 2008. Bedside differentiation of vestibular neuritis from central “vestibular pseudoneuritis”. *J. Neurol. Neurosurg. Psychiatry* 79 (4), 458–460.
- Glasauer, S., Dieterich, M., Brandt, T., 2001. Central positional nystagmus simulated by a mathematical ocular motor model of otolith-dependent modification of Listing's plane. *J. Neurophysiol.* 86 (4), 1546–1554.
- Goldberg, J.M., Fernandez, C., 1971. Physiology of peripheral neurons innervating semicircular canals of the squirrel monkey. I. Resting discharge and response to constant angular accelerations. *J. Neurophysiol.* 34 (4), 635–660.
- Green, A.M., Angelaki, D.E., 2004. An integrative neural network for detecting inertial motion and head orientation. *J. Neurophysiol.* 92 (2), 905–925.
- Gresty, M., Barratt, H., Rudge, P., Page, N., 1986. Analysis of downbeat nystagmus. Otolithic vs semicircular canal influences. *Arch. Neurol.* 43 (1), 52–55.
- Harrison, M.S., Ozsahinoglu, C., 1972. Positional vertigo: aetiology and clinical significance. *Brain* 95 (2), 369–372.

- Helmchen, C., Sprenger, A., Rambold, H., Sander, T., Kompf, D., Straumann, D., 2004. Effect of 3,4-diaminopyridine on the gravity dependence of ocular drift in downbeat nystagmus. *Neurology* 63 (4), 752–753.
- Huh, Y.E., Kim, J.S., 2011. Patterns of spontaneous and head-shaking nystagmus in cerebellar infarction: imaging correlations. *Brain* 134 (Pt. 12), 3662–3671.
- Jen, J.C., Graves, T.D., Hess, E.J., Hanna, M.G., Griggs, R.C., Baloh, R.W., investigators, C., 2007. Primary episodic ataxias: diagnosis, pathogenesis and treatment. *Brain* 130 (Pt. 10), 2484–2493.
- Jung, I., Choi, S.Y., Kim, H.J., Kim, J.S., 2017. Delayed vestibulopathy after heat exposure. *J. Neurol.* 264 (1), 49–53.
- Kattah, J.C., Talkad, A.V., Wang, D.Z., Hsieh, Y.H., Newman-Toker, D.E., 2009. HINTS to diagnose stroke in the acute vestibular syndrome: three-step bedside oculomotor examination more sensitive than early MRI diffusion-weighted imaging. *Stroke* 40 (11), 3504–3510.
- Kim, J.I., Somers, J.T., Stahl, J.S., Bhidayasiri, R., Leigh, R.J., 2000. Vertical nystagmus in normal subjects: effects of head position, nicotine and scopolamine. *J. Vestib. Res.* 10 (6), 291–300.
- Kim, J.S., Oh, S.Y., Lee, S.H., Kang, J.H., Kim, D.U., Jeong, S.H., Choi, K.D., Moon, I.S., Kim, B.K., Oh, H.J., Kim, H.J., 2012a. Randomized clinical trial for apogeotropic horizontal canal benign paroxysmal positional vertigo. *Neurology* 78 (3), 159–166.
- Kim, H.A., Yi, H.A., Lee, H., 2012b. Apogeotropic central positional nystagmus as a sole sign of nodular infarction. *Neurol. Sci.* 33 (5), 1189–1191.
- Kim, J.S., Kim, J.S., Youn, J., Seo, D.W., Jeong, Y., Kang, J.H., Park, J.H., Cho, J.W., 2013. Ocular motor characteristics of different subtypes of spinocerebellar ataxia: distinguishing features. *Mov. Disord.* 28 (9), 1271–1277.
- Kim, C.H., Kim, M.B., Ban, J.H., 2014. Persistent geotropic direction-changing positional nystagmus with a null plane: the light cupula. *Laryngoscope* 124 (1), E15–E19.
- Kim, S.H., Kim, S.S., Ha, H., Lee, S.H., 2016. X-linked adrenoleukodystrophy presenting with positional downbeat nystagmus. *Neurology* 86 (23), 2214–2215.
- Kim, M.B., Hong, S.M., Choi, H., Choi, S., Pham, N.C., Shin, J.E., Kim, C.H., 2018. The light cupula: an emerging new concept for positional vertigo. *J. Audiol. Otol.* 22 (1), 1–5.
- Koo, J.W., Moon, I.J., Shim, W.S., Moon, S.Y., Kim, J.S., 2006. Value of lying-down nystagmus in the lateralization of horizontal semicircular canal benign paroxysmal positional vertigo. *Otol. Neurotol.* 27 (3), 367–371.
- Laurens, J., Angelaki, D.E., 2011. The functional significance of velocity storage and its dependence on gravity. *Exp. Brain Res.* 210 (3–4), 407–422.
- Laurens, J., Straumann, D., Hess, B.J., 2010. Processing of angular motion and gravity information through an internal model. *J. Neurophysiol.* 104 (3), 1370–1381.
- Lee, S.H., Choi, K.D., Jeong, S.H., Oh, Y.M., Koo, J.W., Kim, J.S., 2007. Nystagmus during neck flexion in the pitch plane in benign paroxysmal positional vertigo involving the horizontal canal. *J. Neurol. Sci.* 256 (1–2), 75–80.
- Lee, J.Y., Lee, W.W., Kim, J.S., Kim, H.J., Kim, J.K., Jeon, B.S., 2009. Perverted head-shaking and positional downbeat nystagmus in patients with multiple system atrophy. *Mov. Disord.* 24 (9), 1290–1295.
- Lee, H.J., Kim, E.S., Kim, M., Chu, H., Ma, H.I., Lee, J.S., Koo, J.W., Kim, H.J., Hong, S.K., 2014. Isolated horizontal positional nystagmus from a posterior fossa lesion. *Ann. Neurol.* 76 (6), 905–910.
- Lopez-Escamez, J.A., Molina, M.I., Gamiz, M.J., 2006. Anterior semicircular canal benign paroxysmal positional vertigo and positional downbeating nystagmus. *Am. J. Otolaryngol.* 27 (3), 173–178.

- Macdonald, N.K., Kaski, D., Saman, Y., Al-Shaikh Sulaiman, A., Anwer, A., Bamiou, D.E., 2017. Central positional nystagmus: a systematic literature review. *Front. Neurol.* 8, 141.
- Marti, S., Palla, A., Straumann, D., 2002. Gravity dependence of ocular drift in patients with cerebellar downbeat nystagmus. *Ann. Neurol.* 52 (6), 712–721.
- Merkel, D.M., Zupan, L., Peterka, R.J., 1999. Humans use internal models to estimate gravity and linear acceleration. *Nature* 398 (6728), 615–618.
- Nam, J., Kim, S., Huh, Y., Kim, J.S., 2009. Ageotropic central positional nystagmus in nodular infarction. *Neurology* 73 (14), 1163.
- Oh, S.Y., Kim, J.S., Lee, Y.H., Lee, A.Y., Kim, J., Kim, J.M., 2006. Downbeat, positional, and perverted head-shaking nystagmus associated with lamotrigine toxicity. *J. Clin. Neurol.* 2 (4), 283–285.
- Oh, S.Y., Kim, J.S., Jeong, S.H., Oh, Y.M., Choi, K.D., Kim, B.K., Lee, S.H., Lee, H.S., Moon, I.S., Lee, J.J., 2009. Treatment of apogeotropic benign positional vertigo: comparison of therapeutic head-shaking and modified Semont maneuver. *J. Neurol.* 256 (8), 1330–1336.
- Sheliga, B.M., Yakushin, S.B., Silvers, A., Raphan, T., Cohen, B., 1999. Control of spatial orientation of the angular vestibulo-ocular reflex by the nodulus and uvula of the vestibulo-cerebellum. *Ann. N. Y. Acad. Sci.* 871, 94–122.
- Waespe, W., Wichmann, W., 1990. Oculomotor disturbances during visual-vestibular interaction in Wallenberg's lateral medullary syndrome. *Brain* 113 (Pt. 3), 821–846.
- Yabe, I., Sasaki, H., Takeichi, N., Takei, A., Hamada, T., Fukushima, K., Tashiro, K., 2003. Positional vertigo and macroscopic downbeat positioning nystagmus in spinocerebellar atrophy type 6 (SCA6). *J. Neurol.* 250 (4), 440–443.
- Yakusheva, T.A., Shaikh, A.G., Green, A.M., Blazquez, P.M., Dickman, J.D., Angelaki, D.E., 2007. Purkinje cells in posterior cerebellar vermis encode motion in an inertial reference frame. *Neuron* 54 (6), 973–985.
- Yang, T.H., Oh, S.Y., 2014. Geotropic central paroxysmal positional nystagmus in a patient with human immunodeficiency virus encephalopathy. *J. Neuroophthalmol.* 34 (2), 159–161.
- Yee, R.D., Baloh, R.W., Honrubia, V., 1984. Episodic vertical oscillopsia and downbeat nystagmus in a Chiari malformation. *Arch. Ophthalmol.* 102 (5), 723–725.
- Zee, D.S., Friendlich, A.R., Robinson, D.A., 1974. The mechanism of downbeat nystagmus. *Arch. Neurol.* 30 (3), 227–237.

This page intentionally left blank

Modulation of acquired monocular pendular nystagmus in multiple sclerosis: A modeling approach

17

Ileok Jung^a, Sung-Hee Kim^{b,†}, Hyo-Jung Kim^{c,†}, Jeong-Yoon Choi^{d,e},
Ji-Soo Kim^{d,e,*,†}

^a*Department of Neurology, Korea University College of Medicine, Korea University Ansan Hospital, Ansan, South Korea*

^b*Department of Neurology, Kyungpook National University, Chilgok Hospital, Daegu, South Korea*

^c*Research Administration Team, Seoul National University Bundang Hospital, Seongnam, South Korea*

^d*Department of Neurology, Dizziness Center, Clinical Neuroscience Center, Seoul National University Bundang Hospital, Seongnam, South Korea*

^e*Department of Neurology, Seoul National University College of Medicine, Seoul, South Korea*

*Corresponding author: Tel.: +82 31-787-7463, e-mail address: jisookim@snu.ac.kr

Abstract

Acquired pendular nystagmus (APN) often occurs in association with the disorders affecting the visual system, such as multiple sclerosis (MS). The proposed mechanisms of APN in MS have been a delayed conduction of the visual information for ocular stabilization and unstable neural integrator for feedback controls. We determined the effects of visual inputs on the nystagmus intensity and the effects of saccades on phase shift of the nystagmus in a patient with monocular pendular nystagmus from MS. In this patient, (1) during binocular viewing in the light, the nystagmus was observed only in the eye with more severe visual loss, (2) the nystagmus disappeared in darkness, (3) monocular viewing with either eye markedly suppressed the nystagmus, (4) the nystagmus decreased when the visual inputs became less asymmetric between the eyes, and (5) saccades resulted in a phase shift of the nystagmus. From these results, we propose that the difference in the visual inputs between the eyes is responsible for monocular APN by disturbing visual integration and increasing instability of the feedback.

[†]Author contribution: Jung analyzed the data and drafted the manuscript; S.-H. Kim, Choi and H.-J. Kim acquired and analyzed the data; J.-S. Kim conceptualized the study, acquired and analyzed the data and revised the manuscript.

Keywords

Acquired pendular nystagmus, Monocular pendular nystagmus, Multiple sclerosis, Optic neuropathy, Visual loss

1 Introduction

Acquired pendular nystagmus (APN) often occurs in association with the disorders affecting the visual system (including optic nerve demyelination), or with the lesions involving the dentate-rubro-olivary tract (Guillain-Mollaret triangle) and resultant inferior olivary hypertrophy (Dufour et al., 1972; Farmer and Hoyt, 1984; Kim et al., 2007). APN may be asymmetric, and sometimes monocular (Farmer and Hoyt, 1984; Leigh et al., 1989; Lopez et al., 1996; Yee et al., 1979). APN is usually larger in the eye with a more severe visual loss in multiple sclerosis (MS) (Das et al., 2000). In demyelinating disorders, APN has been ascribed to delayed conduction of the visual information necessary for ocular stabilization (Barton and Cox, 1993; Lopez et al., 1996; Yee et al., 1979), although experimentally manipulating the visual delay in such patients does not affect the frequency of oscillations (Averbuch-Heller et al., 1995).

Another important observation in APN associated with MS is the phase shift of the ocular oscillation following a saccade. This leads to the hypothesis that APN arises from the neural integrator and the phase shift observed during a saccade has been ascribed to resetting of the integrator by the large pulse of neural activity required for generation of a saccade (Choi et al., 2007; Das et al., 2000; Gresty et al., 1982).

Thus, the proposed mechanisms of APN in MS may be summarized as (1) delayed conduction of the visual information for ocular stabilization and (2) unstable neural integrators for feedback controls. To ascertain these hypotheses, we determined the effects of visual inputs on the nystagmus intensity and the effects of saccades on phase shift of nystagmus in a patient with monocular pendular nystagmus due to MS.

2 Methods

2.1 Patient

A 52-year-old woman presented with oscillopsia for 8 months. She had a 17-year history of relapsing and remitting MS that had initially presented with bilateral optic neuritis, more severe in the right eye. With steroid therapy, the visual acuity had almost recovered. Ten years later, she had another attack of right optic neuritis, which was followed by left internuclear ophthalmoplegia a year later. At the time of presentation to the authors, neurological examination showed the best corrected visual acuity of 20/100 in the right eye and 20/25 in the left eye. Both pupils were

equal at 3 mm with diminished responses to the light, but normal responses to the accommodative stimuli. Relative afferent pupillary defect (RAPD) was not evident. Goldman perimetry showed a central scotoma in the right eye. Visual evoked potentials (VEP) disclosed delayed responses in both eyes with a P1 latency of 163 ms in the left and 188 ms in the right eye. Horizontal and vertical pendular nystagmus was observed only in the right eye with a mild fluctuation in amplitude. The nystagmus was suppressed during eccentric gazes. Extraocular movements were full. Horizontal and vertical saccades were normal. The horizontal and vertical smooth pursuit was impaired. She showed no palatal tremor. Other findings of the neurological examination were unremarkable. Laboratory findings were negative for serum anti-aquaporin 4 antibody, β -galatosylcerebrosidase, very long chain fatty acid, NOTCH 3 gene, and paraneoplastic antibodies (anti-Hu, Ri, and Yo). MRIs showed demyelinating lesions in the periventricular white matter and in the paramedian tegmental areas of the midbrain and pons (Fig. 1).

2.2 Study protocol

To determine the effects of visual inputs on the intensity of nystagmus, and to identify if saccadic signals sent to the neural integrator affect the generation of nystagmus, we adopted two study paradigms. The paradigm I was to determine the effect of visual inputs on the intensity (amplitude and frequency) of pendular nystagmus. At first, the patient viewed a stationary visual target with both eyes (binocular) and either eye (monocular). And then 10 neutral density filters from 0.3 to 3.0 log unit (intervals of 0.3 log unit) were placed 1 cm in front of each eye to cover the whole visual fields. With a stepwise increase of the density of the filter in each eye, we were able to modulate the differences in the visual inputs between the eyes. The second paradigm (paradigm II) was to define any phase shift of vertical pendular nystagmus by horizontal saccades.

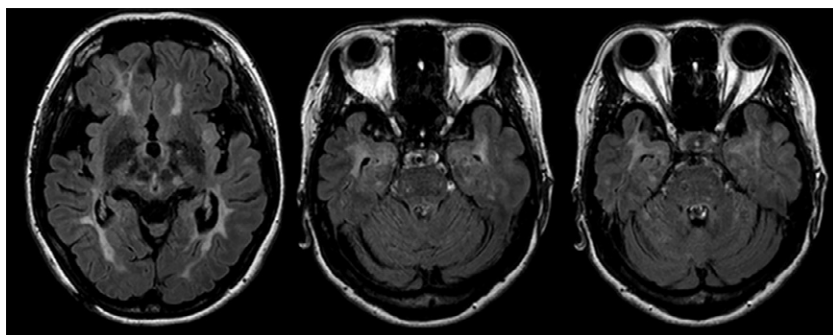


FIG. 1

MRIs of the patient. FLAIR images show demyelinating lesions in the periventricular white matter and in the paramedian tegmental areas of the midbrain and pons.

2.3 Oculography

We recorded spontaneous nystagmus with and without visual fixation, gaze-evoked nystagmus, smooth pursuits and saccades using three-dimensional video-oculography (VOG) (SensoMotoric Instruments, Teltow, Germany) (Yang et al., 2009) and a magnetic search coil (MSC) technique with a 70 cm cubic search coil frame (Skalar, Delft, Netherlands) (Choi et al., 2007).

2.4 Analyses of nystagmus

The acquired eye position data were analyzed using a MATLAB software (version R2011b, MathWorks, Natick, MA). The baseline eye position data were obtained when the eyes were most stable. The intensity of pendular nystagmus was determined by measuring the peak to peak amplitude for 20 s after onset of each stimulus. By averaging the amplitudes of at least 15 to-and-fro cycles of oscillations, we obtained the mean amplitude of nystagmus during each modulation.

2.5 Statistics

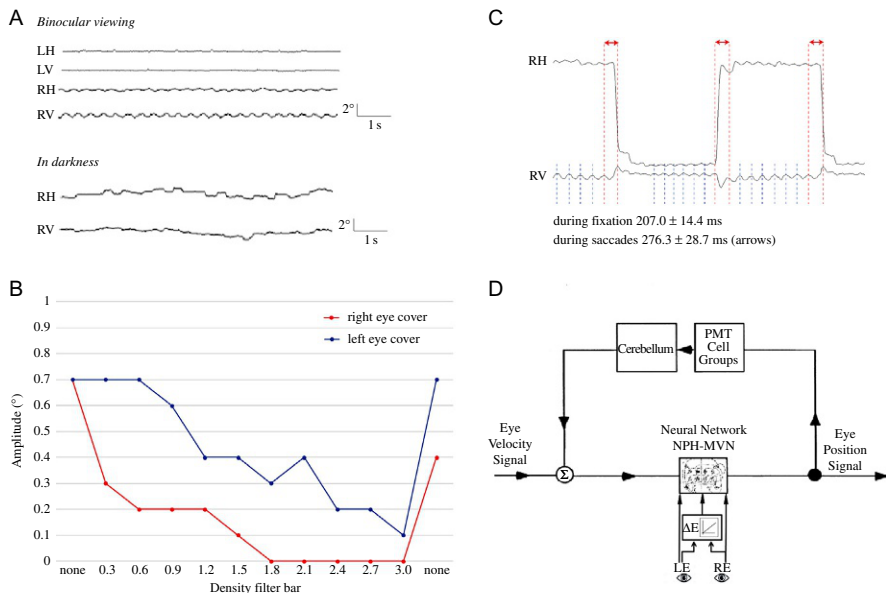
The data were presented as the mean \pm standard deviation (SD), and the differences in the amplitude were evaluated using the *t*-test and Mann-Whitney's *U* test. Statistical analyses were performed using SPSS v.18.0 (IBM Corp., Armonk, NY, USA).

3 Results

3.1 The paradigm I for visual modulation

During binocular viewing, the amplitude of nystagmus was 0.70 ± 0.14 degrees for the horizontal component and 1.31 ± 0.09 degrees for the vertical component. (Fig. 2A) The nystagmus amplitude decreased markedly during either right monocular viewing (left eye occluded) (0.50 ± 0.12 for the horizontal and 1.02 ± 0.15 for the vertical component, $P=0.01$), and left monocular viewing (right eye occluded) (0.58 ± 0.09 for the horizontal and 1.04 ± 0.16 for the vertical component, $P=0.01$). The frequency of nystagmus was measured at 5 Hz, and did not differ between during binocular and monocular viewing. The nystagmus near completely disappeared in darkness (Fig. 2A).

With increasing the density of filter before the right eye, the nystagmus amplitude decreased markedly, and the nystagmus disappeared when the density was 1.8. Increasing the density of filter in the left eye also decreased the nystagmus intensity gradually (Fig. 2B). The frequency of nystagmus remained mostly stable during the modulation.

**FIG. 2**

(A) Spontaneous pendular nystagmus is observed during binocular viewing, but nearly suppressed in darkness. (B) The amplitude of vertical pendular nystagmus is decreased with increase of the density of neutral density filter applied to each eye. (C) The duration of pendular nystagmus is increased during horizontal saccades. RH, horizontal axis of the right eye; RV, vertical axis of the right eye. (D) Our proposed model for acquired pendular nystagmus includes inputs from the visual pathway onto the neural integrator to determine the eye velocity. ΔE is the difference in the visual inputs between the eyes. These asymmetric visual inputs appear to act through a linear transform system onto the neural integrator. RE, right eye; LE, left eye.

Panel D reproduced with permission Leigh, R.J., Das, V.E., Seidman, S.H., 2002. A neurobiological approach to acquired nystagmus. Ann. N. Y. Acad. Sci. 956, 380–390.

3.2 The paradigm II for saccadic modulation

We measure the duration of vertical pendular nystagmus using a magnetic search coil technique. The mean duration of single cycle of pendular nystagmus was 207.0 ± 14.4 ms during the gaze angles of ± 15 degrees bilaterally and increased up to 276.3 ± 28.7 ms ($P = 0.01$) when a saccade was intervened (Fig. 2C). This apparent increase in the duration of nystagmus cycles corresponding to saccades can be interpreted as being due to a resetting of the oscillatory mechanism (Das et al., 2000).

4 Discussion

The main findings of this study may be summarized as follows. In our patient with MS, (1) the nystagmus was observed only in the right eye with a more severe visual loss during binocular viewing in the light, (2) the nystagmus disappeared in darkness,

(3) monocular viewing, achieved by occluding either eye, markedly suppressed the nystagmus, (4) the nystagmus decreased when the visual inputs became less asymmetric between the eyes, and (5) saccades resulted in a phase shift of the nystagmus.

Previous studies have reported monocular pendular nystagmus in patients with visual loss or amblyopia (Barton and Cox, 1993; Dufour et al., 1972; Farmer and Hoyt, 1984; Schneider et al., 2013; Yee et al., 1979). In a patient, the nystagmus disappeared after cataract surgery (Yee et al., 1979). In another study, long term deprivation of vision in one eye caused gaze instability in that eye, which was greater in the vertical plane (Leigh et al., 1989). These findings suggest that ocular stabilization depends upon early visual processing before the inputs from both eyes converge (Leigh et al., 1989, Schneider et al., 2013). It is also proposed that APN arises from delays in the conduction of visual information. From the paradigm I, we were able to confirm the role of visual inputs in generating pendular nystagmus. Of note, the monocular APN disappeared in darkness, decreased markedly while monocular viewing, and decreased when the asymmetry in the visual inputs between the eyes was reduced. These findings indicate that presence of asymmetric visual inputs between the eyes is crucial in generating pendular nystagmus. Then, how are the asymmetric visual inputs led to generation of pendular nystagmus? Combined insults to the central nervous system (Gresty et al., 1982), especially the paramedian tegmental tract or the median longitudinal fasciculus, have been suggested to play an additional role (Das et al., 2000). Our patient also had a history of left INO in addition to bilateral optic neuritis, and MRIs further documented paramedian tegmental lesions in the midbrain and pons. These demyelinating lesions may have interrupted the internal feedback loop and resulted in significant time delay. This delay may have impaired visually mediated stabilization of the eye position and led to ocular oscillation.

The findings of our study indicate that minimum amounts of visual inputs are required to generate pendular nystagmus. In a previous study on APN in MS using a neural network model, the nystagmus was suppressed when the activity of the constituent units in the network ceased for a 100-ms period (Leigh et al., 2002). This finding also supports that visual inputs are essential to generate APN.

During visual fixation, the tonic level of neural firing of the eye muscle plant holds the eyes steady (Robinson, 1964). For conjugate eye movements, synchronization of the visual inputs from each eye may be essential for ocular stabilization and estimation of the ocular dynamics by the brain (Leigh et al., 1989). Thus, when the conduction of visual signal from one eye is delayed, synchronization of visual signals from both eyes will be impaired, and these desynchronized signals arrived at the common neural integrator would generate ocular oscillation (Fahle, 1991; Greschner et al., 2002). Otherwise, decreased visual inputs from one eye may lead to impaired calibration of monocular units in the neural integrator and resultant oscillation of that eye since some neurons in the neural integrators have a monocular firing preference (Schneider et al., 2013; Sylvestre et al., 2003).

In contrast to the intensity, the frequency of nystagmus did not change much during modulation of visual inputs and the slope versus degrees of density filter is

similar to a linear form (Fig. 2D) (Stark, 1974). If the simple visual delay was the cause of the ocular oscillations, altering it should have changed the frequency (period) of oscillations. However, this was not observed in a previous study (Averbuch-Heller et al., 1995). Alternatively, visual delays may affect appropriate calibration of the neural integrators that has monocular components (Schneider et al., 2013; Sylvestre et al., 2003).

Likewise in a previous study on APN from MS (Das et al., 2000) horizontal saccades resulted in a significant phase shift of the nystagmus in our patient. This finding also supports that pendular nystagmus arises from an instability in the feedback control of the neural integrator for eye movements, which depends on a distributed network of neurons in the brainstem and cerebellum (Das et al., 2000; Orban De Xivry and Lefevre, 2007)

5 Conclusion

From the findings in our patient, we suggest that asymmetric visual inputs between the eyes give rise to ocular oscillatory signals, probably via the neural integrator, and untimely feedback due to a delayed conduction results in more severe or monocular nystagmus in the eye with a more severe visual loss.

Acknowledgments

This study was supported by Basic Science Research Program through the National Research Foundation of Korea (NRF) funded by the Ministry of Education, Science and Technology (NRF-2016R1D1A1B04935568).

Disclosure

J.-S.K. serves as an Associate Editor of *Frontiers in Neuro-Otology* and on the editorial boards of the *Journal of Clinical Neurology*, *Frontiers in Neuro-Ophthalmology*, *Journal of Neuro-Ophthalmology*, *Journal of Vestibular Research*, *Journal of Neurology, and Medicine*. Other authors have nothing to disclosure.

References

- Averbuch-Heller, L., Zivotofsky, A.Z., Das, V.E., Discenna, A.O., Leigh, R.J., 1995. Investigations of the pathogenesis of acquired pendular nystagmus. *Brain* 118 Pt 2, 369–378.
- Barton, J.J., Cox, T.A., 1993. Acquired pendular nystagmus in multiple sclerosis: clinical observations and the role of optic neuropathy. *J. Neurol. Neurosurg. Psychiatry* 56, 262–267.

- Choi, K.D., Oh, S.Y., Park, S.H., Kim, J.H., Koo, J.W., Kim, J.S., 2007. Head-shaking nystagmus in lateral medullary infarction: patterns and possible mechanisms. *Neurology* 68, 1337–1344.
- Das, V.E., Oruganti, P., Kramer, P.D., Leigh, R.J., 2000. Experimental tests of a neural-network model for ocular oscillations caused by disease of central myelin. *Exp. Brain Res.* 133, 189–197.
- Dufour, A., Guccione, G., Tamburino, V., 1972. Electronystagmographic considerations on 2 cases of monocular nystagmus. *Rev. Otoneuroophtalmol.* 44, 125–134.
- Fahle, M., 1991. Psychophysical measurement of eye drifts and tremor by dichoptic or monocular Vernier acuity. *Vision Res.* 31, 209–222.
- Farmer, J., Hoyt, C.S., 1984. Monocular nystagmus in infancy and early childhood. *Am. J. Ophthalmol.* 98, 504–509.
- Greschner, M., Bongard, M., Rujan, P., Ammermüller, J., 2002. Retinal ganglion cell synchronization by fixational eye movements improves feature estimation. *Nat. Neurosci.* 5, 341–347.
- Gresty, M.A., Ell, J.J., Findley, L.J., 1982. Acquired pendular nystagmus: its characteristics, localising value and pathophysiology. *J. Neurol. Neurosurg. Psychiatry* 45, 431–439.
- Kim, J.S., Moon, S.Y., Choi, K.D., Kim, J.H., Sharpe, J.A., 2007. Patterns of ocular oscillation in oculopalatal tremor: imaging correlations. *Neurology* 68, 1128–1135.
- Leigh, R.J., Thurston, S.E., Tomsak, R.L., Grossman, G.E., Lanska, D.J., 1989. Effect of monocular visual loss upon stability of gaze. *Invest. Ophthalmol. Vis. Sci.* 30, 288–292.
- Leigh, R.J., Das, V.E., Seidman, S.H., 2002. A neurobiological approach to acquired nystagmus. *Ann. N. Y. Acad. Sci.* 956, 380–390.
- Lopez, L.I., Bronstein, A.M., Gresty, M.A., Du, B., P, E., Rudge, P., 1996. Clinical and MRI correlates in 27 patients with acquired pendular nystagmus. *Brain* 119 (Pt 2), 465–472.
- Orban De Xivry, J.J., Lefevre, P., 2007. Saccades and pursuit: two outcomes of a single sensorimotor process. *J. Physiol.* 584, 11–23.
- Robinson, D.A., 1964. The mechanics of human saccadic eye movement. *J. Physiol.* 174, 245–264.
- Schneider, R.M., Thurtell, M.J., Eisele, S., Lincoff, N., Bala, E., Leigh, R.J., 2013. Neurological basis for eye movements of the blind. *PLoS One* 8, e56556.
- Stark, M.R.C.A.L., 1974. Control of human eye movements I. Modeling of extraocular muscle. *Math. Biosci.* 20, 191–211.
- Sylvestre, P.A., Choi, J.T., Cullen, K.E., 2003. Discharge dynamics of oculomotor neural integrator neurons during conjugate and disjunctive saccades and fixation. *J. Neurophysiol.* 90, 739–754.
- Yang, Y., Kim, J.S., Kim, S., Kim, Y.K., Kwak, Y.T., Han, I.W., 2009. Cerebellar hypoperfusion during transient global amnesia: an MRI and oculographic study. *J. Clin. Neurol.* 5, 74–80.
- Yee, R.D., Jelks, G.W., Baloh, R.W., Honrubia, V., 1979. Unicocular nystagmus in monocular visual loss. *Ophthalmology* 86, 511–522.

Fixation instability in amblyopia: Oculomotor disease biomarkers predictive of treatment effectiveness

18

Matteo Scaramuzzi^{a,b,c}, Jordan Murray^a, Jorge Otero-Millan^d, Paolo Nucci^{b,c},
Aasef G. Shaikh^{e,f}, Fatema F. Ghasia^{a,e,*}

^aCole Eye Institute, Cleveland Clinic, Cleveland, OH, United States

^bSan Giuseppe Eye Clinic, Milan, Italy

^cUniversity of Milan, Milan, Italy

^dDepartment of Neurology, The Johns Hopkins University, Baltimore, MD, United States

^eDaroff—Dell’Osso Ocular Motility Laboratory, Cleveland, OH, United States

^fCase Medical Center, Case Western Reserve University, Cleveland, OH, United States

*Corresponding author: Tel.: +1-216-318-7809, e-mail address: fatemaghasia@gmail.com

Abstract

Amblyopic patients are known to have fixation instability, particularly of the amblyopic eye. The stability of the fixation is affected by the presence of nystagmus, the frequency and amplitude of fixational saccades and inter-saccadic drifts. Amblyopic patients without nystagmus have increased amplitude of the fixational saccades with reduced frequency of the physiologic microsaccades and have increased inter-saccadic drifts. Amblyopia patients who have experienced a disruption in binocularly in early infancy develop fusion maldevelopment nystagmus (FMN) previously called latent nystagmus as it is more evident during monocular viewing conditions. We have found that some amblyopic patients can have nystagmus with slow phases that are not directed nasally and without the reversal in direction on ocular occlusion, features seen in patients with FMN. The current mainstay of amblyopia treatment comprises of part-time occlusion therapy of the non-amblyopic eye. The amount of patching treatment is in the range of 2–6 h/day as determined by the severity of amblyopia. Despite treatment, up to 40% of patients have residual amblyopia. We analyzed the effectiveness of part-time occlusion therapy in amblyopic patients as a function of fixation instability. We categorized amblyopic patients based on their eye movement waveforms obtained during a visual fixation task into those lacking nystagmus, those with FMN and those with nystagmus but no FMN. We did a retrospective chart review to gather information about their clinical characteristics and treatment response. We found that patients with FMN

require a more prolonged duration of treatment and have a poorer recovery of stereopsis compared to patients with nystagmus but no FMN and patients lacking nystagmus. This study suggests that eye movement assessment provides valuable information in the management of amblyopia.

Keywords

Fixation instability, Amblyopia, Microsaccades, Latent nystagmus, Nystagmus

1 Introduction

Fusion maldevelopment nystagmus (FMN) is one of the most common subtypes of pathologic nystagmus seen in children. The National Institutes of Health Committee on Eye Movement and Strabismus classification recommended utilizing a new etiologic description from 2001, replacing the term latent nystagmus. This type of nystagmus has initially been called latent because its severity increases, or became evident when an eye is covered. However, it is now known that true latent nystagmus is rare, with the majority of patients have manifest latent nystagmus seen with both eyes uncovered as identified on eye movement recordings ([Abadi and Scallan, 2000](#)). Amblyopia is a neurodevelopmental disorder that occurs due to de-correlated binocular input to the visual cortex. Investigations in non-human primate models have revealed that loss of horizontal binocular connections within area V1 in infancy is the necessary and sufficient cause of FMN ([Tychsen et al., 2010](#)). The new terminology describes the strong correlation with a binocular fusion maldevelopment that occurs during the infancy, like strabismus, amblyopia or any monocular vision deprivation ([Tychsen, 1992](#)).

Studies by Pediatric Eye Disease Investigator Group (PEDIG) have compared part-time occlusion to full-time occlusion therapy of the non-amblyopic eye and found similar levels of improvement in visual acuity. Thus the current standard of treatment is part-time occlusion ranging from 2 to 6 h/eye depending on the severity of amblyopia ([Holmes et al., 2003](#)). The slow phase velocity (SPV) of FMN increases under monocular viewing conditions and therefore in patients with FMN occlusion was believed to be contraindicated because it could enhance the nystagmus intensity or amplitude ([Duke-Elder and Wybar, 1973](#)). Subsequently, evidence was provided in a small cohort of patients that a significant improvement of visual acuity was obtained with full-time patching during all waking hours ([von Noorden et al., 1987](#)). Similarly, Simonsz demonstrated a decrease in slow phase velocity of nystagmus of the amblyopic eye with full time occlusion over days in five patients with latent nystagmus ([Simonsz, 1989](#)). Despite good compliance, up to 40% of children treated by occlusion therapy are left with residual amblyopia. Some baseline risk factors that predict the presence of residual amblyopia include severe amblyopia at time of diagnosis and older age at treatment initiation ([PEDIG Group, 2011](#)). We asked whether fixation instability could be a contributing factor.

Amblyopes are known to have increased fixation instability (Gonzalez et al., 2012; Subramanian et al., 2013). This instability could be due to the presence of FMN. Amblyopic patients without nystagmus have an increase in the amplitude of fixational saccades with increase inter-saccadic drifts that are not unidirectional unlike the slow phases of nystagmus and are frequently disconjugate; these contribute to the instability in both the fellow and amblyopic eye (Chen et al., 2018; Shaikh et al., 2016; Shi et al., 2012). We have also found increased slow phase velocities in patients with FMN compared to the inter-saccadic drift velocities in amblyopic patients without nystagmus and controls (Kang et al., n.d., submitted under review). During occlusion therapy, the amblyopic eye is the viewing eye. Thus we wanted to investigate whether the fast and slow eye movement properties of the amblyopic eye correlate with the presence of residual amblyopia, the treatment duration, and stereopsis at the end of treatment. We hypothesize that the presence of FMN, particularly those patients with greater slow phase velocity, would have poor treatment response. In addition, we hypothesize that in patients without nystagmus, the presence of increased fixational saccade amplitude and inter-saccadic drift would be correlated with poor treatment response. In the current chapter we focus on the different eye movement waveforms seen during fixation in amblyopia patients, and how patients with FMN compare to patients with nystagmus but no FMN and patients lacking nystagmus.

2 Methods

The records of 80 amblyopic patients from the practice of FG who had eye movement recordings performed between 2013 and 2019 were reviewed. The Cleveland Clinic Institutional review board approved the experimental protocol and written informed consent was obtained from each participant or parent/legal guardian in accordance with the Declaration of Helsinki. After review, 53 patients, who had at least 12 months of follow up after diagnosis of amblyopia and were prescribed patching treatment were included in the study (Table 1).

The clinical categorization of amblyopia subtype and severity at the time of diagnosis were based on PEDIG studies (Manh et al., 2018). Type of amblyopia: Amblyopia associated with strabismus, anisometropia, or both meeting the following criteria: (1) *Strabismic amblyopia*: At least one of the following criteria must be met and criteria are not met for combined-mechanism amblyopia: (a) heterotropia at distance and/or near fixation on examination (with or without spectacles); (b) history of strabismus surgery; (c) documented history of strabismus which is no longer present (and which, in the judgment of the investigator, is the cause of amblyopia). (2) *Anisometropic amblyopia*: At least one of the following criteria must be met: (a) ≥ 0.50 D difference between eyes in spherical equivalent ≥ 1.50 D difference between eyes in astigmatism in any meridian. (3) *Mixed mechanism amblyopia*: Both of the following criteria must be met: (a) criteria for strabismus are met (see above); (b) ≥ 1.00 D difference between eyes in spherical equivalent or ≥ 1.50 D difference between eyes in astigmatism in any meridian.

Table 1 Demographic and clinical parameters at the time of diagnosis of amblyopia.

Patient #	Gender	Category at time of patching	Eye movement waveform	Refractive error right eye	Refractive error left eye	Strabismus near (prism diopters)	Strabismus distance (prism diopters)
1	F	Strabismic Severe	None	+3.5+0.75×120	+3.75+0.75×60	ET 45	ET 45
2	F	Strabismic Severe	None	+6.5 sphere	+6.25 sphere	ET 30	ET 30
3	M	Mixed Severe	None	+5.0 sphere	+1.0 sphere	ET 35	ET 35
4	F	Mixed Moderate	None	+3.0+1.25×65	+1.25+0.25×115	E(T) 4–6	ET 12
5	F	Strabismic Moderate	None	+4.0 sphere	+4.0 sphere	ET 45	ET 30
6	F	Mixed Moderate	None	+8.25+1.75×70	+7.5+1.5×110	Ortho with glasses	Ortho with glasses
7	M	Mixed Moderate	None	+2.5 sphere	+4.5 sphere	Ortho with glasses	Ortho with glasses
8	M	Mixed Moderate	None	Plano+0.50×95	-0.75+3.5×85	XT 20	XT 30
9	M	Anisometropic Moderate	None	Plano+0.50×85	+5.25+2.0×105	Ortho	Ortho
10	M	Anisometropic Severe	None	+7.0+0.50×60	+1.0+0.25×50	Ortho	Ortho
11	M	Mixed Severe	None	+6.5+2.00×70	+0.5+0.5×90	Ortho with glasses	Ortho with glasses
12	M	Anisometropic Moderate	None	Plano+0.75×95	+4.25+2.0×90	Ortho	Ortho
13	F	Anisometropic Moderate	None	+0.25+0.25×90	+5.0+0.5×100	Ortho	Ortho
14	F	Anisometropic Moderate	None	+5.0+0.50×100	+3.0+0.50×80	Ortho	Ortho
15	F	Anisometropic Severe	None	+7.5 sphere	+5.0+0.50×180	Ortho	Ortho
16	M	Anisometropic Moderate	None	+4.0+0.50×105	+0.5+0.5×85	Ortho	Ortho
17	F	Anisometropic Mild	None	-0.25+0.5×90	Plano+2.0×85	Ortho	Ortho
18	F	Anisometropic Moderate	None	-2.75+4.25×95	+1.5 sphere	Ortho	Ortho

19	F	Anisometropic Moderate	None	+0.5+1.0×90	+3.5+1.0×90	Ortho	Ortho
20	M	Mixed Severe	None	+5.25+2.0×75	-0.5+0.5×95	ET 10	ET 10
21	F	Anisometropic Severe	None	-12.0+1.0×105	-0.25+1.25×75	Ortho	Ortho
22	F	Anisometropic Moderate	Nystagmus no FMN	+4.25+1.0×95	+1.75+0.25×80	Ortho	Ortho
23	M	Anisometropic Severe	Nystagmus no FMN	+0.25+0.5×90	-10.75+2.0×50	Ortho	Ortho
24	M	Anisometropic Moderate	Nystagmus no FMN	+7.25+1.5×90	+8.25+1.5×100	Ortho	Ortho
25	F	Mixed Moderate	Nystagmus no FMN	-1.75+3.0×85	-10.0+3.75×85	Ortho with glasses	Ortho with glasses
26	M	Anisometropic Severe	Nystagmus no FMN	+6.75+3.0×90	+0.5 sphere	Ortho	Ortho
27	F	Anisometropic Severe	Nystagmus no FMN	-0.25 sphere	-12.5+3.5×120	Ortho	Ortho
28	M	Mixed Severe	Nystagmus no FMN	+4.5+1.00×60	+1.5+0.50×120	Ortho with glasses	Ortho with glasses
29	F	Anisometropic Moderate	Nystagmus no FMN	+4.0+1.25×85	+1.5+0.5×85	Ortho	Ortho
30	F	Mixed Severe	Nystagmus no FMN	+2.25+0.75×80	+3.5+0.5×135	ET 20	Ortho with glasses
31	M	Mixed Mild	Nystagmus no FMN	+1.25+0.75×90	+0.25+2.0×80	Ortho with glasses	Ortho with glasses
32	F	Mixed Moderate	Nystagmus no FMN	-11.5+0.75×75	-6.5+1.0×105	XT 20	XT 25
33	M	Mixed Mild	Nystagmus no FMN	+6.0+2.0×90	+7.0+1.75×90	Ortho with glasses	Ortho with glasses
34	M	Mixed Severe	Nystagmus no FMN	+1.50 sphere	+4.0 sphere	LET 30	LET 30
35	F	Mixed Moderate	Nystagmus no FMN	+5.5+1.0×100	+6.5+1.0×80	Ortho with glasses	Ortho with glasses
36	F	Mixed Moderate	Nystagmus no FMN	+4.50+2.0×90	+5.5+2.25×90	E(T) 8	E(T) 10

Continued

Table 1 Demographic and clinical parameters at the time of diagnosis of amblyopia.—cont'd

Patient #	Gender	Category at time of patching	Eye movement waveform	Refractive error right eye	Refractive error left eye	Strabismus near (prism diopters)	Strabismus distance (prism diopters)
37	M	Strabismic Moderate	Nystagmus no FMN	+2.75+0.5×180	+2.75+0.50×180	ET 35	ET 35
38	F	Anisometropic Moderate	Nystagmus no FMN	+1.0+0.5×90	+3.75 sphere	Ortho	Ortho
39	F	Mixed Severe	Nystagmus no FMN	+1.50+0.50×70	+3.5+0.5×120	E(T) 8	E(T) 8
40	F	Mixed Mild	Nystagmus no FMN	-1.5+0.75×90	-2.5+1.00×90	XT 35	XT 35
41	F	Mixed Moderate	Nystagmus no FMN	-0.75+0.5×75	+1.5+1.00×90	XT 25	XT 30
42	M	Mixed Moderate	Nystagmus no FMN	+3.5+0.50×110	+1.00+0.50×90	50 RET	50 RET
43	M	Anisometropic Severe	FMN	+5.00+0.50×90	+6.25+1.00×95	Ortho	Ortho
44	F	Strabismic Severe	FMN	+3.50+1.75×90	+3.50+1.75×90	XT 8–10	XT 10
45	M	Mixed Moderate	FMN	-9.5+2.5×165	Plano+0.75×45	ET 4	ET 4
46	M	Strabismic Severe	FMN	+3.0 sphere	+3.0 sphere	XT >60	XT >60
47	F	Mixed Moderate	FMN	+5.0+1.5×80	+6+1.5×95	Ortho with glasses	Ortho with glasses
48	M	Mixed Severe	FMN	-6.75+3.75×90	-9.0+3.75×90	XT 25	XT 45
49	M	Mixed Moderate	FMN	+4.5 sphere	+3.5 sphere	ET 30	ET 25
50	M	Mixed Severe	FMN	+4.5+2.75×85	+3.5+2.75×95	XT 12	XT 12
51	M	Mixed Moderate	FMN	-0.5+1.00×110	+2.50+1.50×55	Flick XT	Flick XT
52	F	Mixed Moderate	FMN	+4.0 sphere	+2.25 sphere	XT 20	XT 20
53	M	Mixed Severe	FMN	+8.0+1.5×90	+7.25+0.5×90	ET 6–8	ET 4

ET=esotropia, XT=exotropia, E(T)=intermittent esotropia and X(T)=intermittent exotropia, ortho=orthotropia.

Severity of amblyopia: Mild amblyopia: if worse eye visual acuity (VA) was <0.30 LogMAR, moderate if ≥ 0.30 and <0.70 , severe if ≥ 0.70 ; VA of the amblyopic eye at baseline. Visual acuity was measured in each eye using the participant's optimal spectacle correction with Snellen linear optotype. For patients younger than 7 years of age, crowding bars HOTV or Allen pictures were used as per the child's ability to perform the test if they were unable to do the Snellen linear optotype. There were only four patients that were diagnosed before their ability to perform optotype testing—they all had manifest strabismus with strong fixation preference. They were all assigned as having severe amblyopia at the time of diagnosis.

Treatment considered was part-time occlusion (2–6 h/day), prescribed depending on the severity of amblyopia. Patients with manifest strabismus were treated according to the American Academy of Ophthalmology Preferred Practice Pattern. Investigators judged compliance with patching treatment to be excellent ($>75\%$), good ($51\text{--}75\%$), fair ($26\text{--}50\%$), or poor ($\leq 25\%$), based on discussions with the parents.

2.1 Eye movement recording and analysis

A high-resolution video-based eye tracker (EyeLink 1000[®], SR Research, Ontario, Canada) was used to measure binocular horizontal and vertical eye positions at a temporal resolution of 500 Hz during a fixation task as described previously. Briefly, eye position data was analyzed after removal of blinks and partial blinks. To measure eye velocity, we differentiated the eye position signal using MATLAB[™] (MathWorks, Natick, MA) diff function. Differential value (velocity signal) was further smoothed with Savitzky-Golay filter, a function that can be applied to a set of digital data points for the smoothing purpose (Shaikh et al., 2016).

Fixational saccades and quick phases of nystagmus were identified using an unsupervised clustering method (Otero-Millan et al., 2014). Drifts were defined as epochs between fixational saccades and blinks. We removed 20 ms data at the beginning and end of each of the drifts to exclude periods of acceleration and deceleration of the eye during fixational saccades and blinks. We characterized fixational eye movements in amblyopic patients based on their waveform characteristics as those without nystagmus, those with nystagmus but without the classic reversal in quick phase of nystagmus and the nasally directed slow phase observed during monocular viewing conditions seen in FMN patients and those with FMN. The form of the slow phase nystagmus appears to be decreasing or linear with dynamic overshoots of quick phases in amblyopia patients with nystagmus unlike the increasing eye velocity waveforms seen in patients with infantile/congenital nystagmus. In addition, patients with nystagmus but no FMN did not have the dissociated vertical deviation frequently seen in FMN patients (Fig. 1).

Of the recruited patients, 21 had no nystagmus, 21 had nystagmus without FMN, and 11 had FMN. The subjects were also grouped based on the type of amblyopia (anisometropic = 19, mixed = 28, strabismic = 6). Patients with anisometropia had no nystagmus or had nystagmus no FMN. All three different waveform characteristics were seen in strabismic and mixed amblyopia patients. There was no difference in the follow up time (none: 56 ± 34 , nystagmus without FMN: 71 ± 37 , FMN: 75 ± 43 , $P = 0.32$).

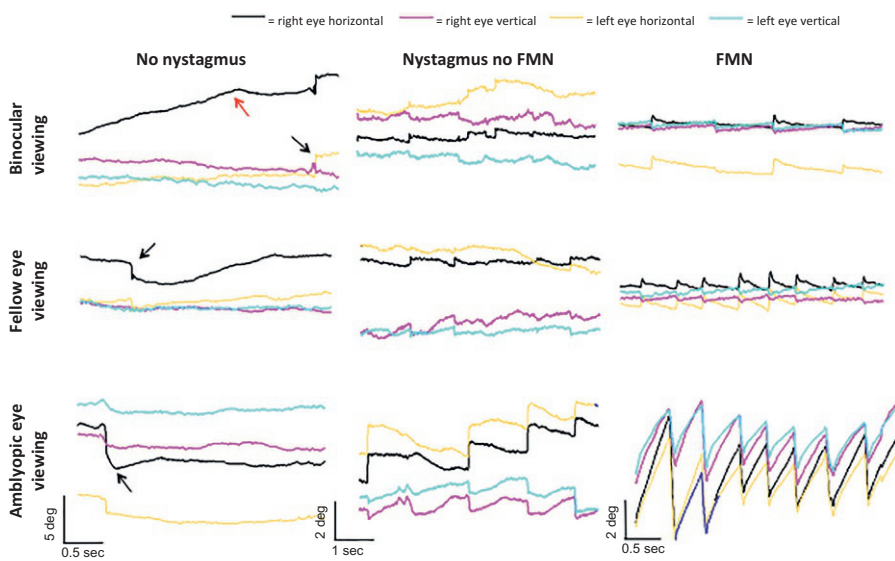


FIG. 1

Representative eye position traces obtained during fixation in amblyopia patients without nystagmus, nystagmus no FMN, and FMN. In patients without nystagmus there is an increase in the amplitude of the fixational saccade with an increase in the inter-saccadic drift. In patients with nystagmus no FMN there is no reversal of the quick phase of nystagmus as seen in patients with FMN. In patients with FMN, there is an increase in slow phase velocity of the amblyopic eye during amblyopic eye viewing condition. Of note, in all three patients abnormalities are seen during binocular viewing condition particularly of the amblyopic eye.

Due to an inadequate number of subjects, we were not able to do subgroup analysis per eye movement waveform within each clinical type of amblyopia. The follow-up duration for amblyopic patients of anisometropic patients was lower than the other two groups (anisometropic = 46 ± 31 , strabismic = 109 ± 32 , mixed = 71.5 ± 32 , $P = 0.0001$).

3 Clinical data and outcome measures

The clinical parameters were extracted from a retrospective chart review for all the enrolled subjects (Table 1). The ages at follow up visits, visual acuity of fellow and amblyopic eye, strabismus measurements in the primary position, stereopsis and compliance to treatment were noted. Stereoacuity was measured with the Titmus Stereoacuity Test. Stereoacuity scores in seconds of arc were: 40", 60", 100", 200", 400", 800", 3500" was the value of patients able to see only the fly; subjects with no detectable (nil) stereoacuity were assigned a value of 7000". For analyses, stereoacuity scores in seconds of arc were converted to log values as follows: 40" (1.60), 60" (1.78), 100" (2.00), 200" (2.30), 400" (2.60), 800" (2.90), 3500" (3.55) and 7000" (3.85). The total duration in months of patching treatment till visual

acuity was stabilized with no further improvement or deterioration ≥ 2 consecutive visits ≥ 6 weeks apart was computed for all the patients with at least 50% compliance. The improvement in visual acuity as expressed in arc minutes were calculated as the difference of acuity at the final visit from that of the acuity at the start of treatment. Patients were stratified based on the degree of vision improvement in response to treatment as <3 arcmin, $3\text{--}6$ arcmin and >6 arcmin. In addition, residual amblyopia at the end of treatment was defined as mild <0.30 LogMAR, moderate if ≥ 0.30 and <0.70 and severe if ≥ 0.70 log MAR scale. Final stereopsis was assessed and patients were classified to have good stereopsis (better than 100 s arc), some stereopsis (100–400 s arc) and gross/absent stereopsis (3500 or absent stereo).

Data analysis and statistics: All analyses were performed in MATLAB (MathWorks, Natick, MA, USA) and GraphPad Prism 7 (La Jolla, CA, USA). A Kruskal-Wallis analysis of variance test was used to compare the demographics and clinical outcomes across amblyopia subtype. We used one-way ANOVA to compare the clinical and oculomotor parameters across fixation eye movement characteristics. An unpaired t-test was used to analyze clinical/oculomotor parameters between the two groups.

4 Results

We investigated the treatment effectiveness of part-time occlusion in amblyopia patients as a function of the fixation instability of the amblyopic eye and the clinical subtype of amblyopia. Besides these, there are several variables such as age at diagnosis, visual acuity at the time of diagnosis and compliance to treatment that could be related to the visual acuity at the end of treatment. The age (in months) when patching treatment was started was similar across eye movement waveforms (no nystagmus = 63 ± 24 , nystagmus no FMN = 56 ± 25 , FMN = 57.9 ± 40.5 , $P = 0.71$) and across the subtype of amblyopia (anisometropic = 76 ± 14 , strabismic = 59 ± 38 , mixed = 65 ± 29 , $P = 0.19$). Similarly, compliance did not correlate with eye movement waveforms (none: 58 ± 21 , nystagmus without FMN: 63 ± 21 , FMN: 59 ± 16 , $P = 0.73$) nor did the visual acuity expressed in arcmin at time of diagnosis (none: 9.3 ± 15.75 , nystagmus without FMN: 7.78 ± 16.5 and FMN: 4.9 ± 3.3 , $P = 0.32$). The compliance to patching (anisometropic: 67 ± 11 , strabismic: 51 ± 17 , mixed: 59 ± 18 , $P = 0.09$) and visual acuity at the time of start of treatment (anisometropic: 8.1 ± 17.4 , strabismic: 9.0 ± 8.5 , mixed: 6.9 ± 12.9 , $P = 0.9$) was comparable across clinical types.

5 Treatment outcome measures as a function of the clinical subtype of amblyopia

Anisometropic patients either did not have nystagmus or had nystagmus without FMN except for only one subject that on initial presentation had anisometropia and FMN. This subject was noted to have intermittent esotropia on subsequent

clinical visits. Thus, we categorized this patient as having mixed mechanism amblyopia for statistical analysis. All the patients with strabismic and mixed amblyopia had strabismus surgery and were either orthotropic with glasses or had microstrabismus with glasses. Fig. 2A plots the visual acuity improvement in arcmin, which was comparable across all three clinical subtypes (anisometropic: 6.9 ± 16.9 , strabismic: 6.4 ± 8.4 , mixed: 4.3 ± 12.3 , $P=0.16$). The total duration of treatment (Fig. 2B) was similar across the three subtypes (anisometropic: 19.2 ± 22 , strabismic: 27 ± 14 , mixed: 19.75 ± 20 , $P=0.16$). Anisometropic amblyopes were more likely to have better stereopsis at the end of treatment compared to the other two groups (Fig. 2C—anisometric: 1.9 ± 0.51 , strabismic: 3.5 ± 0.69 , mixed: 3.0 ± 0.89 , $P < 0.0001$).

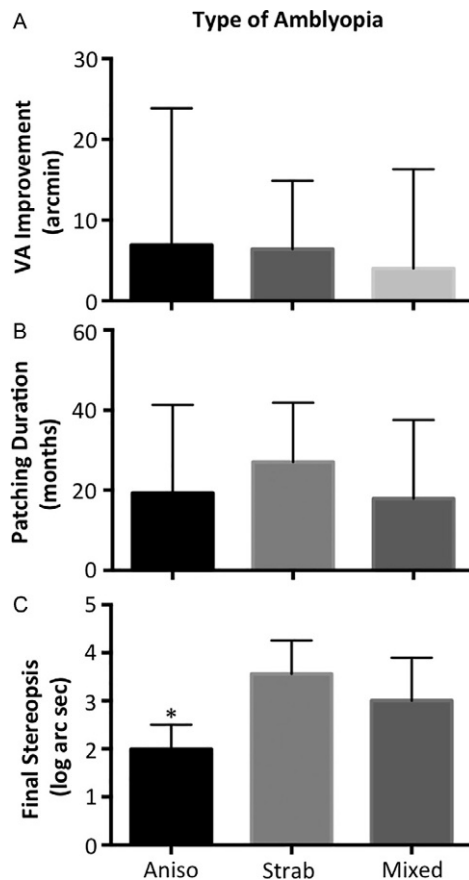


FIG. 2

Clinical outcomes namely visual acuity improvement (A), patching duration (B), and final stereopsis at the end of treatment (C) subgrouped by the type of amblyopia. Visual acuity improvement and patching duration are not significantly different between types. Final stereopsis is significantly better in anisometropic patients.

6 Treatment outcome measures as a function of fixation eye movement waveforms

Patients with FMN had less improvement in visual acuity (Fig. 3A) compared to the other groups; however this difference did not reach statistical significance (none: 7.7 ± 14.5 , nystagmus no FMN: 5.0 ± 16 , FMN: 3.02 ± 3.4 , $P=0.2$). Patients with FMN had a longer duration of treatment (Fig. 3B) compared to the other two groups (no nystagmus: 9.5 ± 6.3 , nystagmus no FMN: 22 ± 22 , FMN: 38 ± 19 , $P=0.01$). The most significant finding is that stereopsis was worse in patients with FMN (Fig. 3C) compared to the other two groups (no nystagmus: 2.4 ± 0.9 , nystagmus no FMN: 2.6 ± 0.9 , FMN: 3.3 ± 0.8 , $P=0.04$).

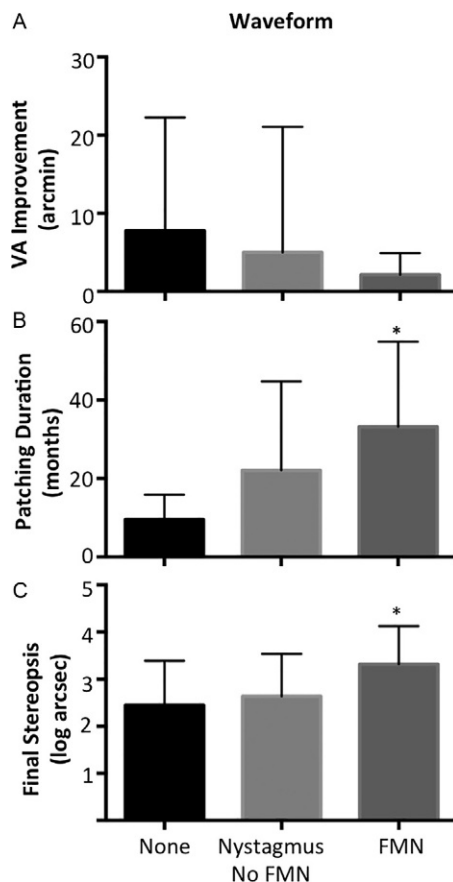


FIG. 3

Clinical outcomes namely visual acuity improvement (A), patching duration (B), and final stereopsis at the end of treatment (C) subgrouped by the fixation eye movement waveforms. Visual acuity improvement is not significantly different between the waveform groups. However, in FMN patients the duration of patching is significantly longer, and the final stereopsis is significantly worst compared to the other two groups.

7 Discussion

The purpose of this study was to identify oculomotor biomarkers that can be used to predict treatment effectiveness of part-time occlusion therapy. In this chapter, we characterized fixational eye movements in amblyopia patients. The subjects enrolled in the study had comparable visual acuity at the time of diagnosis and age at initiation of patching across the groups categorized per their eye movement waveforms. We found that rather than clinical subtype (anisotropic, strabismic or mixed), eye movement characteristics were better in predicting treatment outcomes. This is in agreement with previous studies that have shown that baseline visual acuity and younger age at enrollment were associated with the best improvement, but not the cause of amblyopia (Wallace et al., 2015). We found that children with FMN required a longer duration of treatment compared to those without nystagmus. Despite the improvement in visual acuity, the recovery of stereopsis was poor in patients with FMN.

Very few studies to date have examined occlusion therapy effectiveness in amblyopic patients with FMN. von Noorden et al. (1987) was the first to show in 12 patients with FMN noted on the clinical exam that patching during all waking hours was useful in improving VA, while it was previously considered contraindicated. The study had examined the effects of full time patching with no eye movement recordings. Ours is the first study to, our knowledge, measuring the impact of fixation instability on the effectiveness of part-time patching in amblyopia patients. Our results suggest that patients with FMN are at higher risk of regression with part-time occlusion therapy and require a prolonged duration of treatment. They are also less likely to have good stereoacuity at the end of the treatment despite improvement in visual acuity. Amblyopic patients with nystagmus but no FMN had improvement in both visual acuity and stereoacuity but required a longer duration of treatment compared to those without nystagmus.

The analyses were performed independently for different eye movement waveforms and the type of amblyopia. Strabismic patients have an increase in the drift velocity with higher velocities in patients with nystagmus. Our previous study has shown that the drift velocity and variance increase with an increase in the strabismus angle (Ghasia et al., 2018). All of our patients with strabismic and mixed amblyopia had microstrabismus (defined as <10 prism diopters) at the time of eye movement recordings. In the future, a larger cohort of patients will allow us to independently analyze the effects of eye movement waveforms within each clinical subtype of amblyopia as well as delineate the impact of degree of strabismus.

A significant limitation of the current study is the eye movement recordings were obtained at the end of treatment and the treatment effectiveness was determined based on a retrospective chart review. In addition, only a small cohort of patients with residual amblyopia was treated with atropine and majority of them had no further improvement in visual acuity. The decision to treat was based on discussions with family and the children with greater deficits of visual acuity were more likely to try an alternative treatment. The mean duration of follow up was greater in our study

compared to most amblyopia treatment studies. Thus, we were able to identify regression soon after the treatment was stopped or while it was being tapered for patients who initially had severe amblyopia at diagnosis. The analysis from the current study suggests that eye movement characterization and quantification can play an important role in providing information about prognosis and amblyopia treatment effectiveness. A prospective clinical trial of obtaining eye movement recordings at the time of diagnosis and following the patients longitudinally to determine treatment effectiveness of part-time occlusion will be necessary to confirm the findings of the current observational study. In addition, the study suggests that the timing of amblyopia development seems to play an important role in determining part-time patching treatment effectiveness. Additional prospective studies evaluating alternative treatments such as optical penalization and newer binocular amblyopia treatments in a cohort of amblyopic patients with FMN would help further tailor the treatment.

Acknowledgments

Supported by grants from Blind Children's Center, RPB Unrestricted Grant CCLCM-CWRU, CTSC Pilot Grant Program and Cleveland Clinic RPC Grant (F.F.G.) and Departmental NEI T32 grant (J.M.).

References

- Abadi, R.V., Scallan, C.J., 2000. Waveform characteristics of manifest latent nystagmus. *Invest. Ophthalmol. Vis. Sci.* 41 (12), 3805–3817.
- Chen, D., Otero-Millan, J., Kumar, P., Shaikh, A.G., Ghasia, F.F., 2018. Visual search in amblyopia: abnormal fixational eye movements and suboptimal sampling strategies. *Invest. Ophthalmol. Vis. Sci.* 59 (11), 4506–4517.
- Duke-Elder, S., Wybar, K.C., 1973. Ocular motility and strabismus. In: Duke-Elder, S. (Ed.), *System of Ophthalmology*, vol. 6. C.V. Mosby, St. Louis, p. 824.
- Ghasia, F.F., Otero-Millan, J., Shaikh, A.G., 2018. Abnormal fixational eye movements in strabismus. *Br. J. Ophthalmol.* 102 (2), 253–259.
- Gonzalez, E.G., Wong, A.M., Niechwiej-Szwedo, E., Tarita-Nistor, L., Steinbach, M.J., 2012. Eye position stability in amblyopia and in normal binocular vision. *Invest. Ophthalmol. Vis. Sci.* 53 (9), 5386–5394.
- Holmes, J.M., Kraker, R.T., Beck, R.W., Birch, E.E., Cotter, S.A., Everett, D.F., Hertle, R.W., Quinn, G.E., Repka, M.X., Scheiman, M.M., Wallace, D.K., Pediatric Eye Disease Investigator Group, 2003. A randomized trial of prescribed patching regimens for treatment of severe amblyopia in children. *Ophthalmology* 110 (11), 2075–2087.
- Kang SL, Otero-Millan JM, Beylergil S, Shaikh AG, Ghasia FF n.d. (submitted under review). “Disconjugacy of fixational eye movements in amblyopia.”
- Manh, V.M., Holmes, J.M., Lazar, E.L., Kraker, R.T., Wallace, D.K., Kulp, M.T., Galvin, J.A., Shah, B.K., Davis, P.L., Pediatric Eye Disease Investigator, G., 2018. A randomized trial of a binocular iPad game versus part-time patching in children aged 13 to 16 years with amblyopia. *Am. J. Ophthalmol.* 186, 104–115.

- Otero-Millan, J., Castro, J.L., Macknik, S.L., Martinez-Conde, S., 2014. Unsupervised clustering method to detect microsaccades. *J. Vis.* 14 (2), 18.
- Pediatric Eye Disease Investigator Group (PEDIG) Writing Committee, Wallace, D.K., Kraker, R.T., Beck, R.W., Cotter, S.A., Davis, P.L., Holmes, J.M., Repka, M.X., Suh, D.W., 2011. Randomized trial to evaluate combined patching and atropine for residual amblyopia. *Arch. Ophthalmol.* 129 (7), 960–962.
- Shaikh, A.G., Otero-Millan, J., Kumar, P., Ghasia, F.F., 2016. Abnormal fixational eye movements in amblyopia. *PLoS One* 11 (3), e0149953.
- Shi, X.F., Xu, L.M., Li, Y., Wang, T., Zhao, K.X., Sabel, B.A., 2012. Fixational saccadic eye movements are altered in anisometropic amblyopia. *Restor. Neurol. Neurosci.* 30, 445–462.
- Simonsz, H.J., 1989. The effect of prolonged monocular occlusion on latent nystagmus in the treatment of amblyopia. *Doc. Ophthalmol.* 72 (3–4), 375–384.
- Subramanian, V., Jost, R.M., Birch, E.E., 2013. A quantitative study of fixation stability in amblyopia. *Invest. Ophthalmol. Vis. Sci.* 54 (3), 1998–2003.
- Tychsen, L., 1992. Binocular Vision. *Adler's Physiology of the Eye; Clinical Application*. Mosby, St Louis, MO.
- Tychsen, L., Richards, M., Wong, A., Foeller, P., Bradley, D., Burkhalter, A., 2010. The neural mechanism for latent (fusion maldevelopment) nystagmus. *J. Neuroophthalmol.* 30 (3), 276–283.
- von Noorden, G.K., Avilla, C., Sidikaro, Y., LaRoche, R., 1987. Latent nystagmus and strabismic amblyopia. *Am. J. Ophthalmol.* 103 (1), 87–89.
- Wallace, D.K., Lazar, E.L., Crouch 3rd, E.R., Hoover, D.L., Kraker, R.T., Tamkins, S.M., Pediatric Eye Disease Investigator Group, 2015. Time course and predictors of amblyopia improvement with 2 hours of daily patching. *JAMA Ophthalmol.* 133 (5), 606–609.

Further reading

- Pediatric Eye Disease Investigator Group, 2002. A randomized trial of atropine vs. patching for treatment of moderate amblyopia in children. *Arch. Ophthalmol.* 120 (3), 268–278.
- Pediatric Eye Disease Investigator Group, 2005. Two-year follow-up of a 6-month randomized trial of atropine vs patching for treatment of moderate amblyopia in children. *Arch. Ophthalmol.* 123, 149–157.
- Pediatric Eye Disease Investigator Group, 2008. A randomized trial of atropine versus patching for treatment of moderate amblyopia: follow-up at age 10 years. *Arch. Ophthalmol.* 126, 1039–1044.
- Repka, M.X., Kraker, R.T., Holmes, J.M., et al., 2014. Atropine vs patching for treatment of moderate amblyopia: follow-up at 15 years of age of a randomized clinical trial. *JAMA Ophthalmol.* 132 (7), 799–805.

SECTION

RESEARCH:
Dystonia

VI

This page intentionally left blank

What can kinematic studies tell us about the mechanisms of dystonia?

19

Anna Sadnicka^{a,b,*}, Joseph Galea^c, Mark J. Edwards^a

^a*Motor Control and Movement Disorder Group, Institute of Molecular and Clinical Sciences, St George's University of London, London, United Kingdom*

^b*Clinical and Movement Neurosciences, UCL Queen Square Institute of Neurology, London, United Kingdom*

^c*School of Psychology, University of Birmingham, Birmingham, United Kingdom*

*Corresponding author: Tel.: +44-786-616-9202, e-mail address: asadnick@sgul.ac.uk

Abstract

Clinical movement disorders are classified by an algorithm implemented by a practising movement disorder specialist based on information extracted during the history and clinical examination of a patient. Most simply, dystonia, is a classifier which is reached when a predominant abnormality of posture is noted. In this chapter we summarize studies that have used a variety of techniques to probe beyond the clinical examination and study kinematic features experimentally. We also outline our experimental work in DYT1 dystonia, a group of patients that share a genetically homogenous etiology and can be considered a prototypical dystonic disorder. Our results build on previous studies, confirming that motor variability on a trial-by-trial basis is selectively increased and provide evidence that increases in variability are negatively related to forms of motor learning essential for healthy motor control. Potential neural correlates of increased motor variability are discussed and the implications such work has for the rehabilitation of patients with dystonia are also highlighted.

Keywords

Dystonia, Variability, Adaptation, Motor learning, Rehabilitation

1 Dystonia

Dystonia is a common movement disorder, which is characterized by abnormal postures of the body, often accompanied by tremor ([Albanese et al., 2013](#)). Dystonic postures are typically worsened or induced by action, are mobile and dynamic in nature and can affect specific body parts or be a generalized phenomenon. Dystonia, like many movement disorders, is the physical manifestation of a range of possible

underlying pathologies. These range from conditions causing widespread neurodegeneration (e.g., Parkinson's disease, neurodegeneration with brain iron accumulation), discrete structural lesions (typically of the putamen), and genetic disorders where there is no overt degenerative change and dystonia occurs as an isolated non-progressive phenomenon. DYT1 dystonia is a paradigmatic example of this latter group and is the commonest cause of young-onset isolated dystonia (Bressman et al., 2000). It typically presents with limb dystonia in childhood or early teens, and after a period of progression to segmental/generalized involvement stabilizes and does not progress further (Weisheit et al., 2018). It is caused by a dominantly inherited three base pair deletion in the coding region of the TOR1A gene (Ozelius et al., 1999). People with DYT1 dystonia provide an ideal group within which to study the pathophysiology of dystonia. The dystonia is isolated in nature with no possible confounding effects from associated neurological deficits such as spasticity that can be found in individuals with more complex phenotypes such as dystonic cerebral palsy. Cognition is normal, and the severity of the dystonia itself is typically stable over time, after the initial period of progression is over.

2 Why study kinematics?

Research into the pathophysiology of dystonia has a long history, and the full range of investigative techniques have been applied from genetic and molecular studies, animal modeling, electrophysiology, structural and functional imaging. Broad themes have emerged from this work, for example the concept of aberrant synaptic plasticity, loss of cortical, brainstem and spinal inhibitory function. However, there is a significant difficulty in extrapolating the results of such work to create a mechanistic understanding of the movement disorder that is manifest in dystonia. Many pathophysiological "markers" of dystonia may not bear any relationship to the actual mechanism of the movement disorder itself. For example, some experimental techniques could simply document epiphenomena relating to the excess of movement observed and/or its compensation. Such arguments are supported by the general lack of correlation between the severity of specific pathophysiological markers of dystonia (e.g., cortical inhibition, aberrant plasticity) and the severity of clinical symptoms, and such abnormalities are frequently found in regions of the brain subserving unaffected body parts. Abnormal profiles of inhibition and plasticity are also found across a broad range of neurological disorders, non-specifically modulated across a range of distinct diseases.

It can therefore be argued that the study of the dystonic movement itself deserves more attention. By directly sampling the natural patterns of dystonic movement and characterizing performance within experimental tasks, one can better define kinematic signatures for dystonia and infer the nature of the motor control deficit. There remains no diagnostic test for dystonia and such work offers great potential for better clinical characterization, better severity scores for dystonia and targeted therapeutic interventions (current treatment options are relatively non-specific to pathophysiology).

3 Kinematic studies of dystonia

It is beyond the scope of this article to fully summarize the range of kinematic abnormalities that have been documented in dystonia. Instead we choose two salient and relevant themes; increased variability of movement and the apparent preservation of many motor control elements within the dystonic brain. We initially work from the premise that dystonia is a pattern of movement abnormalities or motor syndrome that can arise from a broad range of etiologies.

Since the very first kinematic studies of dystonia there has been evidence of increased variability of movement ([van der Kamp et al., 1989](#)). For example, one study compared elbow flexion movements in 10 patients with mixed etiological causes for their dystonia with controls measuring elbow flexion kinematics with a potentiometer displayed on an oscilloscope screen ([van der Kamp et al., 1989](#)). They found that even if controls are asked to match the slower dystonic movements that were observed in this study, symptomatic arms of subjects with dystonia have significantly more variability in the amplitude of their movements (quantified by the coefficient of variation) ([van der Kamp et al., 1989](#)). More recently, Fourier analysis was applied to electromyography (EMG) and kinematic data acquired during the performance of a continuous figure of eight writing task in children with dystonia and age-matched healthy controls ([Lunardini et al., 2015b](#)). This method exploited the frequency domain features of the cyclic motor task in order to discriminate between task-correlated and task-uncorrelated components of muscle activity (task-correlated at frequencies related to the cyclic figure of eight movements, task-uncorrelated components at unrelated frequencies). They confirmed their hypothesis that task-uncorrelated variability was increased in comparison to controls and argued that there was a deficit in the dystonic brain to suppress variable and uncorrelated elements of movement ([Lunardini et al., 2015b](#)).

Another feature in dystonia is that many fundamental features of motor control are intact. For example, for many years it was thought that dystonia is an abnormality of posture stemming from the co-contraction of agonist and antagonist muscles. However careful work in multi joint reaching movements using motion analysis and EMG has in fact shown that co-contraction is not an obligatory feature of multi joint movements in dystonia ([Malfait and Sanger, 2007](#)). Another line of work looks at muscle synergy patterns. The presence of muscle synergies in the healthy central nervous system is thought to reflect a general principle adopted to help the musculoskeletal system deal with inherent redundancy of motor control (the fact we have excess resources that allows us to perform the same task in many different possible ways). Synergies, in this context are a co-ordinated activation of a group of muscles with specific activation balances defining a set of muscles working as a single functional unit. This modular organization then allows complex movements or sequences of movements to be achieved by the combination of multiple muscle synergies. Interestingly, in an analysis of performance of children with and without dystonia performing a writing task, dystonic children showed that despite the compromised kinematic outcomes of writing in dystonia, there was a strikingly similar number and structure of the synergy vectors of the two groups of children in the EMG

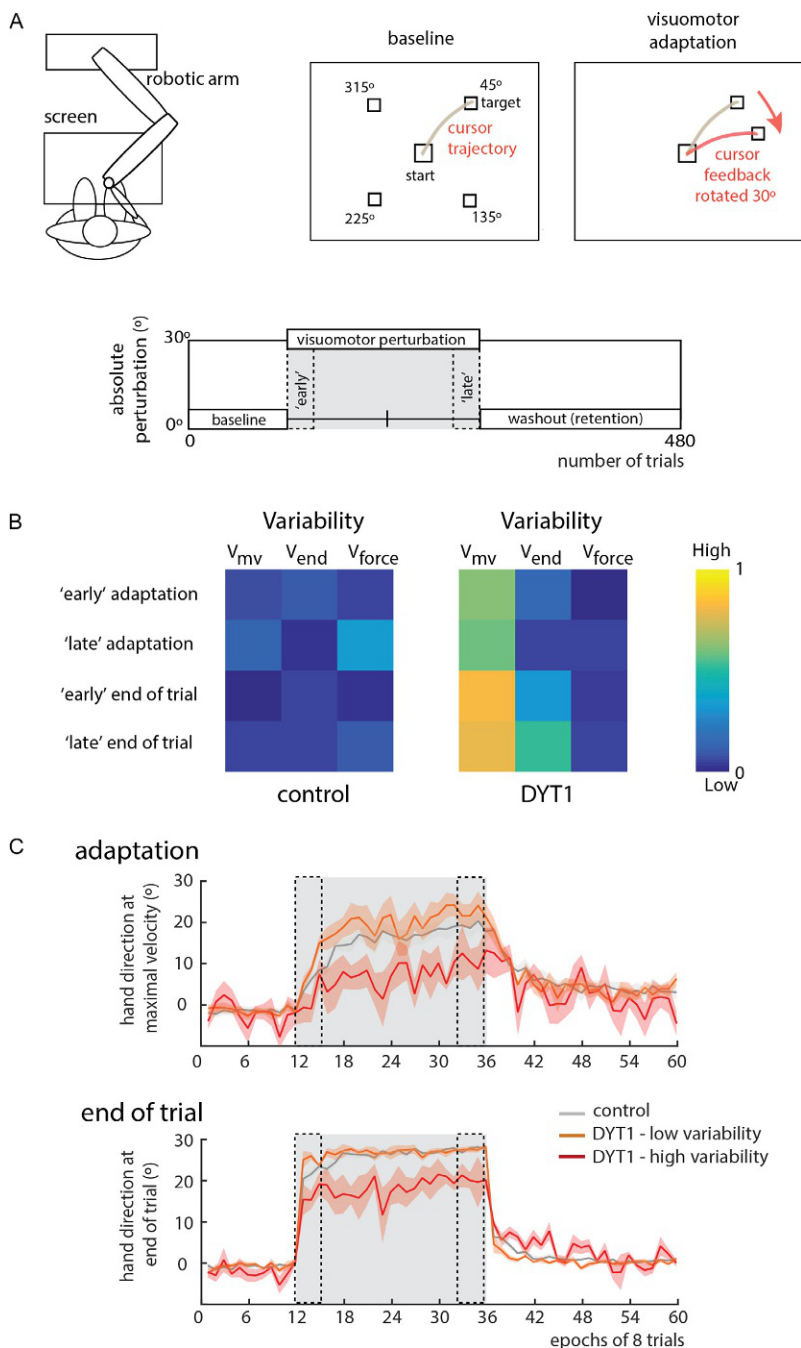
(Lunardini et al., 2017). Similarly, the timing of the activation of the synergy coefficients did not significantly differ (Lunardini et al., 2017). Therefore patterns of effector recruitment remain remarkably similar in this disorder with such obvious clinical motor abnormalities.

4 Variability in DYT1 dystonia

Thus in groups of dystonia due to heterogeneous etiologies increased movement variability is a core feature and many fundamental motor control features remain intact. There are some challenges in the study of mixed groups of patients. For example, studies in childhood dystonia which include dystonic cerebral palsy could also be influenced by additional, albeit lesser insults to the motor system, such as spasticity and weakness. We have therefore chosen to study variability in a homogenous patient group with the genetic DYT1 mutation in an effort to study “dystonic” motor control in isolation.

Motor variability can be defined as the normal variations that occur in motor performance across multiple repetitions of a task (Stergiou and Decker, 2011). Variability has many sources and roles (Sternad, 2018). For example, undesired variability which can potentially corrupt signal transmission with the sensorimotor system can arise secondary to noisy processes within the nervous system, anywhere from the perception of sensory stimuli through to the generation of motor responses (Faisal et al., 2008). Conversely, other types of variability appear to be informative, representing an exploration of motor command space (Tumer and Brainard, 2007). Experimentally, individuals with greater variability of baseline movement parameters relevant to the subsequent learning task are faster learners across reinforcement and motor adaption (error-based) task designs (Wu et al., 2014) (but see He et al., 2016). Moreover, features of such variability appear to be under dynamic regulation. The temporal structure of motor variability can be shown to shift responsively to align to the task design and has different characteristics across different stages of learning (Sternad, 2018; Tumer and Brainard, 2007; Wu et al., 2014). For the healthy motor system, maintaining the dynamic equilibrium of keeping unwanted variability in check while regulating informative elements which assist learning, is therefore an essential role and is an active area of motor control research. In the study of movement disorders such as dystonia understanding shifts in the profile of variability is therefore complex but highly relevant.

Using a robotic manipulandum we designed a task to examine motor variability during reaching movements in the symptomatic arm of 10 manifesting patients with DYT1 dystonia and 12 aged matched controls and investigated whether variability markers were related to motor learning (Fig. 1A) (Sadnicka et al., 2018). For every trial, participants made a fast outward movement from a central starting position toward one of four potential target positions with the aim of stopping in the target box within the fixed time frame of one second. Following a baseline block, sensorimotor adaptation was examined by applying a visuomotor perturbation which distorted

**FIG. 1**

See legend on next page.

visual feedback by 30°. Veridical visual feedback was then reintroduced to examine washout (retention) of the newly learnt visuomotor rotation.

Similar to previous studies, despite the obvious dystonic movements of the symptomatic right arm we found a range of movement parameters to be within normal range. For example, the timing and magnitude of maximal velocity and the maximal force applied were not different across groups. Such findings were again suggestive of a selective motor deficit in DYT1 dystonia. More noteworthy results were found when we started to analyze the patterns of variability of dystonic movements. Principal component analysis of the two-dimensional kinematic data (movements were made across a fixed plane) at different time points revealed that DYT1 dystonia is characterized by a subtle (yet statistically significant) increase in spatial variability. Increases in variability were maximal in phases of movement, which rely on feed-forward motor control (with little or no influence of online feedback). Interestingly such variability appeared random in its nature with no directional preponderance shown in any of the reach conditions. This finding is concordant with the detailed experimental work in children which suggests that the patterns of muscle groups or muscle synergies recruited to tasks are surprisingly intact in a disorder in which the balance between different muscle groups appears so impaired ([Lunardini et al., 2015a, 2017](#)).

FIG. 1

(A) The task was displayed on a horizontal computer screen and performed using a robotic manipulandum. Each trial consisted of making a fast outward movement from a central starting position toward one of four potential target positions. The aim was to stop in the target box within the fixed time frame of one second. Following a baseline block, sensorimotor adaptation was examined by applying a visuomotor perturbation (distorting visual feedback by 30°). True visual feedback was then reintroduced to examine washout (retention) of the newly learnt visuomotor rotation. (B) We examined whether markers of variability in DYT1 dystonia influenced performance indicators in the visuomotor adaptation task. Markers of variability that we expected to be relevant to the task were (i) baseline angular variability at maximal velocity (V_{mv}) and (ii) angular variability at the end of trial (V_{end}). The baseline variability of magnitude of maximal force (V_{force}) applied was selected as a subset of variability that was less relevant to the subsequent learning task. Change of hand direction at maximal velocity (adaptation) and end of trial were used as markers of performance during “early” and “late” phases of the visuomotor perturbation. In controls, there was no obvious relationship between variability markers and performance markers. In DYT1 dystonia markers of learning were negatively correlated with task-relevant variability (V_{mv}). (C) A median split of patients by task-relevant variability into low and high variability groups illustrates this relationship further. In the high variability group both the rate of adaptation (early) and the total magnitude of adaptation (late) were reduced. Ability to correct the visuomotor perturbation at the end of trial after the chance to also use online corrective mechanisms was also significantly negatively related to increased variability. In summary, increased variability relevant to the task was negatively correlated to adaptation performance indicators in DYT1 dystonia (see [Sadnicka et al., 2018](#) for full experimental details).

Given that task-relevant variability and sensorimotor adaptation are related in health (Wu et al., 2014), we then examined how the increased variability in DYT1 dystonia influenced performance indicators in this adaptation learning task. Markers of trial-by-trial variability that we expected to be relevant were (i) variability of movement at maximal velocity and (ii) variability of movement at the end of trial. Variability of force applied by participants was selected as a subset of variability that was less relevant to the task. Learning metrics for both adaptation and at the end of trial (after additional online corrections) were also quantified (see detailed parameter description in legend of Fig. 1B). In controls, there was no obvious relationship between variability markers and performance with low correlation values between variability and subsequent learning metrics (Fig. 1B). In contrast in DYT1 movement variability (at maximal velocity) was clearly related to the ability to learn the visuomotor adaptation. By splitting patients into those with low and high variability this relationship is further illustrated in Fig. 1C. In DYT1 patients with high variability both the rate of adaptation (early) and the total magnitude of adaptation (late) were reduced. Ability to correct for the visuomotor perturbation at the end of trial once online corrections have occurred was also reduced. In summary, increased variability relevant to the subsequent task was negatively correlated to adaptation performance indicators in DYT1 dystonia.

This result was interesting as in health, the correlation between task-relevant variability and motor learning has been plotted as a positive linear relationship suggesting that task-relevant variability is informative to the motor system (Wu et al., 2014). If this line of reasoning is followed one interpretation is that in DYT1 dystonia, this physiological relationship breaks down. Once an upper threshold is breached increased variability no longer assists motor learning. In DYT1 dystonia, increased variability could rather introduce error and uncertainty into the control of movement leading to the poor performance observed in this study (see high variability group in Fig. 1C). Adaptation is a form of error-based learning in which the brain computes a teaching signal which is the difference between the desired movement and the actual movement (which has been perturbed by the influence of visuomotor transformation). Therefore the random spatial variability that we observed could be considered a noise factor which will be added to the teaching signal from each trial, decreasing its accuracy and certainty, and impairing the ability to compute the correction or adaptation coefficient required to update the next movement. This is one very feasible explanation of our results and such an interpretation implies that adaptation itself is intact in dystonia.

What is the relative importance and mechanism driving motor variability within disease models for dystonia? Dystonia is characterized by its involvement of a wide neuronal network and increased variability could be generated by multiple regions and multiple mechanisms. Our data and the literature are perhaps most consistent with the idea that redundant variability or noise is injected at a late phase of movement preparation. One potential neuronal correlate is the finding that there is abnormally enhanced and synchronous oscillatory activity in the *output* nuclei of the basal ganglia of patients with dystonia which is coherent with EMG activity during

dystonic movements (Barow et al., 2014; Chen et al., 2006; Liu et al., 2008). Such oscillatory activity could inject variability onto the elemental movement plan which fits with the literature in dystonia that many basic control components are intact.

It is then interesting to consider if there is evidence that the dystonic motor system is compensating for increased motor variability. In general noise cannot be removed from a signal once it has been added; however processes such as averaging and weighting different components due to prior knowledge are often combined in the nervous system to counter its influence (Faisal et al., 2008). Our task was relatively constrained and higher levels of variability clearly impaired performance. However, a freer task allowing a greater variety of motor control solutions would enable one to evaluate compensatory mechanisms against noise and uncertainty. Already work in children with dystonic cerebral palsy has suggested that when learning the novel skill of throwing a virtual ball children adjusted their motor strategy to be more tolerant to variability in timing (Chu et al., 2016).

Another important line of work which informs neuro-rehabilitation options, is that changing the sensorimotor context for patients can be helpful. Clues for this clinically may be present within sensory trick phenomena in which increased sensory feedback obtained by touching a body part (for example touching chin with hand in cervical dystonia) reduces the expression of dystonia (Patel et al., 2014). If, as our data suggests, poor performance in DYT1 dystonia is related to increases in random variability, it is likely that the motor controller has a lesser ability to extract relevant information from actual sensory feedback as most sensory streams will be polluted by this noisy stochastic component. Therefore, externally generated and augmented feedback may offer real opportunity to reduce dystonic contractions using intact feedback loops that can improve dystonic motor control. For example, in a bimanual myocontrol task in which the modified sum of the EMG amplitudes from the biceps muscles controlled the vertical position of a single red line on a computer screen, if scaled forms of vibratory feedback were given to augment sensory awareness of task-relevant information, children with dystonia were better able to suppress excessive variability (Bertucco and Sanger, 2015; Liyanagamage et al., 2017). Interestingly, occasionally, DYT1 dystonia can also improve with certain actions such as playing piano or knitting (Kojovic et al., 2012), implying that the activation of certain motor circuits reduces the severity of the dystonic manifestations.

5 Directions for future work

The limited number of core clinical movement disorders may in part reflect the limited range of responses that a motor control system can display in response to perturbation by disease. As such dystonia is considered a final common endpoint for a multitude of different etiologies as discussed. However, we also believe that disease specific kinematic signatures are likely to reside within these broad clinical classification systems. The future challenge in this field of investigation is therefore to effectively navigate between kinematic features that are disease specific yielding

insight into pathophysiology and more general patterns of change that are representative of the symptom dystonia and yet perhaps still informative for therapeutic interventions.

6 Conclusions

The pathophysiology of the dystonia's remains an enigma. The analysis of the dystonic movement itself with kinematic techniques offers real opportunity to directly probe dystonic motor control. Within such investigation we need to be mindful of the fact that the term dystonia is often used interchangeably to represent both a motor syndrome in response to a range of pathophysiological insults and also specific diseases (as in the case of the genetically homogenous DYT1 dystonia). Our work in DYT1 dystonia reveals an important role for increased motor variability and delineating the mechanisms behind how such variability is generated and why this occurs remains an important research goal. Overall, the hope is that by reverse engineering dystonic control mechanisms and utilizing intact features of the sensorimotor controller there is an optimistic future for targeted therapeutic interventions.

References

- Albanese, A., Bhatia, K., Bressman, S.B., Delong, M.R., Fahn, S., Fung, V.S., Hallett, M., Jankovic, J., Jinnah, H.A., Klein, C., Lang, A.E., Mink, J.W., Teller, J.K., 2013. Phenomenology and classification of dystonia: a consensus update. *Mov. Disord.* 28, 863–873.
- Barow, E., Neumann, W.J., Brucke, C., Huebl, J., Horn, A., Brown, P., Krauss, J.K., Schneider, G.H., Kuhn, A.A., 2014. Deep brain stimulation suppresses pallidal low frequency activity in patients with phasic dystonic movements. *Brain* 137, 3012–3024.
- Bertucco, M., Sanger, T.D., 2015. Current and emerging strategies for treatment of childhood dystonia. *J. Hand Ther.* 28, 185–193. quiz 194.
- Bressman, S.B., Sabatti, C., Raymond, D., De Leon, D., Klein, C., Kramer, P.L., Brin, M.F., Fahn, S., Breakefield, X., Ozelius, L.J., Risch, N.J., 2000. The DYT1 phenotype and guidelines for diagnostic testing. *Neurology* 54, 1746–1752.
- Chen, C.C., Kuhn, A.A., Hoffmann, K.T., Kupsch, A., Schneider, G.H., Trittenberg, T., Krauss, J.K., Wohrle, J.C., Bardinet, E., Yelnik, J., Brown, P., 2006. Oscillatory pallidal local field potential activity correlates with involuntary EMG in dystonia. *Neurology* 66, 418–420.
- Chu, V.W., Park, S.W., Sanger, T.D., Sternad, D., 2016. Children with dystonia can learn a novel motor skill: strategies that are tolerant to high variability. *IEEE Trans. Neural Syst. Rehabil. Eng.* 24, 847–858.
- Faisal, A.A., Selen, L.P., Wolpert, D.M., 2008. Noise in the nervous system. *Nat. Rev. Neurosci.* 9, 292–303.
- He, K., Liang, Y., Abdollahi, F., Fisher Bittmann, M., Kording, K., Wei, K., 2016. The statistical determinants of the speed of motor learning. *PLoS Comput. Biol.* 12, e1005023.
- Kojovic, M., Parees, I., Sadnicka, A., Kassavetis, P., Rubio-Agusti, I., Saifee, T.A., Bologna, M., Rothwell, J.C., Edwards, M.J., Bhatia, K.P., 2012. The brighter side of music in dystonia. *Arch. Neurol.* 69, 917–919.

- Liu, X., Wang, S., Yianni, J., Nandi, D., Bain, P.G., Gregory, R., Stein, J.F., Aziz, T.Z., 2008. The sensory and motor representation of synchronized oscillations in the globus pallidus in patients with primary dystonia. *Brain* 131, 1562–1573.
- Liyanagamage, S.A., Bertucco, M., Bhanpuri, N.H., Sanger, T.D., 2017. Scaled vibratory feedback can bias muscle use in children with dystonia during a redundant, 1-dimensional myocontrol task. *J. Child Neurol.* 32, 161–169.
- Lunardini, F., Casellato, C., Bertucco, M., Sanger, T.D., Pedrocchi, A., 2015a. Muscle synergies in children with dystonia capture “healthy” patterns regardless the altered motor performance. *Conf. Proc. IEEE Eng. Med. Biol. Soc.* 2015, 2099–2102.
- Lunardini, F., Maggioni, S., Casellato, C., Bertucco, M., Pedrocchi, A.L., Sanger, T.D., 2015b. Increased task-uncorrelated muscle activity in childhood dystonia. *J. Neuroeng. Rehabil.* 12, 52.
- Lunardini, F., Casellato, C., Bertucco, M., Sanger, T.D., Pedrocchi, A., 2017. Children with and without dystonia share common muscle synergies while performing writing tasks. *Ann. Biomed. Eng.* 45, 1949–1962.
- Malfait, N., Sanger, T.D., 2007. Does dystonia always include co-contraction? A study of unconstrained reaching in children with primary and secondary dystonia. *Exp. Brain Res.* 176, 206–216.
- Ozelius, L.J., Page, C.E., Klein, C., Hewett, J.W., Mineta, M., Leung, J., Shalish, C., Bressman, S.B., De Leon, D., Brin, M.F., Fahn, S., Corey, D.P., Breakefield, X.O., 1999. The TOR1A (Dyt1) gene family and its role in early onset torsion dystonia. *Genomics* 62, 377–384.
- Patel, N., Jankovic, J., Hallett, M., 2014. Sensory aspects of movement disorders. *Lancet Neurol.* 13, 100–112.
- Sadnicka, A., Stevenson, A., Bhatia, K.P., Rothwell, J.C., Edwards, M.J., Galea, J.M., 2018. High motor variability in DYT1 dystonia is associated with impaired visuomotor adaptation. *Sci. Rep.* 8, 3653.
- Stergiou, N., Decker, L.M., 2011. Human movement variability, nonlinear dynamics, and pathology: is there a connection? *Hum. Mov. Sci.* 30, 869–888.
- Sternad, D., 2018. It's not (only) the mean that matters: variability, noise and exploration in skill learning. *Curr. Opin. Behav. Sci.* 20, 183–195.
- Tumer, E.C., Brainard, M.S., 2007. Performance variability enables adaptive plasticity of ‘crystallized’ adult birdsong. *Nature* 450, 1240–1244.
- van der Kamp, W., Berardelli, A., Rothwell, J.C., Thompson, P.D., Day, B.L., Marsden, C.D., 1989. Rapid elbow movements in patients with torsion dystonia. *J. Neurol. Neurosurg. Psychiatry* 52, 1043–1049.
- Weisheit, C.E., Pappas, S.S., Dauer, W.T., 2018. Inherited dystonias: clinical features and molecular pathways. *Handb. Clin. Neurol.* 147, 241–254.
- Wu, H.G., Miyamoto, Y.R., Gonzalez Castro, L.N., Olveczky, B.P., Smith, M.A., 2014. Temporal structure of motor variability is dynamically regulated and predicts motor learning ability. *Nat. Neurosci.* 17, 312–321.

Implications of asymmetric neural activity patterns in the basal ganglia outflow in the integrative neural network model for cervical dystonia

20

Alexey Sedov^{a,*}, Ulia Semenova^a, Svetlana Usova^a, Alexey Tomskiy^b, John Douglas Crawford^c, Hyder A. Jinnah^d, Aasef G. Shaikh^{e,f,g}

^aSemenov Institute of Chemical Physics, Russian Academy of Sciences, Moscow, Russia

^bN.N. Burdenko National Scientific and Practical Center for Neurosurgery, Moscow, Russia

^cYork University, Toronto, ON, Canada

^dDepartments of Neurology and Human Genetics, Emory University, Atlanta, GA, United States

^eDepartment of Neurology, Case Western Reserve University, Cleveland, OH, United States

^fNational VA Parkinson Consortium Center and Neurology Service, Louis Stokes Cleveland

VA Medical Center, Cleveland, OH, United States

^gNeurological Institute, University Hospitals, Cleveland, OH, United States

*Corresponding author: +7-903-5795024 e-mail address: alexeys.sedov@gmail.com

Abstract

Cervical dystonia (CD) is characterized by abnormal twisting and turning of the head with associated head oscillations. It is the most common form of dystonia, which is a third most common movement disorder. Despite frequent occurrence there is paucity in adequate therapy, much of which is attributed to its uncertain pathophysiology. Recently we proposed a unifying network model highlighting the role of head neural integrator (hNI) for the pathophysiology of CD. According to our hypothesis the CD is due to abnormal output of hNI; the latter itself is not affected but its dysfunction is secondary to abnormal feedback. We hypothesized that asymmetry in the feedback to hNI is associated with severity in CD; the feedback asymmetry is greater in CD with lateralized head postures, such as turning of head in yaw plane (torticollis) or roll plane (laterocollis). The hypothesis also specifies that feedback to hNI—cerebellum, proprioception, and basal ganglia outflow (pallidus) are connected in a network; thus asymmetry is distributed through the feedback network. In 15 CD patients undergoing deep brain stimulation (DBS) surgery, with their informed consent, we used the opportunity to collect single unit neural responses and local field potential from the globus pallidus to measure whether feedback to hNI is asymmetric. Using machine learning algorithms developed to analyze single unit data, we found: (1) globus pallidus interna (GPi) firing rate, discharge

pattern and gamma oscillation were asymmetric in patients with robust torticollis; (2) there was no asymmetry in these parameters in retrocollis; and (3) in those patients with oppositely directed laterocollis and torticollis. Firing rate was higher in GPi cells ipsilateral to the direction of head rotation; the asymmetry was more pronounced in tonic cells compared to burst neurons. In addition to confirming that CD is associated with an asymmetric pallidal activity, our data showed that neuronal asymmetry correlated with the degree of involuntary head turning. We propose that asymmetric pallidal activity results in asymmetric feedback to hNI causing its dysfunction.

Keywords

Cervical dystonia, Human neural integrator, Globus pallidus, Microelectrode recording (MER), Local field potentials (LFP), Asymmetry

1 Introduction

Cervical dystonia (CD), the most common form of focal dystonia, is characterized by abnormal head posture often combined with neck pain and jerky head oscillations. Information regarding the brain regions that may cause CD is surprisingly limited, and views on the pathophysiological mechanisms of the disease are controversial. In 2002 a pretectal neural integrator, analogous to that in the ocular motor system, was proposed for the control of head movements (Klier et al., 2002). Our recent studies proposed that the head movement abnormalities in CD are due to the malfunctioning of the head neural integrator (hNI) putatively due to impaired feedback from the cerebellum, basal ganglia, or peripheral proprioceptors (Sedov et al., 2017, 2019; Shaikh et al., 2016). According to this model asymmetric feedback to the hNI results in abnormal head postures with or without jerky head oscillations. Support for this hypothesis comes from macaque experiments, where unilateral injection of muscimol into the mesencephalic interstitial nucleus of Cajal (INC) resulted immediately in position-dependent head drifts with intermittent rapid corrective movements, i.e., jerky head oscillation, whereas further progression of the effect led to tonic deviated head postures (Farshadmanesh et al., 2008; Klier et al., 2002). This was interpreted as an immediate bihemispheric imbalance in the hNI, followed by loss in the ability to correct the resulting head drift due to spread of the muscimol through the INC and adjacent midbrain structures. We predict that impaired or asymmetric hNI activity can be due to imbalance in the input to the integrator. The feedback sources to the neural integrator, which include the cerebellum, basal ganglia, and proprioceptors are mutually connected. Therefore the asymmetry in feedback from any of the sources could be reflected in any of the nodes of the network contributing to the hNI. We used the opportunity to measure single unit activity and local field potential (LFP) from the basal ganglia outflow, globus pallidus, during deep brain stimulation (DBS) surgery, asking a key question whether feedback to the hNI in CD is asymmetric. In particular we hypothesize that robust asymmetry in the feedback to hNI is associated with severe lateralized head postures in CD patients.

2 Materials and methods

We measured single unit physiology and LFP from 15 CD subjects undergoing globus pallidus DBS surgery. Surgeries were performed under local anesthesia in Burdenko National Scientific and Practical Center for Neurosurgery. We separated patients into three groups. Group 1 was represented by six patients with robust torticollis. Group 2 included six patients with mild latero-torticollis. Group 3 was presented by control group of three patients with retrocollis. The participants gave written informed consent for the surgery and the involvement in research. Studies were approved by the ethical committee and was performed according to the Declaration of Helsinki.

We recorded and analyzed 865 cells in internal (GPi) and external (GPe) segment of the globus pallidus. Cell localization was controlled by Lead-DBS (<http://www.lead-dbs.org/>). The signals acquired during recordings were pre-processed and analyzed using Spike2 software (CED, Cambridge, UK). The steps for data pre-processing included bandpass filtering (300–5000 Hz for MER) and spike sorting. Spikes were detected using an amplitude threshold and then sorted by means of principal component analysis (PCA). We used method of hierarchical spike train clustering to separate neurons to burst and tonic types (Myrov et al., 2019). We measured 22 objective spike train parameters and oscillations scores in each cell types. We used analysis of variance (ANOVA) and random forest algorithm to determine which parameter is dependent upon the laterality of CD. Oscillation scores (OS) for each frequency band were computed with the spectral analysis of LFP. To estimate the degree of head rotation we used facial feature tracking techniques from video frames with CLM-framework.package (<https://github.com/TadasBaltrusaitis/CLM-framework>).

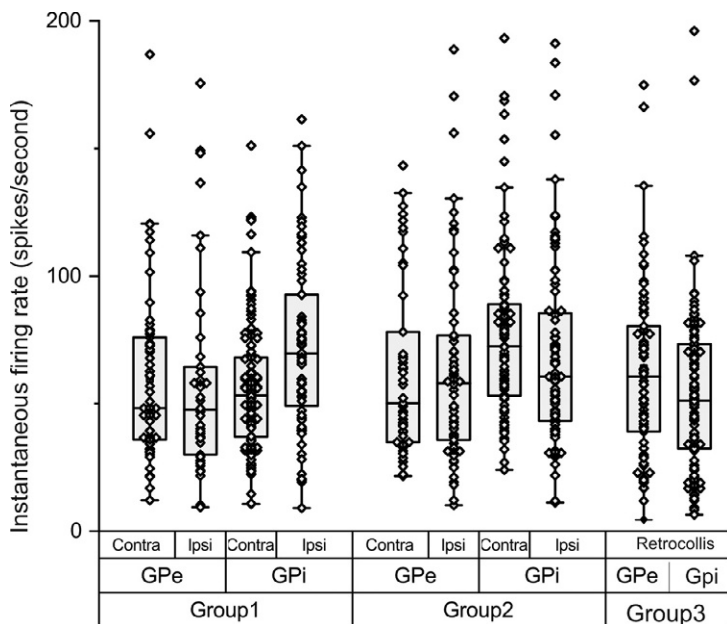
3 Results

We analyzed 22 spike-train parameters in firing rates of GPi and GPe single neurons that were ipsilateral and contralateral to the direction of head rotation. These parameters are outlined in Table 1. Among 22 spike-train parameters only 3 parameters differed in ipsilateral versus contralateral GPi activity in patients who had prominent lateralized head posturing—firing rate (or mean interspike interval), burst index quantifying the pattern of burst firing, and pause index quantifying patterns of episodic burst in the firing rate. In these patients the firing rate was higher in GPi ipsilateral to the direction of dystonia (ANOVA, $P < 0.01$) (Fig. 1). There was no such laterality dependence of firing rate in GPe neurons (Fig. 1). The ipsilateral GPi activity had more bursting response and there were less pauses. Separation of neurons into burst and tonic types showed that the asymmetry was more pronounced in tonic cells compared to burst neurons; the difference was more robust in GPi (Wilks lambda = 0.97, $F(3,191) = 2.22$; $P = 0.08$) compared to GPe (Wilks lambda = 0.98, $F(3,110) = 0.77$; $P = 0.5$) (Fig. 2).

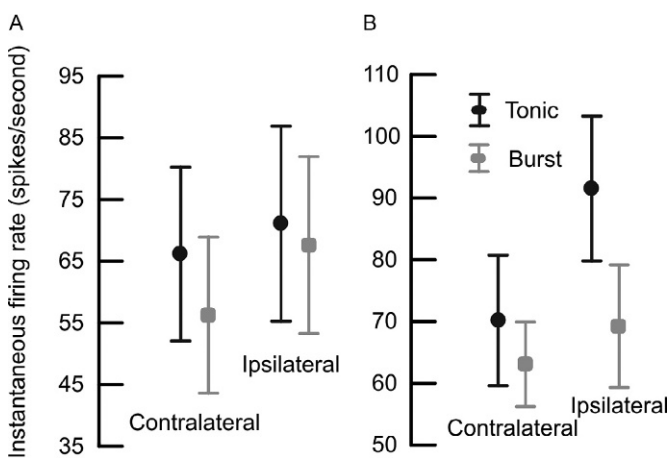
Table 1 Parameters of single unit activity in contra- and ipsilateral globus pallidus.

N	Parameters	GPi			GPe		
		Contra	Ipsi	P value	Contra	Ipsi	P value
1	Firing rate—instantaneous firing rate	57.527	72.486	0.007	50.637	58.961	0.350
2	Coefficient of variation	1.043	0.973	0.260	1.052	1.073	0.946
3	Asymmetry index—ratio of median to mean ISI	0.654	0.682	0.142	0.693	0.688	0.830
4	Frequency variance—ratio of difference in maximum and minimum to maximum FR	43.704	39.258	0.452	39.415	51.453	0.024
5	Local variance—measure of local spike randomness	0.667	0.645	0.668	0.549	0.537	0.418
6	Differential entropy (Nu)—the measure of spiking randomness	0.761	0.786	0.160	0.707	0.716	0.963
7	ISI larger mean—percent of ISI larger than mean ISI	0.326	0.340	0.101	0.312	0.316	0.772
8	Burst index—ratio of number of 10–16 ms ISI to number of ISI > 16 ms	0.653	1.025	0.034	0.445	0.838	0.218
9	Burst spike percent—ratio of spikes in bursts to the total number of spikes	0.223	0.213	0.433	0.224	0.209	0.903
10	Ratio burst time—ratio of burst spikes time to total time	0.072	0.071	0.535	0.087	0.082	0.764
11	Burst rate	1.521	1.703	0.361	1.192	1.070	0.470
12	Interburst interval	0.528	0.523	0.687	0.707	0.695	0.677
13	Mean burst length	0.048	0.041	0.352	0.078	0.077	0.934
14	Mean ISI in burst	0.006	0.005	0.035	0.007	0.007	0.126
15	Mean spikes in burst	8.778	8.720	0.469	9.765	11.000	0.298
16	Pause index—ratio of the number of ISIs > 50 ms to the number of ISIs below	0.056	0.029	0.007	0.054	0.045	0.254
17	O-score 3–8Hz	4.990	4.642	0.608	4.488	4.113	0.302
18	O-score 8–12Hz	2.082	2.271	0.423	2.143	2.221	0.912
19	O-score 12–20Hz	0.894	0.824	0.317	1.190	1.247	0.304
20	O-score 20–30Hz	0.732	0.559	0.164	0.596	0.534	0.924
21	O-score 30–60Hz	1.008	0.872	0.096	0.973	0.714	0.560
22	O-score 60–90Hz	0.980	0.862	0.105	1.192	0.861	0.265

Bold emphasis marks parameters with P < 0.05.

**FIG. 1**

The summary of instantaneous firing rate in individual neurons (each symbol). Box and whisker plot depicts the summary. The length of each box depicts interquartile interval. The horizontal line in the center depicts the median value, boxes depict interquartile interval, while whiskers represent the range. The instantaneous firing rate is plotted on the y-axis while each category is on the x-axis.

**FIG. 2**

The figure depicts the summary of mean and 95% confidence interval of instantaneous firing rate in (A) GPe and (B) GPI neurons. Symbol in the center depicts median while whiskers are 95% confidence interval. Gray line and symbols are burst neurons while black line and symbols are tonic cells.

There was no laterality dependence of the neuronal firing irregularity as quantified by frequency variance, local variance, differential entropy. There was no difference in percent of spikes distributed during the bursts, featuring the prominence of bursts in firing pattern between two hemispheres. Other burst parameters, such as mean burst interval, duration between adjacent bursts or number of spikes within a given burst were not different between hemispheres. The differences noted in those with lateralized posturing in torticollis were not evident in those who had lateraocollis (posturing in roll plane) in one direction while torticollis (posturing in yaw plane) in the other; or those who had retrocollis (posturing in pitch plane). None of the spike train parameters in any groups was asymmetric in GPe neurons, with an exception of small asymmetry in spike frequency irregularity in those who had robust torticollis.

In subsequent analysis we measured the synchronized neuronal activity in form of LFP in each group. We found significant ($P < 0.01$) differences in GPi gamma oscillations in those who had prominent torticollis. There were no significant differences in GPi oscillations in other frequency bands, in those who had prominent retrocollis or torticollis and laterocollis in opposite direction. There was no interhemispheric asymmetry in LFP measured from GPe in any patients.

We measured the strength of coupling between the GPi asymmetry and severity of head turning in nine patients who had robust torticollis. We found significant dependence between the angle of head turning and three asymmetric parameters (Fig. 3A–C).

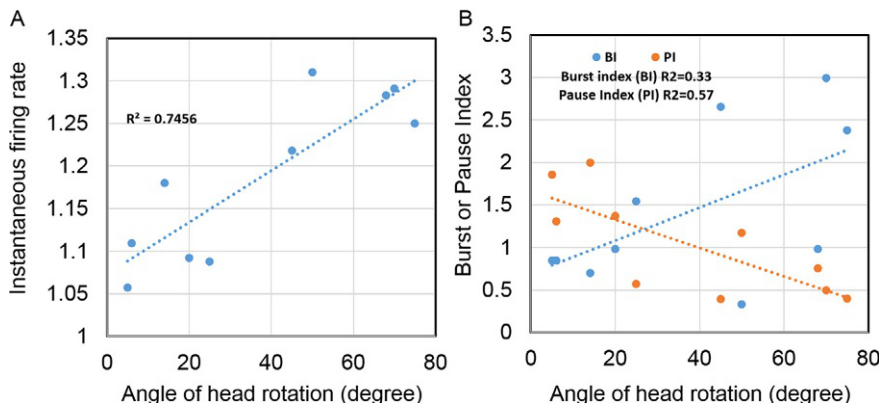


FIG. 3

Example of correlation of (A) asymmetry in instantaneous firing rate and (B) Burst Index or Pause Index and the angle of head rotation. Each data point depicts individual patient, dashed line is a linear fit.

4 Discussion

We measured single unit activity and synchronized discharges, i.e., LFP, in the globus pallidus the main output nuclei of the basal ganglia. In our unifying network model for CD the pallidus is part of interconnected source of feedback to the hNI, the dysfunction of which may lead to CD (Sedov et al., 2017, 2019; Shaikh et al., 2016). We found asymmetry in LFP and single unit activity measured from GPi, similar to previous studies (Lee and Kiss, 2014; Moll et al., 2014). We found differences in LFP and single unit activity in the same group of patients and nuclei; and it further related the asymmetry in firing rate discharge to the robustness in the severity of neck posturing in affected subjects. Another aspect of our study was that in addition to firing rate we found differences in discharge patterns. Specifically, we found that asymmetry were pronounced mainly in tonic cells. In contrast patients who had retrocollis or combinations of oppositely directed laterocollis and torticollis did not have such physiological asymmetry in the pallidus. These results suggest that higher asymmetry in the pallidal activity is correlated with the larger asymmetry in the neck tone. In support of neck muscle tone dependent neck asymmetry, we also found that amount of head rotation correlated with the level of asymmetry in pallidal activity. Due to the anatomically strategic location, the rotation of the head in torticollis is controlled mainly by the ipsilateral neck muscles. The “rate” theory of dystonia predicts that muscle hypertonus in dystonia is correlated with pallidal inhibition (i.e., reduction in firing rate) and thalamic hyperactivity. In contrast we found increased firing rate of GPi ipsilateral to affected neck muscles. It is therefore suggested that GPi hyperactivity is not primary cause of CD but rather reflects imbalanced feedback. Hence the deficits noted in the pallidum in CD patients is consequential, not causal. It is further suggested that asymmetric feedback via the pallidum to the hNI leads to leaky neural integration.

Acknowledgments

The study was funded by the Russian Science Foundation (project 18-15-00009 to Sedov): data collection and analysis. The study was partly supported by the Russian Foundation for Basic Research (project 18-315-00202 to Semenova): estimation of head rotation. The study was also supported by Dystonia Medical Research Foundation (Shaikh); Dystonia Coalition Career Development Award (Shaikh), American Academy of Neurology Career Development Award (Shaikh); and George C. Cotzias Memorial Fellowship from American Parkinson’s Disease Association (Shaikh).

References

- Farshadmanesh, F., Chang, P., Wang, H., Yan, X., Corneil, B.D., Crawford, J.D., 2008. Neck muscle synergies during stimulation and inactivation of the interstitial nucleus of cajal (INC). *J. Neurophysiol.* 100, 1677–1685. <https://doi.org/10.1152/jn.90363.2008>.

- Klier, E.M., Wang, H., Constantin, A.G., Crawford, J.D., 2002. Midbrain control of three-dimensional head orientation. *Science* 295 (5558), 1314–1316. <https://doi.org/10.1126/science.1067300>.
- Lee, J.R., Kiss, Z.H.T., 2014. Interhemispheric difference of pallidal local field potential activity in cervical dystonia. *J. Neurol. Neurosurg. Psychiatry* 85, 306–310. <https://doi.org/10.1136/jnnp-2013-305476>.
- Moll, C.K.E., Galindo-Leon, E., Sharott, A., Gulberti, A., Buhmann, C., Koeppen, J.A., Biermann, M., Bäumer, T., Zittel, S., Westphal, M., Gerloff, C., Hamel, W., Münchau, A., Engel, A.K., 2014. Asymmetric pallidal neuronal activity in patients with cervical dystonia. *Front. Syst. Neurosci.* 8, <https://doi.org/10.3389/fnsys.2014.00015>.
- Myrov, V., Sedov, A., Belova, E., 2019. Neural activity clusterization for estimation of firing pattern. *J. Neurosci. Methods* 311, 164–169. <https://doi.org/10.1016/j.jneumeth.2018.10.017>.
- Sedov, A., Popov, V., Shabalov, V., Raeva, S., Jinnah, H.A., Shaikh, A.G., 2017. Physiology of midbrain head movement neurons in cervical dystonia: physiology of midbrain in cervical dystonia. *Mov. Disord.* 32, 904–912. <https://doi.org/10.1002/mds.26948>.
- Sedov, A., Ussova, S., Semenova, U., Gamaleya, A., Tomskiy, A., Crawford, J.D., Corneil, B., Jinnah, H.A., Shaikh, A.G., 2019. The role of pallidum in the neural integrator model of cervical dystonia. *Neurobiol. Dis.* 125, 45–54. <https://doi.org/10.1016/j.nbd.2019.01.011>.
- Shaikh, A.G., Zee, D.S., Crawford, J.D., Jinnah, H.A., 2016. Cervical dystonia: a neural integrator disorder. *Brain* 139, 2590–2599. <https://doi.org/10.1093/brain/aww141>.

A motor control model of task-specific dystonia and its rehabilitation

21

Anna Sadnicka^{a,b,*}, Jaume Rosset-Llobet^c^a*Motor Control and Movement Disorder Group, Institute of Molecular and Clinical Sciences,
St George's University of London, London, United Kingdom*^b*Clinical and Movement Neurosciences, UCL Queen Square Institute of Neurology,
London, United Kingdom*^c*Institut de l'Art. Medicina & Fisiologia, Terrassa, (Barcelona) Spain***Corresponding author: e-mail address: asadnick@sgul.ac.uk*

Abstract

Task-specific dystonia is a painless deficit of motor control specific to a particular motor skill. In this article we present a motor control model which integrates risk factors for the disorder with the neuroscientific literature of skill learning in health. We particularly focus on the idea that the amount and type of movement variability is critical and show how retraining therapies such as Differential Learning which reintroduces variability into practice can restore motor performance.

Keywords

Task-specific dystonia, Motor control, Model, Rehabilitation, Sensory Motor Retuning, Differential Learning

1 Introduction

Skilled movement represents one of the pinnacles of human development. Professional athletes, dancers and musicians hone their skills through hours of training and there is great beauty in the resulting performance. Worldwide, society has an arts and sports culture embedded in the celebration of such skill. However, the demands placed on the brain and body for such motor excellence are not without risks. In an unfortunate proportion of individuals, a painless deficit of motor control specific to a particular motor skill emerges called task-specific dystonia ([Altenmuller, 2008](#)). The most common subtypes are writing dystonia and musicians' dystonia but the disorder can affect the performance of any skill (from the foot of a flamenco dancer through to golfers' yips) ([Dhungana and Jankovic, 2013](#);

Garcia-Ruiz et al., 2011). Task-specific dystonia is predictably disabling due to its association with skilled tasks that are required for or which define the individuals' occupation. For example, within groups of professional musicians, the prevalence is approximately 1% and the disorder can mark the end of performing careers (Altenmüller et al., 2014).

For centuries, the pathophysiology of the disorder has remained obscure, with disease models oscillating between the domains of psychiatry and neurology (Lin et al., 2006). Task-specific dystonia is currently considered a subtype of dystonia, a neurological disorder characterized by an abnormality of posture (Albanese et al., 2013). However, traditional dystonic neurophysiological markers such as enhanced plasticity (Sadnicka et al., 2014) or reduced inhibition (Kassavetis et al., 2018) are unable to reliably identify patients with task-specific dystonia (ranges overlapping with controls, similar patterns of abnormalities are observed across a range of neurological disorders). Suggesting that subtle and non-specific shifts in excitability may be epiphenoena removed from the core pathophysiology. Neurophysiological abnormalities are also unable to explain why only an individual task is affected, as abnormalities are documented in circuits subserving unaffected body regions (Quartarone et al., 2008). Disease models built on such foundations such as the disordered sensory homunculus of the affected body part (Elbert et al., 1998) are also difficult to reproduce with updated and more reliable methodology (Ejaz et al., 2016) with inconsistent responses noted with retraining based on such principles (sensory re-education) (Butler et al., 2018).

So what does cause task-specific dystonia? We argue that once freed from traditional dystonia disease frameworks a motor control model can be built from existing clinical and experimental data (Sadnicka et al., 2018). The isolated and task-specific deficit clearly ties the problem to a specific motor skill, as at least at onset, the body region affected can be used normally for other tasks. Task-specific dystonia is therefore best understood by the integration of its clinical features with the neuroscientific literature of skill learning in health. In this article, we discuss the range of risk factors for task-specific dystonia and propose mechanisms by which such factors can translate into motor dysfunction. We particularly focus on the idea that the amount and type of movement variability is critical and show how retraining therapies such as Differential Learning which reintroduces variability into practice can restore motor performance.

2 Risk factors for task-specific dystonia

A range of environmental and genetic risk factors are associated with task-specific dystonia. Environmental risk factors can be subdivided according to the components required to perform any task (Fig. 1A); parameters that define the task and the tool; the central nervous system which includes the network that encodes skill performance, modulated by the individual's psychological state; and the periphery or characteristics of the body region that performs the task (Altenmüller and Jabusch, 2010; Sadnicka et al., 2018). As all components are required to work

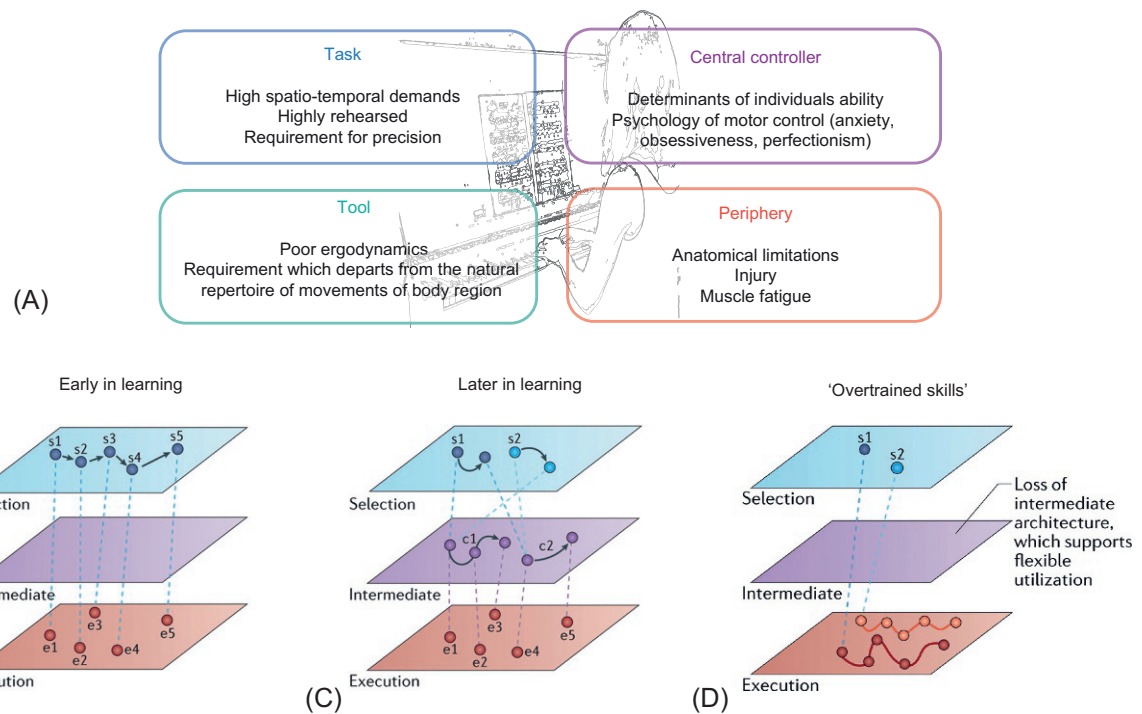


FIG. 1

(A) Risk factors for task-specific dystonia (B) Early skill learning is effortful and involves mapping individual task elements at the selection level (s1-s5) to execution elements (e1-e5) (C) Later in skill learning mechanisms such as chunking are used and chunks (c1, c2) can be flexibly combined in new sequences (s1 versus s2) (D) In "overtrained" skills which are highly optimized the representation at the intermediate level may be lost.

Panels (B)–(D) are taken from Sadnicka, A., Kornysheva, K., Rothwell, J.C., Edwards, M.J., 2018. A unifying motor control framework for task-specific dystonia.

Nat. Rev. Neurol. 14, 116–124.

in concert to maintain task performance, a change in one component prompts a change or shift in others, each component a node within a dynamic network required to function in equilibrium for healthy performance. Subdividing risk factors in this manner reveals a risk profile specific to the individual which can be used to tailor management as patients with task-specific dystonia are heterogeneous.

Naturally, the task-specificity of this disorder focuses one on how *task* can confer risk. The highest relative prevalence is found in musicians; 1 in 100 in some studies, but the real figures are likely to be higher as many affected musicians are not diagnosed (Rosset-Llobet et al., 2009a). Within this group, dystonia preferentially affects the hand required to perform with the highest spatiotemporal demand (Altenmuller and Jabusch, 2009; Rosset-Llobet and Fàbregas-Molas, 2013); the right hand in keyboard players and the left hand in bowed instrument players. The increased incidence in classical musicians over jazz musicians also highlights that the invariant temporal and spatial parameters defined on the sheet music of a classical musician affords risk over the inherent flexibility of notes and timing in jazz. Task-specific dystonia typically affects highly rehearsed skills, most frequently presenting in the decade 30–40 (Rozanski et al., 2015). Therefore, dystonia has a predilection for tasks which push spatiotemporal control to its limits, require invariant accuracy and affects tasks which are highly rehearsed.

The influence of *tool* is beautifully exemplified by the shifting prevalence according to the tools used during different historical eras. For example, many telegraph operators developed motor problems of the finger used with the telegraph key which communicated Morse code (Ferguson, 1971; Suzuki et al., 2012). Here the need for individuated, forceful movements departed from the natural repertoire of finger movements with a precise rhythmical definition is salient. As technology advances, writing is less required and a decline or even extinction of writing dystonia is likely. Furthermore, with increasingly ergodynamic tools in the work place the hope is that this leads to a reduction in prevalence in most occupational domains outside of the arts sphere (for example, there are few reports of computer-related dystonia Suzuki et al., 2012).

In order to perform any skill the *periphery* must be capable of a complex set of task requirements and operate within its physiological constraints (Leijnse et al., 2015; Rosset-Llobet et al., 2009b). Correspondingly, peripheral risk factors for task-specific dystonia include inherent limitations (such as the individual's ability to independently move fingers) and acquired peripheral risk factors which temporarily change the operating parameters of the body region (such as local injury or muscle fatigue due to over practice) (Leijnse et al., 2015).

Centrally mediated risk factors encompass both neural skill control and its psychology. For athletes and musicians, the determinants of the “ceiling” of capacity of the nervous system is an important consideration. Those that reach professional levels of competition or performance usually require a combination of both inherent “talent” (such as their capacity for neural plasticity or processing) and intensive and structured nurture through exposure and training. Correspondingly, musicians who start practicing after the age of 10 have an increased incidence of task-specific

dystonia, which is after the most sensitive/plastic periods of neural development have occurred (Altenmüller and Jabusch, 2009).

The psychology within which the individual rehearses and performs their motor skill is also critical. Compared to unaffected musicians those with task-specific dystonia are six times more likely to exhibit increased levels of anxiety, perfectionism or stress (Ioannou and Altenmüller, 2014). The influence of acute stress and its interaction over motor control is also apparent. For example, a cartographer for the National Guard had to participate in daily drills in which he had to make a dot on a map to show where bombing practice was to occur (Shamim et al., 2011). Although they were practice drills, they were tense situations and he started having difficulty making the dot, the onset of task-specific dystonia (Shamim et al., 2011).

Finally, genetic factors are also thought to be important and are suggested by the male preponderance and positive family history of movement disorders in a proportion of patients (Lohmann et al., 2014; Schmidt et al., 2006). Exactly how genetic and epigenetic factors contribute to the risk profile of an individual remains to be determined. Any process linked to performance of a skill will be influenced by genetics (ranging from the gating of synaptic plasticity through to the determination of personality traits or musical ability).

3 A motor control model of task-specific dystonia

In this section, we discuss how such epidemiological factors can be mapped to mechanism when profiled and interpreted within the rich neuroscientific literature which studies motor skill learning in health.

3.1 Motor skill learning in health

In order to initiate such a discussion we briefly outline core features of motor skill learning in health. A broad definition of motor skill learning is any neuronal changes that allow an organism to accomplish a motor task better, faster, or more accurately than before (Diedrichsen and Kornysheva, 2015). Skill learning is thought to involve various levels of a motor hierarchy. Within this motor hierarchy one fundamental division is between action selection and action execution (Diedrichsen and Kornysheva, 2015). The execution level causes muscle activity, the neurons that project to the spinal cord and synapse on motor neurones which ultimately cause the peripheral muscles to contract. Within the execution level, movement fragments are thought to be encoded within sub-networks of neurons that code for motor synergies which once activated reliably produce specific spatial-temporal patterns of coordinated muscle activity (Diedrichsen and Kornysheva, 2015). The selection level then activates the most appropriate set of motor synergies in a task-specific manner (dotted lines in Fig. 1B) (Diedrichsen and Kornysheva, 2015). With practice, refinement of reaction time-accuracy trade-offs are considered one of the hallmarks

of skill learning (Telgen et al., 2014). This in part is mediated by the formation of intermediate representations which bind together execution elements. For example, experimentally, in addition to sequence completion becoming faster and more accurate, performance starts to show idiosyncratic temporal groups or chunks (Diedrichsen and Kornysheva, 2015). Elementary movements that are bound into one chunk are retrieved faster and more accurately than when the selection level triggers them individually. Such an organization also has the advantage that acquired chunks can be used in the context of novel sequences (Fig. 1C). For example the learning of one sequence (s_1) consisting of two chunks (c_1, c_2) generalizes to the execution of another sequence (s_2) which contains the same chunks in a different order (c_2, c_1) (Sadnicka et al., 2018).

Modular encoding of more abstract features of a task can also endow flexibility to the motor control system. Behaviorally, if an individual is trained on a sequence with temporal (rhythm) and spatial (finger press order) identifiers, a post-training advantage is seen if the temporal features are transferred to a new spatial sequence and vice versa (Kornysheva et al., 2013). Functional MRI data reveals that the temporal and spatial features of the sequence are independently represented in overlapping regions of the pre-motor cortex (Kornysheva and Diedrichsen, 2014). The primary motor cortex in contrast represents the two sequences features (temporal, spatial) in a non-separable fashion (Kornysheva and Diedrichsen, 2014).

Thus as learning progresses intermediate level representations of motor skill features (chunking, modular encoding) are thought to ensure both flexibility and efficiency in motor skill learning (Diedrichsen and Kornysheva, 2015; Sadnicka et al., 2018). Decreasing reliance on the selection level also frees the cognitive system to attend to other related or unrelated tasks whilst the motor system is increasingly automatic in its operation.

3.2 Neural correlates of skill expertise

In high risk groups such as professional musicians and athletes the limitations of the neural networks supporting the skill are likely to be an important contributory factor (Sadnicka et al., 2018). Initially, as we have exemplified in healthy skill learning, chunking a sequence offers a behavioral gain in terms of reaction time and is thought to reduce the overall computational complexity associated with learning an entire sequence as a single horizon/sequence (Ramkumar et al., 2016). However, experimental data suggest that repetitive practice of stereotyped movements can lead to the formation of progressively longer motor chunks (Ramkumar et al., 2016). This shift is thought to reflect a trade-off between cost of computation versus efficiency (Ramkumar et al., 2016). Stereotyped practice is thought to iteratively reduce impediments to more complex computation (for example, the relative offset of cost if an individual is required to produce the same movement many times) and correspondingly the chunk structure appears to progressively elongate maximizing the efficiency of the movement (Ramkumar et al., 2016). Such changes are likely to be accentuated in groups whose profession it is to pursue performance perfection

and efficiency through practice, an extreme version of the normal mode of operation. Furthermore, as chunks increase in length it is also thought that they are increasingly contextual and tied to the individual task or body region. Informatively, poor transfer of these performance gains to other tasks seems to be accentuated if a narrow training repertoire is applied, in contrast to more varied training approaches (Boutin et al., 2012). Practice predating the development of task-specific dystonia is often particularly intensive and stereotyped.

Therefore, in such highly rehearsed tasks, intermediate-level representations that previously conferred flexibility for related tasks could become redundant. If highly stereotyped sequences begin to dominate the movement repertoire, the original transferrable chunk structure could disappear, as the concatenation into long execution bound mega-synergies effectively replaces such intermediate elements (Fig. 1D). Such an architecture within the motor hierarchy could reliably encode an extreme optimization of performance parameters with little variability across movement repetitions. However, the likely cost of such optimization is that the skill representation retains little capacity for flexibility and generalization to other contexts.

3.3 Psychology of motor control

The impact of psychological influences is worth emphasizing as such factors can have an important effect on skill learning. For example, across animal species in stressful situations a reduction in movement variability and exploration is seen, repetition of movements with rigid movement patterns thought to help one regain a feeling of control (Lang et al., 2015). Experimentally, inducing anxiety in healthy controls during baseline practice undermines later sequence learning and at the behavioral level the mechanism appears to be via a reduction in trial-by-trial variability (Sporn et al., 2018). An unnatural reduction of physiologically informative variability secondary to factors such as anxiety or a personality type which favors rigidity of practice are likely to be detrimental. It is well established that in health subsets of variability are informative for skill learning and are dynamically regulated by the motor control system in response to task requirements (Wu et al., 2014).

Another important psychological factor is the influence of attention. For example, the negative effects of self-focus are commonly discussed within the sports science literature (for example, in relation to “the yips” in golfers) and may be equally relevant in forms of motor impairment that share phenomenology in musicians and writers such as motor block or choking under pressure (Edwards and Rothwell, 2011). Triggering factors for task-specific dystonia such as injury, pain and explicit attempts to alter technique or performance will naturally focus attention on the body region. Misdirected attention can then focus on the mechanics of movement rather than on the external consequences or goals of movement and such a strategy has been shown to worsen skill performance (Lewthwaite and Wulf, 2017). Such mechanisms are paramount when considering the cartographer that struggled to mark a dot on the map (Shamim et al., 2011).

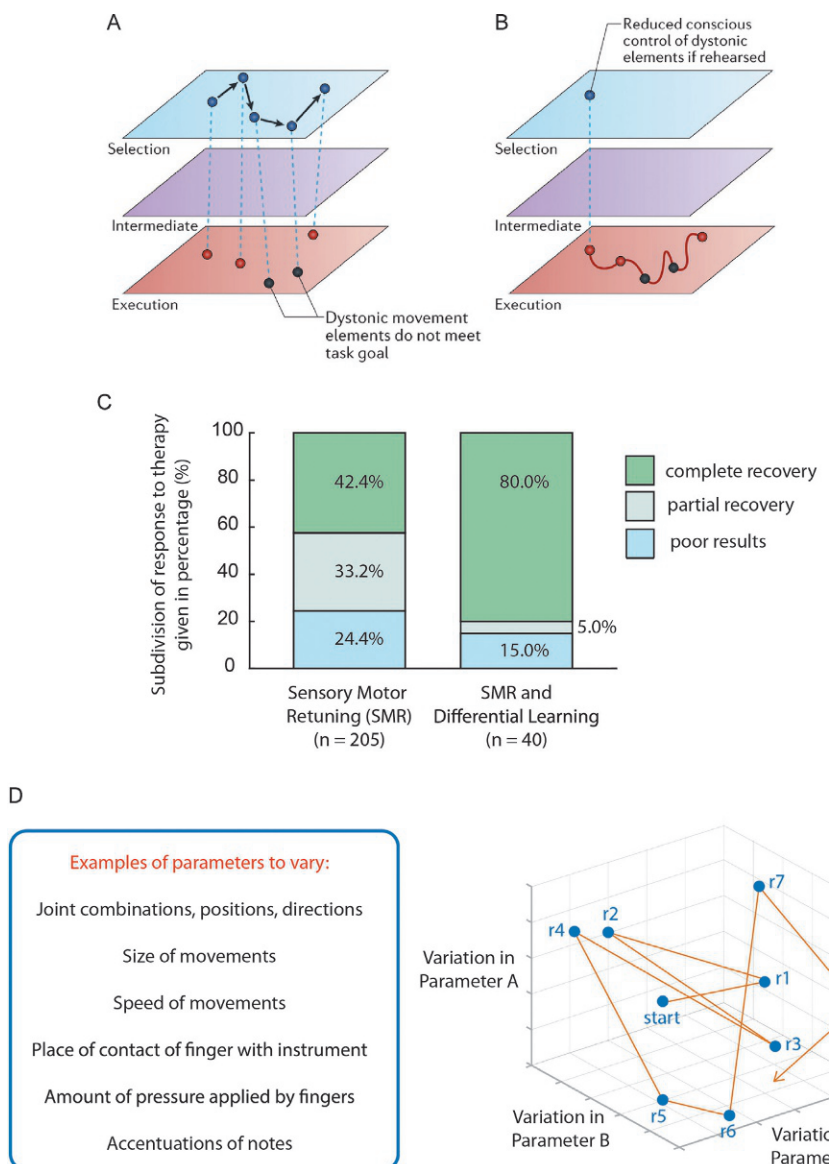
3.4 Onset of dystonia

In many individuals the onset of task-specific dystonia is then commonly precipitated by a triggering event (Rosset-Llobet and Fàbregas-Molas, 2013). Such events include a change in playing technique, injury, a new instrument with a slightly different action/dimension. Conceptually these triggers are best described simply as mismatches between the capacity of the individual's motor control system and the required movement defined by the task and the tool. Some mismatches between capacity and requirement are biomechanical in nature. For example, a task with a high force requirement will limit the capacity to make individuated finger movements leading to greater unintentional and undesired movements of neighboring fingers. Alternatively, changes in capacity due to fatigue or injury of the body can also result in an effector system that responds more erratically to a given motor command. A change in task requirements might also result from external factors, such as changes in the size of a tool or an attempt by the performer to change their instrumental technique. As discussed, in high risk groups, many of their associated risk factors can be interpreted as mechanisms via which the central representation of skill can become particularly narrow in its remit and the required trigger can be a very minor event indeed.

If the individual can accommodate this change in the task requirement by adjusting and scaling its motor commands or finding an alternative combination of neural elements to maintain performance peripherally, an effective compensation has been found. If, however, the new task requirement cannot be accommodated, the performer is pushed outside the boundaries of their learned skill. Task performance then breaks down as no effective compensation is available.

Once a critical mismatch has occurred, novel motor control strategies alien to the existing neural representation of skill must be employed to maintain task performance. However, de novo solutions are unlikely to be able to match or maintain the level of skill performance that was formerly encoded by a hierarchy of neuronal elements optimized over many years of practice (Sadnicka et al., 2018). The skills that are usually affected in task-specific dystonia are characterized by automaticity with little conscious control of movement. By contrast, during de novo learning, task requirements are explicitly mapped to basic execution elements, a time-consuming process that conflicts with the demand for rapid task reproduction within a millisecond timescale. Access to subcomponents of more-abstract movement elements, which previously underpinned some features of expert task performance, is limited. Thus, once task performance has broken down, alternative motor control options are ill-equipped to immediately reinstate motor performance using new elements. Inappropriate and dysfunctional movements are likely to be produced, which are unable to match required task performance levels, marking the onset of task-specific dystonia (Fig. 2A) (Sadnicka et al., 2018).

If dysfunctional or dystonic movements are repeatedly practiced they will become encoded in a similar manner to any other sequence of movements. Conscious access to dystonic movement elements declines, causing frustration for individuals

**FIG. 2**

Neural encoding of task-specific dystonia and its rehabilitation (A) Once a critical mismatch has occurred de novo learning mechanisms are unable to meet task goals. This results in dysfunctional/dystonic movements starting to be encoded within skill network. (B) If dysfunctional/dystonic movements are repeated these will become encoded within lower levels of the hierarchy and there will be less conscious access to dystonic elements. (C) Therapy results before and after adding Differential Learning to Sensory Motor Retuning (SMR). 245 consecutive patients treated at Institut de l'Art, Spain, 2011–2017. Data from a proportion of these patients has been published in preliminary format

(Continued)

with undiagnosed task-specific dystonia as they attempt to implement strategies to address their movement difficulties. Subsequently, skill representations that are activated for a particular context or performance goal will become corrupted, with dystonic movements incorporated into their neural skill network (Fig. 2B) (Sadnicka et al., 2018).

This model for task-specific dystonia is representational and has purposefully resisted providing a direct mapping between the different levels of motor skill learning and specific neural regions as this relationship is likely to be complex. For example, the cerebellar and basal ganglia circuitry form partially parallel loops with multiple cortical regions and may therefore play a role in each of the hierarchical levels of skill learning. Furthermore, emerging treatments for task-specific dystonia such as Differential Learning detailed below target theoretical and behavioral correlates which are thought to involve a broad brain network.

4 Management of task-specific dystonia

4.1 Prevention

One of the important implications of this model is that a proportion of cases of task-specific dystonia could be prevented. As discussed, many occupational forms of task-specific dystonia are characterized by mismatches between the tool or task requirements and the capability of the individual. Improving the ergonomics of tools and limiting task parameters that stress the motor system is likely to be beneficial. However, professional musicians and athletes cannot modify their tool or task requirements to any great extent. Moreover, in response to developing a problem the individual often themselves submits the body to greater and greater demands with the intention of improving aspects of technique or performance. Prevention strategies therefore should focus on modifiable factors; maximizing the “resilience” of relevant representations in the brain, maintaining efficient physiological movements of the periphery, and nurturing a healthy psychological profile.

FIG. 2—Cont'd

(Rosset-Llobet and Fabregas-Molas, 2018). Patients have been classified into three groups depending on their self-reported functional outcome: complete recovery (those who returned to instrumental activity with full recovery, with no dystonia symptoms at all), partial recovery (those with improvement of dystonia symptoms making possible the return to instrumental activity, but still feeling some functional limitation) and poor result (patients who dropped out of treatment or having had certain improvement but not compatible with their musical career). (D) Differential Learning reintroduces noise into training. Parameters are varied in a stochastic manner as shown across repetitions of three theoretical parameters in the three-dimensional scatter and line plot (repetition (r) 1 to 8 demonstrated). Examples of the many parameters that can be varied are given in the box.

Panel (A) is taken from Sadnicka, A., Kornysheva, K., Rothwell, J.C., Edwards, M.J., 2018. A unifying motor control framework for task-specific dystonia. Nat. Rev. Neurol. 14, 116–124.

4.2 Traditional management

Once task-specific dystonia has developed conventional dystonia treatments are often tried. Medications such as trihexyphenidyl have inconsistent effects and are often limited by their side effects (Jabusch et al., 2005; Termsarasab et al., 2016; van Vugt et al., 2014). Botulinum toxin injections, which block the transmission of the nerve to dystonic muscles are often helpful in specialist settings (although some query their long term efficacy) (Kruisdijk et al., 2007; Lungu et al., 2011). However, botulinum toxin injections appear to be acting by suppressing the endpoint of the disease, the inappropriate muscle contractions, rather than addressing the underlying mechanism. Recently a series of patients have received thalamotomy with good outcomes reported (Taira et al., 2006). However, its mechanism of action is entirely unknown, the profile of motor deficits largely uncharacterized and clinical trials are needed before such treatment should be considered mainstream.

Rehabilitation or retraining methods continue to offer a promising treatment option for task-specific dystonia. One of the main form of rehabilitation for task-specific dystonia is Sensory Motor Retuning which was developed by Victor Candia in the 1990s (Candia et al., 1999). Sensory Motor Retuning introduces a novel sensory input by the use of orthotic devices, changing the manner in which the brain perceives the task and facilitating the learning of a healthy performance pattern. For example, splints (to place one or more fingers in a particular position) or rubber bands (that introduce a forced finger flexion or extension in one or more fingers) have commonly been used with the patient performing exercises on the instrument (Rosset-Llobet and Fàbregas-Molas, 2013). Its efficacy is mixed. For example, in a cohort of 205 consecutive patients treated with Sensory Motor Retuning, self-reported functional outcome yields 24% with poor results, 33% with partial recovery with 42% with complete recovery (Fig. 2C). Multifaceted retraining approaches that draw on multiple specific strategies for task-specific dystonia and generic therapy approaches have also been tried (Butler et al., 2018). However when analyzed systematically it remains difficult to clearly identify which elements are the effective ones (Butler et al., 2018; Rosset-Llobet and Fàbregas-Molas, 2013).

4.3 Emerging treatments

The hierarchical motor control model outlined in this paper, invites one to speculate that making a musician's nervous system more flexible could be used in the prevention and treatment of task-specific dystonia. Here, the work of Schöllhorn, a major proponent of Differential Training/Learning, is particularly relevant (Schöllhorn et al., 2012). Differential Learning has the primary aim of enlarging fluctuations or stochastic perturbations that occur over movement repetitions in order to provide additional information to the learner (Schöllhorn et al., 2012). Variation in normally "invariant" parameters are pursued (for example, the joints used, movement geometry, tool used, and environment Fig. 2D) (Schöllhorn et al., 2012).

In task-specific dystonia, if a musician, due to risk factors such as psychological behavior or training workload, shapes a rigid and inflexible representation of their skill, he or she will not easily be able to adapt to internal or external changes. This can lead to dystonia if he or she faces a critical mismatch between an inflexible nervous system and a new task parameter or requirement. Conceptually, Differential Learning therefore offers a targeted manner by which to retrain individuals with task-specific dystonia.

Introducing high doses of variation during retraining is thought to achieve a number of aims. For example, skill networks and neural representations are thought to be “destabilized” facilitating the formation of new functional skill networks (Schollhorn et al., 2010). The use of Differential Learning is also thought to encourage the neural control system to become more flexible and able to accommodate changes the functional parameters of a task (Lungu et al., 2011).

One method of applying this in clinical rehabilitation of task specific dystonia is to perform Sensory Motor Retuning exercises with a change of task parameters every 5 to 10 s (Table 1). The aim is not to look for solutions (a way to play where dystonia symptoms improve or where the patient feels more comfortable) but to introduce

Table 1 Example of a technical exercise on the piano playing C Major scales with both hands over 3 min.

Parameter	Change
Finger joint angle	Metacarpophalangeal joint flexion and interphalangeal complete extension Metacarpophalangeal joint extension and moderate interphalangeal flexion All joints in extension All joints in slight flexion All joints in flexion Metacarpophalangeal join in extension and maximal interphalangeal join flexion
Wrist position	Neutral position Slightly bended Moderately extended Right wrist slightly bended, left slightly extended Right wrist slightly extended, left slightly bended Moving from moderate extension to flexion each scale
Finger force	All fingers pressing keys very softly Right hand pressing keys very softly and left strongly All fingers softly but right and left thumbs Right hand softly but index and left hand strongly but middle Odd fingers softly and even strongly Each three notes change from softly to strongly and vice versa

Each change should be rehearsed for a duration of 10s.

noise (different ways to play, can be more or less functional than the original one). Movements do not have to make any biomechanical or technical sense and outcomes such as the final sound are also considered unimportant as this will otherwise limit the repertoire of movements that can be incorporated into training, hindering motor system fluctuations and reorganization. Recently, 40 patients have finished a protocol that combined Sensory Motor Retuning with Differential Learning (preliminary data published [Rosset-Llobet and Fabregas-Molas, 2018](#)). Notably 80% had complete recovery with only 15% reporting poor results and 5% reporting partial recovery ([Fig. 2C](#)).

5 Conclusions

The proposed motor control model has its roots in observations made by patients and clinicians throughout the centuries. We are now additionally aided by a neuroscientific literature which studies skill learning in health which allows one to elaborate on mechanism and infer potential neurobiological correlates. A motor control model for task-specific dystonia is most able to describe its features and provides a conceptual background to emerging rehabilitative therapies. Promisingly for those in the performance arts such as musicians, Differential Learning shows an encouraging ability to facilitate motor system functional reorganization and flexibility, both a possible preventive tool and therapeutic aid.

References

- Albanese, A., Bhatia, K., Bressman, S.B., et al., 2013. Phenomenology and classification of dystonia: a consensus update. *Mov. Disord.* 28, 863–873.
- Altenmuller, E., 2008. Neurology of musical performance. *Clin. Med. (Lond.)* 8, 410–413.
- Altenmuller, E., Jabusch, H.C., 2009. Focal hand dystonia in musicians: phenomenology, etiology, and psychological trigger factors. *J. Hand Ther.* 22, 144–154, quiz 55.
- Altenmuller, E., Jabusch, H.C., 2010. Focal dystonia in musicians: phenomenology, pathophysiology, triggering factors, and treatment. *Med. Probl. Perform. Art.* 25, 3–9.
- Altenmuller, E., Ioannou, C.I., Raab, M., Lobinger, B., 2014. Apollo's curse: causes and cures of motor failures in musicians: a proposal for a new classification. *Adv. Exp. Med. Biol.* 826, 161–178.
- Boutin, A., Badets, A., Salesse, R.N., Fries, U., Panzer, S., Blandin, Y., 2012. Practice makes transfer of motor skills imperfect. *Psychol. Res.* 76, 611–625.
- Butler, K., Sadnicka, A., Freeman, J., et al., 2018. Sensory-motor rehabilitation therapy for task-specific focal hand dystonia: a feasibility study. *Hand Ther.* 23, 53–63.
- Candia, V., Elbert, T., Altenmuller, E., Rau, H., Schafer, T., Taub, E., 1999. Constraint-induced movement therapy for focal hand dystonia in musicians. *Lancet* 353, 42.
- Dhungana, S., Jankovic, J., 2013. Yips and other movement disorders in golfers. *Mov. Disord.* 28, 576–581.
- Diedrichsen, J., Kornysheva, K., 2015. Motor skill learning between selection and execution. *Trends Cogn. Sci.* 19, 227–233.

- Edwards, M.J., Rothwell, J.C., 2011. Losing focus: how paying attention can be bad for movement. *Mov. Disord.* 26, 1969–1970.
- Ejaz, N., Sadnicka, A., Wiestler, T., Butler, K., Edwards, M., Diedrichsen, J., 2016. Finger representations in sensorimotor cortex are not disrupted in musician's dystonia. In: Society for Neuroscience Annual Meeting 2016. <https://doi.org/10.1038/srep37632>.
- Elbert, T., Candia, V., Altenmuller, E., et al., 1998. Alteration of digital representations in somatosensory cortex in focal hand dystonia. *Neuroreport* 9, 3571–3575.
- Ferguson, D., 1971. An Australian study of telegraphists' cramp. *Br. J. Ind. Med.* 28, 280–285.
- Garcia-Ruiz, P.J., del Val, J., Losada, M., Campos, J.M., 2011. Task-specific dystonia of the lower limb in a flamenco dancer. *Parkinsonism Relat. Disord.* 17, 221–222.
- Ioannou, C.I., Altenmuller, E., 2014. Psychological characteristics in musicians dystonia: a new diagnostic classification. *Neuropsychologia* 61, 80–88.
- Jabusch, H.C., Zschucke, D., Schmidt, A., Schuele, S., Altenmuller, E., 2005. Focal dystonia in musicians: treatment strategies and long-term outcome in 144 patients. *Mov. Disord.* 20, 1623–1626.
- Kassavetis, P., Sadnicka, A., Saifee, T.A., et al., 2018. Reappraising the role of motor surround inhibition in dystonia. *J. Neurol. Sci.* 390, 178–183.
- Kornysheva, K., Diedrichsen, J., 2014. Human premotor areas parse sequences into their spatial and temporal features. *Elife* 3, e03043.
- Kornysheva, K., Sierk, A., Diedrichsen, J., 2013. Interaction of temporal and ordinal representations in movement sequences. *J. Neurophysiol.* 109, 1416–1424.
- Kruisdijk, J.J., Koelman, J.H., Ongerboer de Visser, B.W., de Haan, R.J., Speelman, J.D., 2007. Botulinum toxin for writer's cramp: a randomised, placebo-controlled trial and 1-year follow-up. *J. Neurol. Neurosurg. Psychiatry* 78, 264–270.
- Lang, M., Kratky, J., Shaver, J.H., Jerotijevic, D., Xygalatas, D., 2015. Effects of anxiety on spontaneous ritualized behavior. *Curr. Biol.* 25, 1892–1897.
- Leijnse, J.N., Hallett, M., Sonneveld, G.J., 2015. A multifactorial conceptual model of peripheral neuromusculoskeletal predisposing factors in task-specific focal hand dystonia in musicians: etiologic and therapeutic implications. *Biol. Cybern.* 109, 109–123.
- Lewthwaite, R., Wulf, G., 2017. Optimizing motivation and attention for motor performance and learning. *Curr. Opin. Psychol.* 16, 38–42.
- Lin, T., Shamim, E., Hallett, M., 2006. Focal hand dystonia. *Pract. Neurol.* 6, 278–287.
- Lohmann, K., Schmidt, A., Schillert, A., et al., 2014. Genome-wide association study in musician's dystonia: a risk variant at the arylsulfatase G locus? *Mov. Disord.* 29, 921–927.
- Lungu, C., Karp, B.I., Alter, K., Zolbrod, R., Hallett, M., 2011. Long-term follow-up of botulinum toxin therapy for focal hand dystonia: outcome at 10 years or more. *Mov. Disord.* 26, 750–753.
- Quartarone, A., Morgante, F., Sant'angelo, A., et al., 2008. Abnormal plasticity of sensorimotor circuits extends beyond the affected body part in focal dystonia. *J. Neurol. Neurosurg. Psychiatry* 79, 985–990.
- Ramkumar, P., Acuna, D.E., Berniker, M., Grafton, S.T., Turner, R.S., Kording, K.P., 2016. Chunking as the result of an efficiency computation trade-off. *Nat. Commun.* 7, 12176.
- Rosset-Llobet, J., Fàbregas-Molas, S., 2013. *La Dystonie du Musicien*. Alexitere Editions, Montauvan.
- Rosset-Llobet, J., Fabregas-Molas, S., 2018. Chapter 51: Rehabilitation and Plasticity of Task-Specific Focal Hand Dystonia, first ed. Cambridge University Press.
- Rosset-Llobet, J., Candia, V., Fabregas i Molas, S., Dolors Rosines i Cubells, D., Pascual-Leone, A., 2009a. The challenge of diagnosing focal hand dystonia in musicians. *Eur. J. Neurol.* 16, 864–869.

- Rosset-Llobet, J., Garcia-Elias, M., Montero, J., Valls-Sole, J., Pascual-Leone, A., 2009b. Linburg's syndrome, can it cause focal dystonia? *Mov. Disord.* 24, 1704–1706.
- Rozanski, V.E., Rehfuss, E., Botzel, K., Nowak, D., 2015. Task-specific dystonia in professional musicians. A systematic review of the importance of intensive playing as a risk factor. *Dtsch. Arztebl. Int.* 112, 871–877.
- Sadnicka, A., Hamada, M., Bhatia, K.P., Rothwell, J.C., Edwards, M.J., 2014. A reflection on plasticity research in writing dystonia. *Mov. Disord.* 29, 980–987.
- Sadnicka, A., Kornysheva, K., Rothwell, J.C., Edwards, M.J., 2018. A unifying motor control framework for task-specific dystonia. *Nat. Rev. Neurol.* 14, 116–124.
- Schmidt, A., Jabusch, H.C., Altenmuller, E., et al., 2006. Dominantly transmitted focal dystonia in families of patients with musician's cramp. *Neurology* 67, 691–693.
- Schollhorn, W.I., Beckmann, H., Davids, K., 2010. Exploiting system fluctuations. Differential training in physical prevention and rehabilitation programs for health and exercise. *Medicina (Kaunas)* 46, 365–373.
- Schollhorn, W., Hegen, P., Davids, K., 2012. The non linear nature of learning—a differential learning approach. *Open Sports Sci. J.* 5, 100–112.
- Shamim, E.A., Chu, J., Scheider, L.H., Savitt, J., Jinnah, H.A., Hallett, M., 2011. Extreme task specificity in writer's cramp. *Mov. Disord.* 26, 2107–2109.
- Sporn, S., Hein, T., Herrojo, R.M., 2018. Bursts and variability of beta oscillations mediate the effect of anxiety on motor exploration and motor learning. *bioRxiv*, <https://doi.org/10.1101/442772>.
- Suzuki, K., Takano, M., Hashimoto, K., et al., 2012. Computer mouse-related dystonia: a novel presentation of task-specific dystonia. *J. Neurol.* 259, 2221–2222.
- Taira, T., Ochiai, T., Goto, S., Hori, T., 2006. Multimodal neurosurgical strategies for the management of dystonias. *Acta Neurochir. Suppl.* 99, 29–31.
- Telgen, S., Parvin, D., Diedrichsen, J., 2014. Mirror reversal and visual rotation are learned and consolidated via separate mechanisms: recalibrating or learning de novo? *J. Neurosci.* 34, 13768–13779.
- Termsarasab, P., Thammongkolchai, T., Frucht, S.J., 2016. Medical treatment of dystonia. *J. Clin. Mov. Disord.* 3, 19.
- van Vugt, F.T., Boulet, L., Jabusch, H.C., Altenmuller, E., 2014. Musician's dystonia in pianists: long-term evaluation of retraining and other therapies. *Parkinsonism Relat. Disord.* 20, 8–12.
- Wu, H.G., Miyamoto, Y.R., Gonzalez Castro, L.N., Olveczky, B.P., Smith, M.A., 2014. Temporal structure of motor variability is dynamically regulated and predicts motor learning ability. *Nat. Neurosci.* 17, 312–321.

This page intentionally left blank

Tremor in chronic inflammatory demyelinating polyneuropathy: Proof of unifying network model for dystonia

22

Nataliya Pyatka^a, Alexey Sedov^b, Benjamin L. Walter^c, Hyder A. Jinnah^d,
Aasef G. Shaikh^{a,e,f,*}

^a*Department of Neurology, University Hospitals Cleveland Medical Center and Case Western Reserve University, Cleveland, OH, United States*

^b*Russian Institute for Chemical Physics, Moscow, Russia*

^c*Center for Neurological Restoration, Cleveland Clinic, Cleveland, OH, United States*

^d*Departments of Neurology and Human Genetics, Emory University, Atlanta, GA, United States*

^e*Daroff-DellOsso Ocular Motility Laboratory and Neurology Service, Louis Stokes Cleveland VA Medical Center, Cleveland, OH, United States*

^f*National VA PD Consortium Center, Louis Stokes Cleveland VA Medical Center, Cleveland, OH, United States*

*Corresponding author: Tel.: +1-216-844-1000, e-mail address: aasefshaikh@gmail.com

Abstract

Traditional hypotheses for the pathogenesis of dystonia, the third most common movement disorder, have focused primarily on the basal ganglia. Contemporary theories have emphasized the role of the cerebellum. The modulation of peripheral proprioception also affects dystonia. We proposed a unifying network model for dystonia where the cerebellum, basal ganglia, and peripheral proprioception are connected in a circuit that forms the neural integrator network, ensuring steady position. We suggested that impairment anywhere along this circuit leads to common phenomenology—slow drifts followed by corrective movements, resembling dystonic tremor. We tested this concept in a patient with chronic inflammatory demyelinating polyneuropathy with resulting abnormal proprioception. Quantitative assessment of tremor in this patient revealed drifts in limb position followed by corrective movements and superimposed sinusoidal oscillations—consistent with neural integrator dysfunction. This unique case of chronic inflammatory demyelinating polyneuropathy describes the role of proprioception on the unifying network model for dystonia.

Keywords

Eye movement, Superior colliculus, Basal ganglia, Burst neurons

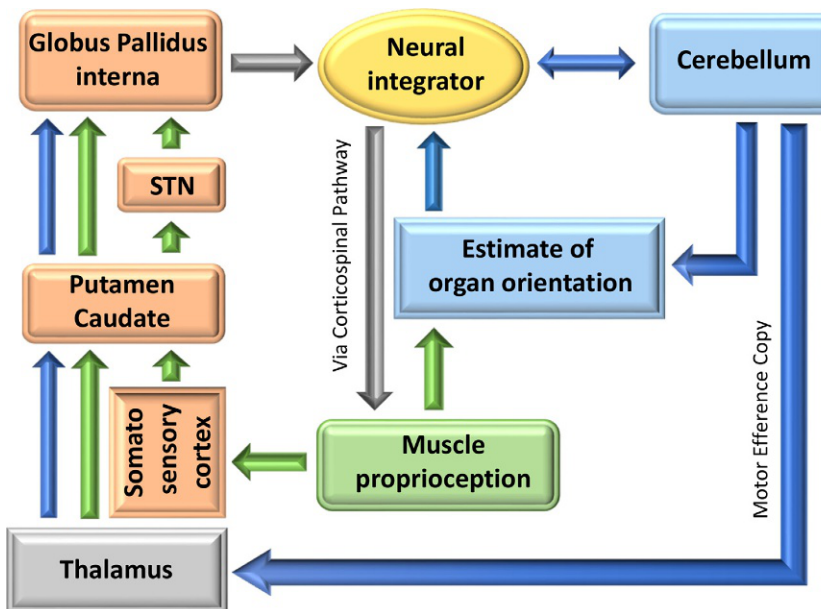
1 Introduction

Dystonia is the third most common movement disorder affecting 3 million people worldwide. It is characterized by a stereotyped pattern of involuntary turning or tilting of the affected organ, often combined with pain and jerky or tremulous movements. Dystonia is stigmatizing and has a profound negative impact on the quality of life, with scores on standardized tests that are comparable to Parkinson's disease, multiple sclerosis, and stroke.

Information regarding brain regions involved in pathophysiology of dystonia is surprisingly limited and often conflicting. Traditional hypotheses for the origin of dystonia have focused on the basal ganglia (Vitek, 2002). In contrast, contemporary theories emphasized the role of the cerebellum (Prudente et al., 2014). Although peripheral proprioception sensors are frequently normal in dystonia, their modulation can effect movement characteristics (Tempel and Perlmutter, 1990). Indeed, a recognized therapy for dystonia with botulinum neurotoxin influences proprioceptive signals (Rosales et al., 1996). These diverse viewpoints lead to important questions. First, how could deficits involving different anatomic structures, such as the globus pallidum and the cerebellum, cause the same disorder? Second, if dystonia is due to deficits in the cerebellum or the globus pallidum, then how could peripheral proprioceptive interventions affect the motor function in dystonia?

We proposed a novel conceptual framework that accommodated currently conflicting information to directly address the above questions. The concept is that abnormal movements in dystonia are due to an impairment in the function of the brain circuit called the neural integrator. This circuit converts a burst of activity (known as a "pulse," a signal related to movement) to steady-state neural firing (known as a "step," a signal related to steady position), assuring a stable position (Shaikh et al., 2016). The neural integrator is part of the final common pathway that projects to the muscles that comprise the peripheral motor plant. The neural integrator is inherently imperfect and its fidelity must be improved by feedback. We conceptualized that the cerebellum, globus pallidum, and peripheral proprioception are mutually connected sources of feedback to the neural integrator (Fig. 1). Impairment anywhere along the feedback network leads to the phenomenology characteristic of dystonia. The signature deficits include: (1) drift in position of the body part followed by rapid correction, leading to asymmetric waveform trajectory with a jerky appearance (Shaikh et al., 2013, 2015b, 2016), (2) sinusoidal oscillations superimposed upon the drifts (Shaikh et al., 2015b), and (3) organ orientation (resting or "null" position) where there are no oscillations (Shaikh et al., 2013, 2015b).

The unifying network model for dystonia predicts that if peripheral proprioception is part of the feedback loop to the neural integrator, then impaired proprioception

**FIG. 1**

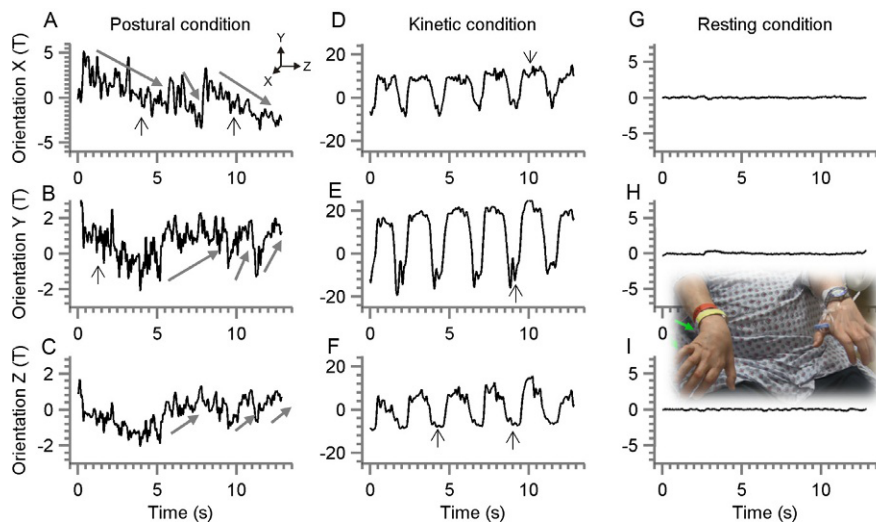
Schematic representation of the integrative network model.

(as seen in certain forms of neuropathies) will lead to drifts in organ position. The drifts will be followed by corrective movements, causing jerky oscillations of the affected body part. We tested this hypothesis in a patient with known history of chronic inflammatory demyelinating polyneuropathy (CIDP) who acutely developed limb dystonia that paralleled worsening of his neuropathy. The hypothesis predicts: (1) drift in hand position during postural condition and subsequent rapid corrective movement that gives the waveform a jerky or saw-tooth appearance, (2) relatively high-frequency sinusoidal oscillations superimposed upon the drifts, (3) worsening of the oscillation amplitude during goal directed movements, and (4) minimal involuntary movements during resting condition. We used quantitative motion analysis to test these predictions in our CIDP patient.

2 Methods

2.1 Clinical case

A 62-year-old man with known CIDP presented with rapidly progressive upper and lower extremity proprioceptive dysfunction. There was an involuntary ulnar deviation of the right hand at the wrist and extension of the fifth digit at the metatarsophalangeal joint but flexion at the interphalangeal joint ([Fig. 2](#)). The abnormal

**FIG. 2**

Example of dystonic tremor during postural (A–C), kinetic (D–F), and resting (G–I) conditions. The angular orientation of the hand with respect to earth's magnetic field (T: tesla) in all three axes of rotations is plotted on the y-axis, while the corresponding time is plotted on the x-axis. In each panel (more clearly seen in panels A–C) the oblique gray arrows depict the drift, followed by rapid corrective movements. The vertical (short) black arrows show an example of sinusoidal oscillations. Inset shows the posturing of the right hand (arrow) consistent with dystonia.

posture of the hand and finger was minimal at rest, but increased during goal directed actions. Such posturing was not seen in the left hand that had jerky hand oscillations. The amplitude of jerky oscillations worsened during goal directed movements. Oscillations were absent at rest. Involuntary posturing of one hand and jerky oscillations of the other hand were diagnostic for bilateral hand dystonia. This subjective clinical assessment triggered instrumented investigation of these oscillations.

2.2 Data acquisition technique

The experiment protocol and the study were approved by the Institutional Review Board at University Hospitals Cleveland Medical Center. Objective data for hand movements were obtained with a wearable motion sensor (Opal Sensor, APDM, Portland OR) that includes a three-axes accelerometer (range ± 200 G, $G = 9.8 \text{ m/s}^2$), a gyroscope (range ± 2000 degree/s), and a magnetometer (range ± 8 G). The noise levels for accelerometers, gyroscope and magnetometer were $120 \mu\text{G}$, 0.025 degree/s, and 2 mG , respectively. All sensors had a sampling frequency of 120Hz in each orientation. Data were transmitted wirelessly to a PC using 2.40–2.48GHz ISM band, at 2Mbps. The sensor synchronized with the host PC instantaneously with

<30ms latency. The sensor had a weight of <25 g (including battery) and had 8 Gb of internal storage. Horizontal hand movements were defined as those around earth's vertical axis (i.e., turning the hand to the right or left). Vertical hand movements were those around earth's horizontal axis. Torsional hand movements were pronation/supination. Measurements were performed while the subject's hands were outstretched (postural condition), reaching for a stationary target (the examiner's finger, kinetic condition), or resting completely on the table (resting condition).

2.3 Data analysis

Hand movement data was analyzed offline using previously published strategy (Shaikh et al., 2008, 2013, 2015b) with several enhancements. Briefly, we computed 3D hand positions vectors in using MATLAB™ (Shaikh et al., 2013, 2015a, b). We then used frequency segregation to isolate hand tremor (sinusoidal oscillations) from dystonia (jerky oscillations), since they occurred together. Subsequent analysis separately analyzed the oscillation parameters of both oscillation types.

3 Results

[Fig. 2A–C](#) depicts an example of postural hand tremor. Kinetic tremor is shown in [Fig. 2D–F](#); and resting tremor is in [Fig. 2G–I](#). Drift in hand position was seen during postural condition (gray arrow, [Fig. 2A–C](#)). Drift moves the hand away from the desired orientation and is followed by a rapid corrective movement. Such drifts and rapid corrective movements result in the jerky appearance of the oscillations (the hallmark of dystonic tremor)). In addition, there were superimposed sinusoidal oscillations. The severity of the jerky and sinusoidal oscillations was worse during goal-directed movements ([Fig. 2D–F](#)). We did not see any oscillations during resting conditions.

Continuous wavelet transformation was decomposed into jerky and superimposed sinusoidal oscillations ([Fig. 3](#)). [Fig. 3A](#) illustrates hand orientation with respect to time (same epoch of patient data set as depicted in [Fig. 2A](#)). [Fig. 3B](#) illustrates wavelet transformation of the signal depicted in [Fig. 3A](#). Y-axis in [Fig. 3B](#) is wavelet level— inversely proportional to the oscillation frequency; x-axis is the corresponding time. Color-code illustrates the power of the waveform frequency at a given time. The yellow box in [Fig. 3A](#) shows high frequency oscillations, while the arrows depict the quick phases. [Fig. 3E](#) and F illustrates continuous wavelet transformation of kinetic tremor during voluntary reaching movements. It is noteworthy that trajectories of reaching movement are seen in the lower frequency spectrum (red/orange bands in [Fig. 3F](#)); sinusoidal oscillations intervene between these voluntary movements. This analysis suggests that tremor in CIDP can have a mixture of jerky and sinusoidal oscillations, as expected given neural integrator dysfunction).

In subsequent analysis we compared the frequency and amplitude of sinusoidal oscillations during postural, kinetic, and resting conditions. The mean

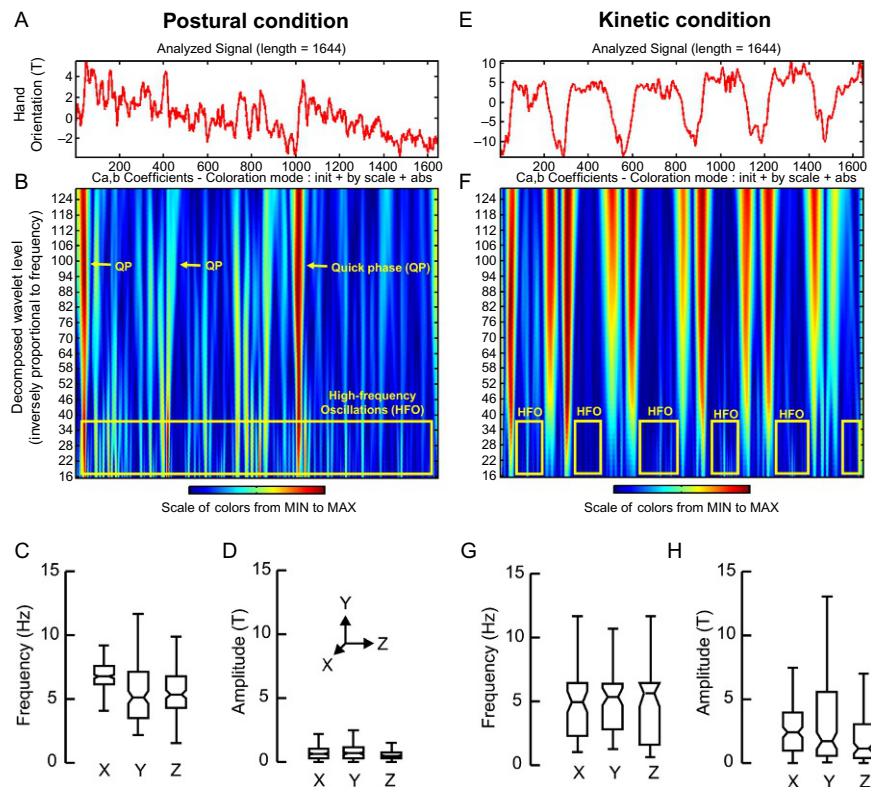


FIG. 3

Same epoch of postural and kinetic tremor as illustrated in Fig. 2. Jerky and sinusoidal waveforms are distinctly separated since the jerky waveform has a much lower frequency compared to the superimposed high-frequency oscillations. The y-axis depicts the wavelet level, inversely proportional to the oscillation frequency. The x-axis is the corresponding time. The color code illustrates the waveform power at a given time. The bottom of the wavelet power spectrum, in the yellow box, shows high frequency oscillations while the arrows depict power in the quick phases that follow the drift. The left panel of column depicts the postural condition, while the right panel depict the kinetic condition. Box plots in the bottom panels depict the summary of frequency (C: postural tremor, G: kinetic tremor) and amplitude (D: postural tremor, H: kinetic tremor). Horizontal line in the middle of the box-whisker plot depicts median values; notch is 95% confidence interval; length of the box is interquartile distance; whiskers illustrate the range.

frequency during postural condition was 7.2 ± 3.0 Hz (Fig. 3C) and the mean frequency during reaching movements was 4.9 ± 2.8 Hz (Fig. 3G). There was no tremor during resting condition. The amplitude of oscillation was 0.7 ± 0.6 T during postural condition (Fig. 3D); the amplitude robustly increased (3.3 ± 3.4 T) during the reaching task (Fig. 3H).

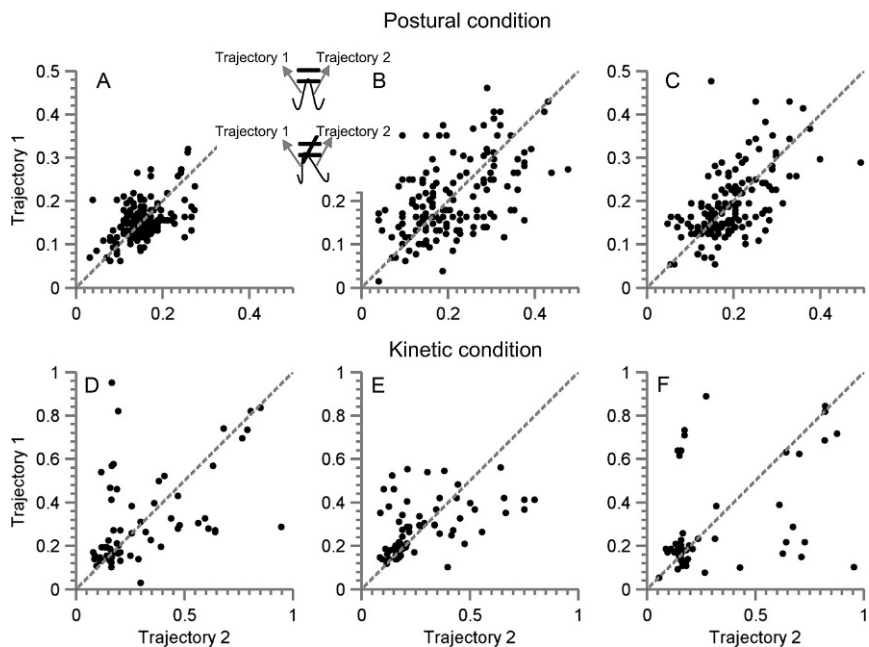


FIG. 4

Quantitative analysis of tremor irregularity. As depicted in inset of panel A, regular tremor will have equal velocity of two opposing trajectories (here trajectory 1 and trajectory 2). In contrast, when the oscillation is jerky, one trajectory will have a relatively lower frequency compared to the other (here trajectory 1 \gg trajectory 2). Trajectory 1 is plotted on the y-axis while trajectory 2 is plotted on the x-axis. Dashed line is the equality line. Each data point depicts one cycle. Panels A–C depict postural tremor trajectory comparison in x-, y-, and z-axes, respectively. Panels D–F illustrate kinetic tremor trajectory comparison in x-, y-, and z-axes, respectively.

We then quantified the jerkiness of the dystonic tremor waveform. We predicted that if the oscillations were sinusoidal, then the velocity of trajectory 1 in one direction (Fig. 4A) would be comparable to the velocity of trajectory 2 in the opposite direction (Fig. 4A). On the contrary, the jerky waveform resulted in asymmetric velocities of trajectory 1 as compared to trajectory 2 (Fig. 4A). Fig. 4 depicts such comparison for tremor in each axis during postural (Fig. 4A–C) and kinetic (Fig. 4D–F) conditions. The velocity of trajectory 1 is plotted on the y-axis while the corresponding velocity of trajectory 2 is plotted on the x-axis. Each data point depicts one oscillation cycle. Sinusoidal oscillation waveforms would have resulted in the distribution of data points around the dashed equality line. In contrast, we found broad dispersion of data points in all three axes during postural condition (Fig. 4A–C). This dispersion suggests that some oscillations were sinusoidal

(because some data points were along the equality line) but many were jerky instead of sinusoidal (as several data points were far away from the equality line). Such dispersion of data points was even more spread out during the kinetic condition (Fig. 4D–F), suggesting worsening of tremor jerkiness during the reaching task, thus confirming an additional diagnostic feature of the dystonic tremor.

4 Discussion

We tested the hypothesis that in a CIDP patient with hand dystonia and tremor, worsening of peripheral neuropathy and putative worsening of the proprioceptive feedback leads to jerky oscillations due to a dysfunction of the neural integrator. We validated the following key predictions supporting this hypothesis: (1) the oscillation waveform would have a slow drift and rapid corrective movement (hence the jerky appearance), as expected given neural integrator dysfunction, (2) there would be relatively high-frequency sinusoids superimposed upon the drifts—a phenomenon analogous to the head tremor in cervical dystonia (Shaikh et al., 2015b), and (3) there would be no involuntary movements when the subject's hand was at rest (i.e., the “null” position).

Tremor is a known characteristic of CIDP (Dalakas et al., 1984). However, our study is the first quantitative description of the tremor waveform kinematics and its classification as a dystonic tremor. Previous literature characterized the tremor in CIDP as coarse and irregular (Dalakas et al., 1984), which is consistent with the clinical definition of a dystonic tremor (Fahn, 1984). The tremor improved with immune therapy on most occasions and in some cases treatment with propranolol reduced tremor intensity (Dalakas et al., 1984). The tremor in CIDP largely varied in frequency (3–6 Hz), which is also a characteristic of dystonic tremor (Shaikh et al., 2008). Eye-blink conditioning is impaired in CIDP patients with tremor, but not in those without tremor; suggesting that cerebellar abnormalities could also be linked to tremor in CIDP (Schwingenschuh et al., 2013). It was proposed that abnormal proprioceptive function reaches the cerebellum and affects its function, leading to tremor (Bain et al., 1996; Kiers et al., 1994; Stanton et al., 2006). Tremor was also reported with benign IgM paraproteinaemic neuropathy (Saverino et al., 2001). These patients also had gait ataxia, in addition to a tremor, again suggestive of cerebellar impairment. Cerebellar hyperactivity was confirmed in PET activation studies (Saverino et al., 2001).

Presence of tremor in CIDP patients with abnormal cerebellar function suggests a “double hit” in the integrative neural network depicted in Fig. 1. The CIDP model of dystonic tremor, the integrative network model, and the “dual-hit” hypothesis further provide insight into why not all patients with cerebellar dysfunction and not all patients with CIDP develop dystonic tremor. It is possible that if a subject has an inherent propensity in the proprioceptive feedback system (that can lead to instability in the integrative neural network) then a second hit, in the form of cerebellar

dysfunction will lead to dystonic tremor. Likewise, inherent instability in cerebellar function alone cannot lead to dystonic tremor, but a second hit, in the form of proprioceptive dysfunction (as seen in CIDP), would then lead to dystonic tremor.

To summarize, we classified coarse and irregular tremor in CIDP as dystonic tremor using quantitative oscillation trajectory analysis. We further suggest that the dystonic tremor in CIDP could be due to an impairment in the function of the circuit called the neural integrator. The neural integrator is a part of the final common pathway projecting to the muscles that comprise the motor plant and its fidelity is improved by feedback. The cerebellum, globus pallidum, and proprioception are mutually connected sources of the feedback to the neural integrator. Impairment anywhere along the feedback network leads to the phenomenology characterizing dystonia.

Acknowledgments

A.S. is supported by career development award from the American Academy of Neurology, George Cotzias Memorial Fellowship (American Parkinson's Disease Association), and Dystonia Medical Research Foundation. There are no financial conflicts of interests. On behalf of all authors, the corresponding author states that there is no conflict of interest.

References

- Bain, P.G., Britton, T.C., Jenkins, I.H., Thompson, P.D., Rothwell, J.C., Thomas, P.K., Brooks, D.J., Marsden, C.D., 1996. Tremor associated with benign IgM paraproteinaemic neuropathy. *Brain* 119 (Pt 3), 789–799.
- Dalakas, M.C., Teravainen, H., Engel, W.K., 1984. Tremor as a feature of chronic relapsing and dysgammaglobulinemic polyneuropathies. Incidence and management. *Arch. Neurol.* 41 (7), 711–714.
- Fahn, S., 1984. The varied clinical expressions of dystonia. *Neurol. Clin.* 2 (3), 541–554.
- Kiers, L., Clouston, P., Zuniga, G., Cros, D., 1994. Quantitative studies of F responses in Guillain-Barre syndrome and chronic inflammatory demyelinating polyneuropathy. *Electroencephalogr. Clin. Neurophysiol.* 93 (4), 255–264.
- Prudente, C.N., Hess, E.J., Jinnah, H.A., 2014. Dystonia as a network disorder: what is the role of the cerebellum? *Neuroscience* 260, 23–35.
- Rosales, R.L., Arimura, K., Takenaga, S., Osame, M., 1996. Extrafusal and intrafusal muscle effects in experimental botulinum toxin-A injection. *Muscle Nerve* 19 (4), 488–496.
- Saverino, A., Solaro, C., Capello, E., Trompetto, C., Abbruzzese, G., Schenone, A., 2001. Tremor associated with benign IgM paraproteinaemic neuropathy successfully treated with gabapentin. *Mov. Disord.* 16 (5), 967–968.
- Schwingenschuh, P., Saifee, T.A., Katschnig-Winter, P., Reilly, M.M., Lunn, M.P., Manji, H., Aguirregomozcorta, M., Schmidt, R., Bhatia, K.P., Rothwell, J.C., Edwards, M.J., 2013. Cerebellar learning distinguishes inflammatory neuropathy with and without tremor. *Neurology* 80 (20), 1867–1873.

- Shaikh, A.G., Jinnah, H.A., Tripp, R.M., Optican, L.M., Ramat, S., Lenz, F.A., Zee, D.S., 2008. Irregularity distinguishes limb tremor in cervical dystonia from essential tremor. *J. Neurol. Neurosurg. Psychiatry* 79, 187–189.
- Shaikh, A.G., Wong, A.L., Zee, D.S., Jinnah, H.A., 2013. Keeping your head on target. *J. Neurosci.* 33, 11281–11295.
- Shaikh, A.G., Wong, A., Zee, D.S., Jinnah, H.A., 2015a. Why are voluntary head movements in cervical dystonia slow? *Parkinsonism Relat. Disord.* 21, 561–566.
- Shaikh, A.G., Zee, D.S., Crawford, J.D., Jinnah, H.A., 2016. Cervical dystonia: a neural integrator disorder. *Brain* 139 (Pt 10), 2590–2599.
- Shaikh, A.G., Zee, D.S., Jinnah, H.A., 2015b. Oscillatory head movements in cervical dystonia: Dystonia, tremor, or both? *Mov. Disord.* 30, 834–842.
- Stanton, M., Pannoni, V., Lewis, R.A., Logigan, E.L., Naguib, D., Shy, M.E., Cleland, J., Herrmann, D.N., 2006. Dispersion of compound muscle action potential in hereditary neuropathies and chronic inflammatory demyelinating polyneuropathy. *Muscle Nerve* 34 (4), 417–422.
- Tempel, L.W., Perlmutter, J.S., 1990. Abnormal vibration-induced cerebral blood flow responses in idiopathic dystonia. *Brain* 113 (Pt 3), 691–707.
- Vitek, J.L., 2002. Pathophysiology of dystonia: a neuronal model. *Mov. Disord.* 17 (Suppl 3), S49–S62.

SECTION

RESEARCH: Parkinson's
disease **VII**

This page intentionally left blank

Oculomotor effects of medical and surgical treatments of Parkinson's disease

23

Salil Patel^a, James J. Fitzgerald^{a,b}, Chrystalina A. Antoniades^{a,*}

^a*NeuroMetrology Lab, Nuffield Department of Clinical Neurosciences, University of Oxford, Oxford, United Kingdom*

^b*Nuffield Department of Surgical Sciences, University of Oxford, Oxford, United Kingdom*

*Corresponding author: Tel.: +44-186-523-4728,
e-mail address: chrystalina.antoniades@ndcn.ox.ac.uk

Abstract

Oculomotor abnormalities are fast becoming a proxy for disease diagnosis and progression. Saccades—ballistic eye movements—are known to be affected by dopaminergic cell loss in the basal ganglia, caused by Parkinson's disease. Pharmaceutical and neurosurgical interventions such as deep brain stimulation and functional neurosurgery have both been noted to have an effect on saccades. Comparing and contrasting these effects may yield insights into Parkinson's disease pathophysiology, and the mechanisms of pharmacological and neurosurgical treatments. Computational models of saccadic control, such as the LATER model, can help to interpret the distribution of saccadic latencies, providing a framework for objectively comparing the effects of pharmaceutical interventions and deep brain stimulation.

Keywords

Saccades, Eye movements, Oculomotor, Deep brain stimulation, Stereotactic neurosurgery, Parkinson's disease, LATER model, Basal ganglia

1 Introduction

Eye movement abnormalities (Anderson and MacAskill, 2013; Antoniades et al., 2007) have been identified in a number of neurodegenerative conditions and their diagnostic potential is becoming increasingly apparent. One such condition is Parkinson's disease (PD), a progressive neurodegenerative disorder that primarily presents with motor symptoms including bradykinesia, tremor and muscle rigidity,

but also features a broad range of non-motor symptoms such as cognitive derangements and autonomic impairments. PD symptoms are frequently treated with the dopamine precursor levodopa and/or dopaminergic agonists. Another treatment used in a more advanced of patients is deep brain stimulation (DBS) where electrical stimulus pulses are delivered to parts of the basal ganglia.

The core pathology in PD involves the degeneration of neurons in the substantia nigra pars compacta (SNc) (Fearnley and Lees, 1991), and consequently the loss of their dopaminergic projections to the striatum. This affects the function of networks involving both cortical areas and parts of the basal ganglia. In addition to motor symptoms, this leads to oculomotor abnormalities, particularly in saccadic eye movements. One of the benefits of the study of eye movements is that they are standardized tasks providing a quantitative, reproducible and accurate measure (Antoniades et al., 2013a). Hence the study of eye movements has great potential as a tool for investigating PD, and indeed a number of studies have identified differences in saccades between PD patients and healthy controls. There is considerable interest in the idea that measures such as this could supplement conventional clinical assessments using rating scales such as the Unified Parkinson's Disease Rating Scale (UPDRS), which are nonlinear and exhibit considerable inter-rater variability (Post et al., 2005).

Several studies have shown saccadic eye movements are affected in patients with PD (Antoniades et al., 2015; Pretegiani and Optican, 2017). Prosaccades are the ballistic movements eyes make when moving toward a visual stimulus (Watanabe and Munoz, 2011). The antithesis—antisaccadic movements—are defined as the ocular movement away from a visual stimulus. Despite sounding mechanically similar, antisaccadic tasks are far more complicated, involving an inhibition of a 'normal' prosaccadic reflex. The antisaccadic error rate (AER) compares how often the patient makes a prosaccadic movement when an antisaccadic movement is required (Everling and Fischer, 1998). The AER has been shown to be significantly higher in patients with PD—illustrating a potential clinical marker for PD onset, severity and interventional success (Antoniades et al., 2013a).

Parkinson's disease has been at the center of research focused on movement disorders over the last few decades. Over that time many of its fundamental mechanisms have been elucidated, effective techniques for medical management were found, and novel surgical techniques developed as an alternative to medical management in certain patients with advanced disease. Here we briefly describe the oculomotor effects of medical and surgical treatments in those individuals who have PD.

2 Effects of PD medication on the oculomotor system

Despite much research into potential biomarkers, current diagnosis and disease staging remain reliant on the clinical assessment of motor symptoms using rating scales, such as part III of the UPDRS mentioned previously. This causes a number

of problems: assessments are subject to inter-observer variability; rating scales are nonlinear; and the scales only enter their working range once more than half of the dopamine producing cells in the brain have degenerated (Goetz et al., 2008).

New treatments, and in particular disease modifying drugs (DMDs), are desperately needed. Only around 1 in 10 newly developed drugs survive rigorous assessment in trials, which are both time consuming and very costly. Failures must be recognized quickly so that resources can be transferred to the next candidate agent. When evaluating DMDs investigators are usually looking for small changes in disease trajectory. The more sensitive a biomarker, and the less affected it is by noise, the sooner a difference will be seen after treatment commences. A sensitive and noise resistant measure, such as saccadic eye movements, is therefore critical to minimizing resource consumption in the evaluation of doomed drugs.

An additional problem arises when the measurement is affected by background symptomatic medication, which the great majority of PD patients are treated with. Symptomatic treatment can obscure progression in standard motor scales almost completely, rendering them insensitive to changes in disease trajectory and thus unsuited to DMD evaluation. When considering saccades as potential biomarkers it is therefore of great interest to understand the effects that antiparkinsonian medications have on them.

Prosaccadic latency (PSL) has been studied extensively in PD, but investigators have disagreed about how it is affected by administration of levodopa. Some have reported that levodopa increases PSL (Cubizolle et al., 2014; Dec-Cwiek et al., 2017; Kitagawa et al., 1994; Michell et al., 2006; Muller et al., 1994), while others describe a decrease (Gibson et al., 1987; Rascol et al., 1989; van Stockum et al., 2012). Other reported effects of levodopa are a reduction in the antisaccadic error rate (Hood et al., 2007), a reduction in prosaccadic accuracies (Gibson et al., 1987), and an improvement of voluntary saccadic amplitude (Rascol et al., 1989). Improvements in the ability to perform sequences of memory guided saccades have also been noted (Highstein et al., 1969) but with no improvement in the hypometria of memory guided saccades, a characteristic abnormality in PD.

A study by Duka and Lupp (1997) demonstrated what happens after administration of such medication to individuals who do not have a neurological condition and therefore classified as healthy controls. A combination of antisaccadic and reflexive tasks was used to examine 20 young healthy male volunteers. Everyone in the study received levodopa and benserazide (100 and 25 mg respectively). Reflexive saccades and antisaccades were measured at 1 and 5 h post drug administration. The results indicated no change in the pro or anti saccadic latencies but an increase in the anti-saccadic error rate.

More work is needed to clarify fully the pattern of changes in saccadic parameters induced by antiparkinsonian medication. At present, even in the case of the most widely studied variable, PSL, authors disagree not just on the magnitude but even the direction of the medication effect. Ideally for applications such as DMD evaluation, we would like a measure that is completely unaffected by medication.

3 Effects of surgical intervention on PD on the oculomotor system

Over the past half century, the accurate electrical stimulation of specific brain areas has revolutionized the treatment of movement disorders. It has also provided the unique opportunity to carry out research into the human brain function and associated pathophysiology. Deep brain stimulation (DBS) has provided us with invaluable information on the importance of the deep nuclei in oculomotor control (Fitzgerald and Antoniades, 2016).

DBS was first used for Parkinson's-induced motor fluctuations in the 1960s (Sironi, 2011). By stimulating specific deep brain structures, it was found that motor symptoms could be dramatically reduced. Modern surgery uses stereotactic frames to site electrodes with sub-millimetric accuracy into deep grey matter structures. A large body of evidence demonstrates the efficacy of DBS in alleviating both motor symptoms and fluctuations (Limousin-Dowsey et al., 1999).

The subthalamic nucleus (STN) and globus pallidus interna (GPi) are the usual targets for stimulation in akinetic-rigid Parkinson's disease (Weaver et al., 2009). Multiple areas of the BG are also involved in oculomotor control, and in addition to improvements in motor function stimulating the GPi and STN affects oculomotor function. By monitoring changes in ocular movements, investigations using DBS as an independent variable can uncover clues regarding the mechanism behind modulation the nature of the oculomotor circuitry, and the function of deep brain nuclei.

In contrast to the disputed effects of levodopa on PSL, there is clear consensus that stimulation at either STN or GPi reduces PSL (Fawcett et al., 2007; Temel et al., 2008; Yugeta et al., 2010). STN-DBS and GPi-DBS both also improve PD-slowed smooth pursuit (Nilsson et al., 2013). However, the effects on antisaccades are more complex. While GPi-DBS reduces the AER, STN-DBS does not (Antoniades et al., 2015). This might occur due to GPi stimulation causing retrograde stimulation of striatopallidal axons ultimately improving information flow from the prefrontal cortico-basal ganglia loops to oculomotor circuitry (Fitzgerald and Antoniades, 2016). Such strengthening, it is hypothesized, may rely on the DBS-induced antidromic activation of striatal medium spiny neurons (MSNs) causing GABA release and subsequent depression of AER. Patients with PD are known to have higher MSN firing rates and this has been suggested as a cause of an abnormally high AER. Computational analysis has shown low MSN excitability is required for accurate information transfer (Guthrie et al., 2013). STN-DBS does not modulate MSNs and hence, has no effect on AER, whereas levodopa does affect AER and is known to act on MSNs (Hood et al., 2007).

We have previously used an oculomotor task to test a prediction of the Bayes theorem that disrupting information processing in the STN with DBS, should abolish the normalization of the neural representation of probabilities. We found out that PD patients who had their Deep Brain Stimulation systems switched off behave similarly

to healthy controls and we assumed that changes induced by switching the system on would have been similar in healthy controls if they had similar DBS systems (Antoniades et al., 2014).

3.1 Computational modeling of oculomotor function in PD

Over the last few decades, a range of computational models of BG function have emerged. One of these, the LATER model (Carpenter and Williams, 1995), describes the presumed underlying neural decision mechanisms associated with saccadic reaction times (latencies).

In brief, LATER (see Fig. 1) provides us with three parameters (median latency, main slope and early slope), which allow us to compare differences in latency distributions between individuals.

Saccadic reaction times vary largely from trial to trial, yet they also appear to follow a simple rule; the reciprocal of latency, or reaction time, obeys a Gaussian distribution. Plotting a cumulative histogram in which latency is represented on a reciprocal scale, and cumulative frequency is plotted on a probit scale (which is the reciprocal of a cumulative distribution and has the useful property that a Gaussian distribution is transformed into a straight line) allowing us to describe these latency distributions with relatively few parameters. This histogram is known as a reciprobit plot (see Fig. 2). The median latency is defined as the intercept with the 50% axis, and slope is directly related to the standard deviation of the distribution. Interestingly when observing these saccadic latency distributions there is often a small, early

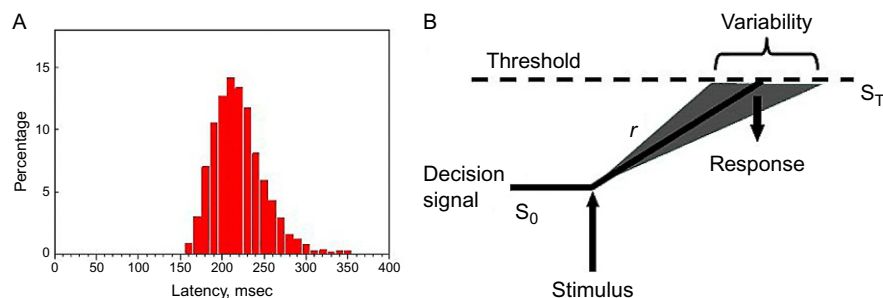
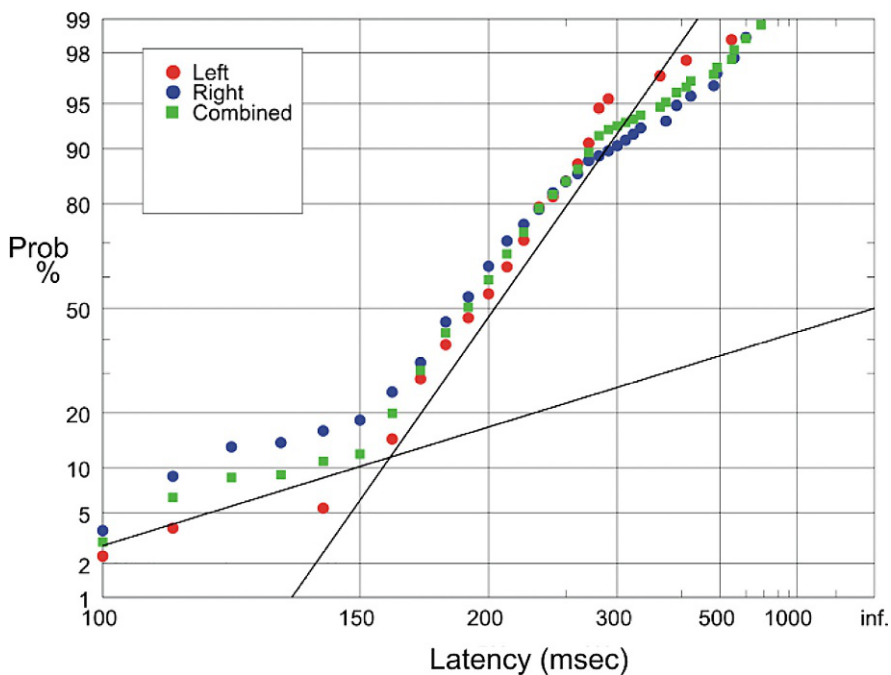


FIG. 1

Using the LATER model to study eye movements. (A) A raw histogram showing a typical distribution of saccadic latencies. (B) LATER can explain why reciprocal latencies are distributed normally. A decision signal rises from a starting level to a pre-determined threshold level, at which point a saccade is initiated by the participant. Latency corresponds to the time taken to reach the threshold level. The rate of rise of the decision signal has a Gaussian distribution meaning that latency data sets will follow a recinormal distribution. On different trials, r is a normal random variate, with mean μ and variance σ^2 , giving rise to a skewed latency histogram.

**FIG. 2**

LATER model distributions showing the main and early populations of saccadic latencies.

component of the distribution that does not fit the main reciprobit slope. This early component, sometimes described as express saccades, is thought to arise in conditions of great urgency or expectation where the action of lower level circuits might escape the normal tonic inhibition from above, and indeed this is supported by the fact that the incidence of these express saccades is increased in tasks with increased urgency. We can model these express saccades with a separate, shallower reciprobit slope. As a result, to compare our observed saccadic latency distributions we use three parameters; the median latency, the main slope (σ) and the early slope (σ_E) (see Fig. 2).

The model attempts to explain why saccadic datasets follow this recinormal law (see Fig. 1B). It states that for a reaction to be made then some kind of decision signal, starting at an initial level S_0 , rises at a constant rate (r) until it reaches a criterion level (S_T). The rate (r) at which the decision signal rises varies from trial to trial, such that it follows a Gaussian distribution and therefore since the latency observed will be proportional to $(S_T - S_0)/r$, this will make the distribution of reaction times recinormal. If this model indeed relates to neurophysiological activity it states that activity in a particular set of neurons must rise until a threshold criterion of activity is reached, at which point a response, such as a saccade, will be made. [Hanes and Schall \(1995\)](#) demonstrated this by recording from the FEF in the Rhesus monkey.

They found that activity in individual neurons increased to a threshold level before a saccade was initiated, and that the rate in rise of activity displayed stochastic variability which resulted in the distribution of saccadic reaction times.

The effects of PD on the LATER parameters have been described previously (Antoniades et al., 2013b). Can such models account for the effect of medication and of stimulation in PD?

A study by Michell et al. (2006) examined the effect of levodopa on neural decision-making processes using saccadic latency distributions. The main finding was that levodopa tends to increase reaction time (significant difference in reciprocal median saccadic latency on vs off medication), although the effect varied substantially between patients.

We have previously used this model to examine a cohort of moderate disease PD patients and found that the population of early saccadic responses is larger than in controls (Antoniades et al., 2013b). We also carried out a study of saccadic latencies in patients undergoing DBS (Antoniades et al., 2012). We found latency to be *increased* immediately following implantation of STN electrodes and before switching the stimulation on, but then *reduced* to a level below baseline once stimulation was switched on. Using the LATER model we looked at the saccadic LATER parameters averaged over the nine patients who took part in this study. The reciprocal median latency, μ , decreased following lead implantation but increased with modulation. The standard deviation of the early population, the σ_E LATER parameter, decreased significantly after stimulation was switched on. This indicates a reduction in the proportion of express saccades, which might be interpreted as indicating a restoration of descending inhibitory control.

More such studies are needed and models such as LATER are useful as the study of distributional parameters gives us a lot more information than simply looking at one single saccadic parameter such as the average of saccadic latencies. This model is still quite simple however, while saccadic control is complex, involving multiple parallel pathways, including some projecting directly to the superior colliculus and others indirectly to the SC via the basal ganglia. It is likely that as more experimental data emerges, more refined models will be needed.

References

- Anderson, T.J., MacAskill, M.R., 2013. Eye movements in patients with neurodegenerative disorders. *Nat. Rev. Neurol.* 9, 74–85.
- Antoniades, C.A., Altham, P.M., Mason, S.L., Barker, R.A., Carpenter, R., 2007. Saccadometry: a new tool for evaluating presymptomatic Huntington patients. *Neuroreport* 18, 1133–1136.
- Antoniades, C.A., Buttery, P., Fitzgerald, J.J., Barker, R.A., Carpenter, R.H., Watts, C., 2012. Deep brain stimulation: eye movements reveal anomalous effects of electrode placement and stimulation. *PLoS One* 7, e32830.
- Antoniades, C., Ettinger, U., Gaymard, B., Gilchrist, I., Kristjansson, A., Kennard, C., John Leigh, R., Noorani, I., Pouget, P., Smyrnis, N., Tarnowski, A., Zee, D.S., Carpenter, R.H., 2013a. An internationally standardised antisaccade protocol. *Vision Res.* 84, 1–5.

- Antoniades, C.A., Xu, Z., Carpenter, R.H., Barker, R.A., 2013b. The relationship between abnormalities of saccadic and manual response times in Parkinson's disease. *J. Parkinsons Dis.* 3, 557–563.
- Antoniades, C.A., Bogacz, R., Kennard, C., Fitzgerald, J.J., Aziz, T., Green, A.L., 2014. Deep brain stimulation abolishes slowing of reactions to unlikely stimuli. *J. Neurosci.* 34, 10844–10852.
- Antoniades, C.A., Rebelo, P., Kennard, C., Aziz, T.Z., Green, A.L., Fitzgerald, J.J., 2015. Pallidal deep brain stimulation improves higher control of the oculomotor system in Parkinson's disease. *J. Neurosci.* 35, 13043–13052.
- Carpenter, R.H., Williams, M.L., 1995. Neural computation of log likelihood in control of saccadic eye movements. *Nature* 377, 59–62.
- Cubizolle, S., Damon-Perriere, N., Dupouy, S., Fouquet-Samier, A., Tison, F., 2014. Parkinson's disease, L-dopa and "express" saccades: superior colliculus dyskinesias? *Clin. Neurophysiol.* 125, 647–648.
- Dec-Cwiek, M., Tutaj, M., Gracies, J.M., Volkmann, J., Rudzinska, M., Slowik, A., Szczudlik, A., 2017. Opposite effects of L-dopa and DBS-STN on saccadic eye movements in advanced Parkinson's disease. *Neurol. Neurochir. Pol.* 51, 354–360.
- Duka, T., Lupp, A., 1997. The effects of incentive on antisaccades: is a dopaminergic mechanism involved? *Behav. Pharmacol.* 8, 373–382.
- Everling, S., Fischer, B., 1998. The antisaccade: a review of basic research and clinical studies. *Neuropsychologia* 36 (9), 885–899.
- Fawcett, A.P., Cunic, D., Hamani, C., Hodaie, M., Lozano, A.M., Chen, R., Hutchison, W.D., 2007. Saccade-related potentials recorded from human subthalamic nucleus. *Clin. Neurophysiol.* 118, 155–163.
- Fearnley, J.M., Lees, A.J., 1991. Ageing and Parkinson's disease: substantia nigra regional selectivity. *Brain* 114, 2283–2301.
- Fitzgerald, J.J., Antoniades, C.A., 2016. Eye movements and deep brain stimulation. *Curr. Opin. Neurol.* 29, 69–73.
- Gibson, J.M., Pimlott, R., Kennard, C., 1987. Ocular motor and manual tracking in Parkinson's disease and the effect of treatment. *J. Neurol. Neurosurg. Psychiatry* 50, 853–860.
- Goetz, C.G., Tilley, B.C., Shaftman, S.R., Stebbins, G.T., Fahn, S., Martinez-Martin, P., Poewe, W., Sampaio, C., Stern, M.B., Dodel, R., Dubois, B., Holloway, R., Jankovic, J., Kulisevsky, J., Lang, A.E., Lees, A., Leurgans, S., Lewitt, P.A., Nyenhuis, D., Olanow, C.W., Rascol, O., Schrag, A., Teresi, J.A., Van Hilten, J.J., Lapelle, N., 2008. Movement Disorder Society-sponsored revision of the Unified Parkinson's Disease Rating Scale (MDS-UPDRS): scale presentation and clinimetric testing results. *Mov. Disord.* 23, 2129–2170.
- Guthrie, M., Leblois, A., Garenne, A., Boraud, T., 2013. Interaction between cognitive and motor cortico-basal ganglia loops during decision making: a computational study. *J. Neurophysiol.* 109, 3025–3040.
- Hanes, D.P., Schall, J.D., 1995. Countermanding saccades in macaque. *Vis. Neurosci.* 12, 929–937.
- Highstein, S., Cohen, B., Mones, R., 1969. Changes in saccadic eye movements of patients with Parkinson's disease before and after L-dopa. *Trans. Am. Neurol. Assoc.* 94, 277–279.
- Hood, A.J., Amador, S.C., Cain, A.E., Briand, K.A., Al-Refai, A.H., Schiess, M.C., Sereno, A.B., 2007. Levodopa slows prosaccades and improves antisaccades: an eye movement study in Parkinson's disease. *J. Neurol. Neurosurg. Psychiatry* 78, 565–570.

- Kitagawa, M., Fukushima, J., Tashiro, K., 1994. Relationship between antisaccades and the clinical symptoms in Parkinson's disease. *Neurology* 44, 2285–2289.
- Limousin-Dowsey, P., Pollak, P., Van Blercom, N., Krack, P., Benazzouz, A., Benabid, A., 1999. Thalamic, subthalamic nucleus and internal pallidum stimulation in Parkinson's disease. *J. Neurol.* 246 (Suppl. 2), II42–5.
- Michell, A.W., Xu, Z., Fritz, D., Lewis, S.J., Foltyne, T., Williams-Gray, C.H., Robbins, T.W., Carpenter, R.H., Barker, R.A., 2006. Saccadic latency distributions in Parkinson's disease and the effects of L-dopa. *Exp. Brain Res.* 174, 7–18.
- Muller, C., Wenger, S., Fertl, L., Auff, E., 1994. Initiation of visual-guided random saccades and remembered saccades in parkinsonian-patients with severe motor-fluctuations. *J. Neural Transm. Park. Dis. Dement. Sect.* 7, 101–108.
- Nilsson, M.H., Patel, M., Rehncrona, S., Magnusson, M., Fransson, P.A., 2013. Subthalamic deep brain stimulation improves smooth pursuit and saccade performance in patients with Parkinson's disease. *J. Neuroeng. Rehabil.* 10, 33.
- Post, B., Merkus, M.P., De Bie, R.M., De Haan, R.J., Speelman, J.D., 2005. Unified Parkinson's disease rating scale motor examination: are ratings of nurses, residents in neurology, and movement disorders specialists interchangeable? *Mov. Disord.* 20, 1577–1584.
- Pretegiani, E., Optican, L.M., 2017. Eye movements in Parkinson's disease and inherited parkinsonian syndromes. *Front. Neurol.* 8, 592.
- Rascol, O., Clanet, M., Montastruc, J.L., Simonetta, M., Soulieresteve, M.J., Doyon, B., Rascol, A., 1989. Abnormal ocular movements in Parkinson's disease—evidence for involvement of dopaminergic systems. *Brain* 112, 1193–1214.
- Sironi, V.A., 2011. Origin and evolution of deep brain stimulation. *Front. Integr. Neurosci.* 5, 42.
- Temel, Y., Visser-Vandewalle, V., Carpenter, R.H., 2008. Saccadic latency during electrical stimulation of the human subthalamic nucleus. *Curr. Biol.* 18, R412–R414.
- van Stockum, S., Macaskill, M.R., Anderson, T.J., 2012. Impairment of voluntary saccades and facilitation of reflexive saccades do not co-occur in Parkinson's disease. *J. Clin. Neurosci.* 19, 1119–1124.
- Watanabe, M., Munoz, D.P., 2011. Probing basal ganglia functions by saccade eye movements. *Eur. J. Neurosci.* 33 (11), 2070–2090.
- Weaver, F.M., Follett, K., Stern, M., Hur, K., Harris, C., Marks Jr., W.J., Rothlind, J., Sagher, O., Reda, D., Moy, C.S., Pahwa, R., Burchiel, K., Hogarth, P., Lai, E.C., Duda, J.E., Holloway, K., Samii, A., Horn, S., Bronstein, J., Stoner, G., Heemskerk, J., Huang, G.D., 2009. Bilateral deep brain stimulation vs best medical therapy for patients with advanced Parkinson disease: a randomized controlled trial. *JAMA* 301, 63–73.
- Yugeta, A., Terao, Y., Fukuda, H., Hikosaka, O., Yokochi, F., Okiyama, R., Taniguchi, M., Takahashi, H., Hamada, I., Hanajima, R., Ugawa, Y., 2010. Effects of STN stimulation on the initiation and inhibition of saccade in Parkinson disease. *Neurology* 74, 743–748.

This page intentionally left blank

Vestibular heading perception in Parkinson's disease

24

**Sinem Balta Beylergil^{a,b}, Sarah Ozinga^a, Mark F. Walker^{b,c},
Cameron C. McIntyre^a, Aasef G. Shaikh^{a,b,c,d,*}**

^a*Department of Biomedical Engineering, Case Western Reserve University, Cleveland, OH,
United States*

^b*National VA Parkinson Consortium Center, Neurology Service, Daroff-Dell'Osso
Ocular Motility and Vestibular Laboratory, Louis Stokes Cleveland VA Medical Center,
Cleveland, OH, United States*

^c*Department of Neurology, Case Western Reserve University, Cleveland, OH, United States*

^d*Movement Disorders Center, Neurological Institute, University Hospitals, Cleveland,
OH, United States*

*Corresponding author: Tel.: +1-216-844-1000, e-mail address: aasefshaikh@gmail.com

Abstract

Postural instability and falls are common causes of morbidity and mortality in the second most prevalent neurodegenerative condition, Parkinson's disease (PD). Poor understanding of balance dysfunction in PD has hampered the development of novel therapeutic measures for postural instability and balance dysfunction. We aimed to determine how the ability to perceive one's own linear motion in the absence of visual cues, i.e., vestibular heading, is affected in PD. We examined vestibular heading function using a two-alternative forced choice task performed on a six-degree-of-freedom motion platform. Sensitivity of the vestibular system to subtle variations in heading direction and systematic errors in accuracy of responses were assessed for each subject using a Gaussian cumulative distribution psychometric function. Compared to healthy subjects, PD presented with higher angular thresholds to detect vestibular heading direction. These results confirm the potential of our study to provide valuable insight to the vestibular system's role in spatial navigation deficits in PD.

Keywords

Motion perception, Veering, Falls, Postural instability

1 Introduction

Parkinson's disease (PD) is a neurodegenerative disorder affecting about 10 million individuals worldwide. PD is the second most common age-related neurodegenerative disease. In addition to tremor, rigidity, abnormally slow movements and decreased reaction time, PD patients also suffer from visuospatial navigational impairments such as lateral drifts while walking (veering) (Bloem et al., 2004; Davidsdottir et al., 2008; Fetsch et al., 2009; Hanakawa et al., 1999; Prokop et al., 1997; Ren et al., 2015; Seichepine et al., 2015; Warren et al., 2001; Young et al., 2010). These visuospatial and navigational deficits lead to gait instability with a prevalence of falls in PD reaching nearly 70% (Bloem et al., 2004; Davidsdottir et al., 2008). Visuospatial deficits and postural instability in PD are poorly and unpredictably responsive to modern pharmacotherapy (Bloem et al., 2001) or state-of-the-art surgical therapies such as deep brain stimulation (DBS), although both treatments provide dramatic improvement in other motor symptoms (Deuschl et al., 2006; Fasano et al., 2015; Krack et al., 2003). There is significant paucity in literature objectively examining balance and the vestibular function in PD in patients. Therefore, there has been limited opportunity to quantify the degree of patient-specific postural instability and its correlation with perception of one's own linear motion, i.e., heading. Poor understanding of the mechanisms of postural instability and navigational impairments in PD has hampered the development of more successful treatments (Bloem et al., 2004).

We set out to understand the physiological underpinnings of the process by which visual, vestibular, and visual-vestibular integrated systems govern heading perception critical for spatial navigation and maintenance of postural stability in PD. As a first step, we focused on the vestibular system, and in particular vestibular heading perception. Our central hypothesis was that PD patients have imprecise and/or directionally biased perception of heading. This hypothesis was tested in experiments utilizing a motion platform with six degrees of freedom and an objective two-alternative forced choice psychophysics task that precisely measures perceived vestibular heading in PD patients.

2 Methods

2.1 Subjects

We studied vestibular heading perception in a group of 14 individuals with PD (all men, median age: 69 years, age range: 52–83 years). The PD subjects were recruited from the movement disorders clinic at the National VA Parkinson Consortium Center at Louis Stokes Cleveland VA Medical Center as well as the movement disorders clinic at the University Hospitals Cleveland Medical Center. The inclusion criteria for PD included the ability to perform informed consent, Hoehn and Yahr stages 2–4 when off medication, and a stable and optimal medical regimen of antiparkinsonian medication for at least 6 months prior to study participation (see Table 1 for demographics). Exclusion criteria were dementia, clinically

Table 1 Clinical presentation.

Patient	Age	Dominant hand/foot	Duration of disease (years)	Most affected side by PD	Number of falls in last 6 months	Duration of DBS (years)	Total UPDRS-III	Medication (Levodopa equivalent dose)
1	76	R/R	11	R	7	0.5	51	1040
2	53	R/R	5	R	2	3	12	60
3	66	L/L	22	L	4	3	48	800
4	52	R/R	12	R	0	3	40.5	1505
5	71	R/R	21	R	900	1	36.5	1100
6	70	L/R	12	R	1	7	50	300
7	69	R/R	9	L	4	1	48.5	0
8	72	R/R	10	L	104	3	47	900
9	83	R/R	14	R	52	2	42	925
10	64	R/R	18	L	0	8	56	0
11	71	R/R	14	L	60	7	41	610
12	79	R/R	17	L and R	2	5	54	500
13	69	R/R	8	L	0	1	25.5	500
14	64	R/R	10	L	26	3	23.5	348

significant depression or anxiety, focal brain lesions, history of intracranial surgery with an exception of DBS surgery, and a clinical diagnosis of atypical Parkinsonism. All patients were successfully treated with antiparkinsonian medications, except two subjects who did not require treatment due to mild disease burden. The median duration of disease of the PD group was 12 years (range: 5–22 years). The stage and diagnosis of the disease was individually assessed by a movement disorders specialist (AS). In addition to clinical diagnosis and assessment, we also measured the third (motor) subsection of the Unified Parkinson's Disease Rating Scale (UPDRS-III) with a possible maximum score of 108. The median UPDRS-III score of the PD group was 44.50 (range: 12–56) (see [Table 1](#) for individual scores). The comparison group was comprised of 16 healthy controls (HC) (10 men; median age: 58.50 years, age range: 35–77 years). Both HC and PD subjects had no clinical evidence for peripheral vestibular dysfunction. All subjects gave informed, written consent, in accordance with the Declaration of Helsinki, under a protocol approved by Institutional Review Boards of the Louis Stokes Cleveland VA Medical Center.

2.2 Experiment setup

We objectively examined the vestibular heading perception function using a two-alternative forced choice task and a motion platform with six degrees of freedom, i.e., hexapod (Moog, North Aurora, NY), that allows for translation along any direction in three-dimensional space ([Fig. 1A](#)). The subjects were securely seated in a padded chair with a five-point safety harness that was affixed to the motion platform of the hexapod. The subject's head was secured inside a cushioned helmet which was fixed to the chair's headrest to immobilize the head relative to the platform. Two reflective markers were placed on the subject's zygomatic arches and one on the chin to ensure consistent head stability across testing blocks with a 3-D motion capture camera (Vicon®, Culver City, CA). In order to eliminate visual cues, the experiments were done in a darkened room and the subjects wore a blindfold.

2.3 Experiment protocol

The experiment consisted of 99 trials conducted in 3 blocks of 33 trials separated by a short break. During each trial, the subjects experienced a step of forward movement. The direction of forward movement was equally randomized across trials at straight-ahead (0°), and 5° , 10° , 20° , 30° to the right or left ([Fig. 1B](#)). Total displacement along the motion trajectory was 0.4 m lasting 1.5 s in duration. The peak velocity and peak acceleration were 0.53 m/s and 1.38 m/s^2 , respectively. These kinematic parameters exceeded vestibular detection thresholds ([Guedry, 1974](#)). After each displacement, the platform remained stationary for 3 s during which the subjects were asked to indicate whether the movement was rightward or leftward relative to their perceived straight-ahead using a right or left handheld input response device.

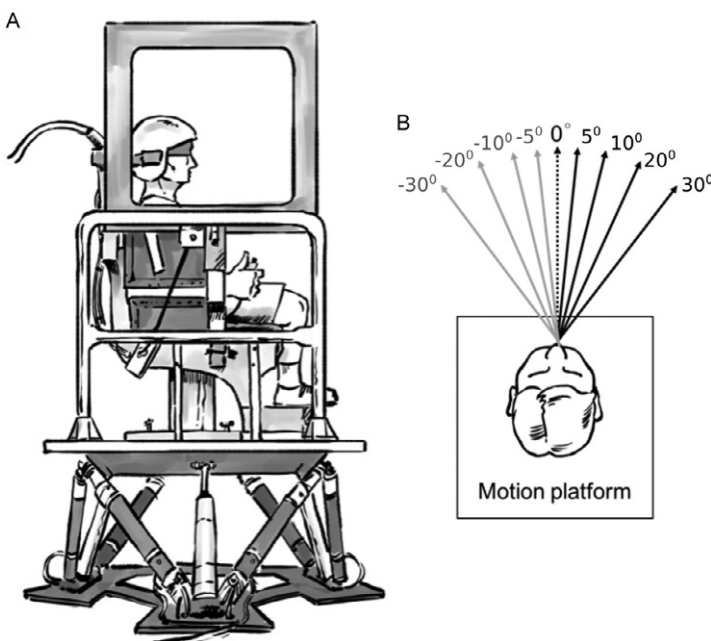


FIG. 1

Vestibular heading perception measurement. (A) The six-degree-of-freedom motion platform (MOOG) used in the experiments. Subjects were passively translated along linear horizontal trajectories in a darkened room while wearing a blindfold that eliminates external visual cues. (B) The direction of forward movement was equally randomized across trials at straight-ahead (0°), and 5° , 10° , 20° , 30° to the right or the left.

2.4 Data analysis

The vestibular heading perception threshold and direction perception bias of each subject were determined by fitting a Gaussian cumulative distribution psychometric function to the percentage of rightward decisions at each level of motion direction derived from the binary responses recorded in the experiment (Wichmann and Hill, 2011). Vestibular thresholds (σ) were defined as the standard deviation of the Gaussian fit. A steeper psychometric function yields low values of vestibular threshold indicating a more sensitive vestibular system to subtle variations in heading direction. Direction perception biases (μ) were determined by the amount of linear translation of the psychometric function along the x -axis. This value indicates the heading direction to which a left or right response of a subject is equally likely and quantifies the degree of asymmetry of subjects in perceived straight-ahead motion.

3 Results

The central hypothesis tested in our experiments was that PD patients have directionally biased and/or imprecise perception of vestibular heading perception. This hypothesis was tested in 14 PD and 16 HC subjects by a two-alternative-forced choice task involving passive en bloc forward heading motion in horizontal line at straight-ahead (0°), 2.5° , 5° , 10° , 20° , and 30° to the right or to the left, randomized across trials. We expected that wide-angle rightward displacement would be associated with most rightward responses, and leftward displacement with leftward responses. There would be an uncertainty in responses ($\sim 50\%$, i.e., by chance) during straight-ahead movement.

We found that the total number of correct responses was significantly lower ($z = 2.80$, $P = 0.005$) in the PD group (median = 64.64, range = 44.44–79.79) compared to the HC group (median = 80.30, range = 47.47–89.89). We then used response data to estimate the psychometric curves. The psychometric analysis was first performed at the group level. Group psychometric curves were obtained by fitting a Gaussian cumulative distribution function to the proportion of rightward decisions averaged over subjects in each subject group at each level of motion direction (Fig. 2A). Discrimination thresholds of the groups as indicated by the standard deviation of the group psychometric curves showed that the average response of PD had

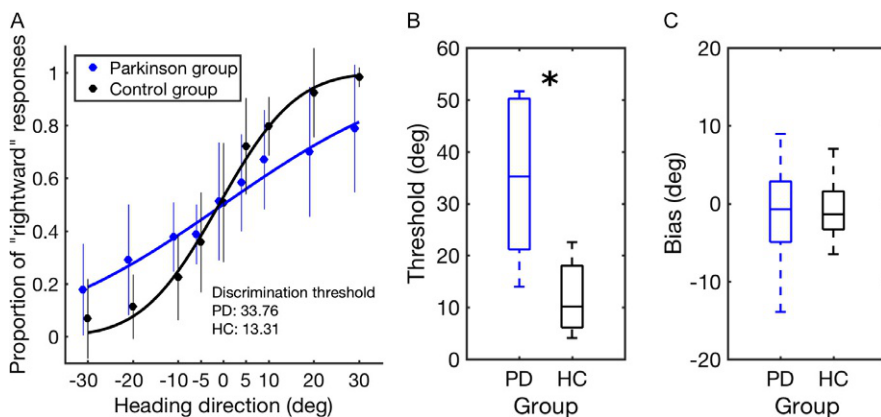


FIG. 2

(A) Psychometric curves of subject groups. A Gaussian cumulative distribution function was fitted to the proportion of rightward decisions averaged over subjects in each subject group. Discrimination thresholds derived from the average psychometric curves of the groups are indicated. Error bars demonstrate standard deviations of the responses at each level of motion direction. Goodness of fit measures of the psychometric curves: $R_{HC}^2 = 0.99$, $R_{PD}^2 = 0.97$. (B and C) Boxplots of discrimination thresholds and vestibular biases of subjects derived from individual psychometric curves. Discrimination threshold of the PD group was found significantly higher than the HC group (Wilcoxon rank sum test, $P < 0.05$, indicated with an asterisk).

a higher discrimination threshold than that of HC ($\sigma_{PD} = 33.76$, 95% confidence interval (CI)=[28.07, 39.45] vs. $\sigma_{HC} = 13.31$, CI=[10.99, 15.62]). On the other hand, bias parameters of PD and HC at the group-level were comparable ($\mu_{PD} = -0.02$, CI=[−2.56, 2.51] vs. $\mu_{HC} = -0.09$, CI=[−2.30, 0.42]).

In a subsequent individual-level analysis, bias and threshold parameters were derived from each subject's psychometric function (Fig. 2B and C) and statistically compared between groups. Two PD and one healthy subject with poor task performance and psychometric functions with goodness-of-fit R^2 values lower than 0.10 were excluded from the statistical comparison as their parameters took unrealistic values. Wilcoxon rank sum tests revealed that discrimination threshold was significantly higher in the PD relative to HC ($z=3.59$, $P < 0.001$, Fig. 2B), while vestibular bias was not significantly different ($z=-0.10$, $P = 0.91$, Fig. 2C).

As the final analysis, we used Spearman's rank-order correlation to test for a possible association between the clinical parameters of the patients and the parameters obtained from the psychometric functions (summarized in Tables 1 and 2, respectively). We found a positive correlation between discrimination threshold and age of the PD patients (Spearman rho=0.65, $P = 0.02$). On the other hand, neither UPDRS-III scores (rho=0.11, $P = 0.72$) nor disease duration were correlated with discrimination threshold (rho=0.08, $P = 0.79$). Additionally, vestibular bias showed no correlation with the total UPDRS-III scores (rho=−0.12, $P = 0.69$), age (rho=−0.38, $P = 0.22$) or disease duration (rho=0.19, $P = 0.53$).

Table 2 Individual percent correct response, vestibular bias and discrimination thresholds of patients.

Patient	Correct response (%)	Vestibular bias (deg)	Discrimination threshold (deg)
1	71.11	0.29	22.02
2	71.72	2.84	21.13
3	78.79	−9.18	17.68
4	67.68	2.25	28.37
5	60.61	−3.66	46.11
6	60.61	8.94	44.58
7	76.32	−13.69	27.04
8	61.62	−13.91	41.99
9	58.59	−4.25	50.21
10	78.79	−0.08	15.66
11	44.44	—	—
12	61.62	−4.95	51.62
13	79.80	−1.40	13.99
14	53.54	—	—

Vestibular bias and discrimination threshold values correspond to the mean and standard deviation of the cumulative Gaussian psychometric function. Vestibular bias and discrimination threshold of Patients #11 and #14 could not be estimated due to poor model fits ($R^2 < 0.10$)

4 Discussion

Maintenance of balance and postural stability during locomotion requires accurate sensing of heading (Barnett-Cowan et al., 2010; Bertolini et al., 2012, 2015; Shaikh et al., 2013, 2017). Common and classic manifestations of PD such as narrow stance, stooped posture with forward flexion of the shoulders, flexion of hips and knees, increased flexion tone, postural sways, and altered percept of verticality are some of the obvious mechanical predisposing factors that result in postural instability and falls. Effectively overcoming such mechanical factors to maintain postural stability and balance depends upon one's ability to integrate proprioceptive, vestibular, and visual information; the basal ganglia being instrumental in modulating this integrative process (Konczak et al., 2007; Maschke et al., 2003; Wright et al., 2007).

Changing the proprioceptive signal alone by modulating muscle tone with pharmacotherapy or DBS, as often seen with the therapeutic interventions in PD, is insufficient to improve balance dysfunction and instability during locomotion. PD patients also have a range of visual deficits that affect postural control and the scaling of movement in response to visual stimuli (Armstrong, 2011; Barbato et al., 1994; Bronstein et al., 1990; Rinalduzzi et al., 2011). Accurate navigation during locomotion also relies on optic flow information (motion of images on the retina during movement) and perceived location of the goal (Fajen and Warren, 2004; Harris and Carre, 2001; Kearns et al., 2002; Turano et al., 2005; Warren et al., 2001). Asymmetries in optic-flow bias the perception of heading direction toward the hemifield with slower optic-flow speed. Thus, PD patients with predominant left-sided symptoms perceive the midline to the right and veer to the right while walking (Chou et al., 2009; Davidsdottir et al., 2008; Duchon and Warren, 2002). However, visual sensory processing changes in PD are not the whole story. Even though peripheral vestibular function and brainstem vestibulo-ocular reflexes are normal in PD, the function of cortical and cerebellar vestibular networks contributing to the multi-sensory integrative processes may be affected (Bertolini et al., 2015; Yousif et al., 2016). Very little is known about the vestibular contribution to the integrative process in individuals with PD.

Our experiments focused on the vestibular heading perception discovering significant inaccuracy in vestibular heading direction discrimination. We found that PD patients had higher angular threshold to detect heading direction, and their perception of self-motion was less sensitive to the variations in heading direction. Our results, while being novel in showing abnormal heading perception in PD, are consistent with previous studies examining abnormal vestibular motion perception in other domains in PD subjects. For example, individuals with PD have difficulty in reliably perceiving the forward tilt of their body—they have a false sense of leaning forward (Bertolini et al., 2012, 2015). The misperception of forward leaning is due to the abnormal interaction of the vestibular signals from the semicircular canals and the otoliths (Bertolini et al., 2015). Such misperception leads to inappropriate compensation and subsequent backward “correction” often leading

to falls. Self-orientation while navigating in the environment is also impaired in PD (Montgomery et al., 1993). Deficiencies in the multisensory integration of vestibular signals is unmasked in PD during dynamic tasks. Maintaining and constantly updating self-orientation during navigation is also impaired in PD (Montgomery et al., 1993).

Why vestibular function is affected in PD? The consequences of dopaminergic neuronal loss in substantia nigra pars reticulata result in abnormal activity in several of the basal ganglia nuclei, including the subthalamic nucleus and connected globus pallidum (internal and external segments). These nuclei are extensively connected to the areas responsible for perception of motion. Ventral subthalamic nucleus stimulation is associated with blood flow changes in premotor cortex; while stimulation of dorsal subthalamic nucleus correlates with changes in the activity of the anterior cerebellar vermis (Hill et al., 2013). The cerebellar outflow is affected by the abnormal bursting and oscillatory subthalamic activity (Rascol et al., 1997; Yu et al., 2007). Stimulation of subthalamus increases neuronal activation in the rat deep cerebellar nuclei (Bostan and Strick, 2010; Moers-Hornikx et al., 2011). The latter modulation may happen through the connections of dorsal aspect of the subthalamus to the deep cerebellar nuclei by the way of pedunculopontine nucleus (Edley and Graybiel, 1983; Noda et al., 1990; Ricardo, 1981; Semba and Fibiger, 1992; Smith et al., 1990; Steininger et al., 1992) or pontine gray (Giolli et al., 2001). Electrical modulation of pedunculopontine nucleus via DBS enhances the perceptual threshold of self-rotation in PD individuals (Yousif et al., 2016). Further downstream from the subthalamo-ponto-cerebellar projections, the cerebello-thalamic pathway connects the vestibular and deep cerebellar nuclei to the ventroposterolateral nucleus of the thalamus (Hoshi et al., 2005; Liedgren et al., 1976; Ni et al., 2010). The vestibular thalamus projects to the parieto-temporal cortex (Akbarian et al., 1992; Middleton and Strick, 2000), which plays a role in vestibular motion perception (Bremmer et al., 2002; Gu et al., 2007). Direct alteration of the cerebellar activity or the modulation of the cerebellar projections to the thalamus changes perception of one's own motion (Bertolini et al., 2012, 2015; Dahlem et al., 2016; Lenz et al., 1988; Shaikh et al., 2013, 2017; Tarnutzer et al., 2012).

We did not find significant correlation between the length of disease duration or severity of motor impairment and vestibular heading perception. Relatively lower number of subjects in this pilot investigation could possibly result in such lack of correlation. Future studies with a larger cohort of PD patients are justified. Our study used a motion platform to generate passive translation. Therefore, it is likely that our outcomes cannot be directly compared to the real-world scenario involving stance and gait abnormalities causing falls in PD. While considering this caveat, it is necessary to utilize the objective motion platform to precisely isolate heading perception distinguishing sensory (vestibular) information. This foundational understanding is necessary to set up future studies that can more explicitly evaluate the role of vestibular perception in gait instability and navigational deficits in a relatively large cohort of patients. Future studies will also include visual and proprioceptive experiments, as well as multi-sensory interactions.

5 Conclusion

We provide a support for the hypothesis that vestibular heading perception is impaired in PD and the impairment is in the form of inaccuracy in perceiving the heading direction. These results provide insights into mechanistic underpinning of navigational deficits, veering and gait instability in PD. These results can be the first step in accomplishing the overall mission to understand the role of multi-sensory input from visual and vestibular system and their integration in navigational deficits and postural instability in PD. In the future, similar concepts can be applied to refining therapeutic measures improving gait instability, abnormal spatial navigation and falls in PD.

References

- Akbarian, S., Grusser, O.J., Guldin, W.O., 1992. Thalamic connections of the vestibular cortical fields in the squirrel monkey (*Saimiri sciureus*). *J. Comp. Neurol.* 326, 423–441.
- Armstrong, R.A., 2011. Visual symptoms in Parkinson's disease. *Parkinsons Dis.* 2011, 908306.
- Barbato, L., Rinalduzzi, S., Laurenti, M., Ruggieri, S., Accornero, N., 1994. Color VEPs in Parkinson's disease. *Electroencephalogr. Clin. Neurophysiol.* 92, 169–172.
- Barnett-Cowan, M., Dyde, R.T., Fox, S.H., Moro, E., Hutchison, W.D., Harris, L.R., 2010. Multisensory determinants of orientation perception in Parkinson's disease. *Neuroscience* 167, 1138–1150.
- Bertolini, G., Ramat, S., Bockisch, C.J., Marti, S., Straumann, D., Palla, A., 2012. Is vestibular self-motion perception controlled by the velocity storage? Insights from patients with chronic degeneration of the vestibulo-cerebellum. *PLoS One* 7, e36763.
- Bertolini, G., Wicki, A., Baumann, C.R., Straumann, D., Palla, A., 2015. Impaired tilt perception in Parkinson's disease: a central vestibular integration failure. *PLoS One* 10, e0124253.
- Bloem, B.R., Grimbergen, Y.A., Cramer, M., Willemsen, M., Zwinderman, A.H., 2001. Prospective assessment of falls in Parkinson's disease. *J. Neurol.* 248, 950–958.
- Bloem, B.R., Hausdorff, J.M., Visser, J.E., Giladi, N., 2004. Falls and freezing of gait in Parkinson's disease: a review of two interconnected, episodic phenomena. *Mov. Disord.* 19, 871–884.
- Bostan, A.C., Strick, P.L., 2010. The cerebellum and basal ganglia are interconnected. *Neuropsychol. Rev.* 20, 261–270.
- Bremmer, F., Klam, F., Duhamel, J.R., Ben Hamed, S., Graf, W., 2002. Visual-vestibular interactive responses in the macaque ventral intraparietal area (VIP). *Eur. J. Neurosci.* 16, 1569–1586.
- Bronstein, A.M., Hood, J.D., Gresty, M.A., Panagi, C., 1990. Visual control of balance in cerebellar and Parkinsonian syndromes. *Brain* 113, 767–779, Pt 3.
- Chou, K.L., Amick, M.M., Gagner, M., 2009. Contrast sensitivity in Parkinson's disease patients with subthalamic nucleus deep brain stimulation. *Mov. Disord.* 24, 766–769.
- Dahlem, K., Valko, Y., Schmahmann, J.D., Lewis, R.F., 2016. Cerebellar contributions to self-motion perception: evidence from patients with congenital cerebellar agenesis. *J. Neurophysiol.* 115, 2280–2285.

- Davidsdottir, S., Wagenaar, R., Young, D., Cronin-Golomb, A., 2008. Impact of optic flow perception and egocentric coordinates on veering in Parkinson's disease. *Brain* 131, 2882–2893.
- Deuschl, G., Schade-Brittinger, C., Krack, P., Volkmann, J., Schafer, H., Botzel, K., Daniels, C., Deuschlander, A., Dillmann, U., Eisner, W., Gruber, D., Hamel, W., Herzog, J., Hilker, R., Klebe, S., Kloss, M., Koy, J., Krause, M., Kupsch, A., Lorenz, D., Lorenzl, S., Mehdorn, H.M., Moringlane, J.R., Oertel, W., Pinsker, M.O., Reichmann, H., Reuss, A., Schneider, G.H., Schnitzler, A., Steude, U., Sturm, V., Timmermann, L., Tronnier, V., Trottnerberg, T., Wojtecki, L., Wolf, E., Poewe, W., Voges, J., Neurostimulation Section German Parkinson Study Group, 2006. A randomized trial of deep-brain stimulation for Parkinson's disease. *N. Engl. J. Med.* 355, 896–908.
- Duchon, A.P., Warren Jr., W.H., 2002. A visual equalization strategy for locomotor control: of honeybees, robots, and humans. *Psychol. Sci.* 13, 272–278.
- Edley, S.M., Graybiel, A.M., 1983. The afferent and efferent connections of the feline nucleus tegmenti pedunculopontinus, pars compacta. *J. Comp. Neurol.* 217, 187–215.
- Fajen, B.R., Warren, W.H., 2004. Visual guidance of intercepting a moving target on foot. *Perception* 33, 689–715.
- Fasano, A., Aquino, C.C., Krauss, J.K., Honey, C.R., Bloem, B.R., 2015. Axial disability and deep brain stimulation in patients with Parkinson disease. *Nat. Rev. Neurol.* 11, 98–110.
- Fetsch, C.R., Turner, A.H., DeAngelis, G.C., Angelaki, D.E., 2009. Dynamic reweighting of visual and vestibular cues during self-motion perception. *J. Neurosci.* 29, 15601–15612.
- Giolli, R.A., Gregory, K.M., Suzuki, D.A., Blanks, R.H., Lui, F., Betelak, K.F., 2001. Cortical and subcortical afferents to the nucleus reticularis tegmenti pontis and basal pontine nuclei in the macaque monkey. *Vis. Neurosci.* 18, 725–740.
- Gu, Y., DeAngelis, G.C., Angelaki, D.E., 2007. A functional link between area MSTd and heading perception based on vestibular signals. *Nat. Neurosci.* 10, 1038–1047.
- Guedry, F.E., 1974. *Psychophysics of Vestibular Sensation*. Springer-Verlag, Berlin-Heidelberg-New York.
- Hanakawa, T., Fukuyama, H., Katsumi, Y., Honda, M., Shibasaki, H., 1999. Enhanced lateral premotor activity during paradoxical gait in Parkinson's disease. *Ann. Neurol.* 45, 329–336.
- Harris, M.G., Carre, G., 2001. Is optic flow used to guide walking while wearing a displacing prism? *Perception* 30, 811–818.
- Hill, K.K., Campbell, M.C., McNeely, M.E., Karimi, M., Ushe, M., Tabbal, S.D., Hershey, T., Flores, H.P., Hartlein, J.M., Lugar, H.M., Revilla, F.J., Videen, T.O., Earhart, G.M., Perlmutter, J.S., 2013. Cerebral blood flow responses to dorsal and ventral STN DBS correlate with gait and balance responses in Parkinson's disease. *Exp. Neurol.* 241, 105–112.
- Hoshi, E., Tremblay, L., Feger, J., Carras, P.L., Strick, P.L., 2005. The cerebellum communicates with the basal ganglia. *Nat. Neurosci.* 8, 1491–1493.
- Kearns, M.J., Warren, W.H., Duchon, A.P., Tarr, M.J., 2002. Path integration from optic flow and body senses in a homing task. *Perception* 31, 349–374.
- Konczak, J., Krawczewski, K., Tuite, P., Maschke, M., 2007. The perception of passive motion in Parkinson's disease. *J. Neurol.* 254, 655–663.
- Krack, P., Batir, A., Van Blercom, N., Chabardes, S., Fraix, V., Ardouin, C., Koudsie, A., Limousin, P.D., Benazzouz, A., LeBas, J.F., Benabid, A.L., Pollak, P., 2003. Five-year follow-up of bilateral stimulation of the subthalamic nucleus in advanced Parkinson's disease. *N. Engl. J. Med.* 349, 1925–1934.

- Lenz, F.A., Tasker, R.R., Kwan, H.C., Schnider, S., Kwong, R., Murayama, Y., Dostrovsky, J.O., Murphy, J.T., 1988. Single unit analysis of the human ventral thalamic nuclear group: correlation of thalamic "tremor cells" with the 3-6 Hz component of Parkinsonian tremor. *J. Neurosci.* 8, 754–764.
- Liedgren, S.R., Milne, A.C., Schwarz, D.W., Tomlinson, R.D., 1976. Representation of vestibular afferents in somatosensory thalamic nuclei of the squirrel monkey (*Saimiri sciureus*). *J. Neurophysiol.* 39, 601–612.
- Maschke, M., Gomez, C.M., Tuite, P.J., Konczak, J., 2003. Dysfunction of the basal ganglia, but not the cerebellum, impairs kinaesthesia. *Brain* 126, 2312–2322.
- Middleton, F.A., Strick, P.L., 2000. Basal ganglia output and cognition: evidence from anatomical, behavioral, and clinical studies. *Brain Cogn.* 42, 183–200.
- Moers-Hornikx, V.M., Vles, J.S., Tan, S.K., Cox, K., Hoogland, G., Steinbusch, W.M., Temel, Y., 2011. Cerebellar nuclei are activated by high-frequency stimulation of the subthalamic nucleus. *Neurosci. Lett.* 496, 111–115.
- Montgomery, P., Silverstein, P., Wichmann, R., Fleischaker, K., Andberg, M., 1993. Spatial updating in Parkinson's disease. *Brain Cogn.* 23, 113–126.
- Ni, Z., Pinto, A.D., Lang, A.E., Chen, R., 2010. Involvement of the cerebellothalamic pathway in Parkinson disease. *Ann. Neurol.* 68, 816–824.
- Noda, H., Sugita, S., Ikeda, Y., 1990. Afferent and efferent connections of the oculomotor region of the fastigial nucleus in the macaque monkey. *J. Comp. Neurol.* 302, 330–348.
- Prokop, T., Schubert, M., Berger, W., 1997. Visual influence on human locomotion. Modulation to changes in optic flow. *Exp. Brain Res.* 114, 63–70.
- Rascol, O., Sabatini, U., Fabre, N., Brefel, C., Loubinoux, I., Celsis, P., Senard, J.M., Montastruc, J.L., Chollet, F., 1997. The ipsilateral cerebellar hemisphere is overactive during hand movements in akinetic Parkinson patients. *Brain* 120 (Pt. 1), 103–110.
- Ren, X., Salazar, R., Neargarder, S., Roy, S., Ellis, T.D., Saltzman, E., Cronin-Golomb, A., 2015. Veering in hemi-Parkinson's disease: primacy of visual over motor contributions. *Vision Res.* 115, 119–127.
- Ricardo, J.A., 1981. Efferent connections of the subthalamic region in the rat. II. The zona incerta. *Brain Res.* 214, 43–60.
- Rinalduzzi, S., Cipriani, A.M., Capozza, M., Accornero, N., 2011. Postural responses to low-intensity, short-duration, galvanic vestibular stimulation as a possible differential diagnostic procedure. *Acta Neurol. Scand.* 123, 111–116.
- Seichepine, D.R., Neargarder, S., Davidsdottir, S., Reynolds, G.O., Cronin-Golomb, A., 2015. Side and type of initial motor symptom influences visuospatial functioning in Parkinson's disease. *J. Park. Dis.* 5, 75–83.
- Semba, K., Fibiger, H.C., 1992. Afferent connections of the laterodorsal and the pedunculopontine tegmental nuclei in the rat: a retro- and antero-grade transport and immunohistochemical study. *J. Comp. Neurol.* 323, 387–410.
- Shaikh, A.G., Palla, A., Marti, S., Olasagasti, I., Optican, L.M., Zee, D.S., Straumann, D., 2013. Role of cerebellum in motion perception and vestibulo-ocular reflex-similarities and disparities. *Cerebellum* 12, 97–107.
- Shaikh, A.G., Straumann, D., Palla, A., 2017. Motion illusion-evidence towards human vestibulo-thalamic projections. *Cerebellum* 16, 656–663.
- Smith, Y., Hazrati, L.N., Parent, A., 1990. Efferent projections of the subthalamic nucleus in the squirrel monkey as studied by the PHA-L anterograde tracing method. *J. Comp. Neurol.* 294, 306–323.

- Steininger, T.L., Rye, D.B., Wainer, B.H., 1992. Afferent projections to the cholinergic pedunculopontine tegmental nucleus and adjacent midbrain extrapyramidal area in the albino rat. I. Retrograde tracing studies. *J. Comp. Neurol.* 321, 515–543.
- Tarnutzer, A.A., Palla, A., Marti, S., Schuknecht, B., Straumann, D., 2012. Hypertrophy of the inferior olivary nucleus impacts perception of gravity. *Front. Neurol.* 3, 79.
- Turano, K.A., Yu, D., Hao, L., Hicks, J.C., 2005. Optic-flow and egocentric-direction strategies in walking: central vs peripheral visual field. *Vision Res.* 45, 3117–3132.
- Warren Jr., W.H., Kay, B.A., Zosh, W.D., Duchon, A.P., Sahuc, S., 2001. Optic flow is used to control human walking. *Nat. Neurosci.* 4, 213–216.
- Wichmann, F.A., Hill, N.J., 2011. The psychometric function: I. Fitting, sampling, and goodness of fit. *Percept. Psychophys.* 63, 1293–1313.
- Wright, W.G., Gurfinkel, V., King, L., Horak, F., 2007. Parkinson's disease shows perceptuo-motor asymmetry unrelated to motor symptoms. *Neurosci. Lett.* 417, 10–15.
- Young, D.E., Wagenaar, R.C., Lin, C.C., Chou, Y.H., Davidsdottir, S., Saltzman, E., Cronin-Golomb, A., 2010. Visuospatial perception and navigation in Parkinson's disease. *Vision Res.* 50, 2495–2504.
- Yousif, N., Bhatt, H., Bain, P.G., Nandi, D., Seemungal, B.M., 2016. The effect of pedunculopontine nucleus deep brain stimulation on postural sway and vestibular perception. *Eur. J. Neurol.* 23, 668–670.
- Yu, H., Sternad, D., Corcos, D.M., Vaillancourt, D.E., 2007. Role of hyperactive cerebellum and motor cortex in Parkinson's disease. *Neuroimage* 35, 222–233.

This page intentionally left blank

A new approach for estimation of spiketrain patterns in basal ganglia

25

Vladislav Myrov^a, Alexey Sedov^{b,*}, Alexey Tomskiy^c, Ludmila Myrova^d,
Elena Belova^b

^aSaint Petersburg Academic University, Saint Petersburg, Russia

^bSemenov Institute of Chemical Physics, Moscow, Russia

^cN.N. Burdenko National Scientific and Practical Center for Neurosurgery, Moscow, Russia

^dMoscow Scientific Research Institute of Radio Engineering, Moscow, Russia

*Corresponding author: Tel.: +7-903-579-5024, e-mail address: AlexeyS.Sedov@gmail.com

Abstract

The pathophysiological model of dystonia proposed that in addition to reduced firing rate in the internal pallidum, changes in the pattern may also play a role in disease manifestation. While common methods for patterns separation depends on arbitrary spiketrain parameters, we considered the new method for neural patterns based on spike density histograms and hierarchical clustering of real datasets. We used the single unit activity recordings from the globus pallidus external (GPe) and the globus pallidus internal (GPi) from 10 cervical dystonia (CD), 7 segmental dystonia (SD) and 8 generalized dystonia (GD) patients undergoing deep brain stimulation surgery. Using novel method, we separated three patterns of activity: burst, burst-like and tonic. Using this separation, we revealed the differences both in firing rate and pattern distribution between dystonia patients. We have shown the suitability of the proposed method for pattern clusterization on real data and assume that further application of this method would facilitate more detailed study of the neural activity in the basal ganglia and the search for neurophysiological biomarkers of movement disorders.

Keywords

Neuronal activity, Neuronal patterns, Cluster analysis, Spike density histogram, Basal ganglia, Dystonia

1 Introduction

Dystonia is a movement disorder characterized by sustained muscle contractions, twisting, repetitive movements, and abnormal postures of the affected body part. Most hypotheses regarding the pathophysiology of dystonia emphasize alterations

in the basal ganglia-thalamocortical motor circuit. The current model for pathophysiology of dystonia proposed that, in addition to reduced firing rate in GPi, changes in the pattern and the degree of synchronization in neuronal activity may cause dystonia (Starr et al., 2005; Tang et al., 2007; Vitek, 2002). We hypothesize that the involvement of a larger volume of muscles in GD compared with SD and CD should lead to significant changes in both firing rates and neuronal activity patterns in GPi. We tested this hypothesis using previously described approach (Myrov et al., 2019) that separates spiketrains into different patterns in order to assay the usefulness of this method for neurophysiological problems.

2 Materials and methods

2.1 Data description

In the present study, we used the dataset of single unit activity recordings: the data from the globus pallidus external (GPe, 638 single units) and the globus pallidus internal (GPi, 741 single units) were acquired from patients with cervical, segmental and generalized dystonia (10, 7 and 8 patients, respectively). The data were collected during deep brain stimulation (DBS) surgeries at the N.N. Burdenko Neurosurgery Institute in 2014–2017. The participants gave written informed consent for the surgery and the involvement in research. Studies were approved by the ethical committee and was performed according to the Declaration of Helsinki.

The signals acquired during recordings were pre-processed and analyzed using Spike 2 software (CED, Cambridge, UK). The steps for data pre-processing included bandpass filtering (300–5000 Hz for MER), alignment and spike sorting. Spikes were detected using an amplitude threshold and then sorted by means of principal component analysis (PCA).

2.2 Method description

To derive the pattern parameters, we have clustered spike trains based on the histograms for neural activity recordings (spike density histograms SDHs). Jensen-Shannon Divergence (JSD) were used as a distance metrics. For grouping spiketrains into the patterns, we have used hierarchical clustering approach; we chose Ward's method for merging the branches (Ward, 1963) because it minimizes the total within-cluster variance at each merging step (Myung, 2003). According to Wards algorithm, at each step the most adjacent clusters are merged. The distance between two clusters is defined as the increase in the error sum of squares after merging the clusters.

The Elbow method was used to determine the optimal number of clusters. To identify significant differences between the pattern distribution for CD, SD and GD, we bootstrapped our data 100 times and performed Mann-Whitney non-parametric test. As significance threshold we chose P value equal to 0.05.

3 Results

We performed independent clustering of SDHs for GPi and GPe data to classify spike trains into the patterns.

The Elbow method revealed three to be the optimal number of clusters. We found 344 burst cells with FR 34 (23–48) and CV 1.46 (1.29–1.77), 563 burst-like cells with FR 61 (47–78) and CV 1.08 (1.00–1.18), and 472 tonic cells with FR 68 (38–101) and CV 0.86 (0.74–0.95) (Fig. 1). Pattern distribution and description for each group can be found in Table 1, typical spiketrains are shown in Fig. 1. The table displays significant differences between firing rate (FR) and coefficient of variance (CV) between particular patterns. One can also notice the differences in both firing rate and firing patterns between GPi and GPe nuclei as well as CD, SD and GD patients.

We found that the percentage of GPi tonic cells was significantly lower in GD patients, but the percentage of GPe tonic cells was higher in CD patient. Firing rate

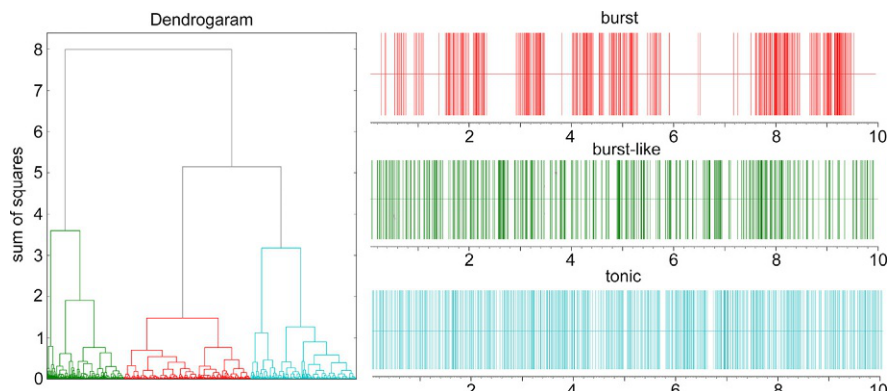


FIG. 1

Dendrogram and typical spiketrains for the patterns.

Table 1 Proportion of patterns with corresponding FR and CV in each state for GPi and GPe data.

Structure	Pattern	CD		SD		GD	
		Distribution (%)	FR	CV	Distribution (%)	FR	CV
GPi	Burst	27.1	29	1.50	22.1	44	1.31
	Burst-like	43.9	63	1.05	45.3	60	1.06
	Tonic	29.0	83	0.86	32.6	56	0.79
GPe	Burst	19.7	36	1.55	27.9	29	1.66
	Burst-like	32.7	52	1.16	34.5	63	1.11
	Tonic	47.6	67	0.87	37.6	72	0.85

of GPi tonic cells was higher and burst cells was lower in CD patients. We also found that percentage of GPe burst cells was lower in CD patients. Firing rate of GPi burst-like cells and all GPe cells was not significantly different.

4 Discussion

This study demonstrates the suitability of previously described method (Myrov et al., 2019) for firing pattern estimation in dystonia patients. This method isolates three clusters of single unit activity with different firing rate and pattern characteristics without any assumptions of underlying statistical models. This division allowed us to describe in more detail the physiological properties of the GPi and GPe cells and to compare specific parameters of activity in patients with CD, SD and GD.

Our estimation approach showed the differences between GPi and GPe firing patterns for each group of patients. We found that characteristics of both GPi and GPe nuclei in CD patients significantly differ from SD and GD. Wherein SD and GD patients have the same characteristics of single unit activity. In addition, we found that the differences were observed in tonic and burst cells while burst-like neurons showed similar activity.

Previous studies showed reduction of GP activity in mouse model of dystonia (Nambu et al., 2011) and in dystonic patients compared to healthy non-human primates (Starr et al., 2005). Neuronal model of dystonia also showed changes in GP firing pattern (Vitek, 2002). According these data we hypothesized linear reduction or pattern changes in GP activity from CD to SD and then GD patients. But we found significant differences only between CD and other patients. This may be due to differences in the pathophysiology of the cervical and other dystonias. We suppose that further division of dystonia patients into different subgroup is needed to find correlation between clinical features and single unit activity. Further application of the method will facilitate more thorough study of the neural activity in the basal ganglia and the search for neurophysiological biomarkers of various subtypes of dystonia.

Acknowledgment

This study was supported by the Russian Science Foundation (RScF 18-15-00009).

References

- Myrov, V., et al., 2019. Neural activity clusterization for estimation of firing pattern. *J. Neurosci. Methods* 311, 164–169.
- Myung, I.J., 2003. Tutorial on maximum likelihood estimation. *J. Math. Psychol.* 47 (1), 90–100.
- Nambu, A., et al., 2011. Reduced pallidal output causes dystonia. *Front. Syst. Neurosci.* 5, 89.

- Starr, P.A., et al., 2005. Spontaneous pallidal neuronal activity in human dystonia: comparison with Parkinson's disease and normal macaque. *J. Neurophysiol.* 93 (6), 3165–3176.
- Tang, J.K.H., et al., 2007. Neuronal firing rates and patterns in the globus pallidus internus of patients with cervical dystonia differ from those with Parkinson's disease. *J. Neurophysiol.* 98 (2), 720–729.
- Vitek, J.L., 2002. Pathophysiology of dystonia: a neuronal model. *Mov. Disord.* 17 (Suppl. 3), 49–62.
- Ward, J.H., 1963. Hierarchical grouping to optimize an objective function. *J. Am. Stat. Assoc.* 58 (301), 236–244.

This page intentionally left blank

SECTION

RESEARCH: **VIII**
Others

This page intentionally left blank

A model-based study of internuclear ophthalmoparesis and ocular-motor fatigue in multiple sclerosis

26

Jonathan B. Jacobs^{a,b,c}, Clara Chisari^d, Margaret M. Skelly^a,
Mark F. Walker^{a,b}, Alessandro Serra^{a,b,e,*}

^aDaroff-Dell'Osso Ocular Motility Laboratory, Department of Neurology, Louis Stokes Cleveland VA Medical Center, Cleveland, OH, United States

^bSchool of Medicine, Case Western Reserve University, Cleveland, OH, United States

^cDepartment of Biomedical Engineering, Case Western Reserve University, Cleveland, OH, United States

^dDepartment of Neurology, University of Catania, Catania, Italy

^eDepartment of Neurology, University Hospitals Cleveland Medical Center, Cleveland, OH, United States

*Corresponding author: Tel.: +1-216-844-3193, e-mail address: axs505@case.edu

Abstract

Internuclear ophthalmoparesis (INO) in multiple sclerosis (MS) is due to demyelination of the medial longitudinal fasciculus (MLF). INO is typically modeled as an increased peak-velocity and peak-acceleration ratio of abducting to adducting eye (pulse-size ratio, PSR). PSR can be affected by fatigue during prolonged ocular-motor tasks (ocular-motor fatigue). We propose that an important component of horizontal disconjugacy in INO is due to a delayed delivery of the saccadic pulse to the adducting eye (pulse-time delay, PTD). We expanded a control-system model to account for both abnormal PSR and PTD reflecting faulty axonal transmission in INO and to provide a better understanding of possible changes induced by fatigue. Saccades were measured in 19 MS patients with INO and 10 controls, using a 10-min saccadic “fatigue test” consisting of repetitive back-to-back 20° saccades. In the horizontal saccades model the unitary MLF connection was partitioned into parallel sub-tracts representing progressive degrees of disease effect. INO patients showed baseline abnormal PSR and PTD with some changes during the fatigue test. Manipulations of gain and transmission delay in the model provided simulated saccades that closely resembled those of INO. Ocular-motor fatigue may be a heterogeneous phenomenon that involves inter-saccadic fluctuation of PSR and PTD and adaptation during demanding ocular-motor tasks. INO as a model of abnormal axonal conduction has a potential role in assessing efficacy of reparative therapies in MS.

Keywords

Saccades, Internuclear ophthalmoparesis, Multiple sclerosis, Fatigue, Medial longitudinal fasciculus

Abbreviations

BGNI	burst generator and neural integrator
PAR	peak-acceleration ratio
PSR	pulse-size ratio
PTD	pulse-time delay
PTD_a	PTD-acceleration
PTD_o	PTD-onset
PVR	peak-velocity ratio

1 Introduction

Internuclear ophthalmoparesis (INO) is a disorder of horizontal saccadic conjugacy and the most common eye movement abnormality in multiple sclerosis (MS) (Frohman et al., 2002; Meienberg et al., 1986; Müri and Meienberg, 1985; Tilikete et al., 2011). Demyelination of the medial longitudinal fasciculus (MLF) in MS causes slowing of the adducting eye during horizontal saccades. The neural network for horizontal saccades control is quite straightforward (Leigh and Zee, 2015; Serra et al., 2018): excitatory burst neurons lying in the paramedian pontine reticular formation (PPRF) generate a velocity command called the pulse of innervation that projects to the abducens motor neurons and abducens internuclear neurons within the abducens nucleus. The pulse of innervation travels from abducens motor neurons onto axons of the ipsilateral abducens nerve to the lateral rectus muscle, and from the abducens internuclear neurons via the MLF to the contralateral oculomotor nucleus and medial rectus muscle via the oculomotor nerve. In normal subjects, both eyes rapidly accelerate to deliver an ipsilateral conjugate saccade that quickly lands gaze on the target. Normal values for the various parameters of horizontal saccades have been established at baseline and after prolonged ocular-motor tasks (Collewijn et al., 1988; Fuchs and Binder, 1983).

In MS, acute or chronic demyelination may result in axonal damage or axonal loss within the MLF, which can no longer efficiently conduct high-frequency signals (pulse of innervation) causing slowing of ipsilateral eye adduction. INO is a cornerstone clinical finding on bedside examination for the diagnosis of MS and it can be reliably quantified and measured over time in the laboratory settings (Chen et al., 2011; Frohman et al., 2002; Leigh and Zee, 2015). INO may be a significant cause of visual disability for patients affected by MS as it interferes with daily activities, presenting with double or blurred vision and inconvenient breaks in binocular fusion during rapid head turning (Mills et al., 2008).

The circuitry responsible for conjugate horizontal saccades can be represented as a basic mathematical model, which was originally developed to account for conjugate saccades and their interactions with disconjugate vergence movements (Zee et al., 1992). It incorporates saccade generator components that are based on electrophysiological measurements of burst neurons in the brainstem of monkeys, a neural integrator unit (pulse-step integration) and ocular-motor plant units (orbital contents), also directly derived from studying macaque and human saccades. This model can simulate conjugate horizontal saccades made by normal subjects and disconjugate saccades, for instance similar to the ones observed in INO.

Multiple studies have utilized INO as a model of abnormal axonal transmission in MS. For instance, combined imaging and electrophysiological studies of the MLF have proposed INO as a biomarker of axonal and myelin integrity (Wang et al., 2015). Modeling of INO has provided insights into understanding of symptoms commonly associated with MS, such as Uhthoff's phenomenon and fatigue (Davis et al., 2008; Matta et al., 2009). Motor fatigue is a common and disabling symptom in patients with MS but its pathophysiological mechanisms remain unclear and no effective treatment is available. INO is typically modeled as an increased peak-velocity or peak-acceleration ratio of abducting to adducting eye (*pulse-size ratio, PSR*) as a consequence of “low-pass filtering” of the saccadic pulse along the demyelinated MLF axons. In other studies, PSR is also referred to as “versional disconjugacy index” (VDI) (Frohman et al., 2002, 2003). In a small MS population with INO, PSR changes have been shown during prolonged ocular-motor tasks (*ocular-motor fatigue*), suggesting INO may represent a reductionist model for motor fatigue in MS (Matta et al., 2009). Other studies have shown changes of saccadic peak velocity, latency and amplitude in MS patients who report symptoms of fatigue (Ferreira et al., 2017; Finke et al., 2012). Our previously unreported observations suggest that a component of horizontal disconjugacy in INO is due to a delayed delivery of the saccadic pulse to the adducting eye. We will refer to this interocular difference in timing of saccade onset as the *pulse-time delay, PTD*.

To better characterize the dynamics of PSR and PTD changes in INO at baseline and during prolonged ocular-motor tasks, we set out to study horizontal saccades in a larger population of MS patients with INO, and to implement a control-system model that can reproduce the complex range of behaviors observed in MS patients, based on the underlying physiological hypothesis of decreased conduction gain and velocity along the population of MLF axons.

2 Methods

2.1 Eye movement recording

We recorded saccades in 19 MS patients (median age 47, 8 females) with chronic mild to moderate INO with full adduction range (13 bilateral, total 32 INO eyes) and 10 age-matched healthy controls, using a 10-min saccadic “fatigue test”

consisting of repetitive back-to-back 20° saccades ($\pm 10^\circ$) in response to a target jump at 0.5 Hz. Eye movements were measured using the EyeLink II (SR-Research, Ontario, Canada), sampled at 500Hz with 16-bit precision. Each eye was calibrated monocularly to allow detection of tropias and phorias. To avoid diplopia, patients were tested monocularly during the fatigue test; the viewing eye was typically the one affected by INO, or the one that appeared more affected on clinical exam in patients with bilateral INO. To prevent phase distortion, eye position was filtered forward and backward using a time-symmetric fourth-order low-pass Butterworth filter with a cutoff frequency of 25 Hz, safely above the spectral profile found by FFT analysis of the data. Velocity and acceleration were calculated using a symmetric central-point differentiator of width 5 (two points before and two after the central point). Neither the filtering nor the differentiation caused shifts in time.

All eye-movement analysis, including detection of voluntary saccades, was performed using custom software (OMtools, available from <http://omlab.org/software/software.html>). A saccade was determined to begin when its velocity exceeded a threshold of 40°/s, and to terminate when the velocity dropped below 40°/s. (We observed that using a lower threshold would often yield negative results for PTD due to differentiation noise as well as small square-wave jerks and other saccadic intrusions occurring during the purposive saccade.) Additionally, we could specify detection in either or both eyes, in either or both directions, and include saccades only within a specified amplitude range. The detection algorithm did not automatically include saccades for analysis; that was left to the judgment of the operator performing the analysis.

For each saccade we measured PSR, both by abducting-to-adducting eye peak-velocity ratio (PVR) and peak-acceleration ratio (PAR), and PTD, both as the time difference of saccade onset between the adducting and abducting eyes (PTD-onset, PTD_o) and as interocular difference in timing of peak acceleration (PTD-acceleration, PTD_a). We excluded from our PSR and PTD analysis the double-stepped saccades we observed in some cases of INO, although we provide an explanation for their dynamics later in the discussion. Saccades were measured for three consecutive time intervals (T1-T3) of 200s each to evaluate for changes possibly induced by ocular-motor fatigue. An average of 44.8 ± 22.5 saccades were collected at each interval per INO. An average of 48.3 ± 16.5 saccades were collected per control in each direction of horizontal gaze. Only saccades of at least 10° of amplitude were included.

Statistical analysis was performed using STATA 12.1 software packages (StataCorp. 2011; Stata Statistical Software: Release 12; College Station, TX: StataCorp. LP). In descriptive analyses, continuous variables were summarized as mean and standard deviation (SD) or median, and categorical variables were expressed as percentages. The numerical dataset was tested for normal distribution with the Shapiro-Wilk test. In case of abnormal distribution, non-parametric tests were performed. Differences between patients and controls were tested using the Fisher exact and Mann-Whitney U tests for dichotomous and continuous variables,

respectively. Nominal data were analyzed by Pearson's Chi Square or Fisher's exact test, where applicable. To assess PSR and PTD differences at each time point (T1, T2, and T3), ANOVA (Bonferroni, post hoc analysis) and Kruskal/Wallis were carried out, when appropriate. A P value lower than 0.05 was considered statistically significant.

2.2 Model simulation

The full model, shown in Fig. 1, is an expansion of an earlier model of INO whose saccade dynamics are adapted from Zee et al. (1992). That original model used a combined burst generator and neural integrator (BGNI) with a large negative feedback and a fast-saturating non-linear feed-forward function to create a pulse-slide-step signal to drive a plant model composed of a single-pole, zero-pole, and complex-pole series of transfer functions.

2.2.1 Single-branch model

To create the first approximation of INO, we split the BGNI output into two paths: one that continued to the plant as before (abducting, or unaffected), while the second was passed through a combination of pure time delay and a low-pass function to model the effects of impaired conduction through the MLF before reaching an identical copy of the plant (adducting, or impaired). Eq. (1) describes the low-pass filter that we used in the MLF pathway component axons:

$$\text{LPF: num}/(sTc + 1), \quad (1)$$

where num is the gain and Tc is the time constant, specified in seconds.

Simply modifying the time constant of the low-pass is sufficient to alter the shape of the pulse-slide-step, decreasing the total energy delivered to the plant and delaying when that energy arrives (Fig. 2A). However this delay does not affect when the *leading edge* of the signal reaches the plant, which is where it begins to move, only how long it takes for the eye to reach its maximal position. It cannot account for an additional type of delay that we have observed in some of our patients, namely that there is an increased delay before the affected eye shows any movement with respect to the unimpaired eye, as modeled in Fig. 2B, where the timing of peak output of a delayed signal (yellow) can appear after that of an undelayed, but filtered one (blue).

To allow simulation of these *en bloc* delays, we added a pure delay prior to the low-pass block. From a modeling perspective, there is no difference in the response if the delay is placed following the LPF block. Finally, by varying its numerator, the low-pass can be modified to act as a transmission gain for the MLF. (It makes sense only to decrease below unity as we are representing a decreased number of axonal fibers.) Adjustments of these three parameters (time constant, delay, and gain) allowed us to reproduce some basic patient saccades, capturing details such as greater hypometricity, slower rise to peak velocity, and greater delay before the onset of eye movement. As powerful as this model is, we still regularly encountered

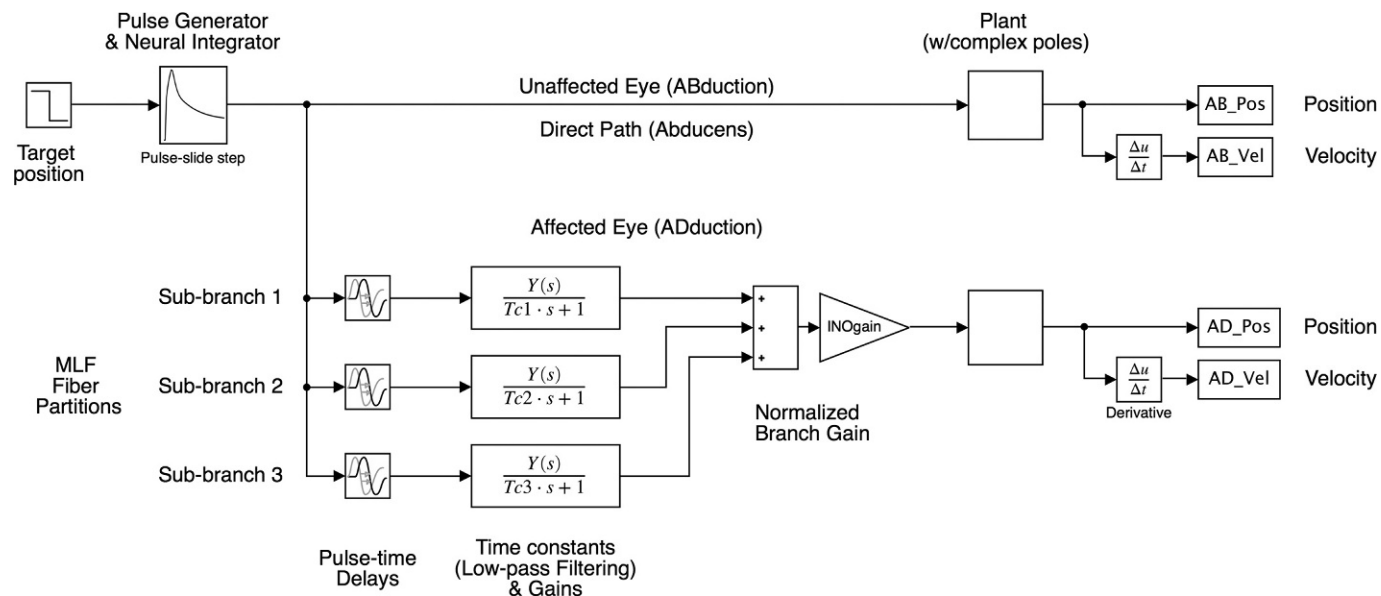


FIG. 1

The INO model. The target change directs the burst generator and neural integrator (BGNI) to generate a pulse-slide-step tuned to the plant dynamics. The signal is divided, with the top pathway driving the abducting eye, and the lower pathway(s) driving the adducting eye through one or more branches of the MLF, which have user-variable gain, delay and time constants.

Based on Zee, D.S., Fitzgibbon, E.J., Optican, L.M., 1992. Saccade-vergence interactions in humans. *J. Neurophysiol.* 68 (5), 1624–1641.

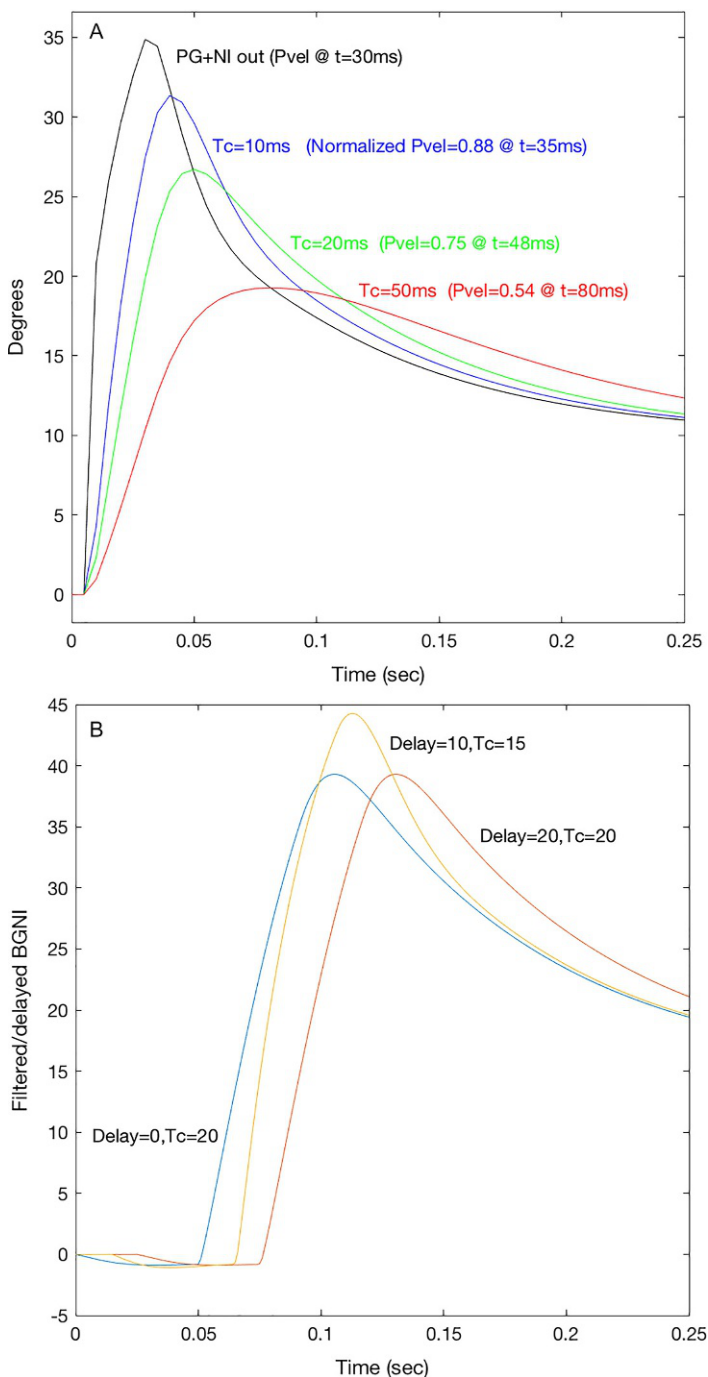


FIG. 2

Model simulations of the effect of time constant on pulse-slide-step from BGNI. (A) As T_c increases, the peak velocity of the resulting saccade is decreased due to the low-pass filtering effect. Also, the initially sharp peak-velocity is broadened and delayed in time. (B) Combined effects of T_c and delay. Because these effects partially overlap, it can be difficult to determine how much of these changes, both at baseline and following fatigue are due to which factor.

saccadic responses that were too complex for it to reproduce. We found multiple instances of saccades with double peaks in their velocity data, as well as others with prolonged plateaus where we expected a normal-shaped peak-velocity profile.

2.2.2 Multiple-branch model

The appearance of such complex saccades suggests the possibility of superposition of signals dispersed in time. To implement this in the model, we chose to split the MLF into three branches, each with its own time constant, gain, and delay block. This is intuitively satisfying physiologically as well, because the MLF contains a great many axons, and there is no reason to believe that they should all be uniformly affected by the demyelinating process of MS. By partitioning the MLF, we can treat each branch differently, for example modeling a population of minimal disease, moderate disease, and severe disease, with parameters unique to each condition. The branches feed into a summation node followed by a gain multiplier of 1/3 to renormalize the combined signal to the same range as in the original model before being fed to the complex plant. Values of all parameters are set using a graphical interface. It is possible to replicate the original single-branch model by disabling the other two branches. The gain multiplier is automatically adjusted to match the number of active branches.

3 Results

3.1 Saccades parameters

In the control group, average PSR values for both velocity and acceleration were close to 1 at each time interval: PVR were 0.978 at T1, 0.977 at T2, and 0.979 at T3; PAR were 0.987 at T1, 0.99 at T2 and 0.992 at T3. Average PTD_o values were 0.0016 s at T1 through T3. Average PTD_a values were 0.002 s at T1, 0.0017 s at T2 and 0.0018 s at T3. PSR and PTD did not change significantly following the fatigue test in the controls.

Patients with INO showed baseline abnormal PSR for both velocity and acceleration values, with baseline PVR and PAR of 1.2 and above. Average of PVR was 1.88 at T1, 1.91 at T2, and 1.9 at T3; average of PAR was 2.23 at T1, 2.25 at T2 and 2.22 at T3, both measures at each time significantly higher than those in the control group. PSR did not change significantly following the fatigue test for the INO group. PTD_o values were 0.010 s at T1 through T3, at each time significantly higher than those in the control group. Average PTD_a values were 0.006 s at T1, 0.005 s at T2 and T3, at each time significantly higher than those in the control group. PTD did not change significantly following the fatigue test for the INO group.

Looking at individual results, seven INOs showed significant decrease of PVR at T3 vs T1, and six INOs showed significant increase of PVR at T3 vs T1. Eight INOs showed significant decrease of PAR at T3 vs T1, and five INOs showed significant increase of PAR at T3 vs T1. One INO showed significant increase of PTD_o at T3 vs T1, and one INO showed significant decrease of PTD_a at T3 vs T1.

Manipulations of T_c , gain, and transmission delay in the model provided simulated saccades that closely resembled those of INO patients during the fatigue test.

3.2 Model simulation: PSR changes

[Fig. 3](#) shows an example of PSR increase after the fatigue test in a patient with INO and in the model.

Panels A and B show a leftward saccade of a patient with INO at the beginning and toward the end of the fatigue test, respectively. This patient has bilateral INO and is viewing with the left eye. After fatigue, the PVR increases from 1.67 to 2.3 due to decrease of peak velocity of both eyes but with a relatively greater decrease in the adducting eye. Panels C and D show the model simulation. To reproduce this subject's saccades, we first matched the timing of the abducting and adducting peak velocities. A T_c of 15ms (with no decreased gain setting or added delay) was sufficient to simulate a right INO, and by itself yielded a PSR of 1.14. Decreasing the gain to 0.68 resulted in a PSR of 1.67 (C), and a further decrease to 0.5 resulted in a PSR of 2.28 (D).

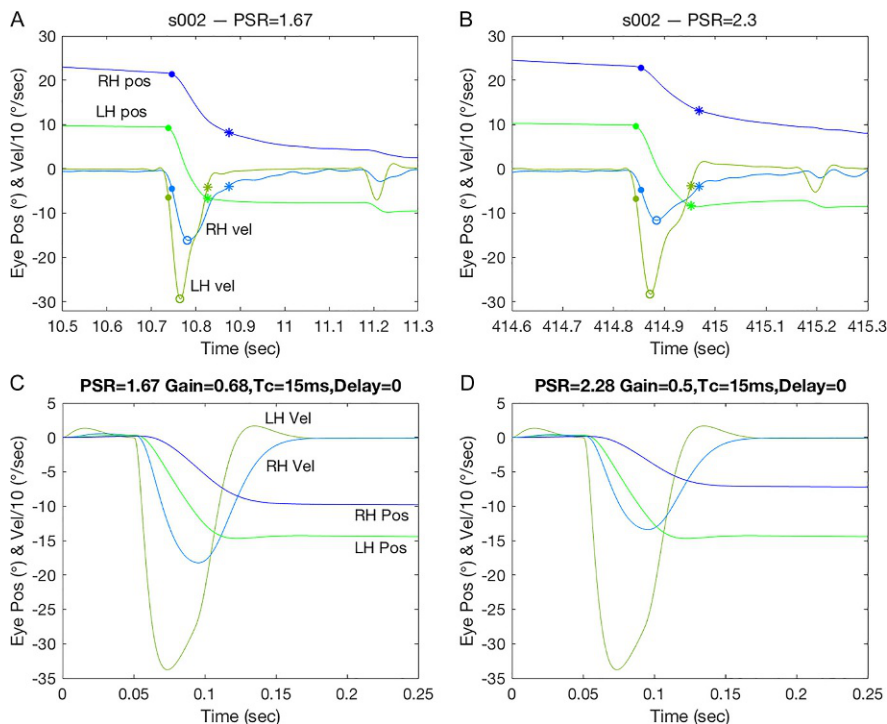


FIG. 3

PSR changes (increase) in INO and in the model. The subject has made a leftward saccade so the right eye response (in blue) is slower and hypometric (A, B). Panels C and D show the model simulations. See text for details. The closed circles mark the time of saccade onset based on velocity; the stars show the end of the saccade; the open circles mark the peak velocity. RH pos: right eye position; LH pos: left eye position; RH vel: right eye velocity; LH vel: left eye velocity.

3.3 Model simulation: PTD changes

Fig. 4 shows examples of PTD variability in the same subject, irrespective of possible ocular-motor fatigue.

Close-up views of the velocity and acceleration traces from two rightward saccades of a patient with INO, both occurring at the beginning of the fatigue test, are shown in panels A and B. This patient has bilateral INO and is viewing with the right eye. These two consecutive saccades from the same subject have very different

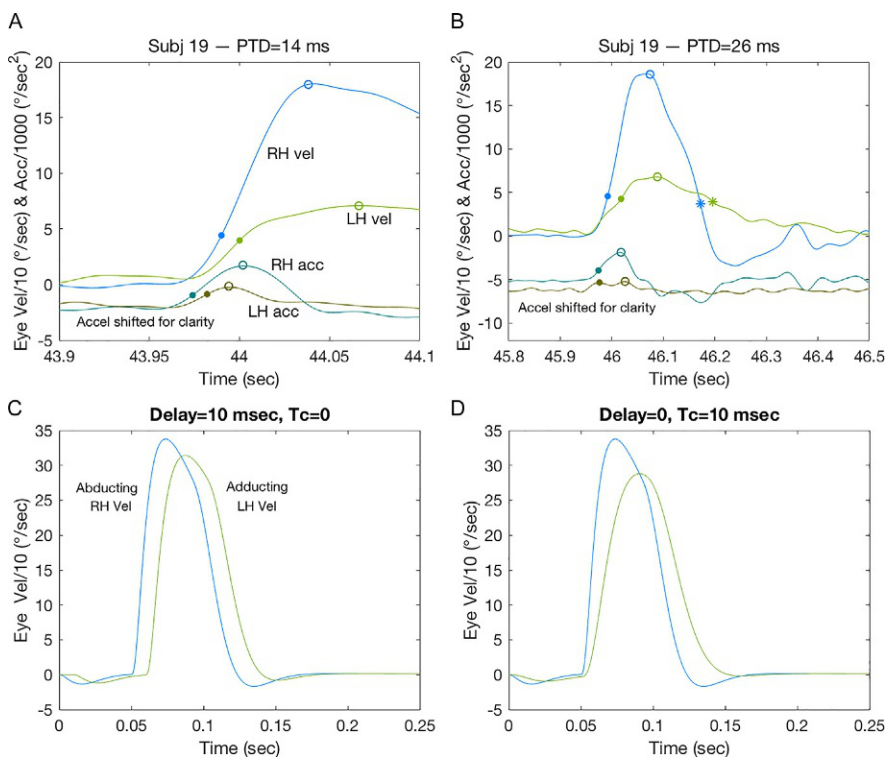


FIG. 4

PTD changes in INO (velocity and acceleration traces shown) (A, B) and in the model (velocity traces only shown) (C, D). In the left panels (A, C), there is a difference in timing between when the adducting and abducting eyes begin their saccades, suggesting the introduction of a pure delay. Panel C shows the abducting eye velocity rising above its baseline before the adducting eye does. This is more clearly seen in the acceleration traces (bottom two lines). In the right panels (B, D), there is little to no difference in when either velocity leaves baseline; this PTD is more likely due to Tc effect. The closed circles mark the time of saccade onset based on velocity; the stars show the end of the saccade; the open circles mark the peak velocity and peak acceleration. RH vel: right eye velocity; LH vel: left eye velocity; RH acc: right eye acceleration; LH acc: left eye acceleration.

PTD, 14 and 26 ms, respectively. Panel A shows that the velocity traces leave baseline at distinctly separate times (as shown by acceleration traces), therefore the PTD is likely due to pure delay. In panel B there is little to no difference between the times the velocity traces leave baseline. In this case it is more likely that the PTD is due to the filtering effect of the Tc component. Panels C and D show the respective cases for the model: (C) Use of pure time delay; (D) use only of elevated Tc.

In many cases, it will be possible to model the subject's findings using solely a single-branch increase in Tc, or by introducing a time delay in addition to that increase in Tc. For larger PTDs, however, it may not be feasible to rely on increased delay and Tc alone.

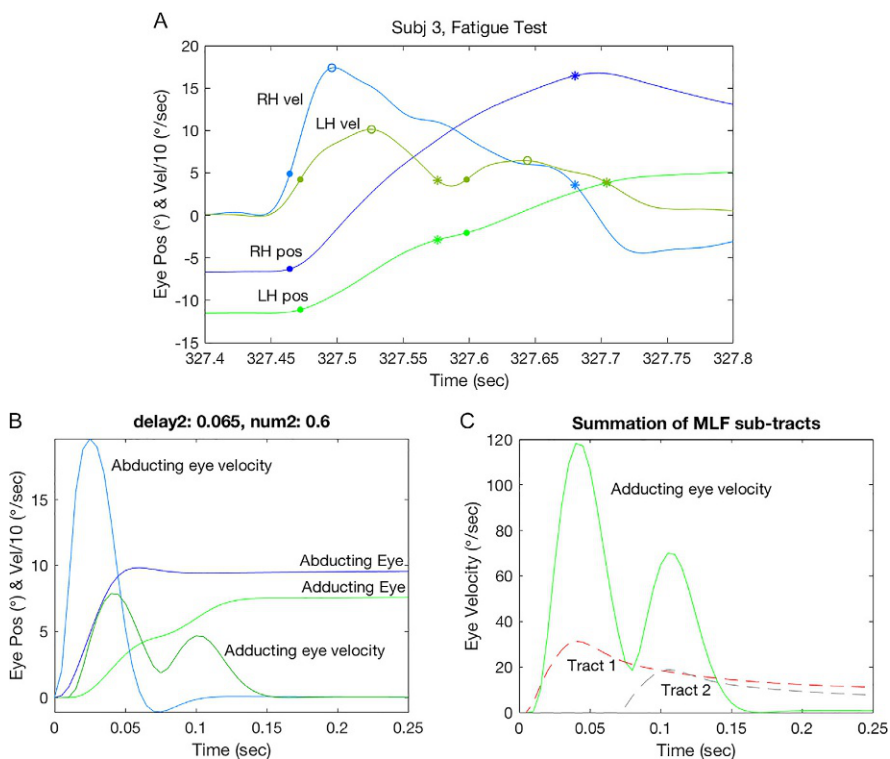
3.4 Model simulation: Complex saccades

The use of additional sub-tracts can generate complex motions of the affected eye by allowing for the superposition of multiple scaled and time-shifted signals transmitted along each branch of the MLF. For example, even using only two of the three sub-tracts, we could simulate double-stepped single saccades, as sometimes seen in INO due to MS.

[Fig. 5A](#) shows a saccade recorded from one of our subjects. Note that the adducting eye (green) has two distinct saccades as the velocity dropped below 40°/s, while the abducting eye (blue) only has a single saccade. Panel B demonstrates the model simulating this by addition of a scaled and delayed pulse from BGNI over the second MLF sub tract. Panel C is a schematized view of the velocity trace, showing the contributions of the initial and secondary pulses.

4 Discussion

The horizontal binocular disconjugacy characteristic of INO has been used to understand common disabling symptoms in MS, such as sensitivity to high temperature and primary motor fatigue ([Davis et al., 2008](#); [Ferreira et al., 2017](#); [Finke et al., 2012](#); [Matta et al., 2009](#)). Because INO is an eye movement disorder accessible to accurate recording and quantification, it has been proposed as an actual model of demyelination and impaired axonal conduction in MS, which may be of greater utility when its study is coupled with advanced neuroimaging techniques ([Sakaie et al., 2011](#); [Wang et al., 2015](#)). Our study of several INOs due to MS, supported by simulations in an improved control model of horizontal saccades, allowed us to expand the characterization of INO in a way that may better correlate with the underlying hypothesis of faulty axonal transmission along the MLF. We believe this study further supports the utility of INO as a strong outcome measure for trials of therapies that can improve axonal conduction, and even reparative agents. This category of treatments has received a great deal of attention and there is experimental evidence that several compounds with remyelinating properties might soon turn useful in patients with MS ([Mei et al., 2014](#); [Najm et al., 2015](#); [Scolding et al., 2017](#)).

**FIG. 5**

Examples of double-stepped saccades in INO and in the model. (A) This patient's adducting saccade (green) shows two separate velocity peaks, while the abducting saccade only has one velocity peak. (B, C) The model can reproduce this by the addition of a second MLF sub-tract with a pure delay and reduced gain. See text for details. The closed circles mark the time of saccade onset based on velocity; the stars show the end of the saccade; the open circles mark the peak velocity. RH pos: right eye position; LH pos: left eye position; RH vel: right eye velocity; LH vel: left eye velocity.

What does our study add to the way INO is typically modeled and measured through eye movement recording? Fundamental studies have shown that INO is best quantified as an abnormal abducting-to-adducting eye ratio of peak velocity, acceleration and saccade amplitude (Chen et al., 2011; Flipse et al., 1997; Frohman et al., 2003; Serra et al., 2008), and these measures have been even formally standardized as “versional disconjugacy index” (VDI) (Frohman et al., 2002, 2003). Abnormalities of the above measures reflect the underlying pathological process of INO where, due to demyelination and axonal compromise and loss, a smaller pulse of innervation is delivered to the adducting eye causing a typical slowing during horizontal

saccades. The classic findings of abnormal peak velocity and acceleration ratio (PVR, PAR) in INO are consistent with the results from our patient population, when comparing to values of normal controls. However, our results emphasize that a component of horizontal disconjugacy in INO is due to a delayed delivery of the saccadic pulse to the affected eye. While controls show physiological delay in saccade onset between the two eyes of <2 ms, with saccade onset calculated based on a 40°/s velocity threshold, our results show that this pulse time delay (PTD_o) in INO patients is significantly higher, with average values of 10 ms. Also, while other studies have considered the interocular time difference in occurrence of saccadic peak acceleration not a sensitive way to distinguish between INO and healthy controls (Flipse et al., 1997), our results show that PTD calculated as such difference (PTD_a) is at least two times greater (average 5–6 ms) than in controls (<2 ms). Adding measures of PTD to INO modeling may provide an adjunctive study outcome when testing for therapies that improve axonal transmission along the MLF tracts. Based on published data from three patients (Serra et al., 2014), we are currently conducting a double-blind placebo-controlled crossover trial examining the effects of dalfampridine, a potassium channel blocker that ameliorates conduction of demyelinated axons, on measures of INO such as PSR and PTD ([NCT02391961](#)). Basic changes observed in our patient population can be reproduced in our model in terms of gain and signal delay, which supports the importance of including PTD as a measure of disconjugacy in INO.

Are measures of PSR and PTD in INO due to MS affected by sustained repetitive ocular-motor tasks? Does INO worsen over time due to ocular-motor fatigue and can this be a model for primary motor fatigue in MS? Evidence from our previous studies suggest that binocular saccadic parameters may change following fatigue (Matta et al., 2009). The idea of an underlying progressive failure of axonal transmission induced by fatigue is supported by the observation that horizontal conjugacy in INO also worsens following increases in core body temperature (Davis et al., 2008), which may share a similar mechanism. Our current study confirms that PSR can increase or decrease after fatigue in some patients with INO. These changes can potentially be both attributed to further worsening of axonal transmission that might even involve conduction block along some of the affected axons. Hypothetically, as the signal deteriorates, the size of the saccadic pulse for the affected eye further decreases resulting in increased PSR following fatigue (Fig. 3). However, the effects of fatigue on INO are likely more complicated. Adaptive mechanisms (potentially of cerebellar origin) could play a role for example in causing a drop in the pulse size for both eyes, resulting in a smaller PSR following fatigue, perhaps as a way to preserve as much conjugacy as possible. We have previously observed that, in cases of severe INO, some patients employ vergence movements to overcome ocular motor fatigue (Matta et al., 2009). It is possible that PTD changes during the fatigue test might reflect fluctuation of axonal transmission fidelity not necessarily in a linear fashion. Fig. 4 shows how PTD can even vary from saccade to saccade in the same subject without showing a consistent increase following the fatigue test

(i.e., average value of PTD at T3 vs T1). Thus, changes of PTD over time could also be relevant as an outcome measure when using agents, such as dalfampridine, that can stabilize axonal transmission by allowing a more consistent conduction of the pulse from saccade to saccade. Our preliminary results from an ongoing phase II trial of dalfampridine to treat INO in MS may support this hypothesis ([ClinicalTrials.gov: NCT02391961](#)).

In summary, ocular-motor fatigue is likely an heterogeneous phenomenon that may affect patients with INO differently, probably based on chronicity of the MLF damage, severity of INO and underlying level of axonal damage and reserve, and development of adaptation mechanisms of gaze control.

We have developed and presented a model of INO that can reproduce a wide range of the saccades we see in our patients who have MS and INO, simulating changes in PSR and PTD. We were also able to simulate complex saccades that could not otherwise be recreated without the use of the MLF sub-tracts we introduced. (It should be noted that, due to the interactions of multiple parameters over multiple branches, there are likely multiple sets of values that can reproduce any or most waveforms. In the future we will attempt to formalize the rules for selection using parameter estimation.) At this time, there are aspects of our patient data that we do not yet match. In particular, we have noted some subjects' saccadic pulses last longer than we can account for with just increased Tc. We believe this could be a result of adaptive mechanisms, possibly independent of INO, that take place in MS, as these prolonged pulses can appear in both eyes. Consequently, attempting to match peak-velocity by way of adjusting Gain and/or Tc results in hypometric saccades. Increasing the pulse width would allow us to retain the decreased peak-velocity while eventually letting the adducting eye reach the target. We plan on addressing this with modifications of the feedback mechanism within the original model's BGNI.

Effects of possible ocular-motor fatigue on saccadic performance in INO are more complex than the current basic model can account for. In this study, we do not address the issue of long- and short-term changes in behavior, which will require the addition of a time-dependent state to automatically update parameters. For example, we observed that increase or decrease of PSR following fatigue may be due to a combination of changes of the adducting and abducting eye peak-velocities, including decrease or increase of the abducting unaffected eye's peak-velocity. A future model should also offer the possibility of mimicking changes of gain and velocity of the abducting eye, that probably represent neural adaptation to ocular-motor fatigue through the use of feedback/feedforward between eyes, combined with learning to allow the performance of each eye to affect the other.

In summary, our model provides a novel background for our observations related to possible ocular-motor fatigue and variability of axonal transmission in INO. In particular, the modification of a basic model to incorporate parallel MLF sub-tracts with distinct conduction gains and delays can reproduce a variety of complex saccades, before and after fatigue, seen in patients with varying degrees of adduction impairment.

Acknowledgment

We are grateful to Dr. J. Cohen and D. Ontaneda for referring subjects to our study.

Funding

This work was supported by Career Development Award #IK2RX001180 from the United States (U.S.) Department of Veterans Affairs, Rehabilitation Research & Development Service.

Disclaimer

The contents do not represent the views of the U.S. Department of Veterans Affairs or the United States Government.

References

- Chen, A.L., Ramat, S., Serra, A., et al., 2011. The role of the medial longitudinal fasciculus in horizontal gaze: tests of current hypotheses for saccade-vergence interactions. *Exp. Brain Res.* 208, 335–343.
- Collewijn, H., Erkelens, C.J., Steinman, R.M., 1988. Binocular co-ordination of human horizontal saccadic eye movements. *J. Physiol.* 404, 183–197.
- Davis, S.L., Frohman, T.C., Crandall, C.G., et al., 2008. Modeling Uhthoff's phenomenon in MS patients with internuclear ophthalmoparesis. *Neurology* 70, 1098–1106.
- Ferreira, M., Pereira, P.A., Parreira, M., Sousa, I., Figueiredo, J., Cerqueira, J.J., Macedo, A.F., 2017. Using endogenous saccades to characterize fatigue in multiple sclerosis. *Mult. Scler. Relat. Disord.* 14, 16–22.
- Finke, C., Pech, L.M., Sommer, C., et al., 2012. Dynamics of saccade parameters in multiple sclerosis patients with fatigue. *J. Neurol.* 259, 2656–2663.
- Flipse, J.P., Straathof, C.S., Van der Steen, J., et al., 1997. Binocular saccadic eye movements in multiple sclerosis. *J. Neurol. Sci.* 148, 53–65.
- Frohman, E.M., Frohman, T.C., O'Suilleabhain, P., et al., 2002. Quantitative oculographic characterisation of internuclear ophthalmoparesis in multiple sclerosis: the versional dysconjugacy index Z score. *J. Neurol. Neurosurg. Psychiatry* 73, 51–55.
- Frohman, E.M., O'Suilleabhain, P., Dewey Jr., R.B., Frohman, T.C., Kramer, P.D., 2003. A new measure of dysconjugacy in INO: the first-pass amplitude. *J. Neurol. Sci.* 210 (1–2), 65–71.
- Fuchs, A.F., Binder, M.D., 1983. Fatigue resistance of human extraocular muscles. *J. Neurophysiol.* 49 (1), 28–34.
- Leigh, R.J., Zee, D.S., 2015. *The Neurology of Eye Movements*, fifth ed. Oxford University Press, New York.
- Matta, M., Leigh, R.J., Pugliatti, M., Aiello, I., Serra, A., 2009. Using fast eye movements to study fatigue in multiple sclerosis. *Neurology* 73 (10), 798–804.

- Mei, F., Fancy, S.P.J., Shen, Y.A., et al., 2014. Micropillar arrays as a high-throughput screening platform for therapeutics in multiple sclerosis. *Nat. Med.* 20 (8), 954–960.
- Meienberg, O., Müri, R., Rabineau, P.A., 1986. Clinical and oculographic examinations of saccadic eye movements in the diagnosis of multiple sclerosis. *Arch. Neurol.* 43 (5), 438–443.
- Mills, D.A., Frohman, T.C., Davis, S.L., et al., 2008. Break in binocular fusion during head turning in MS patients with INO. *Neurology* 71, 458–460.
- Müri, R.M., Meienberg, O., 1985. The clinical spectrum of internuclear ophthalmoplegia in multiple sclerosis. *Arch. Neurol.* 42 (9), 851–855.
- Najm, F.J., Madhavan, M., Zaremba, A., et al., 2015. Drug-based modulation of endogenous stem cells promotes functional remyelination in vivo. *Nature* 522 (7555), 216–220.
- Sakaie, K., Takahashi, M., Dimitrov, I., et al., 2011. Diffusion tensor imaging the medial longitudinal fasciculus in INO: opportunities and challenges. *Ann. N. Y. Acad. Sci.* 1233, 307–331.
- Scolding, N.J., Pasquini, M., Reingold, S.C., Cohen, J.A., 2017. Cell-based therapeutic strategies for multiple sclerosis. *Brain* 140 (11), 2776–2796.
- Serra, A., Liao, K., Matta, M., et al., 2008. Diagnosing disconjugate eye movements: phase-plane analysis of horizontal saccades. *Neurology* 71, 1167–1175.
- Serra, A., Skelly, M.M., Jacobs, J.B., et al., 2014. Improvement of internuclear ophthalmoparesis in multiple sclerosis with dalfampridine. *Neurology* 83, 192–194.
- Serra, A., Chisari, C.G., Matta, M., 2018. Eye movement abnormalities in multiple sclerosis: pathogenesis, modeling, and treatment. *Front. Neurol.* 9, 31. <https://doi.org/10.3389/fneur.2018.00031>.
- Tilikete, C., Jasse, L., Vukusic, S., et al., 2011. Persistent ocular motor manifestations and related visual consequences in multiple sclerosis. *Ann. N. Y. Acad. Sci.* 1233, 327–334.
- Wang, C., Paling, D., Chen, L., et al., 2015. Axonal conduction in multiple sclerosis: a combined magnetic resonance imaging and electrophysiological study of the medial longitudinal fasciculus. *Mult. Scler. J.* 21 (7), 905–915.
- Zee, D.S., Fitzgibbon, E.J., Optican, L.M., 1992. Saccade-vergence interactions in humans. *J. Neurophysiol.* 68 (5), 1624–1641.

Further reading

- Frohman, T.C., Davis, S.L., Frohman, E.M., 2011. Modeling the mechanisms of Uhthoff's phenomenon in MS patients with internuclear ophthalmoparesis. *Ann. N. Y. Acad. Sci.* 1233, 313–319.

Central positional vertigo: A clinical-imaging study

27

Emiliano De Schutter^a, Zachariah O. Adham^b, Jorge C. Kattah^{b,*}

^a*Division de Neurologia, Hospital Del Carmen, Mendoza, Argentina*

^b*Illinois Neurologic Institute, University of Illinois College of Medicine, Peoria, IL, United States*

*Corresponding author: Tel.: +1-309-253-1793, e-mail address: kattahj@uic.edu

Abstract

The diagnosis of central positional vertigo (CPV) is challenging, mainly because symptoms overlap with the common variants of benign paroxysmal positional vertigo (BPPV). Recent correlations of imaging with neurologic exams have improved our understanding of CPV and ability differentiate it from BPPV. Yet, there is still a need to develop better diagnostic algorithms to improve timely diagnosis and early intervention. Here we present a retrospective review of the clinical characteristics, neurologic evaluation and imaging of CPV in a cohort of 27 patients and propose a diagnostic algorithm to be tested in future prospective fashion. Most patients had positional nystagmus (downbeat and apogeotropic horizontal), cerebellar ocular motor abnormalities and truncal ataxia indicative of a central lesion. 61.5% of our cohort had paroxysmal CPV, 30.5% had a non-paroxysmal CPV and 8% paroxysmal-evolving-to-non-paroxysmal CPV. The most common pattern of positional nystagmus evoked with maneuvers was positional downbeat nystagmus (pDBN, 69.2%), apogeotropic horizontal nystagmus (42.3%), geotropic (7.69%) and multiplanar (23.0%). Notably, 13 (50%) of patients had cerebral imaging prior to CPV being on the differential diagnosis, whereas another 50% of patients had CPV diagnosis preceding their work-up. Unilateral lesions on imaging were 4 × less likely to exhibit nausea and vomiting, nearly 2 × less likely to exhibit paroxysmal nystagmus, and 2 × less likely to exhibit nystagmus with habituality. Findings of pDBN or apogeotropic nystagmus alone were enough to diagnose CPV in 50% of our patient cohort, underscoring the importance of clinical evaluation in a time when an “imaging-first” philosophy is gaining popularity in Neurology.

Keywords

Algorithm for evaluation of central positional vertigo, Central positional nystagmus, Imaging of central positional vertigo

1 Introduction

Diagnostic differentiation of central positional vertigo from benign paroxysmal positional vertigo (BPPV) remains difficult, particularly considering that BPPV is the most common cause of vertigo (Baloh, 2017; Dix and Hallpike, 1952; Furman and Cass, 1999; Kim and Zee, 2014; von Brevern et al., 2007). To understand this diagnostic difficulty, a brief historical recount is germane. Since the first publication of positional vertigo and paroxysmal nystagmus in the 1921 by Bárány (Baloh, 2017). Nylen (1931) published the largest series of brain tumors and CPV to date. Although the definition of the nystagmus direction and the positional diagnostic techniques do not allow a precise comparison with our current nystagmus classification, it is remarkable that the diagnosis—80 years later—remains similarly challenging.

Central positional vertigo (CPV), shares several common symptoms with BPPV; however, it is not related to displaced otoconia in the semicircular canals (Kim and Zee, 2014). It results from impaired “*central vestibular* processing of canal and otolith activation, in addition, to prolonged velocity storage in the cerebellar nodulus” (Choi et al., 2015, 2018).

CPV patients have certain key eye movement features that allow clinical recognition, and require a different diagnostic and management plan (Cho et al., 2017; Choi et al., 2015, 2018; Macdonald et al., 2017). Such sentinel eye signs are critical to initiate a work up in search of the most common causes: vascular, neoplastic, demyelinating, infectious, inflammatory or degenerative. These lesions are located in the posterior fossa (Buttner et al., 1999; Cho et al., 2017; Choi et al., 2015, 2018; Macdonald et al., 2017; Nylen, 1931). We applied current diagnostic criteria for positional vertigo (Buttner et al., 1999; von Brevern et al., 2015), and correlated them with final neurotologic, neurologic, genetic, imaging, surgical and pathologic diagnosis. In our series, we made two major comparisons. First, we compared a group clinical diagnosed as CPV prior to imaging with another in which imaging had demonstrated a CNS lesion (obtained without preceding neurotologic evaluation). Second, we compared a group with bilateral lesions on imaging to a group with unilateral lesions.

2 Methods

This is a retrospective observational analysis of clinical records from Saint Francis Medical Center, the main teaching affiliate of the University Of Illinois College Of Medicine in Peoria, Illinois, USA and Hospital Del Carmen in Mendoza (Argentina). The University of Illinois institutional review board approved the consent form and the study for the patients evaluated in Peoria. The study spanned over 17 years (2001–18). Exclusion criteria included previous history of isolated BPPV, idiopathic, isolated positional nystagmus most notably intermittent or interictal pDBN with migraine (Polensek and Tusa, 2010).

We included patients with positional paroxysmal and non-paroxysmal nystagmus who had a neurotologic diagnosis of CPV and neuroimaging studies. We used the diagnostic criteria for positional vertigo from the Barany Society (von Brevern et al., 2015).

We used various reviews and case series for diagnostic criteria of CPV (Buttner et al., 1999; Macdonald et al., 2017; von Brevern et al., 2015). The CPV criteria included positional vertigo or dizziness with paroxysmal and non-paroxysmal positional nystagmus, associated with central ocular motor abnormalities, truncal imbalance or both; all patients failed canal-repositioning therapeutic maneuvers. In addition, we studied a group with imaging studies that demonstrated a central lesion prior to the CPV diagnosis. Patients underwent neurologic and neurotologic clinical exams, imaging and genetic studies, surgical evaluation and postmortem pathologic examination. Multiplanar MRI studies included DWI and ADC sequences and contrast administration in all patients. We performed Video Oculography, including positional testing with and without fixation block in all cases. An autopsy examination was described in one of the cases previously reported (Cha et al., 2007; Kattah and Gujrati, 2005). We summarize the testing protocol in Fig. 1. We looked for nystagmus during attempted straight-ahead fixation and in lateral gaze and checked for pseudospontaneous nystagmus (PSN), in which nystagmus during straight-ahead fixation changes direction or resolves during a 30-deg forward head pitch, and is a sign of horizontal canal BPPV (Asprella-Libonati, 2008). We also performed the Dix-Hallpike (DH) keeping the head in the straight, right or left hanging position for 1 min. When fatigable, geotropic, upbeat/torsional nystagmus developed, we performed an Epley maneuver without further testing. In those patients with positional downbeat (pDBN) or pDBN/torsional, or horizontal nystagmus on DH maneuver—or those without nystagmus—we performed additional positional testing, including head roll maneuvers. In recent cases (cases 20–27), we included prone position testing. The supine head roll (SHR) maneuver served to identify patients with horizontal geotropic or apogeotropic nystagmus. This SHR maneuver involved a rapid head turn and maintenance of the head in one position for 1 min, to determine fatigability or spontaneous reversal of nystagmus direction. We performed each positional maneuver at least twice to determine habituality.

The MRI protocol used in these patients has been previously described (Newman-Toker et al., 2008). MRI of the brain was obtained in 26 patients and CT only in one, in whom MRI was contraindicated (case 25). In one the MRI was not viewed but was interpreted as normal by a radiologist. One patient also had a FDG PET/MRI scan of the brain.

We applied Fisher's Exact Test, to compare characteristics of groups: (1) patients with a clinical CPV diagnosis prior to imaging (CVP-first) vs patients with imaging prior to CPV diagnosis (Imaging-first); and (2) patients with bilateral lesions vs patients with unilateral lesions.

3 Results

3.1 General characteristics

We included 27 patients. The average age was 55 years without gender preponderance. Table 1 and Fig. 1 provide demographic, symptoms and nystagmus characteristics in patients with imaging prior to or after neurotologic examination;

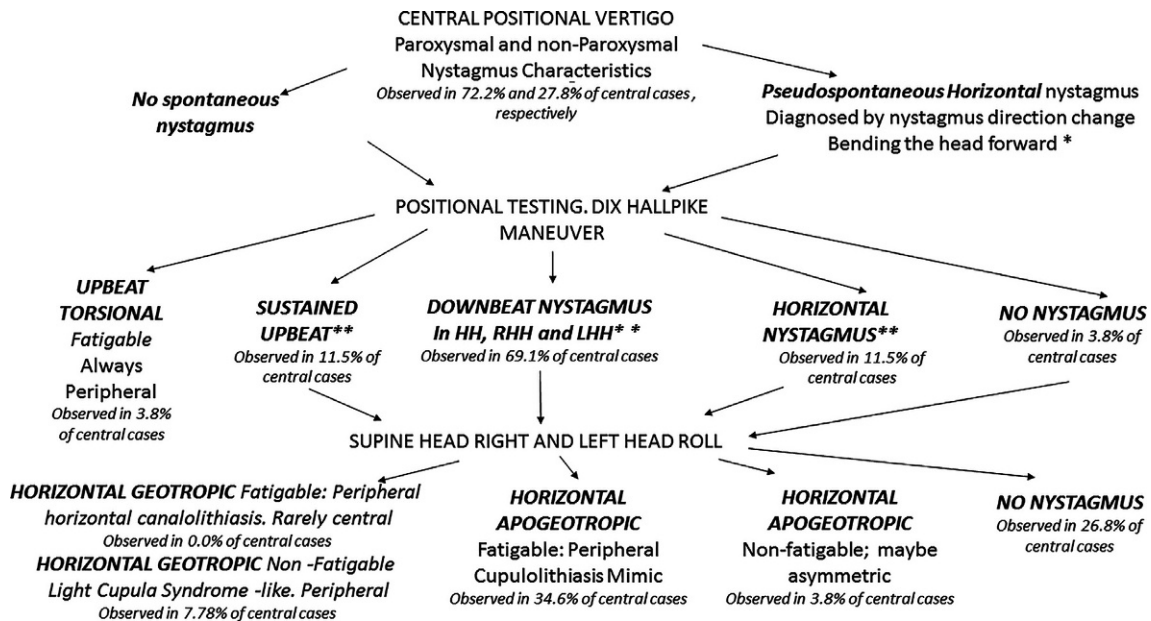


FIG. 1

Flow chart diagram illustrating the diagnostic protocol used in this study and the distribution of different nystagmus types found. Note that the paroxysmal CPV group includes two patients with paroxysmal CPV that eventually became chronic non-paroxysmal. *Important to check the effect of head bending in any patient with spontaneous horizontal nystagmus for direction change. **Several patients had more than one positional nystagmus type.

Table 1 Demographics, positional nystagmus characteristics, imaging and diagnosis in a cohort of central positional vertigo.

PT	Nystagmus in Dix-Hallpike or head roll maneuver	Co-existing nystagmus in primary gaze	Paroxysmal vs non-paroxysmal	MRI findings	Diagnosis
1	Horizontal apogeotropic R: h-LBN SPV 25, L: h-RBN SPV 22.1	None in primary gaze w/o or w fixation	Non-paroxysmal Last >2 min	Several bilateral cerebellar stroke in R nodulus and uvula and partial in L	R vertebral artery occlusion L subclavian steal 60% stenosis of left vertebral artery
2	Positional DBN SPV 10	None initially Eventually primary gaze DBN	Initially paroxysmal Then non-paroxysmal Last >2 min	Normal initially	Episodic ataxia ^a evolving to generalized cerebellar atrophy
3	Positional DBN SPV 11, HS DBN	None initially Eventually developed primary gaze DBN	Non-paroxysmal Last >2 min	Normal initially Loss of Purkinje cells in bilateral nodulus at autopsy	Episodic ataxia ^a evolving to generalized cerebellar atrophy
4	Positional DBN. SPV 8.2	None	Non-paroxysmal Last >2 min	Post-surgical resection of large midline cerebellar mass	Midline vermis dermoid cyst
5	Positional DBN 24 deg/s + apogeotropic horizontal SPV 2 deg/s	None	Paroxysmal	Mild cerebellar atrophy	Idiopathic cerebellar atrophy
6	Positional DBN, SPV 56 deg/s also h-geotropic R h-roll SPV 12.4 deg/s and h-LBN 9.6 deg/s	None	Paroxysmal	Normal initially progressive moderate cerebellar atrophy in serial MRI	Idiopathic cerebellar atrophy
7	First AVS, then positional DBN 12.6deg/s	h-LBN	Paroxysmal	Non-specific T2 bilateral subcortical signal changes	Possibly episodic ataxia/migraine
8	First positional DBN Later DBN	Eventually DBN	Paroxysmal	Non-specific T2 bilateral subcortical signal hyperintensities	Possibly episodic ataxia/migraine
9	Positional DBN, SPV: 6 deg/s	None	Paroxysmal	Reported normal, no films available for review	Genetic variant of EA2 on her son ^b
10	Positional DBN SPV: 28 deg/s	None	Paroxysmal	Cystic midline vermis lesion	Hydatid cyst
11	Positional HH DBN 22 deg/s, sitting UBN 12.6 deg/s	None	Paroxysmal	Unilateral cerebellar flocculus Nodulus and hemisphere Mass	Medulloblastoma

Continued

Table 1 Demographics, positional nystagmus characteristics, imaging and diagnosis in a cohort of central positional vertigo.—cont'd

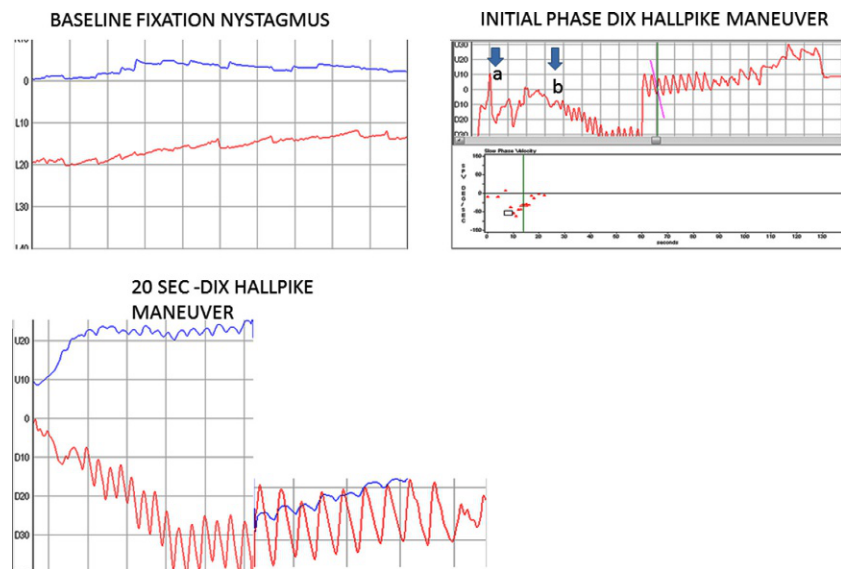
PT	Nystagmus in Dix-Hallpike or head roll maneuver	Co-existing nystagmus in primary gaze	Paroxysmal vs non-paroxysmal	MRI findings	Diagnosis
12	Horizontal apogeotropic R: 8 deg/s, L: 7 deg/s	None in primary gaze w/o or w fixation	Non-paroxysmal Last >2min only with fixation block	<i>Unilateral</i> MCP Posterior Pons stroke	Stroke
13	Positional DBN 11 deg/s	None	Initially paroxysmal, eventually non-paroxysmal	<i>Unilateral</i> right flocculus Nodulus lesion	Right midline cerebellar tumefactive demyelinating lesion
14	Eventually horizontal apogeotropic R: h-LBN SPV: 10, L: h-RBN SPV: 10	Pseudo-spontaneous h-RBN	Paroxysmal	Bilateral flocculus and MCP lesions	Mid-basilar stenosis. Status post basilar artery stent
15	Horizontal apogeotropic R: h-LBN SPV: 13, L: h-RBN SPV: 8	None in primary gaze w/o or w fixation	Paroxysmal	<i>Unilateral</i> right biventer, near nodulus infarct	Subacute stroke
16	Positional DBN HH Positional UBN UR	None	Paroxysmal	Normal	Idiopathic cerebellar degeneration
17	LHH: h-LBN SPV: 5.9 deg/s, RHH; mild h-RBN geotropic	None in primary gaze w/o or w fixation	Non-paroxysmal	Multiple demyelinating lesions ^c	Multiple sclerosis
18	Horizontal apogeotropic RHH: RBN SPV: 1.5, LHH: LBN SPV: 4.5, geotropic	None in primary gaze w/o or w fixation	Non-paroxysmal	<i>Unilateral</i> acute plaque in left cerebellar hemisphere, near nodulus	Multiple sclerosis
19	Horizontal apogeotropic h RBN in dark, apogeotropic h in R+L head roll	h-RBN	Paroxysmal	Mild cerebellar atrophy	Idiopathic cerebellar degeneration and polycystic kidneys
20	Positional DBN SPV 8 deg/s	None	Paroxysmal	<i>Unilateral</i> repaired superior canal dehiscence	Superior canal dehiscence. Unilateral decreased VOR gain all canals
21	Positional DBN 8 deg/s in HH, UBN reversal sitting	Vibration Horizontal RBN	Paroxysmal	Multiple, <i>unilateral</i> AICA and PICA strokes, sparing the nodulus	Intracranial V4 vertebral artery dissection
22	Apogeotropic h-nystagmus, R roll h-LBN 12.2 deg/s and L roll h-RBN. Non-fatigable 10 deg/s Same in DH	Mild h-LGEN with fixation block Supine h-LBN 6 deg/s	Non-paroxysmal	<i>Unilateral</i> , large R cerebellar hemisphere mass with compression of the nodulus	Cerebellar Medulloblastoma

23	Fatigable BPPV in left hanging head SPV 85 deg/s Posterior canal BPPV, responded to Epley maneuver (Fig. 2).	DBN 10 deg/s	Paroxysmal	Mild midline cerebellar atrophy Non-specific T2 subcortical signal hyperintensities	Coincidental posterior canal BPPV in a patient with an idiopathic downbeat nystagmus
24	DBN from 8 deg/s to 20 deg/s UBN URP 6.5 deg/s Apogeotropic h nystagmus R: LBN 6 deg/s; L: LBN 6 deg/s	None in primary gaze w/o or w fixation	Paroxysmal	Normal PET hypometabolism	Idiopathic cerebellar degeneration
25	Apogeotropic h-nystagmus, R roll h-LBN: 25 deg/s; L roll h-RBN. Non-fatigable 22 deg/s	HH: DBN 8 deg/s Prone h-LBN DBN 4 deg/s	Paroxysmal	Medulla compression by severe vertebral/basilar dolichoectasia	Either compression of the caudal brainstem or infarction not detected by CT scan
26	Positional DBN 8 deg/s Left head roll h-RBN 6 deg/s Right head roll h-LBN 7 deg/s	None	Paroxysmal	Gad-65 positive	Autoimmune ataxia
27	Apogeotropic h-nystagmus R roll: LBN 7 deg/s + DBN 6 deg/s and L roll: h-RBN average 12 deg/s + DBN 4 deg/s	HV: DBN HH: DBN Prone DBN/LBN Supine DBN/LBN	Non-paroxysmal	<i>Unilateral</i> infarct right tonsil, uvula and nodulus	mPICA stroke

^aInitial symptoms were episodic and over a decade the patients developed permanent signs of cerebellar dysfunction.

^bThe patient was not tested, but her son showed a gene mutation considered pathogenic.

^cNone of the plaques were located in the cerebellum or brainstem.

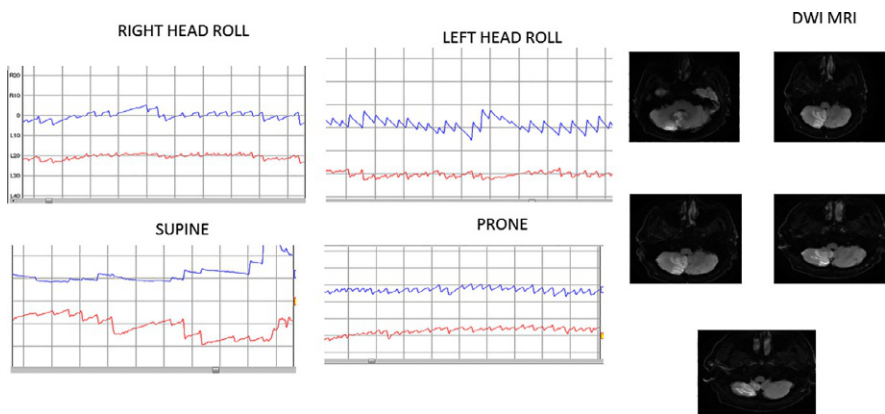
**FIG. 2**

Baseline downbeat nystagmus in a patient with iDBN (*left upper panel*). Dix Hallpike maneuver triggered a characteristic posterior canal BPPV. Note high velocity upbeat nystagmus.

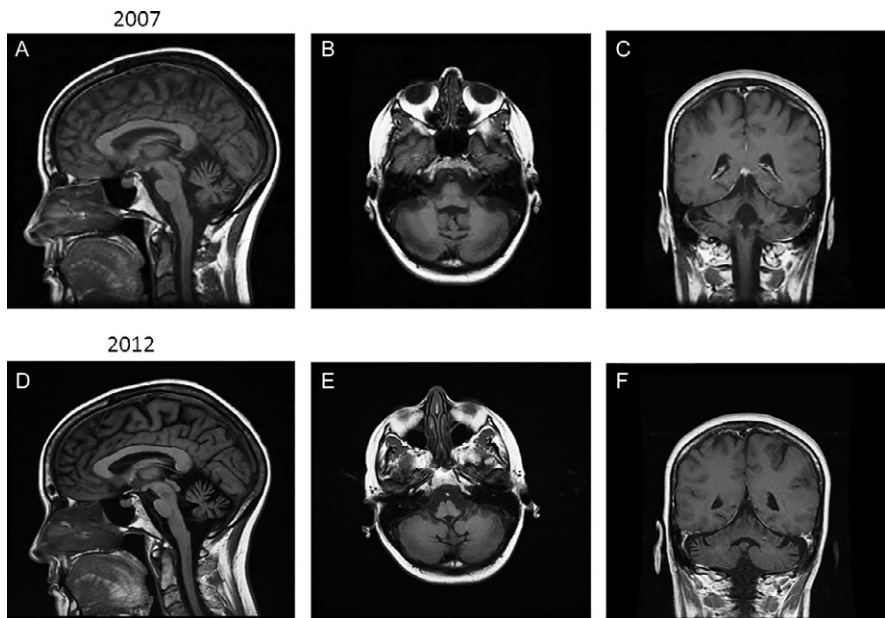
a neurologist or neurotologists before imaging did not evaluate the patients with imaging preceding examination. We also compare patients with unilateral and bilateral lesions on imaging.

The most common pattern of positional nystagmus evoked with maneuvers was positional downbeat nystagmus (pDBN, 66.6%) followed by apogeotropic horizontal nystagmus (40.7%), geotropic (7.4%) and multiplanar (21.0%). Multiplanar includes patients with pDBN plus pUBN when assuming upright position (cases 16 and 25) or pDBN plus horizontal apogeotropic nystagmus (cases 5, 6, 24, 25 and 26, 27; Fig. 1). 66.6% had paroxysmal pattern of nystagmus, 25.9% had a non-paroxysmal (>1 min) pattern, and 7.4% evolved from paroxysmal to non-paroxysmal. We defined latency as the onset of nystagmus after reaching final head position, latency of ≤ 3 s (from offset of positioning); it was observed in 96.2% of the cohort. We observed additional neurologic symptoms in 85.1% of the cohort. 14/27 or 51.8% presented with only vertical nystagmus induced by maneuvers. Only 2/27 patients showed enhancement of nystagmus with fixation (cases 6 and 7) (Figs. 3 and 4).

25.9% of our patients presented with prominent nausea or vomiting, much lower than previously reported, 93.3% (von Brevern et al., 2015). 70.4% of our patients presented with additional ocular motor abnormalities. Positional nystagmus in

**FIG. 3**

Central positional vertigo in a patient with a right PICA stroke that affects the right nodulus and uvula. Note both horizontal apogegotropic and downbeat nystagmus.

**FIG. 4**

Slow progression of cerebellar degeneration over 5 years in a patient with familial cerebellar degeneration and positional downbeat nystagmus.

26% was transiently habituated with repeat positioning (cases 5, 6, 8, 9, 20, 21 and 22), but present at subsequent testing sessions. All patients presented a decrescendo pattern of nystagmus intensity. Interestingly, three patients (cases 9, 11, 12) did not have additional neurological abnormality (isolated CPV). In addition, one patient had limb ataxia and dysarthria (case 25). In 14 patients, episodic vertigo was the reason for consultation to a neurologist; the remaining patients reported primarily unsteadiness while standing and gait difficulty as their primary complaint, however, they also reported positional dizziness, exercise related vertigo and episodic positional oscillopsia.

When a focal lesion was present on MRI, the tonsil/nodulus/uvula and other midline vermis lesions were affected locations. Additional locations included: unilateral middle cerebellar peduncle (MCP), posterior pontine infarct, and bilateral symmetric flocculus and MCP lesions. Two lateral cerebellar hemisphere medulloblastomas were adjacent to the fourth ventricle. In addition, we did not find radiographic evidence of olivopontocerebellar atrophy (OPCA) or basal ganglia changes suggestive of multisystem atrophy (MSA) in our cohort. Etiologies are summarized in [Table 1](#).

Two patients with multiple sclerosis (MS) developed positional vertigo with, non-fatigable, geotropic nystagmus that mimicked a light cupula syndrome as it lasted a few weeks and resolved spontaneously ([Kim et al., 2018](#)) (cases 17, 18). In our entire CPV cohort, we had three patients with provoked nystagmus when tested sitting up with fixation block (hyperventilation-induced DBN in two MS patients and vibration-induced right beat nystagmus in cochleo-vestibular stroke cases 17, 18 and 21), and one patient with PSN (case 7). All our CA, EA and idiopathic DBN (iDBN), except for case 7, had gaze paretic nystagmus, decreased horizontal pursuit gain and poor VOR cancellation. Two patients in this series had unilateral horizontal and vertical vestibular paresis and one had bilateral vestibular paresis (unilateral in one after SCD surgery, one post cochleo-vestibular stroke and bilateral in one CA patient). Two EA patients with pDBN developed in time straight ahead fixation DBN. With the exception of two patients with normal Romberg with inability to perform tandem gait in this cohort, the remaining CPV patients had positive Romberg sway and truncal ataxia, including EA patients examined in an interictal phase.

3.2 CPV-first and imaging-first groups

Thirteen patients (cases 4, 13–22, 26, 27) had first lesions on imaging (Imaging-first), and on subsequent clinical examinations were noted to have positional nystagmus. The acute symptoms explain their initial evaluation at an Emergency Department (ED). 53.8% of these patients had paroxysmal nystagmus, 23% showed fatigability or habituality of nystagmus, none had any clinically appreciable latency in onset of nystagmus, while all showed other neurologic findings on exam—mainly ataxia or inability to do tandem gait. On DH and head-roll maneuvers 53.8% patients showed pDBN, 7.69% had upbeat nystagmus when sitting up after DH. Of those showing pDBN on DH and straight hanging head position, four had also horizontal apogeotropic nystagmus with supine head roll; notably, we did not see PSN in this

group. Of those who showed only horizontal nystagmus on DH ($n=3$), one patient had horizontal nystagmus also with head roll.

In the CPV-first subcohort (cases 1, 2, 3, 5, 6–12, 23, 24, 25), all had additional truncal ataxia and ocular motor cerebellar signs (primarily gaze paretic nystagmus, impaired horizontal pursuit). The most frequent nystagmus in this subcohort was pDBN (78.5%, paroxysmal and non-paroxysmal) followed by apogeotropic horizontal nystagmus (35.7%). Three patients had both pDBN and apogeotropic horizontal nystagmus (cases 4, 26, 27; see Table 1). 71.5% of these patients did not have nausea or vomiting. 8.5% of CPV-first patients had paroxysmal positional nystagmus, with one additional patient (case 13) initially presenting with pDBN and progressed to continuous straight ahead fixation gaze DBN within an 18-month period. In this sub-cohort of CPV-first patients, 71.5% had no nystagmus habituation. In this subcohort nystagmus developed immediately after reaching the final head position in the majority.

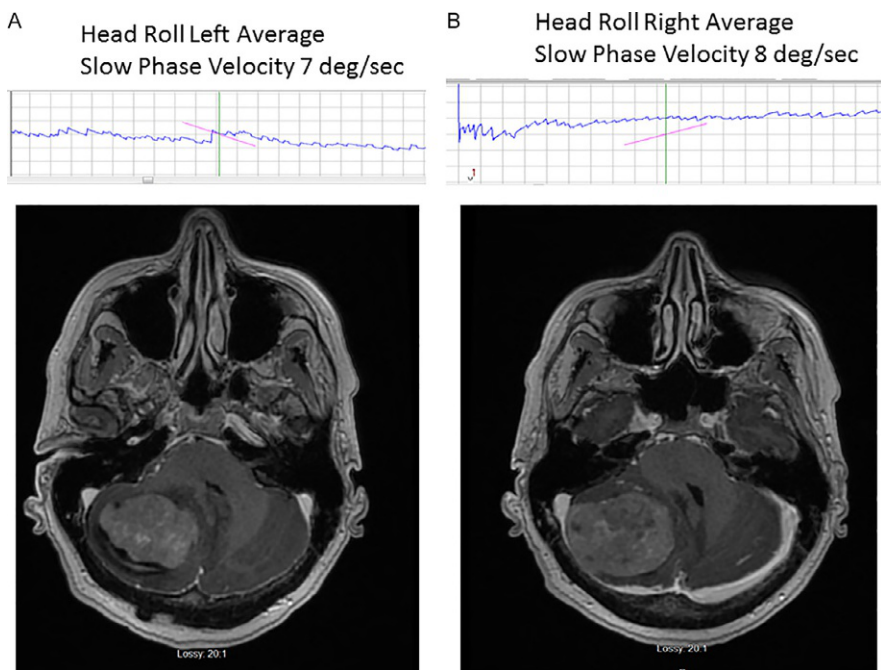
3.3 Unilateral and bilateral lesion groups

With regard to patients showing bilateral lesions on imaging (cases 1–10, 14, 16, 18, 19, 23–26): 33.3% presented with nausea and vomiting, 72.2% exhibited pDBN, 66.6% paroxysmal nystagmus, 27.7% habitual nystagmus. For patients with unilateral lesions on imaging (cases 11–13, 15, 17, 20–22, 27): 11.1% presented with nausea and vomiting, 55.5% exhibited pDBN, 55.5% paroxysmal nystagmus, 22.2% habitual nystagmus, and 22.2% with specific lesion of the nodulus.

4 Discussion

Based on our study of a two groups of patients with central positional vertigo—one group diagnosed before imaging, and the other after—we have developed a diagnostic algorithm (Fig. 1) that we propose as a working hypothesis for future testing, in the spirit of Lance Optican. Before discussing the algorithm, we first compare our data base (which we used, in part, to formulate the model) with prior studies (Fig. 5).

We found 12/27 or 44.4% (cases 2, 3, 6–11, 13, 16, 20, 21) of our cohort presented with only vertical nystagmus on maneuvers, a greater percentage than the previously reported fraction (24.8%) of central positional nystagmus (CPN) cases analyzed in a recent meta-analysis REF. Our cohort had only 2 out of 27 patients with nystagmus enhanced with fixation (cases 6 and 7), this is less than previously reported (von Brevern et al., 2015). Our cohort had additional unique features, including latency ≤ 3 s in 26/27 or 96.2%, persistence of nystagmus for >1 min (8/27 or 25.9%) and abnormal postural symptoms and signs (23/27 or 85.1%). These results are similar to the cases aggregated in a recent meta-analysis by Macdonald et al. (2017), in which 94.7% of their patients had latency ≤ 3 s, and 41.7% showed nystagmus persisting for >1 min. 74.0% of our patients presented with additional ocular motor abnormalities, comparable to the 88.6% previously reported (von Brevern et al., 2015). Our cohort had only 25.9% (cases 8–10, 14, 16, 24, 27)

**FIG. 5**

Horizontal apogeotropic nystagmus in a patient with a large right cerebellar hemisphere mass.

of our patients present with prominent nausea or vomiting, much lower than previously reported, 93.3% (von Brevern et al., 2015).

While CPV accounts only for a small fraction of positional vertigo patients, precise diagnosis is critical to initiate a work-up and possibly rapid intervention. We combined our cohort analysis with parameters recommended by recent studies to create an algorithm or protocol, which allows rapid recognition of “CPV” (Fig. 1). Whereas the Dix-Hallpike maneuver is probably the only positional test needed in patients with typical posterior canal syndrome, performing an extended positional test protocol is imperative in all horizontal canal positional vertigo patients. This extended protocol includes the prone positions.

All our patients had positional symptoms, 85.1% had vertigo, three patients had a sensation of loss of balance and unsteadiness when changing position, at time severe and leading to fall (cases 11, 14 and 15). One of our patients (case 3) reported oscillopsia, a finding previously reported in only four cases of central positional nystagmus series (Feil et al., 2019; Schniepp et al., 2014; Tateno and Sakakibara, 2018). Unlike all previously reported cases of oscillopsia in the setting of CPN, ours presented with pDBN on DH and straight-head-hanging maneuvers (SHHM); all others with oscillopsia had positional torsional, geotropic, and upbeat nystagmus. A recent editorial comment emphasized the high frequency of “vertigo” as a complaint among patients with cerebellar disorders. It is possibly related to an abnormal

perception of motion (Shaikh and Manto, 2019). To facilitate the discussion we will describe the clinical symptoms and findings in the two patients' subgroups and will follow with a subgroup comparison.

4.1 General clinical neurotology findings

Our series, in agreement with previous reports, confirm that nystagmus direction and its temporal characteristics are the most important factors to diagnose CPV. Compared to central lesions, those in the periphery generally resolve spontaneously (Kim et al., 2012). Peripheral lesions generally respond well to canal repositioning maneuvers and failure to respond to canal repositioning justifies an investigation for a central cause (Fife, 1998). Fig. 1 is a summary list of the protocol and signs leading to CPV diagnosis. For example, posterior SCC BPPV results in a pathognomonic paroxysmal, geotropic upbeat/torsional nystagmus. This, even in patients with associated neurologic abnormalities, is always of peripheral origin and responds to canal repositioning maneuvers despite a frequently abnormal neurologic examination, particularly in the context of traumatic brain injury (Ahn et al., 2011) or multiple sclerosis (Frohman et al., 2003) (Fig. 6).

pDBN is more difficult to localize; a diagnosis of canalolithiasis of the anterior canal BPPV can be confidently made when the paroxysmal DBN occurs after conclusion of an Epley maneuver, or when it responds to repositioning maneuvers. Moreover, in some cases, when DH triggers pDBN—leading to a preliminary diagnosis of anterior canal BPPV—testing the contralateral side reveals a typical upbeat/torsional

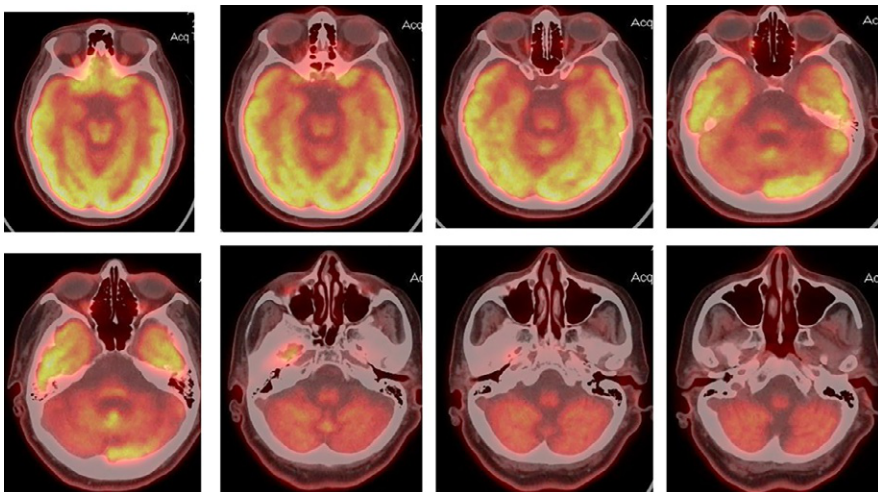


FIG. 6

PET scan of patient with cerebellar degeneration and positional downbeat nystagmus, the MRI showed minor changes, PET scan showed diffuse cerebellar conspicuous hypometabolism (lower panel) , in contrast to normal cerebral metabolism in the temporal lobes.

nystagmus, suggesting ectopic otoconia in the distal non-ampullary arm of the posterior canal (Welgampola et al., 2017) which simply improves with a specific liberatory maneuver. We found combined pDBN during DH with h-apogeotropic nystagmus in head roll maneuvers to be an important sign suggesting CPV. In this series, we include only pDBN patients with imaging abnormalities, or in the context of a cerebellar/brainstem degenerative process; in many cases pDBN may be an isolated finding associated with migraine and other uncertain etiology. Importantly, additional cerebellar ocular motor abnormalities (Leigh and Zee, 2015), and posture and gait abnormalities contributed to lesion localization in this CPV cohort, underscoring the value of a detailed neurologic and neurotologic evaluation among patients with positional vertigo.

5 Comparison between clinical-first and imaging-first subgroups

To better aid clinical decision making, we believe it is germane to compare cases first diagnosed as CPV from clinical exam against those diagnosed as CPV after first identifying brain lesions on imaging. The CPV-first cohort had only 4/14 patient with nausea and vomiting, compared to 3/13 patients who had lesions identified on imaging first. We found 21.4% CPV-first patients with as non-paroxysmal, compared to 46.1% of imaging-first patients. 28.5% CPV-first patients showed habituality of nystagmus, compared to 23.1% imaging-first patients. 4/14 CPV-first patients had no discrete lesion or entirely normal imaging, compared to 10/13 imaging-first patients. Overall, the CPV-first subcohort was 2 × less likely to have non-paroxysmal nystagmus and 2.5 × less likely to have a discrete mass on imaging.

5.1 CPV lesion localization

The clinical and imaging findings in this series support the notion that the midline cerebellar vermis is important in the processing and modulation of simultaneous graviceptive otolith and canalicular angular velocity signals. CPV originates from an abnormal central response to otolith activation during positional testing. In this cohort, two patients with large fourth ventricle tumors presumably caused either bilateral mass effect or infiltration of the midline vermis. In contrast, unilateral lesions had conspicuous imaging findings, most often involved vascular abnormalities or unilateral tumors.

11.1% of those with unilateral lesions had nausea and vomiting on presentation, compared to 33.3% with CA or presumed bilateral lesions. 56.6% of those with unilateral lesions were unable to perform tandem gait, compared to 88.88% of those with bilateral lesions. 33.3% of those with unilateral lesions had lesions in the nodulus/uvula. Moreover, 72.2% of our bilateral CPV lesions had pDBN, in contrast to a lower 55.5% of those with unilateral lesions (Table 1). Overall, unilateral lesions were 3 × less likely to report nausea and vomiting.

6 Limitations

There are several limitations in this study, mostly related to the small sample size and the retrospective nature of the study. Moreover, it is not possible to estimate the precise incidence of CPV in the population that we serve because CPV patients often undergo imaging and neurosurgical or medical treatment without neurologic consultation. A recent report involving a 5400 subject cohort with cerebellar disease identified 57 cases (1%) who had CPV. We restricted this study to CPV patients with specific syndromic etiology (CA, EA and iDBN syndromes) or imaging abnormalities in an effort to define a clinical imaging correlation, thus we excluded migraine patients with ictal or interictal isolated pDBN who could potentially develop late clinical and imaging central abnormalities.

In conclusion, CPV is not common, but critical to diagnose, as it may be the most important neurologic abnormality found; in this series, we uniformly found the nystagmus direction as the most helpful central indicator, additional factors such as nystagmus latency, habituality and duration are selectively helpful. In our series, the lack of improvement with canal repositioning maneuvers, with exception for the coincidental posterior canal BPPV patient with SCA, was also a CPV characteristic. Finally, we encountered vestibular, oculomotor and postural abnormalities in most cases; consequently, atypical positional nystagmus cases require a careful neurologic evaluation, ideally performed prior to MRI. The proposed testing algorithm awaits testing in a prospective study to include examination prior to imaging.

References

- Ahn, S.K., Jeon, S.Y., Kim, J.P., Park, J.J., Hur, D.G., Kim, D.W., Woo, S.H., Kwon, O.J., Kim, J.Y., 2011. Clinical characteristics and treatment of benign paroxysmal positional vertigo after traumatic brain injury. *J. Trauma* 70, 442–446.
- Asprella-Libonati, G., 2008. Pseudo-spontaneous nystagmus: a new sign to diagnose the affected side in lateral semicircular canal benign paroxysmal positional vertigo. *Acta Otorhinolaryngol. Ital.* 28, 73–78.
- Baloh, R.W., 2017. Vertigo. Five Physician Scientists and the Quest for a Cure. University Press, Oxford.
- Buttner, U., Helmchen, C., Brandt, T., 1999. Diagnostic criteria for central versus peripheral positioning nystagmus and vertigo: a review. *Acta Otolaryngol.* 119, 1–5.
- Cha, Y.H., Lee, H., Jen, J.C., Kattah, J.C., Nelson, S.F., Baloh, R.W., 2007. Episodic vertical oscillopsia with progressive gait ataxia: clinical description of a new episodic syndrome and evidence of linkage to chromosome 13q. *J. Neurol. Neurosurg. Psychiatry* 78, 1273–1275.
- Cho, B.H., Kim, S.H., Kim, S.S., Choi, Y.J., Lee, S.H., 2017. Central positional nystagmus associated with cerebellar tumors: clinical and topographical analysis. *J. Neurol. Sci.* 373, 147–151.
- Choi, J.Y., Kim, J.H., Kim, H.J., Glasauer, S., Kim, J.S., 2015. Central paroxysmal positional nystagmus: characteristics and possible mechanisms. *Neurology* 84, 2238–2246.

- Choi, J.Y., Glasauer, S., Kim, J.H., Zee, D.S., Kim, J.S., 2018. Characteristics and mechanism of apogeotropic central positional nystagmus. *Brain* 141, 762–775.
- Dix, M.R., Hallpike, C.S., 1952. The pathology symptomatology and diagnosis of certain common disorders of the vestibular system. *Proc. R. Soc. Med.* 45, 341–354.
- Feil, K., Strobl, R., Schindler, A., Krafczyk, S., Goldschagg, N., Frenzel, C., Glaser, M., Schoberl, F., Zwergal, A., Strupp, M., 2019. What is behind cerebellar vertigo and dizziness? *Cerebellum*. in press.
- Fife, T.D., 1998. Recognition and management of horizontal canal benign positional vertigo. *Am. J. Otol.* 19, 345–351.
- Frohman, E.M., Kramer, P.D., Dewey, R.B., Kramer, L., Frohman, T.C., 2003. Benign paroxysmal positioning vertigo in multiple sclerosis: diagnosis, pathophysiology and therapeutic techniques. *Mult. Scler.* 9, 250–255.
- Furman, J.M., Cass, S.P., 1999. Benign paroxysmal positional vertigo. *N. Engl. J. Med.* 341, 1590–1596.
- Kattah, J.C., Gujrati, M., 2005. Familial positional downbeat nystagmus and cerebellar ataxia: clinical and pathologic findings. *Ann. N. Y. Acad. Sci.* 1039, 540–543.
- Kim, J.S., Zee, D.S., 2014. Clinical practice. Benign paroxysmal positional vertigo. *N. Engl. J. Med.* 370, 1138–1147.
- Kim, J.S., Oh, S.Y., Lee, S.H., Kang, J.H., Kim, D.U., Jeong, S.H., Choi, K.D., Moon, I.S., Kim, B.K., Oh, H.J., Kim, H.J., 2012. Randomized clinical trial for apogeotropic horizontal canal benign paroxysmal positional vertigo. *Neurology* 78, 159–166.
- Kim, M.B., Hong, S.M., Choi, H., Choi, S., Pham, N.C., Shin, J.E., Kim, C.H., 2018. The light cupula: an emerging new concept for positional vertigo. *J. Audiol. Otol.* 22, 1–5.
- Leigh, R.J., Zee, D.S., 2015. *The Neurology of Eye Movements*. Oxford University Press.
- Macdonald, N.K., Kaski, D., Saman, Y., Al-Shaikh Sulaiman, A., Anwer, A., Bamjiou, D.E., 2017. Central positional nystagmus: a systematic literature review. *Front. Neurol.* 8, 141.
- Newman-Toker, D.E., Kattah, J.C., Alvernia, J.E., Wang, D.Z., 2008. Normal head impulse test differentiates acute cerebellar strokes from vestibular neuritis. *Neurology* 70, 2378–2385.
- Nylen, C.O., 1931. A clinical study on positional nystagmus in cases of brain tumor. *Acta Otolaryngol. Suppl.* 15, 1–111.
- Polensek, S.H., Tusa, R.J., 2010. Nystagmus during attacks of vestibular migraine: an aid in diagnosis. *Audiol. Neurotol.* 15, 241–246.
- Schniepp, R., Wuehr, M., Huth, S., Pradhan, C., Schlick, C., Brandt, T., Jahn, K., 2014. The gait disorder in downbeat nystagmus syndrome. *PLoS One* 9, e105463.
- Shaikh, A.G., Manto, M., 2019. Vertigo in cerebellar disease—do the eyes have it or is there more to perceive? *Cerebellum*. in press.
- Tateno, F., Sakakibara, R., 2018. Positional vertigo after isolated cerebellar nodulus stroke: a report of 3 cases. *J. Stroke Cerebrovasc. Dis.* 28, 487–489.
- von Brevern, M., Radtke, A., Lezius, F., Feldmann, M., Ziese, T., Lempert, T., Neuhauser, H., 2007. Epidemiology of benign paroxysmal positional vertigo: a population based study. *J. Neurol. Neurosurg. Psychiatry* 78, 710–715.
- von Brevern, M., Bertholon, P., Brandt, T., Fife, T., Imai, T., Nuti, D., Newman-Toker, D., 2015. Benign paroxysmal positional vertigo: diagnostic criteria. *J. Vestib. Res.* 25, 105–117.
- Welgampola, M.S., Akdal, G., Halmagyi, G.M., 2017. Neuro-otology—some recent clinical advances. *J. Neurol.* 264, 188–203.

Eye-hand re-coordination: A pilot investigation of gaze and reach biofeedback in chronic stroke

28

**John-Ross Rizzo^{a,b,e,*†}, Mahya Beheshti^{a,†}, Azadeh Shafeeesabet^a, James Fung^a,
Maryam Hosseini^a, Janet C. Rucker^{b,c}, Lawrence H. Snyder^d, Todd E. Hudson^{a,b}**

^a*Department of Physical Medicine & Rehabilitation, NYU School of Medicine, New York,
NY, United States*

^b*Department of Neurology, NYU School of Medicine, New York, NY, United States*

^c*Department of Ophthalmology, NYU School of Medicine, New York, NY, United States*

^d*Department of Neuroscience, Washington University School of Medicine, St. Louis,
MO, United States*

^e*Department of Biomedical Engineering, NYU School of Engineering, New York, NY, United States*

*Corresponding author: Tel.: +1-646-501-7828; Fax: +1-212-263-2683,
e-mail address: johnross.rizzo@nyumc.org

Abstract

Within the domain of motor performance, eye-hand coordination centers on close relationships between visuo-perceptual, ocular and appendicular motor systems. This coordination is critically dependent on a cycle of feedforward predictions and feedback-based corrective mechanisms. While intrinsic feedback harnesses naturally available movement-dependent sensory channels to modify movement errors, extrinsic feedback may be provided synthetically by a third party for further supplementation. Extrinsic feedback has been robustly explored in hand-focused, motor control studies, such as through computer-based visual displays, highlighting the spatial errors of reaches. Similar attempts have never been tested for spatial errors related to eye movements, despite the potential to alter ocular motor performance. Stroke creates motor planning deficits, resulting in the inability to generate predictions of motor performance. In this study involving visually guided pointing, we use an interactive computer display to provide extrinsic feedback of hand endpoint errors in an initial baseline experiment (pre-) and then feedback of both eye and hand errors in a second experiment (post-) to chronic stroke participants following each reach trial. We tested the hypothesis that extrinsic feedback of eye and hand would improve predictions and therefore feedforward control. We noted this improvement through gains in the spatial and temporal aspects of eye-hand coordination or an improvement in the decoupling noted as incoordination post-stroke in previous

[†]These authors contributed equally.

studies, returning performance toward healthy, control behavior. More specifically, results show that stroke participants, following the interventional feedback for eye and hand, improved both their accuracy and timing. This was evident through a temporal re-synchronization between eyes and hands, improving correlations between movement timing, as well as reducing the overall time interval (delay) between effectors. These experiments provide a strong indication that an extrinsic feedback intervention at appropriate therapeutic doses may improve eye-hand coordination during stroke rehabilitation.

Keywords

Coordination, Eye, Hand, Stroke, Biofeedback, Re-coordination

1 Introduction

Eye-hand coordination (EHC) depends critically on integrated control of ocular and appendicular sensorimotor systems to accomplish a single goal, such as touching a visual target. Optimal coordination between eye and hand relies on complex feedforward- and feedback-mediated relationships between the visuo-perceptual, ocular and appendicular motor systems, and takes advantage of finely orchestrated synergies between these systems in both the spatial and temporal domains.

Feedforward control is the prediction, planning and subsequent generation of motor commands based on a desired action. Feedback control corrects these commands based on sensory feedback about motor performance, involving error detection and modification either in real-time during the movement (online correction) or following movement termination (offline modification of future movement (Ao et al., 2015)). Feedback derived from motor errors can be classified as either “intrinsic” or “extrinsic.” Intrinsic feedback refers to innate sensory-perceptual information channels that monitor motor performance as judged against desired performance through both comparisons to efference copy and the motor execution compared to the external environment (Sigrist et al., 2013). Intrinsic feedback is what is naturally available. Extrinsic feedback, in contrast, is provided synthetically by a third party or external device to supplement intrinsic feedback. Extrinsic feedback may be leveraged experimentally, typically by enhancing the information provided visually (screens), aurally (speaker, headphones), tactiley (robots, vibrotactile), or a combination of the above (Sigrist et al., 2013).

Evidence-based clinical practice guidelines for post-stroke rehabilitation include biofeedback (extrinsic feedback) as a favorable management recommendation for several post-stroke conditions, including impairments of gait, balance, and motor control (Panel, 2006). While biofeedback has been implemented with success often through visual cues and prompts in stroke rehabilitation, these approaches very often center on correcting the hand/limb component of the intended action. This continues in contemporary rehabilitation despite the fact that most tasks and interventions are visually guided actions that require eye-hand coordination (Seok et al., 2016), and it

assumes that no inherent dysfunction resides on the visual system or in integrating the visual and motor components for coordinated control. Predicting the consequence of a motor plan and any anticipated error is the essence of feedforward control (Wolpert and Ghahramani, 2000; Wolpert et al., 1995); this is true for movement in the hand and also the eye. Improving these predictions should allow one to improve motor performance through the process of motor learning (Shadmehr and Wise, 2005). In stroke, there are motor planning deficits, as hemiparetic patients are unable to properly predict the impact of a given set of neural commands when asked to perform visually guided hand movements (Beer et al., 1999). If these predictions are impaired, external “prompts” or visual cues may help adjust not only hand control, but also eye control and inform a working eye-hand coordination model.

In our study, we provide extrinsic feedback as part of a visually guided pointing task that is focused on remediating eye-hand incoordination, defined as temporal decoupling of eye and hand during attempted coordination, for participants with middle cerebral artery stroke. Separate feedback signals convey, first, the difference between the actual endpoint of the saccade and the intended spatial target, and second, the actual endpoint of the reach. We test the hypothesis that adaptive control mechanisms will be recruited to rescue both temporal and spatial aspects of eye-hand decoupling in these stroke subjects, guiding performance toward neurotypical coupling (normative eye-hand control).

2 Methods

2.1 Subjects

Seventeen (17) neurologically sound control subjects (aged 26.2 ± 4.6) and 13 stroke participants (57.4 ± 14.2) with a known history of middle cerebral artery ischemic stroke were recruited. Among the stroke participants, seven had right hemispheric middle cerebral artery (MCA) stroke and six had left hemispheric MCA strokes (mild-moderate motor impairment [Fugl-Meyer Scale]; <2 modified Ashworth scale). The clinical characteristics of the stroke participants are summarized in [Table 1](#).

2.2 Inclusion and exclusion criteria

A focused stroke history and neurological and musculoskeletal examinations (inclusive of more extensive range of motion analyses) were performed on all participants to determine inclusion/exclusion.

Stroke participants: (1) ≥ 18 years, (2) injury in the middle cerebral artery (MCA) distribution at least 4 months prior to enrollment, (3) ability to complete the Fugl-Meyer Score (FMS) to define arm motor impairment (Fugl-Meyer et al., 1975), (4) a full range of eye movements in horizontal and vertical directions, as assessed by the experimenter, (5) ability to perform pointing tasks, as assessed by the

Table 1 Clinical characteristics of stroke participants.

Subject ID	Age (Years)	Sex	Stroke characteristics ^a	Chronicity (Months)	Fugl-Meyer score ^b
1	78	M	R MCA distribution	24	66
2	61	F	R MCA distribution	84	66
10	39	M	R MCA distribution	55	47
11	70	M	R MCA distribution	2	66
6	60	F	R MCA distribution	30	30
7	73	M	R MCA distribution	72	58
8	51	F	R MCA distribution	146	30
3	34	M	L MCA distribution	19	66
4	39	F	L MCA distribution	16	45
5	70	M	L MCA distribution	32	58
9	60	M	L MCA distribution	52	63
12	47	F	L MCA distribution	17	61
13	65	F	L MCA distribution	7	66
Avg. (SD)	57.5 (14.3)			42 (39)	55.5 (13.3)

^aStroke characteristics, lesion location obtained from medical history with participant and/or family members serving as historian; region and laterality cross-validated for consistency with examination findings.

^bFugl-Meyer Score, a summation of the Upper Extremity Score (out of 66), which reflects the extent of post stroke motor impairment.

experimenter, (6) willingness to complete all clinical assessments, and (7) an ability to give informed consent and complete HIPPA certifications.

Control and stroke participants were excluded if they met any of the following criteria: (1) cognitive dysfunction <24 on the Mini Mental Status (Srivastava et al., 2006), (2) significant injury to an eye, weakness in extraocular muscles or presence of visual field cuts, assessed by the Beery-Buktenica Developmental Test of Visual-Motor Integration (Beery VMI) (Malloy et al., 2003; Temple et al., 2010; Zagan and Mead, 1983), standard clinical tests for visual acuity (Snellen chart) (Tannenbaum, 1971), visual fields (Beck et al., 1985). The 25-item National Eye Institute Visual Functioning Questionnaire and a 10-item neuro-ophthalmic supplement survey were completed to quantify the extent of disability due to perceived visual deficits (Beck et al., 1985), (3) hemi-spatial neglect assessed via the line bisection test (Schenkenberg et al., 1980) and the single-letter cancellation (Johnston and Diller, 1986), (4) major disability, as determined by a score >4 on the modified Rankin scale (Johnston and Diller, 1986; Rankin, 1957), (5) previous neurological illness, confounding medical conditions, or significant injury to the upper extremity, (6) significant depression determined by a score <11 on the Geriatric Depression scale (Volz et al., 2016), (7) pregnancy, and (8) electrical implant devices, e.g., pacemakers or defibrillators.

A video eye tracker (Eye Link II) was used to record eye movements. Subjects were seated on an adjustable chair 60 cm away from Dell 27" monitor screen. The eye tracker was calibrated for each participant before each session. A motion sensor (Polhemus) was affixed to the distal aspect of the index finger of the hand on the to-be-tested arm (the dominant arm for controls, and both arms in participants with stroke). The Polhemus sensor was affixed to the finger by first placing it on the finger and securing it at three locations (proximal and distal phalanx and wrist). A nine-point grid on the table top spanning 12 by 9 cm was used to calibrate the Polhemus sensor. At the beginning of each trial participants were asked to place their sensor-attached fingertip at known locations on the table to calibrate the fingertip to the table.

2.3 Experiment

To assess potential learning effects secondary to the addition of extrinsic feedback focused on ocular motor errors, subjects participated in two experiments involving a pro-saccade look-and-reach task. The first experiment included terminal error feedback of hand position (baseline) and the second experiment (feedback) included extrinsic feedback of reach and ocular motor error (LeVasseur et al., 2001).

In each experiment, controls participated in one session, and stroke participants completed up to two sessions, one per arm (depending on whether they were capable). During each session, a subject made 152 reaches; 76 to a randomly selected sequence of five target locations on a circle centered on the start position of the reach, and 76 starting from a separate randomly selected sequence of the same target circles to the center of the circle (center-out and center-in reaches did not show substantial differences and data were collapsed across these conditions in the analysis). At the beginning of each session, participants were instructed in the task, and it was verified that they understood the task and could execute the required reaches by performing a short series of familiarization trials. Familiarization concluded when subjects had learned to make the basic movement by responding to visually presented targets and go-beeps (see below). Each reach was accomplished by lifting the motion-sensor attached index finger, and only re-touching the table at movement termination (rather than sliding the finger or a stylus across the table). They were additionally instructed to minimize head motion by maintaining a stable (aligned) head/neck posture.

At the start of each trial, participants maintained fixation at a visual indicator (blue "start circle"). In half of each session (76 reaches) the movement began at the screen center toward a peripheral target, and in half of trials movements started at a peripheral position and progressed toward the screen center. The movement target (a small white circle, approx. 0.5° visual angle) was illuminated for 0.5 s, and the look-and-reach movement was cued by the simultaneous presentation of a "GO" beep and extinguishing of the start circle. Participants were instructed to move their eyes and finger as quickly and accurately as possible to the target position on the table. Participants were given feedback at the end of each movement. Feedback of fingertip endpoints was displayed at reach termination in both experiments,

and eye error feedback was displayed at the end of the reach in the feedback experiment. Eye feedback was shown on the screen at the spatial location recorded at the time of peak fingertip velocity, when in healthy controls the eye has typically fixated the target (Hayhoe et al., 2012) [to reinforce the coupling between eye and hand]. The experiment was performed with both hands (one session per hand) in participants with stroke whenever possible. Incomplete or drop-out participant-related data was excluded.

This study was approved by the Institutional Review Board of New York University's School of Medicine. Written informed consent was obtained from all participants.

2.4 Statistical analysis

Data were first median-filtered to remove outliers, and kinematic parameters were estimated after individual trials were aligned to the time of reach onset. Velocity traces were unremarkable and were not studied further. Two-sample *t*-tests were used to compare pairs of means. The results were compared with Welch's *t*-test due to unequal sample sizes and likely heteroscedasticity. As an adjunct to traditional *t*-tests, Bayesian analogues of the reported *t*-tests confirm our statistical results; 95% Bayesian confidence regions around all computed estimates, shown in the figures, display the result of the comparison graphically.

2.5 Results

2.5.1 Demographics

The participants with stroke were uniform in their neuroanatomic injury patterns; a full list of clinical characteristics is presented in Table 1. The mean FMS (Fugl-Meyer Score) was 55.5 ± 13.3 , with a range of 30–66.

3 Eye and hand movement timing/duration

The primary saccade produced by stroke participants during the baseline experiment occurred significantly earlier than in healthy participants regardless of the examined limb. As described previously, these early saccades are likely due to a disinhibition process that likely includes an anticipatory component (Rizzo et al., 2017b). In the second experiment with ocular motor feedback, stroke participants still initiated saccades early compared to controls, but later relative to their own baseline. However control participants began making premature saccades (early) when compared to their baseline data (baseline experiment control: 529 ms, CI[520 537], less-affected arm: 106 ms CI[80 132]; more-affected arm: 82 ms, CI[52 112]; feedback experiment control: 445 ms CI[434 456], less affected 118 ms CI[82 154], more affected 172 ms CI[130 215]). Stroke participants also reversed the trend in their reaching behavior and initiated reaches earlier in both the less- and more-affected arm, while reach

initiation in controls was similar in both experiments (baseline: control: 566 ms, CI[555–577], less-affected arm: 545 ms CI[521 568]; more-affected arm: 600 ms, CI[569 631]; feedback: control: 566 ms CL[555 577], less affected 466 ms CI[439 494], more affected 558 ms CI[542 575]. We define the time interval between the primary saccade and reach onset as our measure of temporal decoupling; this was significantly longer in stroke participants compared to controls in both experiments (baseline control: 26.8 ms CI[16.3 37.4], less affected: 439 ms CI[404 474], more affected: 519 ms CI[476 562]). During the experiment with extrinsic feedback, primary saccades were “re-coordinated” or re-coupled in stroke participants, reducing the time between saccade onset and reach onset and more closely approximating control behavior, re-synchronizing effectors (control: 121 ms CI[105 136], less affected: 348 ms CI[303 394], more affected: 386 ms CI[341 431]). In addition, correlations between saccade and reach onsets for individual reaches across all participants were significantly lower in stroke participants in the baseline experiment (control: $r = 0.63$ CI[0.6 0.65], less affected: $r = 0.36$ CI[0.31 0.41], more affected: $r = 0.31$ CI[0.25 0.37]), but were nearly identical in the feedback experiment (control: $r = 0.42$ CI[0.39 0.45], less affected: $r = 0.42$ CI[0.34 0.49], more affected: $r = 0.41$ CI[0.33 0.49]) (Fig. 1).

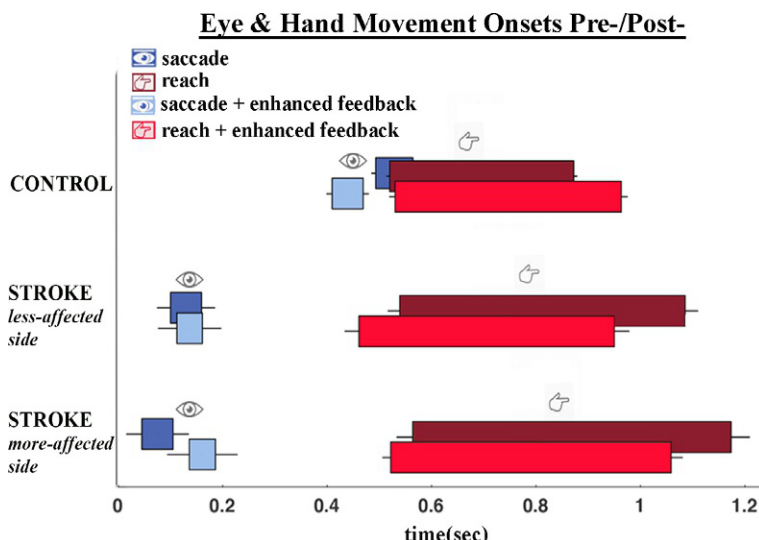
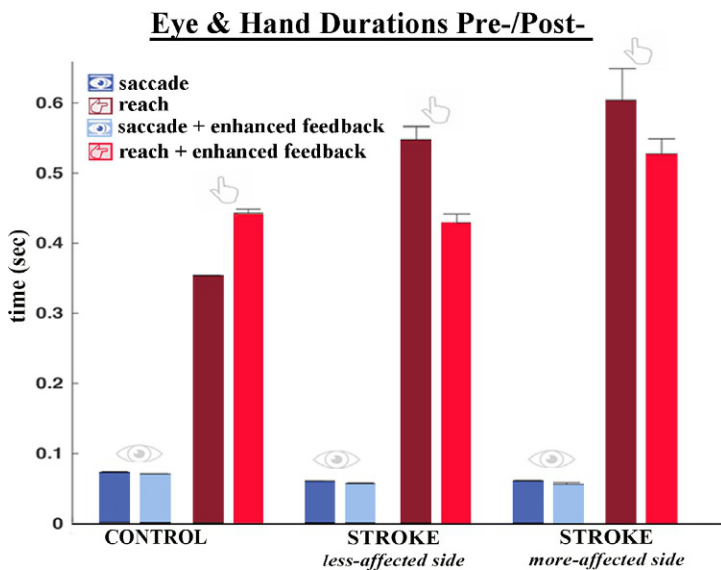


FIG. 1

Eye and hand movement onsets pre-/post-: Movement onset and offset (termination) times for the eye (blue) and hand (red), as represented by the left and right edges of the corresponding bars. Movement onsets/offsets between eye (saccade) and hand (reach) are compared pre-/post- (darker to lighter color) “enhanced feedback” (extrinsic feedback of the eye and hand) for controls, and both more- and less-affected arms in stroke participants.

Participants with stroke typically manifest with prolonged reach durations; during baseline performance, durations were indeed longer, as compared to controls, in addition to the degree of prolongation correlating to arm motor impairment severity. By comparison, at the end of the feedback experiment, reach duration decreased on average in stroke participants in both the less (from 546 ms CI[537 555] to 486 ms CI [477 495]) and more affected limbs (from 604 ms CI[587 622] to 537 ms CI[522 552]), while control participants made significantly longer reaches (from 352 ms CI[348 356] to 433 ms CI[428 438]). Saccade duration was significantly shorter in stroke participants, as compared to control participants in both experiments (baseline, control: 71.2 ms CI[70.2 72.2], less affected: 59.3 ms CI[58.0 60.4], more affected: 59.9 ms CI[58.7 61.0]; feedback, control: 59.1 ms CI[57.7 60.6], less affected: 48.4 ms CI [46.9 49.8], more affected: 49.8 ms CI[48.3 51.3]; Fig. 2), which corresponds to saccades that are usually about 10 mm. shorter in patients than controls (control baseline: 59.0 mm CI[58.6 59.5], feedback: 64.3 mm CI[63.9 64.6]; less affected baseline: 54.4 ms CI[53.7 55.1], feedback: 53.4 ms CI[52.4 54.4]; more affected baseline: 51.4 ms CI[50.7 52.1], feedback: 53.9 ms CI[53.0 54.8]).

**FIG. 2**

Eye and hand durations pre-/post-: Movement durations for the eye (blue) and hand (red), as represented by top edge of the corresponding bars. Movement durations between eye (saccade) and hand (reach) are compared pre-/post- (darker to lighter color) “enhanced feedback” (extrinsic feedback of the eye and hand) for controls, and both more- and less-affected arms in stroke participants.

4 Spatial errors for look and reach

Fig. 3 demonstrates that spatial errors (endpoint distance from the target) decreased after feedback was provided to participants. Endpoint reach errors decreased in control and stroke participants regardless of reaching limb. The accuracy improvement was significant in controls and the more affected arm of stroke participants (baseline experiment: control 9.3 mm, less affected 19.2 mm, and more affected 21.4 mm; feedback: control 6.9 mm, less affected 17.4 mm and more affected 14.6 mm). Interestingly, we also provide evidence that the spatial error of primary saccades improved post-feedback, on average, in the stroke condition, across both arms; this was not the case in controls. The concordance between eye and hand gains in spatial errors is of particular interest and contrary to findings in controls. Remarkably, as noted above, while controls de-synchronize eye and hand movement timing when provided extrinsic eye and hand feedback, stroke participants appear to benefit and re-synchronize, pairing robustly with the concordant spatial gains.

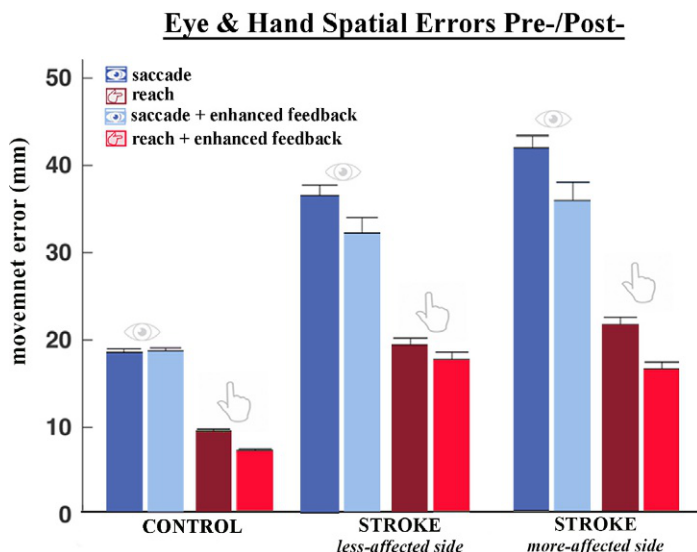


FIG. 3

Eye and hand spatial errors pre-/post-: Spatial errors for the eye (blue) and hand (red), as represented by top edge of the corresponding bars. Spatial errors between eye (saccade) and hand (reach) are compared pre-/post- (darker to lighter color) “enhanced feedback” (extrinsic feedback of the eye and hand) for controls, and both more- and less-affected arms in stroke participants.

5 Discussion

In the present study, corrective mechanisms were recruited to rescue and re-coordinate eye-hand coupling in stroke participants, guiding performance back toward neurotypical coupling through extrinsic feedback that includes endpoint errors of both saccades and reaches. This was evident through gains in temporal resynchronization, spatial accuracy, shorter reach durations, and improved onset correlations between effectors.

Stroke patients often suffer from deficits that affect their ability to make proper use of sensory information (intrinsic feedback) above and beyond their motor deficits (Ward and Cohen, 2004). Their impairments are often noted during dynamic eye-hand coordination tasks, emphasizing potential difficulties in rapidly processing sensory information, as well as in sensorimotor planning, integration, and motor execution. Inefficient handling of sensory information may lead to difficulties in predicting target motion, a deficit in feedforward mechanisms, and in the integration of sensory feedback for error correction (Caeyenberghs et al., 2009, 2010). In fact, predictive control is vital to optimized visuomotor planning (Hudson et al., 2008). Sensorimotor impairment may be multifactorial and compromised secondary to not only ocular motor deficits but also visuospatial planning and visuoperceptual abnormalities (Kaplan and Hier, 1982; Machner et al., 2009; Malhotra et al., 2006; Mennem et al., 2012; Rowe et al., 2009). As described previously, early primary saccades elicited by stroke participants, likely due to a reflexive, upper motor neuron-like disinhibition, may be triggered as an attempt to anticipate spatial targets in time and space (Rizzo et al., 2017b). While this evidence alone, is enough to suggest that related predictions for ocular motor control are likely poor, recent results also support that eye-hand tasks are significantly decoupled in time for both the more and less affected hands, and for targets in either hemifield. In addition to expected reach errors for the hemiparetic limb, there are also spatial errors noted for saccades, in otherwise visually intact participants (Rizzo et al., 2017a).

Feedback delivered extrinsically has been demonstrated to improve the effect of upper limb training in stroke patients (Subramanian et al., 2010). By providing this information explicitly (on-screen) at the end of each reach, an external, synthetic information source is able supplement natural, intrinsic feedback signals that underlie normal adaptation and learning mechanisms (Huang et al., 2005; Kim et al., 2015). Error biofeedback of the limb has been studied extensively (Alhasan et al., 2017; Huang et al., 2005; Urra et al., 2015; Van Dijk et al., 2005), but error biofeedback of the ocular motor system is a plausible, yet previously untested, concept in which primary saccadic endpoints (offline) are displayed on-screen relative to the intended spatial target. In stroke, where disinhibition has been noted in the ocular motor system, eye movements may be prematurely initiated with compromised accuracy (Rizzo et al., 2017b). Providing saccade error feedback may re-focus stroke

participants on eye movement control, while reducing the cognitive/computational demands associated with the corrective actions necessary to improve that control. Improving the accuracy and timing of fixations will in turn improve the quality of visual information available for reach control, ultimately improving overall performance.

These results are consistent with previous studies suggesting that performance feedback may facilitate the neural processing required for motor-error correction and improve the feedforward predictions of motor commands. In stroke participants, extrinsic feedback helps improve reach outcomes, including spatial and temporal errors (Cirstea and Levin, 2007; Maulucci and Eckhouse, 2001; Simonsen et al., 2017). In contrast to a previous study showing longer movement durations following feedback, stroke participants in our study made shorter duration reach movements in the feedback experiment when compared to the baseline experiment (Simonsen et al., 2017). In contrast, studies have shown that visual feedback can be unfavorable for visuomotor adaptation in healthy participants (Sigrist et al., 2013), which is consistent with a trend toward decoupling in our control participants.

Our study evaluated the effect of externally provided, terminal saccade feedback on a relatively simple look-to-reach task that aims to aid eye-hand incoordination. The effectiveness of extrinsic feedback was previously shown to vary based on task complexity and feedback timing (Winstein, 1991; Wulf and Shea, 2002). Studies have also been performed using different types of extrinsic feedback including visual, auditory, haptic, and multimodal; there is no consensus regarding the most effective way to provide such feedback (Sigrist et al., 2013). We believe visual feedback through extrinsic spatial prompting served here to improve eye movement accuracy, adding an emphasis on eye movement control, both of which served to help re-balance the cognitive resources and ultimately central control required to orchestrate eye-hand function post-injury.

Visually guided reaching relies on a constellation of processing resources, including both working memory and executive function (Baddeley, 2003; Baddeley and Hitch, 1974). It is likely that either the use of these resources, their full extent, or both may be impaired following stroke. A source of extrinsic feedback such as the one provided in our feedback experiment may provide error information (or may emphasize error information) that is not fully coded or processed following stroke. When provided with the means to reduce cognitive load in this way, our stroke participants showed evidence of enhanced eye/hand temporal coupling and overall error correction. Future studies should manipulate the complexity of the task, timing of feedback, and different feedback modalities to determine the appropriate dosing, frequency, and detailed form of feedback to optimize therapeutic outcomes. Our results provide a strong indication that employing extrinsic feedback in appropriate therapeutic doses may significantly improve ocular motor capabilities in the setting of eye-hand coordination for stroke rehabilitation.

References

- Alhasan, H., Hood, V., Mainwaring, 2017. The effect of visual biofeedback on balance in elderly population: a systematic review. *Clin. Intervent. Aging* 12, 487.
- Ao, D., Song, R., Tong, K.-Y., 2015. Sensorimotor control of tracking movements at various speeds for stroke patients as well as age-matched and young healthy subjects. *PLoS One* 10, e0128328.
- Baddeley, A., 2003. Working memory: looking back and looking forward. *Nat. Rev. Neurosci.* 4, 829–839.
- Baddeley, A.D., Hitch, G., 1974. Working Memory. *Psychology of Learning and Motivation*. Elsevier.
- Beck, R.W., Bergstrom, T.J., Lighter, P.R., 1985. A clinical comparison of visual field testing with a new automated perimeter, the Humphrey field analyzer, and the Goldmann perimeter. *Ophthalmology* 92, 77–82.
- Beer, R., Dewald, J., Rymer, Z., 1999. Disturbances of voluntary movement coordination in stroke: problems of planning or execution? *Prog. Brain Res.* 123, 455–460.
- Caeyenberghs, K., Van Roon, D., Van Aken, K., De Cock, P., Linden, C.V., Swinnen, S.P., Smits-Engelsman, B.C., 2009. Static and dynamic visuomotor task performance in children with acquired brain injury: predictive control deficits under increased temporal pressure. *J. Head Trauma Rehabil.* 24, 363–373.
- Caeyenberghs, K., Leemans, A., Geurts, M., Taymans, T., Vander Linden, C., Smits-Engelsman, B.C., Sunaert, S., Swinnen, S.P., 2010. Brain-behavior relationships in young traumatic brain injury patients: fractional anisotropy measures are highly correlated with dynamic visuomotor tracking performance. *Neuropsychologia* 48, 1472–1482.
- Cirstea, M.C., Levin, M.F., 2007. Improvement of arm movement patterns and endpoint control depends on type of feedback during practice in stroke survivors. *Neurorehabil. Neural Repair* 21, 398–411.
- Fugl-Meyer, A.R., Jaasko, L., Leyman, I., Olsson, S., Steglind, S., 1975. The post-stroke hemiplegic patient. 1. A method for evaluation of physical performance. *Scand. J. Rehabil. Med.* 7, 13–31.
- Hayhoe, M.M., McKinney, T., Chajka, K., Pelz, J.B., 2012. Predictive eye movements in natural vision. *Exp. Brain Res.* 217, 125–136.
- Huang, H., Ingalls, T., Olson, L., Ganley, K., Rikakis, T., He, J., 2005. Interactive multimodal biofeedback for task-oriented neural rehabilitation. *Conf. Proc. IEEE Eng. Med. Biol. Soc.* 3, 2547–2550.
- Hudson, T.E., Maloney, L.T., Landy, M.S., 2008. Optimal compensation for temporal uncertainty in movement planning. *PLoS Biol.* 4, e1000130.
- Johnston, C.W., Diller, L., 1986. Exploratory eye movements and visual hemi-neglect. *J. Clin. Exp. Neuropsychol.* 8, 93–101.
- Kaplan, J., Hier, D.B., 1982. Visuospatial deficits after right hemisphere stroke. *Am. J. Occup. Ther.* 36, 314–321.
- Kim, C.Y., Lee, J.S., Lee, J.H., Kim, Y.G., Shin, A.R., Shim, Y.H., Ha, H.K., 2015. Effect of spatial target reaching training based on visual biofeedback on the upper extremity function of hemiplegic stroke patients. *J. Phys. Ther. Sci.* 27, 1091–1096.
- LeVasseur, A.L., Flanagan, J.R., Riopelle, R.J., Munoz, D.P., 2001. Control of volitional and reflexive saccades in Tourette's syndrome. *Brain* 124, 2045–2058.

- Machner, B., Sprenger, A., Kompf, D., Sander, T., Heide, W., Kimmig, H., Helmchen, C., 2009. Visual search disorders beyond pure sensory failure in patients with acute homonymous visual field defects. *Neuropsychologia* 47, 2704–2711.
- Malhotra, P., Coulthard, E., Husain, M., 2006. Hemispatial neglect, balance and eye-movement control. *Curr. Opin. Neurol.* 19, 14–20.
- Malloy, P., Belanger, H., Hall, S., Aloia, M., Salloway, S., 2003. Assessing visuoconstructional performance in AD, MCI and normal elderly using the beery visual-motor integration test. *Clin. Neuropsychol.* 17, 544–550.
- Maulucci, R.A., Eckhouse, R.H., 2001. Retraining reaching in chronic stroke with real-time auditory feedback. *NeuroRehabilitation* 16, 171–182.
- Mennem, T.A., Warren, M., Yuen, H.K., 2012. Preliminary validation of a vision-dependent activities of daily living instrument on adults with homonymous hemianopia. *Am. J. Occup. Ther.* 66, 478–482.
- Panel, O., 2006. Ottawa panel evidence-based clinical practice guidelines for post-stroke rehabilitation. *Top. Stroke Rehabil.* 13, 1–269.
- Rankin, J., 1957. Cerebral vascular accidents in patients over the age of 60. I. General considerations. *Scott. Med. J.* 2, 127–136.
- Rizzo, J.R., Fung, J.K., Hosseini, M., Shafieesabet, A., Ahdoot, E., Pasculi, R.M., Rucker, J.C., Raghavan, P., Landy, M.S., Hudson, T.E., 2017a. Eye control deficits coupled to hand control deficits: eye-hand incoordination in chronic cerebral injury. *Front. Neurol.* 8, 330.
- Rizzo, J.R., Hudson, T.E., Abdou, A., Lui, Y.W., Rucker, J.C., Raghavan, P., Landy, M.S., 2017b. Disrupted saccade control in chronic cerebral injury: upper motor neuron-like disinhibition in the ocular motor system. *Front. Neurol.* 8, 12.
- Rowe, F., Brand, D., Jackson, C., Price, A., Walker, L., Harrison, S., Eccleston, C., Scott, C., Akerman, N., Dodridge, C., Howard, C., Shipman, T., Sperring, U., Macdarmid, S., Freeman, C., 2009. Visual impairment following stroke: do stroke patients require vision assessment. *Age Ageing* 38, 188–193.
- Schenkenberg, T., Bradford, D.C., Ajax, E.T., 1980. Line bisection and unilateral visual neglect in patients with neurologic impairment. *Neurology* 30, 509–517.
- Seok, H., Lee, S.Y., Kim, J., Yeo, J., Kang, H., 2016. Can short-term constraint-induced movement therapy combined with visual biofeedback training improve hemiplegic upper limb function of subacute stroke patients? *Ann. Rehabil. Med.* 40, 998–1009.
- Shadmehr, R., Wise, S.P., 2005. *The Computational Neurobiology of Reaching and Pointing: A Foundation for Motor Learning*. MIT Press.
- Sigrist, R., Rauter, G., Riener, R., Wolf, P., 2013. Augmented visual, auditory, haptic, and multimodal feedback in motor learning: a review. *Psychon. Bull. Rev.* 20, 21–53.
- Simonsen, D., Popovic, M.B., Spaich, E.G., Andersen, O.K., 2017. Design and test of a Microsoft Kinect-based system for delivering adaptive visual feedback to stroke patients during training of upper limb movement. *Med. Biol. Eng. Comput.* 55, 1927–1935.
- Srivastava, A., Rapoport, M.J., Leach, L., Phillips, A., Shammi, P., Feinstein, A., 2006. The utility of the mini-mental status exam in older adults with traumatic brain injury. *Brain Inj.* 20, 1377–1382.
- Subramanian, S.K., Massie, C.L., Malcolm, M.P., Levin, M.F., 2010. Does provision of extrinsic feedback result in improved motor learning in the upper limb poststroke? A systematic review of the evidence. *Neurorehabil. Neural Repair* 24, 113–124.
- Tannenbaum, S., 1971. The eye chart and Dr. Snellen. *J. Am. Optom. Assoc.* 42, 89–90.

- Temple, V., Drummond, C., Valiquette, S., Jozsvai, E., 2010. A comparison of intellectual assessments over video conferencing and in-person for individuals with ID: preliminary data. *J. Intellect. Disabil. Res.* 54, 573–577.
- Urra, O., Casals, A., Jane, R., 2015. The impact of visual feedback on the motor control of the upper-limb. 2015, 3945–3948.
- Van Dijk, H., Jannink, M.J., Hermens, H.J., 2005. Effect of augmented feedback on motor function of the affected upper extremity in rehabilitation patients: a systematic review of randomized controlled trials. *J. Rehabil. Med.* 37, 202–211.
- Volz, M., Mobus, J., Letsch, C., Werheid, K., 2016. The influence of early depressive symptoms, social support and decreasing self-efficacy on depression 6 months post-stroke. *J. Affect. Disord.* 206, 252–255.
- Ward, N.S., Cohen, L.G., 2004. Mechanisms underlying recovery of motor function after stroke. *Arch. Neurol.* 61, 1844–1848.
- Winstein, C.J., 1991. Knowledge of results and motor learning—implications for physical therapy. *Phys. Ther.* 71, 140–149.
- Wolpert, D.M., Ghahramani, Z., 2000. Computational principles of movement neuroscience. *Nat. Neurosci.* 3 (Suppl), 1212–1217.
- Wolpert, D.M., Ghahramani, Z., Jordan, M.I., 1995. An internal model for sensorimotor integration. *Science* 269, 1880–1882.
- Wulf, G., Shea, C.H., 2002. Principles derived from the study of simple skills do not generalize to complex skill learning. *Psychon. Bull. Rev.* 9, 185–211.
- Zagar, R., Mead, J.D., 1983. Analysis of a short test battery for children. *J. Clin. Psychol.* 39, 590–597.

Further reading

- Optican, L.M., 2005. Sensorimotor transformation for visually guided saccades. *Ann. N. Y. Acad. Sci.* 1039, 132–148.

Kinematics and the neurophysiological study of visually-guided eye movements

29

Laurent Goffart^{a,b,*}

^aAix Marseille University, CNRS, INT, Institut de Neurosciences de la Timone, Marseille, France

^bAix Marseille University, CNRS, CGGG, Centre Gilles Gaston Granger, Aix-en-Provence, France

*Corresponding author: Tel. +33 491324052, e-mail address: laurent.goffart@univ-amu.fr

Abstract

How do we relate observations and measurements made at the behavioral and neuronal levels? Notions of kinematics have been used to “decode” the firing rate of neurons and to explain the neurophysiology underlying the generation of visually-guided eye movements. The appropriateness of their fitting to events occurring within a medium (the brain) radically different from the physical world is questioned in this chapter. Instead of embedding the eye kinematics in the firing rate of central neurons, we propose that the saccadic and pursuit eye movements in fact reflect the dynamics of transitions of brain activity, from unbalanced states to equilibrium (symmetry) between opposing directional tendencies carried by the recruited visuomotor channels, with distinct transitions characterizing each movement category. While the eyeballs conform to the physical laws of motion, the neural processes leading to their movements follow principles dictated by the intrinsic properties of the brain network and of its diverse neurons.

Keywords

Tracking, Saccade, Pursuit, Symmetry, Equilibrium, Neurophysiology, Kinematics, Complexity

1 Gaze, target and measurements

During the characterization of the neuronal processes which underlie the ability to visually capture a moving object, the neurophysiological studies have been led to embed within the inner functioning of the brain, notions which belong to the vocabulary of kinematics. When they rotate in the orbit, the eyeballs do not change

their shape, and this rigidity allows specifying their orientation with a few numbers (coordinates) whose values depend upon the physical reference frame that has been chosen. Thus, gaze became assimilated to a line (the line of sight) or to an axis (visual axis), shifting from one point in the visual field to another, even though gaze actually refers to an extended field of binocular visuomotor interactions (Hafed et al., 2015; Krauzlis et al., 2017; Otero-Millan et al., 2014).

Attributing point-like values to gaze and targets inevitably leads to numerical differences between them, especially when their measurement is made with higher resolution. However such differences between measured values should not lead us to think that corresponding differences exist within the brain functioning. Objects in the physical world are obviously not points and during visual fixation, all light beams do not converge onto one single photoreceptor. The numerical values attributed to gaze and target directions belong to a “medium” which is not the brain but the set of behavioral measurements. Within the medium of brain functioning, a target, whether it is located in the central or peripheral visual field, is not point-like. From the retinal ganglion cells to their post-synaptic targets, and from the latter to their targets in the cerebral cortex or the brainstem, the divergence of anatomical projections implies that the neuronal image of any physical object, even tiny, recruits an increasing number of neurons (e.g., Nowak and Bullier, 1997).

When we record the activity of neurons in cortical visual areas, we find that they emit action potentials whenever a stimulus appears within a more or less extended region of the visual field. Likewise, when we record neurons in saccade-related regions (e.g., deep superior colliculus), we discover bursts of action potentials whenever a saccade is made toward locations situated within a more or less bounded region of the visual field. The extent of response fields indicates that any visual object, or any saccade toward its location, involves a large set of neurons (Anderson et al., 1998; McIlwain, 1976; Sparks et al., 1976). Moreover, in most visual and saccade-related regions, the neurons are laid out in such a way that neighboring neurons respond to neighboring stimuli in the visual field, or burst during saccades toward neighboring locations. Despite the divergence of anatomical projections and the lateral extent of post-synaptic contacts, the retinal topology is preserved across the layers of neurons.

The consequence of these two basic observations is that neighboring objects in the visual field, or saccades toward their respective location, mobilize neuronal assemblies which involve common cells. This overlap is not taken into account when the focus is made upon the numerical difference between gaze and target directions, the value of which is called *position error* or *motor error*. Such an error signal is indeed considered as the critical factor triggering a saccade and specifying its metrics (amplitude and direction).

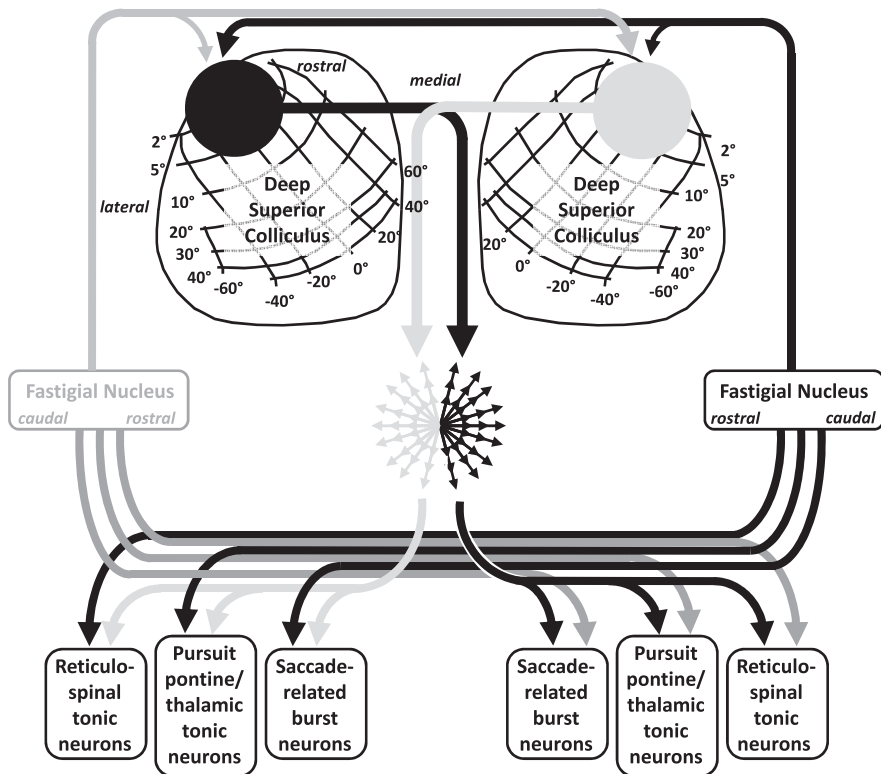
2 Gaze direction as equilibrium

The simplest solution that was proposed to model the execution of saccades is a negative feedback loop reducing this difference, i.e., between a desired direction of gaze and an estimate of its current direction. Desired gaze direction

corresponds to the selected target location. The *motor error* resulting from the comparison between these two estimates would feed the premotor neurons which themselves would emit action potentials at a rate proportional to the size of the error (van Gisbergen et al., 1981). Thus, while the gaze direction moves toward the target, the motor error diminishes and the firing of premotor neurons declines and cease exciting the motor neurons when the error has been zeroed (Robinson, 1975).

In this theoretical framework, a non-zero motor error leads to a saccade. However, recent studies in the monkey reported pathological cases where stable fixation is engaged although gaze is not directed toward the location which was previously fixated during non-pathological (control) conditions. Gaze is directed toward a location which is offset with respect to the target; no saccade is launched in spite of non-zero motor error. For example, when the activity of caudal fastigial nuclei (cFN) is altered by a local and unilateral injection of a pharmacologically-inhibiting agent (muscimol), the monkey does not direct its gaze toward the target (located straight ahead) but toward a location slightly shifted toward the injected side (Goffart et al., 2004; Guerrasio et al., 2010; Ohtsuka et al., 1994; Robinson et al., 1993). By contrast, when the injected drug is a disinhibiting agent (bicuculline), the gaze is deviated toward the opposite side (Sato and Noda, 1992). The ipsilesional fixation offset observed after muscimol injection is not an oculomotor disorder because when the head is free to move, the monkey exhibits an ipsilesional deviation of the head (cervical dystonia) and the eyes in the orbit are deviated toward the contralateral side (Quinet and Goffart, 2005). The relatively similar sizes of fixation offset between the head-restrained and—unrestrained testing conditions suggest an alteration of processes underlying gaze orientation. This deduction is consistent with anatomical studies which report cFN projections to the rostral parts of both SC (May et al., 1990) and not to the nuclei prepositus hypoglossi (NPH) or medial vestibular nuclei (MVN) where tonic neurons projecting to abducens motor neurons are found (Noda et al., 1990). In the rostral SC, the neurons fire in a sustained manner when the same gaze direction is maintained (Dorris and Munoz, 1995), but they also emit bursts of action potentials during fixational saccades (Hafed and Krauzlis, 2012). When muscimol is injected in this part of the SC, the monkey exhibits a fixation offset when it directs its gaze toward a straight ahead target. By contrast, saccades to peripheral targets are accurate (Goffart et al., 2012). A fixation offset has also been reported after muscimol injection in the frontal eye field (Dias and Segraves, 1999), a region which is reciprocally connected with the deep superior colliculus (Sommer and Wurtz, 1998).

These observations stress not only the limitations brought by reducing gaze and target to their measured values, but also the problem brought by assimilating their difference as a command leading to a saccade. However, when we consider gaze direction as the outcome of flow of signals propagating from the optic to the motor nerves, along multiple parallel channels involving neuronal assemblies distributed bilaterally in the brain, we are led to a viewpoint where a change in gaze orientation is not initiated when the flows involve omnidirectional commands that counterbalance each other (Fig. 1; Goffart et al., 2018).

**FIG. 1**

Gaze direction as equilibrium. A saccade or a slow eye movement is not initiated when the visuo-oculomotor system is within a mode where opposing commands (issued for instance by the left and right superior colliculi) counterbalance each other. For generating saccadic and pursuit eye movements, the symmetry breaking involves different groups of neurons. Saccades involve neurons located in the pontomedullary reticular formation whereas slow eye movements involve neurons in the pontine nuclei and the thalamus (see Bourrelly et al., 2018b and Goffart et al., 2018 for more explanations). The bilateral fastigial activity also contributes to the muscle tone which specifies the horizontal orientation (yaw) of the head (Goffart and Pélisson, 1998; Quinet and Goffart, 2005).

3 Transforming the location of a peripheral target into saccade duration

The concept of negative feedback loop was a simple solution to the fundamental problem of understanding how the *locus* of activity elicited by a visual target, in the retina or in the superior colliculus, is transformed into *duration* of motoneurons' bursting activity (Moschovakis et al., 1996; Scudder et al., 2002; Sparks, 2002). The solution was simple because it removed the need to search, within the brain activity, a process encoding saccade duration, as Hans Kornhüber (1971) initially proposed, but

later revisited (Jürgens et al., 1981). With the negative feedback control, a cerebral “chronometer” is not needed; the movement duration is a secondary by-product of a process reducing a difference between spatial magnitudes putatively encoded in the brain activity. This conceptual framework was fertile because it stimulated the making of multiple experiments which brought several new observations compatible with a negative feedback control. However, if the proposed signals (encoding of eye and target directions or displacements) and processes (comparator or resettable integrator) have no neurophysiological substrate, then the theory becomes irrefutable because it is impossible to demonstrate that any putative thing does not exist.

Later, on the basis of neuromimetic modeling, it was suggested that the signals used by models would not be explicitly conveyed by separate groups of neurons, but would correspond to activities involving assemblies of interconnected neurons distributed over several territories (Optican and Quaia, 2002; Robinson, 1992). Consequently, the signals imagined by the models are not tractable anymore with classical unit recording techniques. While the feedback control hypothesis encountered these complications, the hypothesis of Kornhuber (1971) was further developed by the group of Peter Thier (2011). Unfortunately, evidence for chronometric control is not convincing (see Goffart et al., 2017a, 2018 for explanations).

4 Tracking a moving target

The notion of negative feedback control has also been used to explain the guidance of eye movements made when a subject tracked a moving visual target. Two processes would operate in parallel before the target saccade: one process would reduce the difference between gaze and target directions (same as discussed above) while the other would reduce the difference between the eye and target velocities. Recording techniques indeed allow measuring eye movements with such high resolution that instantaneous velocity and acceleration can be calculated. When the performance of a subject tracking a moving target is measured, numerical differences between kinematic parameters of the eye and target can be calculated. Thus, notions such as “velocity error” and “acceleration error” were added to the list of stimuli driving the generation and execution of pursuit eye movements (Lisberger et al., 1987).

However, proposing that the instantaneous velocity of the eyeball (or of any physical object) is a parameter embedded within the inner functioning of the brain is a hypothesis which is difficult to take root in the neurophysiological soil for several reasons. First, neuronal activities propagate within a medium whose number of dimensions is different from the 3-dimensional “space” of kinematics. A simple centrifugal horizontal motion implies one single dimension in physical space but as many dimensions as there are parallel channels transmitting the retinal signals to the abducens and oculomotor nuclei. Second, from the retinal input to the motor output, the pattern of neuronal connectivity (divergence followed by convergence) suggests multiple homothetic transformations (expansions and contractions) between the anatomical relays. In other words, the activity which is elicited by a stimulus, even very small, is not rigid; any gaze or target situation measured here and now

is not reducible to a point of coordinates (x,y,z,t) . Third, compared to its changes of coordinates, a moving target does not yield mirror-like changes of activity in the brain networks: residual activities persist, as shown in the superior colliculus for example (Goffart et al., 2017b). The instantaneous velocity of an eye movement is the outcome of action potentials emitted by motor neurons under the influence of neurons distributed in several other regions and during a longer time interval. Moreover, when correlations between firing rate and velocity are observed, they can be secondary consequences of changes in alertness or motivation (e.g., Takikawa et al., 2002). Saccades are indeed slowed and the firing rate of saccade-related neurons reduced when the alertness declines (e.g., Fuchs et al., 1993; Henn et al., 1984; Soetedjo et al., 2000). Finally, recordings in the cat have revealed stronger correlations between the firing rate of motoneurons and the change in muscle force (Davis-Lopez de Carrizosa et al., 2011). Therefore, the correlation between the firing rate of single neurons and eye kinematics must be interpreted with the greatest caution, especially for those neurons located several synapses upstream from the motor neurons (see Goffart et al., 2018 for more explanations).

5 Target velocity as a stimulus for pursuit

The suggestion that pursuit consists of matching the eye and target velocities can be traced back to the studies of Rashbass (1961) and Robinson (1965). It pervades so much the contemporary sciences of eye movements that most reviews declare visual pursuit as involving a negative feedback loop reducing a difference between estimates of target and eye velocities. However, rigorously speaking, when target distance (position error), velocity or acceleration are said to be stimuli influencing pursuit eye movements, the causal relationship should be restricted to the sets of numerical values which belong to the same medium (the physical world) and for which the tools of kinematics have proven their efficiency.

Rashbass (1961) designed an oculomotor task where gaze, instead of shifting toward a target moving toward the foveal field, drifts away from it, in the same direction as the target motion but with a lower speed. This observation was taken as evidence that target velocity is a stimulus for pursuit eye movements. In this task, the target appears at a slightly eccentric location before moving slowly toward the foveal field. The slow motion must start from an eccentric location whose numerical value is approximately 0.15–0.2 times the target speed. If its speed is less than $10^{\circ}/s$, the target must start from a location which, at most, is situated 2° from the center of the foveal field. The target *center* is then located at the edge of the foveal field. However, as explained at the beginning of our chapter, the fact that the target is a small spot does not imply that its cerebral image is point-like. A saccade is not launched toward its location because the equilibrium that characterizes gaze direction has not been broken; the visuo-oculomotor saccadic system is within a mode where opposing commands still counter-balance each other (Fig. 1). We shall now see that the slow eye movement does not require an encoding of target velocity for its initiation and maintenance.

6 Pursuit as sustained imbalance

The slow eye movement in the same direction as the target motion (but away from its physical location) tells us that its generation involves another kind of symmetry breaking. During horizontal target motions, it results from an imbalance between commands that tonic neurons in the left and right NPH/MVN exert upon the motor and internuclear neurons in the abducens nucleus (McFarland and Fuchs, 1992; Scudder and Fuchs, 1992). Their bilateral equilibrium would be broken by any asymmetrical excitation, for instance in the visual input from the pretectum. The imbalance of activity between the left and right nuclei of the optic tract (NOT) could also be completed by asymmetric input from the left and right paraflocculi.

Unless the drug diffuses toward the pretectum, drifts do not happen during unilateral inactivation of rostral SC: the monkey is able to maintain stable gaze. Its direction is offset with respect to the target with an angle which is relatively constant, even while the monkey pursues a moving target (Hafed et al., 2008). Despite the mismatch between gaze and target directions, the pursuit is preserved. Comparable observations have been shown after caudal fastigial inactivation (see the first figures in Bourrelly et al., 2018a, 2018b). Made in experimentally-induced pathological conditions, they indicate that the target does not have to be centered within the foveal field for being smoothly pursued. Several behavioral experiments in the normal subject actually demonstrated this possibility (Fuchs, 1967; Pola and Wyatt, 1980; Robinson, 1965; Segraves and Goldberg, 1994; Winterson and Steinman, 1978).

Thus, during the Rashbass' task, a velocity signal is not necessary to explain why gaze moves away from an approaching target. The motion of the target image across the foveae yields asymmetrical activity between the left and right NOT (Gamlin, 2006; Hoffmann et al., 2009; Mustari and Fuchs, 1990). Then, the fact that the slow eye movement persists and increases to reach the same speed as the target, in spite of the diminishing velocity error can be explained by the maintenance of the same unbalanced drive from the tonic neurons in NPH/MVN to the motor neurons.

7 Conclusion

During the past five decades, notions of kinematics were used to “decode” the firing rate of neurons and to unravel the neurophysiology of tracking eye movements. The appropriateness of these notions to a medium radically different from the physical world was not questioned. Instead of embedding the eye movement kinematics in the firing rate of central neurons, we propose that saccadic and slow eye movements reflect the dynamics of transitions (from unbalanced states to equilibrium) of bilateral activity carrying opposing directional tendencies.

Thus, the target foveation consists of dynamically adjusting the balance (symmetry) between opposing tendencies emitted in the left and right parts of the brain, as proposed for the control of fixation (Goffart et al., 2012; Guerrasio et al., 2010), saccade trajectory (Bourrelly et al., 2018a; Goffart et al., 2003, 2004; van Gisbergen et al., 1981) and pursuit (Bourrelly et al., 2018b; Hafed et al., 2008).

Concerning the question how eye movements reach the target speed, the acceleration would involve recruitment: increasing the firing and number of motion-related neurons moves the eyes faster whereas decreasing them reduces their velocity. Then, understanding the cerebral control of pursuit eye movement requires characterizing the adjustment of the appropriate population size through recruiting neurons and increasing the occurrence of synchronized action potentials at post-synaptic levels (Goffart et al., 2017a, 2018).

Acknowledgments

The author thanks Professors Gabriella Crocco and Igor Ly for epistemological advices.

References

- Anderson, R.W., Keller, E.L., Gandhi, N.J., Das, S., 1998. Two-dimensional saccade-related population activity in superior colliculus in monkey. *J. Neurophysiol.* 80, 798–817.
- Bourrelly, C., Quinet, J., Goffart, L., 2018a. The caudal fastigial nucleus and the steering of saccades toward a moving visual target. *J. Neurophysiol.* 120, 421–438.
- Bourrelly, C., Quinet, J., Goffart, L., 2018b. Pursuit disorder and saccade dysmetria after caudal fastigial inactivation in the monkey. *J. Neurophysiol.* 120, 1640–1654.
- Davis-Lopez de Carrizosa, M.A., Morado-Díaz, C.J., Miller, J.M., de la Cruz, R.R., Pastor, A.M., 2011. Dual encoding of muscle tension and eye position by abducens motoneurons. *J. Neurosci.* 31, 2271–2279.
- Dias, E.C., Segraves, M.A., 1999. Muscimol-induced inactivation of monkey frontal eye field: effects on visually and memory-guided saccades. *J. Neurophysiol.* 81, 2191–2214.
- Dorris, M.C., Munoz, D.P., 1995. A neural correlate for the gap effect on saccadic reaction times in monkey. *J. Neurophysiol.* 73, 2558–2562.
- Fuchs, A.F., 1967. Saccadic and smooth pursuit eye movements in the monkey. *J. Physiol.* 191, 609–631.
- Fuchs, A.F., Robinson, F.R., Straube, A., 1993. Role of the caudal fastigial nucleus in saccade generation. I. Neuronal discharge patterns. *J. Neurophysiol.* 70, 1712–1740.
- Gamlin, P.D., 2006. The pretectum: connections and oculomotor-related roles. *Prog. Brain Res.* 151, 379–405.
- Goffart, L., Péliisson, D., 1998. Orienting gaze shifts during muscimol inactivation of caudal fastigial nucleus in the cat. I. Gaze dysmetria. *J. Neurophysiol.* 79, 1942–1958.
- Goffart, L., Chen, L.L., Sparks, D.L., 2003. Saccade dysmetria during functional perturbation of the caudal fastigial nucleus in the monkey. *Ann. N. Y. Acad. Sci.* 1004, 220–228.
- Goffart, L., Chen, L.L., Sparks, D.L., 2004. Deficits in saccades and fixation during muscimol inactivation of the caudal fastigial nucleus in the rhesus monkey. *J. Neurophysiol.* 92, 3351–3367.
- Goffart, L., Hafed, Z.M., Krauzlis, R.J., 2012. Visual fixation as equilibrium: evidence from superior colliculus inactivation. *J. Neurosci.* 32, 10627–10636.
- Goffart, L., Bourrelly, C., Quinet, J., 2017a. Synchronizing the tracking eye movements with the motion of a visual target: basic neural processes. *Prog. Brain Res.* 236, 243–268.
- Goffart, L., Cecala, A., Gandhi, N., 2017b. The superior colliculus and the steering of saccades toward a moving visual target. *J. Neurophysiol.* 118, 2890–2901.

- Goffart, L., Bourrelly, C., Quinton, J.-C., 2018. Neurophysiology of visually-guided eye movements: critical review and alternative viewpoint. *J. Neurophysiol.* 120, 3234–3245.
- Guerrasio, L., Quinet, J., Büttner, U., Goffart, L., 2010. Fastigial oculomotor region and the control of foveation during fixation. *J. Neurophysiol.* 103, 1988–2001.
- Hafed, Z.M., Krauzlis, R.J., 2012. Similarity of superior colliculus involvement in microsaccade and saccade generation. *J. Neurophysiol.* 107, 1904–1916.
- Hafed, Z.M., Goffart, L., Krauzlis, R.J., 2008. Superior colliculus inactivation causes stable offsets in eye position during tracking. *J. Neurosci.* 28, 8124–8137.
- Hafed, Z.M., Chen, C.Y., Tian, X., 2015. Vision, perception, and attention through the lens of microsaccades: mechanisms and implications. *Front. Syst. Neurosci.* 9, 167.
- Henn, V., Baloh, R.W., Hepp, K., 1984. The sleep-wake transition in the oculomotor system. *Exp. Brain Res.* 54, 166–176.
- Hoffmann, K.P., Bremmer, F., Distler, C., 2009. Visual response properties of neurons in cortical areas MT and MST projecting to the dorsolateral pontine nucleus or the nucleus of the optic tract in macaque monkeys. *Eur. J. Neurosci.* 29, 411–423.
- Jürgens, R., Becker, W., Kornhüber, H., 1981. Natural and drug-induced variations of velocity and duration of human saccadic eye movements: evidence for a control of the neural pulse generator by local feedback. *Biol. Cybern.* 39, 87–96.
- Kornhüber, H.H., 1971. Motor functions of cerebellum and basal ganglia: the cerebellocortical saccadic (ballistic) clock, the cerebellonuclear hold regulator, and the basal ganglia ramp (voluntary speed smooth movement) generator. *Kybernetik* 8, 157–162.
- Krauzlis, R.J., Goffart, L., Hafed, Z.M., 2017. Neuronal control of fixation and fixational eye movements. *Philos. Trans. R. Soc. Lond. B Biol. Sci.* 372, 20160205.
- Lisberger, S.G., Morris, E.J., Tychsen, L., 1987. Visual motion processing and sensory-motor integration for smooth pursuit eye movements. *Annu. Rev. Neurosci.* 10, 97–129.
- May, P.J., Hartwich-Young, R., Nelson, J., Sparks, D.L., Porter, J.D., 1990. Cerebellotectal pathways in the macaque: implications for collicular generation of saccades. *Neuroscience* 36, 305–324.
- McFarland, J.L., Fuchs, A.F., 1992. Discharge patterns in nucleus prepositus hypoglossi and adjacent medial vestibular nucleus during horizontal eye movement in behaving macaques. *J. Neurophysiol.* 68, 319–332.
- McIlwain, J.T., 1976. Large receptive fields and spatial transformations in the visual system. *Int. Rev. Physiol.* 10, 223–248.
- Moschovakis, A.K., Scudder, C.A., Highstein, S.M., 1996. The microscopic anatomy and physiology of the mammalian saccadic system. *Prog. Neurobiol.* 50, 133–254.
- Mustari, M.J., Fuchs, A.F., 1990. Discharge patterns of neurons in the pretectal nucleus of the optic tract (NOT) in the behaving primate. *J. Neurophysiol.* 64, 77–90.
- Noda, H., Sugita, S., Ikeda, Y., 1990. Afferent and efferent connections of the oculomotor region of the fastigial nucleus in the macaque monkey. *J. Comp. Neurol.* 302, 330–348.
- Nowak, L.G., Bullier, J., 1997. The timing of information transfer in the visual system. In: Kaas, J., et al. (Eds.), *Extrastriate Cortex*. vol. 12. Plenum Press, pp. 205–241.
- Ohtsuka, K., Sato, H., Noda, H., 1994. Saccadic burst neurons in the fastigial nucleus are not involved in compensating for orbital nonlinearities. *J. Neurophysiol.* 71, 1976–1980.
- Optican, L.M., Quaia, C., 2002. Distributed model of collicular and cerebellar function during saccades. *Ann. N. Y. Acad. Sci.* 956, 164–177.
- Otero-Millan, J., Macknik, S.L., Martinez-Conde, S., 2014. Fixational eye movements and binocular vision. *Front. Integr. Neurosci.* 8, 52.
- Pola, J., Wyatt, H.J., 1980. Target position and velocity: the stimuli for smooth pursuit eye movements. *Vision Res.* 20, 523–534.

- Quinet, J., Goffart, L., 2005. Saccade dysmetria in head-unrestrained gaze shifts after muscimol inactivation of the caudal fastigial nucleus in the monkey. *J. Neurophysiol.* 93, 2343–2349.
- Rashbass, C., 1961. The relationship between saccadic and smooth tracking eye movements. *J. Physiol.* 159, 326–338.
- Robinson, D.A., 1965. The mechanics of human smooth pursuit eye movement. *J. Physiol.* 180, 569–591.
- Robinson, D.A., 1975. Oculomotor control signals. In: Lennerstrand, G., Bach-y-Rita, P. (Eds.), *Basic mechanisms of ocular motility and their clinical implications*. Pergamon, Oxford, pp. 337–374.
- Robinson, D.A., 1992. Implications of neural networks for how we think about brain function. *Behav. Brain Sci.* 15, 644–655.
- Robinson, F.R., Straube, A., Fuchs, A.F., 1993. Participation of caudal fastigial nucleus in saccade generation. II. Effects of muscimol inactivation. *J. Neurophysiol.* 70, 1741–1758.
- Sato, H., Noda, H., 1992. Saccadic dysmetria induced by transient functional decortication of the cerebellar vermis. *Exp. Brain Res.* 88, 455–458.
- Scudder, C.A., Fuchs, A.F., 1992. Physiological and behavioral identification of vestibular nucleus neurons mediating the horizontal vestibuloocular reflex in trained rhesus monkeys. *J. Neurophysiol.* 68, 244–264.
- Scudder, C.A., Kaneko, C.R.S., Fuchs, A.F., 2002. The brainstem burst generator for saccadic eye movements: a modern synthesis. *Exp. Brain Res.* 142, 439–462.
- Segraves, M.A., Goldberg, M.E., 1994. Effect of stimulus position and velocity upon the maintenance of smooth pursuit eye velocity. *Vision Res.* 34, 2477–2482.
- Soetedjo, R., Kaneko, C.R., Fuchs, A.F., 2000. Evidence that the superior colliculus participates in the feedback control of saccadic eye movements. *J. Neurophysiol.* 87, 679–695.
- Sommer, M.A., Wurtz, R.H., 1998. Frontal eye field neurons orthodromically activated from the superior colliculus. *J. Neurophysiol.* 80, 3331–3335.
- Sparks, D.L., 2002. The brainstem control of saccadic eye movements. *Nat. Rev. Neurosci.* 3, 952–964.
- Sparks, D.L., Holland, R., Guthrie, B.L., 1976. Size and distribution of movement fields in the monkey superior colliculus. *Brain Res.* 113, 21–34.
- Takikawa, Y., Kawagoe, R., Itoh, H., Nakahara, H., Hikosaka, O., 2002. Modulation of saccadic eye movements by predicted reward outcome. *Exp. Brain Res.* 142, 284–291.
- Thier, P., 2011. The oculomotor cerebellum. In: Liversedge, S.P., Gilchrist, I., Everling, S. (Eds.), *The Oxford handbook of eye movements*. Oxford University Press.
- van Gisbergen, J.A.M., Robinson, D.A., Gielen, S.A., 1981. A quantitative analysis of generation of saccadic eye movements by burst neurons. *J. Neurophysiol.* 45, 417–442.
- Winterson, B.J., Steinman, R.M., 1978. The effect of luminance on human smooth pursuit of perifoveal and foveal targets. *Vision Res.* 18, 1165–1172.

Further reading

- Pellionisz, A., Llinas, R., 1982. Space-time representation in the brain: the cerebellum as a predictive space-time metric tensor. *Neuroscience* 7 (12), 2949–2970.

Deficient head motor control in functional dizziness: Experimental evidence of central sensory-motor dysfunction in persistent physical symptoms

30

Nadine Lehnen^{a,b,c,d,*}, Lena Schröder^{a,d}, Peter Henningsen^a, Stefan Glasauer^{b,c,d}, Cecilia Ramaiolli^{a,b,c}

^a*Department of Psychosomatic Medicine and Psychotherapy, Klinikum rechts der Isar, Technical University of Munich, Munich, Germany*

^b*German Center for Vertigo and Balance Disorders, University Hospital Munich, Munich, Germany*

^c*Institute of Medical Technology, Brandenburg University of Technology Cottbus-Senftenberg, Senftenberg, Germany*

^d*Graduate School of Systemic Neurosciences, Ludwig-Maximilians-University Munich, Planegg, Germany*

*Corresponding author: Tel.: +49-89-4140-6448; Fax: +49-89-4140-6773,
e-mail address: n.lehnen@tum.de

Abstract

Understanding the mechanisms of symptoms that are insufficiently explained by organic dysfunction remains challenging. Recently, it has been proposed that such “functional symptoms” are based on erroneous sensory processing in the central nervous system (CNS), with internal expectations dominating sensory inputs.

In a pilot study, we used a head motor control set-up to assess the interplay between sensory input and expectation on the example of patients with functional dizziness. Eight patients and 11 age-matched healthy controls performed large active eye-head gaze shifts towards visual targets in the natural situation and with the head moment of inertia 3.3-fold increased. The latter induces head oscillations and the expected sensory outcome of the movement, estimated in the CNS, does not match the actual sensory input. Head oscillations were assessed in patients and in healthy subjects and compared to prior results from patients with organic disease (vestibular loss and cerebellar ataxia). Head oscillations in patients with functional dizziness were

different from those of healthy subjects ($F(1,17)=27.26, P<0.001$, partial $\eta^2=0.62$), and similar to those of patients with cerebellar ataxia, and with vestibular loss ($F(2,19)=0.56, P=0.58$). Even in the natural, unweighted, condition, head oscillations were higher in functional dizziness patients than in healthy subjects ($P=0.001$). Since an extensive work-up failed to demonstrate any explanatory peripheral vestibular, motor, or cerebellar organic dysfunction, these motor control deficits are a first indication of erroneous interplay between expectations and sensory input in the CNS that could account for persistent physical symptoms.

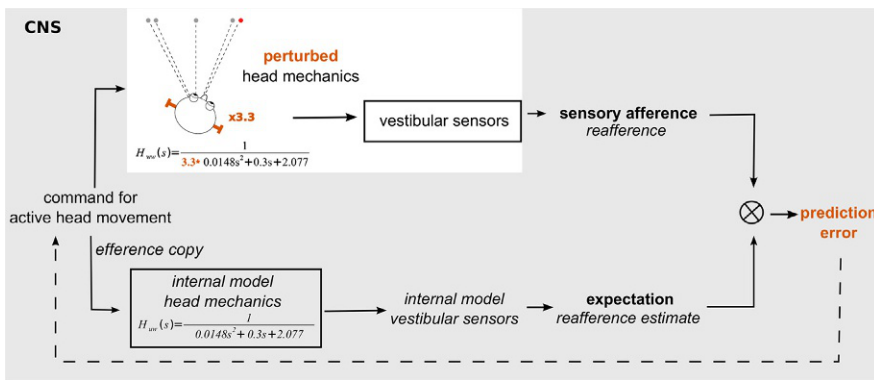
Keywords

Functional dizziness, Bodily distress, Somatic symptom disorder, Perceptual dysregulation, Predictive coding, Somatoform

1 Introduction

Patients with persistent physical symptoms that are unexplained by conventional clinical evaluations and tests present an enduring challenge to their caregivers. Their bodily complaints, like chest pain, bowel irritation, fatigue or dizziness can emerge from different body regions (Henningsen et al., 2018b), are very common in medicine (Carson et al., 2000; Fink et al., 2004, 2005; Haller et al., 2015; Reid et al., 2001), greatly impair functioning and quality of life (Carson et al., 2011), and present a huge social and economic burden (Hiller et al., 2003; Konnopka et al., 2012; Wortman et al., 2018). However, despite the extensive and repetitive work-ups characteristic for this patient group (Den Boeft et al., 2016; Fink et al., 1999; Hansen et al., 2002), symptoms are insufficiently explained by organic dysfunction. A recent concept, which is based on the predictive coding model of brain function (Friston, 2005; Mumford, 1992; Rao and Ballard, 1999; Srinivasan et al., 1982), understands persistent physical symptoms as a result of erroneous sensory processing in the central nervous system, with expectations (prior beliefs) dominating perceptual inference (Edwards et al., 2012; Henningsen et al., 2018a; Van den Bergh et al., 2017). This hypothesis is neurobiologically consistent, but so far, has not been experimentally tested. Here, to test this hypothesis, we apply a framework based on mathematical modeling and analysis of the head motor system (Fig. 1, experimental litmus test first described in Lehnen et al., 2018a).

Head movements as part of large eye-head gaze shifts to visual targets are a well characterized example to study the interaction between expectation and sensory input (Goldberg and Cullen, 2011; Guitton, 1992). Discrepancies between expectations and sensory input, i.e., prediction errors, are used to update motor commands, and alter actions, so that the resulting input conforms to the predictions (Wolpert et al., 1998). This can be experimentally tested by mechanically altering head characteristics (cats: Guitton et al., 1984; monkeys: Tomlinson, 1990; Tomlinson and Bahra, 1986; healthy humans: Guitton and Volle, 1987; Laurutis and Robinson, 1986). Increasing the head moment of inertia in healthy humans, for example, leads

**FIG. 1**

Simplified scheme of head motor control underlying the experimental approach. In this experiment, subjects performed horizontal large combined active eye-head gaze shifts towards visual targets. After a set of gaze shifts in the natural condition, head mechanics were perturbed by a helmet with eccentrically attached masses 3.3-fold increasing the head moment of inertia (weighted condition, drawing, H_{ww} —head with weight—transfer function of the modified head plant indicated in Laplace notation (Peng et al., 1996; Tangorra et al., 2003)). The sensory input resulting from the head movement during the gaze shift (reafference) is measured by vestibular sensors. In the weighted condition, the reafference does not match the expected sensory outcome of the movement (reafference estimate) formed in the central nervous system (CNS, gray background). This is because the reafference estimate is based on a CNS-internal model of the head mechanics (H_{uw} —head unweighted—transfer function of the head plant in the natural situation) formed before the head moment of inertia was increased. The difference between expectation and sensory afference, i.e., the prediction error, can be exploited to update CNS-internal models, motor commands, and actions, so that the resulting input conforms to the predictions.

to unwanted head oscillations, which, using the prediction error to adapt the internal models to the altered head mechanics, can be reduced over trials (Lehnen, 2006; Lehnen et al., 2008; Sağlam et al., 2011). Both intact sensory afference and the ability to adapt internal models are essential to reduce unwanted head oscillations when the head moment of inertia is increased: patients with chronic complete bilateral vestibular loss (missing vestibular afference) do not reduce head oscillations, and cerebellar ataxia patients (who have deficits in forming internal models) only reduce oscillations to some extent (Lehnen et al., 2009a,b; Sağlam et al., 2014; Sağlam and Lehnen, 2014).

Here, we apply this well characterized set-up to patients who suffer from functional dizziness, a very common persistent physical symptom (Brandt et al., 2015; Dieterich and Eckhardt-Henn, 2004; Eckhardt-Henn et al., 2009; Feuerecker et al., 2015). Following the hypothesis that persistent physical symptoms are based on erroneous sensory processing in CNS, with expectations dominating perception, these patients would feel dizzy because they put too much trust into pathological

prior beliefs used to interpret sensory input. Translated into head motor control, we expect these patients to be more reliant on their existing internal models and therefore more resistant to sensory driven updating (prediction error). This would be reflected in deficient head motor control, which should resemble that of patients with organic disease affecting the interplay between sensory input and expectations like vestibular loss, or cerebellar ataxia.

2 Materials and methods

2.1 Subjects

In a prospective pilot study, 8 patients with functional dizziness (aged 35 ± 13 years, mean \pm standard deviation (SD), 5 females) who presented with permanent symptoms to a tertiary vertigo/dizziness center, and 11 age- and gender-matched healthy volunteers (32 ± 6 years, mean \pm SD, 6 females) participated in the study.

A comprehensive neurological history and exam (including neuro-otological and neuro-ophthalmological assessments), neuro-otological and neuro-ophthalmological work-ups (including caloric irrigation, video head impulse testing and subjective visual vertical), as well as MRI scans of the brain did not reveal any organic dysfunction that could sufficiently explain the patients' symptoms. Healthy subjects had no history of balance disorders and a normal neurological exam.

The experimental procedure was approved by the Ethics Committee of the Medical Faculty of the Ludwig-Maximilians-University and was in accordance with the Declaration of Helsinki. All subjects gave their informed consent prior to participation and were free to withdraw from the experiment at any time.

2.2 Experimental procedure

2.2.1 Video head impulse test and head impulse testing device function test

In addition to the clinical work-up, vestibular function during passive head movements was assessed with the video head impulse test (vHIT, in analogy to Bartl et al., 2009). Also, dynamic vision during passive head motion was measured with the Head Impulse Testing Device—Functional Test (HITD-FT, also called functional head impulse test (Ramat et al., 2012; Versino et al., 2014), procedure described in Ramaioli et al. (2014).

2.2.2 Altering head mechanics during eye-head gaze shifts to visual targets

The experimental set-up was designed in analogy to Lehnen (2006). Subjects performed 52 horizontal gaze shifts (combination of eye and head movements) in complete darkness to visual targets flashed in a frontal plane before them and situated 35 and 40 degrees to the left and right. Subjects were asked to keep gaze position

until the next visual target was flashed. In order to prevent visual feedback, targets were flashed for <100 ms. The interval between two subsequent visual targets (1–1.8 s) and subsequent target eccentricity (35, 40, 70, 75 or 80 degrees) were randomly assigned to prevent anticipation. The experiment was repeated twice: once in the natural, unweighted, condition, and then with the head moment of inertia 3.3-times increased by means of a helmet with eccentrically placed masses (weighted condition, Lehnén, 2006; drawing in Fig. 1). All subjects and patients were naïve with respect to this experiment. During the experiment, eye movements were recorded by video-oculography of the left eye and head movements by inertial sensors (EyeSeeCam system with a sampling rate of 220 Hz, in analogy to Bartl et al., 2009).

2.3 Data analysis

Data were analyzed offline using MATLAB® (MathWorks, Natick, MA) and IBM SPSS Statistics.

2.3.1 Video head impulse test and head impulse testing device function test

In analogy to Lehnén et al. (2018b), the vHIT gain was computed as the ratio of median eye and head velocity in a 10 ms window between 55 and 65 ms after head impulse start (head velocity exceeding 20 degree/s), and the HITD-FT score was calculated as the rate of correct answers in all trials.

2.3.2 Altering head mechanics during eye-head gaze shifts to visual targets

Active head movements as part of the gaze shifts were analyzed in the natural and in the weighted condition. Head velocity was derived from the inertial sensors and low-pass filtered with a Gaussian filter with a cut-off frequency of 20 Hz. For each trial, i.e., a single gaze shift towards the visual target, head movements were considered in a time window of 1.6 s starting 45 ms before visual target onset. Only movements corresponding to gaze shifts of 75 and 80 degrees were considered in the analysis. Head start was defined as head velocity reaching 6 degree/s, the head movement ended when head velocity crossed 6 degree/s again. In analogy to Sağlam et al. (2014), the head oscillation ratio was assessed as the absolute ratio of the first negative and positive peaks of head velocity (in percent, see inset in Fig. 2). Detection errors could be corrected manually. If head oscillations fell outside 2 SD from the mean of all trials of one subject or patient in one condition (unweighted/weighted), the trial was removed from the analysis. After removing outliers, 31 ± 4 (mean \pm SD) and 25 ± 7 trials were considered for each subject in the unweighted condition and 26 ± 8 and 22 ± 8 trials in the weighted condition for healthy subjects and for patients with functional dizziness, respectively.

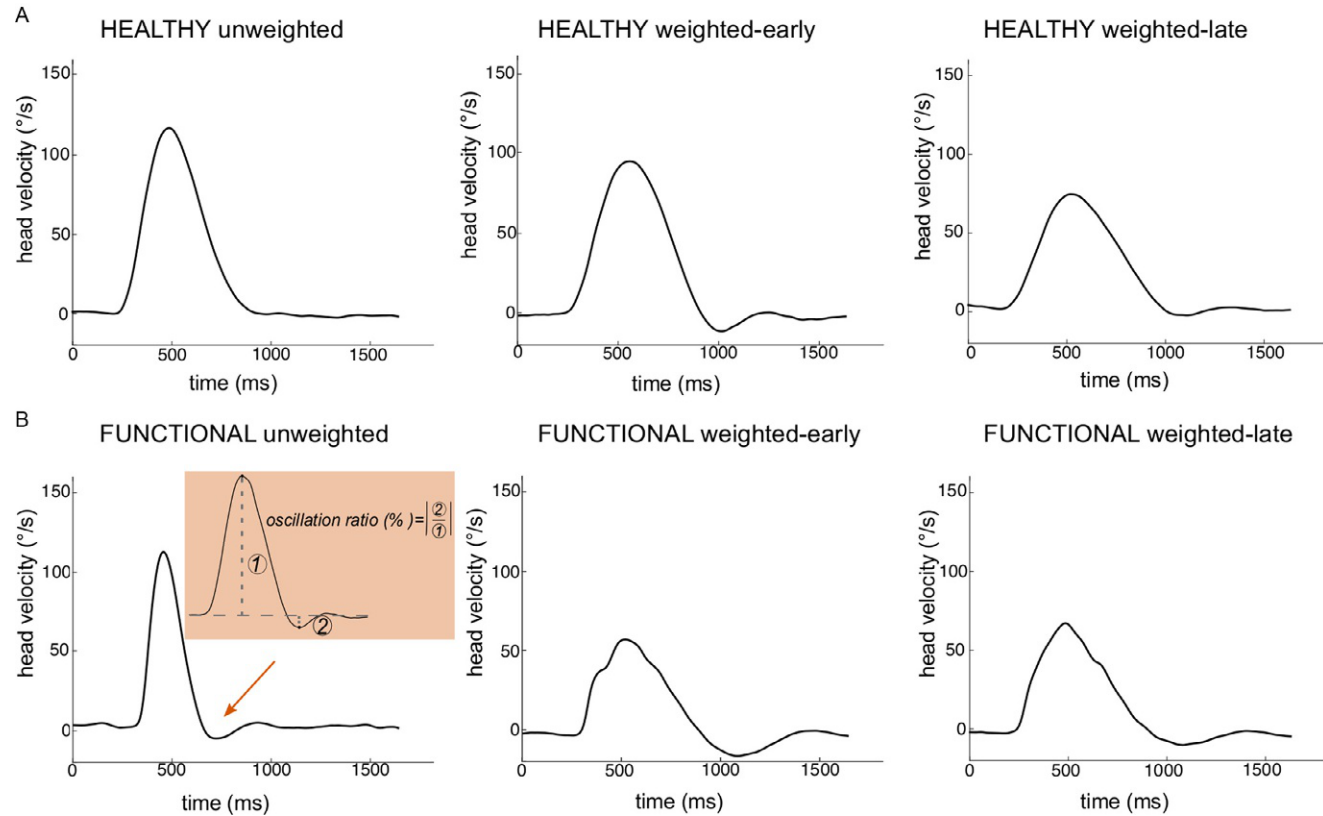


FIG. 2

See legend on opposite page.

2.3.3 Comparison to previously acquired data from patients with chronic vestibular loss and cerebellar ataxia

For comparison, data reported in [Sağlam et al. \(2014\)](#) were reanalyzed in the same way as the data from the functional dizziness patients and healthy subjects of the present study. In [Sağlam et al. \(2014\)](#), 10 healthy subjects (aged 40 ± 6 years, mean \pm SD, 1 female), 9 patients with cerebellar ataxia (aged 57 ± 13 years, 6 females) and 5 patients with chronic vestibular loss (aged 45 ± 7 years, 3 females) participated. In the reanalysis of this data, after outlier analysis, 35 ± 3 (mean \pm SD) and 33 ± 5 trials were considered for healthy subjects, 34 ± 2 and 34 ± 2 trials for patients with cerebellar ataxia and 31 ± 3 and 33 ± 6 trials for patients with chronic vestibular loss, for the unweighted and weighted condition, respectively. A repeated measures analysis of variance (rmANOVA, significance level $P < 0.05$) on head oscillation ratio revealed no difference between the healthy subjects from [Sağlam et al. \(2014\)](#) and the healthy control group investigated for the current pilot study ($F(1,19) = 1.1$, $P = 0.33$), validating following comparisons between the patient groups from [Sağlam et al. \(2014\)](#) and the functional dizziness patients.

2.4 Statistical analysis

Normality was assessed by Kolmogorov-Smirnov testing ($P < 0.05$). Head impulse gains during vHIT and HITD-FT scores for movements to the left and to the right were pooled as there was no side difference (dependent samples *t*-test, $P > 0.05$). A one-way multivariate analysis of variance (MANOVA, $P < 0.05$) was conducted to compare differences in head impulse gains and HITD-FT scores between groups (healthy subjects and patients with functional dizziness).

Differences in head oscillation ratios within three conditions (*unweighted* and *weighted*—split up into *weighted-early* (first 10) and *weighted-late* (last 33) trials) and between the groups (healthy subjects, patients with functional dizziness) were

FIG. 2

Head velocity traces from a healthy subject and a patient with functional dizziness. Representative head velocity traces during an active gaze shift following a 75 degrees target step from a healthy subject (A) and from a patient with functional dizziness (B) in the natural condition (unweighted, left), for the first 10 trials with increased head moment of inertia (weighted-early, middle) and for the last 33 trials with weight (weighted-late, right). The healthy subject performed a smooth head movement without oscillation in the unweighted condition. In contrast, the patient showed head oscillations (note how head velocity undershoots the zero-line, arrow). Inset: to quantify head oscillations, the oscillation ratio was computed as the absolute ratio of the first negative (2) and positive (1) peaks of head velocity. Increasing the head moment of inertia led to head oscillations, more accentuated in the patient. Over the course of the experiment with increased head moment of inertia, both the patient with functional dizziness as well as the healthy participant could reduce head oscillations.

assessed by rmANOVA ($P < 0.05$, Greenhouse-Geisser correction for violation of sphericity). After a significant interaction, a post-hoc independent t -test was calculated to determine differences between groups in the unweighted condition as well as a rmANOVA with subsequent post-hoc Bonferroni tests to compare within factors (*unweighted/weighted-early/weighted-late*) in functional dizziness patients.

Differences between the patient groups (functional dizziness patients and patients with cerebellar ataxia and chronic vestibular loss from [Sağlam et al. \(2014\)](#)) for all three conditions (within factor: *unweighted/weighted-early/weighted-late*) were analyzed with a rmANOVA.

3 Results

3.1 Video head impulse test and head impulse testing device function test

Patients with functional dizziness had intact vestibular function, assessed during passive head movements. Their head impulse gain ($F(1,17) = 0.13$, $P = 0.73$) and HITD-FT responses ($F(1,17) = 1.3$, $P = 0.27$) were not different from those of healthy subjects. Head impulse gains and HITD-FT scores were 1.00 ± 0.06 (mean \pm SD) and $97 \pm 5\%$ for healthy subjects and 0.99 ± 0.1 and $99 \pm 2\%$ for patients with functional dizziness, respectively.

3.2 Altering head mechanics during eye-head gaze shifts to visual targets

[Fig. 2](#) shows representative head velocity profiles from a healthy subject (top panels) and from a patient with functional dizziness (bottom). In the natural, unweighted, condition, the healthy subject performed smooth active head movements without oscillations. In contrast, in the patient with functional dizziness, there was marked head oscillation (note how head velocity undershoots the zero line). Increasing the head moment of inertia (weighted-early condition) led to head oscillations in the healthy subject, and increased head oscillations in the patient with functional dizziness. Head oscillations decreased in both the healthy subject and the functional dizziness patient after several trials with weight (weighted-late condition). This response was true for all subjects and patients. Mean head oscillation ratios (reported as mean \pm standard error of the mean (SEM) in percent) for healthy subjects were 2.33 ± 0.1 for the unweighted and 8.51 ± 0.97 and 6.27 ± 0.33 for the weighted-early and -late condition, respectively. Patients with functional dizziness had head oscillation ratios of 6.02 ± 0.46 (unweighted), 13.17 ± 1.72 (weighted-early) and 11.41 ± 0.58 (weighted-late).

RmANOVA (within-factor *unweighted/weighted-early/weighted-late*) revealed significant differences in head oscillations between patients with functional dizziness and healthy subjects ($F(1,17) = 27.26$, $P < 0.001$, partial $\eta^2 = 0.62$) for the different conditions ($F(1.45,12.36) = 97.42$, corrected $P < 0.001$, partial $\eta^2 = 0.85$)

with a significant interaction ($F(1.45,24.72)=4.28$, corrected $P=0.036$, partial $\eta^2=0.2$). Functional dizziness patients had higher head oscillations than healthy subjects already in the unweighted condition (post-hoc t -test, $P<0.001$). Increasing the head moment of inertia increased head oscillations in the functional patients (rmANOVA, $F(1.18,4.12)=44.42$, corrected $P<0.001$, partial $\eta^2=0.86$, post-hoc Bonferroni $P=0.001$). Head oscillations decreased in these patients in the course of the gaze shifts with weight (see Fig. 3 for a time course of head oscillations with weight, post-hoc Bonferroni $P=0.001$).

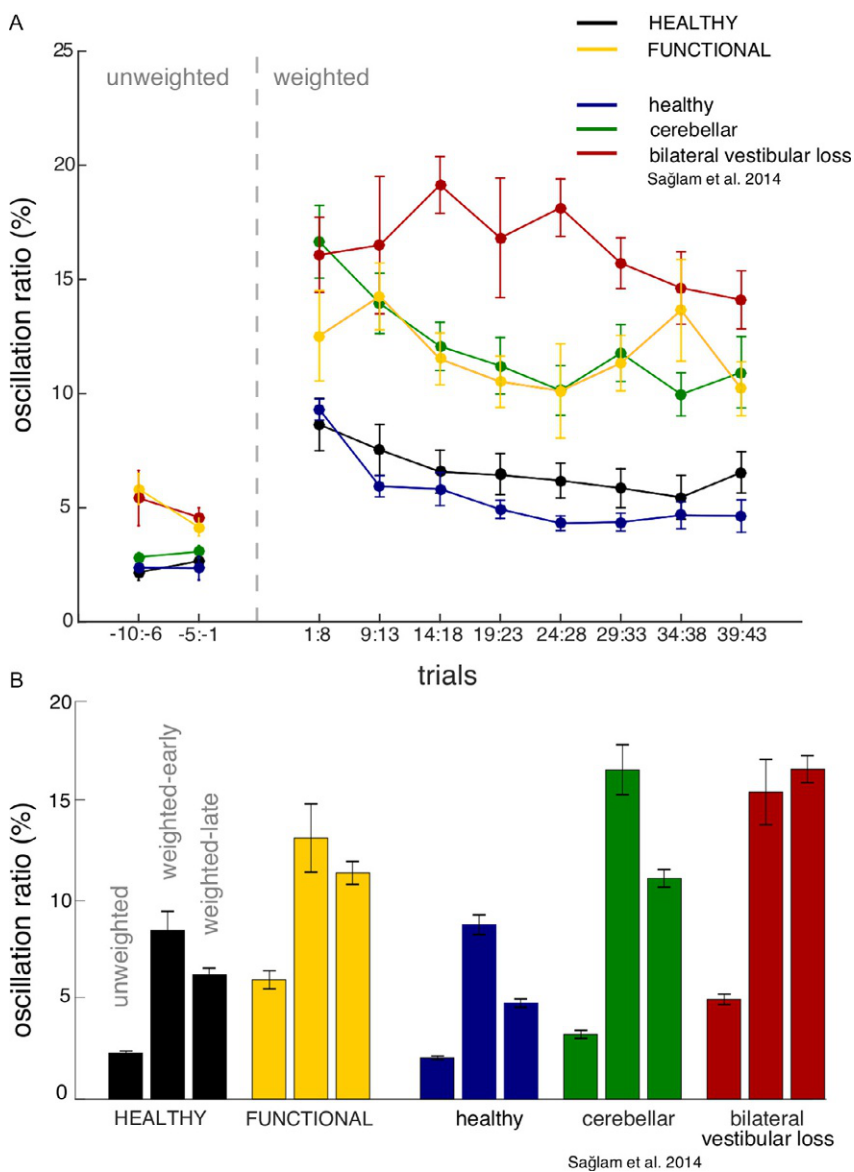
3.3 Comparison to previously acquired data from patients with chronic vestibular loss and cerebellar ataxia

Whilst different from the healthy subjects, the behavior of the functional dizziness patients was not different from that of the patients with cerebellar ataxia, and of the patients with chronic vestibular loss (reanalyzed from [Sağlam et al. \(2014\)](#); rmANOVA between factor: $F(2,19)=0.56$, $P=0.58$, no interaction $F(1.45,27.55)=1.03$, $P=0.39$). Head oscillation ratios were $2.09\pm0.09/8.8\pm0.5/4.84\pm0.21$ for the healthy subjects from the [Sağlam et al. \(2014\)](#) study, $3.27\pm0.20/16.61\pm1.26/11.13\pm0.45$ for the patients with cerebellar ataxia and $5.03\pm0.26/15.48\pm1.64/16.64\pm0.68$ for the patients with chronic vestibular loss (unweighted/weighted-early/weighted-late).

4 Discussion

This pilot study reveals a striking deficit in head motor control in patients with functional dizziness, which bears similarities to that of patients with cerebellar ataxia and to that of patients with severe peripheral vestibular disease (chronic bilateral vestibular de-afferentation). Knowing that an extensive work-up failed to demonstrate any explanatory peripheral vestibular, pyramidal or extrapyramidal motor or cerebellar organic dysfunction, and following the logic of expectation- and sensory-input-dependent motor control (Fig. 1), these motor control deficits are a first indication of erroneous sensory-motor processing in the central nervous system.

Already in the natural, unweighted condition, patients with functional dizziness display increased head oscillations, strikingly similar to patients without any vestibular input (bilateral vestibular loss). As the problem does not lie in peripheral sensory-motor functions, this indicates that patients have difficulties optimizing head motor commands, e.g., to match the commands to the actual mechanical head characteristics, which change over time (through weight gain or alterations in muscle stiffness). Increasing the head moment of inertia and experimentally inducing an incongruence between expected sensory consequences of the head movement and the actual vestibular input further unravels these difficulties. This leads to pronounced head oscillations in the patients with functional dizziness, similar to patients with chronic vestibular loss or cerebellar ataxia, reflecting a problem in the CNS pathway using sensory input to calculate prediction errors and update internal models

**FIG. 3**

Group results for head oscillations. (A) Time course of head oscillations over gaze shifts (each dot represents the average of the oscillation ratios over the trials (gaze shifts) indicated on the x-axis). Head oscillation ratios (means and SEM) for patients with functional dizziness (FUNCTIONAL, yellow) were different from healthy subjects (HEALTHY, black). They were not different from cerebellar ataxia (green) and chronic bilateral vestibular loss (red) patients (Continued)

and motor commands (Fig. 1). From our results, we cannot conclude where in this pathway the problem arises. The similarities to patients with chronic vestibular loss and to patients with cerebellar ataxia point towards a pathology related to the interaction between expectation due to motor planning and sensory input. Patients with chronic vestibular loss cannot access essential sensory vestibular input (Sağlam et al., 2014), whereas cerebellar ataxia patients have difficulties forming internal models (Bastian, 2006; Wolpert et al., 1998) to predict the sensory consequences of action (Izawa et al., 2012; Synofzik et al., 2008; Tseng et al., 2007) and are even discussed to have difficulties more generally in prediction, also regarding purely sensory domains (Baumann et al., 2015; Roth et al., 2013; Therrien and Bastian, 2015). The fact that, in the weighted condition, patients with functional dizziness can decrease unwanted head oscillations to some extent is similar to cerebellar ataxia patients, and differentiates them from patients with chronic vestibular loss, who fail to optimize head motor commands and cannot decrease head oscillations (Sağlam et al., 2014).

Although its exact mechanism remains to be determined, the central sensory-motor dysfunction we find in functional dizziness patients is compatible with the recent hypothesis that persistent physical symptoms are based on perceptual dysregulation (Edwards et al., 2012; Henningsen et al., 2018a; Van den Bergh et al., 2017). In this framework, symptoms in patients with functional dizziness are thought to arise because patients are overly reliant on priorly formed but inaccurate expectations that explain the sensory input as dysfunctional. In analogy, head oscillations in this study's natural, unweighted and weighted conditions would arise because functional dizziness patients stuck to priorly formed internal models and insufficiently incorporated natural or experimental changes to the mechanical head characteristics. It is important, however, to note that patients with functional dizziness reduce head oscillations in the weighted condition and thus seem to be able to update motor commands based on sensory input. On the other hand, they display marked oscillations in the natural condition, where, if they were similarly able to update motor commands, they would have had the opportunity to do so over the thousands of eye-head gaze shifts they had performed in natural life. Thus, the ability to use sensory input might be context-dependent. In a Bayesian decision making or causal

(the healthy subjects from this prior study are denoted in blue). In the unweighted condition (last 10 trials are displayed, labeled with negative numbers on the x-axis), functional dizziness patients displayed increased head oscillations, similar to patients with chronic bilateral vestibular loss. Healthy subjects, functional dizziness patients, and cerebellar ataxia patients (to some extent) could reduce head oscillations in the course of several gaze shift with weight. (B) Mean and SEM of head oscillation ratios for all trials in the unweighted (left bar) and weighted condition, split up into weighted-early (first ten trials, middle bar) and weighted-late (last 33 trials, right bar) summarizing the effects for group and condition.

Data reanalyzed from Saglam, M., Glasauer, S., Lehnen, N., 2014. Vestibular and cerebellar contribution to gaze optimality. Brain 137, 1080–1094. <https://doi.org/10.1093/brain/awu006>.

inference sense, an interpretation of these results might also be that patients—though able to use sensory information to update internal models and motor commands and reduce head oscillations—have a higher tolerance for error, i.e., the threshold for activating adaptation is higher. In our experiment, when the head moment of inertia is increased, the resulting prediction error seems to be deemed relevant enough to be used for updating to some extent, the one in the natural condition not.

Changes in neuro-physiologically measurable head movement parameters like head oscillation ratio might bridge the gap between the symptoms patients suffer from and the absence of any measurable organic dysfunction. The measurable instability in the natural situation nicely reflects patient reports of feeling—not unlike patients with vestibular loss, or with cerebellar ataxia—instable and “wobbly,” in particular when walking, and lends neuro-physiological legitimization to the patients’ reports. Experimental similarities to patients with severe organic disease, such as cerebellar ataxia and vestibular loss, reflect similarities in symptom severity reporting (where functional dizziness patients sometimes exceed patients with organic vestibular deficits, (Best et al., 2006)), disability, as well as in participation and quality of life impairments (Eckhardt-Henn et al., 2003; Lahmann et al., 2015; Tschan et al., 2010).

With the limitations inherent to a pilot approach, this study thus provides a first glimpse into the mechanism underlying functional dizziness as an important example of persistent physical symptom. Its results support the notion that dysfunctions in the CNS interaction between sensory input and expectations about the sensory consequences of one’s own actions play a role in the emergence and manifestation of these symptoms. This first answer to the “how question” of the underlying mechanism does, of course, not include an answer to the etiology question, i.e., why these inference failures manifest. Similarly, it remains to be seen how specific the changes in head motor control are to persistent physical symptoms, as supposed to anxiety or mood disorders, for example. Nevertheless, the measurable alterations in head motor control have the potential for improving positive diagnosis, patient education, and further treatment in this patient group where diagnosis is difficult and often contested, and prognosis is rather poor (van Leeuwen and van der Zaag-Loonen, 2012).

Conflict of interest

N.L. is a shareholder and was a paid consultant to EyeSeeTec GmbH. S.G. is a shareholder of EyeSeeTec GmbH. C.R. was an employee of EyeSeeTec GmbH. L.S. and P.H. declare that the research was conducted in the absence of any commercial or financial relationships that could be construed as a potential conflict of interest.

Author contribution

N.L. did study conception; C.R. collected the data; N.L., L.S., S.G., and C.R. analyzed and interpreted the data; N.L., L.S., and C.R. drafted the initial manuscript; N.L., L.S., P.H., S.G., and C.R. revised the manuscript. All authors have read and approved the final manuscript.

Funding

This study was supported by the German Research Foundation (DFG Research Training Group 2175 “Perception in Context and its Neural Basis” and DFG MA 6233/1-1) and the German Federal Ministry of Education and Research (Grant 01 EO 0914).

Data availability statement

The datasets generated for this study are available on request to the corresponding author.

References

- Bartl, K., Lehnen, N., Kohlbecher, S., Schneider, E., 2009. Head impulse testing using video-oculography. *Ann. N. Y. Acad. Sci.* 1164, 331–333. <https://doi.org/10.1111/j.1749-6632.2009.03850.x>.
- Bastian, A.J., 2006. Learning to predict the future: the cerebellum adapts feedforward movement control. *Curr. Opin. Neurobiol.* 16, 645–649. <https://doi.org/10.1016/j.conb.2006.08.016>.
- Baumann, O., Borra, R.J., Bower, J.M., Cullen, K.E., Habas, C., Ivry, R.B., Leggio, M., Mattingley, J.B., Molinari, M., Moulton, E.A., Paulin, M.G., Pavlova, M.A., Schmahmann, J.D., Sokolov, A.A., 2015. Consensus paper: the role of the cerebellum in perceptual processes. *Cerebellum* 14, 197–220. <https://doi.org/10.1007/s12311-014-0627-7>.
- Best, C., Eckhardt-Herrn, A., Diener, G., Bense, S., Breuer, P., Dieterich, M., 2006. Interaction of somatoform and vestibular disorders. *J. Neurol. Neurosurg. Psychiatry* 77, 658–664. <https://doi.org/10.1136/jnnp.2005.072934>.
- Brandt, T., Huppert, D., Strupp, M., Dieterich, M., 2015. Functional dizziness: diagnostic keys and differential diagnosis. *J. Neurol.* 262, 1977–1980. <https://doi.org/10.1007/s00415-015-7826-0>.
- Carson, A.J., Ringbauer, B., Stone, J., McKenzie, L., Warlow, C., Sharpe, M., 2000. Do medically unexplained symptoms matter? A prospective cohort study of 300 new referrals to neurology outpatient clinics. *J. Neurol. Neurosurg. Psychiatry* 68, 207–210. <https://doi.org/10.1136/jnnp.68.2.207>.
- Carson, A., Stone, J., Hibberd, C., Murray, G., Duncan, R., Coleman, R., Warlow, C., Roberts, R., Pelosi, A., Cavanagh, J., Matthews, K., Goldbeck, R., Hansen, C., Sharpe, M., 2011. Disability, distress and unemployment in neurology outpatients with symptoms “unexplained by organic disease”. *J. Neurol. Neurosurg. Psychiatry* 82, 810–813. <https://doi.org/10.1136/jnnp.2010.220640>.
- Den Boeft, M., Twisk, J.W.R., Terluin, B., Penninx, B.W.J.H., Van Marwijk, H.W.J., Numans, M.E., Van Der Wouden, J.C., Van Der Horst, H.E., 2016. The association between medically unexplained physical symptoms and health care use over two years and the influence of depressive and anxiety disorders and personality traits: a longitudinal study. *BMC Health Serv. Res.* 16, 1–9. <https://doi.org/10.1186/s12913-016-1332-7>.
- Dieterich, M., Eckhardt-Henn, A., 2004. Neurologische und somatoforme Schwindelsyn-
drome. *Nervenarzt* 75, 281–302. <https://doi.org/10.1007/s00115-003-1678-z>.

- Eckhardt-Henn, A., Breuer, P., Thomalske, C., Hoffmann, S.O., Hopf, H.C., 2003. Anxiety disorders and other psychiatric subgroups in patients complaining of dizziness. *J. Anxiety Disord.* 17, 369–388. [https://doi.org/10.1016/S0887-6185\(02\)00226-8](https://doi.org/10.1016/S0887-6185(02)00226-8).
- Eckhardt-Henn, A., Tschan, R., Best, C., Dieterich, M., 2009. Somatoforme Schwindelsyn-drome. *Nervenarzt* 80, 909–917. <https://doi.org/10.1007/s00115-009-2736-y>.
- Edwards, M.J., Adams, R.A., Brown, H., Pareés, I., Friston, K.J., 2012. A Bayesian account of “hysteria” *Brain* 135, 3495–3512. <https://doi.org/10.1093/brain/aws129>.
- Feuerecker, R., Dieterich, M., Eckhardt-Henn, A., Becker-Bense, S., 2015. Nicht-organischer Schwindel. *Fortschr. Neurol. Psychiatr.* 83, 135–141. <https://doi.org/10.1055/s-0034-1385272>.
- Fink, P., Hansen, M.S., Oxhøj, M.L., 2004. The prevalence of somatoform disorders among internal medical inpatients. *J. Psychosom. Res.* 56, 413–418. [https://doi.org/10.1016/S0022-3999\(03\)00624-X](https://doi.org/10.1016/S0022-3999(03)00624-X).
- Fink, P., Hansen, M.S., Søndergaard, L., 2005. Somatoform disorders among first-time referrals to a neurology service. *Psychosomatics* 46, 540–548. <https://doi.org/10.1176/appi.psy.46.6.540>.
- Fink, P., Sørensen, L., Engberg, M., Holm, M., Munk-Jørgensen, P., 1999. Somatization in primary care: prevalence, health care utilization, and general practitioner recognition. *Psychosomatics* 40, 330–338. [https://doi.org/10.1016/S0033-3182\(99\)71228-4](https://doi.org/10.1016/S0033-3182(99)71228-4).
- Friston, K., 2005. A theory of cortical responses. *Philos. Trans. R. Soc. Lond. B Biol. Sci.* 360, 815–836. <https://doi.org/10.1098/rstb.2005.1622>.
- Goldberg, J.M., Cullen, K.E., 2011. Vestibular control of the head: possible functions of the vestibulocollic reflex. *Exp. Brain Res.* 210, 331–345. <https://doi.org/10.1007/s00221-011-2611-5>.
- Guitton, D., 1992. Control of eye-head coordination during orienting gaze shifts. *Trends Neurosci.* 15, 174–179. [https://doi.org/10.1016/0166-2236\(92\)90169-9](https://doi.org/10.1016/0166-2236(92)90169-9).
- Guitton, D., Douglas, M., Volle, M., 1984. Eye-head coordination in cats. *J. Neurophysiol.* 52, 1030–1050. <https://doi.org/10.1152/jn.1984.52.6.1030>.
- Guitton, D., Volle, M., 1987. Gaze control in humans: eye-head coordination during orienting movements to targets within and beyond the oculomotor range. *J. Neurophysiol.* 58, 427–459. <https://doi.org/10.1152/jn.1987.58.3.427>.
- Haller, H., Cramer, H., Lauche, R., Dobos, G., 2015. Somatoform disorders and medically unexplained symptoms in primary care. *Dtsch. Arztebl. Int.* 112, 279–287. <https://doi.org/10.3238/arztebl.2015.0279>.
- Hansen, M.S., Fink, P., Frydenberg, M., Oxhøj, M.L., 2002. Use of health services, mental illness, and self-rated disability and health in medical inpatients. *Psychosom. Med.* 64, 668–675. <https://doi.org/10.1097/01.PSY.0000024104.87632.94>.
- Henningsen, P., Gündel, H., Kop, W.J., Löwe, B., Martin, A., Rief, W., Rosmalen, J.G.M., Schröder, A., van der Feltz-Cornelis, C., Van den Bergh, O., 2018a. Persistent physical symptoms as perceptual dysregulation. *Psychosom. Med.* 80, 422–431. <https://doi.org/10.1097/PSY.0000000000000588>.
- Henningsen, P., Zipfel, S., Sattel, H., Creed, F., 2018b. Management of functional somatic syndromes and bodily distress. *Psychother. Psychosom.* 87, 12–31. <https://doi.org/10.1159/000484413>.
- Hiller, W., Fichter, M.M., Rief, W., 2003. A controlled treatment study of somatoform disorders including analysis of healthcare utilization and cost-effectiveness. *J. Psychosom. Res.* 54, 369–380. [https://doi.org/10.1016/S0022-3999\(02\)00397-5](https://doi.org/10.1016/S0022-3999(02)00397-5).
- Izawa, J., Criscimagna-Hemminger, S.E., Shadmehr, R., 2012. Cerebellar contributions to reach adaptation and learning sensory consequences of action. *J. Neurosci.* 32, 4230–4239. <https://doi.org/10.1523/JNEUROSCI.6353-11.2012>.

- Konnopka, A., Schaefer, R., Heinrich, S., Kaufmann, C., Lupp, M., Herzog, W., König, H.H., 2012. Economics of medically unexplained symptoms: a systematic review of the literature. *Psychother. Psychosom.* 81, 265–275. <https://doi.org/10.1159/000337349>.
- Lahmann, C., Henningsen, P., Brandt, T., Strupp, M., Jahn, K., Dieterich, M., Eckhardt-Henn, A., Feuerer, R., Dinkel, A., Schmid, G., 2015. Psychiatric comorbidity and psychosocial impairment among patients with vertigo and dizziness. *J. Neurol. Neurosurg. Psychiatry* 86, 302–308. <https://doi.org/10.1136/jnnp-2014-307601>.
- Lauritis, V.P., Robinson, D.A., 1986. The vestibulo-ocular reflex during human saccadic eye movements. *J. Physiol.* 373, 209–233. <https://doi.org/10.1113/jphysiol.1986.sp016043>.
- van Leeuwen, R.B., van der Zaag-Loonen, H.J., 2012. Unexplained dizziness does not resolve in time. *Acta Neurol. Belg.* 112, 357–360. <https://doi.org/10.1007/s13760-012-0082-5>.
- Lehnen, N., 2006. *The Effect of Increased Head Inertia on Eye-Head Control in Human Gaze Shifts: Analysis and Mathematical Modeling of a Motor System*. Doctoral dissertation, Ludwig-Maximilians Universität München.
- Lehnen, N., Büttner, U., Glasauer, S., 2008. Head movement control during head-free gaze shifts. *Prog. Brain Res.* 171, 331–334. [https://doi.org/10.1016/S0079-6123\(08\)00648-1](https://doi.org/10.1016/S0079-6123(08)00648-1).
- Lehnen, N., Büttner, U., Glasauer, S., 2009a. Head-free gaze control in humans with chronic loss of vestibular function. *Ann. N. Y. Acad. Sci.* 1164, 409–412. <https://doi.org/10.1111/j.1749-6632.2009.03774.x>.
- Lehnen, N., Büttner, U., Glasauer, S., 2009b. Vestibular guidance of active head movements. *Exp. Brain Res.* 194, 495–503. <https://doi.org/10.1007/s00221-009-1708-6>.
- Lehnen, N., Henningsen, P., Ramaioli, C., Glasauer, S., 2018a. An experimental litmus test of the emerging hypothesis that persistent physical symptoms can be explained as perceptual dysregulation. *J. Psychosom. Res.* 114, 15–17. <https://doi.org/10.1016/j.jpsychores.2018.08.007>.
- Lehnen, N., Kellerer, S., Knorr, A.G., Schlick, C., Jahn, K., Schneider, E., Heuberger, M., Ramaioli, C., 2018b. Head-movement-emphasized rehabilitation in bilateral vestibulopathy. *Front. Neurol.* 9, 562. <https://doi.org/10.3389/fneur.2018.00562>.
- Mumford, D., 1992. On the computational architecture of the neocortex—II the role of cortico-cortical loops. *Biol. Cybern.* 66, 241–251. <https://doi.org/10.1007/BF00198477>.
- Peng, G.C.Y., Hain, T.C., Peterson, B.W., 1996. A dynamical model for reflex activated head movements in the horizontal plane. *Biol. Cybern.* 75, 309–319. <https://doi.org/10.1007/s004220050297>.
- Ramaioli, C., Colagiorgio, P., Sağlam, M., Heuser, F., Schneider, E., Ramat, S., Lehnen, N., 2014. The effect of vestibulo-ocular reflex deficits and covert saccades on dynamic vision in opioid-induced vestibular dysfunction. *PLoS One* 9, e110322. <https://doi.org/10.1371/journal.pone.0110322>.
- Ramat, S., Colnaghi, S., Boehler, A., Astore, S., Falco, P., Mandalà, M., Nuti, D., Colagiorgio, P., Versino, M., 2012. A device for the functional evaluation of the VOR in clinical settings. *Front. Neurol.* 3, 39. <https://doi.org/10.3389/fneur.2012.00039>.
- Rao, R.P.N., Ballard, D.H., 1999. Predictive coding in the visual cortex: a functional interpretation of some extra-classical receptive-field effects. *Nat. Neurosci.* 2, 79–87. <https://doi.org/10.1038/4580>.
- Reid, S., Wessely, S., Crayford, T., Hotopf, M., 2001. Medically unexplained symptoms in frequent attenders of secondary health care: retrospective cohort study. *BMJ [Br. Med. J.]* 322, 656–659. <https://doi.org/10.1136/bmj.322.7289.767>.
- Roth, M.J., Synofzik, M., Lindner, A., 2013. The cerebellum optimizes perceptual predictions about external sensory events. *Curr. Biol.* 23, 930–935. <https://doi.org/10.1016/j.cub.2013.04.027>.

- Sağlam, M., Glasauer, S., Lehnen, N., 2014. Vestibular and cerebellar contribution to gaze optimality. *Brain* 137, 1080–1094. <https://doi.org/10.1093/brain/awu006>.
- Sağlam, M., Lehnen, N., 2014. Gaze stabilization in chronic vestibular-loss and in cerebellar ataxia: interactions of feedforward and sensory feedback mechanisms. *J. Vestib. Res.* 24, 425–431. <https://doi.org/10.3233/VES-140538>.
- Sağlam, M., Lehnen, N., Glasauer, S., 2011. Optimal control of natural eye-head movements minimizes the impact of noise. *J. Neurosci.* 31, 16185–16193. <https://doi.org/10.1523/JNEUROSCI.3721-11.2011>.
- Srinivasan, M.V., Laughlin, S.B., Dubs, A., 1982. Predictive coding: a fresh view of inhibition in the retina. *Proc. R. Soc. Lond. B Biol. Sci.* 216, 427–459. <https://doi.org/10.1098/rspb.1982.0085>.
- Synofzik, M., Lindner, A., Thier, P., 2008. The cerebellum updates predictions about the visual consequences of one's behavior. *Curr. Biol.* 18, 814–818. <https://doi.org/10.1016/j.cub.2008.04.071>.
- Tangorra, J.L., Jones, L.A., Hunter, I.W., 2003. Dynamics of the human head-neck system in the horizontal plane: joint properties with respect to a static torque. *Ann. Biomed. Eng.* 31, 606–620. <https://doi.org/10.1114/1.1566772>.
- Therrien, A.S., Bastian, A.J., 2015. Cerebellar damage impairs internal predictions for sensory and motor function. *Curr. Opin. Neurobiol.* 33, 127–133. <https://doi.org/10.1016/j.conb.2015.03.013>.
- Tomlinson, R.D., 1990. Combined eye-head gaze shifts in the primate. III. Contributions to the accuracy of gaze saccades. *J. Neurophysiol.* 64, 1873–1891. <https://doi.org/10.1152/jn.1990.64.6.1873>.
- Tomlinson, R.D., Bahra, P.S., 1986. Combined eye-head gaze shifts in the primate. II. Interactions between saccades and the vestibuloocular reflex. *J. Neurophysiol.* 56, 1558–1570. <https://doi.org/10.1152/jn.1986.56.6.1558>.
- Tschan, R., Wiltink, J., Best, C., Beutel, M., Dieterich, M., Eckhardt-Henn, A., 2010. Validation of the German version of the vertigo handicap questionnaire (VHQ) in patients with vestibular vertigo syndromes or somatoform vertigo and dizziness. *Psychother. Psychosom. Med. Psychol.* 60, e1–12. <https://doi.org/10.1055/s-0029-1243206>.
- Tseng, Y.-W., Diedrichsen, J., Krakauer, J.W., Shadmehr, R., Bastian, A.J., 2007. Sensory prediction errors drive cerebellum-dependent adaptation of reaching. *J. Neurophysiol.* 98, 54–62. <https://doi.org/10.1152/jn.00266.2007>.
- Van den Bergh, O., Witthöft, M., Petersen, S., Brown, R.J., 2017. Symptoms and the body: taking the inferential leap. *Neurosci. Biobehav. Rev.* 74, 185–203. <https://doi.org/10.1016/j.neubiorev.2017.01.015>.
- Versino, M., Colagiorgio, P., Sacco, S., Colnaghi, S., Quagliari, S., Manfrin, M., Benazzo, M., Moglia, A., Ramat, S., 2014. Reading while moving: the functional assessment of VOR. *J. Vestib. Res.* 24, 459–464. <https://doi.org/10.3233/VES-140531>.
- Wolpert, D.M., Miall, R.C., Kawato, M., 1998. Internal models in the cerebellum. *Trends Cogn. Sci.* 2, 338–347. [https://doi.org/10.1016/S1364-6613\(98\)01221-2](https://doi.org/10.1016/S1364-6613(98)01221-2).
- Wortman, M.S.H., Lokkerbol, J., van der Wouden, J.C., Visser, B., van der Horst, H.E., Olde Hartman, T.C., 2018. Cost-effectiveness of interventions for medically unexplained symptoms: a systematic review. *PLoS One* 13, e0205278. <https://doi.org/10.1371/journal.pone.0205278>.

Mathematical Modelling in Motor Neuroscience: State of the Art and Translation to the Clinic. Gaze Orienting Mechanisms and Disease

EDITED BY
Stefano Ramat and Aasef G. Shaikh

Our understanding of the nervous system has made enormous progress since the discovery of the neuron as its constitutive processing element at the beginning of the 20th century. Thanks to advances in anatomy, cell biology, biochemistry, pharmacology and genetics, which have been made at an ever-increasing rate, the cellular foundations of the nervous system have been elucidated. Growing in parallel, new techniques for recording neuronal activity and imaging the brain have made possible the field of systems neuroscience, which seeks to understand of how populations of neurons govern behavior; engineering principles, mathematical modelling and a range of computational approaches have played key roles.

Motor neuroscience deals with understanding of how the brain is able to produce and control movement, i.e. our means to interact with the surroundings. Within this field of research, the study of how the brain controls eye movements has lead the way, emerging as the best understood human sensorimotor system due to the fruitful collaboration between basic science, clinical studies and mathematical modelling. Mathematical models allow us to forge hypotheses to account for functional properties of a biological system in a concise and unambiguous manner, and to quantitatively test such hypotheses by comparing experimental data and model predictions. This approach has proven especially fruitful in the ocular motor system, partly because of certain advantages offered by eye movements, but also because basic sciences have clarified the neural populations involved and their characteristics. Thus, basic knowledge such as anatomical connections, neuronal discharge properties and pharmacology, have been incorporated in mathematical models. Importantly, models developed for normal behavior have been extended to account for quantified clinical findings, providing unique opportunities to experimentally test the ability of models to account for pathological data. An important part of the scientific method has been to apply the results of experimental tests of a model's predictions to refine or revise the model.

The celebration of the career of Dr. Lance Optican, a leader in the field of systems neuroscience, was the occasion for organizing the conference "Mathematical Modeling in Motor Neuroscience. A short course and scientific meeting" in June 2018 in Pavia, Italy. Lance's models have guided ocular motor research over the past 30 years, and the articles collected in these two volumes, which originated from that conference, witness the relevance of his work, while providing a snapshot of the state of the art of the field.

Key Features

- Provides the authority and expertise of leading contributors from an international board of authors
- Presents the latest release in the Progress in Brain Research series
- Includes the latest information on mathematical modeling in motor neuroscience



ACADEMIC PRESS

An imprint of Elsevier
elsevier.com/books-and-journals

ISBN 978-0-444-64254-7



9 780444 642547